Laboratory Directed Research and Development FY2001

Annual Report

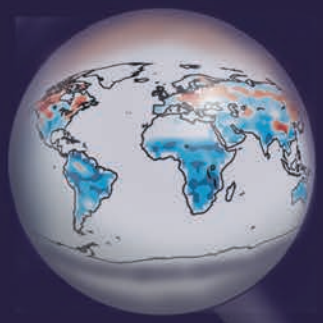

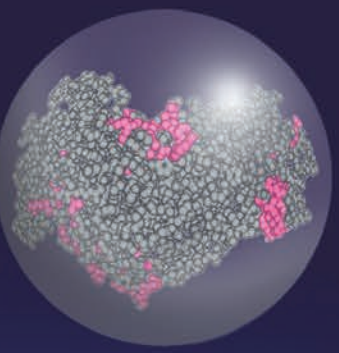

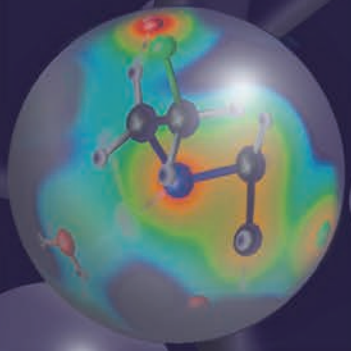

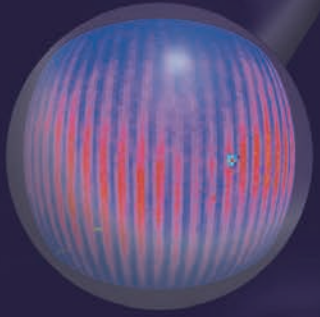

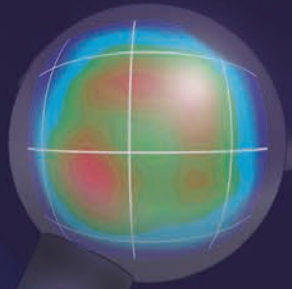

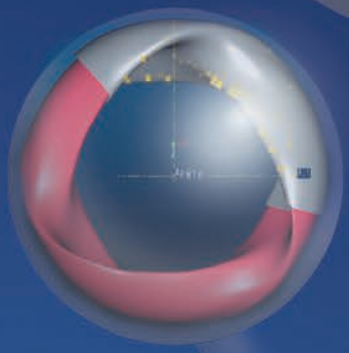

Lawrence Livermore National Laboratory

Making History Making a Difference

1952-2002

This work was performed under the auspices of the U.S. Department of Energy by University of California Lawrence Livermore National Laboratory under contract No. W-7405-Eng-48.

Laboratory Directed Research and Development FY2001

Annual Report

UCRL-LR-113717-01

Lawrence Livermore
National Laboratory

Making History
Making a Difference

1952-2002

Acknowledgments

This *Annual Report* provides an overview of the FY2001 Laboratory Directed Research and Development (LDRD) Program at Lawrence Livermore National Laboratory (LLNL) and presents a summary of the results achieved by each LDRD project. At LLNL, Laboratory Director C. Bruce Tarter and Deputy Director for Science and Technology Jeffrey Wadsworth are responsible for the LDRD Program and delegate responsibility for the operation of the Program to the Director of the Laboratory Science and Technology Office, Rokaya Al-Ayat. The LDRD Program at LLNL is in compliance with Department of Energy (DOE) Order 413.2 and other relevant DOE orders and guidelines.

The LDRD Program extends its sincere appreciation to the principal investigators of the FY2001 projects for providing the content of this report, and to the publications team, whose names are listed below. A special thanks goes to Emmeline Chen, Robert Kirvel, Whitney Lacy, Donald McNichols, Katherine Walter, and Gloria Wilt for editorial assistance and to LDRD staff members Andrew Hazi and Kenneth Jackson for their technical review. We also thank the other members of the LDRD team for their many contributions to this publication: Carol Booth, administrative specialist; Mary Callesen, administrator; Nancy Campos, database administrator, and Cathleen Sayre, resource manager.

Scientific Editor

Rokaya Al-Ayat

Publication Editor

Karen Kline

Publication Designer

Daniel Moore

Publication Staff

Coralyn McGregor, editor
Peter Murphy, editor
Louisa Cardoza, compositor

Contents

Section 2 Atmospheric and Geosciences

Section 3 Biotechnology and Health Care Technologies

Section 4 Computing, Modeling, and Simulation

Section 5 Energy and Environmental Technologies

Section 6 Lasers, Electro-Optics, and Beams

Section 7 Materials Synthesis and Characterization

Section 8 Nuclear and Atomic Science and Technology

Section 9 Space Science and Technology

Appendix

Program Overview

Laboratory Directed Research and Development Program

Established by Congress in 1991, the Laboratory Directed Research and Development (LDRD) Program provides the Department of Energy (DOE)/National Nuclear Security Administration (NNSA) laboratories, like Lawrence Livermore National Laboratory (LLNL or the Laboratory), with the flexibility to invest up to 6% of their budget in long-term, high-risk, and potentially high payoff research and development (R&D) activities to support the DOE/NNSA's national security missions. By funding innovative R&D, the LDRD Program at LLNL develops and extends the Laboratory's intellectual foundations and maintains its vitality as a premier research institution. As proof of the Program's success, many of the research thrusts that started many years ago under LDRD sponsorship are at the core of today's programs.

The LDRD Program, which serves as a proving ground for innovative ideas, is the Laboratory's most important single resource for fostering excellent science and technology for today's needs and tomorrow's challenges. Basic and applied research activities funded by LDRD enhance the Laboratory's core strengths, driving its technical vitality to create new capabilities that enable LLNL to meet DOE/NNSA's national security missions. The Program also plays a key role in building a world-class multidisciplinary workforce by engaging the Laboratory's best researchers, recruiting its future scientists and engineers, and promoting collaborations with all sectors of the larger scientific community.

The LDRD Portfolio Management Process

The LDRD Program management process at LLNL has three major components that ensure the quality of each fiscal year's portfolio: (1) a top-level strategic planning process to identify key science and technology areas for LDRD investment; (2) a call to the Laboratory scientific and technical community for innovative and relevant proposals within the DOE/NNSA mission areas; and (3) a scientific peer-review process to select an LDRD portfolio from these proposals.

In addition to LLNL's LDRD Program management process, the DOE/NNSA oversees the Laboratory's Program to ensure that the Program accomplishes its objectives. This oversight includes financial certification reviews, appraisal process reviews, program plan reviews—both in the field and at headquarters, individual project reviews, and onsite reviews of both technical content and management processes. In an independent FY2001 report to Congress,[1] the General Accounting Office stated,

> *All the LDRD projects we reviewed met DOE's guidelines for selection [and] had created the internal controls necessary to reasonably ensure compliance with DOE's guidelines. The key controls in place included using DOE's guidelines to control and conduct the project-selection process…and ensuring appropriate DOE oversight and review of the results of the process."*

[1] *U. S. General Accounting Office (2001). Report to Congressional requesters: National laboratories oversight of Laboratory Directed R&D Program (OUO). GAO-01-927. p.3.*

Lawrence Livermore National Laboratory

Fifty Years of Science in the National Interest

In 2002, its 50th Anniversary year, LLNL,a premier applied-science laboratory, proudly carries forward its primary national security mission: to ensure the safety, security, and reliability of the nation's nuclear weapons stockpile without underground nuclear testing, and to prevent and counter the spread and use of weapons of mass destruction—nuclear, chemical, and biological.

The Laboratory uses the scientific and engineering expertise and facilities developed for its primary mission to pursue advanced technologies for other important national security needs—homeland defense, military operations, and missile defense, for example—that evolve in response to emerging threats. In terms of broader national needs, the Laboratory executes programs in energy security and long-term energy needs, environmental assessment and management, bioscience and technology to improve human health, and breakthroughs in fundamental science and technology. With this multidisciplinary expertise, the Laboratory serves as a science and technology resource to the U. S. government and as a partner with industry and academia.

One of three DOE/NNSA laboratories, LLNL has been managed since its inception in 1952 by the University of California (UC). This half-century association with UC has enabled the Laboratory to establish an atmosphere of intellectual freedom and innovation that attracts and maintains the world-class workforce needed to meet challenging national missions.

Structure of the LDRD Program

Project Categories

The LDRD Program at LLNL consists of three major project categories: Strategic Initiative (SI), Exploratory Research (ER), and Laboratory-Wide Competition (LW). Throughout the year, the Program also funds a few projects in a fourth category, Feasibility Study/Project Definition (FS).

Strategic Initiative

The Strategic Initiative (SI) category focuses on innovative R&D activities that are likely to set new directions for existing programs, help develop new programmatic areas within LLNL's mission responsibilities, and enhance the Laboratory's science and technology base. Projects in this category are usually larger and more technically challenging than projects funded in other categories. An SI project must be aligned with the strategic R&D priorities of at least one of four Laboratory Strategic Councils: (1) the Council on Bioscience and Biotechnology, (2) the Council on Energy and Environmental Systems, (3) the Council on National Security, and (4) the Council on Strategic Science and Technology.

Exploratory Research

The Exploratory Research (ER) category is aligned with the strategic R&D needs of a Laboratory Directorate (ERD) or Institute (ERI). Typically, fewer than half of the proposals that researchers submit to their Directorates and Institutes are forwarded to the ER selection committee for review.

Laboratory-Wide Competition

Projects in the third LDRD category, Laboratory Wide Competition (LW), emphasize innovative research concepts and ideas with limited management filtering to encourage the creativity of individual researchers. The LW Competition is open to all LLNL staff in programmatic, scientific, engineering, and technical support areas. Researchers submit their project proposals directly to the LW selection committee. The number of projects selected in this category ranges from one-third to one-fifth of those submitted.

Feasibility Study/Project Definition

This special project category, Feasibility Study/Project Definition (FS), provides the flexibility to define and develop potential projects in the other three categories. To increase its responsiveness to Laboratory scientists and engineers, the LDRD Program funds FSs throughout the year. Principal investigators can submit FS proposals through their directorate or directly to the LDRD Program Office.

The FY2001 LDRD Portfolio

Investing to support national security missions

Portfolio Structure

The FY2001 LDRD portfolio was carefully structured to continue the Program's vigorous support for the strategic vision and long-term goals of NNSA and LLNL. The FY2001 projects described in this *Annual Report* have undergone a stringent selection process and on-going management oversight. Analysis shows that the overwhelming majority of this portfolio—94%—supports the Laboratory's national security mission. This level of support far exceeds the National Security Program percentage of LLNL's overall budget, estimated to be 70% for FY2001.

In FY2001 the Program funded 195 projects. Figure 1 shows the number of projects in each of the four project categories.

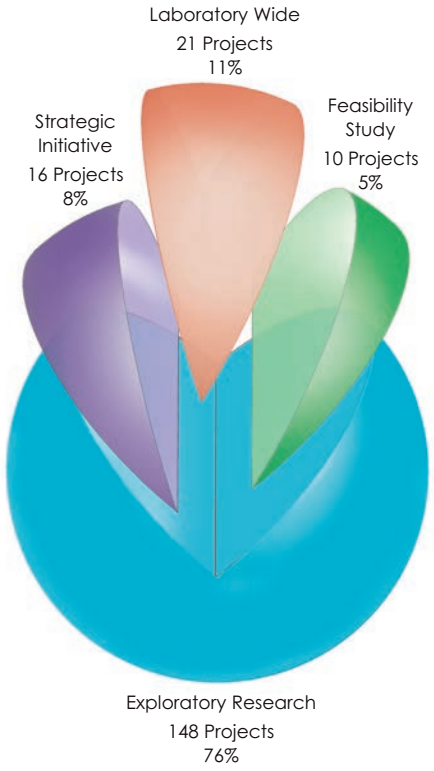

Figure 1. Number and percentage of LDRD projects in each of the four project categories. In FY2001, 195 projects were funded.

Strategic Initiative

In FY2001, the LDRD Program funded 16 SI projects out of 28 proposals submitted. The SI category represents 8% of LDRD projects for FY2001. Projects in this category range from research in computational biology to space science and technology.

Exploratory Research

In FY2001, of the 178 proposals the Directorates and Institutes forwarded to the ER selection committee, 148 were funded. Exploratory Research accounts for 76% of LDRD projects for the fiscal year. Examples of projects in this category include global and climate simulations, research on remote detection of bioaerosols, and ultrafast production of highly stable nanostructures on semiconductors.

Laboratory-Wide Competition

Of the 63 LW proposals submitted, the Program funded 21. The LW category represents 11% of LDRD projects in FY2001. Projects in this category range from applying adap-

tive optics to extend the range of human visual acuity to x-ray lasers that probe the properties of high-density plasmas.

Feasibility Study

Feasibility Studies are limited to a maximum duration of six months and a budget not to exceed $50 thousand. Total funding for FSs is limited to 1% of the LDRD Program budget. In FY2001, the Program funded ten FS projects—5% of LDRD projects.

Portfolio Funding

In FY2001, the DOE/NNSA authorized the LLNL LDRD Program to fund $55.2 million for projects: approximately 66% was allocated for ERs, 27% for SIs, 6% for LWs and 1% for FSs. Figure 2 shows the distribution of funding among the four LDRD project categories.

Strategic Initiatives accounted for all seven projects in the top funding level. The average funding for an LDRD project in FY2001 was $238 thousand; most ERs were funded at this level. Funding for LWs averaged $160 thousand per project. Figure 3 shows the number of projects in various levels of funding.

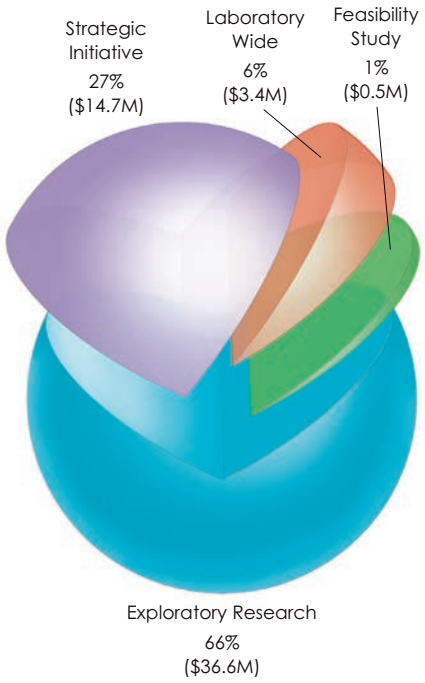

Figure 2. Distribution of funding (in $ million) among the four LDRD project categories. Total funding for FY2001 was $55.2 million.

Project Competency Areas

Although LDRD projects often address more than one scientific discipline, each project is classified into one of nine competency areas that are relevant to NNSA and Laboratory missions. The nine competency areas are:

- Advanced Sensors and Instrumentation
- Atmospheric and Geosciences
- Biotechnology and Health Care Technologies
- Computing, Modeling, and Simulation
- Energy and Environmental Sciences
- Lasers, Electro-Optics, and Beams
- Material Synthesis and Characterization
- Nuclear and Atomic Science
- Space Science and Technology

Figure 4 shows the percentage of LDRD funding and number of projects in each competency area in FY2001. Consistent with the Laboratory's strategic needs, Computing, Modeling, and Simulation received the most funding (24%) and has the largest number of projects (46), while the smallest competency area was Space Science and Technology, which received less than 5% of the funding for ten projects. This investment strategy enables the Laboratory to meets its special responsibility for nuclear weapons research, including advanced simulation and computing, the prevention and counterproliferation of weapons of mass destruction, international security, arms control, and energy and environmental management.

Portfolio Highlights

Six FY2001 projects—two projects each from the SI, ER, and LW categories—highlight the diverse scope of LDRD research. These projects demonstrate the Program's emphasis on science and technology R&D to meet the evolving needs of the DOE/NNSA's national security mission.

Strategic Initiative

Ultrafast materials probing with the Falcon–linac Thomson x-ray source

P.T. Springer, Principal Investigator (01-SI-007, p. 6-17)

The goal of this project is to develop and demonstrate a novel x-ray probe to study the ultrafast dynamics of matter on the timescale of atomic motions—a picosecond or less. Such experiments include observing the motions of atoms in a material or a chemical reaction when the material is excited with a laser. With collaborators at the University of California, Los Angeles, LDRD researchers are using state-of-the-art techniques to synchronize the ultrashort light pulse (less than 100 femtoseconds) from the LLNL's multiterawatt Falcon laser with a high-energy (100 megaelectron volt) linear accelerator (linac). Thomson scattering of laser photons off a tightly focused low-emittance beam of relativistic

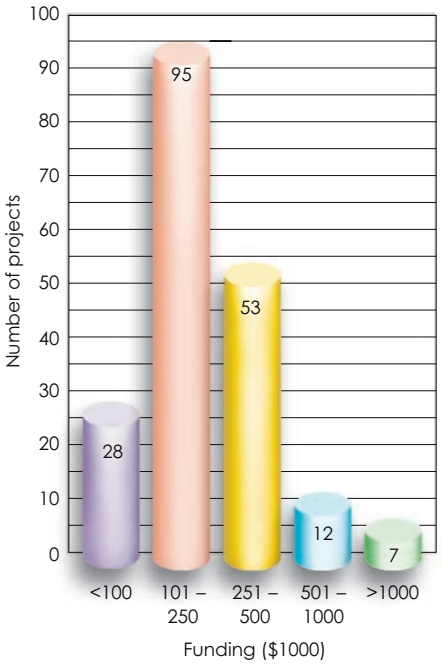

Figure 3. Number of projects at various levels of funding (in $ thousand). The average funding for an LDRD project in FY2001 was $238 thousand.

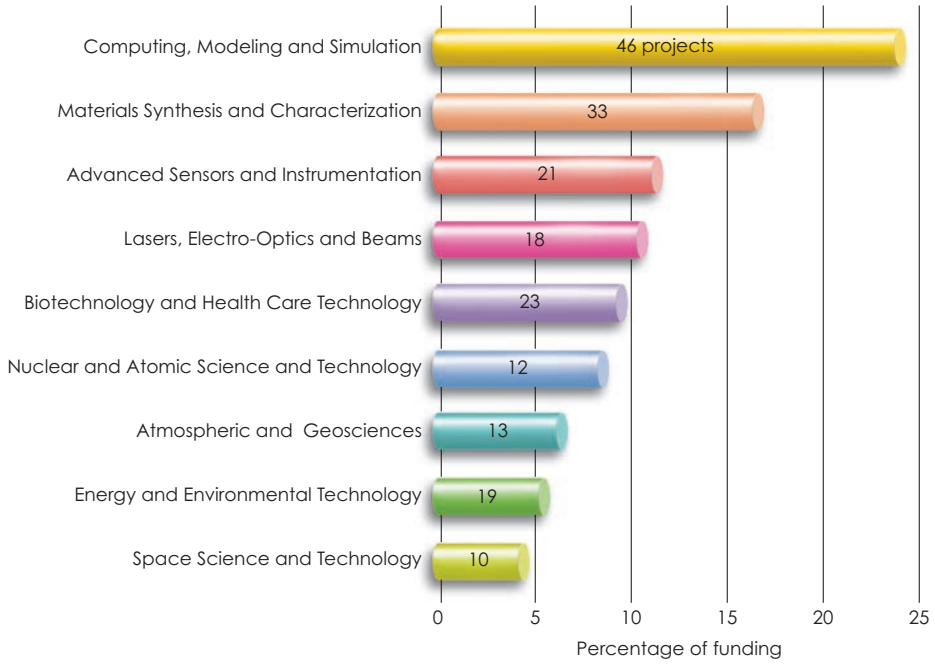

Figure 4. Percentage of LDRD funding and number of projects in each competency area in FY2001.

electrons from the linac produce bursts of tunable hard x rays with a pulse duration of less than 100 femtoseconds. This x-ray beam is expected to make possible unprecedented dynamic measurements of high-atomic-number materials that are important for the Stockpile Stewardship Program.

In FY2001, the project successfully completed major laser and linac modifications and improvements required to optimize x-ray production. In FY2002, the project will focus on producing, characterizing, and using the high-energy Thomson beam in pulse-probe experiments.

Broad-spectrum biological assays using liquid-based detection arrays
F. Milanovich, Principal Investigator (99-SI-016, p. 1-4)

One of the most significant shortfalls in our nation's ability to counter threats from bioterrorism is the lack of a detection system that can quickly and accurately detect the presence of many pathogens simultaneously. This project is developing a fast, inexpensive, portable, high-throughput, parallel pathogen-detection prototype to aid the nation in its fight against bioterrorism (see box story on p. 6). This technology, called liquid array, uses optical encoding of small-diameter beads that serve as templates for biological capture assays. Once exposed to a fluid sample, the beads can be individually identified and probed for target pathogens at rates of several thousand beads per second. Because each bead can be separately identified and ascribed with a different assay, many parallel assays can be performed simultaneously.

In FY2001, the project team made excellent progress in developing a portable, easy-to-use pathogen-detection device that makes it possible for first responders to run sophisticated diagnostics in the field. At year's end, the project was in the process of identifying potential commercial partners. This work has resulted in a number of patents.

Exploratory Research

Colloidal transport of actinides in the vadose zone
A. B. Kersting, Principal Investigator (00-ERD-011, p. 5-2)

Toxic contaminants generated during the nuclear weapons program have resulted in over six billion cubic meters of contaminated soil and rock at DOE facilities. Sixty million cubic meters of this contaminated material lie within the vadose zone—the area between the surface and the underlying groundwater aquifers. To develop effective cleanup and containment methods for environmental restoration of sites contaminated with radioactive nuclear waste, this project focused on understanding how and under what conditions colloids (particles smaller than 1 micrometer) influence the transport of actinides in the subsurface.

Using vadose-zone water and rock samples from a tunnel system in Rainier Mesa at the Nevada Test Site, the research team evaluated the competing controls on colloidal transport through careful laboratory experimentation, and developed a verifiable transport model that supports both experimental and field results.

In FY2001, the team continued its investigation of the assumption that actinides are immobile in the subsurface by documenting, for the first time, plutonium transport associated with colloids detected in groundwater 1.3 kilometers from their original source.

Negating chemical-agent dispersion during missile defense
G. T. Nakafuji, Principal Investigator (00-ERD-014, p. 4-8)

What happens to the chemical weapon payload carried by an intercepted ballistic missile? The goal of this project is to help determine whether proposed, high-altitude ballistic-missile-defense intercept systems are effective in preventing lethal dispersion of a chemical warfare agent from an intercepted chemical warhead. The project has both computational and experimental components.

Experiments during FY2001 were conducted in collaboration with scientists at the University of California, Santa Barbara's supersonic, rarefied, pulsed-air wind tunnel. The experiments yielded remarkable results for observing the breakup of liquid in drops ranging in diameter from 2 millimeters to more than 1 centimeter at altitudes between 30 and 70 kilometers. The rarified conditions at such altitudes result in extended breakup time scales that reveal features of droplet breakup that have never before been reported in the literature.

Laboratory Wide Competition

Metal–insulator transition in lithium and lithium hydride
M. Bastea, Principal Investigator (00-LW-037, p. 7-12)

LLNL scientists have recently demonstrated the metallization of fluid hydrogen

and oxygen under high dynamic pressures. The goal of this project is to search for the opposite phenomenon—a nonmetallic, high-pressure phase of metallic lithium (Li), a first in the history of physics—and to find the metallization conditions of lithium hydride (LiH), which provides the unique opportunity to understand the effects of coupling two elements with opposite tendencies at extreme conditions. The transition of condensed matter between electrically conducting and insulating states is a topic of wide scientific interest. Phase transitions in the two materials studied in this project—Li and LiH—have several applications to LLNL's stockpile stewardship mission in laser-target fabrication and experimental design.

Shock reverberation experiments at LLNL and experiments conducted at Sandia National Laboratory's Z-pinch accelerator in FY2001 provided data on the behavior of Li under conditions of very high pressure. This research, which builds on LLNL's special experimental capabilities in shock and high-pressure physics, will lead to new physical insight and improved theoretical models for the behavior metals and other solids under conditions of very high pressure.

Direct imaging of protein–DNA complexes using carbon-nanotube atomic force microscopy and single-molecule optical detection

A. Noy, Principal Investigator
(01-LW-007, p. 3-21)

Living cells have developed sophisticated DNA repair mechanisms to maintain their genetic code integrity. However, errors in the repair process itself or interactions between the damaged DNA and cellular proteins may lead to cancer. Structural studies have provided some information about the local damage in the DNA, but several pivotal questions remain unanswered, for example, how proteins find a damaged site among normal base pairs, and how they recruit the other proteins needed for the repair process. Looking at the large-scale picture of DNA repair and tracking individual proteins as they assemble on the damaged DNA may provide some answers.

This project is developing a new experimental method that combines two powerful techniques—carbon nanotube atomic force microscopy (AFM) and single-molecule optical detection—to collect nanometer-resolution images that capture, for the first time, the transient DNA–protein interactions that are crucial for understanding DNA damage repair.

In FY2001, researchers concentrated on using simultaneous AFM and single-molecule optical detection to investigate how XPA, a repair protein, binds to DNA.

Recent LDRD Program Accomplishments

Over the years, LDRD-sponsored projects have realized major scientific and technical breakthroughs that have been widely reported in the technical community. Highlighted here are a few of the achievements of recent LDRD projects.

Patents

The table below shows the number of patents resulting from LDRD-funded research during each of the past five years. Projects sponsored by LDRD consistently account for a large percentage of the patents issued for LLNL research, especially considering that the LDRD Program funding represents only 6% of the total LLNL budget, with the exception of FY2000, when the Program received only 4% of the budget.

	1996	1997	1998	1999	2000	2001
Total LLNL patents	83	64	78	84	93	89
LDRD patents	35	29	39	45	35	42
LDRD patents as percentage of total	42	45	50	54	38	47

Awards

- **DOE Defense Program Award of Excellence for Technical Excellence in Advanced Simulation and Computing (ASCI)**

LDRD principal investigators G. Galli (00-ERD-031) and F. Gygi (01-ERD-044) received this 2001 DOE award for their simulation on shocked deuterium using first-principles molecular dynamics techniques. The simulation showed that it is possible to observe a shock front at the microscopic scale, thus opening the way to direct shock simulations from first principles, without experimental input. This work is applicable to stockpile stewardship.

- **LLNL FY2001 Science and Technology Award: Crystals, Biomineralization, and the Origins of Life**

Team members: J. De Yoreo, M. McBride, C. Orme, A. Noy, and T. Land

The team received this annual LLNL award for their outstanding scientific and technical achievements in developing new understanding of biomineralization and crystal growth, in partnership with scientists from the Virginia Polytechnic Institute and the University of South Alabama. Determining the mechanisms by which living organisms control materials design and synthesis on a molecular scale is one of the grand challenges facing materials science. Much of this work was conducted with LDRD funding, beginning in FY1995 (95-ERP-144) and most recently in FY2001 (01-ERD-040).

Post-September 11 Response Supported by LDRD Investments

Recent events have highlighted the importance of the LDRD strategic investment approach to addressing emerging national priorities. Many of the capabilities the NNSA laboratories fielded in response to post-September 11 events were the result of previous LDRD Program investments. Continuing terrorist activities underscore the fact

From the Dugway Proving Grounds to the Salt Lake City Olympics

LDRD investments pay off for national security and homeland defense

A battery-powered device the size of a notepad computer can rapidly detect and identify many biowarfare agents simultaneously and accurately. This LLNL-patented technology[1], developed over a period of a decade at LLNL with LDRD and other funding sources, is the basis of the instrument that was selected over a slate of eight competing instruments to provide one component of biosecurity at the Salt Lake City Olympics. The instrument, the SmartCycler®, performed thousands of environmental measurements as part of the Homeland Security team deployed in the Salt Lake City area during the 2002 Winter Olympics. Under license from LLNL, the SmartCycler® is marketed by Cepheid of Sunnyvale, CA.

Supported by LDRD funding since 1996[2], a team of LLNL scientists, led by Fred Milanovich and Ray Mariella, developed miniaturized polymerase chain reaction (PCR) technology, now licensed to Cepheid, that can be packaged into instruments that are fast, accurate, and reliable, yet portable, user-friendly, and tough enough to withstand operating conditions in medical clinics, in civilian emergencies, and on the battlefield.

The Cepheid machine used at the Olympics contains 16 sample chambers operating independently to perform simultaneous analysis of environmental samples that may contain many potential pathogens. Using fluorescence-based PCR assays in combination with advanced flow cytometry technology, this real-time instrument simultaneously obtains detailed genetic information about the virulence and epidemiology of each pathogen in the sample by amplifying unique regions of its DNA, thus eliminating the need for culturing cells or microorganisms.

The latest LLNL version of the PCR instrument is the Handheld Advanced Nucleic Acid Analyzer (HANAA), which is a four-chamber, real-time, battery-powered instrument—the first of its kind. Since September 11 and the subsequent anthrax attacks, this technology has been deployed as part of Homeland Security. A six-chamber version of the HANAA, called the BioSeeq® built by Environmental Technologies Group (ETG) under sublicense from Cepheid, is expected to reach the market in 2002 and is already in great demand from first-response agencies, hospitals, and medical clinics.

When LLNL researchers first began to develop the PCR/flow cytometry technology in the early 1990s, their goal was to build the highest-performance instrument possible and make the technology available to support the Human Genome Project and medical applications. Design considerations that would later prove essential, such as reliability in the field, portability, and ease of use by nontechnical personnel, were not a consideration. At that time, countering the spread of biological weapons of mass destruction had yet to become a major national concern.

The Gulf Crisis in 1990–91 and the collapse of the Soviet Union in 1991 heightened the threat of biological warfare and terrorism to our national security. In response, the Department of Defense (DoD) raised the priority of research directed towards counterproliferation of biological and chemical weapons. When the PCR/flow cytometry project first received LDRD funding in FY1996, LLNL was unknown in the biodefense field. But with its multidisciplinary capabilities in national security programs, bioscience, engineering, and computations, LLNL had the expertise to meet this new challenge. Clearing the initial hurdle—demonstrating the usefulness of the PCR and flow cytometry technologies for military applications and thereby gaining credibility in the biodefense community—sent the project team to the Dugway Proving Grounds in Utah in October 1996 for the DoD-sponsored Joint Field Trials.

At Dugway, the field-portable versions of LLNL's flow cytometer correctly detected and identified 87 percent of all the unknown bacterial warfare simulants, with no false positives, outperforming all other participants in the trials. After the 1996 trials, the team improved the PCR assays with multiplex assay methods for faster performance, longer-wavelength laser excitation, and better reagents for increased sensitivity. A year later, the new device was successfully tested.

Since then, a stream of funding—from LDRD, DOE, and Work for Others—for various aspects of this challenging problem has made possible continuous improvements in technology and instrument development. The result is commercially available products like the SmartCycler® and BioSeeq®.

The terrorist attacks of September 11 and the anthrax attacks that followed turned the threat of biological weapons into reality for the nation's civilian population. Because of the LDRD Program's long-term investments in emerging national security missions, LLNL has successfully transferred biodetection technologies to the private sector to help combat bioterrorism.

[1] Northrup, M. Allen, R. P. Mariella, A. V. Carrano, and J. W. Balch, "Silicon-based sleeve devices for chemical reactions", US Patent No.5,589,136 (31 December, 1996).
[2] LDRD project 96-DI-009, *Biological warfare: detection, identification, and tracking technology,* (F. P. Milanovich, R. P. Mariella, Jr., and R. Langlois).
[3] LDRD project 94-ERD-009, *Diode-laser-based flow cytometer,* (R. P. Mariella, Jr.).

that the nation needs to invest now in the science and technology that will effectively anticipate emerging threats. Below are three examples of technologies developed with LDRD Program funding that were fielded in response to terrorist attacks on the U.S.

- **Hyperspectral Infrared Imaging System (HIRIS)**

HIRIS was developed to detect and identify the chemical composition of gas plumes by their spectral signatures. A passive longwave-infrared imaging system that simultaneously collects spectral, spatial, and temporal data of the same scene at hundreds of different infrared wavelengths, HIRIS monitored chemical emissions from World Trade Center fires after September 11, 2001.

- **Handheld Advanced Nucleic Acid Analyzer (HANAA)**

This miniaturized polymerase chain reaction (PCR) analyzer was developed for on-site detection of biological weapons agents. Nucleic acid analysis via PCR was chosen over immunoassay for this application because of PCR's unmatched ability to obtain detailed genetic information about a particular pathogen's virulence and epidemiology. HANAA was fielded at the Salt Lake City Olympics (see box story on facing page).

- **Micropower Impulse Radar**

Micropower impulse radar generates ultrashort, picosecond-pulsewidth electromagnetic signals that span the upper radio- and lower microwave-frequency spectrum. As in conventional radar, targets within the illuminated regions of the transmitted signals scatter, absorb, and reflect the incident signal. The reflected signals, when post-processed, can be used to describe and characterize the targets. This technology was modified for use as a debris-penetrating radar to search for live victims that might have been trapped in the building debris during search-and-rescue efforts at the World Trade Center.

National Security

LDRD projects have resulted in scientific advancements that have applications ranging from energy production and environmental concerns to DOE and Department of Defense (DoD) national security programs. Livermore and other NNSA Laboratories have effectively applied the world-class science and technology developed through LDRD-funded research to projects that support specific requirements identified by DOE and other agencies.

Listed below are a few examples of technologies used in DOE and DoD defense and counterterrorism programs that were initiated using LDRD funds.

- **Portable DNA Analyzers for Biological Incidents**

LDRD funded the research, development, and initial demonstration of DNA analyzers. These battery-powered instruments are finding applications in both counterterrorism and battlefield situations (see box story on facing page). LDRD also initiated our capabilities in finding unique biological signatures for pathogens likely to be used in biological terrorist attacks. Advances in this area have been recently demonstrated in a real-life situation. Using the LLNL-developed DNA-based test system, biologists at Northern Arizona University detected an outbreak of the plague in prairie dogs so quickly that they were able to issue a health warning within hours.

A current LDRD project is exploring similar DNA-based technologies for rapid and high-throughput identification of hoof and mouth disease, a viral agent. Results from these research activities are of great interest to the NNSA's Chemical and Biological National Security Program (CBNP), the Centers for Disease Control, the Department of Agriculture, and local animal-health agencies.

- **Biological Early Warning Systems for the Department of Defense**

LDRD funded the early applied research that enabled the Laboratory to develop the Joint Biological Early Warning System (JBREWS) for the Joint Program Office for Biodefense in the DoD. JBREWS is a self-configuring, self-healing radio frequency sensor network to support both sensor data acquisition and command-and-control functions. The sensor network architecture had an outstanding performance in a DoD advanced-concept technology demonstration.

- **Combat Simulation**

LDRD projects contributed significantly to the early development of the Joint Conflict and Tactical Simulation (JCATS), an entry-level simulation that can model conflicts from the campaign level to individuals fighting inside a multistory building. Using actual terrain and elevation data, JCATS models the world in 3D, permitting detailed examination of individual and small-unit performance in realistic rural or urban backdrops. Dynamic aggregation/deaggregation, a JCATS-unique feature, allows users to create and control large formations of troops or police officers while the underlying simulation continues to track and record activity at the individual level. Aggregation enables a few players to control large-scale complex games while maintaining the ability to dynamically telescope in and concentrate on key events in the simulation run.

In FY2001, the JCATs team received a Modeling and Simulation Award from the DoD's Modeling and Simulation Office.

- **Conventional Munitions**

LDRD has funded numerous projects to improve our understanding of high explosives. This has permitted the Laboratory to engage in all aspects of munitions research from the rational design of new explosives to the safe disposal of munitions. LDRD has also funded studies in fundamental hydrodynamics that have led to warhead design optimization. Using the science acquired from LDRD-funded research, Livermore has contributed to numerous DoD-sponsored projects for the development of conventional weapons.

- **High-Power Laser Diodes and Diode-Pumped Solid-State Lasers**

In the late 1980s and early 1990s, Livermore LDRD supported the development of high-power semiconductor diode laser arrays, a compact and efficient technology that forms the basis for most future laser systems. The LDRD

Program sponsored the introduction of microchannel cooling techniques for these emitters and the development of the world's highest-power arrays. At more than 10 kilowatts each, the units had active areas the size of several postage stamps. Over the past decade, LDRD funds also helped support work using the high-power diode laser arrays to optically excite solid-state laser media and replace the much larger and less efficient flashlamps in diode-pumped solid-state laser systems.

The Laboratory's expertise in this high-power technology is leading to new military laser prototypes. In September 2001, the Laboratory and the Army's High Energy Laser Strategic Test Facility (HELSTF) unveiled the highest average power single-beam solid-state laser in the world, a 10-kilowatt laser that could demonstrate a new short-range air and missile defense capability. The ultimate objective is to develop a next-generation system to produce a 100-kilowatt laser prototype. Potential targets include enemy tanks, attack helicopters, and antitank missiles.

- **Cybersecurity**

Over the past several years, LDRD funded an SI project (99-SI-005) to develop a comprehensive approach and a model for information assurance activities that enable researchers, policy makers, and computer security experts to understand and begin to address the problems posed by the nation's reliance on massive computer networks. We have concentrated LLNL's efforts on developing the Information Operations, Warfare, and Assurance (IOWA) software. IOWA is a suite of software toolsets that can be used for modeling and visualizing information networks, analyzing vulnerabilities, and simulating attacks and fixes. During the last year, we completed extensive quality assurance and documentation, leading to a production version of the first software toolset. The toolset is currently in use by sponsors within the DOE and other federal intelligence agencies.

The FY2001 LDRD Annual Report

The *FY2001 LDRD Annual Report* provides a summary of LDRD-funded projects for the fiscal year. Each article, submitted by the principal investigator, summarizes the project scope, motivation, goals, relevance to DOE/NNSA and LLNL mission areas, and the progress achieved in FY2001.

Articles are arranged in sections that correspond to the nine LDRD competency areas. Within each section, articles appear in numerical order of their tracking code (e.g., 01-ERD-100) a unique identifier that consist of three elements. The first element is the fiscal year the project began (01 for FY2001); the second element is the LDRD project category (ERD for Exploratory Research in the Directorates); and the third element identifies the order in which the proposal was received (100).

The Appendix includes a compilation of LDRD research-generated publications, a principal investigator index, a project title index, and an index of projects by tracking code.

Advanced Sensors and Instrumentation

Section 1

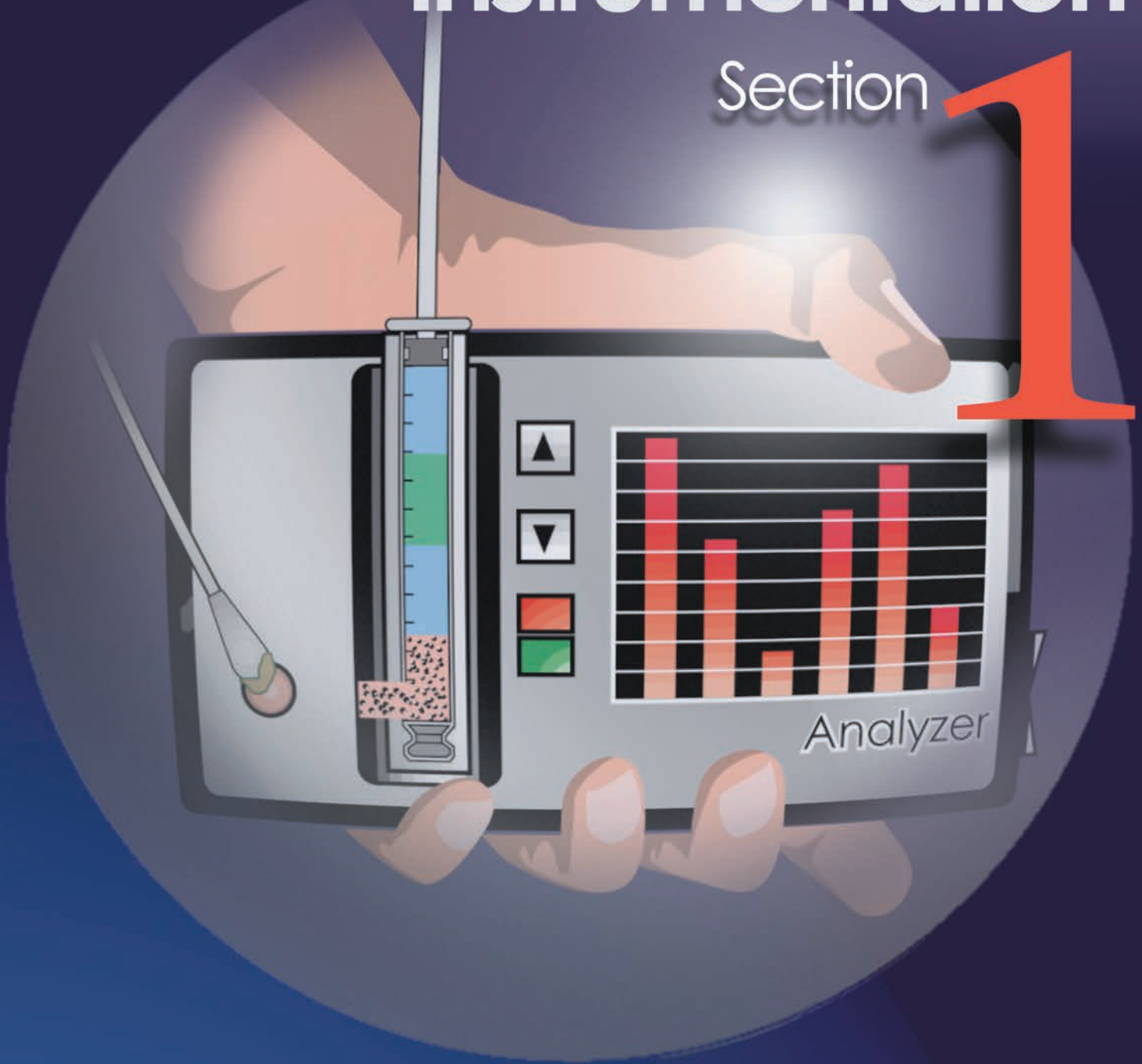

Section 1 Advanced Sensors and Instrumentation

Real-time mass-spectrometric detection and identification of biological aerosols

K. Langry

Most techniques for pathogen detection, such as polymerase chain reaction (PCR), flow cytometry, and conventional mass spectrometry, require time-consuming sample preparation and complex reagents, and have slow response (time scale of minutes). The objective of this project was to demonstrate the feasibility of real-time aerosol analysis with a system that can detect and identify individual biological aerosol particles in milliseconds with no sample preparation and no reagents.

The bioaerosol analysis system we envision would operate by pulling aerosols directly from the atmosphere into a vacuum chamber where an intense infrared (IR) laser pulse would be delivered to each bioaerosol particle, disrupting it and yielding various molecular ions. The masses of these ions, determined by time-of flight mass spectrometry (TOF-MS), would be used to identify the microorganisms that constitute the particle.

An aerosol mass-spectrometry system would be ideally suited for autonomous, continuous, long-term operation at ground-based sites and aboard airborne sampling platforms. The system would significantly expand the capabilities for detection of biological agents in military and civilian applications.

The experimental approach taken in this project was first to demonstrate that molecular signatures of various common bacteria could be obtained from spores using the matrix-assisted laser desorption/ionization (MALDI) technique with TOF-MS. This was achieved in the first year of the project (FY1998) using UV-MALDI. During FY1999, we demonstrated that unique bacterial signatures can be obtained with matrix-free samples by TOF-MS using a pulsed IR laser.

In FY2000, we planned to demonstrate that with a pulsed IR laser we could disrupt aerosolized spores passing through the source of a TOF-MS and generate mass spectra unique to the bacteria from which they originated. The development of mass spectra from aerosolized biological material proved to be a technical challenge. It was also an administrative challenge, because of the necessity of developing a safe protocol for generating and analyzing biological aerosols. This was accomplished late in this final year of the project (FY2001) with approval of an Integrated Work Statement.

As protocols for handling and analyzing the aerosols were developed during FY2001, we addressed the technical challenge of interfacing the electronic timing circuits of the laser system with the mass spectrometer. We detected mass spectra from biological aerosol particles using a pulsed UV (266-nm) laser.

Our work in this project has established the feasibility of rapid identification of biological aerosols with IR laser desorption followed by time-of-flight mass spectroscopy (see Figure). Making real-time aerosol analysis work will depend on accurate timing of the firing of the IR desorption laser, which must take place within a window of less than 1 μs and with a timing that depends on particle mass. Just as critical will be accurately determining the timing of events leading up to laser firing (charging the capacitors that drive the Nd:YAG pump laser, thermally equilibrating the optical parametric oscillator crystal that delivers the IR pulse, and allowing for the recovery time of the laser rods). Once these timings are known, it should be possible to assemble and evaluate a prototype system.

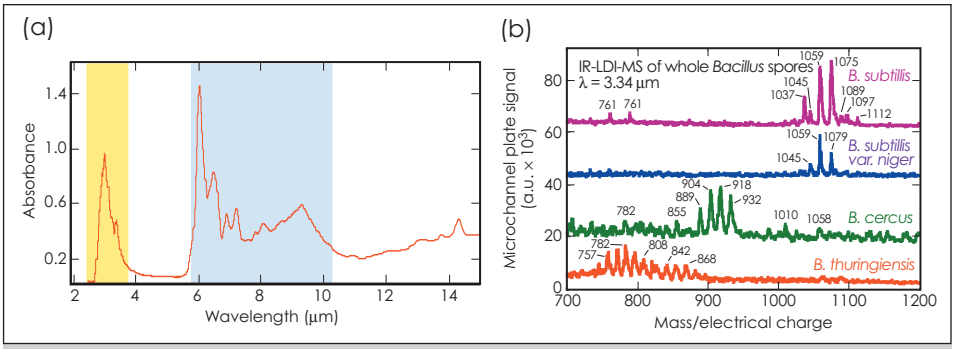

(a) The infrared (IR) spectrum of *B. subtilis* spores exhibits two major absorption bands, one centered around 3.3 μm (yellow) and the other at 6.2 μm (blue). These two wavelengths are characterisitic of dipicolinic compounds that make up a large portion of *B. subtilis* spores. (b). A thin film of spores from four different *Bacillus* species were pulsed with a 3.34-μm IR laser beam and produced the unique time-of-flight mass spectra shown here.

Single-fluorescent-molecule confocal microscopy: A new tool for molecular biology research and biosensor development

S. M. Lane, C. W. Hollars, T. R. Huser, R. L. Balhorn

The ability to detect and identify a single molecule represents the ultimate limit in detection sensitivity. Because of advancements in microscopic techniques over the past decade, this capability is being used with fluorescent molecules for a variety of applications. Our goal is to exploit this inherent sensitivity of single-molecule detection (SMD) in the development of ultrasensitive immunoassays for use in biological, medical, and national security applications. This achievement would improve sensitivity by a factor of 1000 or more over that of current, state-of-the-art, nonamplified analysis of biological molecules, which is typically limited to nanomolar detection limits.

During FY2000, we had successfully used a dual-label approach for the single-molecule analysis of a protein target molecule at nanomolar levels. The scheme used three antibodies to the target, two tagged with spectrally distinct fluorophores. This approach drastically reduces the occurrence of false-positive detected events because it requires the simultaneous signal detection of the two fluorophores at the same place on the sample to within the resolution of the microscope (about 250 nm). In this analysis, the labeled target is captured using the third antibody, which is attached to the surface of a glass microscope slide using silanization methods. We were unable to realize the ultimate sensitivity of this analysis because of the nonspecific attachment of the labeled antibodies to the surface of the slide—probably due to incomplete silanization of the surface, which provided areas of exposed glass to which the proteins and antibodies readily and nonspecifically attach.

In FY2001, our experimental effort was focused on developing a more suitable silanized surface. We investigated both the nonspecific attachment of fluorescently labeled antibodies on glass surfaces prepared with numerous silane species and silanization protocols. Where these efforts produced a reduction in nonspecific binding, we were able to demonstrate improved sensitivity at ultralow target concentrations.

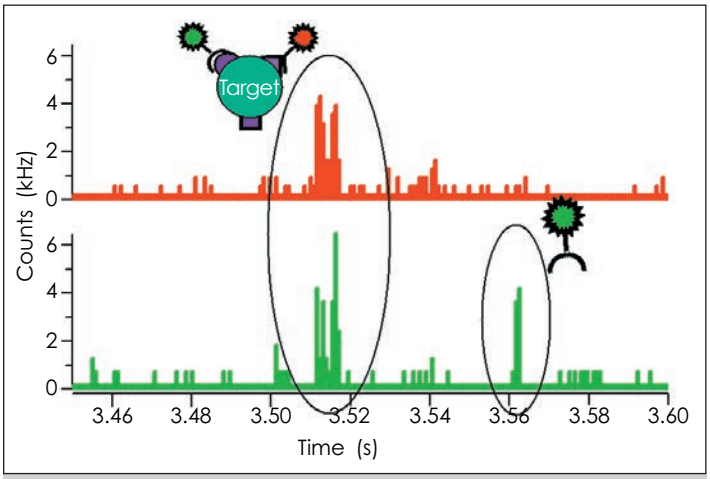

Two-color fluorescence intensity traces of a freely diffusing target/labeled-antibody solution. The coincident burst at about 3.51 s indicates the detection of a target molecule, which is distinguished from the detection of a lone antibody at about 3.56 s.

By probing freely diffusing target molecules, we circumvented the nonspecific binding that limits the surface-capture method just described. Fluorescent molecules are detected through observation of short, intense photon bursts when the fluorescent molecules diffuse through the focal spot, as the Figure shows. Coincident emission of a photon burst in both emission channels indicates a doubly labeled target molecule; unbound antibodies or targets with one attached antibody are single-channel events. Because the target is detected in solution, no surfaces are involved, and limitations caused by nonspecific binding have been removed. However, this approach is limited by a small detection volume (1 fl). Thus, at femtomolar concentrations, detecting a sufficient number of positive events to perform a realistic assay would require impractical lengths of time.

On the basis of these results, future efforts in this area will focus on developing a single-molecule assay that utilizes a microchannel with dimensions on the order of 0.5 × 100 × 100 mm. This device would have 10^3 to 10^4 times greater throughput than the previously discussed 1-D approach. The development of a practical flow channel of these dimensions and the use of a video-rate, charge-coupled device (CCD) camera to image the fluorescent molecules in the flow field will dramatically increase the detection volume, and thus reduce the analysis time of ultralow concentrations to minutes or possibly seconds.

Dynamic focusing of acoustic energy for nondestructive evaluation

J. V. Candy, J. G. Berryman, D. H. Chambers, R. D. Huber, K. A. Fisher, A. L. Meyer, G. H. Thomas

MAIN TOC

Our goal in this project was to research and develop a nondestructive evaluation (NDE) technique for dynamically focusing acoustical energy to both detect and characterize flaws in parts undergoing ultrasonic testing. Our approach incorporated detailed simulations, algorithm development, hardware, proof-of-principle experiments, and the design and construction of a prototype flaw-detection/localization/imaging system.

The dynamic-focusing method that we have designed uses time-reversal (T/R)—a technique for focusing on a reflective target or mass through a homogeneous or inhomogeneous medium excited by a broadband source. Our T/R processor detects flaws (or scatterers) by utilizing its primary attribute—the ability to iteratively focus on the strongest flaw. A T/R processor simply receives the multichannel time series radiated from the region under investigation, collects the array data, digitizes, time-reverses the sensor-array signals, and then re-transmits the signals back through the medium to focus. A patent using the T/R decomposition approach to identify flaws in parts for NDE is pending.

Our T/R technique has application to many areas of high interest to the Laboratory. These include (1) detecting flaws in lenses for laser-based optics and also in component parts of weapons systems as part of the Stockpile Stewardship Program; (2) developing revolutionary, noninvasive medical treatments; (3) designing new methods for secure communications; and (4) designing seismic applications such as locating underground structures.

During FY2001, we expanded the scope of the project to include the initiation of collaborations with researchers at both Stanford and Iowa State Universities to investigate T/R processing techniques for random media and multimode scattering structures, respectively. We also developed—conceptually and theoretically—an approach to treating tissue masses using T/R focusing. Finally, we completed a prototype T/R system and performed a wide variety of proof-of-principle, ultrasonic NDE experiments. These included flaw detection and localization in aluminum, laser optics, and a layered composite part. As one of the experiments, we selectively focused on the strongest flaw in an aluminum part and then on the weakest flaw (see Figure), thereby demonstrating the focusing capability using T/R processing. The idea was to compare the iterative focusing capability of the T/R processor [Figs. (b,c)] to an eigen-decomposition approach using the T/R operator directly in the part [Fig. (a)] The results demonstrate that both approaches are capable of focusing ultrasonic energy on the strongest flaw—very important to detecting flaws in high-power laser optics.

The results of our work have appeared or will soon appear in a number of refereed journal articles.

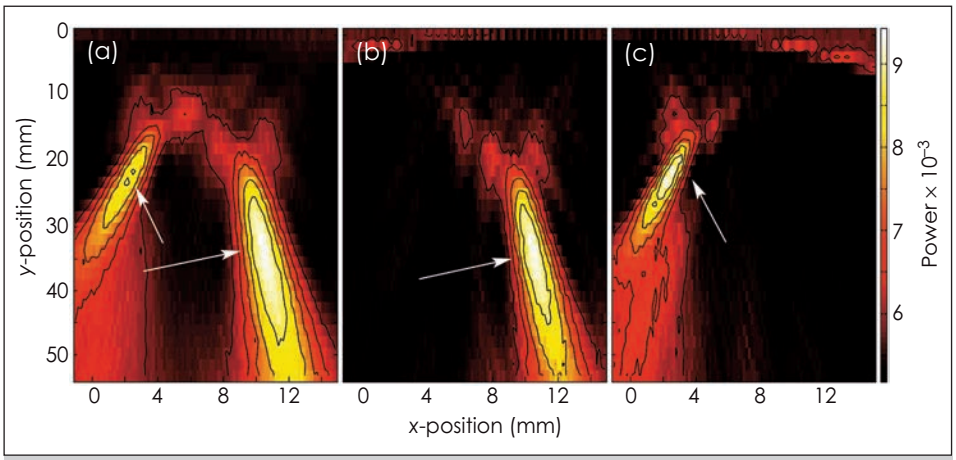

Selective focusing using the time-reversal prototype system on an aluminum part with two flaws: (a) raw image (unfocused array illumination); and array source localization on (b) the strongest flaw, and on (c) the weakest flaw.

Broad-base biological assay using liquid-based detection arrays

F. Milanovich, B. Colston, J. Albala, S. Visuri, K. Venkateswaran

MAIN TOC

The release of a biological agent by terrorists represents a serious threat to the safety of U.S. citizens. At present, over 50 pathogens and toxins are on various agency threat lists. Many of these pathogens have symptomatic delays of days to weeks, delays that seriously compromise effective diagnosis and treatment. This translates into two major deficiencies in our ability to counter biological terrorism: (1) the lack of any credible technology to rapidly detect and identify all the pathogens or toxins on current threat lists, and (2) the lack of a credible means to rapidly diagnose thousands of potential victims.

In this project, we have been developing a rapid, inexpensive, high-throughput, multiple target, pathogen-assay technology. The technology, which we call the Liquid Array (LA), utilizes optical encoding of small-diameter beads that serve as the templates for biological capture assays. Our goal was a detection technology capable of simultaneously identifying hundreds of different bio-agents and/or rapidly diagnosing several thousand individuals.

We pursued this research in three thrusts. In the first, we explored the fundamental interactions of the beads with proteins and nucleic acids in complex mixtures. This provided us with a complete understanding of the limits of the technology with respect to throughput and complex environment. A major spinoff of this work is in the rapidly emerging field of proteomics—the protein complement of genomics. In the second thrust, we looked at a model human-disease state to assess the application of the LA in a highly challenging, real-world medical diagnostic. Finally, we developed a novel concept that would utilize the bead assay in the simplest possible instrument format. A portable, affordable biodetection instrument would provide ease of use for emergency first responders and a point-of-care diagnostic capability for physicians.

During FY2001, we used the LA technology to further elucidate the dynamics of two different bacterial DNA-repair systems (UvrABC and RAD 51BC). Initial results confirmed the ability of these proteins to discriminate between damaged and undamaged DNA bound to individual bead sets. However, because proteins bind to each other and DNA much more weakly than antibody–antigen reactions, discrimination of individual interactions in this relatively complex environment continues to be a challenge.

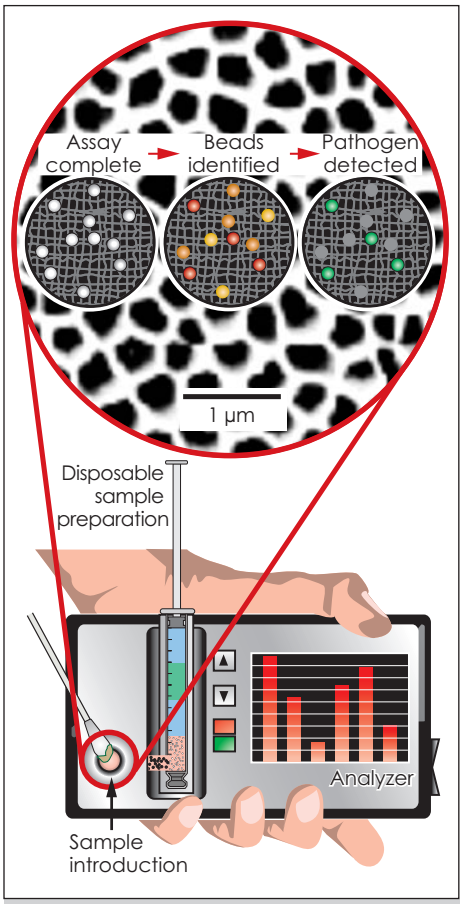

A disposable apparatus for making multiplexed measurements. For imaging and analysis, reagents are loaded and serially dispensed from a multiseptum syringe onto a membrane.

In collaboration with researchers at the University of California, San Francisco (UCSF), and the California Department of Health Services (DHS), we demonstrated multiplex assays for diagnosing a cancer-inducing virus (human herpes virus 8) prevalent in AIDS victims and for determining vaccine efficacy for preventable childhood diseases (mumps, measles, rubella, and chicken pox). We validated both assays on hundreds of real serum samples against benchmarked standards, and we are preparing this research for publication in first-tier scientific journals.

Finally, we made excellent progress in the development of a portable pathogen-detection device. Minimal operator involvement is required beyond sample introduction, so that untrained personnel such as first responders can run sophisticated diagnostics onsite. We designed and constructed several disposable sample-preparation prototypes (see Figure) and were able to demonstrate that their performance was comparable to that of existing bench-top methods. In addition, we constructed a brassboard analyzer for reading the bead assays and developed, in collaboration with researchers at the University of California, Davis and DHS, a panel for screening respiratory viruses. At year's end, we were identifying potential commercial partners for transferring this technology.

Our work has resulted in a number of patents and articles in refereed journals.

Cooperative mobile sensing networks

R. Roberts, G. Armstrong, R. Hills

Large networks of ground-based sensors are increasingly important for data collection and interpretation, with applications ranging from providing tactical situation awareness, to monitoring suspected chemical weapons facilities, to providing meteorological data, to modeling the spread of forest fires. Advances in sensor miniaturization and communication technologies make it feasible to develop systems of sensors that are autonomously deployed over varied terrains and are assembled into a network by small, unmanned air vehicles (UAVs).

We are investigating the use of UAVs as mobile, adaptive communications backbones for ground-based sensor networks. The UAVs provide communication connectivity to sensors that cannot communicate with each other because of terrain, distance, or other geographical constraints. In these situations, UAVs provide a vertical communication path for the sensors, thereby mitigating geographic obstacles often imposed on networks.

During FY2001, we continued to develop the global path-planning algorithm that we initiated in FY2000. Our numerous improvements to the basic algorithm include (1) addition of weights to sensor nodes, (2) addition of terrain constraints in path planning, and (3) improvements that decreased computational complexity.

Significant progress in UAV automation algorithms included (1) developing a control structure that allows a UAV to navigate around a subnet of sensors and locally adapt its route based on the movements of sensors within the subnet, and (2) investigating algorithms in which two UAVs cooperatively reassign sensors moving between subnets so that the path lengths of the two subnets are minimized.

We also investigated software technologies to support file passing between sensors and a ground station using UAVs. We identified and obtained software technology that provides a store-and-forward service. This software has been tested on a desktop network and is awaiting flight tests.

To support our investigation, we are developing a software tool called STOMP, for simulation, tactical operations and mission planning. STOMP maintains and displays the states of objects (e.g., sensors and UAVs) over a digital terrain elevation data (DTED) background (see Figure). The STOMP architecture allows external events (input from a real UAV) to be processed with simulated events (input from a simulated UAV). A message handler associated with each object determines the appropriate action for each type of event. Thus, STOMP can simultaneously respond to real and virtual objects.

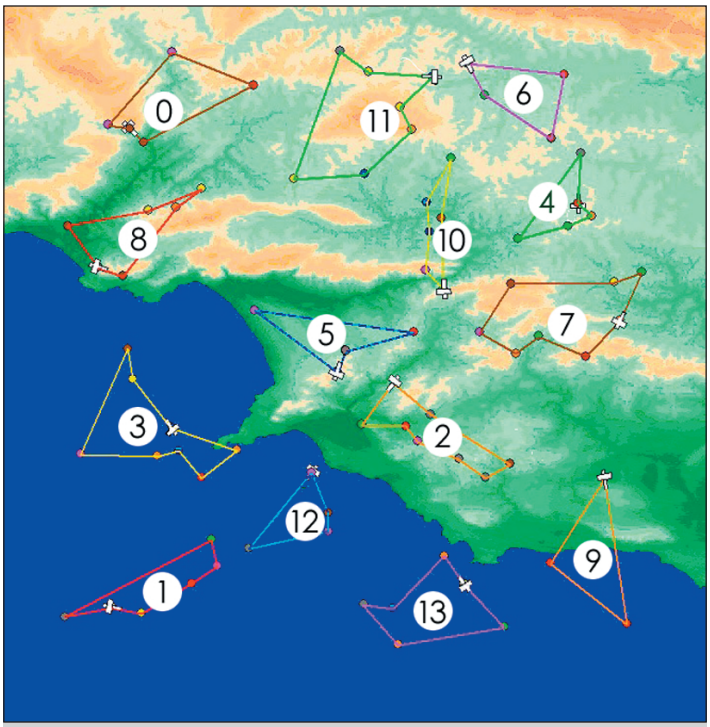

An image from the simulation, tactical operations, and mission planning (STOMP) display, illustrating the subnets and routes of 14 unmanned air vehicles (UAVs) servicing 79 sensors.

Finally, in FY2001 we established a collaboration with the University of California, Davis. Our objective is to investigate algorithms that allow a UAV to adaptively search for point targets (e.g., a lost sensor), loiter in the vicinity of the target to collect data, and move on to the next target after data collection is complete. A second part of this collaboration is to further the development of STOMP.

In FY2002, we plan to (1) continue our development of automation algorithms, in particular algorithms that allow UAVs to cooperatively adjust their subnets based on the importance of sensors within the subnets; (2) flight test our communications modules and software, thereby demonstrating a prototype system; and (3) continue development of STOMP to the point where it can serve as a ground station for the control of real UAVs.

High-sensitivity, optically polarized nuclear magnetic resonance of surfaces in materials science and biology

M. Balooch, S. E. Hayes, J. A. Reimer, A. K. Paravastu

The goal of this research has been to expand the usefulness of modern solid-state nuclear magnetic resonance (NMR) by overcoming its primary limitation: low sensitivity due to modest achievable nuclear spin polarizations at thermal equilibrium. Nuclear spins in semiconductors could be spin-polarized beyond thermal equilibrium values through spin-selective excitation of electrons using polarized light. Optically polarized (or laser-enhanced) NMR (OPNMR) could be used to bring certain dilute spin systems in semiconductors into the detection limit of solid-state NMR, but the usefulness of this new technique has been limited by an incomplete understanding of the origin of the OPNMR signal.

This project will provide a new NMR capability for LLNL that has both high sensitivity and spatial selectivity and that can be used to analyze systems with dilute nuclear spins. Examples are surfaces or interfaces (i.e., semiconductor/insulator barriers and nanoclusters) or very small quantities of samples (e.g., biological samples and trace analysis). Applications range from biology to stockpile stewardship and other national security missions.

During FY2001, our OPNMR apparatus was upgraded for improved sample-temperature control, laser excitation at a range of frequencies, and sensitivity to multiple NMR-active nuclei. With this new equipment, we have been probing the OPNMR effect resulting from laser irradiation at energies both above and below the band gap of bulk GaAs, at temperatures varying from 4 to 50 K, and through detection of multiple NMR frequencies to answer open questions about OPNMR signal generation. The two requirements for optical polarization of nuclei are (1) spin-selective optical excitation of electrons and (2) electron-nuclear spin exchange. The first requirement for OPNMR is well understood in atomic systems in which electronic energy levels are characterized by distinct amounts of angular momentum and excited states are accessible only through irradiation with specific polarizations of photons. In semiconductors such as GaAs, analogous selection rules are believed to exist because of atom-like symmetries near the band edge. In FY2001, we discovered OPNMR enhancements through laser irradiation as far as 0.30 eV below and 0.80 eV above the band gap of bulk GaAs (see Figure)—a result that was not predicted by present understanding of the OPNMR phenomenon. These findings have significant implications in proposed experiments that involve selective enhancement of samples through band-gap engineering.

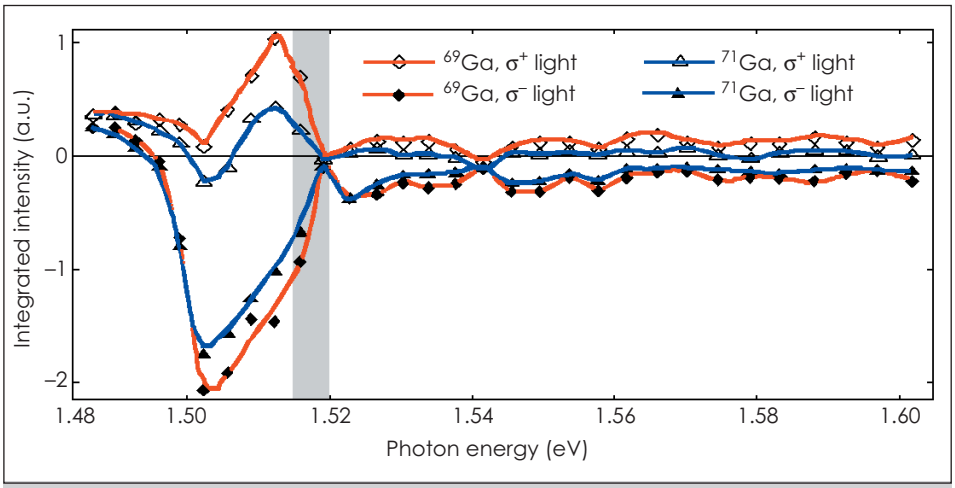

Gallium-69 and ^{71}Ga optically polarized nuclear magnetic resonance (OPNMR) of bulk GaAs at 10 K shows many orders of magnitudes enhancement in signal intensities compared to dark NMR below the band gap of GaAs (shown as shaded area).

In summary, we have observed new effects relating to the dependence of OPNMR of laser photon energy and sample temperature of bulk GaAS that contradict present models. The results are being analyzed to provide fundamental insights into the role of angular momentum in solid-state physics. Our results suggest that direct enhancement of nuclear spin polarization may not be limited to a few classes of probe materials.

Ultrawideband communications

F. Dowla, A. Spiridon, D. Benzel, T. Rosenbury, S. Azevedo

In most intelligence applications, it is important to collect data rapidly and transmit it covertly and reliably. In these applications, robust, short-range, covert wireless communications systems are needed that have low probability of detection, low probability of intercept, and low-power, small-size sensor communication hardware that is suitable for both clandestine urban and battlefield operations. Commercial communication systems that operate in fixed frequency bands are easily detectable, prone to jamming by the enemy, and may lack the requisite robust communication links between the sensors collecting the data, a critical issue for demonstrating the real-time performance of a distributed sensor network.

Our goal in this project is to develop advanced ultrawideband (UWB) communication transceivers and radios that would fulfill these important needs of our country's defense and intelligence communities.

Our goal for FY2001 was to build a highly covert UWB radio with a data capacity of 200 kilobits per second (kbps) and a range of 100 m. With our first-generation transmitters, we were challenged to meet simultaneously the requirements for both data capacity and range. Although our initial design exceeded the data capacity by more than an order of magnitude (>2 Mbps)—the transmission range was limited to a few meters. However, we designed, implemented, simulated, and experimentally tested (with both data and voice communication) several prototype UWB radios that meet those requirements. As the Figure shows, in one variation of our design the radio transmitted up to a range of 110 m at 115 kbps with a bit error rate (BER) of better than 0.0001. For this test, the data capacity was limited by the capabilities of the laptop computer being used as part of the test equipment. Our new UWB waveform design permits data transmission at megabits per second.

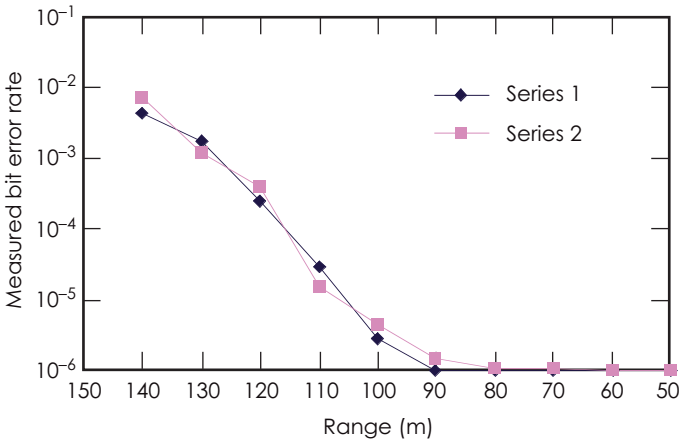

Performance of a prototype ultrawideband (UWB) radio being developed for covert operation. In both test series, the bit error rate and range met design goals. Series 1 represents the model; Series 2 represents the empirical results.

In another significant success during FY2001, we verified experimentally that our UWB communication system had an improved level of performance, with a lower BER in the presence of multipath signal propagation. Most communication systems have difficulties in the presence of the multipath signal distortion caused by obstacles and reflectors. We invented a highly robust algorithm that can compensate for channel distortions.

In FY2002, we plan to reach a number of significant milestones that include (1) developing a detailed architecture design of our UWB radio, (2) completing final reports on modeling and propagation, (3) demonstrating improved signal-processing techniques at the receiver, and (4) quantifying the level of covertness of UWB radios. We also plan to complete (1) three working units of UWB radios with a data capacity of 1 Mbps, a range of 250 m, and a requirement of less than 0.5 W for two channels; and (2) robust, handheld, voice-communication UWB radios.

Dynamic InSAR: Using InSAR to image seismic waves remotely from space

P. Vincent, A. Rodgers, D. Dodge, D. Rock, B. Walter, C. Schultz, J. Zucca

Seismology has provided most of what we understand about the interior of the solid Earth and plays a dominant role in monitoring global manmade seismic activity such as underground mining and nuclear-test activity. Information is limited by indirect measurement and the relatively sparse spatial sampling provided by a global distribution of (point-based) seismometers. Interferometric synthetic aperture radar (InSAR) is a radar remote-sensing technique we are using to investigate the possibility of imaging an entire seismic-wave field. Two SAR images acquired at different times can be combined interferometrically to measure subcentimeter changes in elevation of the ground occurring between imaging times.

Applications of this capability relevant to LLNL's national security missions include (1) improving seismic monitoring of nuclear explosions; (2) detecting underground facilities, and (3) assessing bomb damage to underground facilities. Other applications include advancing understanding of earthquake-rupture physics, pinpointing the source of harmonic tremors in volcanoes, and developing an open-ocean tracking and early-warning system for tsunamis.

Our near-term goal is to determine the feasibility of using InSAR to image seismic waves remotely from airborne and space-based platforms. The challenge is to find an archived SAR image of a seismic wave that is moving at 3 to 8 km/s. The precise space–time location of a candidate seismic wave must be accurately predicted as a function of distance from its source, an intersection must be found with the satellite's imaging swath, and the intersection must occur before the seismic waves have decayed below InSAR's detection thresholds. If these challenges can be overcome, our long-term goal would be to encourage the development and implementation of this new dynamic InSAR imaging capability on future SAR satellite and airborne platforms.

Rocket-motor detonation at the Utah Test and Training Range (UTTR) used to measure seismic surface waves for a future synthetic aperture radar (SAR) experiment. The condensation cloud from the atmospheric shockwave can be seen propagating outward. To determine the surface displacements from the explosions, seismic waves (not visible) were recorded using three radial lines of buried seismometers and accelerometers installed from 100-m to 1-km distances from the explosions.

During FY2001, we searched archives of commercially available SAR data from satellites for a seismic wave from a source such as an earthquake or explosion. We developed the algorithms to perform this search out to 180 degrees (half-way around the globe). Thus far, candidate intersections are too distant from their source; hence, the predicted surface displacements are too small to warrant the purchase of the relevant SAR data now. However, we are continuing our search as new data from global seismic events become available.

We are working to coordinate a SAR imaging experiment of a triggered seismic (explosion) source so that we can control the image-capture process. To predict the surface displacements for such an experiment, and to investigate the potential applications listed above, we have run simulations using LLNL's E3D seismic simulation code. To determine the surface displacements from an explosive source, and to calibrate our E3D seismic simulations, we collected seismic data from the detonations of large, 20-ton rocket motors at the Utah Test and Training Range (UTTR) near Salt Lake (see Figure). These data—along with simulations—are being used to calibrate a future, triggered SAR collection experiment.

Luminescent markers

C. G. Stevens, F. Magnotta, A. Pertica, T. Meier

Recent events have highlighted the need for advanced technologies for intelligence gathering and special forces operations. We propose to develop and demonstrate a new covert marker and detection technology that would have military and intelligence applications. For example, knowledge of vehicular traffic patterns can provide a significant source of intelligence: observing vehicle movement from a point of origin would establish its connection with other locations (e.g., a missile launch site) and aid in understanding personnel networks in and between terrorist cells. Military applications could include marking and tracking high-value targets, providing covert identification of supply-drop locations, and locating special forces personnel and downed pilots.

In this project we are developing a new luminescent marker and detection technology that is both bright (using a special viewer) and covert. The marker is based on the synthesis and application of rare-earth compounds that absorb light across a broad visible–ultraviolet spectral region and then efficiently emit light in a narrow resonance band in the near-infrared, beyond visible detection. This approach maximizes detectability by absorbing a large fraction of the sunlight spectral band. It also minimizes false positives, because the narrow line emission allows comparison to neighboring background wavelengths over a small spectral range. A high degree of background discrimination results if this interval is much smaller than changes in the background spectral characteristics.

We synthesized the material in a high-temperature (800 to 1000°C) oven equipped with a flow system for H_2/N_2 reducing gas mixtures. By using various combinations of time, temperature, and reducing atmosphere, we obtained fine crystalline powders with several levels of doping. We have synthesized samples containing the correct crystalline form at better than 90%.

Three spectral properties are of most interest to us: luminescence line widths, luminescence efficiency, and absorption cross section. The luminescence spectrum exhibits a very sharp, prominent peak near 700 nm, having a linewidth of 0.2 nm. This feature is followed by a series of smaller peaks. About 45% of the luminescence intensity is found in the major peak. The measured absorption cross section of a small single crystal, averaged over the band, was 5×10^{-19} cm^2; we estimate that the quantum efficiency for total luminescence is 80 ± 20%. Knowing the values for these key optical properties, we can estimate the performance of a standoff sensor of a marked object. A target painted with a 100-μm-thick varnish containing a 5% loading of marker material should generate a luminescent radiance of 6×10^{17} photons/s·cm^2·sr under solar radiation with a zenith sun angle of 60°.

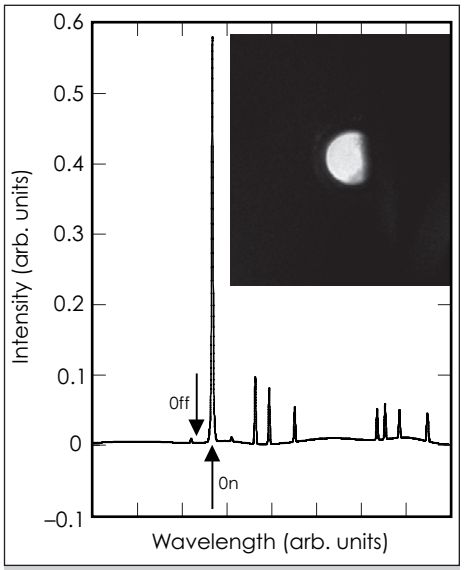

Image of marked object made with a laboratory viewing system. The image represents the difference in light intensity at the two wavelengths shown, on and off the resonance band of the marking compound.

We have designed and fabricated a luminescence viewer incorporating extremely narrow-band filters to observe the marked object on and off the narrow luminescence feature. Using a charged-coupled device camera to record the image, we have tested the viewer in the laboratory, with a 1-cm-diam spot on a target 2 m from the viewer. The Figure shows the viewer output, which represents the difference between the signals at the two wavelengths indicated in the accompanying high-resolution luminescence spectrum.

The micrometer- sized crystallites in the marker have a significantly higher refractive index than available varnishes, resulting in a highly scattering formulation. Reducing the crystallite size to the 100-nm range will create an optimum formulation. Once optimized, radiances such as that mentioned above would allow a small viewer to "see" a marker 20 km away with better than 100-to-1 signal-to-noise ratio. We are conducting preliminary tests of a viewer for long-range outdoor use. This was a one-year LDRD project; based on its results, several proposals for further work have been submitted to DoD sponsors.

Nanoscience and nanotechnology in nonproliferation applications

B. D. Andresen, J. G. Reynolds, T. M. Tillotson, P. R. Coronado, S. R. Kane, S. E. Letánt, B. R.

MAIN TOC

Chemical and biological weapons (CW and BW) are now recognized as major threats to national safety and security. One approach to combating CW and BW is to monitor production activities through collection and detection methods. Commercial, polymer-utilizing tools developed for CW field collections have good selectivity. However, such tools also must have unprecedented levels of sensitivity. The high sensitivity is needed because only trace [parts per billion (ppb)] or ultratrace levels [parts per trillion (ppt) or less] of CW- and BW-related materials are found in the environment. Specific selectivity is necessary to distinguish CWs and BWs from naturally occurring compounds.

Nanostructured materials—materials that have surface features and pore structures on the nanometer scale—can potentially be more specific, yet more versatile, than traditional polymers. Materials attractive for this use are silica sol-gels, mesoporous silica and carbon nanotubes, and porous silicon (Si). In this project, we are tailoring—through chemical and surface modification—these nanostructured materials to be the new generation of highly efficient, small accumulators of and sensors for CW and BW compounds.

This project capitalizes on the strengths of LLNL, utilizing expertise in synthesis and development of nanostructured materials and their application to forensics.

During FY2001, we progressed in the development of silica sol-gels, carbon nanotubes, and porous Si as accumulators and sensors. We began modifying silica sol-gels to provide designed cavities and reaction sites that increase specificity for target CW compounds. For example, we synthesized specific cavities in the nanostructured framework by first incorporating organic substituents and then removing them by air oxidation (see Figure). To increase the selectivity of these cavities, we began designing binding sites for CW compounds by adding metals such as scandium and lanthanides into the silica framework. We fine-tuned the synthetic methods by using alkoxide condensation reactions. For better selectivity in aqueous environments, fluorinated groups were incorporated into the sol-gel matrix, thereby making the material hydrophobic.

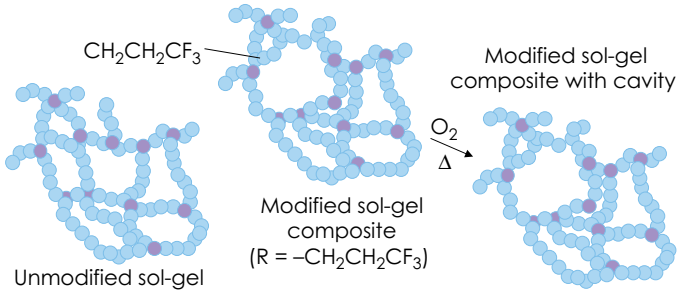

Effects on pore structure of incorporating an organic substituent group (R) into a silica sol-gel framework. Note the physical space in the structure after the R group is oxidized away.

Using commercially available, single-wall nanotubes, we developed new activation techniques that enhance their collection activity. Initial test results with nanotubes in unique (patentable) collection configurations showed that these modified carbon nanotubes have 3 to 4 times the activity of Carboxen—a polymer that is the industry standard for the collection of CW-related compounds. Silicon polymers were used as binders in the development of thin-film coatings that contain these materials; such coatings are important for the ultimate, real-time application of nanostructured collectors.

Recent work in universities has shown that the photoluminescence properties of the surface of porous Si can be used in the detection of CW and BW. Our approach is to utilize photoluminescence for detection through anchoring CW-active enzymes on the porous Si. By the end of FY2001, we had begun production to isolate the CW-active enzyme, produced test pieces of porous Si, and developed linkages for the enzyme to the porous surface.

In FY2002, we will continue enhancing the specificity of these materials by (1) designing cavities in the sol-gel materials, (2) increasing the size of the nanotubes and modifying the activation procedures, and (3) attaching the CW-active enzyme to the surface in the porous Si materials. Our overriding goal will be to prepare new materials that have increased collection efficiencies and analytical specificity.

Satellite-deployed digital video on demand

C. Bennett, M. Carter, C. Clower, R. Priest

MAIN TOC

The ability to obtain real-time video imaging anywhere on the face of the Earth would provide an extremely valuable intelligence tool that could be of great benefit to national security and the detection of proliferation of weapons of mass destruction. Such surveillance capability also would provide improved crisis response in times of national emergency and contribute to both strategic and tactical intelligence in support of DOE missions in national security and counterproliferation.

This research project investigates the possibility of deploying a constellation of satellite platforms that combine several unique LLNL capabilities and LDRD-developed technologies to obtain real-time video imaging of any spot on the Earth within minutes. These technologies include high-performance, light-weight diffractive optics (00-SI-003), very light-weight, ultralow-power, interrogated laser communications (99-ERD-011), and large-area, 2-D, mosaic focal-plane arrays developed from the massively compact halo object (MACHO) project (90-DR-011).

In FY2001, we explored various technical approaches to this problem using satellite constellations ranging in altitude from low Earth orbit (LEO) to geosynchronous orbit (GEO). We found that to assure global coverage, 125 satellites are required at an altitude of 500 km, while only three are required in GEO. Key issues are the comparative cost analysis for equivalent performance of the two groups of satellites, and the role that LLNL technology might play in this analysis.

Due to the enormous number of small LEO satellites that have been launched, a wealth of cost data is available regarding such systems. In contrast, because far fewer large GEO systems exist, the uncertainties in the cost of developing advanced technology are enormous for these systems. Based on our system requirements assumptions and available cost models, we found that an LEO constellation is less expensive than a GEO constellation by a large margin. However, by virtue of the uncertainties inherent in developing advanced technology, LLNL research and development have the potential to dramatically alter the affordability of such systems.

Geolocation using passive synthetic apertures

M. R. Portnoff

Determining the geographic location of a source that is emitting radio-frequency (RF) energy on the Earth's surface is referred to as geolocation. The ability to perform accurate geolocation is required for a variety of civil and national-security applications—including search and rescue, delivery of emergency services, and support to military operations.

Traditional approaches to geolocation typically require either three widely spaced sensors, each with small-aperture antennas, or two widely spaced sensors, each with large-aperture antennas. The signals received by the sensor suite are jointly processed using some variety of triangulation algorithm to determine the location of their common source. However, these traditional approaches have two significant problems: (1) they require multiple sensors that are both expensive and usually in high demand, and (2) practical deployments often deliver less-than-desirable accuracies.

Our goal in this project is to develop and characterize data-processing algorithms that provide an order-of-magnitude improvement in geolocation accuracy over traditional methods. Our approach is nontraditional and seeks to incorporate previously unexploited information—it relies on new data processing, not new hardware.

The concept is based on a single antenna–receiver combination deployed on a moving platform. With appropriate collection geometries and suitable emitted signals, we can exploit the platform motion and process the received signal to synthesize an effective antenna aperture hundreds to thousands of times larger than the actual physical antenna. We refer to this larger effective aperture as a passive synthetic aperture (PSA). For a sufficiently large PSA, we have developed a method to determine both the range and bearing to the emitter.

Although our approach was motivated by the success of synthetic-aperture radar (SAR) techniques, the geolocation problem is significantly more difficult than the SAR problem. SAR is an active sensor which uses an interrogating waveform that is not only known, but is also optimized for the application. Furthermore, an active sensor can determine the range to a target simply by measuring the round-trip travel time of the transmitted pulse. In contrast, geolocation relies on passive sensing. That is, the system must accommodate whatever waveform the source emits, and the travel time from the source to the sensor cannot, generally, be measured so simply.

During FY2001, we developed two methods for PSA formation that are specific to both continuous-wave (CW) and narrow-band (NB) signals. One method is linear; the other is nonlinear. With further analysis, we determined that these methods can be extended, with little or no modification, to certain other, more complicated, signals of interest. Although additional signal-specific methods could be derived for other classes of target signals, we are now focusing on the CW/NB linear-processing method because of its relative simplicity and applicability to many signals of interest.

To gauge our success, we compared the spatial resolution of our PSA approach to that of an equivalent-size real aperture. Because an aperture synthesized with a moving receiver cannot outperform a physical aperture of the same size, the performance of the equivalent-size physical aperture provides an upper bound on the best possible performance of a synthetic aperture. For many signals of interest, we have shown that it is possible for a PSA to achieve this performance bound. Furthermore, for a number of application scenarios, we have demonstrated that the performance obtained by applying the PSA method would be valuable.

Our goal for FY2002 is twofold: we will (1) develop the signal-processing algorithms to implement the PSA-formation methods we developed in FY2001, and (2) demonstrate the validity of these algorithms by processing real or simulated data.

Development of a two-dimensional proportional counter at elevated pressures

S. J. Luke, D. A. Archer, R. Lochner, D. Moltz, S. Prussin, D. Chivers

The development of advanced radiation detectors that optimize the measurements of weak gamma radiation sources in the presence of background radiation is needed to detect clandestine nuclear materials for national security, medical imaging, and astrophysics applications. Such detectors must increase the signal-to-noise ratio by maximizing the probability for detecting a source photon while minimizing the probability that a detected event is due to background radiation.

The goal of this project was to develop, test, and demonstrate a prototype high-pressure noble-gas radiation detector based on a system that takes account of the likely source location, determines the trajectory of the photon, and tends to reject signals from random locations. The definition of a photon's trajectory is accomplished by constructing an imaging system using a high-pressure noble-gas detector, comprised of a drift region followed by a proportional counter that operates at elevated pressures and has 2-D position sensitivity. The 2-D position-sensitive detector plane must operate at pressures above 5 atm and provide sufficient gain and energy resolution to allow accurate reconstruction of the photon trajectory. While high-pressure noble-gas detectors have been demonstrated previously, none of those designs provides the characteristics required for the detection of special nuclear materials.

This project will provide key experimental benchmarks for detector simulations codes. The technology outcome of this research is of interest to the DOE Office of Nonproliferation and International Security and to the Defense Threat Reduction Agency.

In FY2001, we began by demonstrating that a 1-D readout system for the gas detector could be operated at elevated pressures. The 1-D detector established system parameters for a 2-D device, provided information on detector noise and gas gain under elevated pressures. The results showed that the total noise can be greatly reduced from prior experiments and that reasonable energy resolution can be obtained, even when averaged over the very large number of microwells (2500) included in the detector. The plot in the Figure shows that the energy resolution for the detector is approximately 8 to 10% full width at half maximum, which is close to the physical limit for the energy resolution of the system in its present configuration.

Next, to compare readout systems we designed two 2-D read-out systems for the detector with sufficient electronics to demonstrate 2-D spatial resolution. The first of these systems, a 2-D extension of the microwell concept in which each well acts like an independent proportional counter, was tested in the gas chamber at 1 atm to compare to the 1-D measurements. The system produced simultaneous signals from both the anode and cathode outputs from orthogonal spatial read-outs. This measurement demonstrated the ability to define x and y coordinates for photon interactions in the detector.

The second system we designed was based on microstrip technology, which operates with continuous, orthogonal anodes and cathodes. Rather than a microwell system, where each well acts like an independent proportional counter, this system contains continuous, orthogonal anodes and cathodes. Because of technical difficulties in manufacturing and the complexity of the procurement process, the detector was delivered after the project ended.

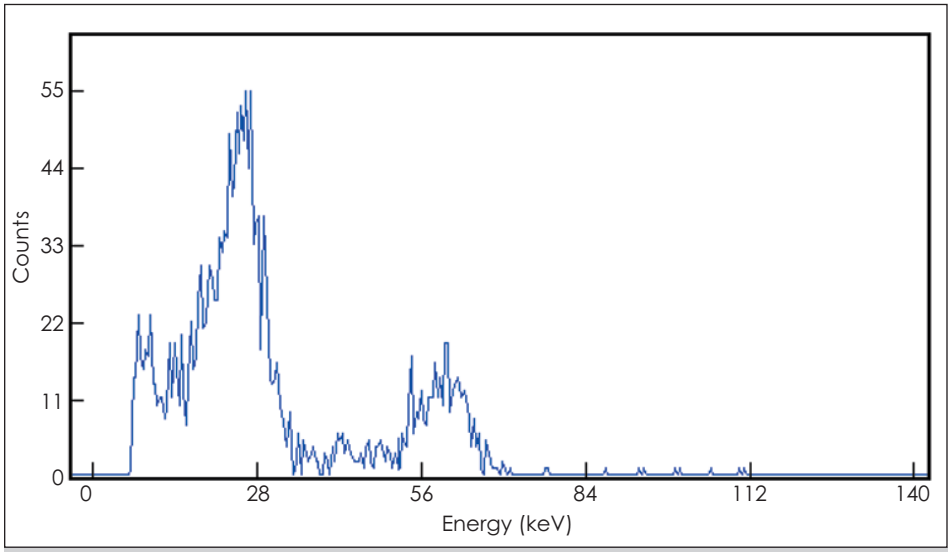

Pulse height distribution obtained from the detector using a ^{241}Am source, with a microwell read-out and 1 atm of Xe.

Integrated microfluidic fuel processor for miniature power sources

J. D. Morse, A. F. Jankowski, R. T. Graff, J. P. Hayes

Miniature fuel cells have attracted significant interest in recent years as a viable alternative for powering portable electronics. While hydrogen is the ideal fuel, reformate fuels are a viable option for the miniature fuel-cell power sources being developed at LLNL. These miniature fuel cells represent a unique approach because they use thin-film solid-oxide electrolytes that operate in the 350 to 600˚C range and are tolerant of CO-poisoning effects. An integrated, microfluidic fuel processor that is capable of reforming hydrocarbon-based fuels having high specific-energy contents would provide significantly longer-lasting power sources than are now available. This work leverages LLNL's expertise in microfluidic devices, microfabrication techniques, and materials science.

Potential applications for miniature fuel-cell power sources include their deployment in the autonomous sensor networks being developed to meet national security requirements, as well as battery replacements for a range of consumer electronics products—including cell phones and handheld computers.

The objective of this project is to design, fabricate, and test a microfluidic fuel processor that converts an easy-to-store liquid fuel—such as methanol—to hydrogen as the fuel flows from the reservoir through a glass microchannel that has been coated with catalytic material. During FY2001, we designed, fabricated, and initiated testing of prototype fuel processors. The primary design, illustrated in Fig. (a), consists of a glass microchannel that is coated with a catalytic material and connected to the fuel reservoir by microfluidic interconnections. Resistive heaters positioned along the reaction zone allow the fuel mixture to be heated as fuel flows through the microchannel. With water added to the methanol, the steam-reforming reactions are assisted by the catalyst at temperatures in the 200 to 300˚C range, which is compatible with our solid-oxide fuel-cell operating temperature. Steam reforming reacts methanol and water, generating byproducts of hydrogen, carbon monoxide, and carbon dioxide.

With adequate surface area of the catalytic material and applied heat, the microfluidic reformer produces hydrogen-gas fuel with minimal power input required to sustain the microreaction. Thus, the design details of the microchannel fuel processor must specifically match the necessary volume, catalyst surface area, flow velocity, and thermal signature of the glass microchannel. The hydrogen and other byproducts are then delivered to the fuel-cell manifold by microfluidic interconnects. This system approach allows for an integrated solution that addresses issues of fuel storage, processing, and delivery. The goals of this effort are reforming sufficient methanol to generate 500 mW of electrical power from a fuel cell.

Figure (b) illustrates the experimental apparatus assembled to evaluate the performance of our fuel processor. Initial testing demonstrated conversion of the methanol–water fuel mixtures at very small flow rates, corresponding to the effective surface area of the catalyst support. Thus, for a platinum catalyst coated by evaporation into glass microchannel reactors having a total length of 4 cm, we observed that conversion to byproducts, including carbon dioxide, began at 240˚C. Further quantification of conversion efficiency will determine the optimal flow velocity of specific microchannel designs and catalyst materials.

In FY2002, we will continue to explore the optimal catalytic material for incorporation within our microfluidic device. We will also further evaluate additional issues, such as the heat-transfer characteristics of the reformer itself, effective heat-exchange designs, and specific flow rates.

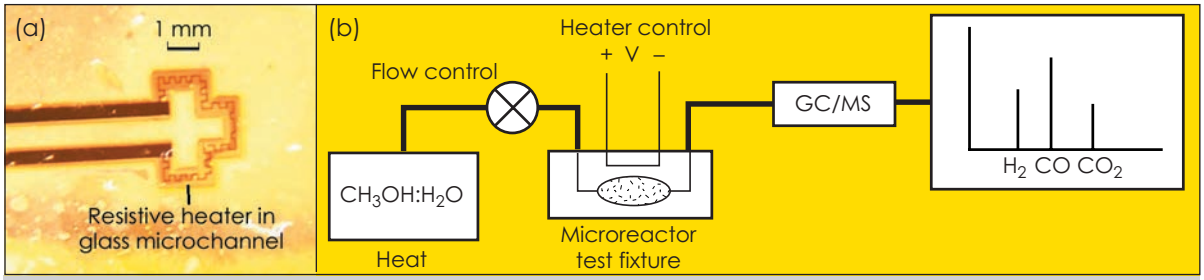

A new, microfluidic fuelprocessor, showing (a) the glass-microchannel reactor with its integrated resistive heater, and (b) the experimental apparatus (where GC/MS is a gas-chromatography mass spectrometer).

Establishing that time-reversal methods are effective for improving communications channels

A. J. Poggio, A. Meyer, J. V. Candy

The typical communications channel is subjected to a variety of signal distortions, including multipath interference, which corrupts the information being transmitted and reduces the effective channel capacity. The mitigation of multipath interference is an ongoing concern for communication systems operating in complex environments, for example, within buildings, urban environments or heavily wooded areas. Communications between mobile units and distributed sensors, so important to national security, are dependent upon flawless information movement in complex environments. Finding a better method of channel equalization, i.e., the removal of channel distortion to extract the transmitted information, is important to the Laboratory's national security mission.

A novel processing method, time-reversal signal processing (TRSP) implicitly compensates for multipath interference in complex communications environments by using the equivalent of imbedded phase conjugation in processing the signals (see 99-LW-045). TRSP has already been used for detecting flaws in materials by utilizing its ability to iteratively focus signal energy on the dominant flaw. The processor simply receives the multichannel time series scattered from the region under investigation, collects the array data, digitizes, time-reverses the sensor-array signals, and then re-transmits the signals back through the medium to focus. For point-to-point communications without transmitter and receiver arrays, the time-reversal aspect is similar but the process is quite different. There is neither an array (although this is envisioned as a logical step in later development) nor is there iterative transmitting to enable focusing. The TRSP application in point-to-point communications is effected as follows:

1. A pilot signal known to both transmitter (**A**) and receiver (**B**) is sent by **A** to **B**. **B** then stores the received signal, which is a version of the pilot propagated through the environment.

2. **A** then transmits the required information signal. that has been convolved with the pilot signal. The received signal at **B** (information propagated through the environment) is then convolved with the signal from step (1) that has been reversed in time and finally convolved with the pilot.

The resulting signal is the information signal convolved with the autocorrelation of the pilot (known) and the autocorrelation of the propagation descriptor or Green's Function (unknown) that accounts for the effects of the medium. The latter is a peaked function of lag and becomes increasingly impulsive with increases in complexity of the environment. This characteristic enables extraction of the information from a received signal that is highly corrupted by effects in the propagation medium.

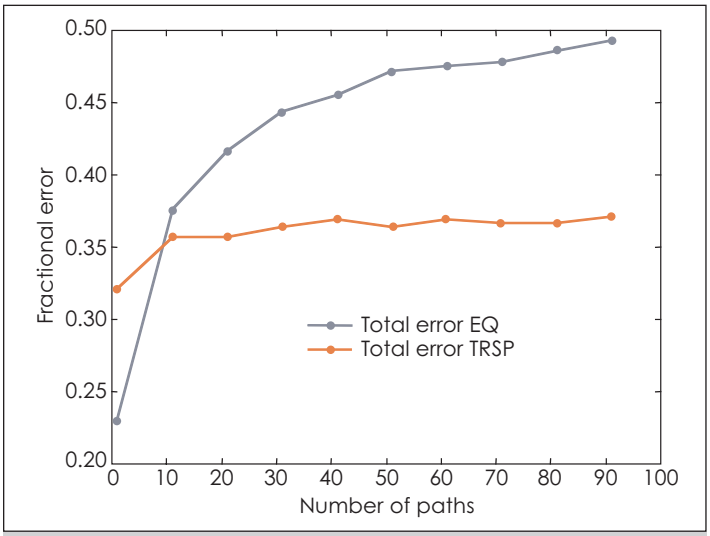

The time reversal (TR) method outperforms classical equalization (EQ) in complex multipath environments, except where EQ is optimized for a similar situation (usually a few paths).

The objective of this project is to demonstrate (1) the feasibility of using TRSP to compensate for the deleterious effects of multipath, and (2) that TRSP is a viable option for equalization and can offer advantages over classical, more complex, methods.

In FY2001, simulations were carried out using a varying number of scatterers that caused multipath. The pilot signal was a pseudorandom sequence of finite length and the information signal was a known biphase modulated signal. The performance metric was the mean squared error between the estimated information signal and the true information signal. The TRSP method was compared to the classical equalization approach involving a linear transversal filter to identify advantages.

The TRSP generally outperformed classical equalization except when the equalizer was uniquely tuned and optimized for the particular environment, a computationally demanding process (see Figure). While the classical equalizer was a better performer than TRSP in simpler environments, it asymptotically approached a greater error than the TRSP as the density of scatterers increased. In fact, any deviation from the conditions under which tuning was performed caused classical equalization to suffer dramatically. On the other hand, TRSP demonstrated its robustness by maintaining the consistency of its performance over a broad variety of test conditions.

Based on the simulations executed during this feasibility study, the TRSP approach is an excellent candidate for mitigating the effects of severe multipath. TRSP competes with the performance of equalization schemes, especially in the presence of a large number of scatterers causing multipath, requires straightforward signal processing operations, and is robust in the presence of noise.

Development of a detector to measure the angular dependence of the cosmic-ray-induced neutron background flux at ground level

J. Morgan, M. Frank, S. Prussin

The ability to detect and measure low-intensity sources of radiation is important for arms control, nonproliferation, and the prevention of nuclear smuggling activities. Often the background radiation level interferes with the detection of these sources. Most of the neutron component of background radiation comes from the interactions of cosmic rays with the upper atmosphere, and the subsequent propagation of these neutrons to ground level. Knowledge of the directionality of this background radiation can be used to improve the signal-to-noise ratio of background radiation measurements. This project will test the feasibility of a new type of neutron detector that is capable of measuring the energy and angle-resolved cosmic-ray-induced neutron flux at ground level. LLNL has taken the lead in developing new detector concepts for national security applications.

We plan to evaluate the new detector concept developed at the University of California, Berkeley (UCB) by developing a prototype and testing its ability to measure the angular distribution of low-energy neutrons with the required sensitivity. This detector, based on conventional ^{3}He detectors and a new, boron-loaded moderator to provide the directionality, will be used to verify the recent UCB calculations of the energy and angle spectrum of these cosmic-ray induced neutrons. Once verified, these calculations can then be used to improve the design of detector systems for low-level signals.

The Figure illustrates a calculation of the directionality of the neutron signals that a standard ^{3}He detector will measure. Over common soil, the thermal region of the neutron flux is predicted to have an up/down asymmetry of about a factor of 3, which makes a significant contribution to the detector noise. But with the proper shielding, calculations predict that detector noise can be reduced by almost an order of magnitude. If these calculations are confirmed by experiment, then by accounting for the natural directionality of the thermal flux at the Earth's surface and by modifying the absorption/scattering environment in the vicinity of the detector, the signal-to-noise ratio may be increased by the same amount.

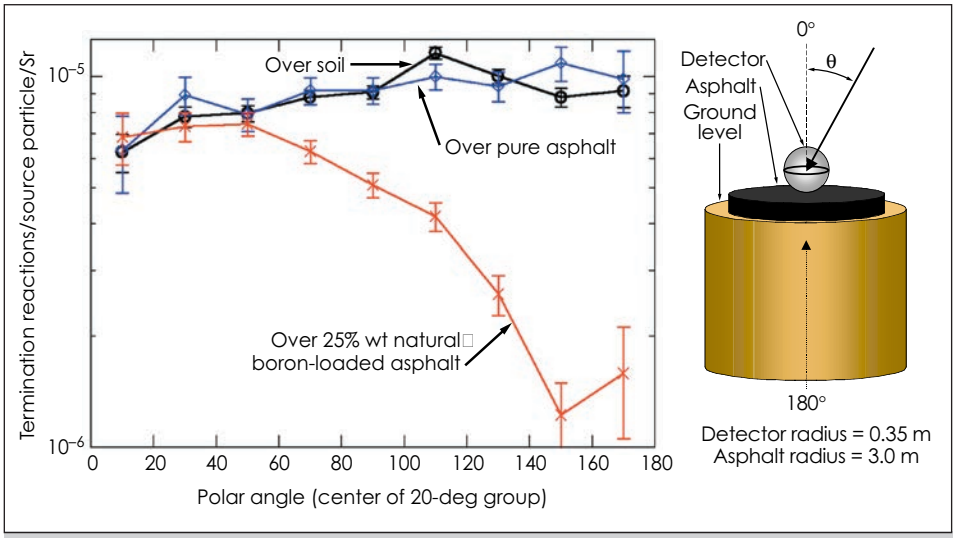

Calculated direction of arrival of neutron interactions in a ^{3}He detector at ground level with various shielding configurations: soil, pure asphalt, and boron-loaded asphalt

In FY2001, the project focused on constructing the detector system. The detectors were tested and relatively calibrated, the electronic components were assembled and the data acquisition assembled and tested. The structure comprising the shielding for the detectors is in the final stages of completion and the support structure for the detector assembly was designed and is ready for construction. A van was equipped with a mobile power unit to deploy the system in remote locations.

As a follow-on from this project, in FY2002 we will begin to make preliminary measurements of the angle-resolved low-energy neutron flux. If the calculations are confirmed, we will use the results to begin designing detection systems for border control and nuclear search. Other potential applications include using the detector to make measurements of the angle-resolved neutron flux in the Antarctic region, where this flux may have a significant effect on geochronologies developed from radiation measurements on shales removed from the area.

An early warning system to detect illicit use of nuclear materials and facilities

N. Suski, L. Gray, W. Ruhter, D. Manatt, D. Poland

Recent experiences, primarily with Iraq and North Korea [Democratic Peoples' Republic of Korea (DPRK)] have highlighted several shortcomings of current comprehensive safeguards implementation. The Additional Protocol, approved in 1997, provides the International Atomic Energy Agency (IAEA) the right to obtain information from member nations pertaining to nuclear research, development and manufacturing, and allows the IAEA inspectors unprecedented access to nuclear facilities and activities. With the Additional Protocol, the IAEA now has the authorization to use an expanded suite of tools, including broader information collection and evaluation at the national level, satellite imagery, environmental sampling, remote and unattended monitoring, complementary access, and other measures.

This project, which is relevant to the DOE's International Safeguards mission, examines the feasibility of implementing an early warning system to detect illicit use and/or diversion of nuclear materials from a commercial nuclear spent-fuel reprocessing facility. This study focuses on the ability to use advanced measurement technologies, data transmission, and information management systems in a commercial reprocessing plant as part of an integrated safeguards system.

A large-scale, well-developed plutonium (Pu) and uranium (U) extraction (PUREX) process has been optimized to produce high-purity Pu that is free from radioactive contamination with maximum concern for conservation of source materials. The successful separation worldwide of hundreds of tons of Pu has instilled a high level of confidence in the PUREX-based process. Other techniques, such as the pyrometallurgical processing used in the Integral Fast Reactor (IFR) fuel cycle, are still in the research and development stage. Using the PUREX process, a large-scale commercial spent fuel reprocessing plant typically processes about 200 to 800 tons of spent fuel per year, of which approximately one percent (2 to 8 tons) is Pu.

For detection purposes, important attributes of any nuclear materials processing technology include detailed knowledge of material properties and process parameters at any point in the process. Material properties include isotopic assay, chemical composition, radiological properties, mass, and/or volume. Process indicators that could be used to detect material diversion or facility misuse include flow rates, temperature, pressure, equipment state, off gases, and use of reagents and process energy. Important facility-design information includes purpose, nominal capacity, general arrangement, (particularly with reference to the form, location and flow of nuclear material), layout of important items of equipment that use, produce or process nuclear material; and description of features of the facility relating to material accountancy, containment, and surveillance.

The conclusion of this study is that opportunity exists for integrating facility and process operations data into the safeguards monitoring system. Several areas require additional research and development, including monitoring of material flow and inventory; containment and surveillance technologies; and information management, including data transmission, data fusion, data visualization and all source analysis. Research and development is needed in the use of noble-gas fission products for safeguards monitoring, ambient temperature radiation detection, solution monitoring utilizing novel approaches such as micropower impulse radar (MIR), and smart camera technologies. Development and utilization of simulation technology will have a dramatic affect on the design cycle for data transmission and communication infrastructures for remote monitoring systems.

Carbon nanotube array sensors

C. Lee, A. Noy, N. Ben-Barak, B. Woods, S. Swierkowski

This project examines the feasibility of using aligned arrays of carbon nanotubes as sensing elements in nanoscale transducers and sensors. Carbon nanotube sensors, orders of magnitude smaller and more sensitive than microscale sensors, can make measurements on very-small-length scales and with sensitivity unattainable using current technology. The key challenges of this feasibility study are to (1) grow nanotubes in a controllable uniform array, using catalytical chemical vapor deposition (CVD) process, and (2) incorporate such arrays into a signal readout system based on modified micro-electronic techniques.

Arrays of hollow nanometer-scale carbon nanotubes offer several unique advantages as a material for the active component of a transducer/sensor. First, they have exceptional mechanical strength yet are laterally compliant due to their long, slender geometry. Second, their length can be varied from several nanometers to tens of micrometers, which gives a high degree of control over the sensor geometry. Third, carbon nanotubes are conductive, offering the natural choice of a capacitive detection scheme for signal readout.

Carbon nanotube array sensors have applications in remote sensing for DOE's nonproliferation and intelligence missions. Because their scale is compatible with biological cells, nanotube array sensors can also be used for biodetection.

As a specific demonstration, we are building an acoustic sensor using the nanotube array grown on the electrode surface. sensor. Because of its very small size, such a sensor could eventually be used for an artificial human cochlea—the snail-shaped canal of the inner ear that contains the essential hearing organs. The working principle behind this artificial "ear" follows that of the stereocilla, the hairs that line the walls of the human cochlea. When an acoustic or pressure wave impinges upon the hairs, their motion is translated into a signal sent through the nervous system. An array of nanotubes in a similar configuration will have a strong directional sensitivity and a high signal-to-noise ratio. Furthermore, the small size of the array will facilitate motion detection on the nanometer-length scale including, perhaps, cellular or even biomolecular motion.

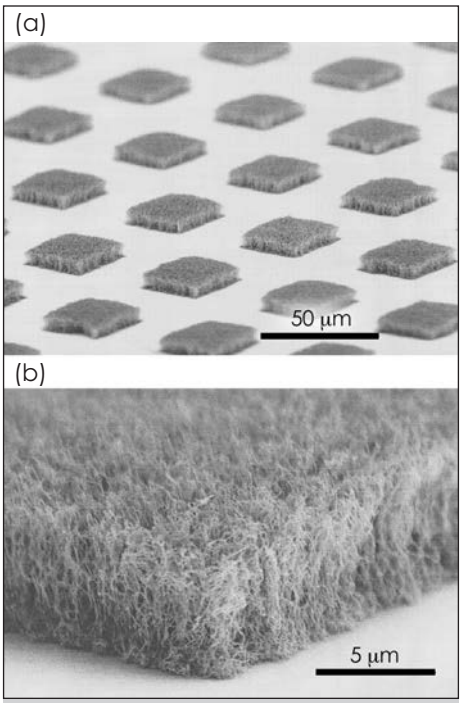

(a) Scanning electron microscope micrographs of patterned carbon nanotube arrays grown on a silicon surface. Each square is one array. (b) Close up of one array.

In FY2001, two tasks were carried out in parallel. The first task was to establish the feasibility and the necessary conditions for fabricating dense arrays of carbon nanotubes on silicon substrates using readily available shadow mask patterns. Several candidate compounds were evaluated as catalysts for the CVD growth of carbon nanotubes. Thin, 5-nm films of iron acted as the catalyst most compatible with our requirements for fabrication conditions and final array geometry. The CVD capabilities were upgraded to permit fabrication of the arrays of the required density. Surprisingly, the hydrodynamics of gas flow in the process tube during CVD has a profound influence on the geometry of the final array. We tested several flow regimes and found the conditions for reliable growth of uniform arrays. Figure (a) shows a scanning electron microscope photograph of a series of nanotube arrays that were grown on a porous silicon substrate. Figure (b) shows a close up of one of the arrays. Note that the nanotubes have tangled are have not grown completely uniformly in the vertical direction.

The second task was to design and fabricate a micro-electronic-based signal readout system. An interdigital comb pattern was chosen for ease of fabrication by standard micromachining techniques. The spacing of the combs was defined so that the distance between each tine was one-quarter of the wavelength of a specific frequency wave. A series of combs were laid out to span a fixed bandwidth. An impinging wave was detected capacitively as the nanotubes on consecutive tines deflect in a manner analogous to wind blowing over a wheatfield. By the end of the project, the lithography masks were completed; the comb parts are awaiting fabrication.

The development of this sensor is continuing with follow-up funding. In addition, we are exploring the possibilities of using these patterned arrays as nanoscale filters in microfluidic channels and as microscale diffraction gratings or optical beam dumps. A patent is in progress for this work.

Diffraction-limited adaptive optics and the limits of human visual acuity

S. S. Olivier, S. C. Wilks, C. A. Thompson

Visual acuity of the normal human eye is limited by significant high-order optical aberrations that cannot be corrected by standard corrective eyewear. Adaptive optics (AO), a technology used in astronomy to correct for image blurring arising from atmospheric turbulence, can compensate for these aberrations and provide normal eyes with supernormal vision.

In collaboration with the Department of Ophthalmology at the University of California, Davis (UCD), we are using LLNL's unique expertise in high-resolution optical wavefront control with liquid-crystal spatial light-modulator devices to carry out detailed studies of the visual performance benefits of improved ocular aberration correction for the general population. This project seeks to determine the ultimate resolution of the human eye and the ideal optical correction, considering wavefront aberrations and neurological factors.

Beyond the fundamental contribution to basic vision research, this work will advance the revolution in the vision correction industry for the development of next-generation corrective eyewear and surgical procedures designed to take the general population beyond the "20/20" visual acuity standard.

High-resolution liquid-crystal adaptive-optics system for human vision correction that will be used at the University of California, Davis beginning in FY2002 to study the limits of human visual acuity.

This work will also have application in developing supernormal vision for specific defense and national security missions. In addition, this research will have direct application to the development of new clinical ophthalmic instrumentation that will greatly enhance current capabilities to diagnosis and treat the diseases that are the primary causes of human blindness.

In an earlier LDRD project (98-ERD-061), we developed expertise in using high-resolution liquid-crystal wavefront-control technology to provide high-precision beam control for high-power laser systems. In the present project, we are applying that expertise to high-precision correction of optical aberrations in the human eye. This high-precision capability will be critical in reaching our objective of using AO to enable assessment of the ultimate physiological and neurological limits of human visual acuity.

During FY2001, we designed and constructed an AO system for human vision correction using new liquid-crystal, spatial light-modulator technology. The system senses and corrects the aberrations present in the human eye. First, a dim beam of infrared light is directed into the eye and focused onto the retina. A small fraction of this light is reflected from the retina and serves as a "beacon" for sensing the aberrations present in the eye. The light from this beacon is relayed to the liquid crystal and then to a wavefront sensor that determines the residual aberrations. This wavefront information is used to calculate signals that are sent to the liquid crystal to compensate for the aberrations. Simultaneously, the subject can look through the system, off the face of the spatial light modulator, to a computer monitor that displays a visual acuity target. By varying the characteristics of this target and recording the patient's perceptions, we can study the limits of human visual acuity.

In FY2002 we will transfer the AO system to a laboratory in the UCD Medical Center (see Figure), where we will work with faculty and staff in the Department of Ophthalmology to perform initial clinical trials of human visual acuity after correcting the subject's ocular aberrations.

A high-speed, photon-counting camera for the detection of extrasolar planets

J. N. Ullom, M. F. Cunningham, B. Macintosh, T. Miyazaki, S. E. Labov

MAIN TOC

The search for extrasolar planets—planets orbiting stars outside our solar system—is motivated by the desire to discover small planets similar to Earth. Since small planets are difficult to detect, the first step is finding giant planets with large orbits, like Jupiter. Solar systems containing these planets may have smaller, Earth-like planets traveling closer to the parent star. However, current methods detect extrasolar planets indirectly by observing a planet's gravitational influence on its parent star. These methods are primarily sensitive to giant planets with small orbits. A new method is needed to directly observe planets with large orbits. Direct observation can also provide additional information about a planet's composition and/or orbit.

Directly observing an extrasolar planet from Earth is challenging because of the relative proximity of the planet to its parent star. Although a large, terrestrial telescope can provide the angular resolution necessary to visually separate the planet from the star, atmospheric turbulence limits the telescope's performance. In addition, the parent star appears much brighter than the planet. Adaptive optics (AO) can increase a planet's brightness, but they have little effect on residual star glare.

To overcome these difficulties, we are developing a high-speed, photon-counting camera that is sensitive to individual optical and infrared photons. This camera, which brings together cryogenic sensing elements and cryogenic digital electronics, will capture a series of images, taking each frame during the short timescale (~100 ms) when star glare consists of discrete speckles of light. In any given frame, some pixels may have speckles, while others may be speckle-free. The speckle-free pixels can then be combined to build a final image uninterrupted by star glare and atmospheric turbulence.

Once the camera's sensing elements are developed and tested, sensors will be integrated with a novel read-out multiplexer that allows the response of many sensors to be measured by a relatively small number of amplifiers. If successful, this project will make it possible to acquire and process data from arrays containing thousands of pixels. Results will provide the proof-of-concept needed for LLNL to build larger instruments for major observatories and space-based missions.

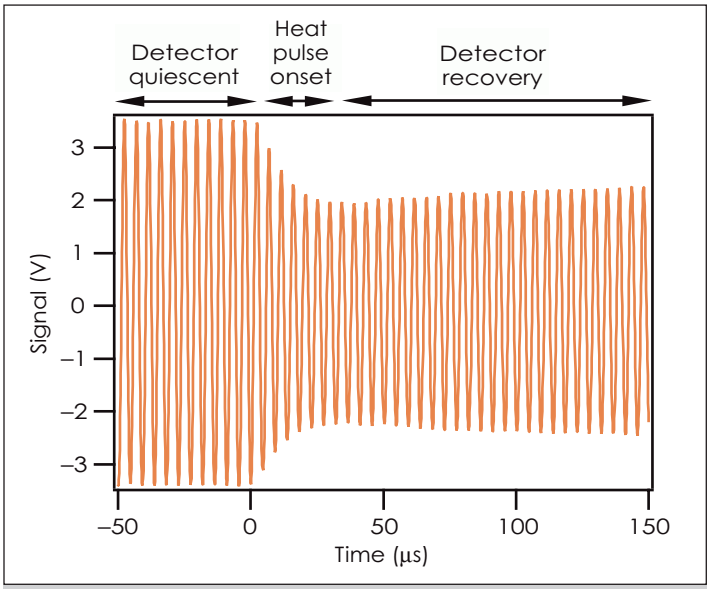

A sensor's measured response to a heat pulse while under ac bias. The amplitude of the signal changes when the heat pulse is applied. After the heat pulse is applied, the compression of the bias envelope is proportional to the pulse energy.

This project builds on existing LLNL expertise in two areas: AO and cryogenic photon sensors. We are using the new read-out technology to develop detectors that perform high-resolution spectroscopy of fissile material at about five times the spectral resolution of existing equipment. The ability of these detectors to discern the presence of nuclear material will be used in support of LLNL's nuclear nonproliferation mission. The technology developed for this project has other applications, such as the development of x-ray detectors for the National Aeronautics and Space Administration (NASA).

Our progress during FY2001 includes developing a high-yield process for fabricating large arrays of thin-film photon sensors. Prototype sensors composed of multilayers of molybdenum and copper were built and operated. These sensors are suitable for detecting x-rays and gamma rays. Similar to other energy-dispersive detectors, the sensors identify photons by measuring their energy. However, the performance levels of the new sensors, which have an energy resolution better than 25 eV for 6-keV photons and better than 70 eV for 60-keV photons, are roughly five times better than those of commercial detectors.

The sensors have a superconducting transition temperature of 0.1 K. At this temperature, the absorption of a single photon produces a brief (100 μs to a few ms), detectable increase in a sensor's temperature. To test the sensors, a demagnetization refrigerator capable of cooling to 0.08 K was constructed. In addition, a frequency-based read-out technique was developed where each sensor is operated under ac bias at an identifying frequency. By enabling each amplifier to measure signals from multiple sensors, this technique makes operating arrays with large numbers of sensors feasible. The Figure shows a sensor's response to an applied heat pulse.

One goal for FY2002 is to sum the ac signals from multiple sensors to demonstrate a complete multiplexed read-out system. Another goal is to shrink the characteristic dimension of the sensors from 500 to 25 μm so that they can detect single optical and infrared photons.

Atmospheric and Geosciences

Section 2

Section 2 Atmospheric and Geosciences

Toward a new era of research in aerosol–cloud–climate interactions at LLNL

C. C. Chuang, D. J. Bergmann, J. E. Dignon, P. S. Connell, P. J. Cameron-Smith

One of the largest uncertainties in simulations of climatic change is the influence of anthropogenic aerosols on the Earth's radiation budget. By scattering or absorbing solar radiation, aerosols directly change the planetary albedo. Aerosols—unlike CO_2—also have a significant indirect effect by serving as cloud condensation nuclei. The large spatial and temporal variabilities in aerosol concentrations and chemical characteristics have made it difficult to assess the magnitude of aerosol effects on atmospheric radiation. These variabilities are the leading sources of uncertainty in predicting future climatic variations.

In this project, we built on LLNL's expertise in aerosols and chemistry to identify the responsible processes in aerosol–cloud–climate interactions and thereby to improve the level of scientific understanding regarding the effects of aerosols upon climate. This project addresses the DOE's energy and environment missions and has important consequences for energy planning and for making informed decisions about strategies for avoiding anthropogenic climatic change and adapting to future climatic change.

During FY2001, we added a number of improvements to LLNL's integrated, massively parallel atmospheric chemical transport (IMPACT) model for a better representation of aerosol physics. These included modules for simulating the gravitational settling velocity and dry-deposition velocity of aerosols as well as a radiation package for calculating changes in solar radiative fluxes by aerosols.

To study aerosol climatology, we developed a new version of IMPACT that has a compact chemical mechanism (about 21 prognostic species). This new version, together with the meteorological fields simulated by the Middle Atmosphere Community Climate Model 3, predicts the global distributions of sulfate, organic and black carbon, dust, and sea salt, as well as their seasonal variations. By applying the monthly averages of OH, HO_2, and H_2O_2 from previous IMPACT simulations with a fully interactive chemical mechanism (about 100 prognostic species), sulfate is formed through both gaseous and aqueous oxidation of SO_2 and dimethyl sulfide (DMS). Other types of aerosols, either emitted by nature in the form of particles or formed much more quickly from their gaseous phase precursors, are assumed to be injected into IMPACT as particulates. This compact version of IMPACT is faster than the full-chemistry version by a factor of 10. We analyzed the simulated sulfur cycle to ensure that results using the compact version are in good agreement with those from the full-chemistry version. To validate the accuracy of the compact version, we compared the simulated aerosol concentrations with field measurements at different geographical locations. We found that most of the simulated concentrations are in general within one deviation of the mean of the measurements.

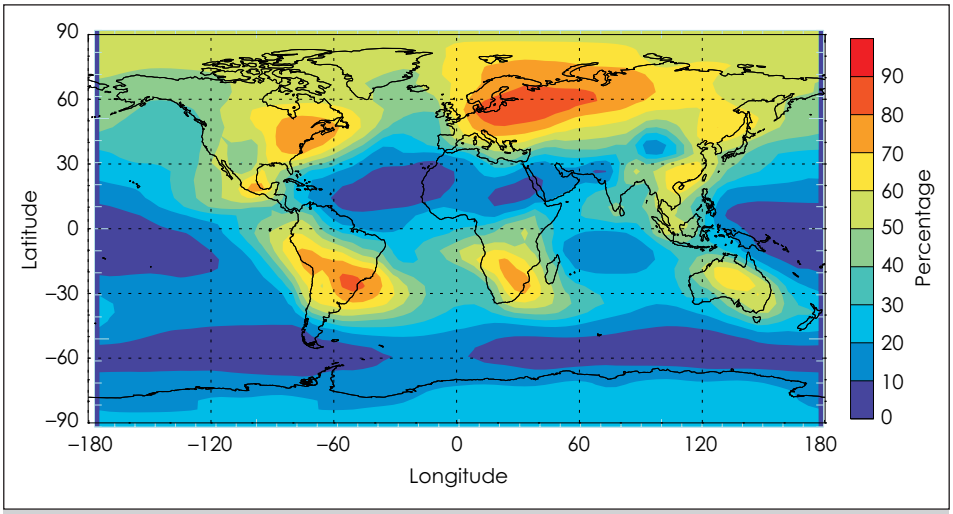

Percentage of the annual-average aerosol concentrations from anthropogenic sources, as simulated using a new version of LLNL's integrated, massively parallel atmospheric chemical transport (IMPACT) model.

To address the importance of anthropogenic emissions in the spatial pattern of aerosol concentrations, we examined the percentage of the simulated annual-average aerosol concentrations from anthropogenic sources. As shown by the Figure, anthropogenic emissions result in significant increases in aerosol abundance, particularly over Europe—where over 80% of aerosols are derived from anthropogenic sources.

We are now poised to perform multiyear simulations to characterize future variations in climate. Our simulations will incorporate the emission scenarios that are newly developed by the Intergovernmental Panel on Climate Change. This work will provide us with a more quantitative range for aerosol effects on climate when compared to the range of climatic effects from greenhouse gases.

MEDIOS: Modeling Earth deformation using interferometric observations from space

P. Vincent, S. Larsen, P. Goldstein, J. Zucca, W. Walter, B. Foxall

Interferometric synthetic aperture radar (InSAR) is a remote sensing technique in which two radar images acquired from space at different times are combined interferometrically to measure subcentimeter changes in ground elevation that occur between the imaging times. InSAR has become the standard geodetic tool in academia and industry for mapping surface displacements from a variety of sources such as faults, glaciers, fluid reservoirs (oil, gas, geothermal, and volcanic), and soil and aquifer compaction. The quasi-continuous InSAR maps of surface displacement fields provide the added constraints needed for more sophisticated models of these sources.

LLNL, through this LDRD project, has acquired the expertise to process and invert InSAR data associated with these types of sources. While many academic research organizations are using InSAR, we have pioneered its application to sources of surface deformation related to national security, including underground nuclear test monitoring and characterization, and underground facility detection and characterization. The size of InSAR data frames (typically 100 × 100 km) makes it an ideal wide-area search technique for national security applications.

The goal of this project has been to build an InSAR data inversion tool that can be applied to virtually any type of surface deformation to produce highly accurate models of the subsurface process responsible for the observed surface displacement field. We developed the inversion tool using an elastic half-space for computational efficiency. To demonstrate this capability we focused on three major categories of subsurface processes that align with LLNL's missions: (1) nonproliferation and defense, (2) energy-resource exploitation, and (3) seismic hazard mitigation.

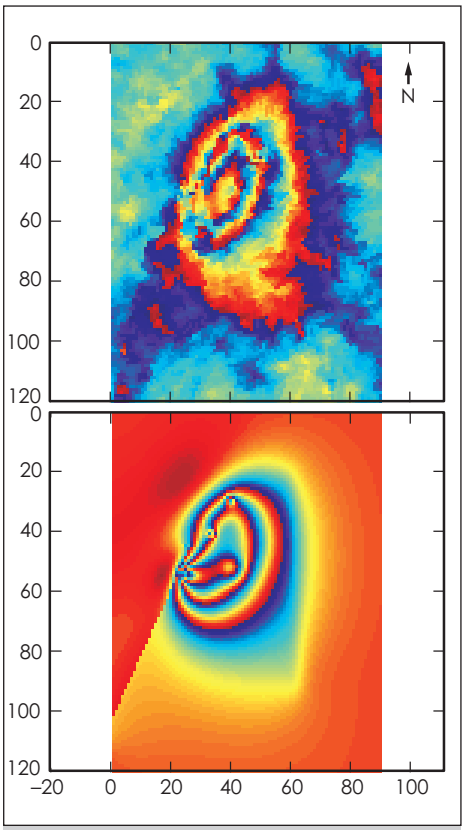

Best fit model (bottom) from inversion of InSAR data (top) of a cluster of five past underground nuclear tests. Axis units represent 30-m bins, so image dimensions are 2.7 km across × 3.6 km down. One color cycle = 28 mm of near-vertical deformation.

We have successfully applied our InSAR data inversion tool to simultaneously invert for multiple sources and source types in categories 1 and 3; work on category 2 is in progress. For example, we inverted InSAR data from a cluster of five past underground nuclear tests (category 1) on Pahute Mesa at the Nevada Test Site (see Figure). The inversion tool derives a best-fit model for these InSAR data, which consist of five collapsed point sources: one for each of the five nuclear tests; three normal faults bounding the north, east, and west sides of the region, corresponding to mapped surface traces; and a single closing subhorizontal fracture below the surface, representing the integrated damage zone above all five shots.

Using the commercial finite-element modeling code MARC/MENTAT, we have also produced more realistic time-dependent forward models of the underground nuclear test cluster that simulate the time-dependent deformation revealed by the InSAR data. We hope to couple the more accurate, time-dependent finite-element models into our inversion tool in a future project that utilizes LLNL's high-performance supercomputing resources.

Satellite-based observation of the tectonics of Southern Tibet

F. J. Ryerson, R. Finkel, J. Van der Woerd, P. Tapponnier, A. S. Meriaux

The Tibetan Plateau represents an area comparable in size to the western U.S., but with an average elevation close to 5000 m above sea level. Understanding the timing and mechanisms responsible for uplifting such a huge region remains one of the outstanding problems in continental geodynamics. The Plateau is surrounded by large strike-slip faults oriented at high angle to the direction of convergence between India and Asia. At one extreme these faults have been viewed as the geodynamically unimportant byproduct of distributed ductile deformation in the lower crust and mantle. At the other, the faults are interpreted as localized, lithospheric shear zones that are absorbing large motions between relatively rigid blocks. The resolution of this issue requires quantitative information on the rates of slip along these faults. Low slip rates (millimeters per year) would be compatible with distributed deep deformation, whereas fast rates (centimeters per year) rule it out.

In this project, we have been determining the slip rates of the Karakorum Fault, the Karakorum–Jiali Fracture Zone (KJFZ), the Jiali Fault, the Altyn Tagh Fault (ATF), and the Red River Fault using a combination of satellite-image interpretation, field mapping, and cosmic-ray exposure dating. The work will lead to a better understanding of the mechanical properties of the Earth's crust, with implications for the earthquake cycle, monitoring nuclear tests, and resource recovery.

For the ATF, cosmic-ray exposure dating of tectonically offset geomorphic markers yields a millennial slip rate of 34 ± 4 mm/y. This morpho-chronological slip rate supports localized lithospheric deformation in which the ATF absorbs as much of India's convergence relative to Siberia as does the Himalayan Frontal Thrust (HFT, see Figure). If extrusion of a rigid Tibet occurs along the ATF, then there must be equivalent features at its southern boundary. The HFT has no lateral component of motion and is therefore kinematically incompatible with lateral motion in the north. However, the Karakorum Fault, which lies to the northwest of the HFT, may form part of a network of faults that define the actual, kinematic southern boundary of this "central Tibet plate."

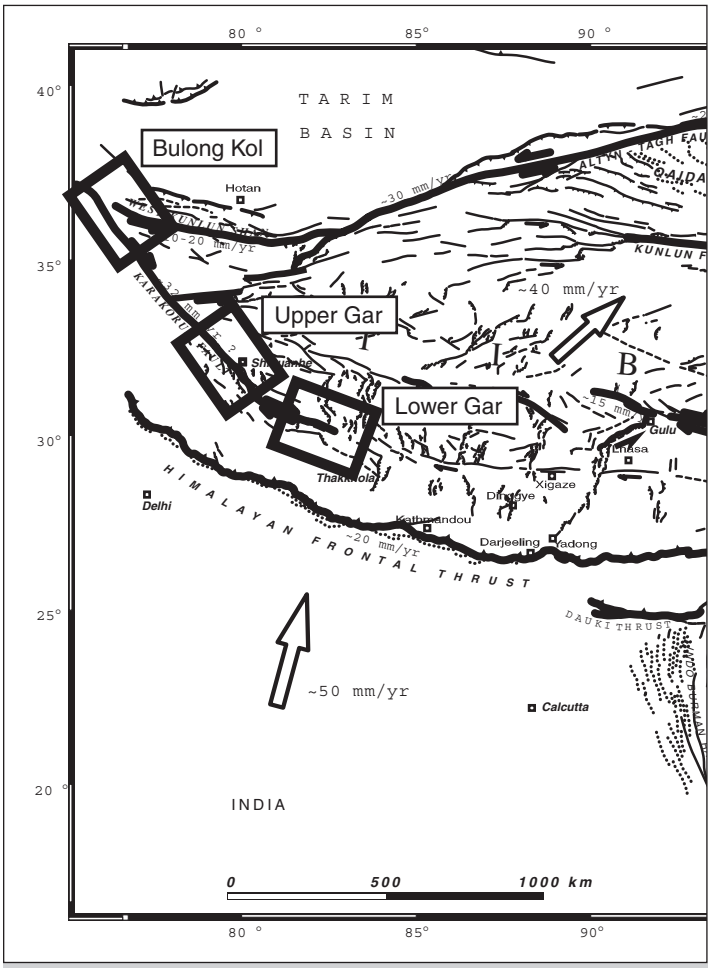

Tectonic map of Tibet showing the study areas along the Karakorum Fault. Also shown are the Altyn Tagh Fault (ATF) and the Himalayan Frontal Thrust (HTF).

By the end of FY2001, we had collected samples from tectonically offset morphological features ranging from tens of meters to kilometers in three areas along the Karakorum Fault: the lower Gar Valley, the upper Gar Valley, and Bulong Kol (see Figure). Near Bulong Kol, cosmogenic dating of a 40-m fluvial offset yields a slip rate of about 6.5 mm/yr. In the lower Gar Valley, a glacial moraine offset by about 350 m was dated at 32.3 ± 9.5 × 10^3 yr, yielding a slip rate of 10.8 ± 3.6 mm/yr. Relative to the ATF rates, these Karakorum rates are lower than expected. The disparity may be due to either some combination of along-strike variation in slip rate, or a fault system comprising multiple strands. The latter would imply subparallel faults, each moving at a relatively low rate, but in aggregate yielding a cumulative rate comparable to that of the ATF. Analysis of the samples taken during FY2001 in the upper Gar Valley should help to resolve this issue.

During FY2002, we will concentrate on the cosmogenic dating of the samples collected in the upper Gar Valley. These data will allow us to constrain the slip rate on the Karakorum Fault and to determine if there is any spatial variation in the rate that can be used to better understand how deformation is carried across the southern portion of the Tibetan plateau.

Stuffing carbon away: How mineralogy and precipitation control long-term carbon sequestration in soils

J. R. Southon, C. A. Masiello, P. Reimer

As humans continue to add the greenhouse gas carbon dioxide (CO_2) to the atmosphere, understanding the processes that can be used to sequester carbon becomes increasingly important. Such studies must focus on carbon reservoirs that are large enough to receive significant quantities of CO_2 and stable enough to retain the CO_2 for many years.

Soils are a promising natural reservoir for carbon storage because the soil carbon pool is approximately twice the size of the atmospheric carbon pool. Limited measurements on radiocarbon (^{14}C) in soil show that some soils are excellent at removing carbon from the atmosphere, retaining high organic carbon concentrations for hundreds to thousands of years, while other soils return their organic matter to the atmosphere within decades. This project is the first to use the carbon-cycle analytical strength of ^{14}C to approach problems of mineral carbon storage in nonvolcanic-soil systems. By identifying some of the conditions under which soil carbon storage is maximized, this study will contribute useful knowledge to inform land-use planning to enhance sequestration beyond current levels (for example, by returning agricultural land to forest or pasture).

This research supports the DOE's terrestrial carbon sequestration program through better understanding and improved models of how various soils store carbon. Collaborators include researchers at the University of California, Santa Barbara, the University of California, Irvine, Lawrence Berkeley Laboratory, and the U.S. Geological Survey.

Coastal California soils provide excellent field sites for the study of soil mineralogy and precipitation, two potential controls on carbon storage. Our field sites are two sets of California coastal soil terraces, one near Eureka and another near Santa Cruz. Within each set of terraces, only soil mineral development varies; all other pertinent parameters (rainfall, plant systems, and soil parent material) are nearly constant. Precipitation at Santa Cruz is half that at Eureka, allowing us to create a two-dimensional matrix of soil properties. We are using radiocarbon to determine the turnover time of soil organic matter on each of these terraces.

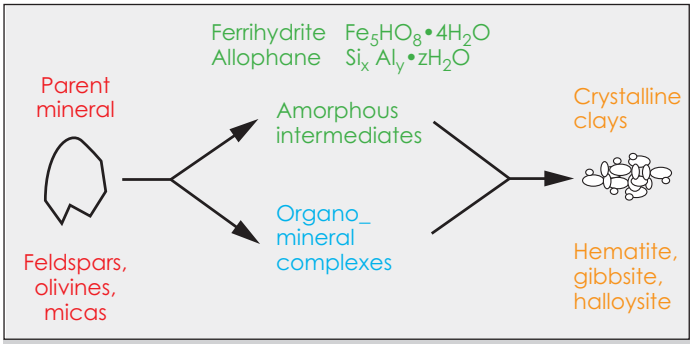

Weathering of soils from primary minerals though carbon-sequestering metastable intermediates to crystalline secondary minerals. Our research shows that intermediates, called organomineral complexes, are important in storing carbon.

As soil terraces weather, their primary, crystalline parent material (bedrock) transitions to various metastable intermediates and finally to secondary, crystalline clays, as shown schematically in the Figure. In FY2001 we examined the relation between the concentrations of two types of metastable intermediates and the capacity of soils to hold organic matter, as measured by soil carbon concentration and radiocarbon age. As a control, we compared the correlation between organic carbon storage and metastable weathering product content with the correlation between organic carbon storage and clay content. We found that organometal complexes were highly correlated with organic carbon storage, while amorphous mineral content and clay content were not significantly correlated. Grain size, as a measure of clay content, is commonly used as a proxy for carbon turnover times in carbon cycle models. Results show that this parameterization is a poor predictor of carbon turnover, and that at our field site, local soil mineralogy is a better proxy for soil carbon storage rates.

Our FY2002 research will focus on the role of water in the storage of soil carbon, both as a weathering agent influencing the trajectory of mineral development and as a medium transporting carbon to deep, mineral-rich horizons. The transport of dissolved organic carbon down soil profiles is one of the linchpin processes determining whether or not carbon reaches deeper horizons and can be sequestered.

In FY2002 we will also examine the chemical characteristics of carbon sequestered in soil minerals using ^{13}C nuclear magnetic resonance. We will test whether specific carbon functional groups are preferentially bound to specific soil minerals, or if carbon binding occurs nonspecifically.

Micro- and nanodeformation of aqueous films for seismic applications

D. L Farber, B. P. Bonner, M. Balooch, W. Siekhaus

Seismology—in the broadest sense, the study of Earth's dynamical response to mechanical stimuli—is a singularly powerful tool for investigating a wide variety of scientific, technical, and environmental problems. Seismic research impacts an extraordinarily wide range of human activities, including earthquake hazard mitigation, tracking movement of pollutants underground, and hydrocarbon exploration. The LLNL mission addresses nontraditional but critical seismic problems, such as predicting the ground response to explosive or earthquake loading at locations for which there is no local calibration, and forensic seismology, the detection of clandestine explosions. This project addresses the most fundamental and long-standing problem in seismic remote sensing of the Earth: the role fluids play in transmission, modulation, and dissipation of seismic energy.

We have developed new technologies based on atomic force microscopy (AFM) and nanoindentation to attack this problem at the submicrometer length scales where the critical physical mechanisms operate. Our results are directly applicable to the prediction of weapons effects on the surface and underground, and to the DOE's energy and environment missions.

During FY2001, we used depth-sensitive nanoindentation and force modulation to study aqueous films in a nanocrystal for the first time. We were able to accomplish this by taking advantage of the ability of certain sheet minerals (the swelling clay, montmorillonite) to confine extremely thin water layers (0.25 nm/layer) between silicate sheets that make up the crystallites. At ambient temperature, the number of water layers intercalated by surface forces can be controlled by modulating the activity of the water. The samples were evaporated onto optically flat, fused-silica substrates to create thin films in which the sheets are oriented parallel to the substrate. The Figure shows an AFM image of the prepared sample.

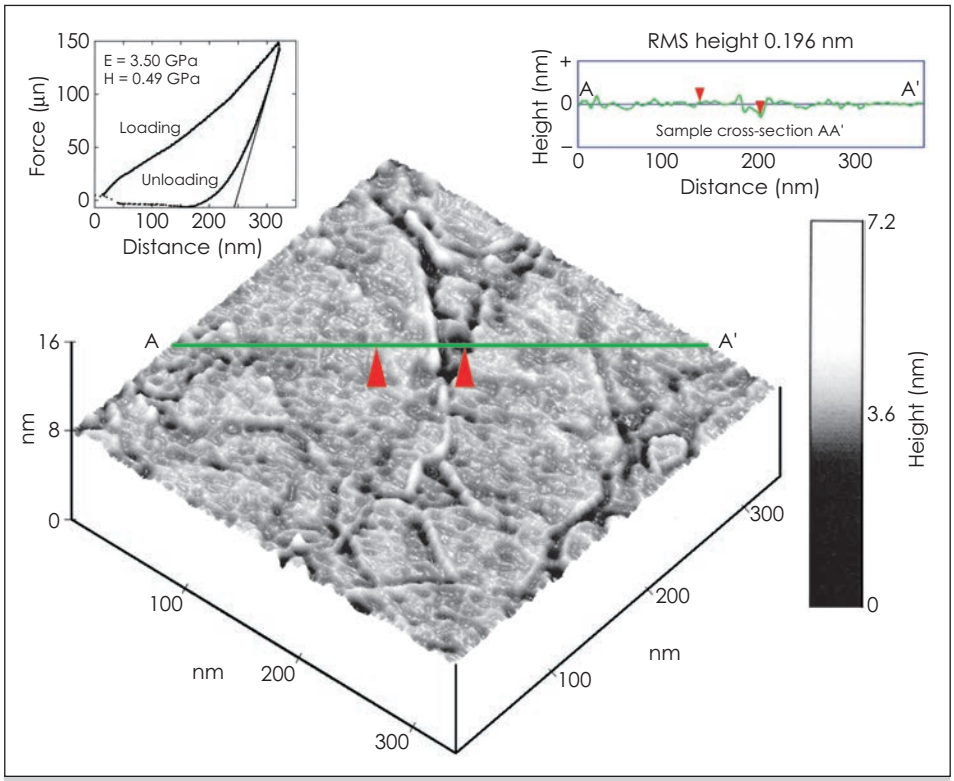

Atomic force microscope (AFM) image of deposited sample of nanocrystalline sheet silicate. The inset shows force-displacement for nanoindentation. Note the large hysteresis, which indicates energy dissipation.

Samples were tested in dry nitrogen and ~30% relative-humidity air. Our initial results demonstrate that the Young's modulus (E) decreased from ~11 to 4 GPa with hydration. Interestingly, the character of force penetration curves also changed from a nearly ideal viscoelastic response in humid air (shown in the inset to the Figure) to local softening (probably cracking) in the dry case (not shown). Force modulation experiments indicate that strong frequency-dependent damping appears only for the hydrated sample. The dramatic stiffness reduction and strong attenuation caused by monolayers of water demonstrate, for the first time, the critical effect of water at a scale that could not be observed by previous technology. In addition, the measurements of frequency-dependent viscoelastic properties are the first for nanocrystalline material of any type.

In FY2002, we will extend our measurements on montmorillonite to other sheet silicates to observe the effects of additional layers of water and to generalize our conclusions. We will begin to use molecular dynamics and effective medium modeling to apply our results to field-scale predictions. We will also use the AFM to directly measure force-displacement curves for quartz–quartz and quartz–water contacts, to determine if contact adhesion effects play a role in seismic attenuation.

Simulating fine-scale atmospheric processes: A new core capability and its application to a wildfire behavior study

M. M. Bradley, M. J. Leach, C. R. Molenkamp, C. H. Hall, L. A. Wilder, L. A. Neher

MAIN TOC

This project focuses on developing, testing, and prototyping a unique capability to couple weather-prediction models that span a range of spatial and temporal scales with a state-of-the-science, physics-based combustion model developed at Los Alamos National Laboratory (LANL). Our primary goal is to protect lives, property, and natural resources; our scientific goal is to understand wildfire processes and to represent that understanding in computer models. The emerging system of models will accurately simulate both wildfire behavior and local weather, taking into account their mutual interactions and the effects of complex terrain. The system also will predict smoke dispersion and its health effects. A geographic information system (GIS) will efficiently process model input data and analyze the human and economic consequences of predicted fire behavior.

The dramatic example of the wildfires that threatened to release radioactive material from DOE facilities at Los Alamos, Hanford, and Idaho Falls in 2000 demonstrates that this work supports DOE national security missions.

As a proof-of-concept demonstration, this project will simulate the early stages (in Tunnel Canyon) of the October 20, 1991 East Bay Hills wildfire in California, which claimed 25 lives and destroyed 3000 dwellings. In addition, we plan to simulate hypothetical fires in nearby unburned areas in response to requests from local emergency-management agencies, which would use the results to prepare for future wildfires.

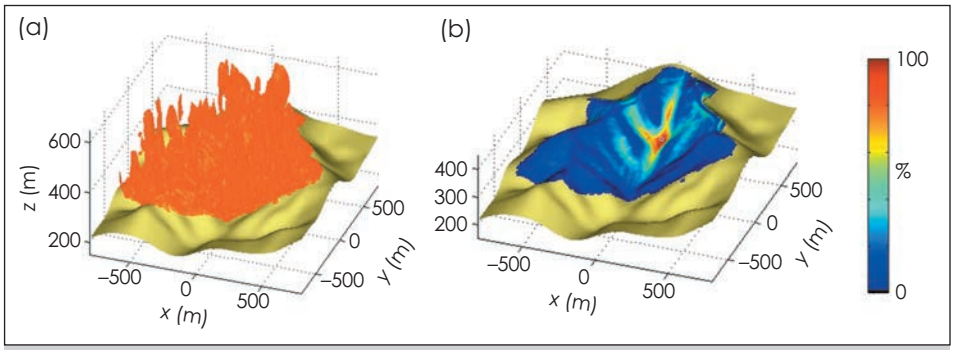

Modeling the burning of a uniform eucalyptus grove in Tunnel Canyon, Oakland, CA., at 11:15 a.m. PDT, 15 min after ignition: (a) 325° temperature contour, and (b) percent fuel burned.

In FY2001, we acquired the latest versions of the models used in LANL's high-gradient flow solver HIGRAD and its combustion simulator FIRETEC, and implemented them on LLNL's TeraCluster 2000 computer. We began integrating these models with our operational regional weather prediction model, the Coupled Oceanographic and Atmospheric Mesocale Prediction System (COAMPS).

For our initial simulations, we prepared 1991 global weather analysis data from the European Center for Medium-Range Weather Forecasting for ingest by COAMPS, processed complex geospatial terrain and fuel data for input to HIGRAD and FIRETEC, and developed MatLab-based scripts that significantly streamline running the coupled system of models and analyzing the output. We completed several COAMPS, HIGRAD, and FIRETEC interactive fire/weather simulations for the early phase of the East Bay Hills fire as part of a sensitivity study on the effects of wind speed and fuel types.

The Figure shows results from a simulation of a fire in a hypothetical eucalyptus grove in Tunnel Canyon in Oakland, where the East Bay Hills fire started.

In FY2002, using numerical analysis techniques, sensitivity studies, scale analyses, diagnostic studies, and comparisons of model simulations with real-world observations, we plan to (1) examine important physical and numerical issues regarding the atmospheric models' inter-scale coupling, treatment of conservative properties, the need for up- and down-scale energy exchange, and sensitivity to fuel characteristics; and (2) evaluate the effect of up-scale energy transfer from the East Bay Hills fire on the HIGRAD solution and on COAMPS-simulated processes. The primary evaluation metric will be the ability of the models to replicate observed fire behavior, as provided by historical data and the eyewitness accounts of fire-fighting professionals.

A high-resolution, global-climate simulation

P. B. Duffy

One major barrier to more realistic simulations of global climate has been the relatively coarse resolution used in global-climate models. Because of the extreme computational demands of global-climate simulations, global-climate models typically use resolutions of about 300 km (i.e., the smallest features in these simulations are 300 km across). As a result of this coarse resolution, global-climate models typically do not produce results that are meaningful on regional scales (e.g., within California). As a step towards solving this problem, in this project we are experimenting with running global-climate models at resolutions as fine as about 50 km, which requires roughly 200 times more computer time than a comparable simulation at the standard resolution of 300 km. These simulations, the highest-resolution global-climate simulations ever attempted, are made possible by the extraordinary computing resources available to LLNL and other DOE laboratories. The goal of these simulations is to lead the way towards improved simulations of climate on both global and regional spatial scales. Our work also showcases the use of computational resources on the scale of the Advanced Simulation and Computing (ASCI) program for addressing important national programs beyond stockpile stewardship.

During FY2001, we performed three high-resolution global-climate simulations: (1) a 12-yr simulation of the present climate at about 75-km resolution; (2) a companion 12-yr simulation of the effects of increased greenhouse gases, also at 75-km resolution; and (3) a simulation of the years 1978–1995 at about 50-km resolution. At the close of the year, the first two simulations had been completed; the last was still in progress. As expected, the high-resolution simulations of today's climate are generally more realistic than comparable coarse-resolution simulations. The Figure shows an example of this, in which the simulations of present-day precipitation over the U.S. agree more closely with observations as the resolution becomes finer. Because topography itself is better represented in the finer-resolution simulations, the improvement gained from these simulations is especially significant in quantities that are strongly influenced by topography, such as surface temperature and precipitation—two quantities that also have strong societal impacts.

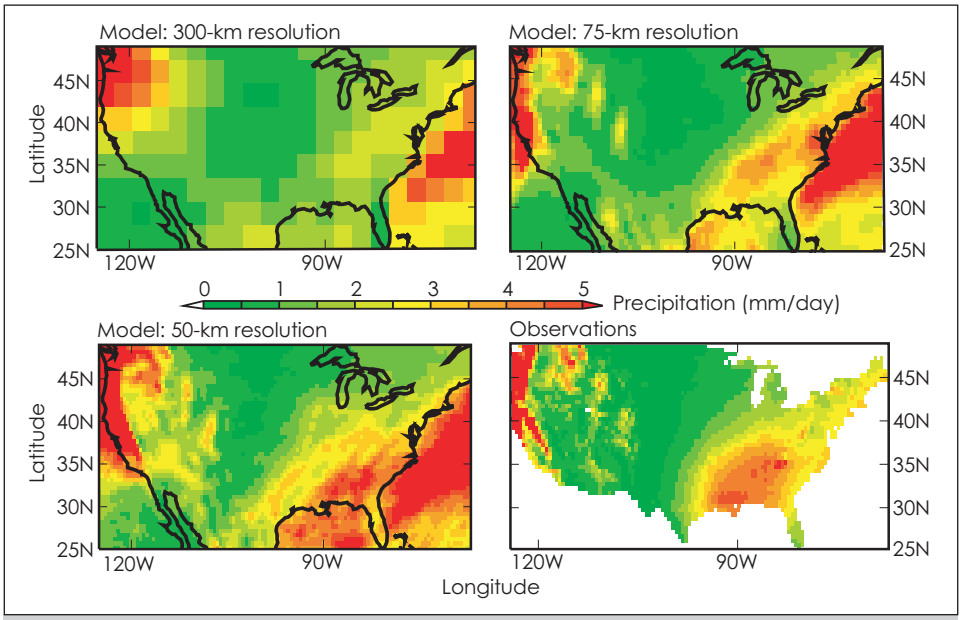

Wintertime precipitation over the United States, as observed and as simulated in three global-climate simulations of different resolutions. The finer-resolution simulations are more realistic.

Preliminary results from these simulations have generated wide interest among climatologists; we have received numerous requests from other groups to analyze aspects of our results. So far, we have made limited results available to other groups; eventually, all our results will be available.

Our experimental high-resolution simulations have demonstrated the feasibility and value of running global-climate models at high resolution. In future work (for which we have received initial funding from the DOE), we will use the high-resolution model to produce improved simulations of climatic change on global and regional spatial scales.

Accelerated carbonate dissolution as a carbon dioxide separation and sequestration strategy

K. G. Caldeira, K. G. Knauss, G. H. Rau

MAIN TOC

Simulations of global warming indicate that unabated release of carbon dioxide (CO_2) could increase global land temperatures an average of 8°C (14.4°F) by the end of the century. One strategy to diminish climate change is to store fossil-fuel CO_2 where it would be isolated from the atmosphere. Proposed storage reservoirs include deep saline aquifers, the terrestrial biosphere, and the oceans.

We are developing a novel method for sequestering fossil-fuel carbon in the ocean by accelerating the natural weathering reactions associated with carbonate minerals. This process would react power-plant effluents with crushed carbonate minerals and seawater in a reactor vessel to form calcium and bicarbonate ions in solution. The carbonate-dissolution method of ocean CO_2 disposal uses existing technologies, abundant carbonate minerals, and seawater to neutralize CO_2-induced acidity. The method would convert most of the fossil-fuel CO_2 to the bicarbonate form, which does not readily exchange with the atmosphere. Also, because the waste water generated by the carbonate-dissolution method would be much more benign than directly injected CO_2; the effluent could be released into near-shore ocean waters.

Our goal is to test, through experiments and computer modeling, whether this method can be applied economically on a large scale and whether it would contribute significantly to the global management of carbon. This project directly supports the DOE's energy and environmental missions.

Since the project began in mid-FY2001, we have been working on an integrated approach that combines bench-top experimentation and computer modeling. The bench-top experiments are designed to develop the chemical kinetic data required for an engineering analysis of our carbon-sequestration method. We have (1) designed and built the experimental apparatus [Fig. (a)], and (2) completed our first experiment involving dissolution of calcium carbonate in a stirred reactor vessel using a simulated flue gas [Fig. (b)].

(a)

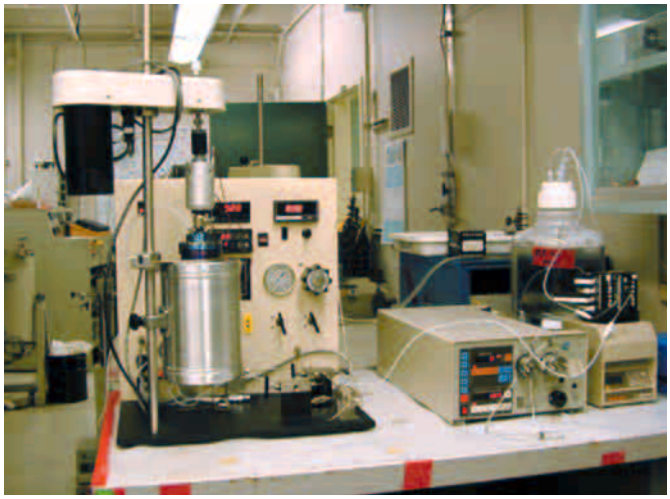

(b)

Experimental equipment being used to test the carbonate-dissolution method of CO_2 capture and sequestration, showing (a) our bench-top apparatus; and (b) a closeup of the reactor vessels (cylinders in the rear), the stirring apparatus (foreground), and calcium carbonate crystal (foreground, right side).

Computer modeling is needed to understand how and where the resulting effluent could be released into the ocean and to determine what happens to the fossil-fuel carbon in the long term. For example, we must know how much of it will stay in the ocean and how much will leak out to the atmosphere, where, and when. In FY2001, we completed detailed thermodynamical chemical calculations, and used LLNL's ocean general circulation model (OGCM) to simulate the fate of the effluent after its release into the ocean.

Our initial experimental and computational results indicate that carbonate-dissolution is a safe and effective method of storing carbon in the ocean.

In FY2002, we plan to perform a suite of experiments to help us understand the kinetics of the reactions under realistic conditions, for example, using real seawater and mining-grade carbonate minerals. These experiments would give us a better idea of the chemistry of the effluents. We would then use OCGM simulations to help us understand (1) the consequences of releasing this effluent into the ocean, and (2) how effective this process would be as a CO_2-separation-and-sequestration strategy.

Adaptive tracking of atmospheric releases

D. J. Larson, R. Calhoun

When dangerous chemical or biological releases occur in the atmosphere, emergency responders and decision makers must assess exposure rates of the affected population, establish evacuation routes, and allocate medical resources. This project focuses on improving the scientific basis for making such decisions.

Future rapid-response teams, some of which may come from LLNL, will use a variety of atmospheric sensors and atmospheric computer models to predict and characterize the movement of chemical or biological releases in urban environments; LLNL is likely to contribute expertise in this area. Merging the information and capabilities of computer models with real-time atmospheric data from sensors will represent a key advance. The resulting product will dynamically interpolate and extrapolate the raw sensor data into a coordinated "picture" or interpretation of the developing flow scenario.

The scientific focus of the project was the exploration and development of algorithms that may serve to fuse laser infrared radar (lidar) data, which measure wind speed much as a police radar measures vehicle speed, and a dispersion model into a single system. Our goal was to provide the scientific foundation for a combined lidar/model approach capable of accurately tracking the evolution of atmospheric releases on distance scales of about 20 km. The fundamental idea is to create feedbacks, so that lidar data can be used for wind field inputs into a dispersion model. The model would, in turn, guide lidar data acquisition by directing more intensive scanning to regions where more data are key to improving the modeling.

Three major accomplishments were achieved in FY2001. First, we created a database of synthetic lidar data that can be used to test algorithms relating to a combined lidar/dispersion model. The data, which represent nocturnal atmospheric drainage flows in the Salt Lake City Basin, came from calculations on the LLNL Advanced Simulation and Computing (ASCI) White supercomputer with a computational fluid dynamics model running in large-eddy simulation mode. A simple modification of the resulting air-flow data produced radial velocity wind field data (see Figure), which may be directly compared with real lidar data and substituted for them. A short animation (in the CD-ROM version of this article) represents drainage flow from the mountains; the assumed position of the lidar was that of an actual lidar that took data in DOE's Urban Dispersion Project in the fall of 2000.

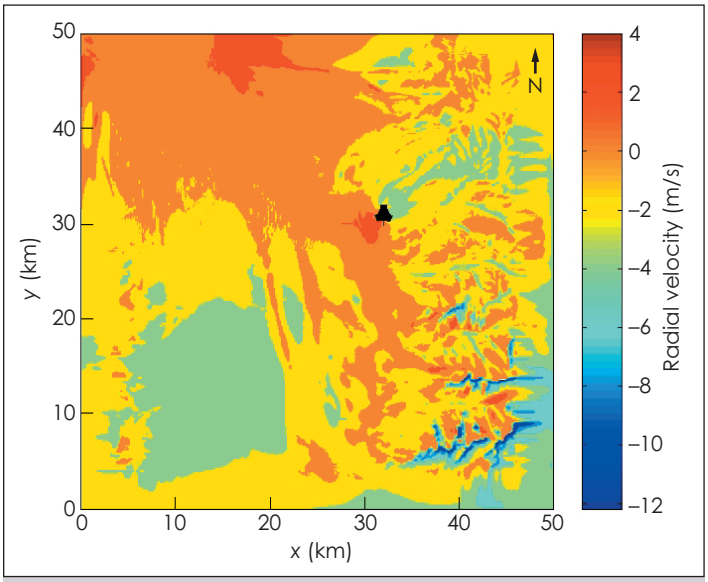

Synthetic laser infrared radar (lidar) data representing night-time drainage airflow from the mountains around Salt Lake City, Utah, as imaged by a lidar whose position is indicated by the black symbol. Such synthetic data can be used in developing a combined lidar/computational model to track and predict the course of atmospheric releases.

After studying the "Terminal Winds" project at the Lincoln Laboratory of the Massachusetts Institute of Technology and analyzing algorithms and approaches used by other scientists on related or relevant projects, we determined that an approach using the Gauss–Markov theorem will be useful in designing an advanced sensor integration system for incorporating lidar into numerical models. In particular, the theorem will assist in building a single interpretation of a flow field based on possibly conflicting sensor data.

We began development of a script-based "test" laboratory that samples the database and provides input to a dispersion model, which was ported and tested on the Frost computer platform at LLNL, where the CFD runs were completed. Our results demonstrate that specially sampled data from numerical models can indeed be a useful surrogate for actual lidar data, which currently can be gathered only at great expense.

The PI is now an Assistant Professor of Mechanical and Aerospace Engineering at Arizona State University (ASU). LLNL and ASU have recently established a collaboration entitled "Advanced Sensor Integration into NARAC's Atmospheric Data Assimilation Program" which we believe will benefit from the groundwork provided by this LDRD.

Critical analysis of the atmospheric importance of iodoalkane emissions using the LLNL IMPACT model

P. S. Connell

Ozone (O_3) is a key atmospheric chemical species in the investigation of global atmospheric change. It is a photochemically active atmospheric participant, has important spectral interactions with long-wavelength radiation in the atmosphere (related to climate change) and with the short-wavelength region of the solar spectrum (related to ultraviolet reduction and to tropospheric photochemistry), and is subject to large-scale atmospheric transport.

Recent analyses show that observed trends of O_3 decrease in the lower stratosphere, under both transport and photochemical control, are more pronounced than at higher altitudes, where local photochemical control is predominant. Ozone near the tropopause has been thought to be primarily under transport control, but it is possible that particularly effective ozone-destroying compounds, such as atomic iodine (I), may contribute to ozone photochemical loss in this region.

In this project, we have used a core LLNL capability, the IMPACT 3D chemistry-transport model of the global stratosphere and troposphere, to predict the atmospheric abundance of I as introduced to the atmosphere by CH_3I, a naturally emitted compound, and by CF_3I, a proposed industrially produced compound for fire-fighting.

For inorganic iodine, the basic ozone-destroying catalytic cycle is the pair of reactions $I + O_3 = IO + O_2$ and $IO + O = I + O_2$ which correspond to the net reaction $O + O_3 = 2O_2$

This net reaction can take place directly, but is significantly accelerated by the presence of the iodine radical species, which are themselves regenerated, not consumed. IO reactions with ClO and BrO, which are also fast, provide alternative cycles that increase ozone loss. Chemical-kinetic considerations, however, suggest that iodine is much more efficient at destroying ozone than chlorine.

In the simulations performed in this project, we ran the IMPACT model for two-week periods, initialized from restart files for the appropriate period from the IMPACT reference atmosphere runs, using meteorology provided by the MACCM3 global climate model from the National Center for Atmospheric Research. Iodine compounds were initialized to zero. Boundary conditions for CH_3I and CF_3I were set to 1 part per trillion (ppt) by volume at the surface between 30°S and 30°N, representing, for CH_3I, the natural background, and for CF_3I, low-latitude emissions corresponding to hypothetical usage by developing nations. Mid-latitude emissions, between 30°N and 60°N, represent usage by industrialized nations. The two-week simulations used 64 nodes of an IBM SP parallel computer.

We calculate an e-folding lifetime of three to six days for CF_3I, depending on the pattern of emissions in latitude and on the season. For low-latitude emissions, interactions with convection produce a substantial enhancement in upper tropical troposphere abundance of both CF_3I and its iodine-containing degradation products (see Figure), which will produce a significantly greater ozone depletion potential (ODP) than would be expected using the conventional approach of a well-mixed troposphere. Transport of the products dominates stratospheric photolysis of CF_3I as a source of lower-stratospheric iodine, and this is also contrary to the conventional approach for determining ODP. The predicted IO abundance in the lower stratosphere would be on the order of 1 ppt for a surface CH_3I abundance of several parts per trillion. Both of these values are in rough agreement with the scattered observations that have been reported. These concentrations, although low, are high enough, given the efficiency of iodine for catalyzing ozone destruction, to compete with chlorine-moderated ozone destruction in the lowest stratosphere and to warrant further observations of atmospheric iodine over a range of latitudes and seasons.

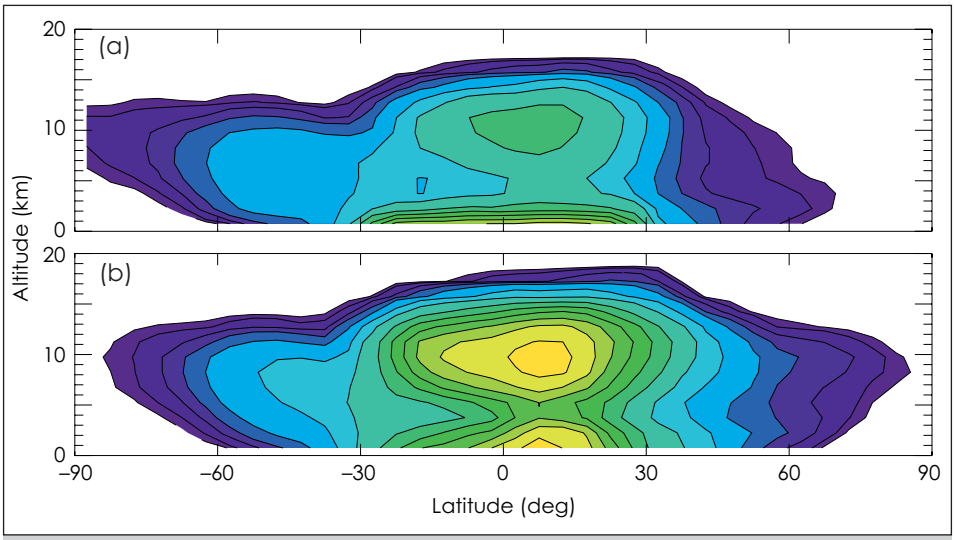

IMPACT simulated distributions of (a) CF_3I and (b) its iodine-containing products in July for emissions at low-latitudes. Contour lines are mixing ratios. Note the local maxima near the equatorial tropopause (10–15 km altitude), demonstrating rapid convective lofting of near-surface air to the stratospheric gateway. This exposes ozone in the lower stratosphere to destruction by iodine catalysis.

Natural variability and anthropogenic influence on climate: Surface-water processes in the Indonesian seas over the last 120 years

T. P. Guilderson, M. Kashgarian, K. Caldeira

The intimate coupling of the surface of the ocean and the overlying atmospheric boundary layer implicitly link variations in atmospheric characteristics to the underlying sea-surface temperature field. The Indonesian Seaway is a conduit for cross-equatorial, transoceanic exchange between the western Pacific and Indian Oceans. The Indonesian through-flow (ITF) has been recognized as an important contributor to the global thermohaline circulation and global climate. Enhanced vertical mixing in the Indonesian Seas drives large fluxes of heat and freshwater into the water column; when this water is ultimately incorporated into the ITF, it contributes to the regional freshwater and heat budget. It is this redistribution of heat and salt that—in concert with regional or basin-scale processes such as the El Niño Southern Oscillation (ENSO)—sets the stage for the global thermohaline circulation.

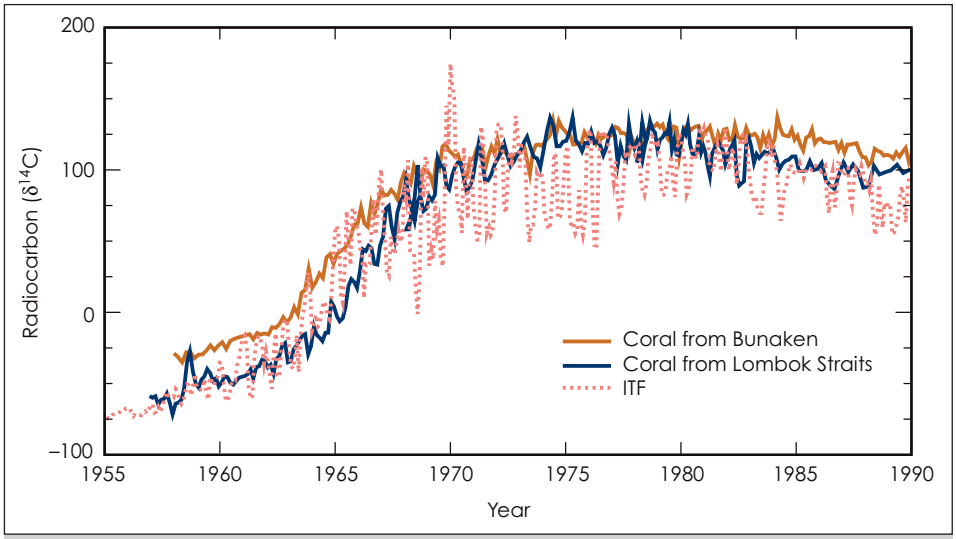

High-resolution surface-water $\delta^{14}C$, as recorded in corals from the Sulawesi Sea and Lombok Straits in Indonesia and compared with that simulated by the Lamont Ocean–Atmosphere Model forced with observed winds but with a fixed Indonesian through-flow (ITF) transport. The model results are taken from the inflow grid-cell equivalent in space to Bunaken.

Sensitivity tests using the high-resolution Lamont coupled ocean–atmosphere model imply that the amount of ITF changes the proportion of southern and northern waters mixing in the thermocline. The other interpretation of the model results is that changing the ITF results in a basin-wide response of the thermocline.

Our goal is to determine if there is evidence for decadal modulation of the vertical mixing in the Indonesian Seas and, if so, how it affects the vertical structure of the Pacific thermocline. Coral–δ carbon-14 (^{14}C) time series can be used in conjunction with experiments using oceanic models to study the processes governing water-mass mixing and movement in the Indonesian Seas over time scales long enough to study the linkage between processes in the Indonesian Seas and decadal modulation of ENSO. In this study, we focused on the ITF, although our general approach and results have broader applicability in making ocean models more realistic. In addition, the time history of ^{14}C in the surface ocean reflects the uptake and redistribution of bomb-^{14}C; a reasonable proxy for anthropogenic carbon dioxide (CO_2). This research supports the DOE's mission in climate modeling and environmental research.

Since funding began in mid-FY2001, we completed—with the help of summer undergraduate students at LLNL's Center for Accelerator Mass Spectrometry (CAMS) and at Harvard University—a high-resolution, post-bomb, coral-based $\delta^{14}C$ record from Bunaken in the Sulawesi Sea. A comparison of the coral–$\delta^{14}C$ data to date with those simulated in the Lamont Ocean Atmosphere model has begun (see Figure) and shows serious discrepancies in how well the model recreates the observed tracer field.

To study the effect of vertical mixing parameterizations, we began a series of sensitivity tests using LLNL's variant of the Geophysical Fluid Dynamics Laboratory (GFDL) Modular Ocean Model. These sensitivity experiments relate the vertical mixing parameterization to the vertical density structure through the Brünt-Vasaila buoyancy number explicitly defined by the model's own density stratification. An associated sensitivity test will be to utilize eddy kinetic forcing under the assemblage of k-profile parameterization mixing, a common parameterization scheme used in many ocean models. We also updated the Los Alamos Parallel Ocean Program (LANL-POP) model to include radiocarbon as a passive tracer.

In coordination with a collaborator at the University of California, San Diego, we made preliminary measurements on a suite of Western Pacific sclerosponges to study the Suess Effect: the rate of uptake of anthropogenic CO_2 by the ocean.

An overview of our application of high-resolution $\delta^{14}C$ and modeling activities was presented at the International Atomic Energy Agency's Conference on the Study of Environmental Changes Using Isotope Techniques.

Earthquake time series determined from direct cosmogenic dating of fault scarps

L. Benedetti, R. Finkel

MAIN TOC

The simplest view of the process that creates earthquake scarps is that "characteristic earthquakes" repeat at regular intervals in the same place with about the same slip for each event. This concept now forms the basis for understanding earthquake hazards. But, is the characteristic earthquake concept a good approximation to the physics of the earthquake process? Historical information for the Mediterranean region suggests that the frequency of major events varies substantially with time. For small events, compilations that comprise many thousands of earthquakes have been shown to exhibit fractal characteristics in magnitude, space, and time. Whether large seismic events are really part of the same fractal set is still undetermined. This is a critical question that can be addressed only by investigating magnitude–frequency characteristics for large earthquakes over millennial time scales.

We are developing a new method for dating seismic events by building on the capabilities of LLNL's Center for Accelerator Mass Spectrometry (CAMS). This project enhances the Laboratory's competency in cosmogenic isotopes by establishing a new CAMS capability for measuring clorine-36 (^{36}Cl) in samples of surface rock. Our new methodology provides previously unattainable data on earthquake history and the slip distribution of a fault. Moreover, it will allow better assessments of seismic risk in highly populated areas. This research supports the DOE's mission in geosciences and national security.

We use cosmogenic, ^{36}Cl surface-exposure dating to determine the approximate date that a rock was exposed to cosmic rays. Interactions between neutrons and muons from the cosmic rays and target elements in the rocks such as calcium-40 (^{40}Ca) produce cosmogenic isotopes such as ^{36}Cl. Because production of ^{36}Cl decreases exponentially with depth, ^{36}Cl accumulates mostly while the rock is at the surface. The summing of major earthquakes on a fault creates cumulative scarps. With each new earthquake, a new section of free face is exposed on the scarp, with the samples highest on the scarp having the longest exposure and therefore the highest ^{36}Cl concentration. We can model this distribution for a scarp that was created by *n* events with varying recurrence time. The position of discontinuities in the nuclide concentration and the values of the nuclide concentrations allow us to determine a magnitude–frequency spectrum for the fault.

We have chosen to study two areas in the central Apennines where normal fault scarps with heights of tens of meters are exposed and where little erosion has taken place.

During FY2001, we sampled several continuous profiles at sites in Greece: along the Sparta fault [(Fig. (a)] and along the Kaparelli fault (north of the Gulf of Corinth). The best results were obtained for the Sparta fault, which cuts through limestone bedrock to produce a 20-km-long, very well-preserved, normal fault scarp that reaches a height of 10 to 12 m. Samples from the best-preserved sections of this scarp were parsed into 10-cm sections for analysis. The ^{36}Cl and chloride concentrations in the carbonate were determined for 82 Parori subsamples and 64 Anogia subsamples [Fig. (b)] by isotope-dilution accelerator mass spectrometry at LLNL's CAMS.

Our results confirm that an earthquake on this fault destroyed ancient Sparta in 464 BCE [see Fig. (b)]. Four earlier earthquakes in the last 13,000 yr had similar slip amplitudes (about 2 m) and time intervals ranging from 500 to 4,500 yr. The observations also confirm that the Sparta scarp is postglacial, supporting the hypothesis that similar scarps elsewhere in the Mediterranean region have a similar age. The absence of any event since 464 BCE could suggest an event is imminent.

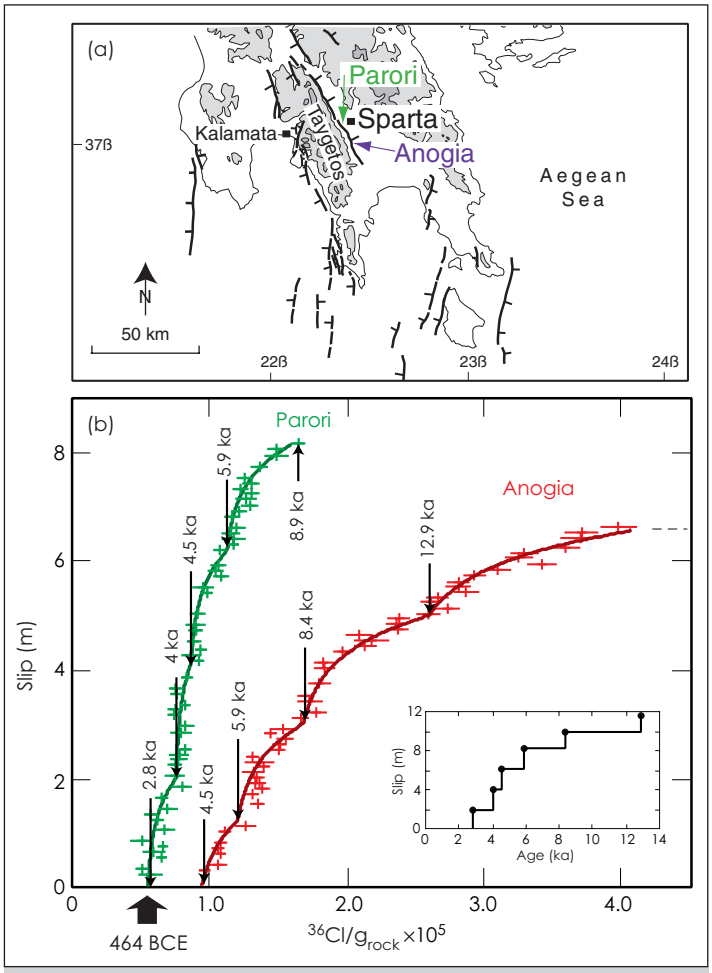

Earthquakes in southern Greece: (a) active faults (arrows show sampling site locations), and (b) ^{36}Cl data and modeled results. Crosses are ^{36}Cl concentrations per gram of rock for each sample; lines are synthetic profiles. Inset is time vs. slip of event deduced from the models. Time is in thousands of years (ka) before the present.

Improving prediction of behavior in geological environments not directly observable

R. D. Aines, R. L. Newmark, J. J. Nitao, W. G. Hanley, A. L. Ramirez, S. Carle, S, Sengupta, K. M.

MAIN TOC

Understanding geological environments that are relevant to Laboratory missions requires optimizing knowledge about the configurations of environmental systems for which sufficient direct observations cannot be made. Even though the properties of such systems can often be measured, complex systems still are dramatically data-limited because of either poor access or the sheer complexity of the issue. Applications could include (1) underground systems ranging from environmental contamination to military bunkers; (2) nuclear-waste disposal systems; (3) fossil-energy extraction systems; and (4) complex, hostile environments such as battlefields or clandestine underground facilities.

We are currently investigating an earth-sciences application. Our new, probabilistic method uses existing forward models to transform uncertainty in the sample space (e.g., lithology or permeability) to uncertainty in the measurement space (e.g., temperature or electrical current). These predicted measurements can then be used to estimate the likelihood of actual measurements, which in turn reduces the uncertainty in the original sample space via conditional probability methods. We accomplish this by integrating the general knowledge represented by models with specific knowledge represented by data, using a statistical method called Bayesian inferencing and a highly efficient, staged Metropolis-type search algorithm originally developed to estimate thermodynamic properties. From this, we obtain a distribution of all of the configurations and parameter values of the system that are consistent with existing data. We call our combination of probabilistic and deterministic approaches the "stochastic engine."

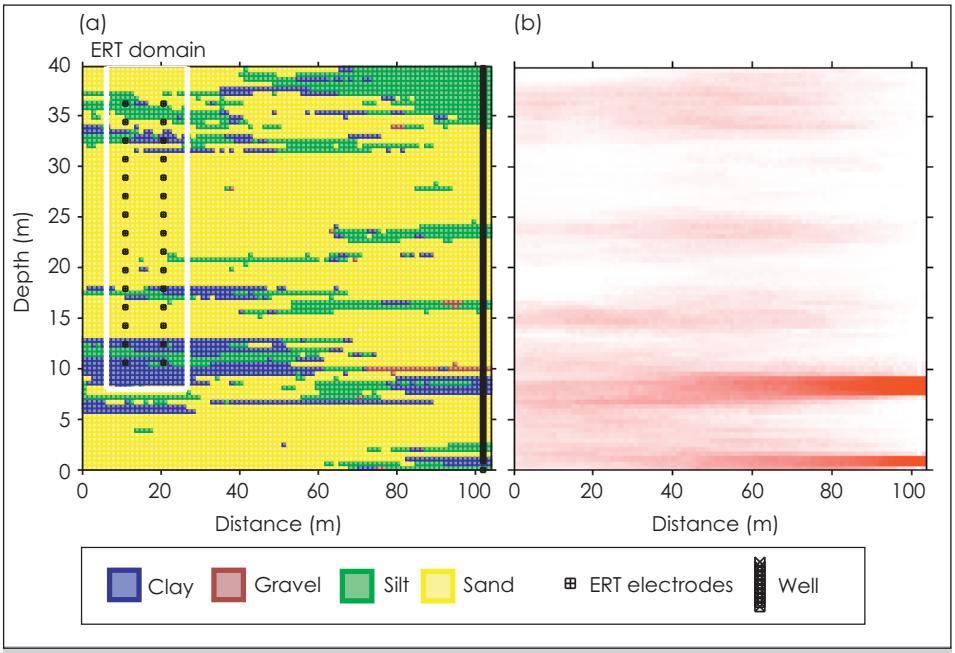

Lithology at the A/M outfall site at DOE's Savannah River Site (SRS). (a) One representation that we used to predict electrical resistance tomography (ERT) results for comparison to the observed data. Representations such as this are accepted or rejected to build up a description of the probability of the site's lithology. (b) One such result, the probability of occurrence of clay at each pixel. Red indicates a probability of 1 and white a probability of 0.

Our method is flexible and is best applied to nonlinear, multidimensional problems.

Because the method is fully automated, large data sets of a variety of types can be used to refine the system configurations. This aspect will be valuable in extending the method to other problems where rapid decisions must be based on limited amounts of data. Our initial earth-sciences application uses models for rock type (lithology), flow and transport, geochemistry, and geophysical imaging; the base representation (system configuration) being refined is the lithology at each underground location.

During FY2001, we demonstrated a two-stage analysis of synthetic electrical resistance tomography (ERT) data and hydraulic-flow information, coupled to a base representation of lithology. Using actual data from a highly contaminated area at DOE's Savannah River Site (SRS), we used our stochastic engine to resolve the lithology using ERT data (see Figure). Savannah River Site will use these methods in the design and implementation of steam cleanup of the largest trichloroethylene (TCE) source in the DOE complex. We also created a Web-based interface that will allow collaborators like SRS to enter data and observe the results of LLNL supercomputer calculations in an interactive mode.

In FY2002, we plan to expand the existing earth-sciences application to three dimensions using large SRS data sets on massively parallel computers. We will (1) condense the complex state space into a set of metastates with roughly equivalent properties; (2) extend our method to include active process analysis, in which an ongoing data stream is used to continuously update our understanding of the system configuration; and (3) evaluate extending our investigation to other types of state spaces—such as chemical parameters in a reacting system or the movement of a plume in the atmosphere.

An integrated climate- and carbon-cycle model

S. L. Thompson

Coupled climate- and carbon-cycle modeling is required to understand and predict the future environmental impacts of fossil-fuel burning. At present, atmospheric CO_2 concentrations are prescribed, not simulated, in large climatic models. To produce credible simulations of the entire climatic system that predict time-evolving atmospheric-greenhouse forcing, we need to use models of manmade emissions as the fundamental input.

Predicting atmospheric CO_2 concentrations represents a substantial scientific advance because of the large natural sources and sinks of carbon that are likely to change as a result of climatic change. Estimates of the amount of manmade CO_2 that will accumulate in the atmosphere depend on understanding the carbon cycle. For this reason, models that use CO_2 emissions as input must directly address greenhouse-related questions of interest to policymakers—such as the amount of CO_2 we can emit before causing a dangerous level of climate change.

The goal of this project is to develop a global-scale, integrated climate- and carbon-cycle (INCAA) model to (1) predict the fate and climatic effect of fossil-fuel-derived CO_2 and aerosols, and (2) evaluate the climatic impact of proposed energy policies. INCCA requires models of the global climate to be coupled with terrestrial and oceanic ecological and biogeochemical components. Our approach relies on the use of existing models of the atmosphere, ocean, land surface, and aerosol chemistry that are well developed and published. Where necessary, we are modifying codes for use on terascale, high-performance computers and for coupling into a comprehensive simulation system.

In this project, we are uniquely positioned to make rapid progress in this high-priority area of global-change prediction because we can leverage previous and ongoing LLNL developments in climatic science and terascale parallel computing. Two initiatives launched recently by the White House—the U.S. Climate Change Research and the Climate Change Technology—both highlight the need for an improved climate-carbon prediction capability. INCCA positions LLNL to play an important role in these initiatives.

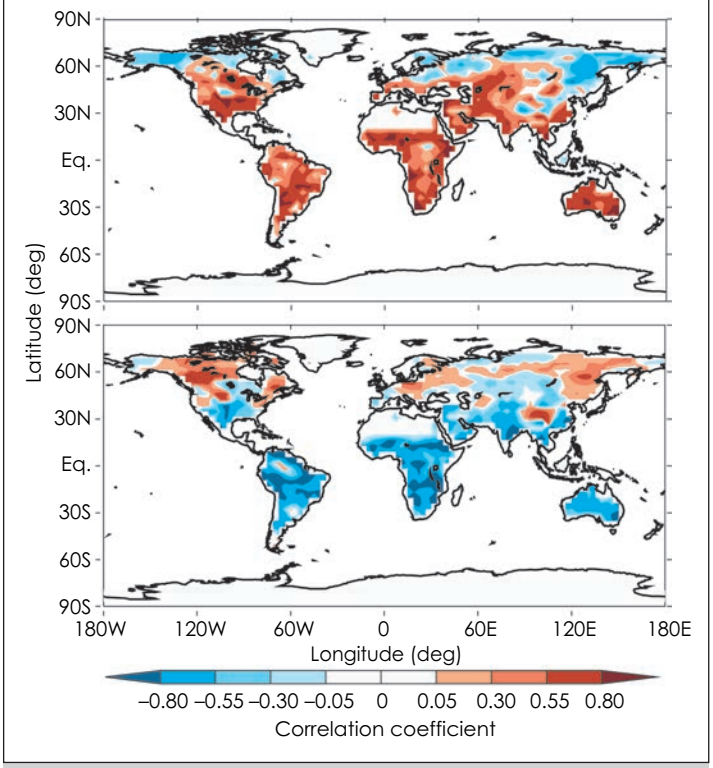

Model-simulated correlations between carbon uptake and interannual variations in climate: (top) net carbon flux and precipitation, and (bottom) net carbon flux and surface temperature. Precipitation controls carbon uptake—except in colder areas where temperature is the limiting factor.

During FY2001, we acquired and tested component models from the National Center for Atmospheric Research (NCAR) and from our collaborators at the University of Wisconsin, applied the coupled terrestrial biosphere–climatic model, and developed the coupled oceanic–biogeochemistry model. An ensemble of 16 multiyear simulations with a coupled climatic and vegetation model subset of INCCA showed that it could reproduce the observed interannual variability of CO_2 uptake by plants that is caused by climatic variations. The correlation between carbon uptake over land and temperature and rainfall variability is shown in the Figure. Model results such as these will help us to understand how the global biosphere reacts to climatic change, something that is difficult to do from observations alone.

We also modified a biogeochemical model for the oceanic carbon cycle; at the end of the year, we were running it within a coupled atmosphere–ocean climatic model. As a prerequisite to coupling it to our overall system, we simplified an existing atmospheric-chemistry model so that it runs ten times faster with little loss of fidelity.

In FY2002, we will (1) test the fossil-fuel aerosol model coupled to a climatic model, (2) continue applications with a new massively parallel version of our coupled climatic and terrestrial-biosphere model, and (3) most significantly, complete the coupling of the full climatic and carbon-cycle system. The last will allow us to start on comprehensive predictive simulations of the effects of carbon-cycle change on future climatic change.

Biotechnology and Health Care Technologies

Section 3

Section 3 Biotechnology and Health Care Technologies

Chimeric proteins to detect DNA damage and mismatches

S. L. McCutchen-Maloney, K. M. Robbins, C. Giannecchini, M. Malfatti

MAIN TOC

The overall goal of this project was to develop chimeric proteins composed of a DNA mismatch or damage-binding protein and a nuclease, as well as methods to detect DNA mismatches and damage. We accomplished this through protein engineering based on using polymerase chain reactions (PCRs) to create chimeric proteins with novel functions for damage and mismatch detection. This project addressed fundamental questions relating to disease susceptibility through single nucleotide polymorphisms (SNPs) detection capability and also supported and enhanced LLNL's competency in the emerging field of proteomics.

In nature, DNA is constantly being subjected to damaging agents such as exposure to ultraviolet radiation and various environmental and dietary carcinogens. If DNA damage is not repaired, mutations in DNA result that can eventually manifest in cancer and other diseases. In addition to damage-induced DNA mutations, SNPs, which are variations in the genetic sequence between individuals, may predispose some individuals to disease. Therefore, methods to detect DNA damage, mutations, and SNPs are useful not only in basic research but also in the health and biotechnology industries. Current methods of detection often use radioactive labeling and rely on expensive instrumentation that is not readily available in many research settings. Our methods to detect DNA damage and mismatches employ simple gel electrophoresis and flow cytometry, which alleviate the need for radioactive labeling and expensive equipment.

In FY1999 and FY2000, we created 12 chimeric proteins, expressed and purified these proteins, and developed methods for mismatch detection using gel electrophoresis and flow cytometry with multiplex detection capability. The project received two patents for this work.

In FY2001, we explored SNP detection by developing methods based on the ability of the chimeric proteins to detect mismatches. Using flow cytometric multiplex assays and fluorescent beads to which the DNA substrates where attached, we showed that several of the chimeras possess greater affinity for damaged and mismatched DNA than for native DNA. This affinity was demonstrated in assays in which we looked both at preferential degradation of damaged or mismatched DNA after addition of a chimeric protein and at preferential binding of the chimeric proteins to damaged or mismatched DNA. In our experiments, we used DNA samples containing damage or mismatches and a control sample containing no damage or mismatches. When a chimeric protein was added to the DNA samples, the damage- or mismatch-recognition portion of the chimeric protein bound the samples containing the DNA damage or mismatch, allowing the nuclease portion to degrade the DNA. Thus, we measured both the preferential binding to and the preferential degradation of these same samples. This was shown in gel-based assays (see Figure) as well as in multiplex flow cytometry assays.

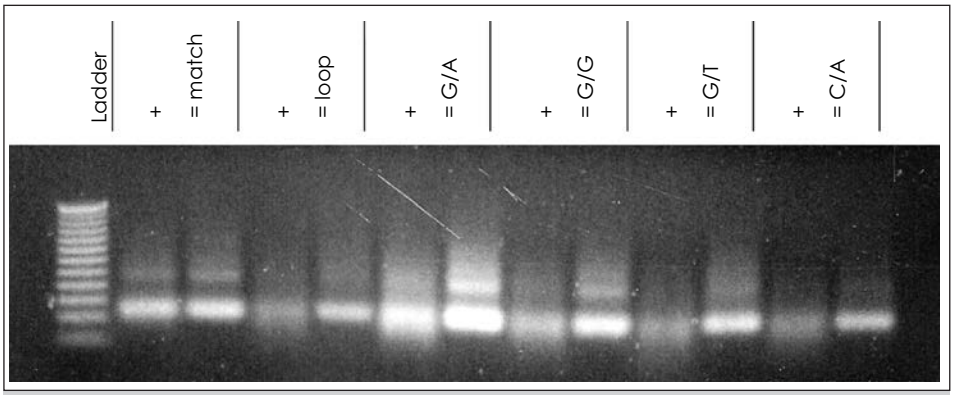

Gel-based mismatch detection using a chimeric protein comprised of a nuclease and a mismatch detection protein (Nuc-MutS). The chimeric protein did not degrade the match (the perfectly matched double-stranded substrate at the far left) but degraded all the mismatches: loop (a double base-pair mismatch), G/A, G/G, G/T, and C/A. The + designates the addition of the chimeric protein and the = represents the negative control with no protein added

In the final year of this project, we also focused on the MutS protein, which in nature functions to detect mistakes in DNA replication by its mismatch-detection capability in a micro-organism that lives under extreme thermal conditions (75˚C). Because of its thermophilic stability, this protein has great potential as a SNP detection tool. However, the results of our multiplex experiments were inconclusive, potentially because of nonspecific interaction of the protein with the beads.

In summary, the chimeric proteins and methods developed in this project have application for detecting SNPs and DNA damage as well as for genetic testing (with further development).

Using mass spectrometry to probe noncovalent interactions between biomolecules

S. J. Shields

MAIN TOC

To counter bioterrorism and to understand, treat, and prevent human disease by developing antibodies for pathogens, we must be able to determine protein conformation, characterize protein–ligand noncovalent interactions, and determine protein conformation changes induced by ligand binding. Characterizing and understanding the cascade of biomolecular interactions is at the heart of biomolecular sensor development. Research efforts implemented by LLNL and the DOE include the design, synthesis, and characterization of small-molecule ligands that noncovalently bind to and act to inhibit the function of biological toxins such as tetanus, botulinum, and cholera by blocking the protein's active site.

Noncovalent interactions are energetically weak associations between molecules (1 to 5 kcal/mole) and consist of (1) hydrophobic interactions, in which nonpolar functional groups interact on the basis of their repulsion from water; (2) electrostatic interactions, in which oppositely charged atoms interact; (3) hydrogen bonds, in which a hydrogen atom is shared between two electronegative atoms; and (4) van der Waals interactions. Because noncovalently bound complexes are weak and their nature depends on the solvent involved, it is difficult to detect them and to determine regions of interaction. Nevertheless, the ability to detect and characterize these interactions is critical in developing molecules to inhibit protein function involved in human disease from naturally or intentionally released pathogens.

This project is aimed at developing mass spectrometric (MS) methods to structurally characterize noncovalent interactions in protein–ligand biomolecular complexes. This work has focused primarily on the complex between tetanus toxin c-fragment protein (TTc-F) (MW 51.8 kDa) and doxorubicin (MW 0.543 kDa). The binding of doxorubicin to one specific region on the surface of TTc-F has been computationally predicted, but had not been observed before this work.

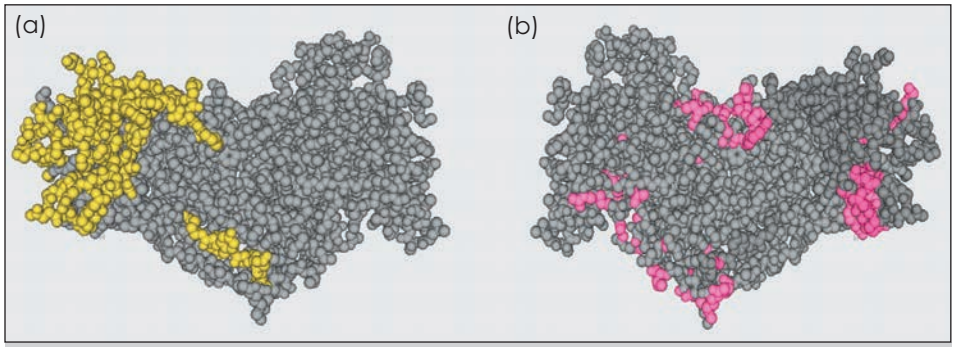

Crystal structure of tetanus toxin c-fragment protein (TTc-F). (a) Yellow indicates doxorubicin binding regions found in FY2001 experiments. (b) Red indicates the region of 3-D structure change induced by formation of TTc-F:doxorubicin complex.

In early FY2001, limited proteolysis experiments on TTc-F:doxorubicin complexes revealed not one but two binding regions at TTc-F:doxorubicin molar ratios of 1:5 and 1:10. These are shown by the yellow amino acids in the crystal structure of TTc-F [Fig. (a)]. Because two regions were observed, and only one was predicted, it is possible that nonspecific surface interactions occur when doxorubicin is present in large excess. Indeed, it was found that at molar ratios greater than 1:10 (TTcF: doxorubicin), doxorubicin binds nonspecifically to many regions of the surface of TTc-F. The presence of nonspecific interactions indicates that it will be essential to develop ligands with specificity.

The limited proteolysis experiments at a 1:5 molar ratio identified a subtle change in the 3-D structure of TTc-F induced by doxorubicin binding. The amino acids in red [Fig. (b)] correspond to regions where a change in conformation was detected. These regions are directly adjacent to or surround the binding regions, which suggests that TTc-F responds to doxorubicin by "tightening" around the molecule. This was surprising, because it was predicted that doxorubicin interacted only with the protein surface. These MS methods are the only methods sensitive enough to detect such subtle structural changes of large biomolecular complexes.

In FY2002, we will focus on extending the limited proteolysis and develop cross-linking and hydrogen/deuterium exchange studies to a larger and more complicated biomolecular system: a protein–DNA complex involved in the DNA repair of damaged DNA. We will examine the protein–DNA interaction by determining the amino acids of the protein and the deoxynucleotides of the DNA that interact and will examine the change in protein 3-D structure induced by protein–DNA complex formation. These studies are critical to the continued development of structural biology at LLNL and to the development of biological sensors to detect disease.

Applications of carbon-nanotube-based atomic force microscopy to proteomics and biological forensics

A. Noy, A. Malkin, J. J. De Yoreo

MAIN TOC

Determining the structure of biological molecules on the nanometer scale is one of the major challenges facing modern molecular biology. Conventional methods typically rely on x-ray analysis of protein crystals—a labor-intensive and time-consuming process. In addition, the difficulty of using x rays to analyze proteins increases with the size of the protein. However, the biggest challenge lies in obtaining the protein crystals for the analysis. Using current state-of-the art techniques in protein crystallization, it will take more than 100 yr to determine the structures of all the proteins coded by the human genome. Perhaps this estimate is over-optimistic considering that most of the easy-to-crystallize proteins have already been studied, and several large classes of proteins—membrane proteins, for example—are notoriously resistant to crystallization efforts. Developing new imaging techniques that do not require crystallization is very important for determining the structure of proteins. These new techniques will be invaluable for identifying the structure and function of biological agents that pose a national security threat, such as pathogenic viruses.

Over the past few years, we have demonstrated a powerful imaging technique that uses atomic force microscopy (AFM) for studying the structures and dynamics of macromolecules and macromolecular crystals. Because the resolution of the technique is limited by the size of the probe tips, the goal of this project is to develop the use of carbon nanotubes as probes for high-resolution AFM. This project supports the DOE's counterproliferation mission.

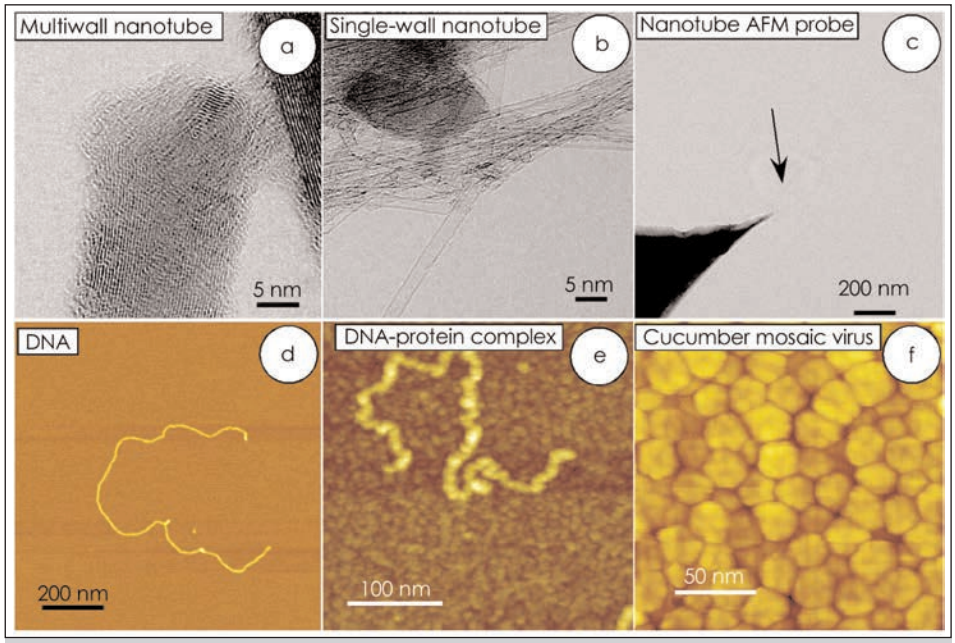

New imaging techniques using carbon nanotubes are determining the structures of proteins: (a–c) show transmission electron microscope (TEM) images of carbon nanotubes and a carbon nanotube [indicated by arrow in (c)] used as a tip for atomic force microscopy (AFM); (d–f) show examples of biological imaging.

During FY2000, we developed the technology for mounting bundles of single-wall carbon nanotubes onto commercial AFM probes and demonstrated that these nanotube probes exhibit substantially better resolution than conventional AFM probes. However, mounted carbon-nanotube tips still fell short in several key areas: (1) the probe-tip radii (~4 to 5 nm) were still too large to obtain the desired level of structural information, (2) the probes were unstable in a fluid environment, and (3) the manufacturing process was extremely labor-intensive and poorly controlled. As a result, we decided to shift our focus and use a catalytic chemical vapor deposition (CVD) process to produce the carbon nanotubes and carbon nanotube tips for AFM.

During FY2001, we designed, built, and refined the apparatus for CVD synthesis of carbon nanotubes. Establishing process conditions and controls allowed us to produce "designer" multiwall and single-wall carbon nanotubes of controlled dimensions and structure [see Figs. (a,b)]. We also developed and tested the protocols for growing carbon nanotubes on the AFM tips using this technology [Fig. (c)]. This new generation of probes exhibited a significant increase in resolution over the older generation of the AFM probes. In addition, the reproducibility of the probes has drastically improved. We are now able to fabricate AFM probes that terminate either in a single carbon nanotube or in a bundle of two to three nanotubes. We also used AFM probes made of carbon nanotubes to image proteins, viruses, and DNA adsorbed on a mica surface. The images in Figs. (d–f) demonstrate that this technique is indeed a valuable tool for obtaining unique and important structural information about these objects. A paper is in preparation.

Development of tritium accelerator mass spectrometry for biomedical sciences research

K. H. Dingley, A. Love, M. L. Chiarappa-Zucca

Tritium (^{3}H) is a widely used radioisotope tracer in biological and environmental research, although quantitation by traditional methods (e.g., liquid scintillation counting) requires large samples and long analysis times. In contrast to traditional methods, accelerator mass spectrometry (AMS) provides up to a thousandfold improvement in sensitivity for the measurement of ^{3}H in milligram-sized samples, while reducing instrument time to minutes. Consequently, ^{3}H AMS would have a profound affect upon the biological research community by facilitating radiotracer studies with low chemical and radiological doses of compounds that are physiologically, pharmacologically, or environmentally relevant. Therefore, ^{3}H AMS can be used to improve our understanding of disease susceptibility and to advance healthcare; it also has potential applications in national security.

Routine and successful use of ^{3}H AMS requires small, simple AMS instrumentation and refined, standardized sample-preparation methods. To address these needs, the specific aims of this project were to (1) characterize a small, dedicated ^{3}H AMS spectrometer; (2) develop routine and robust methods for preparing biological samples; and (3) with the aid of our university collaborators, demonstrate the application of ^{3}H AMS in the biomedical sciences.This project enhances LLNL's competency in advanced instrumentation and diagnostic tools in support of LLNL and DOE's biomedical research and environmental programs.

The spectrometer was completed in FY2000. In FY2001,we finalized our method for preparing samples. Our method is based on sample-preparation procedures used for measurement of deuterium–hydrogen ratios (D/H). In analyzing stable hydrogen isotopes, hydrogen gas is injected into a stable-isotope mass spectrometer; however, for ^{3}H AMS the hydrogen must be in a solid form. Therefore, we modified the D/H sample-preparation methodology to capture the hydrogen as a solid in the form of titanium hydride. A major improvement in the detection limit of our method was obtained through the use of a heated manifold. This method has been used to prepare and accurately quantify ^{3}H in different types of sample matrices, such as plasma, DNA, protein, tissue, and urine. We were also able to adapt our method to separating and analyzing both ^{3}H and ^{14}C from the same sample, a major breakthrough for future applications in dual-isotope labeling studies in which sample size is limiting. A manuscript describing our ^{3}H AMS sample-preparation procedure is being prepared for submission to a refereed journal.

Our technique is enabling LLNL biologists and our university collaborators to conduct studies of national interest that would otherwise be impossible. For example, over the last year, ^{3}H AMS has been utilized in three collaborative projects. At the University of California, Berkeley (UCB), it is being used to (1) measure the rates of cellular proliferation in rat tissues (and will be used to determine if dietary carcinogens increase cell proliferation), and (2) establish the amount of ^{3}H in tree cores collected in potentially contaminated environments. At the University of California, Davis, ^{3}H AMS is being used to investigate the hormonal basis of musth in elephants. Through this work, we have demonstrated the great potential of AMS as a new tool for quantifying ^{3}H in small biological samples at very low (attomole) levels.

The Laboratory is the only institution in the world with a bio-^{3}H AMS capability. Because of the successful development of our sample-preparation methodology, it has been strongly recommended for incorporation into LLNL's National Resource for Biomedical Accelerator Mass Spectrometry, which is funded by the National Institutes of Health.

Engineering titanium for improved biological response

C. A. Orme, E. DiMasi, J. P. Bearinger, J. L. Gilbert

MAIN TOC

Titanium has been used in orthopedic and maxillofacial surgery for many years because of its biocompatibility and its ability to form a direct bond with bone. However, the mechanism by which titanium and its passivating oxide film encourage osteosynthesis is still unknown. In general terms, it is known that the oxide film provides a kinetic barrier that prevents the titanium from corroding and that it provides a substrate to which the constituents of bone can bond.

We have designed a set of experiments to visualize the early-time response of oxide films to electric fields and to solution variations typical of those found in the body near bone. These studies are meant to determine how chemical and electric stress affect corrosion resistance and the formation of a biolayer on a time scale of hours to days. This research, which combines LLNL core competencies in electrochemistry and materials science, supports LLNL's mission in nuclear waste storage (the Yucca Mountain Project) and improved biomaterials.

For this project, we have chosen techniques, namely electrochemical atomic force microscopy (EC AFM), step polarization impedance spectroscopy (SPIS), and surface x-ray diffraction (SXRD), that can be used in fluid environments and that yield information about changes on the atomic scale.

During FY2001 we compared the morphology and electrical response of commercially pure Ti (CPTi) (dental) and the alloy Ti64 (orthopedic) to phosphate-buffered saline solution (PBS) and to PBS to which we added hydrogen peroxide (H_2O_2) to mimic wound environments. The addition of H_2O_2 did not greatly change the surface morphology of either sample. In all cases, oxide domes formed upon immersion and grew out laterally; the growth is slower in the H_2O_2 solution. The electrical responses differed, however. For Ti64 the resistance is largely unchanged by the addition of H_2O_2. The resistance of CPTi, which is approximately linear with voltage in PBS, becomes independent of voltage in H_2O_2 solutions. This suggests that additional TiO_2 is not formed under anodic conditions but rather that a new, low-resistance, porous form of oxide grows. We suggest that CPTi forms a Ti–peroxy (CNOO) layer, whereas the alloy does not. The development of a porous film during wound healing may be beneficial for an implant, because the microstructure may allow protein or mineral phases to bind within the pores of the oxide, forming a graded interpenetrating interface. At the same time it is also important that a tenacious, nonporous (high resistance) barrier remains protecting the metal from detrimental dissolution.

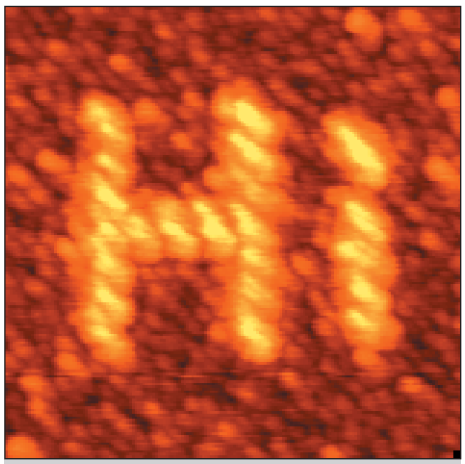

Atomic force microscopy (AFM) image (0.7 μm × 0.7 μm) of oxide grown on titanium using a voltage applied between the AFM tip and the substrate. Photomicrograph by summer students R. Sivamani and E. Bochner.

We completed surface x-ray scattering surveys of Ti sputtered onto silicon (which we found unsuitable for studying the oxide layer, in part because it was polycrystalline) and of single-crystal rutile (TiO_2) in air, water, and dilute H_2O_2. The rutile exhibited a roughened, reconstructed, and/or relaxed surface structure with essentially no difference between the dry crystal, the crystal in contact with water, and the crystal exposed to 2% H_2O_2.

We have created oxide patterns (see Figure) on Ti substrates that we will use as templates for the nucleation of calcium phosphate (bone) minerals in FY2002.

In FY2002, we will continue our characterization of oxide film structure and the manipulation of the biolayer formation to gain more fundamental understanding of the adsorption process. Using surface x-ray diffraction, we will look for (1) the ordering of calcium ions near the TiO_2 substrate in the initial stages of nucleation, (2) evidence for the porous Ti-peroxy film that we think may form in the presence of H_2O_2, and (3) differences in the ordering of calcium ions near the (001) and (110) facets of rutile. To manipulate the biolayer formation, we will use patterned oxide surfaces to control where minerals nucleate and proteins adsorb.

Acoustic filtration, fractionation, and mixing in microfluidic systems

A. Wang, K. Fisher, L. Tarte, C. Lee

MAIN TOC

Developing a robust method for sample pretreatment that combines filtration, fractionation, and mixing of particles is an integral first step in the development of miniaturized, microfluidic biological-analysis systems. Sample preparation in these miniaturized systems relies on a high degree of functionality to perform biological or chemical analysis. Typically, the cost of a part increases with its functionality, yet the danger of sample-to-sample contamination makes inexpensive, disposable parts attractive.

This project was concerned with the research and development of a technique to manipulate small particles (1 to 10 μm) using acoustic energy coupled into a fluid-filled sample "standing wave" chamber made of plastic or glass. These resulting miniaturized systems combine high functionality with an inexpensive, disposable sample chamber.

This acoustic-based, microelectromechanical system (MEMS) will supply the basic fluidic functions necessary in an analysis system used to detect pathogens and biological warfare agents in support of LLNL missions in counterproliferation and defense against bioterrorist threats. The system has considerable ramifications for the microfluidic module (MFM) project that is a subtask of the Laboratory's autonomous pathogen-detection system (APDS).

During FY2001, we extended our understanding of the complex behavior of the acoustically driven standing-wave chambers by applying a commercial 3-D multiphysics finite-element package (ABAQUS). With this sophisticated computational model, the electroacoustic response of the piezoelectric transducers (PZTs)—used as acoustic sources—and the fluid-structure response of the chamber are analyzed simultaneously. From this numerical modeling, we made several significant improvements in the mixing and particle-trapping (filtering) performance of the actual devices. Also, because the new chambers have been acoustically optimized, they can now be operated at lower drive voltages (5- to 15-V peak to peak, or approximately one-third the levels of our FY2000 designs) with the same fluidic performance. The performance of our new devices is strongly dependent on geometrical shape and construction tolerances.

We developed a new process for fabricating sample chambers using an anodic bonding of silicon layers on borosilicate. The resulting chambers have the planar geometrical tolerances required to facilitate robust and stable standing-wave patterns.

Experimental efforts in FY2001 were directed towards filtering and fractionating a flowing sample volume. A typical process, particle rinsing, is simulated in the Figure. A mixture of 10-μm polyurethane beads and a reagent [de-ionized (DI) water and blue dye] is sent through the sample chamber. The particles are trapped and begin to collect at specific nodal positions in the acoustic field. When a sufficient number of particles has been trapped, a neutralizer (simulated here as DI water) is sent into the sample chamber, where it rinses out the blue dye. Procedures such as this one are commonly employed to reduce background noise in a flow cytometer.

During FY2001, we expanded the scope of the project to include applications for trapping or extracting particles and or pathogens from large volumes of water—such as those routinely found in municipal water-treatment systems. Finally, we submitted a Record of Invention (ROI) for the current prototypes and are in the process of completing a detailed publication.

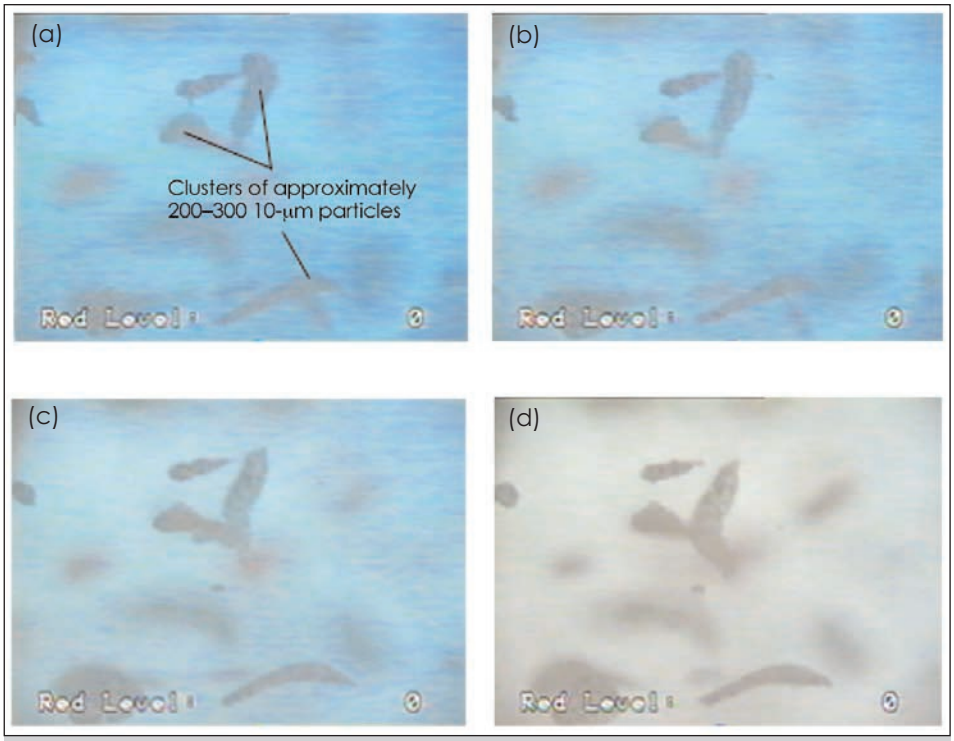

Images taken at 10-s intervals show stationary particle clusters while the blue fluid is being replaced with clear. Volumetric flow is 0.15 ml/min.

A force-feedback instrument for telerobotic minimally invasive surgery

R. R. Miles, K. Seward, F. Tendick, W. Benett, L. Bentley, P. Stephan

MAIN TOC

The number of minimally invasive (MI) surgical procedures has risen steadily since the introduction of the concept in the late 1970s. In most MI procedures, the surgeon inserts rigid instruments through small incisions and manipulates them directly. Telerobotic, or master–slave robotic systems, have been recently introduced in the last few years to carry out MI procedures (such as those in the abdominal cavity) that require greater control and dexterity than humans can provide.

Two drawbacks limit the application of telerobotic systems to still more demanding procedures such as fetal surgery, beating-heart surgery, and tumor removal. First, the mechanical joints used in such systems are larger than desirable. Second, control of the manipulators is not as precise as necessary because the positional and force feedback sensors and the actuating motors are placed at the proximal end of the device, near the surgeon, rather than at the distal end, where the end-effectors are located. Control errors result from mechanical compliance (the deformation of the system under load) between the sensors and the manipulator.

The goal of this project is to improve the state of the art of MI telerobotic tools in several respects. First, we plan to improve dexterity by designing a manipulator with a wrist joint capable of a full three degrees of rotational freedom, to mimic that of the human wrist. We plan to reduce the overall size of the manipulator to enable surgery in more confined areas and to reduce patient trauma enough that local rather than general anesthesia can be used. Second, we plan to design microscale sensors to be inserted at the manipulator to increase the accuracy of system's position and force feedback, and to develop a haptic feedback loop to give the surgeon a better "feel" of the instrument's motion. Third, we plan to design a compact actuator to be inserted near the end-effector to improve fine-motor control.

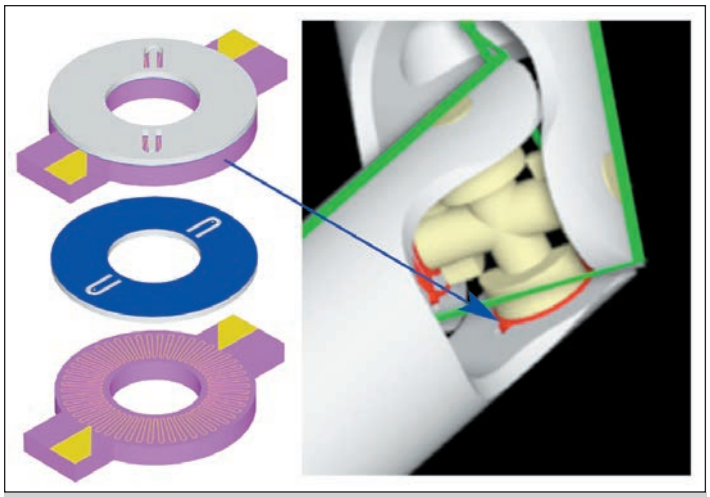

Resistive–capacitive embedded angular position sensor (left) to be inserted in an end-effector (right); such devices may eventually be used in telerobotically controlled, minimally invasive surgery.

This project supports nascent programmatic efforts in medical technologies and has several potential military applications, including the use of remotely controlled surgical tools in the battlefield; nondestructive remote inspections; and controlling, enhancing, and miniaturizing sensors for military and local law-enforcement bomb squads.

In FY2001, we completed the prototype design of a wrist joint that is capable of meeting the dexterity requirements for this application. We completed the design and began fabricating the microscale position sensors. The Figure shows a rendering of the resistive–capacitive sensor to be inserted in the end-effector.

We have taken some steps toward building the joint and sensors to verify the designs. F. Tendick, a member of the UCSF Department of Surgery, is leading the control effort for the project. Tendick's two students and a postdoctoral fellow worked on developing the nonlinear control algorithms required for a proposed compact push–pull actuator using shape-memory alloy as the "muscle." A test-bed was designed and built for testing these algorithms.

Disposable polymerase chain reaction device

E. K. Wheeler,W. Benett, K. Ness, P. Stratton, J. Richards, T. Weisgraber, A. Papavasiliou

MAIN TOC

The September 11, 2001 attack on the United States and the subsequent anthrax scare have raised antiterrorist vigilance to new heights. Although the September 11 attack was orchestrated with hijacked planes, the next threat could be nuclear, chemical, or—as recently evidenced—biological. Many countries that may support terrorist activities are likely to have biological weapons capabilities; biological weapons are probably also accessible to domestic terrorists. Planning and equipping for a biological attack requires detection devices that are robust in the field, easy to use, and relatively inexpensive. This project will advance LLNL's competencies in microtechnology and instrumentation and will provide new capabilities for homeland defense against terrorists.

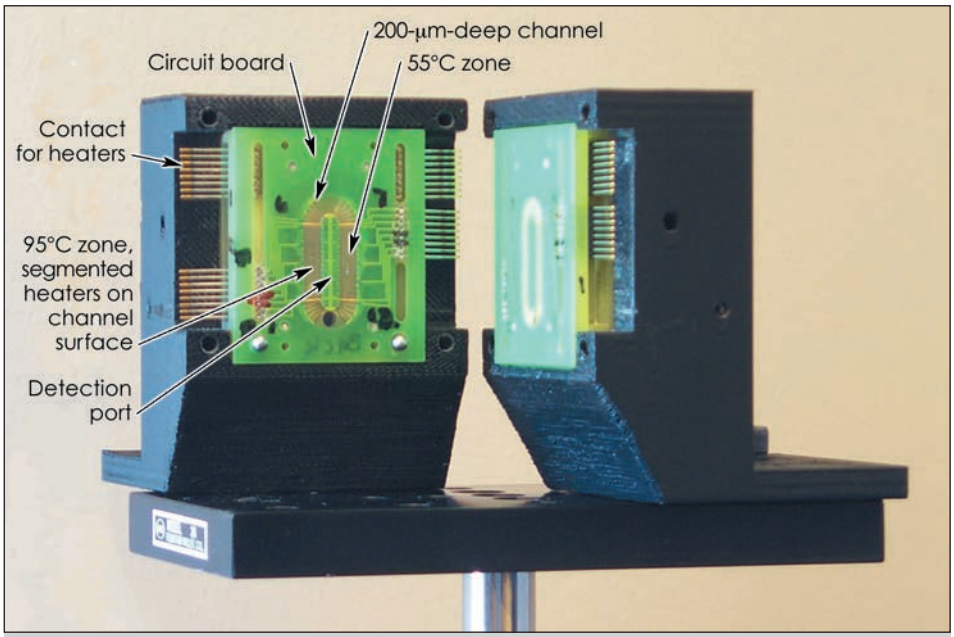

Convectively driven, compact, disposable polymerase chain reaction (PCR) thermal cycler.

To initiate the appropriate course of action, first responders (local emergency response personnel, military, or intelligence personnel) to a biological attack must identify the specific organism used in the release. For this purpose, polymerase chain reaction (PCR) assays are becoming increasingly important because they can amplify a target segment of DNA (by thermal cycling of the necessary reagents) and enable identification of biological pathogens. However, the sophisticated tools needed to assess a potential biological release not only are unaffordable to many first-response agencies, but also require highly trained individuals.

In this project, we are designing and demonstrating a compact, disposable PCR unit based on a novel thermal cycler. The end device from this project will allow first responders at the scene of a biological assault to quickly identify the nature and extent of the attack. By building on LLNL's expertise in designing portable PCR units, we are seeking to develop low-cost, disposable PCR units to be used by first responders. Forensic organizations or environmental specialists looking for the source of contamination in food or water will also benefit from this device.

During FY2001, we focused on modeling design iterations and fabricating prototypes of our novel thermal-cycling chambers for PCR amplification. Our new design for the thermal chamber uses fixed, nonfluctuating, hotter- and cooler-temperature regions through which the sample fluid flows, driven by thermal convective forces. The advantage of this approach is the potentially large energy savings, which increases the probability that small batteries will suffice as the power source for the system.

Initial particle imaging has shown that natural convective forces are strong enough to drive the fluid around the chamber at reasonable speeds. Because the convective thermal cycler is higher risk than traditional temperature cycling and has never been used to drive a PCR amplification, we applied existing modeling codes to verify that sufficient driving forces can be generated and to select optimal materials and geometric parameters.

The first iteration of our convectively driven cycler with zone heating has been fabricated (see Figure). As the fluid in the hot section heats to 95°C, it circulates to the cooler section because of natural convective forces. A patent application for our naturally driven, convective, PCR thermal cycler has been submitted.

In FY2002, we will address preparing samples and minimizing the power consumption of the thermal chamber. Although the thermal cycler is the heart of the PCR amplification, sample integration and detection are crucial to our end deliverable of an integrated, easy-to-use, low-power, robust, and disposable PCR device.

Nanoscale modeling of radiation damage at the DNA base level

C. L. Hartmann-Siantar, M. A. Descalle, C. J. Mundy, A. A. Quong, A. Woodin

Our goal is to describe the initial physical and chemical events leading to radiation-induced DNA base damage—building the key foundational components necessary to describe how radiation damages living cells. To accomplish this, we have combined unique LLNL capabilities in electron-interaction physics, reactive-species chemistry, and Monte Carlo radiation transport to initiate a nanometer-scale radiation-simulation system that directly predicts both ionization and chemical damage to DNA components.

Radiation damage to DNA occurs through two effects: (1) direct ionization by charged particles; and (2) indirect, chemical damage through oxidative products resulting from charged-particle interactions in the cytoplasm, which is primarily composed of water. Because all types of ionizing radiation set in motion energetic electrons, understanding the damage these electrons initiate is fundamental to building a complete understanding of radiation damage. Therefore, we have focused our attention on electron-initiated radiation damage.

The effectiveness of cellular damage-repair mechanisms depends on the chemical nature of DNA damage. Thus, certain types of DNA damage are more dangerous than other types. The challenge is to accurately predict the types and likelihood of DNA damage, ranging from base modification to DNA strand breaks. While previous work has demonstrated the overall feasibility and value of DNA-scale radiation simulations, that work has not predicted the direct chemical nature of DNA damage, nor has it accounted for all electron-interaction processes.

The system we are developing will be the first to directly predict the chemical nature of radiation-induced damage to a DNA base, founded on ab initio calculation of both electron and reactive-species interactions. This project enhances LLNL capabilities for detecting, describing, and predicting the effects of ionizing radiation in biological systems.

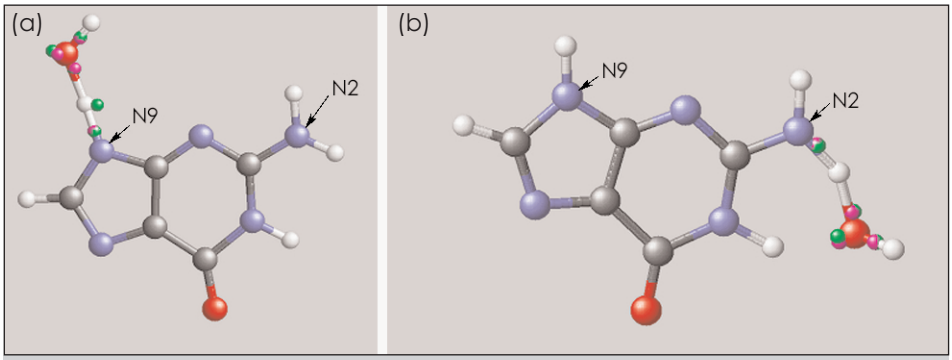

Ab initio molecular dynamics models provide the first insight into the nature of the chemical interaction of an OH radical with the DNA base guanine. Two possible sites for this interaction are (a) at the N9 site, and (b) at the N2 site.

In FY2001, we made significant progress in three areas.

First, we wrote a new, 3-D Monte Carlo single-scatter electron-transport code. Electron-interaction cross sections were taken from the LLNL Evaluated Electron Data Library (EEDL). The EEDL includes elastic scattering, impact ionization, excitation, and bremsstrahlung production, tabulated by atom. The transport code was designed and tested for both single elements and compounds, using atomic fractions to combine individual atomic cross sections, and was benchmarked against calorimeter measurements in beryllium, copper, aluminum, and iron for electron energies from 100 keV to 1 MeV. Using the electron-interaction data generated from ab initio calculations, this code will stochastically predict the spatial distribution of electron-induced ionizations and starting points of initial free radicals.

Second, we initiated theoretical studies of low-energy (0 to 20 eV) electron–water collisions, performing ab initio coupled-channel calculations of elastic scattering and dissociative excitation, including accurate ground and excited target wave functions. These studies were conducted to improve the accuracy of electron-interaction data. We also identified the negative ion resonance states that lead to dissociative electron attachment in the 7 to 10 eV region and initiated studies of electron-induced water+ (H_2O+) dissociative recombination (a process that produces OH radicals). Our results agreed with the first quantitative measurements on electron-induced H_2O dissociation.

Last, we employed ab initio molecular dynamics methods to elucidate the possible reaction mechanisms of guanine and other bases interacting with an OH radical. This work provided the fundamental data necessary to simulate chemical base damage. Through state-of-the-art analysis by tracking the electronic and nuclear degrees of freedom, we found that electron transfer could precede proton transfer. The Figure shows the two possible mechanisms for oxidation of guanine. At the N9 site Fig. (a) shows concerted motion of the proton (white sphere) and electron (green sphere); Fig. (b) shows deprotonation at the N2 site. At both sites, the electron has already transferred to the OH moiety.

This project is providing fundamental atomic and molecular information required to elucidate the important physical, chemical, and biological steps involved in radiation damage. Follow-on research will translate that knowledge into practical solutions for detecting, describing, and predicting the effects of radiation in living systems.

Structural genomics of human DNA repair and microbial pathogen proteins

M. Coleman, B. W. Segelke, P. T. Beernink

The growing number of genes identified in human, animal, and microbial genomics projects challenge us to understand their biological function. The new research field called proteomics aims to elucidate protein structure and function, which is unknown for most of the newly discovered genes. Proteomics projects using high-throughput structure determination, or structural genomics, have run into bottlenecks that must be overcome if we are to move forward quickly towards understanding biology at a molecular level. This project is overcoming these bottlenecks by increasing the throughput of protein production for crystallization trials. Our work will increase the value of genomic information generated at LLNL and for DOE's Human Genomes Program by providing novel screening, production, and crystallization technologies.

Microbial pathogens and human DNA repair processes are of interest to DOE laboratories and to LLNL's Biology and Biotechnology Research Program (BBRP). Our studies have significant health and national security implications, as is evident from the number of human diseases associated with pathogens and with defects in DNA repair pathways, the latter including xeroderma pigmentosum, Cockayne syndrome, ataxia telangiectasia, and Fanconi's anemia. This project makes use of the IMAGE Consortium gene collection at (BBRP), which provides clones for many genes of programmatic interest, and of BBRP's expertise in the automation of routine microbiological tasks. The new procedures, technologies, crystals, and crystal structures we obtain are likely to constitute significant intellectual property and to be of interest to pharmaceutical, structural genomics, and other biotechnology companies.

The biggest bottlenecks for structural genomics studies are protein production, purification, and crystallization, because most proteins do not express well and have only moderate solubility, making them poor candidates for structural studies. We are developing techniques for rapid production screening and functional analysis of proteins produced in a cell-free system, which enable us to examine many genes for their suitability for production and crystallization. We are engineering increased solubility of identified targets to ensure that many more proteins make it to crystallization trials. Our efficient, automated crystallization screening protocol, called CrysTool, allows us to screen many more proteins for crystallization, increasing the likelihood of success.

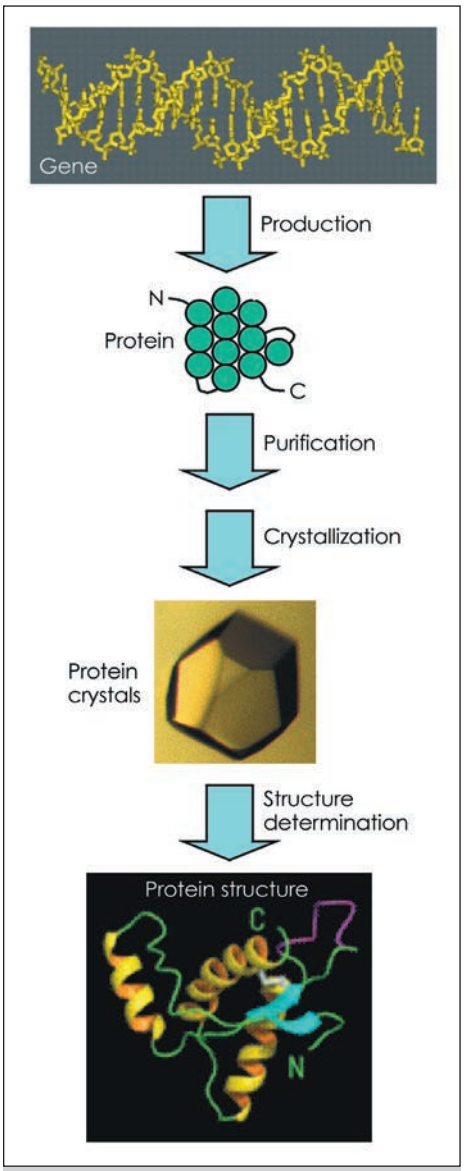

Process steps in structural genomics. We have made substantial progress in overcoming bottlenecks in protein production and crystallization.

In FY 2001 we implemented several innovative screening techniques for cell-free protein production, examined some 80 genes from the IMAGE gene library (and other genes of programmatic interest obtained from within BBRP). We identified about 20 proteins that are suitable for large-scale protein production, including RUVB, HEX1, and SMARCAL1 proteins, novel DNA repair and metabolism proteins discovered at LLNL. Using a standard fluorescence-based protein-folding assay, we distinguished soluble proteins (which can be purified) from insoluble proteins (which will need further engineering before they can be purified). We purified 11 proteins, several of which have sufficient yield (>5 mg) for crystallization trials. Further optimization should provide sufficient yield for all proteins of programmatic interest. We identified ten other proteins as targets for protein engineering, and we began engineering for two of them.

Efforts are under way to build an efficient, automated crystallization facility. We configured a Packard Instruments liquid-handling robot with custom components and interfaced with CrysTool for automated crystallization design and setup. We can demonstrate throughput of more than 1000 experiments per day.

Having completed most of our proof-of-principle experiments, we will standardize and automate our structural genomics process in FY 2002. We will fully implement protein engineering to ensure crystallization of proteins of highest programmatic interest. We will apply new procedures and resources to the scale-up of production screening, production, and crystallization trials. We expect to produce more than 30 novel, purified proteins in FY 2002 and to have about 20 new protein crystals.

Development of a combinatorial approach for synthesis of multidentate reagents

M. Cosman, R. L. Balhorn, F. C. Lightstone

Combinatorial synthesis is an important capability to establish at LLNL. Combinatorial chemistry provides information about the 3-D structure and molecular binding of chemical compounds to efficiently design drugs and other chemical compounds to desired specifications. LLNL has developed techniques for identifying sets of small molecules that bind to specific sites on the surfaces of proteins; this has enabled the design of organic-based multidentate reagents that can be used to bind to toxins and threat organisms. These new reagents could be effective replacements for antibodies used in counterbiological warfare detection technologies. The combinatorial approach for synthesizing reagents is important for drug discovery in general and is very relevant to the DOE and LLNL missions in counterbioterrorism, biosensor development, biomolecular engineering, and detection and decontamination of toxins.

This project proposes to establish a combinatorial synthesis capability and conduct a proof-of-principle demonstration of the capability. To accomplish this goal, we will (1) develop nuclear magnetic resonance (NMR) methods that can rapidly screen large numbers of small molecules for their ability to bind to proteins, (2) confirm their binding sites, and (3) identify those of their functional groups that do not interact with the protein and can be used to attach the molecule to a linker.

Recently, several NMR methods have been developed to enable rapid screening of up to 100 combinatorial compounds at a time. The screening can be accomplished with very low quantities of proteins (nanomolar range) and use proteins with low solubility (a category that includes many of the most biologically relevant proteins). Moreover, NMR can determine the structure of the bound form of the lead compound, thereby reducing the number of variables that need to be optimized in computer simulations. To discover high-affinity ligands—the entities that are coordinated with the central atom of the molecular complex and bind very well with it—using experimental information, we must take into account conformational changes in both protein and ligand upon binding; the studies are conducted under physiological conditions in solution. Other NMR experiments can be used to provide detailed information about the protein binding site and ligand orientation, which can then be used to link two or more small compounds in order to increase both affinity and specificity.

The crystal structure of Tet C with doxorubicin (in red) docked to binding site 1.

In FY2001, we used the tetanus toxin C (Tet C) protein as our test target. The development of molecules that bind to this protein have several applications in medicine and counterbiological warfare. Lead compounds were identified using computer docking studies in which various small molecules were fitted into potential binding sites on the surfaces of the protein structure and rank-ordered for best complementary fit in terms of shape and charge. Several NMR methods were then evaluated for their ability to test binding activity for each top candidate, both separately and then within a mixture. The transfer NOE (nuclear Overhauser effect) experiment, which is based on dipole–dipole interactions between nuclei, provided consistently reliable data for a wide range of different classes of ligands, as well as information about the structure of the bound form of the ligand. The Figure shows the 3-D crystal structure of Tet C. Doxorubicin (in red), one of the ligands studied, is docked computationally in one of four possible binding sites. Our results have established the utility of NMR binding studies in drug discovery, which can now be incorporated into several ongoing LLNL projects.

Noninvasive, noncontact heart monitoring of hemodialysis patients with a micropower impulse radar technique

J. Chang, D. Poland, P. Welsh, J. Trebes, T. Rosenbury

MAIN TOC

Kidney dialysis patients often have heart and vascular problems. Frequent heart monitoring could lead to early detection and treatment of these problems and provide some of the basic data necessary for understanding the development and progress of these medical complications. A noninvasive, noncontact method of monitoring the heart during hemodialysis would provide the opportunity for this monitoring without the discomfort of electrocardiogram (EKG) connections or the intrusion of a doctor and stethoscope. Current monitoring techniques are intrusive, uncomfortable, and labor intensive, especially considering that hemodialysis is performed on each patient in a dialysis center three times a week for 4 h each time.

The micropower impulse radar (MIR)—ultrawideband radar—is based on a technology developed at LLNL for laser-beam characterization for national security mission applications. The features of this technology, which include high resolution, low power, compactness, and potentially low cost, make micropower impulse radar a good candidate for applying unique LLNL national-security capabilities to the field of diagnostic medicine. Micropower impulse radar generates ultrashort picosecond-pulsewidth electromagnetic signals that span the upper radio- and lower microwave-frequency spectrum. As in conventional radar, targets within the illuminated regions of the transmitted signals scatter, absorb, and reflect the incident signal. The reflected signals, when post-processed, can be used to describe and characterize the targets.

The objective of this study is to determine if an MIR device can be developed that has sufficiently high sensitivity and specificity to detect the presence of cardiac arrhythmia. This project has two major goals. The first is to characterize MIR field distribution in the human body. This can be accomplished by using a 3-D finite-difference time-domain numerical modeling technique. The second goal, developing the device at LLNL and subsequently evaluating the performance in a clinical setting, will be accomplished by simultaneously collecting radar-based cardiac data and EKG data from a limited number of patients selected by our collaborators at the Renal Research Institute (RRI) and the Beth Israel Medical Center (both in New York).

In a 6-mo study in FY2001, we determined the basic system requirements of the prototype and needs of the clinician. We specifically focused on detecting the cardiac rhythm of individuals of various body types by using LLNL's electromagnetic 3-D Visible Man modeling capabilities and LLNL-collected dielectric data to design the prototype radar. By leveraging previous LLNL investigations into potential medical applications of the MIR technique (e.g., detection of intracranial hematoma and pneumothorax), we evaluated a prototype radar device. A data-acquisition and signal-processing algorithm was developed to process and interpret the radar return signatures.

Preliminary evaluation of the prototype sensitivity to varying body sizes and illumination orientation have shown encouraging results. The team has developed a human-subject studies protocol, which is awaiting final approval by the Beth Israel Medical Center and LLNL Institutional Review Board.

With a prototype that indicated a capability to remotely sense minute motions such as cardiac rhythm, respiration, and general motion, the project team responded to the Federal Emergency Management Agency and DOE request to assist with the search-and-rescue efforts at World Trade Center in the aftermath of the September 11, 2001 terrorist bombing. The prototype device was modified for use as a debris-penetrating radar to search for live victims that might have been trapped in the building debris.

In FY2002, several patients requiring regular hemodialysis and normal healthy individuals will be selected to undergo cardiac monitoring with the MIR detector at the Beth Israel Medical Center at the discretion of the attending physician.

Developing a quantitative Taqman polymerase chain reaction assay for atmospheric collection of *Coccidioides immitis* for ecological studies

J. I. Daniels, W. J. Wilson, T. Z. DeSantis, J. H. Shinn, G. L. Andersen, S. M. Johnson, D. Pappagianis

MAIN TOC

Coccidioides immitis is the infectious fungal pathogen responsible for coccidioidomycosis, a human disease endemic to the western United States—particularly in the Central Valley of California, where it is known as "Valley Fever." This fungus grows in soil and can produce spores (i.e., arthroconidia) that can be introduced into the air. The predominant pathway for human infection is by inhalation; in some cases, the health effects can be detrimental medically and economically.

Unfortunately, very few details are known about the climatic, ecological, and anthropogenic factors that control the life cycle of *C. immitis* in the environment—specifically, those that would promote spore formation and subsequent inhalation. Yet, *C. immitis* remains (1) an exposure concern for workers at LLNL's Site 300, (2) a potential threat to the health and welfare of students at the future campus of the University of California in Merced, and (3) a problem for the productivity of workers in the Central Valley. *C. immitis* is listed among the biological agents addressed by the Anti-Terrorist and Effective Death Penalty Act (1996).

Focusing unique scientific capabilities related to polymerase-chain-reaction (PCR) technology and analyses and the particle air-sampling strategies developed at LLNL for biological and environmental research on this fungal pathogen will enhance our competency in understanding the ecology of infectious disease in the environment and improve our ability to collect and detect specific microorganisms in the environment. It will also advance the national security mission and the environmental, safety, and health goals of the Laboratory that are directed toward reducing or eliminating environmental transmission and human exposure to naturally occurring or anthropogenically introduced microorganisms.

To quantify, from a DNA signature, the *C. immitis* spores collected in environmental samples—particularly air—we have been (1) developing, standardizing, and validating sensitive Taqman PCR assay protocols; and (2) evaluating the feasibility of collecting air samples in *C. immitis*-endemic areas in the Central Valley of California using advanced nuclepore air-filter media. Such a membrane allows us to use the physics of high-volume air sampling to filter larger samples of air than previously possible, so that the physical location of *C. immitis* in air and eventually soil might be identified using the advanced Taqman-PCR assay. The Figure shows our success in detecting known quantities of killed *C. immitis* spores in air sludge; we are pursuing improvements to detect even smaller quantities than the 1×10^3 spores that are shown.

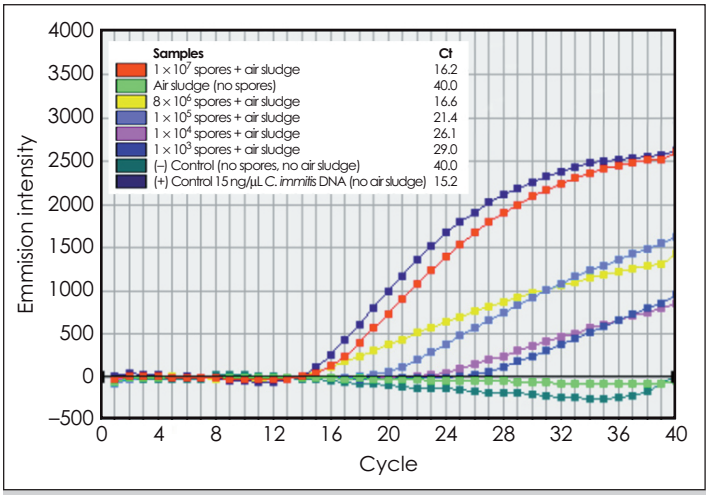

Taqman polymerase-chain-reaction (PCR) assay showing amplification of DNA extracted from different known numbers of *Coccidioides immitis* spores after inoculation into and recovery from air-filter concentrate (sludge) and comparison to controls. Earliest cycle time (Ct) where an amplification signal exceeds zero emission intensity corresponds to the unique DNA content of that sample, which is related to the number of spores that are present.

Finally, our collaborators at the University of California, Davis School of Medicine were instrumental in demonstrating that *C. immitis* spores can be killed for safe handling during investigations involving its detection genetically in laboratory samples and environmental media (i.e., in air-filter concentrate).

At year's end, we were completing our calibration curves for detecting *C. immitis* spores collected on air-filter membranes. The evaluation of the air-filter samples taken from the area endemic for *C. immitis* using our Taqman-PCR-assay protocols will follow. These results will put us in position to pursue studies with unique and advanced technical tools that will characterize and predict the environmental and ecological conditions that must be understood for controlling or eliminating *C. immitis* in the environment.

Structure and function of regulatory DNA: A next major challenge in genomics

L. J. Stubbs, J. Kim, D. M. Wilson III

About 5% of the human genome sequence carries out all of the most important genetic functions, such as coding for specific proteins; the remaining 95% is largely nonfunctional. Finding the relatively small number of important functional sequences and discovering how they work is a major challenge for biomedical researchers. We have developed an unprecedented map of the functional sequences in one human chromosome, HSA19; this foundational work was recently published in the journal *Science*. This project was designed to help LLNL maintain the advantage provided by this achievement by developing a focus in regulatory genomics. This new field aims to locate and study the so-called regulatory elements (REs) in the DNA sequence. REs function like on-and-off switches that control the action of adjacent protein-coding genes, dictating when and where each human protein is made in response to aging, environment , and health.

The scientific foundations for understanding gene regulation are important to a broad range of applications, ranging from human susceptibility to disease, to molecular medicine, and to managing microbes in the environment. Regulatory genomics is one of the research initiatives of DOE's Office of Biological and Environmental Research.

Our work in FY2001 involved two major goals. Our first goal was to complete the computational analysis of HSA19 DNA, with the aim of more precisely predicting the positions of all genes and their REs. We have done this by combining results of several different sequence analysis programs.

Our second goal was to establish efficient methods for testing predicted REs to confirm their function. We developed a high-throughput strategy to test if predicted REs can activate a "reporter gene," which encodes a fluorescent protein (luciferase). We isolated human REs, fused them to the luciferase gene, and transferred the fused gene into cultured human cells; if the human sequence is in fact an RE, the gene will be activated and the cells will glow (see Figure).

Although this reporter assay strategy is widely used, we have streamlined the procedure so that dozens of different REs can be tested reliably at once (see Figure). Being able to do these assays in parallel is important if we are to test REs for more than 30,000 human genes. Now we can test 46 predicted REs at once instead of just one; we can also assay multiple plates of 96 wells per week so we can look at a large number of REs. Using our technique, we have measured the function of a number of known controls and of two predicted HSA19 regulatory elements.

In FY 2002 we plan to establish a team to study the protein components that bind to RE DNA and that are a critical part of the gene activation process (symbolized by shapes attached to the RE sequence in the Figure). We plan to carry out pilot studies to identify these proteins as the project develops. Other plans for FY2002 include (1) continuing to develop RE testing methods and applying them to confirm the function of predicted REs for at least 100 HSA19 genes, and (2) testing mouse counterparts of some human REs, to identify structural and functional differences between species. With collaborators at LLNL, Lawrence Berkeley National Laboratory, and the California Institute of Technology, we will explore the use of informatics tools to help us correlate RE structure and function, testing the hypothesis that common structures are associated with REs that control gene activity in specific types of cells. We will also begin devising and testing methods by which our isolated and tested RE sequences can be used as "hooks" to trap the proteins that are critical to their function.

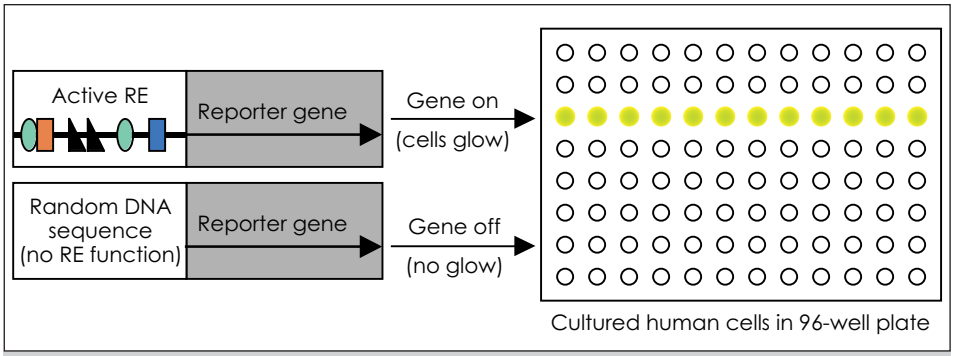

An active human regulatory element (RE) sequence, fused to a fluorescent "reporter" protein gene, will cause cultured human cells to glow; a random sequence will not. To help us find the REs for more than 30,000 human genes, we are devising protocols to test dozens of possible sequences in parallel.

Sensor development using microdot-array fiber-optic sensors

J. Carter, J. Marion, B. Colston, S. Brown, D. Maitland, K. Langry, M. McBride, R. Alvis, T. Wilson

MAIN TOC

The goal of this project is to develop and demonstrate a reproducible, minimally invasive, optical-fiber-based sensor for rapid and in vivo measurements of biological biomarkers using the microjet printing process. If successful, this project will provide clinicians with a new diagnostic tool for making enzyme, blood/gas, and ion measurements.

In addition to the intended medical application, this type of miniaturized chemical sensor would also benefit the Laboratory's national security mission in chemical- and biological-agent detection.

The microjet process for printing indicator chemistries on image-guide fibers is a unique method for creating chemical sensors designed to detect and quantify one or more ligands or analytes in a fluid or airborne medium. The indicator chemistry contains one or more light-energy-absorbing dye(s) whose optical characteristics change in response to the target ligand or analyte. By spectrally monitoring these changes using fluorescence spectroscopy, the target ligand or analyte can be detected and quantified with great sensitivity. If multiple ligand-specific indicator chemistries are printed in a known pattern, these ligands or analytes can be simultaneously detected and measured using optical imaging techniques to spatially register each microdot. We have coined the acronym MiDAS (microdot array sensors) for this new sensor-fabrication methodology.

Historically, commercial development of fiber-optic chemical sensors has been slow because of the inherent difficulty of reproducibly and inexpensively fixing indicator chemistries on the tips of optical fibers. The lack of a reproducible technique results in high inter- and intrasensor variability, which increases the cost of sensor manufacturing since *each* sensor requires individual calibration.

During FY2001, we demonstrated that microjet technology can be utilized for overcoming these difficulties by "printing" indicator chemistries directly on the tips of optical fibers. The Figure shows a six-around-one pattern of microdots, each containing an ion indicator dye printed on the tip of a 500-μm-diam optical-fiber image guide. The Figure shows the excellent reproducibility of our fiber-printing process. Average and standard deviations for the diameter and roundness of these microdots are 93.3 ± 2.2 μm and 0.00072 ± 0.00023 μm, respectively. The fluorescent intensity of the indicator dye varies less than 2%. This example clearly demonstrates the capabilities of microjet technology for reproducibly printing a pattern of identical but spatially discrete sensing regions. Our approach is being investigated for use as a biosensor for in vivo multianalyte measurements.

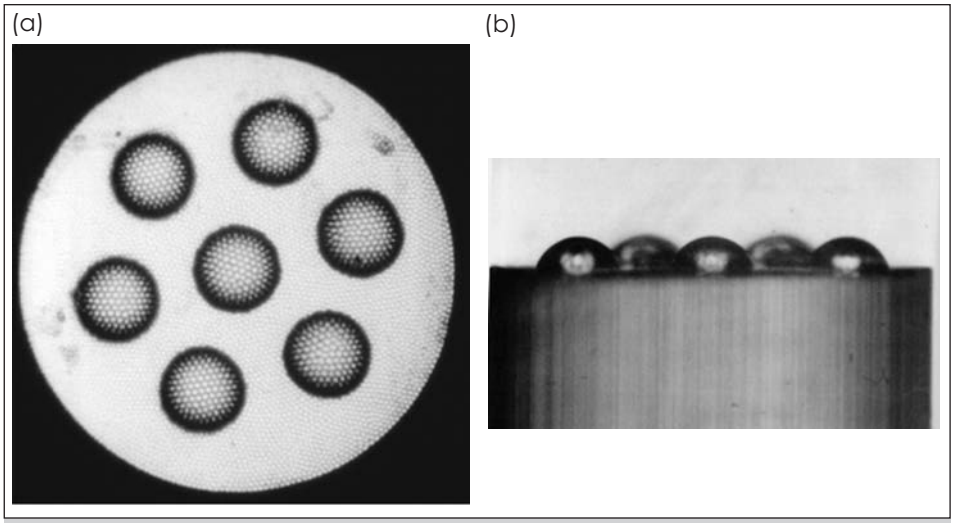

Ninety-mm-diam microdot array sensors "printed" on a 500-μm-diam optical-fiber image guide, showing (a) top view, and (b) side view.

During FY2001, we acquired a printing system for LLNL and began making engineering design changes so that it can be used for printing onto image-guide optical fibers. Meanwhile, we are working with a commercial supplier for our microprinting needs.

In FY2002, we will complete (1) all engineering-design work on the microprinting station, and (2) the development of the enzyme-based biomarkers. The latter will be combined with the continuing ion and blood/gas sensor work from FY2001.

Basis for thermostability in microbial DNA repair proteins

M. P. Thelen, C. Venclovas, M. Colvin

MAIN TOC

Microbes known as archaebacteria can thrive at high temperatures and pressures and in supramolar concentrations of salt or acid. Curiously, the proteins in these microbes are much more stable under such extreme conditions than the more fragile proteins in other organisms. To understand the basis for this stability, we must compare the molecular structures of proteins from archaebacteria with those of similar proteins from other organisms.

In this project we are investigating thermophilic proteins (those suited for temperatures of 60°C to over 100°C) and mesophilic proteins (suited for usual ambient temperatures of roughly 0°C to 40°C). There are no unifying principles to explain the stability of proteins at temperatures over 40°C. Finding such principles would enable the design of new heat-stable proteins that would be useful in many biotechnology applications such as polymerase or ligase chain reactions for amplifying specific DNA sequences. This capability would in turn accelerate research towards preventing diseases caused by aberrant protein folding and aggregation, such as bovine spongiform encephalopathy (BSE, or "mad cow disease") and similar debilitating human syndromes.

This project benefits from LLNL expertise in protein biochemistry, molecular biology, genome sequencing, and computational modeling. Much of the microbial sequence information now available to us is a direct result of DOE initiatives in genomics at LLNL and the Joint Genome Institute. Because of these capabilities, we can interrogate multiple microbial sequences for subtle differences in encoded proteins between thermophilic and mesophilic proteins, which is a new step towards elucidating protein folding and stability.

Several 3-D molecular structures are known at the atomic level for some of these proteins with molecular weights in the 10 to 50 kDa range, but few of these matched structures have been determined. In FY2001, to detect features that confer thermostability in proteins, we used protein multiple-sequence alignment techniques. To understand the thermodynamic stability of some proteins, we performed molecular dynamics (MD) calculations to simulate their denaturation, or melting. As a first test, we chose the ribonuclease H protein, or RNaseH, whose function in DNA replication is well characterized. A large number of homologous RNaseH sequences are present in the microbial genome databases, and high-resolution molecular structures have been determined for both the *Thermus thermophilus* (thermophilic) and *Escherichia coli* (mesophilic) proteins. Moreover, RNase H is relatively small and monomeric, a characteristic currently required for protein MD simulations at reasonable time scales.

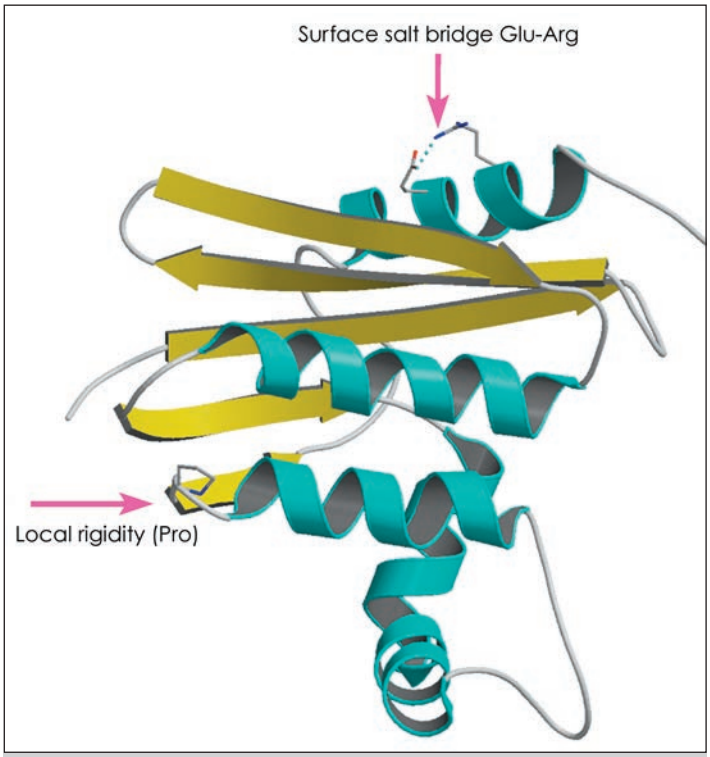

Crystal structure of thermophilic RNaseH. Arrows indicate sites found to contain residues different from those in RNaseH proteins from 17 different mesophilic bacteria. These sites might be important for thermostability by increasing local main-chain rigidity or by introducing favorable electrostatic interactions.

The Figure shows our conclusions from comparisons between the *T. thermophilus* protein and RNaseH homologs selected from 17 mesophilic organisms, including *E. coli*. Of the 145 residues in the thermophilic RNaseH, only 30 are absolutely conserved in all mesophilic RNaseH proteins. However, we were particularly interested in any positions where all mesophilic proteins contained the identical residue, but the thermophilic protein was different. In such cases we used computer modeling to examine these positions more closely in the 3-D structures. Two residue substitutions were identified that could contribute thermostability to a mesophilic protein (arrows).

In a complementary approach, MD simulations of thermal melting in the individual *T. thermophilus* and *E. coli* RNaseH proteins indicated a higher rate of deviation in the mesophilic protein structure, as anticipated for a less-stable molecule. This is a novel application of MD that could be pursued in future studies of the stability, folding and misfolding of proteins.

Development of synthetic antibodies

R. Balhorn, M. Cosman, K. Fidelis, F. Lightstone, J. Satcher, S. Shields, L. Zeller

MAIN TOC

Much of what we've learned about molecular targeting is based on lessons learned from the immune system, an elegant, highly successful mechanism for detecting and eliminating molecular and microscopic foreign entities from the human (or animal) body. Central to the immune system's operation are antibodies—macromolecules that are designed to recognize and target foreign molecular structures. Antibodies enable vast, microscopic, seek-and-destroy operations that serve to fight off infections, cancer, and many other diseases. We believe that it is now possible to develop molecular targeting agents that improve upon the characteristics of natural antibodies and directly deliver lethal substances to cancer cells. The concept of molecular recognition can also be extended to developing powerful new detectors for biological-warfare (BW) agents. Like the natural immune system, detectors relying on molecular-recognition concepts promise to simultaneously detect numerous types of harmful biological agents within a single, compact instrument.

The goal of this project is to develop an integrated computational and experimental process that can be used to create synthetic high-affinity ligands (HALs) that selectively bind to unique sites on any type of protein or surface structure. This capability will make it possible for LLNL to develop a number of new, high-profile programs of interest to (1) national security (e.g., sensor-reagent design for detecting BW agents), (2) human healthcare (e.g., molecular targeting agents for cancer therapy and the design of new types of pharmaceuticals that exhibit minimal side effects), and (3) our armed forces (e.g., new corrosion-blocking surface treatments and the design of nanostructured materials).

For our first target molecule, we chose the extra-cellular domain of the cancer-cell receptor HLA-DR 10—which is found only on non-Hodgkin's lymphoma and B-cell lymphocytes—because the unique regions of this particular molecule that distinguish it from HLA-DR receptor proteins on other cells (i.e., the binding site of the Lym-1 antibody) have already been identified. We proposed five tasks to establish and demonstrate the approach for HAL design for this protein: (1) construct a homology model of HLA-DR10, (2) identify unique "pockets" on the surface of the protein, (3) use docking techniques to predict ligands that bind to these pockets, (4) experimentally confirm those ligands that bind, and (5) synthesize a set of resin-based linkers that can be used to link pairs of ligands that bind different sites together to create the HAL.

During the 6-mo duration of this project in FY2001, we completed the first three of these tasks. Using the crystal structures of four closely related HLA-DR molecules, we generated a homology model of HLA-DR10 for use in docking. We then used surface plots of the modeled structure to identify two adjacent pockets containing HLA-DR10-specific amino acids that are recognized by the HLA-DR10-specific antibody Lym-1 (see Figure). Computational docking runs of 300,000 small molecules were performed for Site 1; a set of 100 ligands predicted to bind to the site was identified. At the end of FY2001, we were applying a combination of mass spectrometry and nuclear magnetic resonance (NMR) spectroscopy to identify those ligands that actually bind to the protein. As a final step, one ligand from each site will be linked together and the set tested for its ability to compete with the Lym-1 antibody for binding to HLA-DR10.

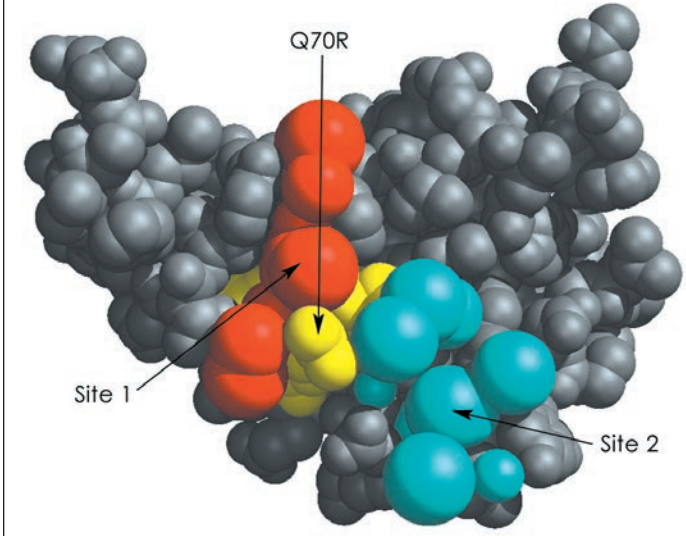

Ligand binding sites ("pockets" in the protein surface) on the cancer-cell receptor HLA-DR10 are shown filled with red or blue spheres. One of the amino acids, Q70R (yellow), that is unique to HLA-DR10 and is recognized by the Lym-1 antibody, is located between the two binding sites.

Subcellular imaging and dose estimation for isotopically enhanced molecular targeting

J. N. Quong

The goal of radiation therapy is to kill only the cancer cells while minimizing the radiation damage to normal cells. Current methods for radiation dose estimation are based on crude, whole-body measurements and centimeter-scale dose averaging, neither of which addresses how radiation is deposited at the cellular level.

One approach to delivering radiation therapy more accurately is using targeted radiopharmaceuticals (TRPs) to seek out cancer cells via cancer-specific targets on the cell surface. However, the distribution of these drugs within tumor and normal cells is currently not known. Such knowledge would provide important information for understanding the interaction between the drugs and cells and lead to more effective cancer treatment while minimizing damage to healthy tissue. This project builds on LLNL's capabilities in radiation and computational physics to advance healthcare technologies.

We propose using secondary-ion mass spectrometry (SIMS)— a technique that has been used for over 20 yr to analyze inorganic samples in materials science and the geosciences—to localize TRPs at the cellular and tissue levels. This work is part of the new bionuclear focus in the Glenn T. Seaborg Institute (GTSI), and supports LLNL's thrust into biological applications and its strategic alignment with the University of California, Davis (UCD) in a Joint UCD/LLNL Cancer Center.

Our goal in this project is to develop an integrated imaging/simulations system to characterize the distribution of TRPs in biological tissue and to simulate dose distributions at the microscopic level. To do this, we must (1) determine a biological sample-preparation technique that does not alter the biochemical distribution and composition of the sample while preserving microstructure and morphology; (2) develop standards for each isotope of interest for quantitative SIMS measurements for input into the dose-estimation software program; (3) extend PENELOPE—a well-tested and validated Monte Carlo photon- and electron-transport code—to calculate 3-D radiation-dose deposition from the measured, internal, source-drug distribution.

This project began in mid-year. During the time available in FY2001, we obtained images of various elemental distributions from tumor and liver tissues. The Figure illustrates the importance of sample-preparation technique, which is critical to proper method selection and data analysis. In addition, we began (1) characterizing the effects of various cell/tissue-processing protocols on elemental distributions, (2) preparing standards required for SIMS quantitation, and (3) extending the Laboratory's MIRAGE computer code to translate the 3-D isotope-concentration maps measured with SIMS into radiation-transport and energy-deposition calculations.

Our goals for FY2002 are to (1) characterize the radioisotope distribution using SIMS, (2) simulate the radiation-dose distribution at the microscopic scale using the TRP distribution from SIMS imaging as input, and (3) further validate the imaging/dose distribution system with another clinically used TRP.

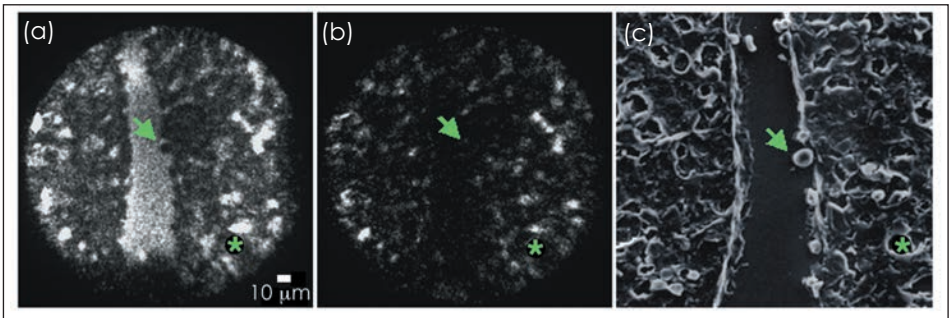

SIMS images of a section of a chemically fixed liver showing distribution of (a) K^+ and (b) Na^+ ions, and (c) a SEM image of the same region. The arrow points to the same physical location in each image. The higher-intensity K^+ image in (a) indicates overall higher concentrations of K^+ than Na^+. Also shown is higher K^+ in the region between the two lobules. Individual liver cells contain K^+ but not Na^+, as expected. These distributions do not correlate with the known in vivo distributions of these ions and verify that chemical fixation alters the distribution of diffusible ions such as Na^+ and K^+. The asterisk in the SEM image indicates another artifact of the preparation—the apparent high concentration of K^+ and Na^+ (bright spots) in physical voids—probably resulting from pooling of solutions used during preparation.

Measuring DNA repair pathway function: A step toward determining health risk from radiation

I. M. Jones, H. Mohrenweiser, D. O. Nelson

MAIN TOC

Although it has been known for decades that human exposure to ionizing radiation increases the incidence of cancer, predicting which individuals are at most risk from radiation exposure is still a distant goal. Such predictive ability is needed to guide policies that regulate radiation exposure and ensure that medical treatments provide maximum benefit with minimum risk.

Differences between people in susceptibility to radiation are largely based on their genotype, the genes inherited from their parents. Among the important genes in this connection are those that produce proteins that repair DNA damaged by radiation. These proteins are of two types, base excision repair (BER) proteins that repair single strand breaks and oxidized bases in DNA, and double strand break repair proteins that repair broken chromosomes.

Using technologies and information from the Human Genome Project, we had determined before beginning this LDRD project that the DNA sequence of DNA repair genes varies within the human population. An average of 3 to 4 different variants were found that affect the protein for each of 37 genes studied. The average frequency of these variants is 5%. Given the many genes in each DNA repair pathway and their many variants, our technical ability to determine an individual's repair genotype greatly exceeds our ability to interpret the information.

A long-term goal of this project is to relate DNA repair genotypes to health risk from radiation. The goal of our initial effort was to begin developing pilot data and identifying statistical methods that could be used to test the hypothesis that many different genotypes have similar DNA repair capacity phenotypes (function). Relations between genotype and phenotype could then be used to group genotypes with similar function and ultimately test the association of groups of genotypes with health risk from radiation. Genotypes with reduced repair function are expected to increase risk of radiation-induced health effects.

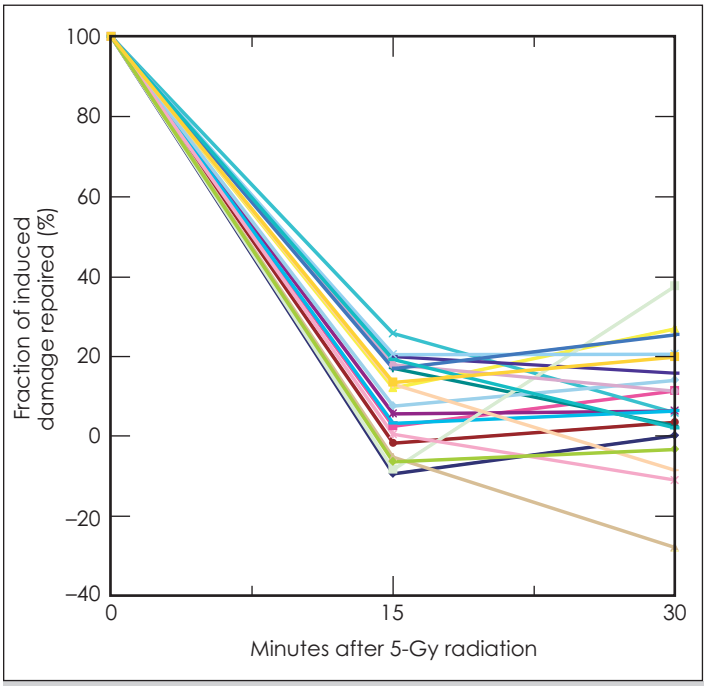

Repair of DNA damage induced by 5 Gy of radiation in cells from 26 healthy people as a function of time after exposure. Relating such differences in repair behavior to an individual's inherited DNA repair genes and to health risk from radiation exposure is a major challenge.

This study focused on the BER pathway. The BER genes are known, variants of the genes have been identified at LLNL, and LLNL has recently developed an assay for BER function using white blood cells.

During FY2001, we focused on developing our BER capacity phenotype assay and studying BER phenotype–genotype relations. Data from the blood cell assay were extended and statistical techniques used to estimate both the variation among samples collected from the same individual and the variation between individual averages. Considerable variation was observed between samples collected over a 6-mo period from each individual. Preliminary estimates based on nine individuals indicate that approximately 10% differences in repair function between groups of 100 individuals could be detected with 80% power and 5% risk of false positives. When data analyses are completed, the assay development results will be published.

A set of 50 cell lines with known BER genotype was selected for a pilot study of phenotype–genotype relations, and the methods were adapted for study of cell lines. The BER phenotype measurements completed on 26 of these cell lines from healthy people reveal considerable variation between individuals. The measurements suggest that there are quantifiable differences between people in the ability to repair damage from ionizing radiation (Figure). We have also begun to evaluate the relevance of emerging statistical learning and data mining techniques to predicting genotype–phenotype relations. Relating variation in the BER phenotype to variation in BER genotype will be the next key step toward epidemiological studies of health risk. The results of this project will be applicable to large molecular epidemology studies of cancer risk associated with variation in DNA repair in radiation-exposed population. This project supports DOE's biological research mission.

Accelerator analyses for protein research

J. S. Vogel, P. G. Grant

Sequencing the human genome and discovering genes within that code are triumphs of modern technology in biological research. We know that (1) coded material is expressed as proteins to produce biochemical effects, (2) proteins are sequences of amino acids found either by high-resolution mass spectrometry (MS) or through improved chemical sequencing, and (3) linking proteins to their originating genes is straightforward. However, expression—or production—of a protein in a specific cell depends on many factors: other genes and cellular signals that trigger expression or control modification of the product. Advanced technology is required to study expressed proteins and their relation to cell dynamics and controlling processes.

In this research, we are applying physical measurements of accelerated ions to the problem of precise protein quantitation, which avoids uncertainties resulting from the variable chemical properties of proteins. This project builds on the expertise within LLNL's Center for Accelerator Mass Spectrometry (CAMS) for applying nuclear technology to biological research to advance LLNL's biological sciences mission and strengthen our program in proteomics.

Improved quantitation of protein interactions is central to several areas of biological research at LLNL and at collaborating campuses of the University of California (UC). For example, because toxins and drugs take effects by producing or interacting with specific proteins, the potency of new drugs and the danger of toxic chemicals can be reliably estimated only by finding the amounts of proteins directly affected by these compounds. Similarly, understanding the virulence of pathogens in biological threats requires precise macromolecular quantitation.

Our approach uses two technologies to quantitate the protein in a sample while quantifying the elemental or isotopic markers of protein interaction: (1) quantitation of areal density with accelerated protons and (2) isotope dilution by accelerated mass spectrometry (AMS).

Accelerated protons pass through the protein and its thin supporting substrate. The amount of proton energy that is lost is a direct measure of the material in the path. In our technique, a proton beam scans the sample to measure the total mass. The protons also induce heavy elements within the protein to produce distinctive x rays, thereby quantifying the elemental abundance. Protein–metal affinities are measured directly with high precision.

By using AMS to quantify the ^{14}C incorporated into molecules as labels for tracing chemical interactions, compounds can be quantified to high precision with very low levels of radiocarbon. To find the mass of the protein that is binding the compound, material with distinctive carbon-13(^{13}C) signatures is added. By measuring both $^{14}C/^{12}C$ and $^{13}C/^{12}C$ ratios, AMS provides direct quantitation of the interaction. We also combine the techniques by quantifying the protein by energy loss and then measuring its ^{14}C content by AMS.

In FY2001, we surveyed substrates for uniformity of energy loss and found the best performance from silicon nitride wafers. These thin films give weight resolution of a few nanograms for protein samples,as seen in the Figure, where the transition from blue to green represents about 2 ng of protein for each pixel. The AMS equipment was modified to obtain ratio measurements with 0.3% resolution, sufficient for about 50-ng precision in quantifying micrograms of protein. In a refereed publication, we demonstrated our method's reproducibility in quantifying drug interactions with proteins separated by electrophoresis. We are investigating tube and flow-through electrophoresis to provide lower isotope contaminations and easier protein quantifications.

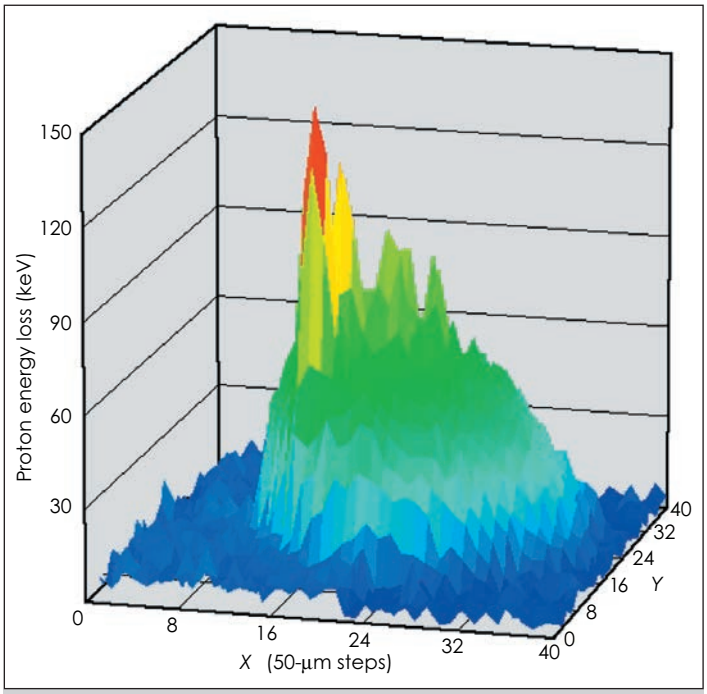

Proton energy-loss image of 1 µg of protein on 1000-Å film of silicon nitride at 50-µm resolution. Peak loss (red) is 160 ng of protein.

In FY2002, we will apply our proton-mass-measurement technique to quantification of elemental abundances within proteins from tumors, with the goal of characterizing how tumors differ from healthy tissue. To quantify protein affinity, we will apply isotope-dilution methods during measurements of protein binding to environmental chemicals.

Direct imaging of protein–DNA complexes using carbon-nanotube atomic force microscopy and single-molecule optical detection

A. Noy, M. H. Corzett, M. Cosman

Complex interactions that occur between DNA and DNA-repair proteins are central to the process of maintaining the genetic information in living cells. Common sources of DNA damage include metabolic processes, production of free radicals, and carcinogens from tobacco smoke, improperly cooked food, or even chemotherapy. If the structural damage to DNA is not repaired or is repaired with errors, it can lead to tumor-causing events at the chromosome and cellular levels. Learning how cellular proteins process damaged DNA on a molecular level is essential to understanding and controlling cancer initiation.

The purpose of this project is to use single-molecule imaging techniques to study the mechanism of DNA binding and DNA-damage recognition for proteins that are active in the initial stages of DNA repair. We are concentrating on the actions of xeroderma pigmentosum (XPA), a protein that is active in damage recognition during nucleotide excision repair pathway. Little is known about the mechanism of action for this protein. We are trying to obtain information about these processes by investigating the interaction of this protein with undamaged DNA and with DNA that contains adducts derived from benzopyrene (BP). These synthetic adducts are an ideal model system for studying DNA damage.

This project enhances (1) the scientific understanding of DNA repair and DNA–protein interactions in general, and (2) LLNL's capabilities in nanoscale instrumentation in support of DOE's biotechnology mission.

During FY2001, we developed a new and unique approach that combines in situ carbon-nanotube atomic force microscopy (AFM)—a capability that we developed for another LDRD project (00-ERD-008)—and single-molecule fluorescence detection. We prepared and purified quantities of XPA protein and also synthesized and purified BP–DNA adducts and linked them to short synthetic-DNA pieces. At the end of the year, we were ligating these adducts into longer pieces of DNA for imaging studies.

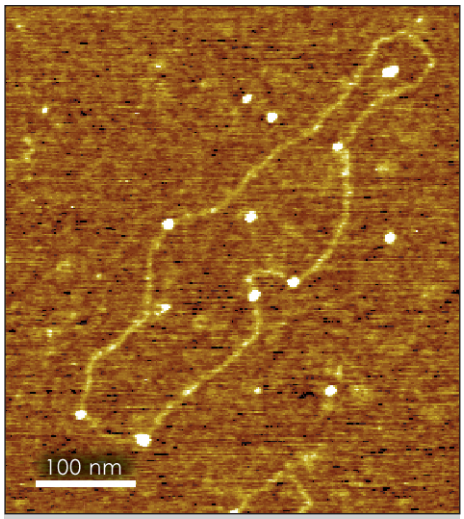

Atomic force microscopy (AFM) image of a single pBr322 DNA plasmid (the circular structure) with six xeroderma pigmentosum (XPA) repair proteins (bright dots) bound to it—the first image ever obtained of a DNA-repair protein bound to DNA.

In our study of nonspecific XPA–DNA interactions, we first established protocols for binding DNA and proteins to the cleaved mica surface for imaging, and then studied binding of XPA to short and long pieces of DNA using high-resolution AFM and carbon-nanotube probes. We obtained the first image of a DNA-repair protein bound to DNA (see Figure). The imaging results confirmed that the binding affinity of XPA is highly dependent on the presence of Zn^{2+} ions.

Significantly, our imaging results helped us to answer a long-standing question: Which of the two possible mechanisms of a damage search is realized in the XPA case? The fact that we see a number of proteins simultaneously bound to DNA strongly favors the scenario in which XPA protein binds to the DNA and then scans along the helix checking for damage—as opposed to the random-sampling mechanism in which the protein diffuses on and off DNA until it finds the damage site.

We also set up and demonstrated the optical detection of labeled XPA proteins on a single-molecule level and began integrating optical detection into DNA-binding experiments.

In FY2002, we plan to complete the synthesis of long, adduct-containing DNA pieces. We will then study specific DNA-damage recognition by XPA. We also plan to set up a number of experiments designed to study the dynamics of DNA-damage search and recognition by XPA in which we use high-speed, single-molecule, optical-imaging techniques.

Single-molecule techniques for advanced in situ hybridization

S. Lane

One of the most significant achievements of modern science is completion of the human genome sequence, completed in the year 2000. Despite this monumental accomplishment, researchers have only begun to understand the relationships between this three-billion-nucleotide genetic code and the regulation and control of gene and protein expression within each of the millions of different types of highly specialized cells. Several methodologies have been developed for the analysis of gene and protein expression in situ, yet despite these advancements, the pace of such analyses is extremely limited. Because information regarding the precise timing and location of gene expression is a crucial component in the discovery of new pharmacological agents for the treatment of disease, there is an enormous incentive to develop technologies that accelerate the analytical process.

With this project, we propose to leverage LLNL technology and expertise to accelerate and enhance the sensitivity of gene- and protein-expression analyses. By employing techniques and instrumentation for the detection of low levels of gene expression, we plan to achieve precise, simultaneous localization of multiple genes or proteins in a single sample in the absence of amplification steps. The results of this research will help to increase the pace of scientific advances required for understanding the regulation and control of gene and protein expression.

During the first few months of this project—near the close of FY2001—we began using a new approach to the problem of discriminating a small number of labeled targets against spurious background signals. Our approach involves the use of plasmon-resonant silver or gold particles fabricated from seed particles with 1- to 5-nm diameters that have an antibody shell conjugated to their surface. These particles can be grown to arbitrary sizes, producing different colored labels, with a commercially available silver enhancer procedure. Using dark-field microscopic techniques, these particles scatter narrow bands of light very efficiently and are 1 million times brighter than single fluorescent molecules. These attributes allow for the nonamplified detection of single particle–target complexes in a multiplexed analysis.

Using biotinylatyed-labeled expression probes and antibiotin-labeled plasmon resonant particles (PRPs), we investigated the expression of the well-characterized Peg3 gene and compared our results with the current state-of-the-art immunohistochemicial (IHC) analysis. The Figure shows the location of the labeled target is consistent for the two approaches. However, for the IHC analysis the signal required chemical amplification for definitive interpretation; the PRP analysis did not. This exclusion of the amplification steps enables greater multiplexing and quantification capabilities for the PRP analysis, as well as reduced artifacts.

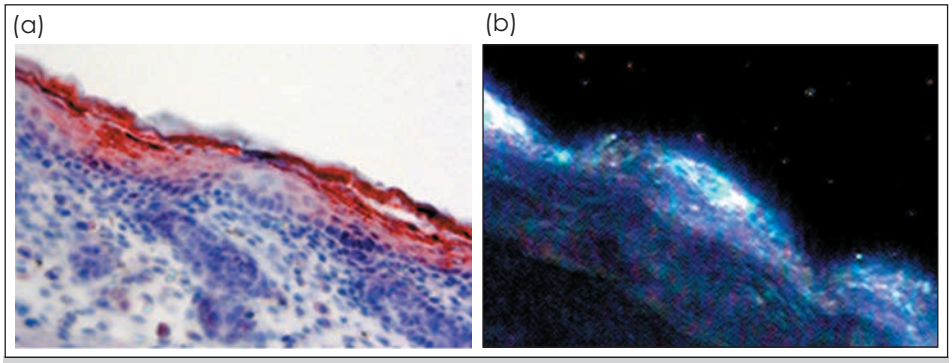

Expression of the Peg3 gene in mouse-embryo tissue sections isolated from the same organism using (a) amplified immunohistochemicial (IHC) and (b) nonamplified plasmon resonant particle–in situ hybridization (PRP–ISH) analyses. Both images indicate the most expression of the gene in the skin regions, as indicated by the red dye in (a) and the bright features in (b).

In FY2002, our work will include the fabrication or separation of monodispersed distributions of PRPs, thereby allowing for the simultaneous multiplexed analysis of several genes. As a second means of circumventing the background fluorescence in tissue analysis, we will explore time-gated fluorescence in combination with quantum-dot labels.

Nuclear magnetic resonance methods for structural characterization of membrane proteins implicated in multiple sclerosis

R. S. Maxwell, M. Cosman, J. Ulloa

Myelin oligodendrocyte glycoprotein (MOG) is an integral membrane protein of the central nervous system implicated as a target for auto-aggressive antibodies in multiple sclerosis (MS). The conformation of MOG in association with the myelin membrane is as yet unknown, and the exact nature of the interactions between this protein and disease-inducing immune responses has not been determined.

Membrane-associated proteins are difficult to study by traditional methods, such as solution-state nuclear magnetic resonance (NMR) and x-ray diffraction, so new structure characterization tools for this important class of biomolecules are urgently needed. Solid-state NMR approaches are available for the study of proteins that are not soluble or crystallizable. This project sets out to apply a combination of novel solid-state and solution-state NMR methods to yield insight into the conformation of MOG in a biologically relevant environment.

The structural knowledge we obtain about this important MS antigen will contribute to our understanding of its function *in vivo*. Our work will also contribute to the development of therapeutics to inhibit the antigen–antibody interaction and thus prevent demyelination in MS patients. Further, the NMR methods developed in this project should be applicable to other difficult-to-study proteins, protein complexes, and other large macromolecules. Other applications include structural and molecular biology of proteins involved in cellular processes, protein-controlled precipitation and dissolution reactions, biomolecular engineering, and biomaterial (bone and prosthetic) growth and rejection by living tissue.

Because of its extensive biochemical, biocomputational, and bioanalytical capabilities, including both solid- and solution-state NMR expertise, LLNL is uniquely suited to investigate the structure and dynamics of MOG. The analytical and physical methods we are developing will have significant impact on biochemical research ongoing at LLNL, including the development of molecular biosensors for the detection of toxins and other biowarfare agents for the DOE's counterproliferation mission. Also, this project will offer a direct contribution to bettering human health.

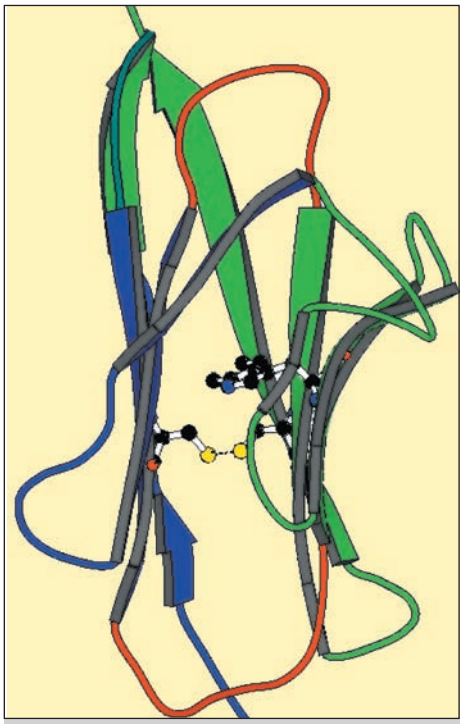

Structural model of the extracellular domain of the protein myelin oligodendrocyte glycoprotein, a target for auto-agressive antibodies in multiple sclerosis, based in part on the nuclear magnetic resonance methods developed in this project.

In FY 2001 we completed preliminary protein expression and purification experiments. We carried out circular dichroism studies in micell environments at various values of pH and temperature. Combined with solution-state NMR studies, these studies allowed us to develop preliminary models of the structure of the extracellular domain of MOG (see Figure), which we have recently published. Further preliminary results show that the extracellular domain of MOG undergoes significant conformational change upon changes in environment, but this issue has not been addressed in physiologically relevant conditions. We have obtained and purified the transmembrane domain of MOG and have begun baseline NMR measurements. Work has also begun to calibrate our solid-state NMR experiments and has oriented phospholipid membrane mimics in order to study the transmembrane domain in detail.

In FY 2002, we will continue to investigate the conformational changes in the extracellular domain caused by changes in micell and bicell media, particularly in physiologically relevant conditions. To gain further structural insights and to constrain subsequent molecular dynamics calculations, we plan to measure ^{1}H and ^{15}N spectral parameters, including scalar and residual dipolar couplings and chemical shifts. These data will provide insight into conformational changes that might be important for MOG pathogenesis and will aid in the assignment and analysis of the solid-state experiments. Finally, we will begin nitrogen-15–hydrogen-1 solid-state correlation experiments to investigate conformational changes in the cellular domains of MOG.

Genomics and proteomics to better understand pathogens

J. P. Fitch, E. Garcia, S. L. McCutchen-Maloney

The deliberate or accidental exposure of hundreds or thousands of people to pathogenic organisms could result in significant loss of life, with high economic and social costs. Addressing the threat of biological terrorism requires improved understanding of the mechanisms by which pathogens harm humans.

Countering the threat of biological weapons of mass destruction is a mission of the DOE. The NNSA Chemical and Biological National Security Programs (CBNP) are developing improved detectors, modeling, remediation technologies, and demonstration of systems for civilian biological and chemical defense. The CBNP is applying genomics and other technologies to accelerate the development of biological assays to detect pathogens; these assays could be validated by public health users such as the Centers for Disease Control.

In this project, we are identifying and characterizing the genes and proteins involved in the virulence mechanisms of pathogenic bacteria and of bacteria involved in host–organism response. Integrating knowledge obtained from genomic and proteomic tools can help us understand such bacteria better and could lead to the creation of new classes of detectors, vaccines, and treatments. We are likely to find traits associated with pathogens that could permit detecting genetically engineered organisms.

We initially focused on the bubonic plague bacterium, *Yersinia pestis*, because its virulence mechanisms can be induced in vitro. These mechanisms are found in several animal and plant pathogens and in other human pathogens with significantly different clinical manifestations, so our work will be applicable to other microbes, including *Salmonella, Y. pseudotuberculosis*, and fire blight.

In FY2001, we made significant progress on both the genomic and proteomic approaches. We designed a series of DNA microarrays that simultaneously determine genetic activity for every gene in *Y. pestis*. A preliminary test array discovered five potential virulence genes that are regulated with the temperature shift associated with going from environmental (26°C) to human body (37°C) temperatures. We screened proteins using mass spectrometry (MS) by comparing protein expression before and after virulence factors were induced in vitro. We demonstrated and published a new approach that spotted DNA on the MS substrate to detect regulatory proteins in *E. coli*, and we are applying the technique to *Y. pestis*.

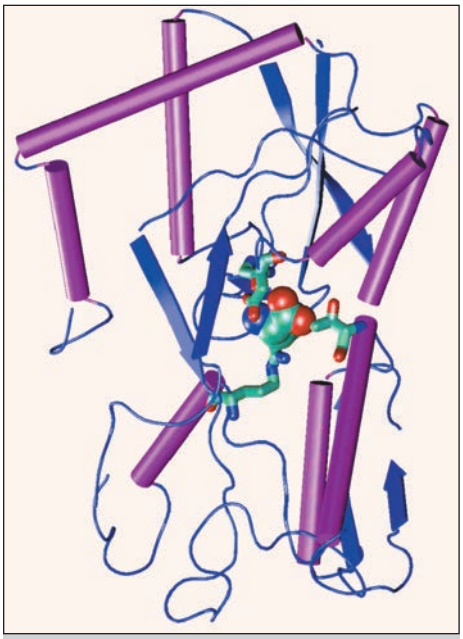

Model of a protein encoded by a newly discovered thermally regulated putative virulence gene. Coils, arrows, and cylinders represent coils, beta-strands, and helices, respectively. The structural model predicts several possible functions for this protein that can be tested in focused experiments.

We achieved several computational milestones, including the development of a computational structural model (see Figure) of one of the putative *Y. pestis* virulence factors identified in our gene expression studies. The model helps us focus experiments to determine what binds to this protein and ultimately to determine its role in *Y. pestis* virulence. Using techniques ranging from differential equations to fuzzy logic, we investigated new modeling approaches that combine large amounts of experimental data into biological hypotheses that can be represented mathematically. We tested the differential equation approach on a DNA repair pathway with published biochemical data; the results are to be published in *Nucleic Acids Research*.

When the Sanger Institute (UK) completes the DNA sequence for *Y. pestis* in FY2002, we will update our DNA microarrays and proteomic systems to accommodate this information. A comprehensive model of virulence will eventually need to integrate data from multiple sources, including DNA sequence, whole-genome expression profiling, comparative genome analysis, MS identification of new virulence proteins, and computed functional prediction of new virulence proteins. In FY2002, we will improve our modeling and data management paradigm to integrate all of sources of data. The ultimate biological test of virulence models will be to confirm that they correctly predict the response of a genetic network to the selective deletion of genes from the pathogen.

Computing, Modeling, and Simulation

Section 4

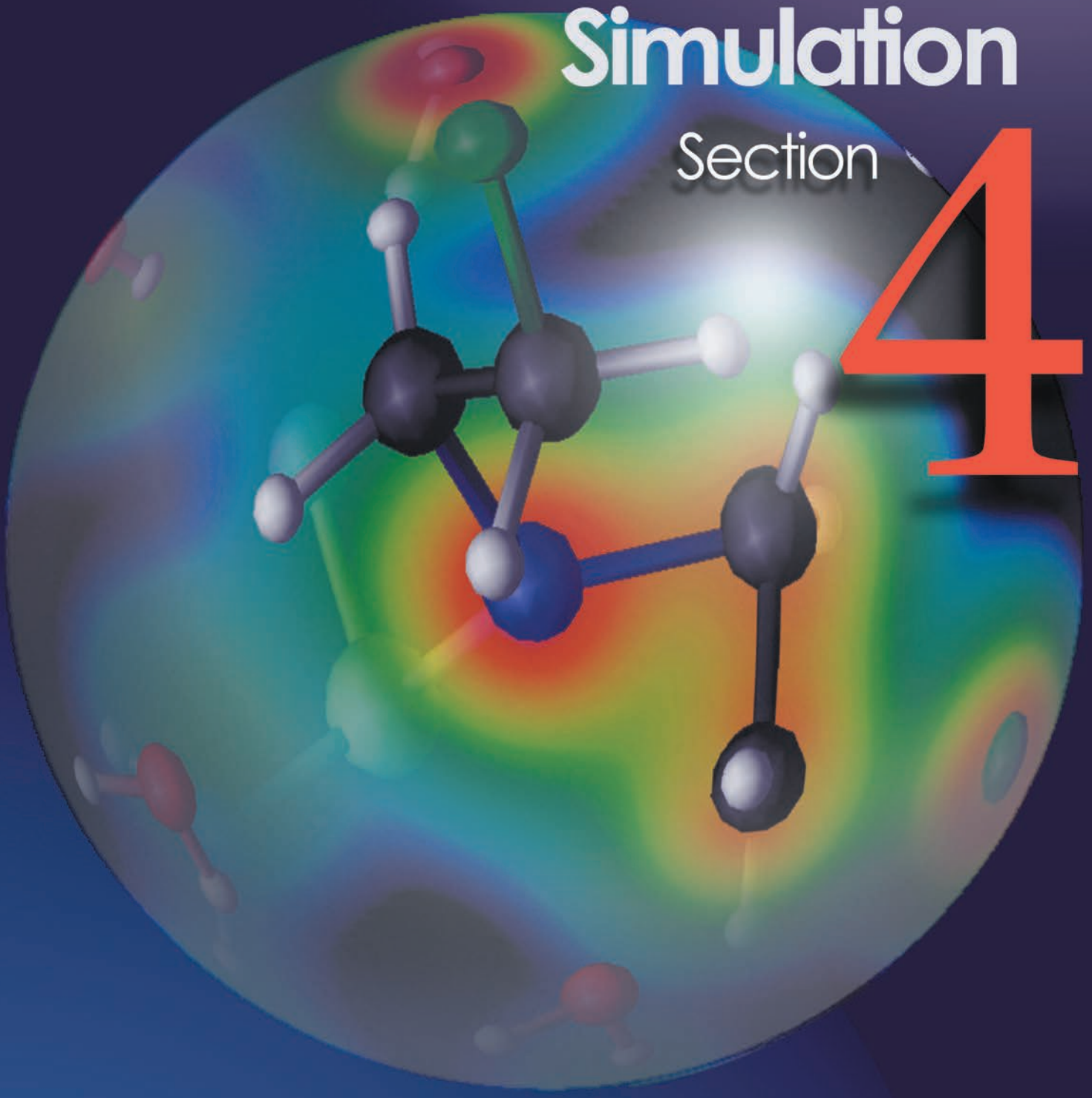

Section 4 Computing, Modeling, and Simulation

Strategic Initiative in computational biology

M. E. Colvin, G. Galli, F. Gygi, D. Barsky, F. C. Lightstone, E. Schwegler

The biological sciences are undergoing a rapid transformation that promises to alter almost every aspect of human endeavor from food production to health care. The sequencing of the full genomes of humans and many other organisms, in combination with a molecular-level understanding of biological phenomena, is increasing the role of predictive models in biological research. This transformation will be largely dependent on computer simulations to do everything from predicting macromolecular structure to designing new drug molecules. Because of its capabilities in advanced simulation and high-speed computing, LLNL is well positioned to play a major role in the emerging field of computational biology.

The goal of this project has been to develop new, state-of-the-art biological modeling methods and to test them on biological problems. This project has been very successful, as demonstrated by several dozen scientific papers, numerous invited talks, and fruitful collaborations. The simulation tools we have developed have also proved valuable to emerging Laboratory programs in biological defense and advanced sensors for counterproliferation missions.

This project continued only into the first month of FY2001. In that period, we completed developing components of the first-principles molecular dynamics (FPMD) program needed for simulating and analyzing biochemical reactions. We evaluated these and other computational biology methods for specific biological problems, including the interaction of the DNA chemical backbone with an Mg atom, the chemical activation of an anticancer drug, and the binding of potential ligands to different sites on the botulinum toxin protein.

We completed the implementation of holonomic constraints on interatomic distances in the JEEP FPMD code. This new functionality makes it possible to control the distance between any pair of atoms during the simulation without affecting the conservation of the total energy. The distance can be kept constant or can be allowed to grow linearly with time, which permits the automatic exploration of some simple reaction paths.

Additionally, a new visualization code (map3Dv) was completed for the analysis of the results of FPMD simulations. This code has four features: (1) interactive visualization (with respect to rotation, translation, and zoom) of atoms and bonds; (2) interactive visualization of transparent isosurfaces of electronic charge density or of molecular orbitals (see Figure); (3) interactive calculation of bond distances, bond angles, and torsion angles; and (4) off-line rendering of all the above features for batch processing of movies or for production of very-high-resolution pictures.

Map3Dv is a C++ code that uses the public VTK visualization toolkit. It is running on the Compaq alphaservers, on the SGI visualization platform in the Livermore Computing Center, and on Linux workstations. In the area of applying and evaluating the computational biology methods, we made progress on FPMD ground-state calculations on solvated dimethyl phosphate, including a magnesium counter ion. We completed a series of molecular docking calculations that identified potential ligands to two sites on the heavy chain of botulinum A toxin. Finally, we evaluated quantum-chemical methods for studying aqueous-phase chemical structures and reaction energies. In particular, we completed the optimization of the anticancer drug metabolite phosphoramide mustard using a dielectric continuum solvation model and evaluated the structure using the average structure determined from FPMD simulations.

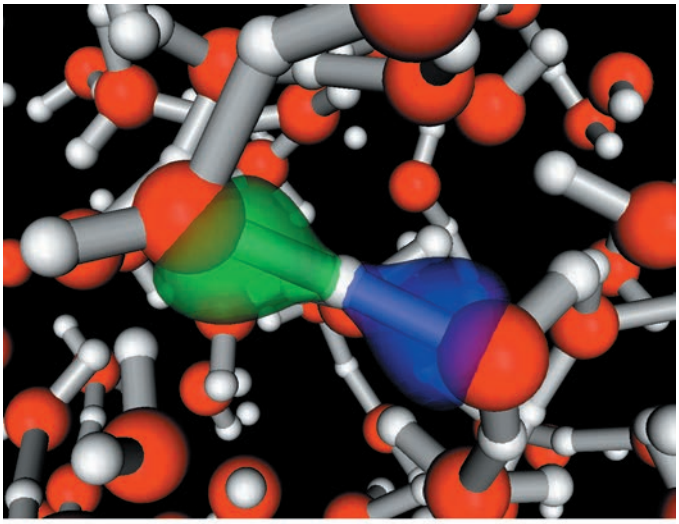

Transparent isosurfaces (green and blue) of maximally localized orbitals involved in the transfer of a proton between water molecules in the liquid state. This visualization was realized with our new visualization code map3Dv using results from simulations carried out with our first-principles molecular dynamics code JEEP.

Quantitative tomography simulations and reconstruction algorithms

H. E. Martz, M. B. Aufderheide, D. M. Goodman, A. Schach von Wittenau, C. M. Logan Jackson, D. Slone

In this project, we sought to improve the accuracy of tomographic reconstruction by including the true physics of the radiographic process with the tomographic reconstruction process. Computed tomography and transmission radiography are useful quantitative diagnostic tools for stewardship of the nuclear weapons stockpile. These techniques are at the heart of LLNL's contribution to meet the goals of the NNSA's Advanced Radiography Campaign.

This project had two main components. First, we sought to enhance our simulation of the radiographic process by improving our modeling of detector and source physics in x-ray radiography and by validating these algorithms against experimental data. Second, to perform the physically accurate forward and back projections required in the tomographic inversion process, we merged this more accurate simulation capability with the constrained conjugate gradient (CCG) optimizer. This was expected to improve reconstructions by preventing the mixing of radiographic artifacts with the object reconstruction. After three years of work, we achieved 2% agreement with data, merged the codes, and applied this algorithm to several test cases.

Our simulation efforts focused on the HADES computer code, which uses ray tracing to simulate radiography—we improved the code's modeling of detectors and sources. To determine detector response, we used MCNP, a code that simulates photon and electron transport using Monte Carlo techniques. This information is then saved in a format that HADES uses. During FY2001, we applied these techniques to modeling the x-ray transmission through copper bars of known width (step wedges), which had been radiographed with the Lab's 9-MV linear accelerator (linac) using a commercial, amorphous-silicon, flat-panel detector. We demonstrated that HADES is accurate at the 2% level—this accuracy in a general radiographic problem represents a significant advance. Our results will be reported at the IEEE Medical Imaging Conference in early FY2002 and have been submitted for publication.

In FY2001, our tomographic efforts concentrated on treating the full nonlinear problem of radiography within a tomographic reconstruction code. Most existing tomography algorithms linearize radiography because they assume Beer's law and require logarithms of the experimental images as input. However, no experimental data obey Beer's law because x-ray sources are almost never monochromatic. To treat the full nonlinear problem, in FY2001 we coupled the superior radiographic simulation capabilities of HADES to the CCG optimizer. Optimizing the full problem proved to be challenging: derivatives of the system become complex, require careful attention to the presence of different materials, and make forward- and back-projection steps complex.

To make this problem tractable, it was necessary to (1) require that the user fix the location of materials within the object (a reasonable requirement in many applications), (2) modify the CCG optimizer to treat multiple materials, (3) operationally link HADES and the modified CCG codes, and (4) make major modifications to the HADES dataflow to compute both forward and back projections over multiple views. In addition to modifying existing forward and back projectors, we decided to have HADES calculate the gradients and search directions required by CCG rather than pass large amounts of redundant data between the two codes. All this work was completed in FY2001, and is a major breakthrough.

In FY2001, we applied these algorithms to a number of fairly simple problems, demonstrating that this new tomographic algorithm works and is able to separate object reconstruction from radiographic artifacts. Our investigations also show a number of challenges in using the algorithm. First, the computational and memory cost for reconstructions is considerable. Second, the quality of the reconstruction is extremely sensitive to the accuracy of the description of the radiographic system. Third, the code is only a prototype—it needs considerable refinement before it can be a production tool. These issues were beyond the scope of the current project and will require future investigation.

Lattice Boltzmann simulation of microfluidic devices

D. S. Clague, E. K. Wheeler

In microfluidic devices, fluids, beads, and other biological matter are transported through networks of micrometer-sized channels for sample preparation, separations, and assays. Understanding the transport behavior of target species in these devices is of paramount importance. The lattice Boltzmann (LB) simulation effort has grown out of a need for computational tools to assist the designers of microfluidic and of biological microfabrication and microelectromechnaical systems (bioMEMS) devices to predict and understand the behavior of beads and macromolecules in microflows. The LB simulation capability, which is a significant advancement over current methods, takes into account the multiple, competing physical phenomena that take place in actual devices—for example particle dynamics, external fields, and near-field particle–particle, and particle–wall interactions.

This research will clearly enhance the Laboratory's competency in this scientific arena, and will enable the design and development of new devices for detecting biological agents and for biomedical research.

Our goal has been to develop a simulation capability to explore the incremental, additive effects of these interactive forces to (1) facilitate understanding, and (2) explore new means of effecting particle manipulations. In particular, work has focused on characterizing particulate behavior in dielectrophoretic separators. Particle mobilities are not only influenced by the colloidal interactions, but also by non-Newtonian fluid effects and particle geometries. Therefore, we enhanced the LB capability to handle power-law fluids (many fluids containing biological species—biofluids—exhibit nonuniformity in viscosity caused by variations in fluid velocity, also known as shear-thinning behavior) and bead-and-spring representation of species. With these enhancements, the LB capability will be applicable to a broader class of biofluidic systems.

As described above, the viscosities of biological fluids tend to depend on the local shear rate. As a result, particle mobilities can be significantly affected and exhibit nonintuitive behavior. To take this into account, in FY2001 we modified the collision operator in the LB formulation to account for local changes in the shear rate. Results from the new, enhanced LB capability are compared with theory in the Figure.

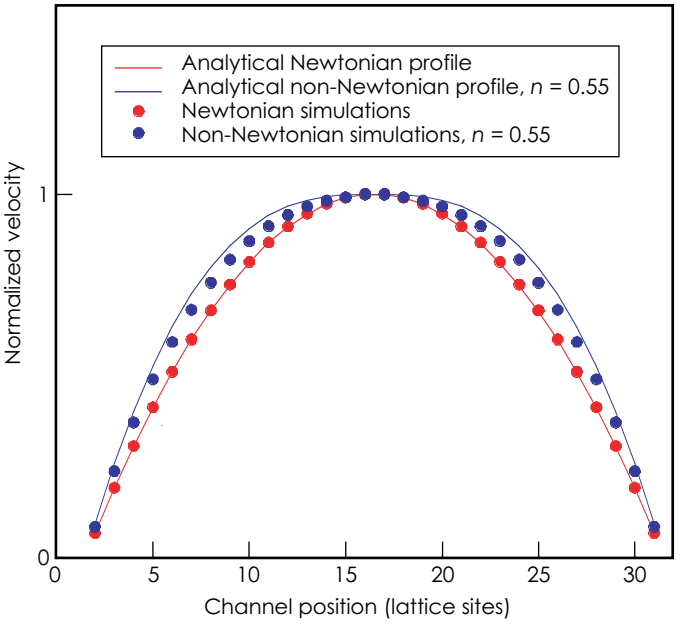

Lattice Boltzmann prediction of power-law fluid behavior compared with theory.

We compared the shear thinning and thickening behavior as predicted by the enhanced LB capability with power-law fluid theory for flow between parallel plates. As shown in the Figure, the simulated results are in good agreement with theory. Furthermore, as discussed above, we enhanced the LB simulation capability to account for more complex particle features. Many species of interest (e.g., DNA strands) are best represented as long chains; hence, one aim of this year's effort was to develop a bead-and-spring representation of macromolecules.

To accomplish this, we successfully incorporated the Finite-Extension-Nonlinear-Elastic-Dumbbell (FENE-Dumbbell) model into the LB capability. The model provides both a building block for representing long-chain macromolecules in the LB simulation capability and the "spring" that bridges the beads—and which also causes the bulk fluid to have non-Newtonian behavior.

The new enhancements that we developed over the past year have expanded the applicability of the LB capability. With the bead-and-spring representation of macromolecules, researchers will be able to study the influence of the chain dynamics of target species—such as a biological agent—on transport properties and conformational issues relevant to detection. Furthermore, the ability to capture the shear-thinning behavior—without any increase in computational time—positions this capability to be applied to many new problems involving biofluids.

Scalable algorithms for visualization and analysis of terascale science

M. A. Duchaineau, V. Pascucci, P. Lindstrom, R. J. Frank, E. C. LaMar

MAIN TOC

Every week, the multiphysics simulation codes on LLNL's supercomputers produce dozens of terabytes of data that are important to the Stockpile Stewardship Program (SSP) and to other programs. Great strides are being made to increase the efficiency and accuracy of the codes by harnessing tens of thousands of processors using scalable algorithms. However, as part of LLNL's goal of computing over a hundred trillion operations per second, a capability must be created to efficiently and accurately handle the huge flow of data this entails, and to provide LLNL's scientists with a scalable, interactive exploration capability.

The goal of our scalable algorithms for visualization and analysis of terascale science (SAVAnTS) project was to obtain orders-of-magnitude improvements in scientific visualization efficiency. We employed multiresolution compression and data-flow optimizations to increase the speed of interactive exploration and to decrease the storage space required for the data-analysis tasks.

The basic mathematical and computational tools we exploited and developed are wavelets—a popular way to represent images for compression and analysis tasks—and spatial hierarchies—the data structures that can lead to fast, sparse computations that exploit coherence in space, time, frequency, and scale. For the large-scale scientific geometry found at LLNL, these tools form a computational infrastructure that is critically needed. For example, the sparse information content of a 3-D pressure field is readily revealed by a wavelet transform, which makes it possible to reduce the data size by factors of 10 to 100 without losing any of the information needed by the scientist.

However, creating such multiresolution compression and display capabilities for Laboratory applications requires overcoming three difficult challenges: (1) appropriate grids must be devised on highly convoluted scientific surfaces, (2) novel wavelet transforms are required that operate effectively on arbitrarily large data sets, and (3) display algorithms must be devised that read exactly the fraction of the compressed data required for any given moment of interaction and also optimize the way this information is sent to graphics hardware. These requirements led to a suite of optimization problems that we addressed during the course of our project.

During FY2001, we devised (1) a hierarchy-building process for surfaces that exploits time coherence; (2) fast, new algorithms to extract material boundaries from volume-fraction information and produce a 3-D hierarchy; (3) a shrink-wrap surface remapper that optimizes display accuracy; (4) a volumetric-based surface compressor that overcomes the complex-topology limitations; (5) a spatial-index reordering that automatically optimizes cache coherence; and (6) a memory-insensitive technique for surface simplification.

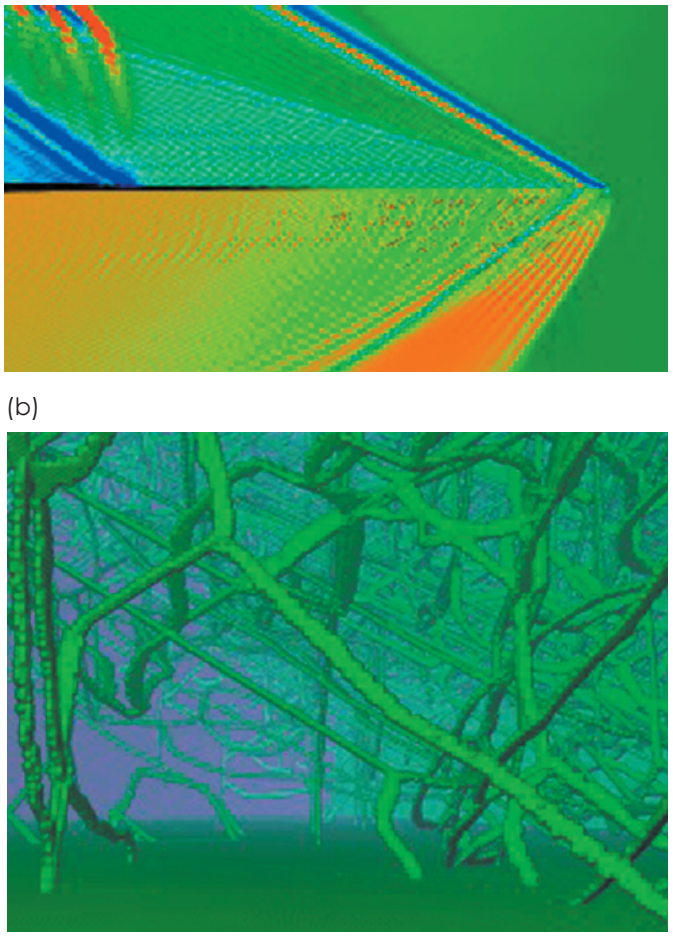

Two large-scale computations aided by our multiresolution compression and display techniques: (a) supersonic cracks in a crystal, and (b) dislocations in breaking metal.

Several large-scale simulations were performed in early FY2001 on several thousand processors of the initial-delivery Advanced Simulation and Computing (ASCI) White supercomputer at LLNL. Aided by our methods, scientists were able to obtain the first successful studies of supersonic crack propagation [Fig. (a)] and the formation of complex junction structures during the brittle failure of metals [Fig. (b)]. Our prototype software for wavelet compression and hierarchical display optimization made it possible to store 25 times more information than was previously possible and also to interact quickly with this wealth of data. The software was shown to scale to 5120 processors, and compression computation added only 10% to the simulation runtime.

Sapphire: Scalable pattern recognition for large-scale scientific data mining

C. Kamath, E. Cantu-Paz, I. K. Fodor, N. Tang

There is a widening gap between our ability to collect data and our ability to analyze it. This problem of data overload has become a serious impediment to scientific advancement in areas as diverse as counterproliferation, Advanced Simulation and Computing (ASCI), astrophysics, computer security, and climate modeling. To improve the way in which scientists extract information from their data, we are developing a new generation of tools and techniques based on data mining, which is the semi-automated discovery of patterns, associations, anomalies, and statistically significant structures in data. In the first step—data pre-processing—high-level features are extracted from the data; in the second step—pattern recognition—the features are used to identify and characterize patterns in the data.

During this 3-yr project, we developed scalable algorithms for the pattern-recognition task and improved their performance, without sacrificing accuracy. We demonstrated our techniques using an astronomical application—the detection of radio-emitting galaxies with a bent-double morphology in the Faint Image of the Radio Sky at Twenty Centimeters (FIRST) survey.

In FY2001, we focused on three tasks: (1) improving the performance of decision-tree algorithms, (2) identifying bent-double galaxies in the FIRST survey, and (3) incorporating our research into software to make it easily accessible to LLNL scientists. In decision trees, we build a model in the form of a tree structure to discriminate among different objects. To improve the performance of decision-tree algorithms, we focused on ensembles of trees, where the results of several trees are combined through simple voting. We invented two new ways of creating ensembles by randomizing the decision at each node of the tree. Using public-domain data sets, we showed that both techniques were more accurate than single trees and competitive in accuracy with other techniques for creating ensembles—but faster by a factor of 2 to 6. In one technique, an ensemble of ten trees could be created in less time than it took to create a single tree. We are in the process of filing patents on this work.

For the bent-double problem, we focused on galaxies composed of three blobs. Using principal-component analysis and exploratory-data analysis techniques, we first identified the key features discriminating bent-doubles from non-bent-doubles. This reduced the number of features from 103 to 31. We next input these features to both our decision-tree software and the generalized linear-model from the commercial software S-PLUS. Varying the number of input features, we created three models for each of the two classifiers. These models were used to classify unseen galaxies, and the results were communicated to our LLNL collaborators on the FIRST project. Galaxies where all six models agreed were considered bent-doubles with high probability, while those with some disagreement resulted in a lower probability.

We completed the beta version of the Sapphire software in early FY2001 and Version 1.0.0 in late FY2001. The latter includes the recent algorithms developed for ensembles and the evolutionary algorithm-based oblique decision trees that we had developed last year. In these algorithms, instead of a decision based on a single feature, we make a decision based on a linear combination of features. We also enhanced the decision trees with several pruning options, splitting criteria, and split finders.

During FY2001, we co-edited one book; published 17 papers in conferences, journals, and books; and presented our work at 15 conferences and workshops. We also filed three new records of invention and three patent applications based on work done in FY2000. During the year, we co-organized two workshops and one week-long program at the Institute for Pure and Applied Math at the University of California, Los Angeles (UCLA), gave three tutorials at conferences, and actively participated in university collaborations.

Our research and software is providing a new generation of data-mining tools and techniques that will improve the way scientists interact with large-scale, multidimensional, time-varying data in the DOE mission areas of stockpile stewardship, nonproliferation, and climate modeling. These tools will also enable new scientific advances derived from very large data sets resulting from long-duration astrophysical observations.

Modeling and simulation for critical infrastructure protection

D. E. Sackett

In the computer and information-based society of today, U.S. national security depends upon the integrity of the nation's information infrastructure. From the use of the Internet to purchase consumer goods, to international funds transfers, to logistical support for the U.S. military, the computing and communications infrastructure supports important functions at all levels. This infrastructure is a prime target for hackers, terrorists, and opposing foreign governments. Maintaining the security of this critical U.S. infrastructure requires the development of capabilities to predict, prevent, recognize, and react promptly to attempted intrusions.

In this project, we have been developing the technological underpinnings and the prototype tools for mapping large networks and then evaluating the usefulness of our technologies and tools. We have also been assessing vulnerability to attacks on the infrastructure using LLNL's Open LabNet as a testbed. The technical challenges have included automated characterization of networks, vulnerability identification, and assessment of the consequences of intrusions.

In FY2001, we added capabilities to the toolset of LLNL's Information Operations, Warfare, and Assurance (IOWA) network mapping database. These capabilities incorporate active discovery methods that more quickly and thoroughly gather information about the network than was previously possible. We then concluded our effort to automatically describe and evaluate the Open LabNet network and to identify vulnerabilities using IOWA (see Figure). In particular, we evaluated the advantages and limitations of the IOWA tools for mapping Open LabNet and the potential enhancements of the IOWA tools that would greatly increase their usefulness for applications to network defense. The IOWA functionality that is the most noteworthy is our integration of IOWA capability with the Laboratory's Nevada Vulnerability Database (NEVADA). The IOWA tools allow the user to automatically generate a map and detailed description of the network, and NEVADA identifies likely vulnerable nodes. This combination is very useful in securing a network against intrusion.

We also assessed and documented the long-term promise of our vulnerability-characterization technology. We concluded that completely automating this process—particularly for multistep intrusions—would be extremely complex because of the difficulty of completely characterizing the behavior of the computers on the network. However, we evaluated active methods (targeted probing) for gathering information to further describe the network, and implemented one method as a test case. This effort demonstrated how active methods can quickly generate specific, needed information.

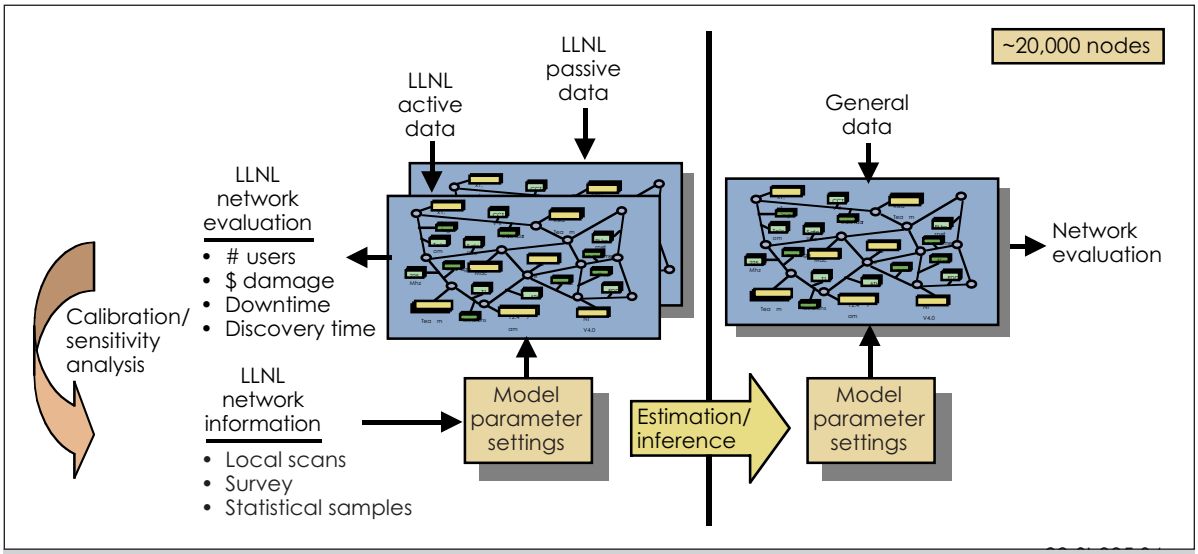

The Open Labnet mapping process tested and calibrated the Information Operations, Warfare, and Assurance (IOWA) toolset.

During FY2001, we also addressed potential enhancements and integration efforts that would significantly increase the usefulness of the IOWA tools in performing active, real-time network defense and computer-incident forensics. We concluded that a high-leverage effort would be the integration of LLNL's Network Intrusion Detector (NID) system and Logger, LLNL's new firewall-log analyzer, with our IOWA/NEVADA system. Inputting the output from NID and Logger to the IOWA database would allow the user to graphically trace an intrusion and analyze how it occurred. Reconfiguring this integrated toolset to detect and respond to intrusions as they occur would yield an extremely important capability.

Coupled ab initio molecular dynamics and Poisson–Boltzmann solvation model

F. Gygi, J. L. Fattebert

This project aimed at developing high-performance software for first-principles molecular dynamics (FPMD) simulations of molecules in the presence of a solvent. First-principles molecular dynamics is an atomistic simulation method that couples a quantum mechanical description of electrons with a classical description of nuclei. It is being used at LLNL in simulations of condensed matter under extreme conditions and for biological applications. For example, FPMD has been used recently to investigate the properties of hydrogen under high pressures. These data are important to stockpile stewardship, fusion, and planetary and astrophysics.

Because most biochemical reactions occur in aqueous solution, simulations must take into account the effect of solvation in water if they are to produce realistic results. The large computational cost of FPMD simulations often precludes a full simulation of a biomolecule surrounded by a large number of water molecules. Simplified models of solvation have been developed, in which the solvent is represented by a polarizable continuum model. Coupling such models to FPMD algorithms can potentially extend considerably the scale of FPMD simulations of biomolecules.This project has developed and implemented a new approach to the simulation of solvated molecules by coupling a Poisson–Boltzmann solvation model to the FPMD method.

During FY2001, we completed the development of a solvation model that can be coupled to a first-principles, electronic-structure calculation in the framework of density functional theory (DFT). An optimal parametrization of the model was determined in order to reproduce the cohesive energy of water. Care was taken to obtain parameters that represent the solvent (water) but that are independent of the solute. The model was also designed to simplify the calculation of the ionic forces needed for molecular dynamics.

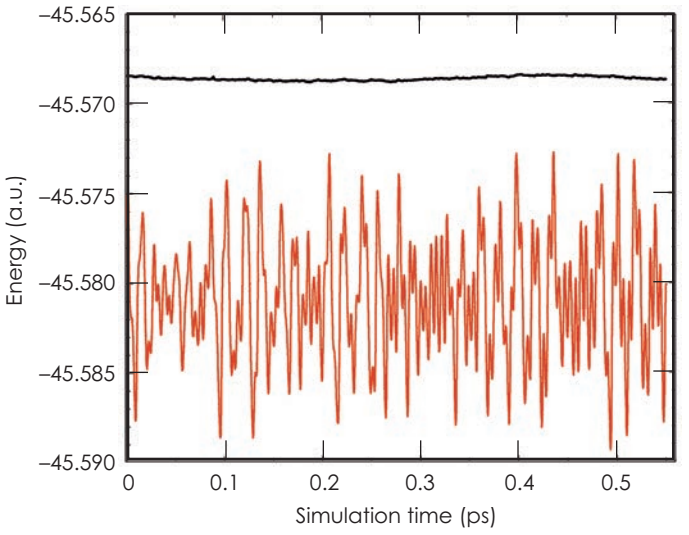

Total energy (black) and Kohn–Sham energy (red) during a simulation of an acetic acid molecule in an aqueous solution. The total energy shows no appreciable drift.

We completed a parallel implementation of the multigrid Poisson–Boltzmann solver. This implementation, based on the message-passing interface (MPI) and the open message-passing (OpenMP) standard, has been successfully ported to IBM-SP, Compaq TeraCluster2000 (TC2K), and Linux platforms. To facilitate coupling this solver to multiple FPMD codes, the solver was implemented as a C++ library. The solver library can be currently coupled to two codes: MGMol (a finite-difference, real-space code) and JEEP (a plane-wave code).

Finally, the use of the Poisson–Boltzmann model coupled to an FPMD simulation was successfully demonstrated on several organic molecules; it showed excellent numerical behavior. In particular, the total energy is accurately conserved during the course of a simulation, which is an essential prerequisite for molecular dynamics simulations (see Figure). We also verified that solvation energies computed for a series of organic molecules in equilibrium geometries reproduce accurately the results obtained in the literature.

We initiated two collaborations within the Laboratory in which the software developed in this project will be used to compute solvation properties of dimethyl-phosphate (a model fragment of the DNA backbone) and to investigate reaction barriers of phosphoramide mustard, an anticancer drug.

Our work has appeared in refereed publications.

Negating chemical-agent dispersion during missile defense

G. T. Nakafuji, R. A. Greenman, T. G. Theofanous

The threat of ballistic missiles carrying chemical, biological, or nuclear payloads is driving the development of new, high-altitude, theater ballistic-missile-defense (BMD) systems that are designed to intercept incoming ballistic targets at altitudes in excess of 30 km. However, the BMD community lacks vital pieces of knowledge that are required for understanding the post-intercept survival and fallout of chemical-warfare (CW) agents.

Our goals are to address issues involving the hydrodynamic breakup of a CW agent following a successful, high-altitude (>30 km) intercept of a missile bearing that agent. Our project has both computational and experimental components and includes a strong collaboration with scientists at the University of California, Santa Barbara (UCSB). This research will enhance LLNL's capabilities to model BMD intercepts and their outcome and will aid in the development of new counterproliferation and demilitarization methodologies.

During FY2001, we successfully characterized liquid breakup in the 30- to 70-km altitude range for specific Newtonian fluids and extended the ALE3D code capability in the slip-flow regime.

The Weber number—the ratio of the gas shear-flow force to the surface tension force of a drop—is a parameter used for characterizing droplet breakup. Higher Weber numbers result in more dynamic droplet-breakup mechanisms. We discovered the existence of wave penetration and shear breakup for Weber numbers as low as 10 to 20 (in some fluids) in low-pressure, supersonic conditions. This is in direct contrast to liquid-breakup results in the literature that predict vibrational or bag breakup in these ranges. The wave-penetration-driven breakup is caused by long-wavelength perturbations in the liquid–gas interface that grows and disrupts the drop. This observed breakup behavior is highly dependent on the fluid properties. For some fluids, the departure from previously identified breakup regimes is pronounced; for fluids like glycerin, the conventional breakup mechanisms (splitting and bag breakup) can still exist. We experimentally determined that significant differences in breakup behavior are observed for drops—tested at the same Weber number—exposed to either supersonic, rarefied, or subsonic, normal-pressure conditions. Our computational results indicate strong variations in surface pressure on the drop that are due to compressibility effects.

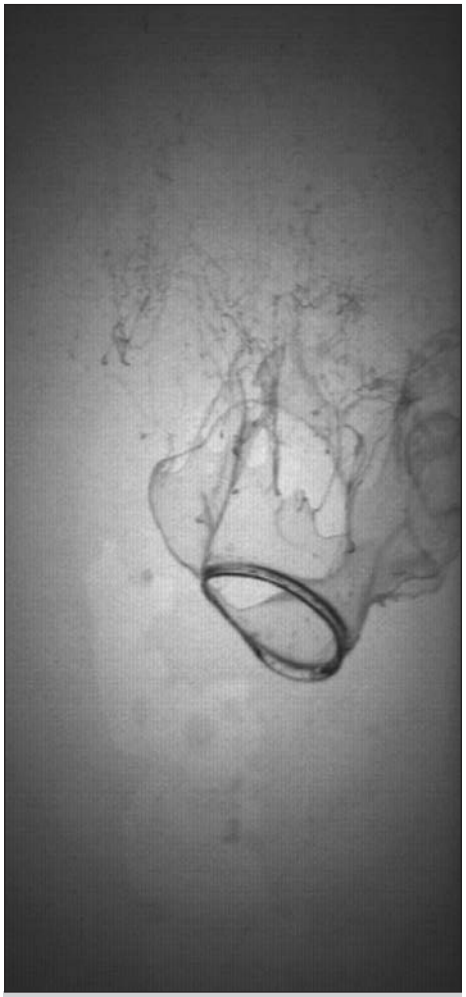

Bag breakup of glycerin in rarefied, supersonic flow.

The rarefied conditions result in extended breakup time scales that reveal features of droplet breakup that have never been reported in the literature. The extended time scale allows the ALE3D code to calculate the evolution of the drop prior to breakup conditions. The arbitrary-Lagrange-Eulerian formulation of ALE3D allows discrete tracking of the gas–liquid interface upon which the appropriate surface tension and boundary models can be applied. The rarefied conditions for drops breaking at high altitude are at the upper end of the slip-flow regime—which is characterized by velocity and temperature discontinuities at the gas–liquid interface and results in reduced surface flow of the drop.

Our experiments during FY2001 were conducted in collaboration with scientists at UCSB's supersonic, rarefied, pulsed-air wind tunnel, a facility that was designed and constructed for examining the physics of droplet breakup. These experiments yielded remarkable results (see Figure) for observing the breakup of liquid in drops ranging in diameter from 2 mm to 1 cm.

In another unique experiment at UCSB, we examined the breakup of large (>1-cm diam) drops. These experiments reveal that droplet breakup cannot be fully described by Weber numbers. A strong inertial effect appears to influence breakup as the drop size is increased.

Our plans for FY2002 include further examination of size-scaling effects and possible expansion of the project to the investigation of low-altitude breakup of drops.

Adaptive methods for laser–plasma simulation

M. R. Dorr, F. X. Garaizar, J. A. F. Hittinger

The ability to predict and control the interaction of intense laser light with plasmas is important in the design of large-scale, laser-driven fusion experiments. Various interaction mechanisms can significantly affect the transport of laser energy to the target. A major challenge in the computational modeling of these interactions is the need to accommodate a wide range of scales—the numerical propagation of laser light in a plasma typically requires wavelength-scale resolution, whereas the diameter of a single laser beam might span two-thousand wavelengths. Moreover, modeling a region of plasma that extends outside the beam does not require such high resolution. Present-day simulators, based solely on uniform grids, must nevertheless use the same fine gridding everywhere. Such inefficiency ultimately limits the size and speed of the simulations that can be performed.

The goal of our project is to investigate the use of parallel adaptive mesh refinement (AMR) as a means of spanning these diverse scales in the simulation of laser–plasma interaction. We are developing a research code called Adaptive Laser Plasma Simulator (ALPS), which employs parallel AMR to solve a coupled system of equations that models laser–plasma filamentation. ALPS simulates problems in two or three spatial dimensions. The mathematical model solved by ALPS consists of a fluid approximation of the plasma combined with paraxial models of the light propagation. The mesh-refinement strategy is block-structured and involves the synchronized integration of the plasma and light equations on a hierarchy of refinement levels.

This research will enhance LLNL's competency in computational physics and high-performance computing in support of the inertial-fusion program and the Stockpile Stewardship Program.

In FY2001, we improved the laser-light propagation algorithm in ALPS to obtain better matching of solutions at the interfaces between coarse and fine grids. The complex linear system solver used in the integration of the paraxial light model was replaced by a more efficient multigrid solver. To increase the robustness of the code for strongly driven, high-intensity problems, we incorporated a new discretization of the plasma equations with better positivity-preserving properties. More general boundary conditions were also added.

As a result of these improvements, we were able to begin using ALPS to simulate a pair of laser beams crossing in a plasma flow. Such problems are important in laser-driven fusion experiments where, under certain conditions, a resonant coupling of the light-beat wave and an ion-acoustic wave can result in the transfer of energy from one beam to the other.

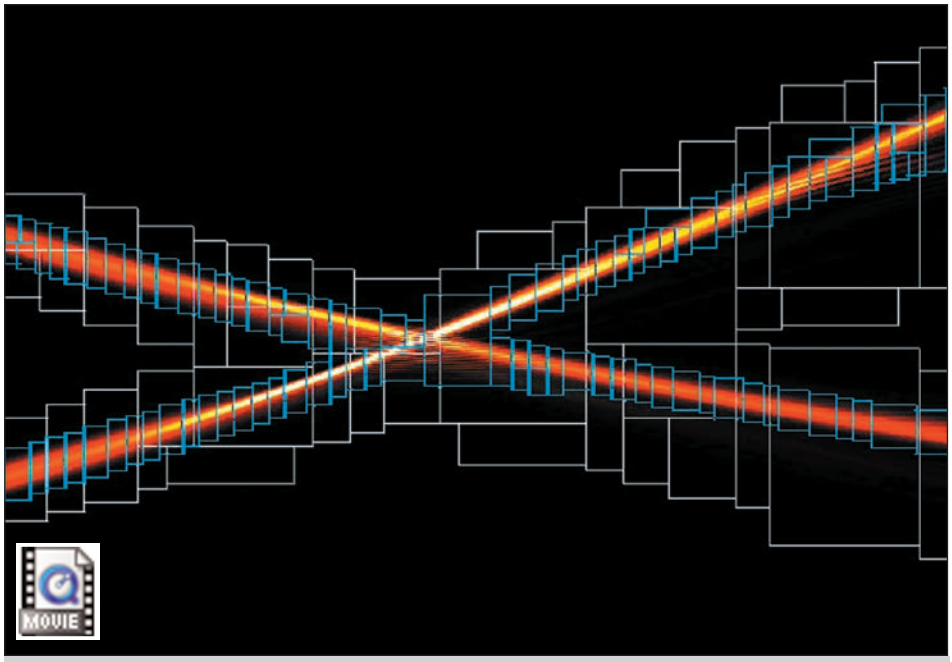

Adaptive calculation of crossed laser-beam intensity in a plasma flow. The white and blue boxes indicate the first and second mesh-refinement levels, respectively.

The Figure shows the ALPS-computed light intensity for one such problem. Here, the upward flow of the plasma and decreasing plasma density results in an upward deflection of the beam and a transfer of energy to the beam propagating from the lower left to upper right (black denotes the lowest intensity and white the highest intensity). AMR enabled the very high resolution required in the interaction region. We also tested ALPS on problems involving 3-D, random-phase plate beams using 128 processors of the TeraCluster2000 (TC2K) at LLNL.

In FY2002, we will extend our plasma model to include Landau damping of ion-acoustic waves by first adding a Krook term followed by a more general model derived from kinetic theory. We will continue the development of practical mesh-refinement criteria, and we will further validate the code by comparing its prediction of energy transfer between crossed laser beams with experimental data to be obtained on the Omega Facility at the University of Rochester.

Rapid problem setup for mesh-based simulation

W. D. Henshaw

Many computational simulation projects at LLNL involve the solution of partial differential equations in complex 3-D geometries. A significant, recognized bottleneck in carrying out these simulations arises in converting some specification of a geometry, such as a computer-aided design (CAD) drawing to a computationally appropriate 3-D mesh that can be used for simulation and analysis.

Even using state-of-the-art mesh generation software, this problem setup step requires weeks or months, which is often much longer than required to carry out the computational simulation itself. It is the objective of this project to build tools and algorithms that will reduce this setup time to less than a day.

This project is developing rapid setup technology, called Rapsodi, for computational physics and engineering problems that use unstructured and hybrid meshes to represent complex geometry.

Although the constraints imposed on computational meshes by Laboratory applications make completely automatic mesh generation extremely difficult, it is clearly possible to significantly reduce the amount of manual labor involved. By developing novel, automated, component-based mesh construction procedures and automated CAD geometry repair and cleanup tools, this project will significantly reduce the amount of hand crafting required to generate meshes for scientific simulation codes. This project will augment the Laboratory's computer simulation capabilities in support of stockpile stewardship and other national security missions.

In FY2001, we developed tools for the interactive repair of structural errors in CAD geometries such as invalid trimming curves and duplicate or missing surfaces. We developed tools for simplifying CAD geometries by removing unwanted details or extracting a subset of the model. We also developed an algorithm to determine connectivity and a global triangulation for CAD geometries that may consist of hundreds of trimmed surface patches. This algorithm automatically repairs most topological errors in the model, such as gaps and overlaps between surfaces. Using the global triangulation, we devised a fast algorithm for projecting points onto the CAD surface and incorporated it into our hyperbolic surface grid generator. This yielded a much more robust code that is about 100 times faster than the previous version. A fast, robust 2-D hybrid mesh generator, based on the advancing-front method, was followed by an initial version of a 3-D hybrid grid generator and methods for moving grid computations and optimizing grid quality.

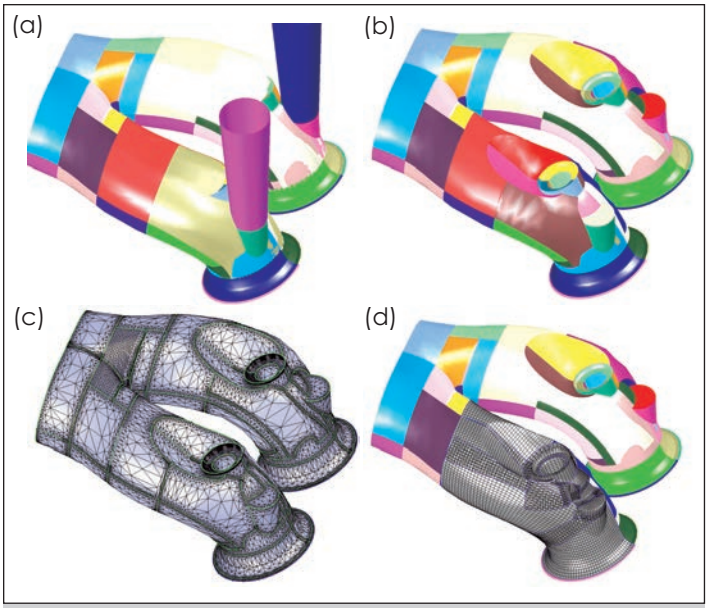

Rapsodi can be used to repair computer-aided design (CAD) models, determine the connectivity and global triangulation and construct grids.

The Figure illustrates the application of the tools developed in this project to an automotive manifold. Starting from a broken CAD geometry (a) Rapsodi tools repair the surfaces (b), determine the connectivity and build a global surface triangulation (c), and construct grids on the geometry (d). Rapsodi reduced the time required to perform these steps from over a week to less than a day.

In FY2002, we will continue to develop our algorithms for CAD repair, topology generation, and mesh generation, and will apply our tools to a variety of CAD geometries for Laboratory and other DOE applications.

New directions for algebraic multigrid methods: Solutions for large-scale multiphysics problems

V. E. Henson

MAIN TOC

Many simulation codes that are important for DOE missions entail solving extremely large problems, requiring the use of parallel computers employing hundreds or thousands of processors. These problems are highly ill-conditioned, which makes them very difficult to solve by any method. Storage and run-time requirements make the use of so-called direct solvers infeasible; iterative solvers often fail outright, or converge so slowly as to make their use impractical. Our research project focuses on the algebraic multigrid (AMG) methods, which are commonly used to solve such problems when direct or iterative solvers are unsatisfactory. AMG methods can work because the essential relations between "smooth error" and the solver are abstracted algebraically from the operator matrix; determining and using those relations in traditional, geometric iterative methods is effectively impossible.

In the first two years of the project we have made significant progress by developing algorithms that enable solutions for difficult problems at the heart of multiphysics simulation codes, including many of the simulations carried out under the Advanced Simulation and Computing (ASCI) program. In FY2000, we integrated a parallel AMG code into two of LLNL's major simulation codes (Kull and ALE3d), and we developed new algorithms to address problems of greater and greater difficulty. In FY2001, we developed new coarsening, interpolation, and relaxation schemes that produce superior results on many problems (particularly convection–diffusion problems and certain elasticity problems), and introduced systems versions of our scalar methods.

Multigrid methods work by recursive application of a two-grid method. The two-grid method itself rests on the observation that "smooth" errors in a problem originally represented on a fine grid cannot be reduced by standard iterative techniques (such as Gauss–Seidel, Jacobi, or conjugate-gradient), but that they can be represented accurately and eliminated efficiently on a coarse second grid, with fewer grid points. The key ingredient for creating an effective AMG algorithm is to characterize smooth errors algebraically and to build operators that represent them accurately.

In FY2001, we focused on developing a new type of element-based AMG algorithm, called AMGe, which is based on our discovery that individual finite-element stiffness matrices implicitly contain critical information about the nature of the smooth-error components. We also devised an "element-free" form of AMGe, applicable to problems not based on finite elements. Development of the AMGe method successfully leveraged the efforts of the Nonlinear Solvers and Differential Equations Project at LLNL's Center for Applied Scientific Computing (CASC).

AMGe yields superior results in several types of problems particularly in difficult elasticity problems. The applicability of AMGe is limited, however, because it is effective only on problems that fulfill certain assumptions about the nature of the smooth error that are intrinsic in the algorithm.

In FY2002, our goal is to develop a new approach, which we call Spectral AMGe, that makes no assumptions on the nature of the smooth error. This method uses the eigenvectors of an agglomeration-based local operator matrix as the basis for the coarse space, which automatically determines the smooth errors representable on the coarse grid. Because the eigenvectors are a property of the operator matrix, no assumptions are placed on the nature of the smooth error. Preliminary experimentation suggests that this approach will lead to the most robust, effective AMG method of any yet developed.

Our research on AMG has made CASC one of the world's leading centers of AMG research, increasing the Laboratory's visibility and importance in the worldwide scientific community. We have published five papers on this work in refereed journals, and are often invited to give lectures at other institutions and at conferences in the United States and abroad. This work has attracted many of the world's leading AMG researchers as collaborators and short-term and sabbatical visitors.

Predicting precise deformation of nonrigid objects

K. L. Blaedel, D. W. Swift, A. A. Claudet

Dimensional characterization of nonrigid objects presents many challenges. For example, when a nonrigid object is mounted in an inspection apparatus, the effect of the fixturing is significant. If the object is not used under the same load conditions as those to which it was subjected during inspection, its dimensional characteristics will deviate from reported values.

Designing specialized fixturing to duplicate "as-installed" conditions does not resolve the problem. For rigid objects, measurement standards are generally of a known pedigree that can be traced to a central authority, such as the National Institute of Standards and Technology. There is no comparable traceability to a single source for nonrigid objects. Specialized fixturing for specific cases precludes standardization across different objects and different manufacturers.

The problem of nonrigid metrology is of direct interest to LLNL in at least three ways. First, it has implications concerning the characterization of thin, hemispherical shells. Second, it has application to the metrology of thin photomasks for extreme-ultraviolet lithography. Third, it can help in the inspection of potassium dihydrogen phosphate (KDP) crystals for advanced laser systems. Further, nonrigid metrology has industrial applications to the fabrication of sheet-metal objects.

The goal of this project is to formulate the research problem (itself a substantial task) and develop a generally applicable method for assessing the dimensional characteristics of nonrigid objects.

Our central idea for the metrology of nonrigid objects is the concept of a "free shape," i.e., the geometry of the object when no external loads (such as those produced by fixturing and gravity) are present. Because it is impossible to measure the free shape directly, a method for inferring it must be developed, and some metric must be developed for acceptance or rejection of objects whose free shape is known.

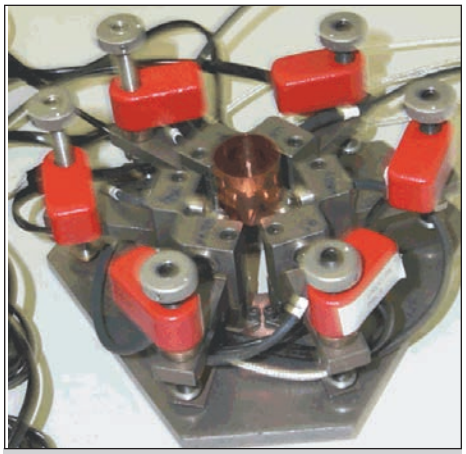

Thin-walled copper cylinder in fixture for metrological measurements. Finite-element calculations based on these measurements allow us to determine the "free shape" of this cylinder, i.e., the shape it would take on if it were not subject to any external deforming forces.

In FY2001 we fabricated a thin-walled copper test cylinder and suitable fixturing apparatus. The cylinder was carefully manufactured under conditions intended to facilitate analysis. The fixturing apparatus applies known loads at three points at 120-deg intervals around the cylinder. When the cylinder is in the fixture (see Figure), the only loads acting on it are those from the three actuators and gravity. Several load conditions were prescribed and 3-D measurements of the cylinder were taken. The loads were computed to create five equal steps, which deformed the cylinder by up to about 2% of its wall thickness. Knowing the loads and the resulting deformations, we carried out a finite-element analysis of the cylinder to extrapolate to its geometry at zero load—the free shape.

We have developed an "energy metric" as one way of characterizing the deviation of the intended geometry of an object (such as our test cylinder) from its actual geometry, as measured by the free shape. To compute this metric, we first calculate the force required to push each node of the free-shape finite-element model of the object to the corresponding node of the as-designed object. Then we multiply each force by the corresponding displacement, and sum these products over the entire object; the result is the energy metric, which represents the quality of the as-built object.

The approach described above represents substantial progress toward a standardizable technique for characterizing the quality of nonrigid objects, and for predicting their behavior under prescribed loads.

Numerical technology for large-scale computational electromagnetics

R. M. Sharpe, D. A. White, N. J. Champagne

The key bottleneck of implicit computational electromagnetics (CEM) tools for large, complex geometries is the solution of the resulting linear system of equations. The goal of this project is to research and develop numerical technology that alleviates this bottleneck for large-scale CEM by greatly reducing the time required to solve the associated hybrid linear systems of equations.

The mathematical operators and numerical formulations used in this arena of CEM yield linear equations that are complex-valued, unstructured, and indefinite. Also, simultaneously applying multiple mathematical modeling formulations to different portions of a complex problem (hybrid formulations) results in a mixed structure linear system, further increasing the computational difficulty. Typically, these hybrid linear systems are solved using a direct solution method, which was acceptable for Cray-class machines but does not scale adequately for Advanced Simulation and Computing-(ASCI-) class machines. Additionally, LLNL's existing linear solvers are not well suited for the linear systems that are created by hybrid implicit CEM codes.

During FY2000, our activities first focused on establishing a test suite of sample matrices to evaluate the solver research. Next, we chose the ISIS++ solver framework (developed at Sandia National Laboratories, Livermore) as a basis for our research. We extended this package to treat complex-valued, hybrid linear systems. In addition to the native iterative methods in the package, we added several direct solvers to address the hybrid linear system.

Our FY2001 activities began with an implementation of a Shur-complement approach for solving block-structured hybrid linear systems, which greatly improves the speed of solution. In addition, we identified and addressed the key research issues associated with preconditioners. Some of these issues amount to extending existing preconditioners to apply to the operators in CEM; others concern developing more physics-based operators.

We identified the need for a research effort on both matrix-based and operator-based preconditioners. The matrix-based methods can be applied to any linear system of equations after the matrix has been assembled. We began work on sparse approximate inverse preconditioners and on incomplete lower/upper preconditioners (ILUs). This work will continue in FY2002, as we have hired a new employee whose doctoral research was in parallel ILU methods.

We began a portion of the work on direct operator-based methods with R. J. Adams of the University of Kentucky. The methods involve recasting integral equations of the first kind into integral equations of the second kind, which we expect to greatly improve the basic conditioning of the linear system. An overall improvement of the system conditioning has been shown to significantly reduce the solution time. We made some progress in this direction, and further work on it is being actively pursued.

The next task was to begin research into so-called fast multipole solution methods (FMM). Working at LLNL during summer 2001, a graduate student from Brigham Young University developed a single-level multipole algorithm. The next step will be to extend the single-level FMM to a multilevel FMM algorithm. These methods have been shown to reduce the operation count from $N*N$ to $N*\log(N)$ for linear systems to which they apply.

In FY2002 we will initially focus on completing the additional matrix-based preconditioners and then on completing the operator-based work for important operators used in CEM. All of this work will be incorporated into our existing solver framework for delivery to LLNL researchers and to the CEM community at large.

Physical and chemical properties of hydrogen-bonded liquids under pressure

G. Galli, E. Schwegler, R. Q. Hood

Hydrogen bonds are the most prominent "weak" interactions in solids, liquids, and gases. They determine the crystal packing of many organic molecules, the 3-D structure of biological macromolecules, and the bonding properties of water—the most important liquid in physical and biological sciences. However, the nature of hydrogen bonds and their changes under pressure are largely unknown.

We are investigating the structural and dynamical properties of low-Z, hydrogen-bonded liquids and liquid mixtures under pressure, using computer simulations—in particular, quantum molecular dynamics (MD) techniques. The data we obtain in our simulations are relevant to the performance of inertial fusion targets and also to models describing the interiors of planets like Jupiter, Uranus, and Neptune.

In FY2001, we carried out (1) a series of simulations of fluids (water, hydrogen fluoride, oxygen, deuterium, and hydrogen) under pressure at given, fixed thermodynamic conditions, and (2) the first fully ab initio simulation of shock propagation in liquid deuterium.

Our predictions for water were confirmed by diamond-anvil-cell experiments conducted at the Commissariat l'Energie Atomique (CEA)(in France) and by neutron-scattering experiments carried out at the Rutherford Laboratory in England. Since the CEA experimental results were made available to us in mid-year, we have been collaborating with the CEA group; we are now performing extensive simulations in which we match exactly several diamond-anvil-cell experiments. Our simulations of shocks in deuterium have (1) allowed us to propose an interpretation of controversial laser-shock experiments carried out at LLNL several years ago using the Nova laser, and (2) shown that it is possible to observe a shock front at the microscopic scale.

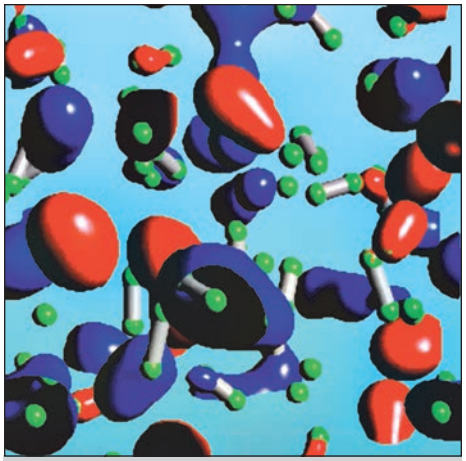

Snapshot of a deuterium quantum simulation showing atoms (green), atomic bonds (gray), and charge-density isosurfaces (blue and red) reveals the inherent disorder of the liquid.

Thus, they have opened the way to direct shock simulations from first principles, without experimental input.

We also (1) coupled ab initio density simulations with quantum Monte Carlo (QMC) calculations and computed the optical gap of liquid hydrogen as a function of pressure, and (2) successfully related the electronic properties of the system to the structural changes—notably molecular dissociation—that were occurring under pressure. The Figure shows both the atomic structure (in particular atomic positions and bonds) and the electronic structure (e.g., charge densities) of the liquid. Although this is still work in progress, our results point to a metallization mechanism under pressure that differs from that inferred from conductivity data obtained in gas-gun experiments. Further analyses are needed to fully understand the origin of the discrepancy. We expect this coupled ab initio MD and QMC investigation to have an important influence on studies of disordered molecular fluids and—in particular—compressed hydrogen.

We also contributed to developing and using algorithms to describe molecular dissociation and dynamical processes under pressure.

Our research during FY2001 was the subject of twelve invited talks and one published article. Our simulation on shocked deuterium received a Department of Energy (DOE) Defense Program Award of Excellence for Technical Excellence in Advanced Simulation and Computing (ASCI) and a joint Defense and Nuclear Technology (DNT) and Computations Award of Excellence. (These were awarded to G. Galli and F. Gygi.)

Our work on shocked deuterium received funding from the ASCI program and is no longer funded by LDRD. The work on all the other fluids (water, oxygen, and other hydrogen-bonded mixtures) will be continued in FY2002. Our main goal will be to compute the properties of these fluids at megabar pressures and to study in detail molecular dissociation under extreme conditions.

Analysis of radionuclide migration through a 200-meter vadose zone following a 16-year infiltration event

A. F. B. Tompson, D. K. Smith, G. B. Hudson

MAIN TOC

The CAMBRIC nuclear test was conducted beneath Frenchman Flat at the Nevada Test Site (NTS) in 1965. The device was positioned 74 m beneath the ambient water table, which is itself 220 m beneath the ground surface (see Figure). Beginning approximately 10 yr later, groundwater adjacent to the test location was pumped steadily for 16 yr to elicit information on radionuclide migration in the saturated zone. The pumping-well effluent—containing mostly "mobile" radionuclides such as tritium, carbon-14, clorine-36, krypton-85, iodine-129, and ruthenium-129—was monitored, discharged to an unlined ditch, and allowed to infiltrate into the ground or to flow towards Frenchman Lake, just over 1 km away. This created an unexpected and remarkable second experiment, which is the focus of this project. To better understand the movement of radionuclides between the ditch and the water table, the migration of the effluent through the 220 m of unsaturated media—the vadose zone—has been analyzed in conjunction with geological data, new radionuclide measurements, isotopic age-dating estimates, and flow and transport models.

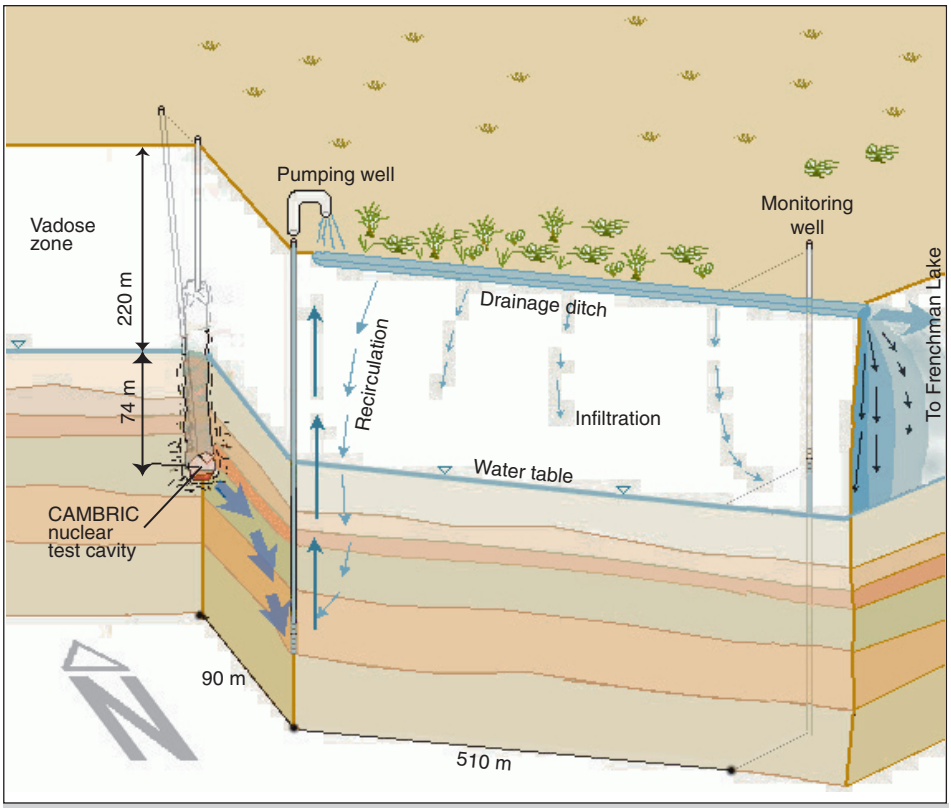

Schematic of the pumping experiment surrounding the CAMBRIC nuclear test at the Nevada Test Site (NTS), showing reinfiltration of ditch effluent towards the water table and the monitoring well.

Measurements at the water table, in a monitoring well 100 m from the ditch, have indicated rising levels of tritium since 1993, roughly 13 to 15 yr after the initial discharge of the effluent into the ditch. In FY2000, results from modeling and tritium age dating suggested that 2 to 5 yr of this transit time occurred solely in the vadose zone. Additional chemical and modeling results obtained in FY2001 also suggest considerable recirculation of the original pumping-well discharge back into the pumping well. This was determined from additional tritium age dating as well as evaporated stable-isotope signatures in the pumping well (Figure).

Surprisingly, no carbon-14 was observed at the water table, suggesting its preferential retention in the vadose zone possibly because of precipitation or other chemical reaction.

Altogether, the results indicate that about 20% of the pumped radionuclides from the original experiment—originally attributed to the test itself—were actually recycled, and would imply that a reanalysis of the original test results is warranted. In addition, the modeling results themselves can be used to confidently quantify the flux of radionuclides reaching the water table underneath the ditch, which is of considerable concern to ongoing environmental and waste-disposal programs at the NTS. Furthermore, the long-term nature of the experiment, the variety of chemical measurements and isotopic interpretations, and their incorporation into a unified modeling analysis all have contributed to a unique perspective for interpreting radionuclide migration.

Because of the legacy of radioactive wastes identified in the surface or in the unsaturated zone at many sites in the DOE complex, our experience is important to accurate predictions of contaminant migration and remedial design in the vadose zone.

Reactive transport modeling of geological carbon dioxide sequestration

J. W. Johnson, J. J. Nitao, C. I. Steefel

The increasingly urgent need to curb anthropogenic carbon dioxide (CO_2) emissions ranks high among the grand scientific challenges of this century. In the near term, significant reductions can only be achieved through innovative sequestration strategies that prevent atmospheric release of large-scale CO_2 waste streams. Among these, injection into confined geological formations—in particular, saline aquifers—represents arguably the most promising alternative.

Successful implementation of this approach relies on our ability to predict the relative effectiveness of subsurface CO_2 migration and sequestration as a function of key formation properties; this will enable us to identify those sites where optimal sequestration performance can be obtained. Quantifying this functional relationship requires a modeling capability that explicitly couples multiphase flow and kinetically controlled geochemical processes, interfaces with comprehensive thermodynamic/kinetic databases, and exploits modern visualization tools. The development of screening criteria for target sequestration sites, together with the reactive transport simulators that facilitate the evaluation of potential sites are critical to several DOE energy and environment programs.

In this project, we developed a unique simulation capability that meets these criteria, then used it to model CO_2 injection at Statoil's North-Sea Sleipner facility—the world's first saline-aquifer storage site. This new capability integrates a state-of-the-art reactive transport simulator (NUFT), supported by geochemical software and databases (SUPCRT92 and GEMBOCHS) and by a dedicated graphics utility (Xtool).

For the Sleipner application, in FY2001 we completed a series of 20-yr simulations, each spanning 10-yr active-injection ("prograde") and post-injection ("retrograde") phases. From these, we quantified, for the first time, (1) the influence of intra-aquifer permeability structure and aquifer/cap-rock composition on migration/sequestration balance; (2) the relative effectiveness of hydrodynamic, solubility, and mineral trapping; and (3) the isolation performance of shale cap rocks.

Intra-aquifer permeability structure controls the path of immiscible CO_2 migration, thereby establishing the spatial framework of plume–aquifer interaction and the potential effectiveness of solubility trapping (CO_2 dissolution into formation waters) and mineral trapping (CO_2 precipitation as carbonate minerals). Actual effectiveness of these sequestration processes is determined by compositional characteristics of the aquifer and cap rock. By retarding vertical and promoting lateral plume migration, intra-aquifer shales significantly expand the spatial extent of plume–aquifer interaction, thereby enhancing the potential for solubility and mineral trapping.

Approximately 85% by mass of injected CO_2 remains and migrates as an immiscible fluid phase (subject to hydrodynamic isolation beneath the cap rock), roughly 15% dissolves into formation waters, and less than 1% precipitates as carbonate minerals. This partitioning defines the relative effectiveness of structural, solubility, and mineral trapping on a mass basis.

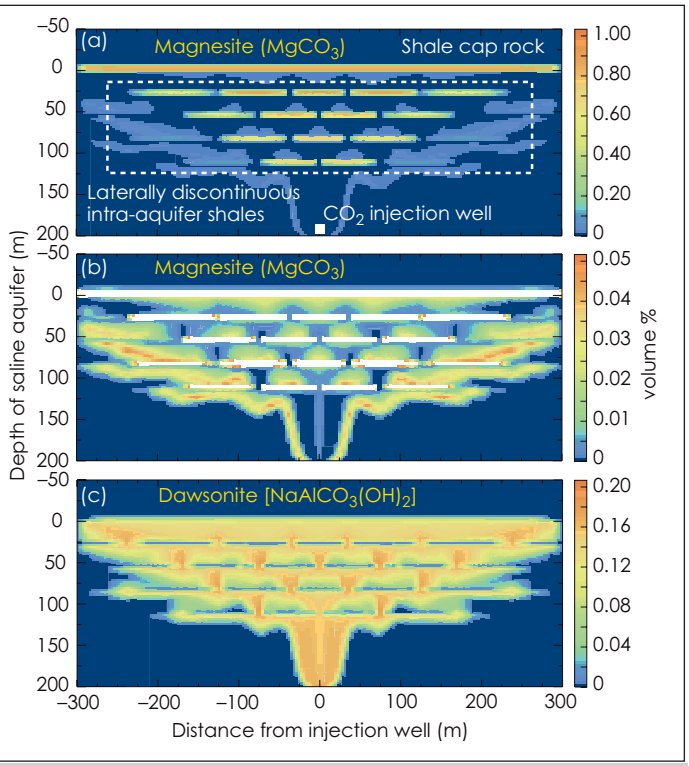

Simulated mineral trapping after 20 yr (a) within intra-aquifer and cap-rock shales, (b) along boundaries of the immiscible CO_2 plume, and (c) within the plume itself.

The significance of mineral trapping, however, lies in its effective reduction of permeability within the aquifer along plume boundaries, and especially within iron/magnesium-rich shales—where it increases their integrity against upward CO_2 migration. The prograde extent of mineral trapping is continuously enhanced during the retrograde phase, reducing basal cap-rock permeability by 22% in our 20-yr simulations. Hence, mineral trapping has enormous strategic significance: it continuously improves isolation security of the voluminous immiscible plume and solubility-trapped CO_2. The Figure illustrates the location and volumetric extent of magnesite and dawsonite precipitation that cause the local reduction in permeability.

During FY2001, we presented our research at four national meetings. Our presentation to the American Association of Petroleum Geologists received a "Best Paper" award from their Division of Environmental Geosciences.

Compensation for thermally induced and geometric errors of machines using an open-architecture controller

D. Born, J. L. Klingmann

In most manufacturing environments, more than half of the errors in fabricated parts are caused by thermal sources. At times, the only viable approach to achieve the desired accuracy is to lose productivity while waiting for thermal transients to diminish or by reducing speeds to reduce heat generation.

Thermal-error compensation—modifying the toolpath to cancel these errors—is another approach to improve accuracy, though this method has not been practical for predicting thermal error in real time. The purpose of this project is to investigate an efficient, practical, model-based method of thermal-error compensation for typical manufacturing environments.

The technology we are investigating is applicable to target fabrication for weapons physics experiments in support of the Stockpile Stewardship Program. Much of the aging equipment inventory at LLNL and across the DOE Complex is being replaced by modern machine tools, many of which are productive but are susceptible to thermal errors. In addition, the efficiency improvement that this project may offer has broad application throughout the DOE Complex manufacturing facilities and at industrial sites working on DOE projects. Compensation methods applied to these new machines will allow the plants and laboratories to operate with the ease of the modern machines but at an improved accuracy level.

Our strategy for compensation is to deterministically combine temperature readings in a machine model to predict toolpoint error. The model used is based both on the geometry of the machine and hypotheses about likely deformation modes. Using the integral of the temperature profile to predict the deformation minimizes the number of temperature sensors. Our approach places temperature sensors at the Gaussian integration points of the structural elements. This small, finite number of temperatures is measured continuously on the machine.

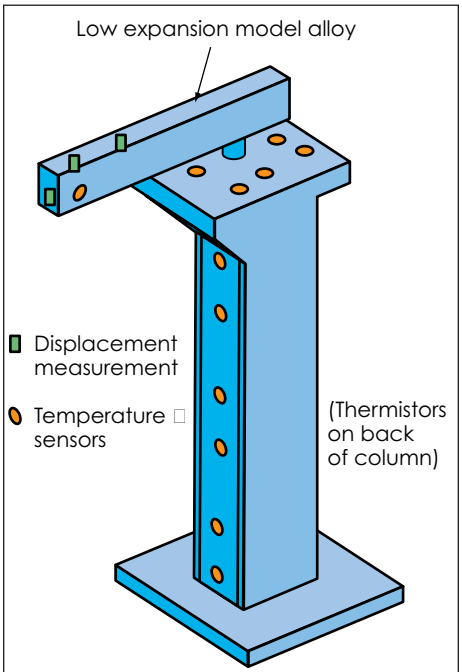

Simplified machine tool structure for developing a thermal compensation model.

During FY2001, our efforts focused on developing a virtual machine that could be used to investigate temperature-sensor locations and the sensitivity of the system to disturbances. To be sure that this virtual machine was a realistic model of a machine in a variable environment, we needed to compare experimental data to the model. The model was based on a simple structure, depicted in the finite-element model shown in the Figure, and has many of the features that make up a typical machine-tool structure. A thermal load was applied to the experimental structure with a heat tape and temperatures were measured. This same temperature profile was then input into the finite-element model and the experimental displacements were compared to the model-predicted displacements. As the heat flowed from the top of the tower, a gradient developed both across the width and length of the tower. The steady-state displacement measurements agreed reasonably well with the finite-element model. The changes in height at the two probe locations were within 2% and 0.1% of the finite-element predictions.

In this experiment, we found the test to be extremely sensitive to changing boundary conditions, such as the ambient environment. Before moving into further testing of the proposed thermal compensation methods, a thorough error budget of the current experiment needs to be conducted to understand the uncertainties. Future work in this area could then be conducted, first in compensating this simple model and then on more complex structures and machines.

New approaches to quantum computing using nuclear magnetic-resonance spectroscopy

M. E. Colvin, V.V. Krishnan

Quantum computing relies on the superposition principle of quantum mechanics; that is, until it is measured, any quantum system can simultaneously exist in all possible states. Thus, although a classical bit must be either 0 or 1, a quantum bit (qubit) simultaneously contains a 0 component and a 1 component and can evolve concurrently along many paths. A quantum computer, therefore, has a high speed relative to a classical computer.

Practical quantum computers would bring about dramatic changes in computation and information processing. They promise superior computational power for solving certain problems that are currently intractable using classical computers. For example, applications such as efficient database searches and cryptography would benefit from the development of practical quantum computers.

Nuclear magnetic resonance (NMR) is uniquely capable of constructing small quantum computers because each line in an NMR spectrum represents the complex interplay among the various interacting spins of the molecule—these transitions can be designed to perform quantum computing. To date, the several algorithms that have been implemented successfully using this method can also (1) test theoretical predictions and facilitate the development of better protocols, and (2) investigate the feasibility of practical quantum computers. However, although a number of researchers have demonstrated the use of NMR computers, there are many areas of potential development, including ways to increase the number of qubits, development of more cost- and time-efficient physical implementations of quantum computation, and methods for the theoretical evaluation of quantum-computer performance.

LLNL's strengths in computing, physics, and materials science offer many opportunities for contributing to the development of quantum computing. In this project, we have been focusing on one particular new idea, use of an anisotropic medium to increase the speed and number of qubits in a NMR-based quantum computer. Our long-term goal is to build scientific credibility in the field and to provide a core of expertise in quantum computing.

During FY2001, we reached several important milestones that enabled us to form the necessary basis for a quantum-computing platform. Our major accomplishments included (1) developing an algorithm to measure the actual time cost of quantum-computer algorithms; (2) completing a general-purpose, ensemble quantum-computing simulator (enQC-lator); and (3) collecting a set of experimental data on a system containing molecules oriented in a liquid-crystal medium. The Figure shows the results from encoding and decoding quantum information of a "Cat state" (analogous to Schrodinger's Cat) algorithm on a three-qubit quantum computer as simulated using our enQC-lator. This tool can be used to critically evaluate and design new algorithms for quantum computing prior to actual experimental implementation.

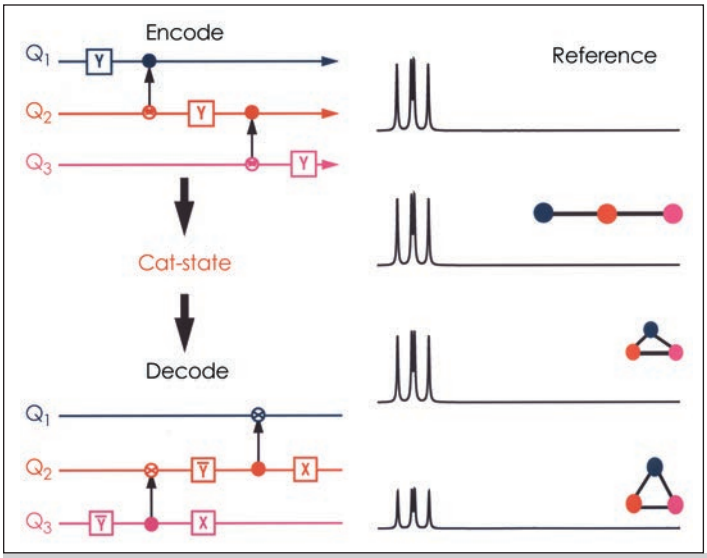

Cat-state bench-mark performance using our ensemble quantum-computing simulator (enQC-lator) in a three-qubit quantum computer, showing descriptions of the computing code (left) and results (right) for different molecular geometries. Vertical arrows represent transfer of qubit information, and boxes represent the radio-frequency, pulses of a given phase. The reference spectrum corresponds to "no operation," while the reduction in the spectral intensity reflects the effect of coupling topology on quantum computing that is based on nuclear magnetic resonance (NMR).

In FY2002, we will concentrate on three important aspects of the project: (1) incorporating efficient quantum computing in the liquid-crystal matrix (3 to 6 qubits), (2) evaluating the performance of quantum computing using multidimensional NMR methods, (3) evaluating methods that will reduce artifacts, and (4) applying quantum computing in isotropic and anisotropic solvent conditions.

Improving advanced simulation software through scientific component technology

S. Kohn, B. Bosl, T. Dahlgren, T. Epperly, G. Kumfert, S. Smith

Numerical simulations play vital roles in the DOE's science mission as basic research tools for understanding fundamental physical processes. As simulations become increasingly sophisticated and complex, no single person—or even single laboratory—can develop scientific software in isolation. Instead, computational scientists must construct simulation software by combining separate software modules developed by experts in physics, chemistry, mathematics, and computer science. Often, combing these software packages in a single application is difficult because of differences in implementation language, programming style, or calling interfaces.

To address problems of complexity, re-use, and interoperability for laboratory simulation software, we are developing software component technology for high-performance parallel scientific computing. Our research focuses on the unique requirements of scientific computing on Advanced Simulation and Computing- (ASCI-) class parallel machines—such as fast, in-process connections among components; language interoperability for scientific languages; and data-distribution support for massively parallel computers. This initiative supports DOE and LLNL missions in national security, energy technology, and environmental stewardship.

In FY2001, our primary accomplishments were the addition of new capabilities to our Babel language interoperability tool, a demonstration of Babel capabilities in LLNL's high-performance preconditioners (HYPRE) parallel linear solver library, and continuing collaboration with members of the DOE's Common Component Architecture (CCA) working group on the development of community-wide standards for high-performance component technology.

Our Babel tool addresses language interoperability issues for high-performance parallel scientific software by generating "glue" code that allows a software library to be called seamlessly from any supported language. In FY2001, we added language capabilities for Java and Python in addition to improving existing language support for Fortran 77, C, and C++. We also significantly increased the robustness of our software through the use of an extensive regression test suite that includes over 3000 tests.

In collaboration with members of the HYPRE development team at LLNL, we integrated some of the Babel language interoperability technology into HYPRE, which supplies critical linear solver technology for the ASCI program. This collaboration provided valuable feedback for improvements in the Babel tool, showed that parallel Babel run-time overheads were small (less than 1% of the total run time), and provided language interoperability and object-oriented capabilities to the HYPRE library.

Finally, we are continuing to collaborate on community technology standards with members of the CCA working group (see http://www.cca-forum.org). The CCA is establishing component technology standards and developing a component infrastructure for DOE high-performance simulation software. The DOE's Office of Science has selected the CCA as one of the recipients of a Scientific Discovery through Advanced Computing (SciDAC) award, a 5-yr research effort consisting of DOE laboratories and academic partners and intended to deliver component technology to computational-simulation efforts within the DOE. The CCA will use the Babel language interoperability technology developed at LLNL as a foundation for the community's common component infrastructure.

In FY2002, we plan to add support for Fortran 90 in the Babel language interoperability tool. Fortran 90 is a common programming language in the application community, and our language interoperability technology will enable Fortran 90 developers to use common mathematical software libraries that are developed using other programming languages. We will develop remote communication capabilities and implement a prototype to investigate parallel redistribution issues for complex scientific data. Working with members of LLNL's Advanced Laser Plasma Simulator (ALPS) project, we will use Babel technology to develop an advanced scripting layer for the ALPS framework. This scripting layer will allow computational scientists to more easily analyze ALPS simulation results and to compare ALPS results against those from other computational tools.

Djehuty: A next-generation stellar-evolution code

D. S. Dearborn, P. P. Eggleton

Stars provide the fundamental quantitative units for measuring the universe. They are the foundation for determining distances and ages and the factories driving chemical evolution. Stars continue to be used as physics laboratories for constraining the properties of fundamental particles (cross sections, masses, etc.) and hot plasmas [opacities, equations of state (EOS), etc.].

Current practices in stellar evolution employ 1-D calculations that quantitatively apply to only a minority of the observed stars (single nonrotating stars, or well-detached binaries). Even in these systems, astrophysicists depend on models of complex 3-D processes such as convection. With the advent of massively parallel computers and the development of codes to use them, LLNL is uniquely situated to move the calculation of stellar properties to the next level of physical understanding.

This project has leveraged abilities from across the Laboratory to develop a 3-D stellar-evolution code that operates on massively parallel computers with the best available physical data (opacities, EOS, etc.). Our code will be a testbed to validate—using astronomical observations—the physical data and advanced numerical algorithms being developed for the Stockpile Stewardship Program. The forefront astrophysical research enabled by Djehuty will attact to LLNL new scientific talent with expertise in hydrodynamics, and nuclear- and atomic-physics disciplines, all of which are essential to fulfill the nuclear weapons stewardship mission of the Laboratory.

At the close of FY2000, we had successfully executed Djehuty—our 3-D hydrodynamic simulation of a star—on LLNL's TeraCluster2000 (TC2K) computer. This was the first-ever 3-D simulation of a whole star. Although it was a single-processor run, with partial physics and an under-resolved (4×10^5-zone) mesh, this progress enabled a series of subsequent runs in FY2001. The series of runs studied different mesh constructs, tested and improved the accuracy of our 3-D models, and began to optimize our physics.

Djehuty now has an accurate EOS, astrophysical opacities for use with its radiative-diffusion-transport package, and a nuclear-reaction network for hydrogen, helium, and carbon burning. The gravity implementation is complete only for spherical stars, but it is adequate for our first major 3-D science study of convective cores. During FY2001, we constructed the large (5×10^7-zone) meshes needed for realistic stellar modeling and began moving our operation from a parallel to a massively parallel environment. The latter was possible because our 3-D stellar models have now been decomposed and run in parallel operations on up to 256 processors.

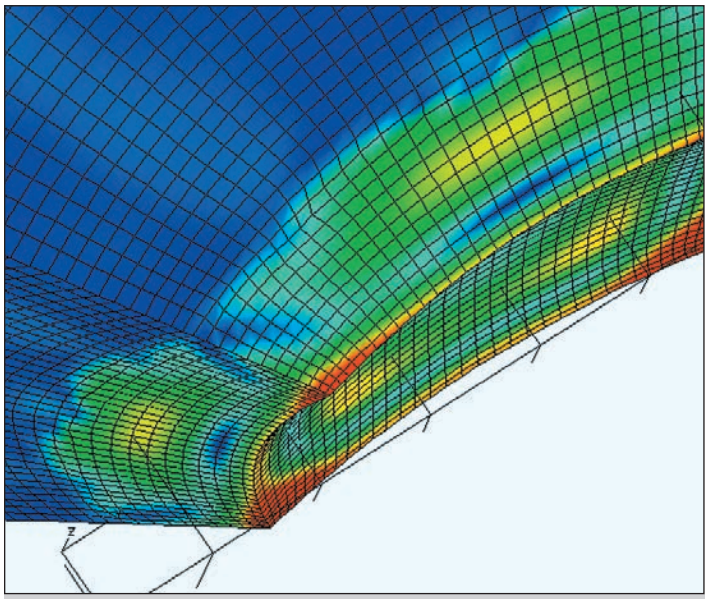

The velocity field driven by hydrogen fusion in a 4-solar-mass star, as shown for a segment of the star. The segment is about half a million kilometers across.

With the basic elements of Djehuty functional, we made a number of extended parallel runs to address a long-standing, well-characterized discrepancy between the convective core size predicted by 1-D stellar models and observed stars. Though it is an early, not well-resolved calculation, the results are encouraging. As the Figure shows, the convective region in our 3-D calculation extends beyond the point predicted in the 1-D modeling. This is important because it (1) is a validation step necessary before presenting Djehuty to the astrophysical community, and (2) has permitted us to find and fix a number of code problems. Work on our generalized gravity algorithm identified a problem in the solver package for radiative diffusion. We performed a major upgrade of that package, and have now resumed running test cases. Coding for the generalized gravitational solver continues; testing this new physics package will begin in the next few months.

Algorithm development continues for both the physical processes and the data exploration needed for studying rapidly rotating stars and binaries. More importantly, this work has attracted a number of excellent post-docs and students to LLNL.

Generalized methods for finite-element interfaces

M. A. Puso

With the increasing complexity of finite-element models, it has become essential to mesh individual parts of a finite-element model independently such that nodes at part boundaries are not aligned. Current finite-element techniques for connecting (i.e., gluing, tying) these dissimilar meshes together at the boundary often cause serious errors in a stress analysis. Aware of this fact, engineering analysts work to avoid dissimilar meshes—often to no avail. Furthermore, the trend for teams of analysts to work independently on different weapons subassemblies makes the need for accurate dissimilar-mesh connection more acute.

The goal of this project is to solve the problem of connecting dissimilar meshes through research in accurate numerical methods that will obviate the need to produce conforming meshes. If successful, this new technology can potentially save vast amounts of time and money across the DOE Complex. For example, a large weapons model often takes a month to build, and will undergo many revisions over a matter of years. Analysts estimate that a method for connecting dissimilar meshes may save up to 25% of their time in meshing over the course of a project, without sacrificing accuracy. This project enhances LLNL's competency in computational mechanics in support of stockpile stewardship.

Recently mathematicians have developed the "mortar method" theory for connecting 2-D, flat interfaces. In FY2001, we extended the mortar method to connect arbitrary 3-D curved meshes so that optimal convergence is achieved. In this way, mesh refinement of the dissimilar mesh will have the same asymptotic rate of convergence as the conforming mesh. Consequently, the use of dissimilar meshing will not compromise the quality of a mesh.

Our FY2001 work focused on answering the following: (1) How are projections from adjacent dissimilar interfaces to be made? (2) What type of integration will be used for the numerical evaluation of the variational projection operators? (3) What Lagrange multiplier interpolation fields are to be used? (4) How will conservation of momentum be preserved?

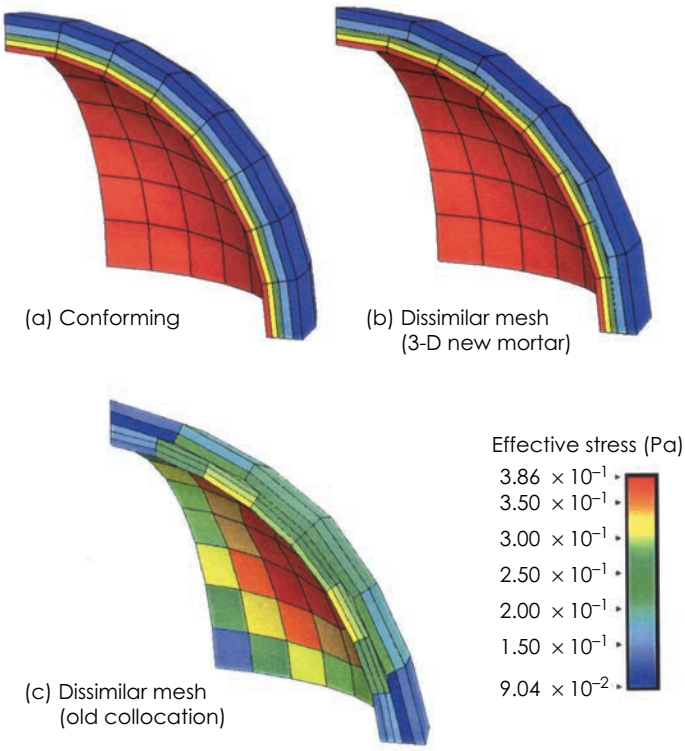

Stress contours of pressurized sphere: (a) conforming mesh, (b) dissimilar mesh (new method), (c) dissimilar mesh (old collocation method). Using our new method, the dissimilar mesh differs by only 0.29% from the conforming mesh.

In FY2001, after considering several projection methods, a simple, yet inefficient closest-point algorithm was ultimately employed. Because of the convexity of the lower-order elements, the interface surface could be easily divided into pallets and integrated using Gauss Radau rules. Several Lagrange multiplier fields were tried. So far, we obtained good results from discontinuous constant fields, but we have yet to identify that such fields are stable. Finally, we have developed a technique that can conserve angular momentum across the interface without re-orienting the mesh.

Our new methods appear to work remarkably well. For example, the Figure shows the stresses results of a pressurized sphere. Using the new method, the stresses in the conforming mesh [Fig. (a)] differ by only 0.29% from those in the dissimilar mesh [Fig. (b)]. Results with the old collocation method were off by 58%.

In FY2002, we will extend our new mortar method to higher-order element meshes and contact surfaces. Some of the simple schemes used for low-order elements will not work for the high-order elements. Furthermore, contact surface applications will require more efficient approaches. The current mortar methods are biased to one side of the interface. For contact, we would like to develop an unbiased approach so that "self-contact" problems and automatic generation of contact surfaces can be handled in a consistent manner. Our ultimate goal is a mortar-method implementation that incorporates our 3-D contact smoothing.

Higher-order mixed finite-element methods for time-domain computational electromagnetics

N. J. Champagne, D. A. White, R. M. Sharpe

MAIN TOC

Computational electromagnetics (CEM) is the most cost-effective approach for electromagnetic design and analysis and (because of safety issues) is often the only way to proceed. LLNL does not have a robust, unstructured-grid, time-domain CEM code. Although some research on mixed finite-element methods (MFEM) for time-domain CEM has been performed in academia, no commercial or government codes use this methodology. If successful, the MFEM methodology developed under this project will ultimately lead to a new electrothermal mechanical modeling capability for engineers. This project builds on LLNL's competency in computational engineering in support of the Laboratory's national security mission.

Computational electromagnetics is a core competency of LLNL. This project is aligned with the goal of developing large, parallel, complex computational modeling and simulation tools. Many applications are inherently temporal in nature (e.g., very rapid rise times), and a robust time-domain capability that scales up to the required complexity is essential. In addition, multiphysics solutions are becoming more important, and this activity is essential to facilitate close coupling with the analysis codes of other disciplines such as mechanical engineering.

Our approach is to research and apply modern, MFEM to the solution of partial differential equations on 3-D unstructured grids. In MFEM, basis functions are chosen for the various physical quantities involved so that the basis functions satisfy the associated types of boundary conditions. This has several benefits, such as proper modeling of electromagnetic boundary conditions across material discontinuities, numerical stability, and strict conservation of charge and energy. In addition, the use of higher-order approximations, which leads to problems in both finite-difference and finite-volume schemes, will enable efficient modeling of electrically large problems.

In FY2001, for implementing higher-order MFEM, we determined that it would be more efficient to use a validated, frequency-domain electromagnetics code (EIGER) than to create a comparable time-domain framework to test the new higher-order structures. (The EIGER development project is a joint activity of LLNL, Sandia National Laboratories, the University of Houston, and the Space and Naval Warfare Systems Center, San Diego.) A general-order representation for elements (segments, triangles, quadrilaterals, tetrahedrons, prisms, and bricks) has been put into the framework. The types of higher-order bases added so far include the scalar bases, curl-conforming vector bases (except for segments), and divergence-conforming vector bases of general order for elements such as triangles, quadrilaterals, and prisms.

The Figure shows the benefits of higher-order modeling in a simple CEM problem. The root-mean-square error in the radar cross section of a perfectly conducting sphere, which decreases as the number of unknowns in the basis function is increased, is most effectively reduced (lowest line in Figure) by using a fourth-order element with a second-order basis function. Here λ is the free-space wavelength of the electromagnetic radiation. Thus, the use of higher-order elements and bases can reduce the solution error while using fewer unknowns in the computational simulation.

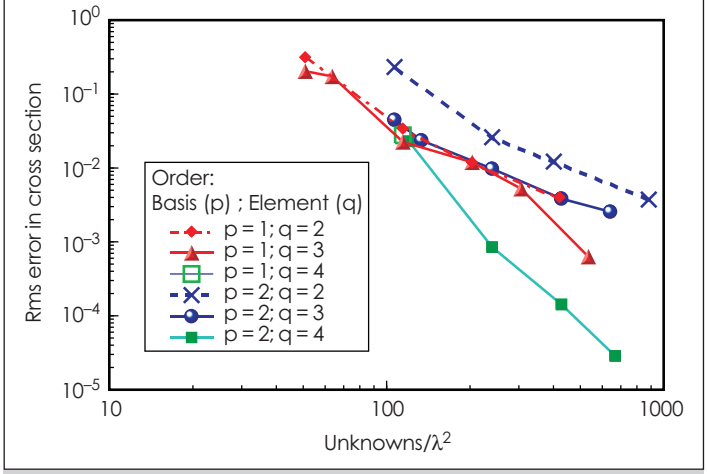

Reduction of the root-mean-square (rms) error of the radar cross section of a perfectly conducting sphere as the number of unknowns increases. Fastest convergence is obtained using a fourth-order element with a second-order basis function.

Our FY2002 work will consist of mathematical analysis and computational experiments to quantify the accuracy and robustness of the higher-order finite-element method. We plan to verify the higher-order rates of convergence for time-domain computations and investigate higher-order time-integration schemes, both explicit and implicit. Fast methods will be required for solving linear systems at every time step. We will apply the solver libraries from the LDRD project "Numerical Technology for Large-Scale Computational Electromagnetics" (00-ERD-021) to the linear systems. We will also design a framework to facilitate future changes or additions to the time-domain or solver methods. Naturally, many iterative refinements to the software will be carried out during this second year of the project.

Exploratory research into the extended finite-element method

K. D. Mish

The finite-element method has become the standard tool of computational mechanics in the national laboratory community, and it accounts for the vast majority of computational analyses performed in support of LLNL's mission. General-purpose finite-element LLNL physics codes such as DYNA3D and ALE3D represent the pinnacle of simulation-based practice in mechanical engineering.

Unfortunately, conventional unstructured finite-element applications are optimized for the design of idealized mechanical systems, whereas LLNL's Stockpile Stewardship mission (for example) is more concerned with the analysis of as-built systems. With sufficient effort, efficient mechanical analysis of such systems can be achieved with tools optimized for general mechanical design. However, the discrepancies between idealized and as-built mechanical configurations may be considerable and may, in fact, render analyses based on the former woefully inadequate. Thus, extending the domain of applicability of finite-element techniques to as-built mechanical simulations, such as those found in various LLNL programs, would be very useful. Further, given the volume of such simulations being conducted, there is a need to automate the analyses to the greatest extent possible.

Extended finite-element (XFEM) techniques provide a means for addressing the "as-built vs idealized" issues, because this family of improvements to conventional finite-element modeling permits a broader range of mechanics simulations of the actual configuration of the mechanical system. In addition, XFEM remedies some of the most onerous limitations of finite-element modeling relevant to LLNL's needs (e.g., localization and singular response near cracks and imperfections). This project will substantially extend LLNL's core competence in computational science and engineering and its capabilities in nuclear weapons engineering and manufacturing technologies in support of DOE's national security mission.

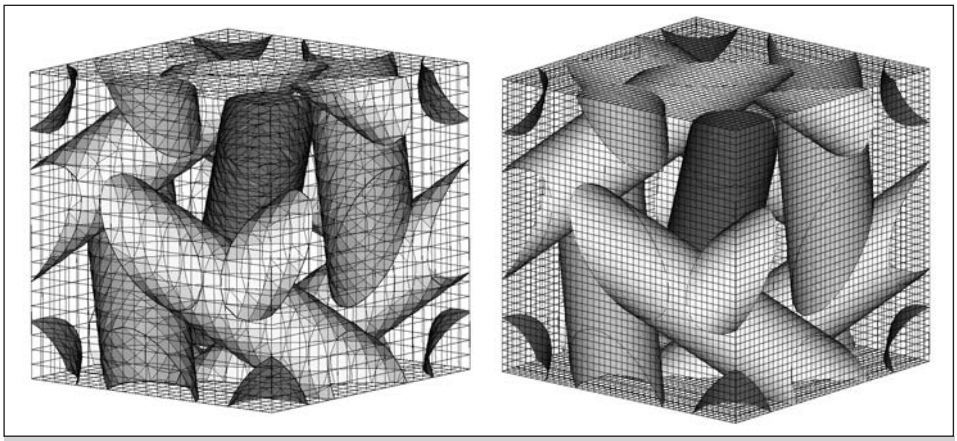

Structured, extended finite-element meshes for unit cell analyses of fiber-reinforced composites: left, coarse mesh; right, refined mesh. Such meshes require much less effort to prepare than those in conventional unstructured finite-element analyses, but yield comparable results.

Design of a scalable high-performance framework for XFEM simulations began in this project during FY2001. Although XFEM closely resembles conventional finite-element codes in many respects, substantial differences make it difficult to reuse code modules from existing finite-element tools. In addition, many of the programmatic drivers for XFEM at LLNL are oriented to manufacturing operations, which involve long-duration physics; scalable nonlinear implicit XFEM analyses, which can computationally span such long time intervals, are therefore of primary importance.

In FY2001, preliminary work also began on demonstrating the range of science and engineering problems that are amenable to solution with XFEM modeling techniques. One important case study, recently developed by our collaborators at Northwestern University, concerns the multiscale mechanical response of composite materials. This problem is attacked by decomposing a structurally anisotropic composite material into unit cells, which are the smallest components capable of representing the composition of the macroscopic material. Mechanical analysis of these unit cells, combined with consistent scale-bridging response-superposition techniques, now permit materials scientists to predict the response of engineered materials (such as composites or functionally graded materials) by standard mechanical simulation methods.

The Figure shows how structured XFEM techniques can be used to capture the unit-cell response of a fiber-reinforced composite (with fibers shown in light and dark gray). The fibers are embedded in a material matrix, which is not shown. Results obtained with the structured XFEM meshes shown agree in detail with those obtained in simulations performed using conventional unstructured finite-element techniques, but the XFEM meshes required an order-of-magnitude less effort to prepare, reducing weeks of preparation to days and providing the results largely without human intervention. This demonstrates the fundamental goal of this project—analysis automation.

Hyperspectral image-based broad-area search

D. W. Paglieroni, D. E. Perkins

From the standpoint of the national security and nonproliferation missions of the DOE laboratories, two of the most important tasks faced by image analysts are broad-area search and site monitoring. In each, the objective is to detect occurrences of targets of interest—typically, solid targets of military significance or gaseous targets such as active plume sources. In a broad-area search, large swaths of the countryside are imaged, usually once. In site monitoring, smaller areas of interest are imaged, potentially several times. To detect targets, one must compare a target's spatial and spectral signatures to signatures of pixel clusters extracted from overhead images.

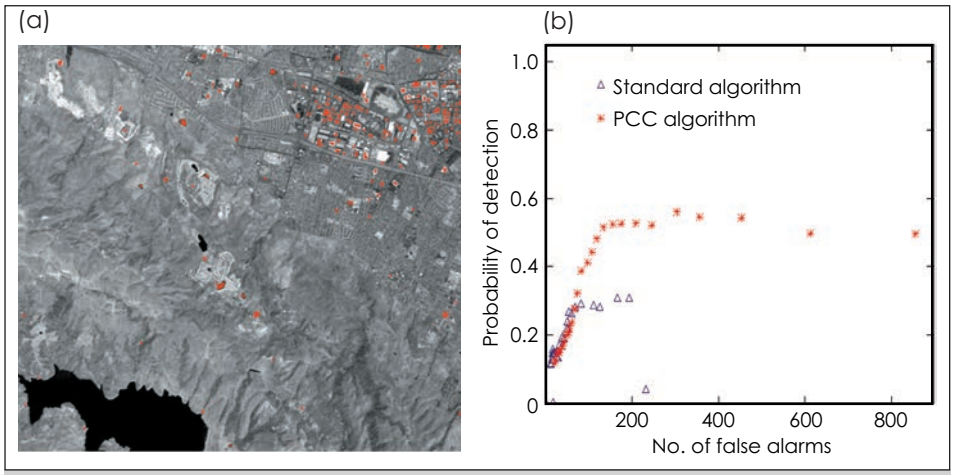

Comparison of target-identification techniques, showing (a) target cues for small, square buildings, and (b) statistical performance of pixel cluster cueing (PCC) vs the industry standard RX algorithm. In this example, PCC has the better statistical performance.

Hyperspectral images consist of hundreds of single-band images stacked on top of one another, each corresponding to a different frequency in the infrared. As such, they provide a much greater context for both spatial and spectral signatures than conventional single-band images, and are thus potentially far more useful for broad-area search and site monitoring. Unfortunately, image analysts do not always have time to prepare reports on all the conventional single-band imagery presented to them, let alone on voluminous hyperspectral imagery.

To address the analysis-throughput problem without compromising target-detection performance, it is useful to employ a model in which imagery from a broad-area cueing sensor is used to task cued sensors to acquire suspected point targets. The cueing sensor is a hyperspectral imager that operates in push-broom mode—it acquires imagery as the collection platform (e.g., an aircraft) flies. This imagery is routed to an onboard processor with algorithms that perform automatic target cueing (ATC) in real-time (i.e., at image-acquisition rates). However, available ATC algorithms are based on anomaly detectors that classify individual pixels as either "anomaly" or "background clutter." They routinely either miss too many targets or produce too many false alarms.

The goal of our hyperspectral image-based broad-area search (HIBAS) project is to develop, test, and evaluate two radically different ATC algorithms based on pixel clustering (as opposed to anomaly detection). We developed the first of these—known as pixel cluster cueing (PCC)—in FY2001. The second—known as K-Means Re-Clustering—is being developed by our collaborators at the University of California, Davis. PCC is a local-clustering (region-growing) approach, and K-Means Re-Clustering is a global clustering (unsupervised pixel classification) approach. These are opposite approaches, and the objective at this point is to compare their performance in various scenarios.

During FY2001, we acquired hyperspectral images and statistically compared target identifications obtained with PCC and with the industry-standard RX algorithm. Figure (a) shows targets identified with the RX algorithm (red clusters on a background image); Fig. (b) shows that PCC can efficiently detect more targets at a given false-alarm rate than the RX algorithm. The plots of detection probability vs. the number of false alarms are generated by varying a decision threshold; they are based on a strict metric that undercounts hits and overcounts misses, but is nonetheless useful for algorithmic comparison. Our work was presented at several conferences.

In FY2002, we plan to (1) complete the K-Means Re-Clustering algorithm, (2) augment PCC to optionally process individual spectral subbands, (3) improve our spatial signature analysis, and (4) introduce spectral-signature analysis into the ATC process. Finally, we will compare results obtained from industry-standard algorithms (such as RX) against the HIBAS algorithms in a study of ATC performance on hyperspectral imagery from a particular flight campaign used throughout the remote-sensing community for which the locations of real targets are known.

Modeling tools development for the analysis and design of photonic integrated circuits

T. C. Bond, J. K. Kallman, G. H. Khanaka, M. D. Pocha

MAIN TOC

Using photonic integrated circuits (ICs), highly compact, low-latency (subpicosecond), wide-bandwidth (terahertz), ultrafast (100 Gb/s) digital-logic and secure-information systems are feasible. However, because industry focuses on high-bandwidth, fiber-optic telecommunications, commercial software is limited to meeting a restricted suite of problems. Thus, as devices increase in complexity, new components cannot be modeled accurately using existing numerical methods. Our goal is to create state-of-the-art, user-friendly simulation resources for the design of photonic ICs.

The unique modeling capabilities developed during this project will have application to several Laboratory missions that rely heavily on photonics for secure communication and remote sensing, including advanced laser science, surveillance, stockpile stewardship, and high-bandwidth diagnostics. In addition, high-performance computing, including the Advanced Simulation and Computing (ASCI) platforms, can profit from high-density optical interconnects.

During FY2001, we focused on modeling basic, all-optical gates realized on both active and passive optical waveguides—specifically, inverter and sampling modules. Such devices are important for optical memories, high-speed switching, and routing. An inverter [Fig. (a)] encompasses the proper integration of laser gain elements with dielectric waveguides, with both optical inputs and outputs. The demonstration of such a basic function, exploiting the gain-leverage and gain-quenching effects, allows the possibility of a full Boolean-logic Technology and hence the realization of logic circuits. We generated suites of 1-D codes using analytical and numerical approaches, in both the frequency and time domains, to analyze the rate equations for multisegmented, 1-D lasing devices. We demonstrated both the gain-lever and gain-quenching effects for a two-section, voltage-controlled, Fabry-Perot edge-emitting, multiquantum-well (MQW) laser coupled to a lateral waveguide. Our time-domain codes, which include the longitudinal dependence of the parameters, are written in Java, allowing the development of a flexible, graphical user interface (GUI). Gain and modulation depth can be obtained using longer control regions and wider lasers, operating close to threshold. Also, the modulation response improves at the expense of the current, and at higher frequencies (>10 GHz) switching is feasible but level restoring is insufficient.

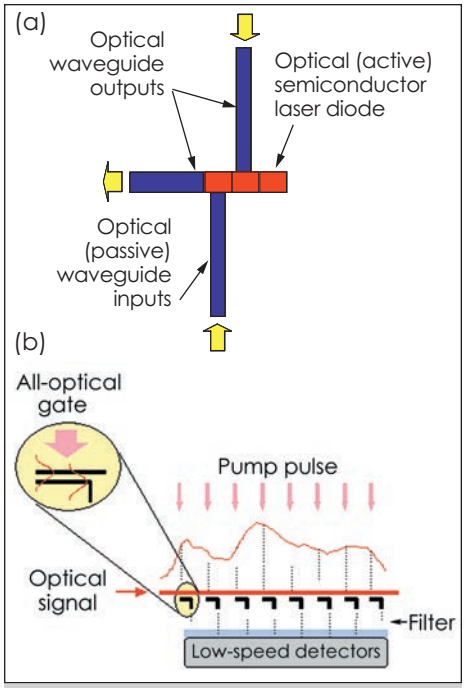

Configuration of (a) an all-optical inverter exploiting the gain quenching effect; and (b) an all-optical tapped delay line, where each sampling gate is a nonlinear directional coupler.

The sampling modules exploit third-order nonlinearities and are used in a tapped, optical-delay-line architecture [Fig. (b)] to sample sequential, short-time slices of a transient signal. This allows the use of low-bandwidth detectors to record switched time slices in parallel. We used a beam-propagation method to solve 2-D, nonlinear Maxwell equations; results matched our expectations. Analysis of the materials, such as fullerene and poly-toluene-sulfonate, is important to achieve faster speeds and reduced device size, factors that influence a final system that integrates several gates and samples subpicosecond signals. At this stage, we demonstrated the feasibility of 100% switching for a 1-ps sampling rate.

At year's end, we were examining and optimizing various parameters, such as length, doping, and mirror reflectivity, that affect the gates in the inverter and sampling modules in terms of modulation efficiency (level restoring), gain (fan-out), and time response (clock-rate).

In FY2002, we plan to enhance our design tools by including additional physical effects (i.e., spatial hole burning, wavelength dependencies, and multimode structures) and by extending the solvers from 1-D to 2-D and 2-D to 3-D, respectively, for the inverter and sampling gates. We will also continue (1) designing other devices for the final system integration, such as AND, NOR, and XOR gates, waveguides and interfaces; and (2) validating our results against experimental results.

Positrons and positronium in insulators

P. A. Sterne, P. Asoka-Kumar, R. Q. Hood, R. H. Howell, A. Bug

Positrons in insulators pose a wide range of outstanding physics questions. In metals, the theory of positrons is well established, and first-principles calculations of positron characteristics are routinely used to identify defects. In insulators—in addition to the delocalized and defect-trapped states seen in metals—the positron can also bind with an electron to form positronium, an electron–positron "atom." Because this complicated behavior is not captured in existing theories, there is no general theory for interpreting positron experiments on insulators.

In this project, we are developing a detailed quantum-mechanical description of positrons in insulators. The combination of experimental capabilities, extensive computational resources, and advanced, quantum-simulation computer codes makes LLNL uniquely suited for this project. The project's successful conclusion will create opportunities for positron annihilation to solve defect-related problems in a wide range of insulators with potential applications to a range of programs—including the Stockpile Stewardship Program and advanced laser programs.

Positronium is widely used to measure free volumes in polymers. This technique uses an empirical model that is calibrated with positron-lifetime measurements on zeolites with well-defined, symmetric pore sizes. However, this empirical model lacks a firm theoretical foundation. Asymmetric and irregularly-shaped pores do not follow the calibration for symmetric pores, and chemical effects are ignored—even though they are often significant. The widespread use of this empirical model, even when it is questionable, highlights the need for a better theory of positronium in insulators.

During FY2001, we developed a path-integral Monte Carlo (PIMC) approach for positronium in insulators with large, open-volume regions, such as zeolites. The Figure compares the electron–positron overlap contributing to positron annihilation in the empirical and PIMC approaches for the silica sodalite zeolite structure. In the empirical model, positronium is treated as a particle confined in a spherical well. The resulting positron lifetime is determined by "pickoff" annihilation between the positron and the zeolite electrons surrounding the open-volume region. Electron–positron annihilation is assumed to occur within some shell near the surface of the open volume, resulting in the overlap illustrated in the Figure. In PIMC simulations, the positronium distribution and the positron overlap with the electrons in a zeolite cage are modeled explicitly. The resulting overlap is clearly shifted towards the side of the cage. The lifetimes given by the two approaches are similar, but the regions of space contributing to the annihilations are clearly different. The PIMC simulations are therefore highly sensitive to chemical changes and asymmetries in the cage structures; they can incorporate size, shape, and chemical effects that cannot be included within the empirical model.

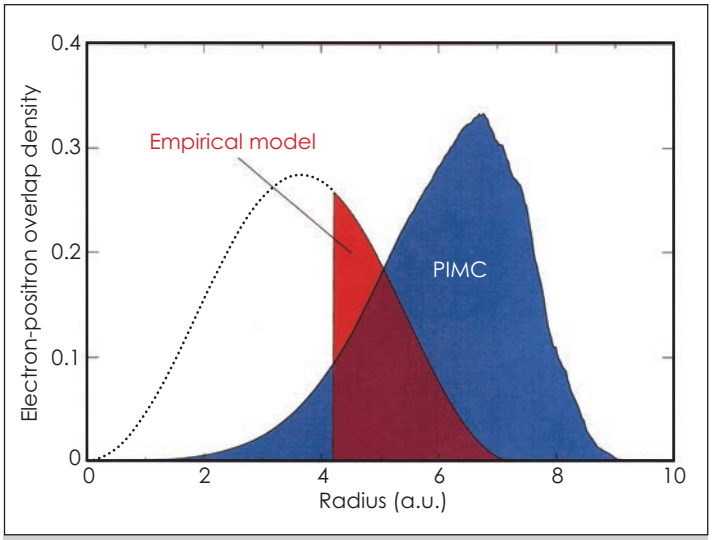

Electron–positron overlap in silica sodalite. Note the shift in overlap towards the sides of the cage in the path-integral Monte Carlo (PIMC) calculation.

We also measured positron lifetimes for a series of zeolite-y samples that are similar to sodalite, but with a larger unit cell. Initial measurements show clear trends that correlate with changes in silicon/aluminum content and with the choice of charge-compensating cation. Because zeolites are sensitive to environmental contamination, we developed a procedure to remove water and measure the samples in vacuum and under different environmental conditions.

In FY2002, we will extend the PIMC approach to more complicated systems and, to validate our theoretical model, perform positron experiments on a broad range of zeolite samples. To understand the fundamental quantum-mechanical nature of positronium in defect-free insulators, we will also implement a variational Monte Carlo approach. Close interaction with ongoing experiments will continue to guide the development of these theoretical approaches.

Smart nanostructures from computer simulation

J. C. Grossman, A. J. Williamson, A. Puzder, G. Galli

Recent rapid growth of interest in nanoscience has been inspired by breakthroughs in the production of high-quality semiconductor and metallic nanoparticles. A growing literature reports promising technologies at the nanoscale, ranging from recording devices only 1-nm across to nanomanipulation devices that could inject drug molecules directly into DNA. The ability to (1) control the critical dimensions of a single nanoparticle, and then (2) assemble multiple particles into organized structures raises the possibility of constructing a new generation of nano-electronic devices such as lasers, single-electron transistors, and photovoltaic materials. Also, nanostructures exhibit novel physical properties such as quantum confinement, Coulomb blockade, confined excitons, exciton–exciton binding, and charged excitons.

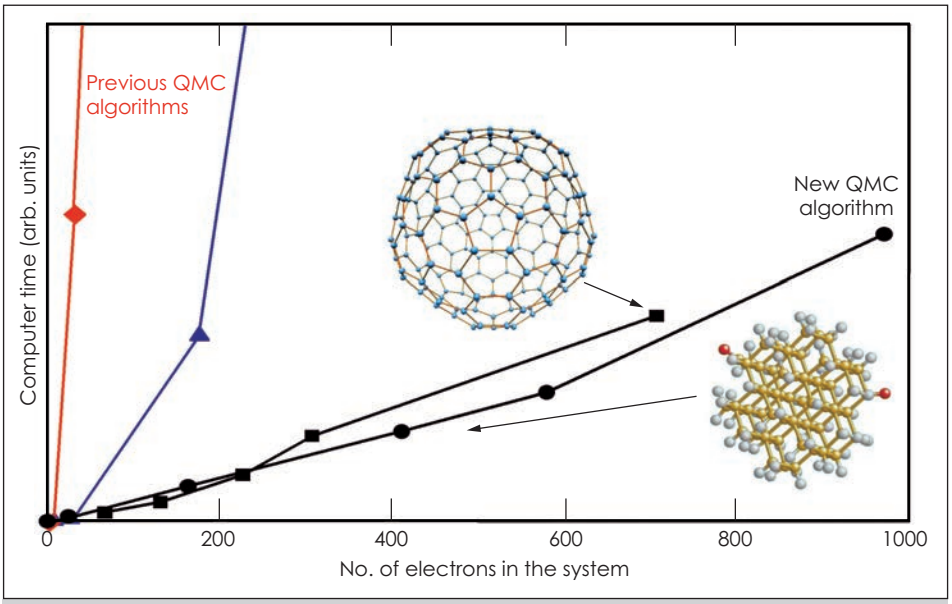

Time required to process a single step in quantum Monte Carlo (QMC) calculations. Our new approach scales linearly as the system size (diamonds, triangles, and circles are for silicon nanostructures; squares are for carbon fullerenes).

Our focus on surface structure and passivation effects, ground- and excited-state optical properties, and interactions between nanoclusters to form quantum "molecules" will (1) help interpret the spectroscopic measurements being performed at LLNL, and (2) provide information not directly accessible to experiments (e.g., effects of charging, shape changes, and different surfactant molecules on the optical properties of nanoparticles). This information is required to design smart nanostructures with tailored physical properties, a technology that will be critical to Laboratory missions in healthcare and in countering the threat of biological warfare and bioterrorism.

A significant difficulty faced by current nanostructure-simulation methods is the large range of size scales spanned by different nanostructure systems—from single nanoparticles as small as 20 atoms to 3-D arrays of nanoparticles containing several million atoms. LLNL's expertise and computational resources provide the ideal platform for bridging these length scales to provide a coherent model of the electronic properties of semiconductor nanostructures ranging from a few to one million atoms.

During FY2001, our significant algorithmic advances in quantum Monte Carlo (QMC) formalism reduced the scaling of the QMC code from scaling as n^3 to n, where n is the number of electrons. The Figure shows this new linear scaling approach applied to carbon and silicon nanostructures (a representative image of each is shown in the Figure). Previous implementations of QMC are also shown for these systems. This reduction of scaling in QMC has a tremendous impact on the applicability of this very important and highly accurate theoretical method. For example, increasing the system size from 20 atoms to 100 atoms would have taken 250 times longer for the computer to calculate with the old QMC algorithms; with our new algorithm it only takes 5 times longer. As a result, we can boost the range of problems we can address with chemical accuracy by several hundred atoms.

Using these newly developed computational tools, we have been able to address one of our primary goals in this project: to examine the impact of surface chemistry on optical properties of quantum dots. For silicon dots (from 1 to 2 nm in diameter), our results clearly demonstrate a strong dependence of the optical gap on the particular way in which the nanostructure is passivated. Further, we have explored the impact of surface reconstruction on the optical gap and found that such reconstruction also plays a key role in determining optical properties.

In FY2002, we will continue investigating three aspects of the properties of carbon, silicon, germanium, and cadmium selenide nanoparticles: (1) the structural effects of adhering different surface passivants to the nanostructure and imperfect passivation, where parts of the surface are left exposed; (2) theoretical interpretations of measured optical properties such as quantum-confined valence and conduction band edges, excitonic band gaps, and charging spectra; and (3) how the electronic states of individual nanoparticles couple when either small clusters or 3-D, close-packed arrays of nanoparticles are constructed.

Shear localization and fracture in shocked metals

G. H. Campbell, F. X. Garaizar, M. Kumar, J. S. Stölken, D. P. Trebotich

Ductile metals are used in engineering applications because of their ability to yield and deform before failure. However, under certain conditions of dynamic loading, metals can fail prematurely. This behavior is often associated with shear-localization phenomena, with shear bands acting as precursors to crack formation.

The Laboratory's defense-related missions often require an understanding of how metals respond to high-explosive (HE) loading and whether those metals fail or fracture. However, HE loading differs from the traditional ways of performing high strain-rate mechanical tests. In HE loading, first to occur is the passage of a strong, detonation-induced shock through the metal. This shock completely changes the microstructure of the metal by inducing intense dislocation multiplication, sometimes accompanied by the formation of deformation twins. This change in microstructure strongly modifies the mechanical response of the metal, changing its yield strength, work hardening rate, and strain to failure. Only after this complete change of microstructure does the metal start to deform from the action of the high-pressure HE-detonation gases. Thus, the shocked microstructure controls the mechanical properties response of the metal.

Although failure and fracture phenomena have been observed in metals for some time, modeling this behavior in a continuum-simulation code has met with very limited success. To gain a fundamental understanding of shear localization and fracture, we are conducting model experiments—using the unique capabilities of LLNL's Center for Applied Scientific Computing (CASC)—with the incorporation of new microstructure and failure models into Eulerian codes. Our multidisciplinary project closely couples modeling, simulation, and experiment. In our approach, we first determine the mechanical response and fracture properties of preshocked metals and then use experiments to guide model development. The preshocked microstructure is induced by laser-shock processing (LSP), a method that is considerably easier and less expensive than HE-driven recovery experiments.

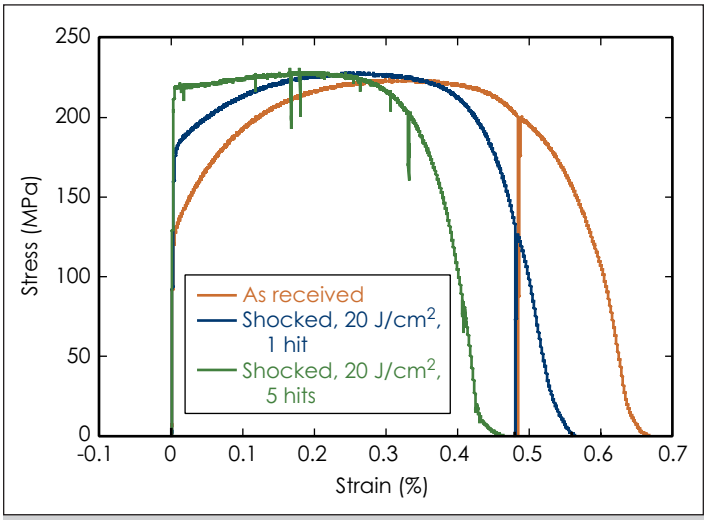

Stress-strain responses of copper samples, both unprocessed and after being subjected to two laser-shock processing (LSP) conditions.

During FY2001, we characterized the microstructures created by LSP in three materials: copper (Cu), tantalum (Ta), and Ta–W alloy. We determined the laser-fluence threshold for inducing spall (in order to avoid it) in the mechanical-test specimens. We also discovered a threshold between shock-induced plastic deformation and, at higher fluences, shock-induced twinning deformation. We measured the mechanical response of specimens subjected to LSP—a representative example from tests of Cu specimens is shown in the Figure. The effects of LSP are clearly visible on these load-displacement curves. The yield stress after LSP is nearly 70% higher than that of the unshocked material. The initial rate of work hardening (as shown by the slope of the line immediately following yield) is markedly reduced. The latter effect directly leads to instability and localization of strain. Finally, we see that the total elongation to failure is also reduced.

In our modeling effort, we performed a mathematical analysis to determine the best approach to obtaining a numerical solution of the equations of elasto-plasticity. We started the development of a fully 3-D Eulerian simulation code using CASC's structured adaptive mesh refinement application infrastructure (SAMRAI). This approach facilitates the development of code to be run on the large parallel platforms available at LLNL.

In FY2002, we will continue our experimental work by beginning fracture-mechanics tests and high strain-rate mechanical tests of LSP materials. We will also begin simulations with simplified materials models in preparation for implementing advanced, physics–based materials-response models and on internal boundary schemes for modeling shear bands and crack propagation.

Pressure-induced chemical reactivity

M. R. Manaa, D. R. Herschbach

Fundamental knowledge concerning the mechanism of high-pressure chemistry is still meager, despite its importance in determining equations of state (EOS), and elucidating structural phase transitions and chemical reactivity in condensed phases. These constitute crucial information that is particularly valuable for developing accurate models of processes under high pressure and temperature—such as those experienced by energetic materials under shock conditions. Even for the simplest of energetic materials—diatomic nitric oxide (NO)—chemical reaction rates and product formations are still unknown, and so is the first response of an explosive molecule to a sudden violent assault.

Our goal is to enhance our understanding of the basic chemistry involved in extreme-condition processes. The experimental results will be crucial to calibrating and guiding our molecular-to-mesoscale simulations of the chemistry of explosives under shock conditions. Ultimately, our work will allow the construction of chemical reaction-rate laws that can be implemented in hydrodynamics codes that will provide accurate descriptions of the properties of high explosives (HE).

In this project, we are conducting a joint experimental and computational effort to study the detailed chemistry of NO under high pressure. The experiments are conducted using a diamond-anvil cell and cryogenic techniques in combination with infrared (IR) and Raman spectroscopy. The aim is to monitor the rate of disappearance of NO and the appearance of products at a series of temperatures and pressures above and below the onset of the disproportionation reaction. High-level quantum electronic-structure methods are being used to locate equilibrium structures of stable intermediates and energy barriers for different mechanistic schemes. To validate our computational approach to other materials of interest, we are also conducting condensed-phase simulations that are identical to the experimental conditions.

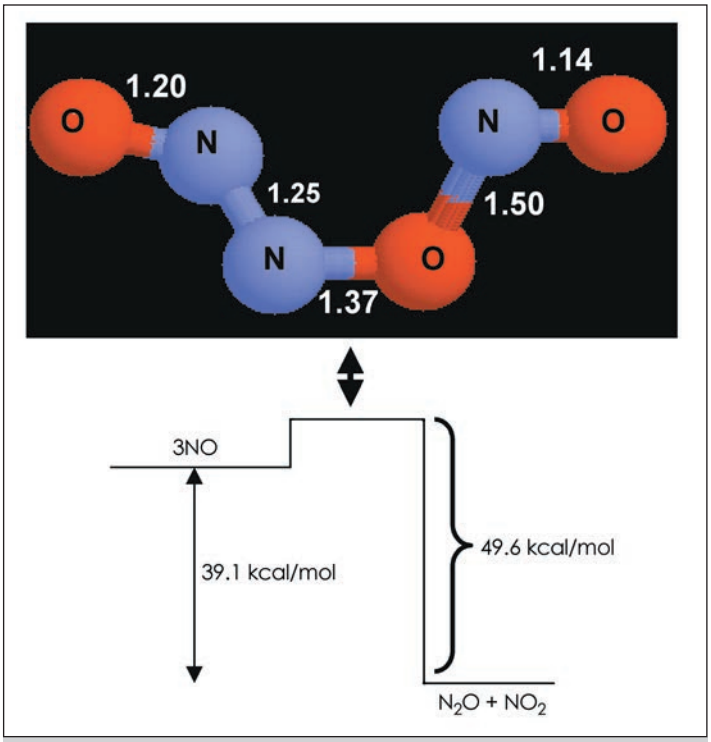

Calculated bond distances and relative energies of a stable N_3O_3 complex.

During FY2001, we implemented ab initio methods in conjunction with molecular-dynamics simulations to determine the chemical reaction rates of detonating HE. Specifically, we carried out ab initio determinations for the heat of reactions ($3NO \rightarrow N_2O + NO_2$ and $2NO_2 \rightarrow N_2O_4$) and searched for equilibrium structures of the N_3O_3 complex. The Figure shows one such stable structure that is 10.5 kcal/mol higher than the separated reactants. The Figure also displays the optimized molecular bond distances for this structure. Interestingly, this complex is located in the product channel of N_2O and NO_2. Further calculations showed the absence of any barrier toward formation of these products. We also calculated the IR and Raman spectra of this complex for later comparison with experimental results. Pending experimental confirmation, a reaction mechanism along the computational determinations suggests a gas-phase analogy of condensed-phase chemistry.

Life-performance—including long-term aging—of polymer systems with significant microstructure

G. B. Balazs, S. DeTeresa, C. Chow, P. Raboin, H. Martz, J. Caruthers

Polymeric components, although often required to function for many years, can exhibit significant performance degradations caused by a variety of mechanisms, including chemical reactions, thermal stresses, and vibration-induced fatigue. Notwithstanding these aging stimuli, engineering components must still perform to original design specifications over their intended lifetimes. Predictive models for aging behavior are needed because it is impractical to test the performance of materials and/or components over complete lifetimes, and clearly impossible to do so for new materials that have only been available for a fraction of a component's design lifetime. Current models are typically an extrapolation of historical data with the hope that the aging process is linear; rational models that acknowledge the underlying chemical and physical processes of aging are thus essential.

The development of these rational models for complex polymeric materials has enormous technological implications. These materials are (1) critical in a variety of current systems of interest to LLNL, (2) employed in numerous DOE and Department of Defense applications, and (3) being used in industrial and consumer applications worth hundreds of billions of dollars each year. The main goal of this project is *not* simply to solve the problem for one particular polymer system, but rather to develop a methodology for integrating polymer-aging parameters into modeling codes so that component lifetime can be predicted.

In FY2001, we assembled a multidisciplinary team to bridge the molecular to continuum domains. As a point of departure—and to provide a sufficiently complex material to allow the development of a research methodology extendable to other polymers—we are studying a silica-filled, porous-foam silicone polymer. This past year, four separate but linked areas of this project proceeded in parallel.

The first area of research that we completed was the synthesis of polymer samples and the determination of primary damage mechanisms. We found that these mechanisms include the removal of water from the silica filler–polymer interface and radiation-induced polymer-chain crosslinking. The second area of research was the measurement of a full suite of the mechanical parameters of the polymer, to be incorporated into the development of hyperelastic models. Indeed, experimental data from the polymer was analyzed by our academic collaborator (Purdue University) using two different hyperelastic constitutive equations. In the future, the data from the chemical damage mechanisms will be fed into these constitutive models so that these models are not simply static, but also acknowledge the molecular and microstructural aging of the material.

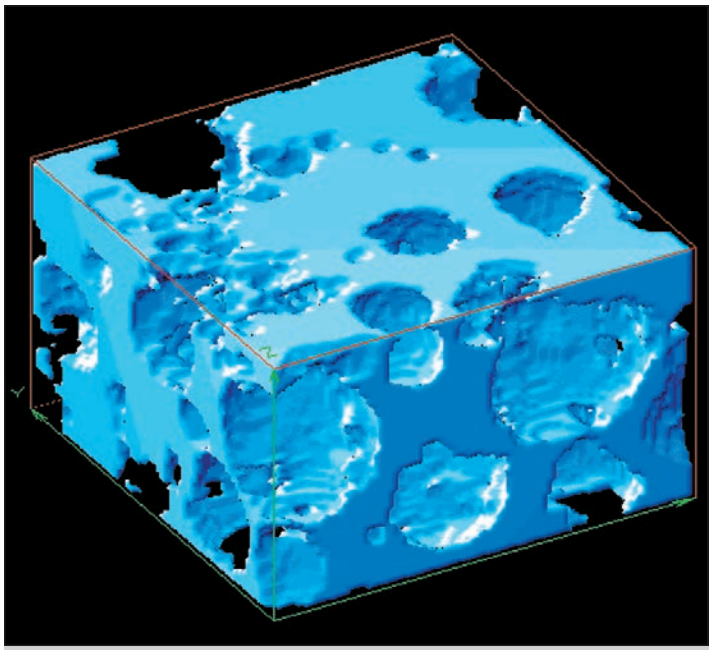

Reconstruction of polymer foam from computed tomography (CT) image data.

The third area of research was the analysis and transformation of computed tomography (CT) image data on the polymer foam (using mathematical algorithms developed for this project), including data obtained while the polymer was in a compressed state. An example of a reconstruction of image data for the foam is shown in the Figure.

In the fourth project area, we successfully incorporated a subset of this data into a finite-element analysis (FEA) code and completed a preliminary code run.

Planned FY2002 work includes refining the molecular and structural aging mechanisms of the polymer, further developing the constitutive models using these data (see earlier discussion), possibly analyzing a larger and more realistic set of CT data, and enhancing the incorporation of image data into the FEA codes.

Modeling and characterization of recompressed damaged materials

R. Becker

Ductile metals subjected to shock loading can develop internal damage through nucleation, growth, and coalescence of voids. The extent of damage can range from a well-defined spall plane induced by light shocks to more widespread damage cause by strong shocks. Because damaged materials are often part of a dynamic system, significant additional deformation can occur in extensively damaged materials. To represent material behavior in simulation codes for stockpile stewardship calculations, both the damage and the recompression processes must be modeled accurately. Currently, no experimentally based models of recompression behavior are available for use in numerical simulations.

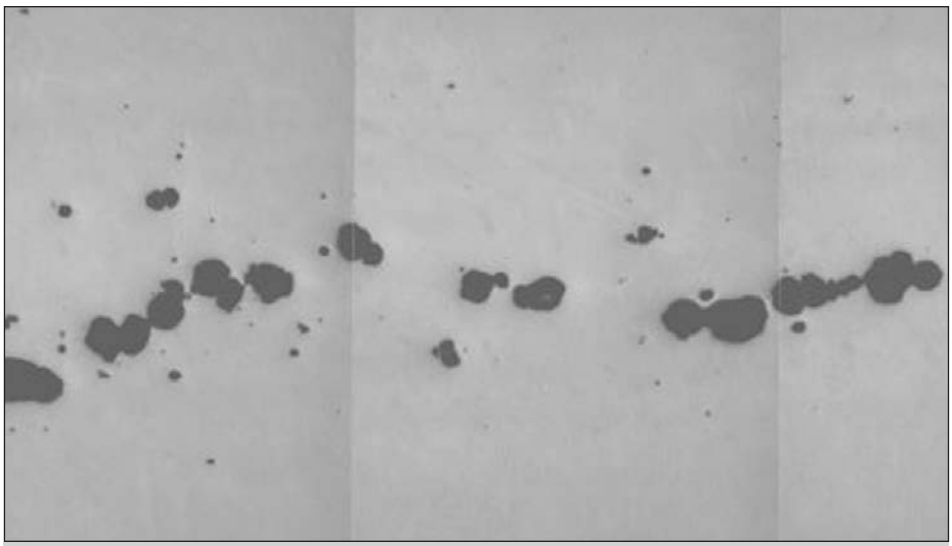

Optical micrograph of gas-gun target showing incipiently linking voids.

The goals of this project are to (1) perform recompression experiments on samples containing controlled and well-characterized damage, (2) develop a model capturing the recompression behavior and residual strength, and (3) implement the model in an Advanced Simulation and Computing (ASCI) code (ALE3D). Our recompression model, together with a failure model based on underlying physical mechanisms, will provide a more accurate representation of material behavior—information that is needed for simulations of explosively loaded materials such as those required by the Stockpile Stewardship Program.

Our experimental work has three sequential stages: (1) use a light gas gun with a soft-capture capability to create, in the gas-gun targets, controlled initial damage in the form of a spall plane, (2) measure the material response during the recompression of samples excised from the gas-gun targets, and (3) assess the residual strength of the recompressed material.

In FY2001, we used an LLNL gas gun with a newly developed soft-recovery capability to create spall damage within copper gas-gun targets. The gas-gun targets, from which recompression specimens would later be machined, were sectioned and optical micrographs were taken (see Figure). To characterize the magnitude and extent of the damage, we digitized and analyzed montages of micrographs for the volume fraction of voids. The level of damage ranged from insignificant to incipient fracture along a spall plane. From each of the gas-gun targets, we extracted four cylindrical specimens for subsequent recompression experiments. Having multiple samples with the same loading history and damage facilitates determining the effects of recompression rate as a function of damage level.

Modeling work was preformed in support of some aspects of our gas-gun and recompression experiments. First, to determine the extent of the uniformly damaged region in the gas-gun targets we simulated our gas-gun experiments using an existing damage-evolution model. This information was then used to specify the size and location of the specimens that were cut from the gas-gun targets for subsequent recompression experiments. We performed additional 3-D simulations to examine the effects of slight flyer misalignment on the induced damage distribution and on the free-surface-velocity diagnostic.

During FY2002, we plan to complete the recompression tests and to assess the residual strength of the samples by performing modified tensile experiments on them. Then, we will use data from the recompression tests either to modify an existing damage-evolution model or to develop a phenomenological representation of the recompression behavior. Finally, we will combine our model with an existing damage-evolution model in the ASCI code ALE3D for evaluation. This will be a first-cut model based on limited data, but it is a major step along the way toward developing an accurate and robust simulation capability for recompressed damaged materials.

Double-shell target design for the NIF: Noncryogenic ignition and nonlinear mix studies for stockpile stewardship

P. Amendt, J. Colvin, M. J. Edwards, L. Suter, R. Tipton

One of the central roles of the National Ignition Facility (NIF) in the Stockpile Stewardship Program is gaining an understanding of nonlinear mix in a convergent geometry. The NIF baseline, cryogenic, single-shell target provides by design a weakly nonlinear environment for hydrodynamic instability growth of outer surface perturbations. This target is tailored toward demonstrating ignition and high gain, but is not well suited as a testbed for studying highly-evolved, nonlinear mix. Double-shell targets, which could provide a test bed for stockpile-relevant studies of nonlinear mix, are commonly viewed as inherently more unstable because of (1) the absence of ablative stabilization of short-wavelength modes on the outside of the inner shell, and (2) a high-Atwood-number interface between the fuel and the dense, high-Z inner shell.

A goal of this project is to find methods for mitigating the sources of instability to the point where ignition with double-shells appears achievable. Developing a simulation and diagnostic capability for understanding highly evolved mix in such an ignition target would provide an essential role for the NIF in stockpile validation. Moreover, the dual use of double-shell targets as a vehicle towards ignition and as a testbed for stockpile-relevant studies provides a unique opportunity to study nonlinear mix under the extreme physical conditions of thermonuclear burn.

During FY2001, we made outstanding progress in the design of a double-shell target. First, we successfully carried out the first-ever 2-D integrated calculations of a hohlraum including the double-shell target. For these calculations, we used the baseline Los Alamos National Laboratory (LANL) double-shell design. We found that intense, high-energy x-ray emission from hohlraum blowoff in the region just below where the laser is absorbed had a strong impact on the symmetry of the high-Z inner shell of the double-shell target. However, we were able to satisfactorily tune away this source of flux asymmetry by moving the laser cones much closer to the hohlraum midplane. At this point, we were able to achieve ignition of the LANL double-shell design and obtain near-spherical performance.

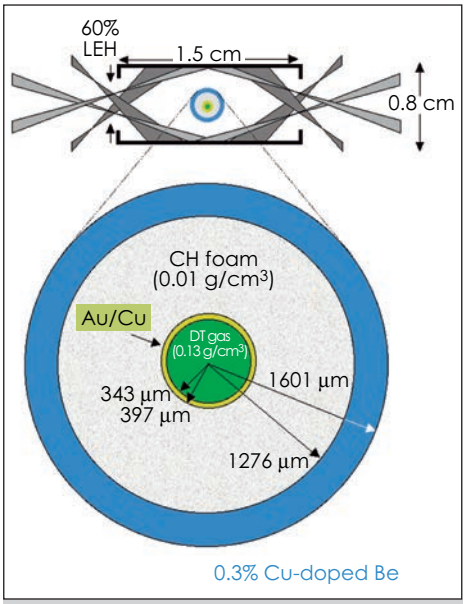

Design for a double-shell ignition target driven by a 250-eV hohlraum.

Following this success, we focused on designing a more robust-igniting double-shell target with reduced sensitivity to damaging mix. Our key improvements to the LANL design included smaller and thicker inner shells. This modification provided the shell with an overall significantly lower aspect ratio [see Fig. (a)], which reduces the effect of perturbation feedthrough from the outer surface to the inner surface of the inner shell. Calculations with the hydrodynamics code CALE and implementation of the Ramshaw nonlinear-mix model both suggest that our baseline design has increased the possibility of achieving ignition on the NIF with double-shell targets.

In FY2002, we expect our research to evolve towards designing an appropriate experimental program on the Omega laser at the University of Rochester to validate our nonlinear-mix models. We have proposed a five-target series on Omega to investigate double-shell implosion physics. Although detailed specifications of the proposed targets are still evolving, our goal is to mimic the NIF double-shell ignition design in as many relevant aspects as possible despite the energy limitations of the Omega laser. During this startup phase of experimentation, we will also investigate target-fabrication issues and continue using CALE for nonlinear-mix simulations of double shells. Optimization strategies for the double-shell design will evolve as more experimental data become available and as our stability calculations mature.

Overcoming the memory wall in symmetric multiprocessor-based systems

B. R. de Supinski, A. Yoo, S. A. McKee, F. Mueller, T. Mohan

The time to access main memory dominates the performance of large-memory codes that are typical of production computing at LLNL. This leads to poor central processing unit (CPU) utilization because main memories are orders of magntiude slower than CPUs. Worse, Moore's law indicates that this "memory wall" problem will increase over time.

This project focuses on improving memory performance in symmetric multiprocessors (SMPs) through dynamic access ordering (DAO) mechanisms. DAO mechanisms—techniques that change the order of memory accesses from that generated by the issuing program—have shown significant promise for alleviating this problem. These techniques combine simple compiler modifications with run-time mechanisms to exploit memory-hardware characteristics such as interleaved memory banks and hot-memory pages.

Previously, researchers have focused on techniques for uniprocessor systems with special-purpose hardware. However, SMP systems need DAO mechanisms that consider the additional memory-access issues (e.g., cache coherency) that arise in the multiprocessor systems in use at LLNL. The goals of this project are to: (1) extend DAO mechanisms to SMPs using hardware commonly available in existing systems, (2) measure the performance of this implementation in existing systems, and (3) determine the performance cost of using existing hardware through simulations that explore minimal hardware modifications that would efficiently implement our techniques. Our SMP-aware DAO mechanisms will decrease the run times of large-memory LLNL codes by increasing the effective memory bandwidth and decreasing or masking memory latency. If successful our results will lead to significant decreases in the run times of many of LLNL's simulation codes that are essential for the Stockpile Stewardship Program.

During FY2001, using new tools that we implemented for this project, we gathered input data for our analytic model for UMT, a 3-D neutral particle transport code for unstructured meshes used at LLNL. These tools demonstrate that the access patterns of UMT are highly irregular and are not well suited to traditional memory system optimizations such as hardware prefetching. Further, parallel memory microbenchmarks that we implemented demonstrate that the linear extrapolation of single processor memory performance does not adequately capture the expected memory system performance for codes with access patterns like that of UMT on SMPs in use at LLNL.

Two of our FY2001 milestones were selecting our experimental system and deciding what hardware we would use to implement our techniques. We established a collaboration with SRC Computers that includes the use of their SMP computer in Colorado Springs. Because this computer's memory controllers and cache coherence controllers are implemented with field programmable gate arrays, we can implement our techniques directly in hardware at reasonable cost. In FY2001, we implemented a simulation of this SMP.

In FY2002, we will modify our SMP simulation to model SMP-aware DAO techniques on the SRC hardware. We will then implement the first SMP-aware DAO techniques and refine the techniques on the basis of our initial results.

Eventually, we will investigate the performance of SMP-aware DAO techniques in the presence of message-passing memory traffic. This traffic can require significant memory-system bandwidth and may have an impact on the value of DAO techniques for the clusters of SMPs that are commonly in use at LLNL. We also plan to explore techniques that extend DAO techniques to computer-based systems that use system on a chip (SOC) and processor in memory (PIM) technologies, important emerging trends in computer architecture that are likely to be used in future LLNL systems.

First-principles molecular dynamics for terascale computers

F. Gygi, J. L. Fattebert

First-principles molecular dynamics (FPMD) is emerging as a very powerful atomistic simulation approach that combines a classical description of nuclei with a quantum mechanical description of electrons. Recent advances in electronic structure methods, notably density functional theory (DFT), have made FPMD a truly predictive approach that provides information on the structural, dynamical, and electronic properties of a physical system. FPMD has been successfully applied to several areas of research at LLNL in materials science, chemistry, biochemistry, and nanotechnology.

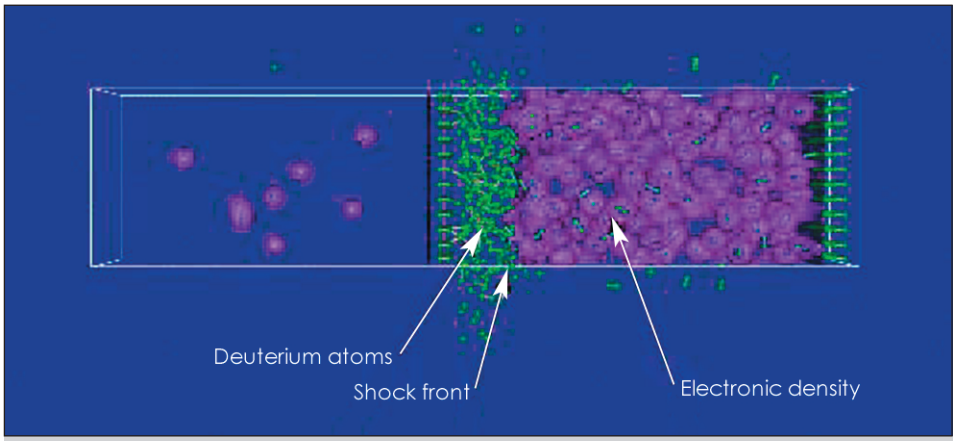

Snapshot taken during a simulation of shock propagation in liquid deuterium, showing the formation of a shock front on an atomic scale. Deuterium atoms are green dots; the electronic density is represented by a dark-red isosurface.

Because of the detailed description of electronic structure that is required, the computational cost of FPMD simulations is high. This makes it necessary to use supercomputers for any FPMD simulation involving more than a few tens of atoms. Being able to run large-scale FPMD simulations on terascale computers will allow simulations to get one step closer to experiments by providing important data that either complement experimental results or replace difficult experiments. The Stockpile Stewardship Program will be a major beneficiary of these enhanced simulation capabilities.

We are developing scalable FPMD software for use on the large parallel computers installed at LLNL and on future terascale computers. Straightforward implementations of FPMD incur a computational cost of $O(N^3)$ for N atoms (where O stands for "on the order of"). More recent approaches have been shown to reduce this cost to $O(N)$ (or linear scaling) for simplified models. Our approach is twofold: we are working on (1) new algorithms to make the conventional $O(N^3)$ approach more efficient on large parallel computers, and (2) $O(N)$ algorithms through the development of two FPMD codes. One code is JEEP (an implementation of a conventional $O(N^3)$ algorithm); the other is MGmol (a finite-difference, real-space, multigrid-based implementation of a linear scaling algorithm). To maximize portability, the software (being written in C++) implements parallelism through the message-passing interface (MPI) and the OpenMP standard.

During FY2001, we completed a mixed MPI/OpenMP implementation of the JEEP code, with specific focus on the use of the symmetric multiprocessor (SMP) nodes of the Advanced Simulation and Computing (ASCI) White computer installed at LLNL. Our analysis of computational bottlenecks led to a reduction of simulation time—we can now simulate 1320 atoms on 165 nodes of the ASCI White platform in less than 40 s/iteration. This improved efficiency made it possible to run the first ab initio simulation of the propagation of a shock in liquid deuterium (see Figure), which revealed details of the electronic properties of the shock front as yet unexplored. In particular, we found that electronic excitations occur at the shock front.

Other new features added to the JEEP code allow for new types of simulations: (1) inclusion of spin-polarization; and (2) implementation of the Mermin functional formalism, which allows for the simulation of excited states and metallic systems. The JEEP code was also successfully ported to other platforms [IBM-SP, Compaq TeraCluster2000 (TC2K), and Linux]. Our major work on the MGmol code included the addition of mixed MPI/OpenMP parallelism and porting the code to the IBM-SP and TC2K platforms. We also obtained important performance improvements by designing a C++ interface to the Scalable Linear Algebra Package (ScaLAPACK) library of distributed linear algebra.

Our work has been published in a number of refereed publications.

In FY2002, we plan to develop intermediate-level parallelism in the JEEP code for use on very large parallel computers (more than 4000 central processing units—CPUs). We will also pursue the development of the MGmol code and use it to achieve linear scaling.

Foundations for petaflop computing

M. K. Seager, K. J. Minuzzo, S. P. Vernon, H. E. Jones

Over the next decade, the computational demands of stockpile stewardship and other applications of national interest, such as computational biology, will far exceed the capabilities that will be achieved through the Advanced Simulation and Computing program, with its goal of 100 teraFLOP/s computing speeds. A large class of stockpile stewardship problems cannot make efficient use of the memory-cache architecture of commercial state-of-the-art microprocessors. In the worst cases, this memory bottleneck limits computational performance to 3% of available microprocessor performance. Furthermore, the speed difference between processors and memory is widening. New technologies and system architectures are required to address this "distance-to-memory" problem and to enable petaflop computing before the year 2010.

For FY2001 the focus of this project was on solving the distance-to-memory problem by doing fundamental research to develop low-temperature silicon (Si) processing technologies that permit fabrication of magnetic memory structures directly on top of microprocessors, and on simulating the computational performance of the resulting system architectures to predict the benefit of this technology on codes for stockpile stewardship and other LLNL missions.

Our research on device physics is focused on two areas. First, we are developing low-temperature Si processing technology using pulsed ultraviolet (UV) lasers to crystallize amorphous thin-film Si layers and electrically activate *p*- and *n*-type dopant materials to form vertically integrated *p*–*n* junction and Schottky barrier diodes. Second, we are developing microfrabrication technology to vertically integrate the diodes with magnetic random accesss memory (MRAM) elements based on magnetic tunnel junction (MTJ) technology. The integrated devices can be used as building blocks to form high-density, electrically switched MRAM arrays directly on top of a microprocessor (see Figure).

We have measured the effect of laser fluence and pulse sequence on the structure and transport properties of doped and undoped amorphous Si films from 75 to 150-nm thick. On/off ratios were obtained of 10^3 in vertical *p*–*n* junction diodes formed in 100- and 125-nm Si films, but the devices have significant leakage. We believe that the low on/off ratio (10^9 is required) is due to grain-boundary conduction, which will be reduced by improving the uniformity of the laser illumination. We are replacing the excimer laser with a solid state laser with better uniformity of illumination and better pulse-to-pulse repeatability. Technical effort in FY2002 will concentrate on using the upgraded laser system to develop a sequential lateral solidification process for growing large-grain crystalline films and developing integrated diode–MTJ arrays with submicrometer feature sizes.

To evaluate and predict the computational performance of scalable scientific algorithms on existing and future computer architectures at LLNL, we have established a systems modeling and simulation capability leveraging expertise at the University of Texas. Our focus has been on assessing how MRAM technology could be used to improve the performance of core algorithms that exhibit marginal performance on state-of-the-art computer architectures. This will be done by profiling and characterizing several core algorithms known to exhibit poor cache performance and assessing how microarchitecture changes influence the algorithm's performance.

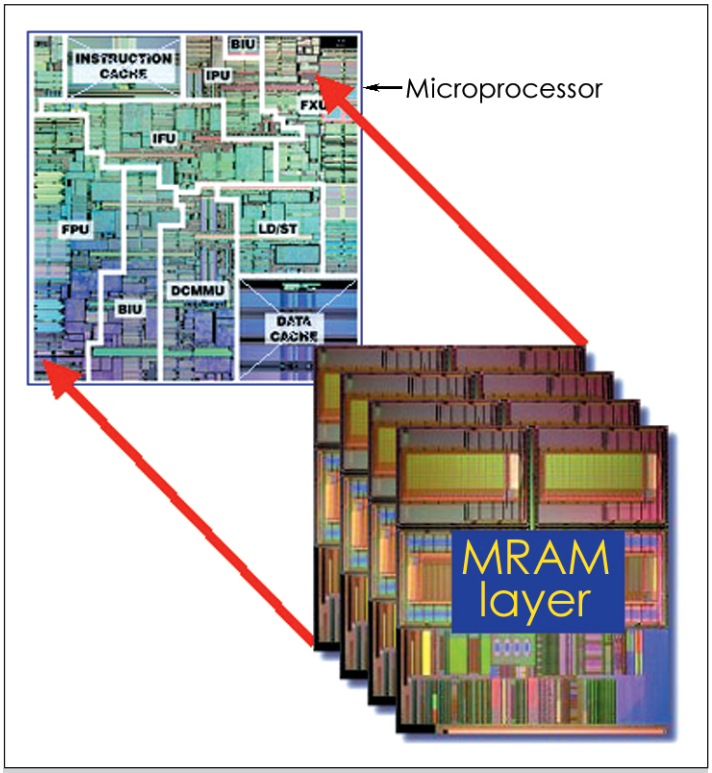

Vertically integrating a diode with an magnetic tunnel junction makes it possible to stack multiple magnetic random access memory (MRAM) layers directly on top of the microprocessor.

Using the profiling and simulation infrastructure, we have documented the predominant memory latency effects for our targeted applications over various workloads. We have also done sensitivity analysis of these applications to combined adjustments of Level 1 and Level 2 cache parameters, and find that performance improvements of factors of 10 or more can be achieved. This work is preliminary. Further study is needed using our simulator, which can instrument the dynamic execution context. This will eventually be used to drive initial designs of an MRAM model. In FY2002, we will combine the efforts of our technology scalability studies and algorithm characterization in order to produce several candidate MRAM-based designs optimized for characterization of scientific applications.

Computational methods for collisional plasma physics

D.W. Hewett, A. B. Langdon, D. J. Larson, B. F. Lasinski, C. H. Still

High-intensity lasers and particle beams are used to probe material properties or drive inertial confinement fusion implosions, which produce very energetic, high-temperature plasmas. Understanding these plasmas requires self-consistent electromagnetic field computation. Though recent advances in technology demand modeling capability at ever higher energy densities and fluxes, present modeling capability of such plasmas is well developed in only two limits: (1) collisionless configurations in which the plasma is so energetic that the individual particles travel distances comparable to or greater than the target spot before colliding with another particle, and (2) collision-dominated configurations in which the particles have very small mean-free paths between collisions. We are building a new modeling capability that will bridge the gap between these limits to support long-pulse (nanoseconds) and short-pulse (subpicosecond) high-intensity laser experiments. Such tools play an essential role in understanding and harnessing high-energy-density physics phenomena—an ongoing subject of LLNL research for stockpile stewardship.

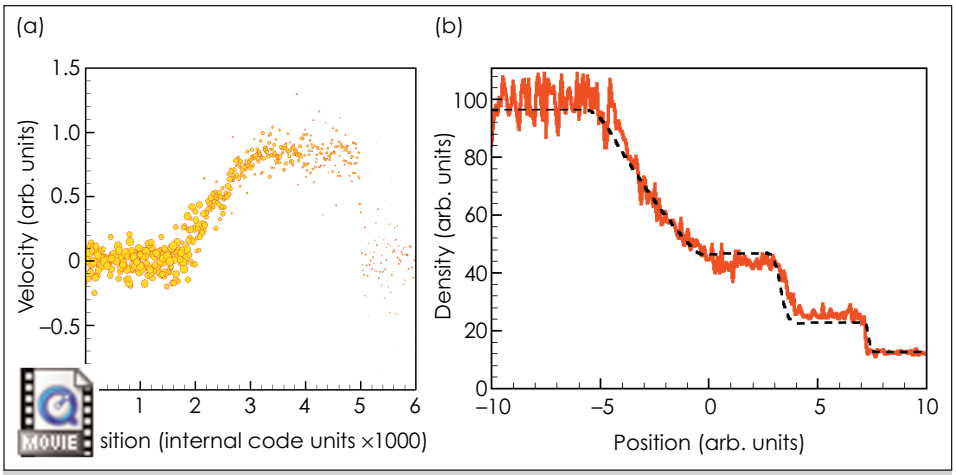

Using particles created with our new computer model, KEYDRO, we have successfully reproduced the density profile of the standard hydrodynamic code solution for the Sod shock-tube problem. (a) Particle velocity vs. position plot of KEYDRO particles in the problem; (b) the density profile derived from these KEYDRO particles (solid line) closely matches the density profile of the hydrodynamic solution (dotted line).

Our research is progressing on two fronts. First, we are modernizing and enabling new versions of collisionless models for massively parallel processing (MPP) of our 3-D particle-in-cell (PIC) capability, for use both as a platform to develop partially collisional algorithms and as a simulation tool. PIC is a collisionless, kinetic model that easily simulates long mean-free-path particle trajectories by stepping particles forward in time in electromagnetic fields generated from the space charge and electric current of the particles themselves. During FY2001, routines essential for algorithm extension to MPP 3-D PIC were developed, and early proof testing of the needed collisional extension to particle dynamics is underway.

The second thrust continues development of a new model that borrows concepts both from the collisionless, kinetic capability of PIC and the fluid algorithms that work well in the collision-dominated regime. Our new computer model, kinetically extended hydrodynamics (KEYDRO), attempts to retain the strengths of each. Like PIC, KEYDRO assigns a mass and net charge to each macro particle, which is allowed to thermally move about in the self-consistent electromagnetic field. Unlike PIC, each KEYDRO particle then carries additional thermodynamic information. These particles are fragmented, yielding numerous additional, smaller particles that probe for emerging features. Subsequent merging eliminates redundancy and provides economy in regions where new features fail to appear.

In FY2001 we developed data structures essential to particle handling and the mathematical underpinnings of fragmentation in both space and velocity. We demonstrated the ability to fragment and merge KEYDRO particles in the collisionless limit without loss of kinetic details. Further, we discovered that collision-dominated, fluid physics can be accommodated consistently with the existing fragmentation and merging capability. This led us to investigate the collision-dominated region. Shock-tubes provide validation for our now collision-dominated model by allowing comparison with both analytic solutions and well-validated experimental tests. A shock-tube is a cylinder with gases, dissimilar in density and temperature, which are initially separated by a thin membrane. When the membrane is broken, a shock wave propagates into the low-density region and a rarefaction wave propagates back into the high density. As the Figure illustrates, we have successfully used KEYDRO particles to replicate the characteristic density profile produced by the standard hydrodynamics code solution of the well-known Sod shock-tube problem.

In FY2002, our MPP 3-D PIC code effort will focus on implementing and testing a collision algorithm. We plan to (1) simulate laser–plasma instability problems in which the effects of finite collisionality are expected; and (2) model current experiments to provide validation. The KEYDRO effort will focus on developing a partially collisional algorithm within this new modeling paradigm.

Study for a novel multilayer mix experiment

T. A. Peyser, T. R. Dittrich, D. P. Rowley, K. S. Budil

Turbulent mixing of materials under the influence of an acceleration or caused by the passage of a shock is a major area of research both in the scientific community and at LLNL. Acceleration or shock-induced hydrodynamic instabilities play an important role in astrophysics, in inertial-confinement fusion, and in defense applications. Many experiments in classical fluid dynamics and at high-energy-density laser facilities have been designed to study these problems. However, both experimental approaches have had significant drawbacks. Typically, the classical fluid-dynamics experiments are limited to relatively low accelerations and weak shocks, and—in order to achieve high accelerations—the high-energy-density laser experiments are limited to small physical scales and low-Z materials.

In this project, we conducted a computational study to assess the feasibility of using a high-explosive- (HE-) driven, multiple-collision accelerator to study turbulent mixing of two dissimilar materials. Our goal was to determine if the large-scale and unique geometry of the multiple-collision accelerator would permit the study of several sources for hydrodynamic instabilities that are not directly accessible with existing experiments. Our research has direct relevance to the Laboratory's stockpile stewardship mission.

Although extensive calculations and experiments have investigated the use of multiple-collision accelerators for other purposes, none have studied the physics of turbulent mixing. We carried out a program of calculations to determine if this technology could be adapted to the issue of turbulent mixing. To determine the scaling of the proposed experiment to the phenomena of interest, we performed 1-D calculations using existing Laboratory hydrodynamic computer codes. The scaling was based on nondimensionalizing the gas-dynamic equations—while assuming that the viscous, thermal, and radiative transport were negligible. This results in the well-known Mach number scaling relationship that relates the length, time, pressure, and density between a proposed experiment and the phenomena the experiment is intended to simulate.

We began our initial investigations by restricting the HE driver of the experiment to configurations and geometries already tested and fielded at LLNL. This established an outer dimension for the problem and a total amount of available drive energy. In a multiple-collision accelerator, conservation of momentum implies that an object of large mass moving with large velocity can impart a significant increase in velocity to an object of smaller mass when the two undergo a collision.

We found that a four-object system undergoing multiple collisions did not impart a sufficiently high velocity to the final mass for us to satisfy this required scaling relationship. In the final collision, the energy of the collision was not large enough to result in shock heating of the fourth mass to a temperature above the melt curve of the materials under investigation. In a six-object system, however, the energy in the final collision was sufficient to result in melting of the final mass, thereby making it meaningful to consider the use of this technology for fluid-dynamic experiments.

At the end of the project, we concluded that this HE-driven, multiple-collision accelerator technology should be considered for fluid-dynamic experiments. Further calculations would be necessary to optimize the dynamics of the system and to determine the diagnostic requirements for any proposed experiments.

Seismic arrays track armor

D. B. Harris, S. C. Larsen, D. B. McCallen, D. W. Rock, J. P. Lewis, D. H. McMahon, J. L. Levatin

Several important military and surveillance applications require imaging structures or tracking vehicles through geologic media of poorly known but presumably heterogeneous structure. Passive and active seismic methods are among the most promising techniques for solving both of these problems. Many past attempts at imaging and tracking using seismic methods yielded poor results because of insufficient attention to characterizing the propagation medium or to adapting algorithms to handle large uncertainties in medium parameters.

In this project we are examining two problems: tracking vehicles on the battlefield with passive surface seismic sensor arrays (essentially a 2-D problem) and delineating underground structures with signals obtained with passive or active methods using similar arrays (a 3-D problem). Passive methods use signals originating in the vehicle or structure; active methods use surface sources (e.g., explosions) to generate signals that are reflected from the structure. The simpler tracking problem was our FY2001 starting point. Our initial work demonstrated a basic capability to track individual vehicles with two arrays. We found that measures to suppress the sensitivity of tracking algorithms to uncertainties in the velocity of the propagation medium are required even in fairly homogeneous media. The more complex structure-imaging problem will be the principal subject of our work in FY2002.

We take both empirical and model-based approaches to solving these problems. Small-scale field trials, such as the tank-tracking exercise discussed below, provide data to test means for characterizing geologic media, to characterize representative media, and to test tracking and imaging algorithms. Computer models generate synthetic data for more realistic, larger-scale problems to determine (for example) the best configuration and number of sensors for detecting or mapping an underground structure. The models are being built on E3D, an established LLNL 3-D full-physics elastic wave propagation code. We plan end-to-end validation of these models by simulating data from field trials.

We developed basic software to support tracking and imaging applications. The software includes a matched-field processor for vehicle tracking, a framework for vehicle simulation (developed as a preprocessor for E3D to drive the code with equivalent seismic sources), and initial work on a 3-D topography capability for E3D, essential for simulation in varied terrain. The matched-field processor borrows an idea from antisubmarine warfare, in which a target is tracked by comparing the data received by a sensor network with a large number of sound fields predicted by a model for a corresponding number of potential target locations.

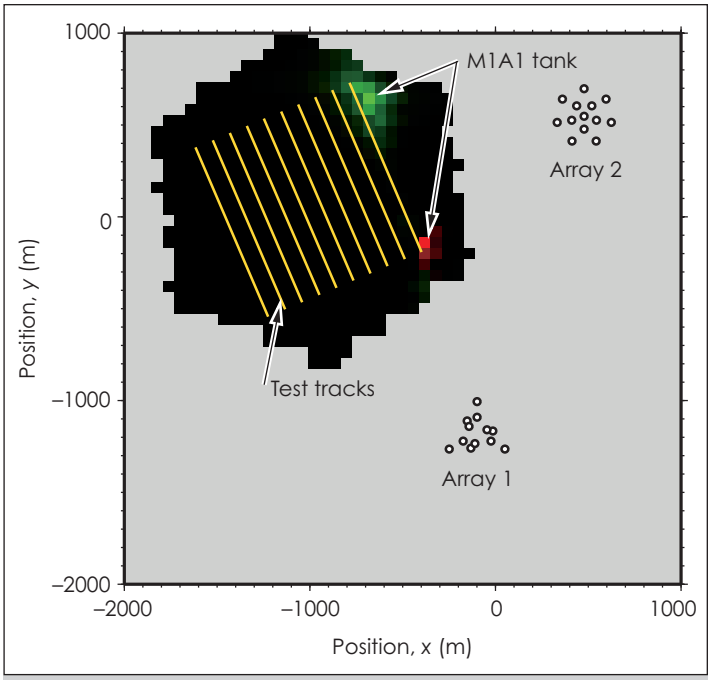

The matched field processor for vehicle tracking correctly locates a moving tank at two separate instants in time using data from two seismic arrays.

In June 2001 we carried out a vehicle tracking experiment at the Nevada Test Site (NTS). Two M1A1 tanks, provided by the Nevada Army National Guard, were driven singly and in pairs along test tracks. Two arrays were deployed nearby, one with 12 and the other with 13 research-grade seismic sensors (see Figure).

The Figure shows a detection statistic that is large (bright) where the tank is most likely to be. The first snapshot (red) was taken as the tank began moving along a track; the second (green) was taken a few minutes later as the tank approached the end of the track. Our results suggests the feasibility of tracking such vehicles with sensor arrays distributed at intervals of several kilometers in highly attenuating geologies; less dense networks may suffice in rock. Matched-field processing is applicable to this problem when modified to account for uncertainties in medium velocity. The computational loads appear tractable; the calculations with two arrays can be carried out approximately ten times faster than real time on a Sun Ultra 10 workstation. Location accuracies of 100 m appear possible with inter-array spacings of about 2 km.

In preparation for our work in FY2002, we evaluated several locations at the NTS and elsewhere for passive and active data collection above underground structures. In FY2002 we will complete vehicle tracking work, extend simulations to buried-structure problems, modify our matched-field processor for imaging underground structures, and collect data to test simulation and imaging algorithms.

Mesochem: Chemical dynamics on a mesoscopic scale

L. E. Fried, D. I. F. Calef, C. J. Wu

This project is developing a new modeling capability in the area of soft-matter dynamics. The term "soft matter" has arisen in the physics community to describe systems where (1) diffusion, hydrodynamics, and possibly chemical reactions are strongly coupled; and (2) the dynamics involve domains between 10 nm and 1 mm in diameter. This definition includes a broad range of physical and chemical systems such as polymers, liquid crystals, droplet formations, emulsions, and cellular structures. As a matter of rapidly growing scientific interest in soft-matter dynamics, *Physical Review E* has recently added "Soft Matter Physics" to its subject list.

Clearly, there is also appreciable interest in soft matter throughout LLNL programs, particularly because the aging and constitutive behaviors of soft-matter systems affect Stockpile Stewardship Program concerns such as materials aging and high-explosives (HE) detonation. For example, the particle size and shape of pentaerythritol tetranitrate (PETN) HE strongly affects its shock-initiation characteristics. A recent micrograph of material from a heated PETN detonator as it penetrates a silicon substrate shows a microstructural evolution into fractal geometries. These effects are also present in PETN that is aging under ambient conditions, where the grains grow and shrink (recrystallize) by exchanging mass through gas diffusion.

Other soft matter used commonly at LLNL includes foams, pads, cushions, and adhesives. Many new, advanced materials under development at LLNL, such as nanostructured energetic materials and aerogels, are also soft matter. Although LLNL has a world-class ability to model material properties on the atomic and macroscopic scales, the structures characteristic of soft matter occur between these two limiting regimes. Our present ability to model the aging and dynamical properties of soft-matter systems is quite limited.

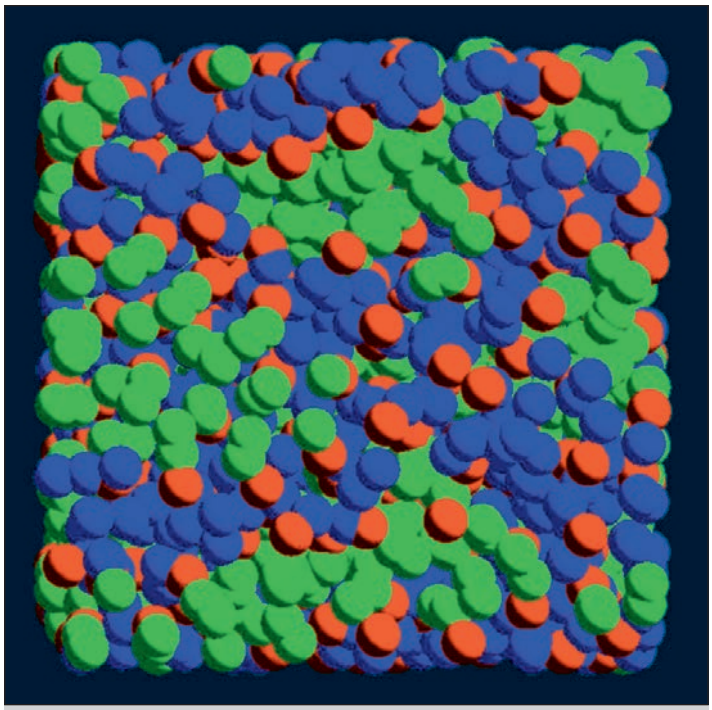

Simulated phase separation of an AB2 polar chain molecule (red and blue spheres, respectively) in a solvent (green spheres). Dissipative particle dynamics (DPD) can find phase separations much more rapidly than can conventional molecular dynamics (MD).

In this project, we are developing Mesochem—a flexible code for modeling chemical reactions in soft matter on the mesoscopic (from 10 nm to 10 mm) scale. Mesochem will help LLNL address a wide range of programmatic challenges, while generating a scientifically unique model of nanoscale-to-mesoscale matter.

In FY2001, we completed the first stage of the development of the full Mesochem code. We derived equations that incorporate chemistry into dissipative particle dynamics (DPD) while preserving the simplicity and desirable physical properties of ordinary DPD and implemented these equations in a DPD program. We (1) validated the program against results published in the literature, (2) performed calculations for mixing and demixing of fluid mixtures, and (3) demonstrated that the Mesochem code can correctly model amphiphilic (head-tail) molecular mixtures commonly found in soaps and biological membranes. The Figure shows the results of a DPD simulation of amphiphilic molecules in a solvent.

In FY2002, we will begin extending the DPD code to include the chemical reactions of nanoscale energetic materials. These will be the first simulations in which a rigorous, mesoscale theoretical approach is combined with chemical reactivity. We also plan to determine the feasibility of an ab initio Mesochem that couples information obtained from atomistic simulations into the chemical DPD framework.

Fermion Monte Carlo

M. H. Kalos

This research offers a major advance in our capability to use exact Monte Carlo methods for solving the Schroedinger equation for many-fermion systems. The Schroedinger Equation for many-fermion systems has been under study for six decades, but no accurate methods have emerged without uncontrolled approximations. The key difficulty is that of dimensionality: a 20-electron system is described by a partial differential equation in 60 dimensions; traditional numerical methods fail in this high-dimensional space. Monte Carlo methods have been impeded by the "Fermion Sign Problem," i.e., wave functions must be antisymmetric in the exchange of identical particles. The standard Monte Carlo approach exploits the fact that the Schroedinger equation in imaginary time is a diffusion equation, which is local, but the Pauli exclusion principle imposes a nonlocal boundary equation, a profound impediment to Monte Carlo methods. The solution to the fermion problem has been one of the major unsolved problems in computational quantum mechanics.

Our research in fermion Monte Carlo at LLNL over the last year and a half has demonstrated a new class of methods capable of overcoming this difficulty. The central idea of the new method is the use of correlated random walks for objects that carry algebraic signs. The project has four general themes: (1) improve the computational efficiency; (2) develop robust computer programs for different applications; (3) perform new physics and chemistry, including benchmark computations; and (4) make Laboratory-wide research connections. This project continues to develop tools for scientific challenges at LLNL, including chemistry, biology, atomic structure, equations of state, properties of materials, and nuclear structure.

In FY2001, definitive results for the triplet state of the hydrogen molecule were obtained. We have begun a collaboration with Professor William A. Lester of the University of California, Berkeley Chemistry Department, where a graduate student has learned our method and has replicated some results. We have begun calculations on the 54-body system of helium-3 atoms and on the ground state of the lithium-2 molecule; both are stable and appear to be correct, but definitive results require progress on second-stage-importance sampling. We have made significant progress on the theory of second-stage-importance sampling, and concluded that a straightforward general method is applicable to systems in general. A paper on our method was published in *Physical Review Letters* and we delivered two invited conference talks on the research.

In FY2002, we plan to: (1) improve the efficiency for extensive and molecular systems; (2) study the dependence of the computational complexity upon the number of particles; (3) validate the methods against known properties; and (4) develop the finite-temperature generalization of the method.

Discrete differential forms: A novel methodology for robust computational electromagnetics

D. A. White

MAIN TOC

Existing Cartesian-grid finite-difference methods for modeling electromagnetic problems are simple, stable, and work quite well for rectangular geometries. However, such standard methods require a prohibitively fine mesh for quantitative field predictions on large electromagnetic problems with nontrivial geometry. In addition, these popular methods are incompatible with the unstructured grid finite-element methods used for thermal and mechanical analyses.

To overcome these limitations, we are investigating advanced discrete differential forms (DDFs), a new methodology for numerical solution of partial differential equations on 3-D unstructured grids. The key idea is that different DDFs are used to represent different physical quantities—for example, 1-forms are is used to represent field-like quantities (electric field) and 2-forms are used to represent flux-like quantities (electric current). The Figure illustrates a 2-form representation.

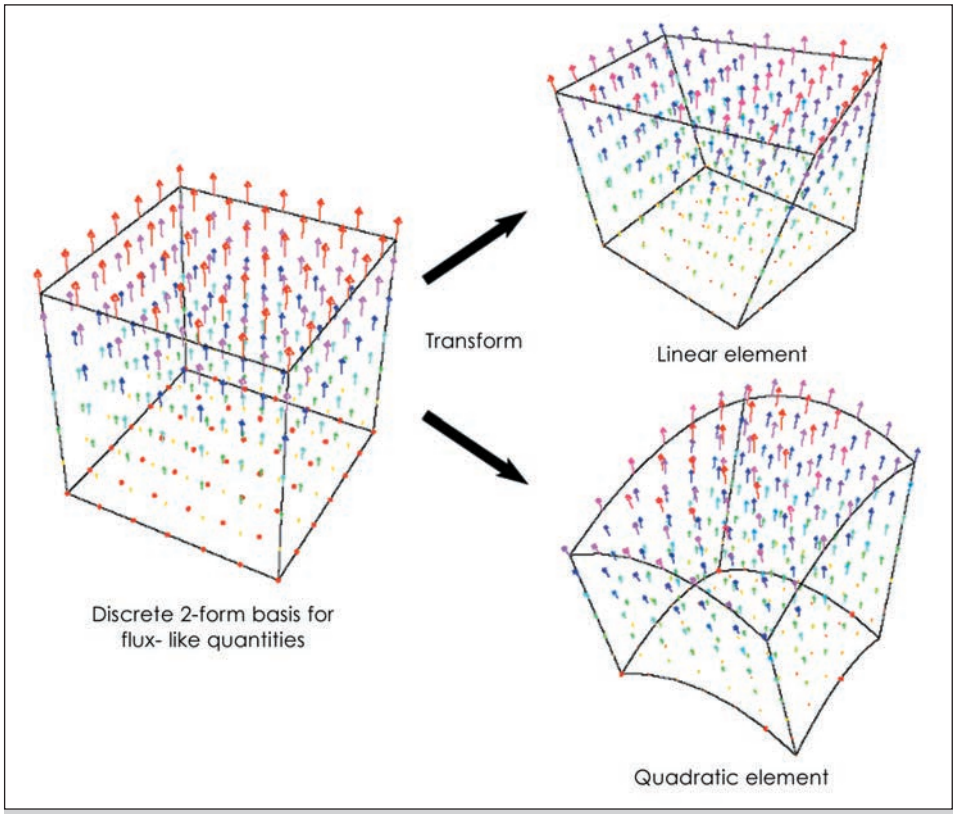

Discrete differential forms, such as the 2-form illustrated above, will lead to accurate multiphysics simulations on 3-D unstructured grids.

We expect that our research will yield a provably stable, conservative, higher-order accurate method for electromagnetics and coupled electrothermalmechanical systems. Stable, conservative, higher-order methods exist for other disciplines such as computational fluid dynamics, but because of the unique characteristics of Maxwell's equations, there is no established comparable method for computational electromagnetics. Many problems of interest to LLNL—such as electromagnetic heating of biological tissue, elastic-magnetic waves in the earth, and effect of stress on integrated optics—are unsolved problems because of the lack of a coupled electrothermalmechanical modeling capability. We expect to determine the feasibility of solving such problems using our DDF methodology.

Our research plan consists of three primary tasks. First, we will research the numerical properties (stability, conditioning, dispersion, etc.) of higher-order DDF basis functions. (Basis functions are local functions defined on a mesh, and the computed field is a linear combination of the basis functions.) Next, we plan to develop a DDF-based finite-element class library that can be used by code developers who want to add our DDF technology to their simulation codes. In fact, an LLNL group is already investigating the use of our class library in a next-generation multiphysics simulation code. Finally, we will demonstrate the efficacy of our DDF basis functions by solving canonical electromagnetics problems and comparing our results to those obtained by alternative methods, and publish our results.

We made significant progress during FY2001. We now understand the basic properties that higher-order discrete differential forms must satisfy. However, these basic properties do not uniquely define the basis functions; defining the basis functions requires a unisolvent set of degrees of freedom (DOF). We determined that the simplest set of DOF (a uniformly spaced interpolation) does not lead to a *p*-convergent approximation, and we successfully constructed sets of nonuniformly spaced interpolation points that are *p*-convergent. By *p*-convergent, we mean that the error of approximation shrinks exponentially with increasing order *p*. This is a new result, and we are submitting a paper detailing our construction.

In FY2002, we will continue researching various methods for formulating DDF basis functions and will investigate the numerical properties, such as stability and conditioning, of these alternative formulations. Formulations that score well will be included in our finite-element class library. By the end of FY2002, we will complete the class library and begin using it to solve some simple, conical-electromagnetics problems.

Understanding the transient sky

H.-S. Park, S. Nikolaev

The night sky displays many kinds of transient objects, some well known (meteors, asteroids, comets, and variable stars) and others more astrophysically interesting (cataclysmic variables, quasars, novae, supernovae, and bright microlensing events). Accurate and systematic monitoring of the variability of many stellar objects has interested astronomers for decades, but such monitoring requires automated telescopes and automated data processing.

LLNL operates an automatic telescope camera system, called the Livermore Transient Optical Imaging System (LOTIS), that was designed to follow up gamma-ray burst triggers from satellites by finding the optical counterparts of the bursts and looking for optical phenomena that can be correlated with the bursts. While not imaging gamma-ray bursts, LOTIS systematically acquires images of the entire night sky. Analysis of this large data set (40 Gbytes/day) requires large computing power, such as that offered by the Laboratory's supercomputing cluster.

The goal of this project was to produce an all-sky database while performing benchmark tests to verify the suitability of the supercomputing cluster for handling large amounts of data of this sort. This project builds on Laboratory capabilities in image processing and high-speed computing, and will have application to remote sensing for national security. Automated techniques for extracting information from time-dependent features in complex images constitute a key enabling technology for efficient processing of image-based intelligence data.

In FY2001, we analyzed a small set of archived data (three months of data on the cataclysmic variable star SS Cygni) to determine the quality of the data. SS Cygni, one of the most heavily observed of all variable stars, is believed to be a binary system consisting of a red dwarf star and a white dwarf. The strong gravity of the dense white dwarf pulls a stream of gas from the companion star, and an accretion disk around the white dwarf causes the outbursts.

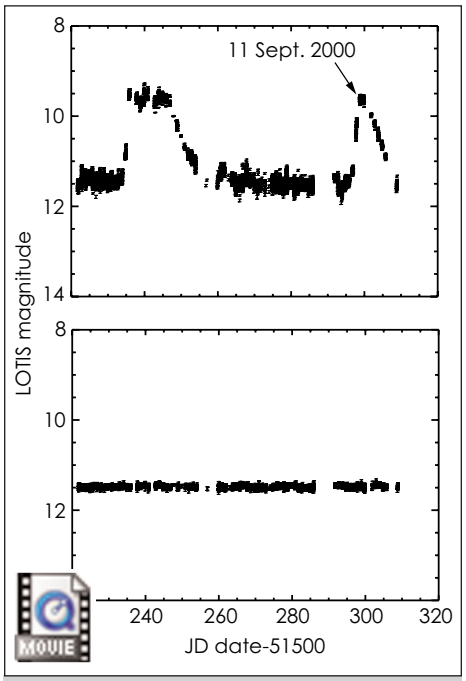

(Above) Light curve for the cataclysmic variable star SS Cygni extracted from LOTIS data; (below) light curve of a nonvariable reference star.

We analyzed images taken from June to September 2000. During this period, LOTIS acquired 60 to 80 images of SS Cygni per night. The images were taken over a wide range of weather and sky conditions, including three full-moon cycles and nights that were foggy, rainy, or (often) clear.

To extract quantitative light curves from the images, we first separate intensity variations due to local conditions from the variability of the star itself by looking at the intensities of nearby nonvariable reference stars. We have automated the five photometric data analysis steps: (1) dark subtraction, (2) astrometric correction, (3) isolation of individual stellar objects, (4) normalization of the intensity with the reference stars, and (5) entering the results (stellar magnitudes vs time) into a database.

The Figure shows the light curves we obtained for SS Cygni, whose quiescent visual magnitude is $V \approx 11.5$, and for a reference star of about the same visual magnitude; the data for the reference star indicate a relative photometric accuracy of $DV \approx 0.03$ for the SS Cygni data. The light curve for SS Cygni shows two outbursts; our continuous coverage permits us to observe and measure the rising phase of the outbursts, something that is only rarely possible otherwise.

In FY2002 we are extending our algorithms to cover a larger field of view, which will yield a database containing many more objects.

Material strength at high pressure

D. H. Lassila, B. P. Bonner, V. V. Bulatov, E. A. Chandler, J. U. Cazamias, J. A. Moriarty

MAIN TOC

Various aspects of the Laboratory's national security mission depend on accurate computer code simulations of plastic flow (i.e., nonreversible deformation) under high hydrostatic pressures. Current strength models cannot be extrapolated to high pressure because they are not based on the underlying mechanisms of plastic deformation.

The principal mechanism by which plastic deformation occurs in metals is the generation and motion of dislocations (line defects) in the crystal lattice. The primary goal of LLNL's multiscale modeling effort is to account for the unit mechanisms associated with dislocation motion, multiplication, and interaction in strength models used in computer code simulations.

The multiscale modeling efforts use results of simulations at small length scales, e.g., dislocation mobility, in simulations of plastic deformation at larger length scales. Dislocation dynamics simulations are the critical links that make this connection possible.

This research project focuses on new developments of physically based dislocation dynamics simulation capability for predicting the strength of body-centered cubic (bcc) metals under high pressure. This work involves coordinated modeling, simulation, and experimental studies of the physics associated with dislocation phenomena at high pressures and high strain rates.

Although the fundamental nature of plastic deformation of metals at high pressure is similar to that at low pressure, involving the generation, motion, and interaction of dislocations, these unit mechanisms can be substantially different at high pressures and high strain rates. As part of FY2001 research, we examined various dissipative mechanisms of dislocation mobility over a range of pressures in full atomistic detail, for example, the relation between atomistic rearrangements of dislocation networks under applied stress, as shown in the Figure. Results in FY2001 included new information on the effect of inertia (effective mass) and state of stress on dislocation mobility. These studies are coupled with ongoing work to develop interatomic potentials.

An all-parallel dislocation dynamics code to run on the latest parallel computing platforms at LLNL is under development. The design separates two distinctly different aspects of code development: a framework that will handle the data in the parallel environment, written in C++, and the disclocation dynamics physics model that resides on each processor. The code framework is essentially complete, and crude physics models are being implemented to allow assessment of computational performance.

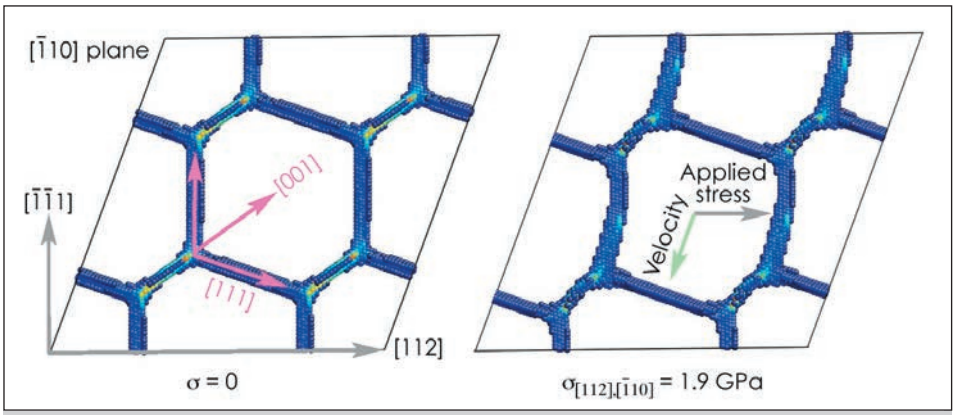

A network of screw dislocations in a specific crystallographic plane [$\bar{1}$10] in body-centered cubic molybdenum in a relaxed state (left) and under applied stress (right). The network moves under the action of stress by kinks splitting off the trailing node and rebuilding the junction at the leading node. This gives rise to a net velocity of the network in a direction opposed to the applied stress.

The experimental work is being performed on high-purity oriented single crystals. In FY2001 we procured, characterized, and purified tantalum and molybdenum (Mo) crystals and performed initial diamond anvil cell experiments on oriented Mo crystals. A Bridgman cell capability has been designed and built for deformation experiments up to 400 kbar. Also, we are developing a "soft recovery" technique that will allow us to recover shock-loaded single crystals intact.

In FY2002, our experimental capability development will be completed and we will begin to measure strength at high pressure and to determine deformation-induced dislocation structure for validation of dislocation dynamics simulations. Deformation experiments will measure material strength to validate simulation results, including deformation-induced dislocation structures. To determine dynamic yield strength, we plan to use a 100 to 700-kbar diamond anvil cell, a 30 to 400-kbar Bridgman cell, and gas-gun experiments.

Strategic Initiative in applied biological simulations

M. E. Colvin, G. Galli, F. Gygi, D. Barsky, F. C. Lightstone, E. Schwegler, C. Venclovas

Our goal is to use LLNL's unique computer resources and expertise in simulation to make scientific advancements in biological problems important to LLNL and the broader scientific community. This project involves collaborations with experimental biologists in areas where computations can advance biological understanding, including studies of the enzymes that repair DNA damage, DNA-binding anticancer drugs, food-borne cancer-causing chemicals, the multiprotein "machines" that replicate DNA, and protein–molecule interactions relevant to new cancer treatments and autoimmune diseases. The simulation capabilities used in the projects have broad application to other DOE missions, including biodefense and environmental cleanup.

In FY2001, we applied simulations to a number of biological problems. Using LLNL's first-principles molecular dynamics (FPMD) software, we investigated the autodissociation of water, the magnesium-ion catalyzed dissociation of water, the activation of phosphoramide mustard (see Figure) and the hydrolysis of dimethyl phosphate. Simulating the autodissociation of a water molecule solvated in water yielded results that closely match experiment. For the intramolecular ring closing of phosphoramide mustard, we find that activation energy is determined by the interactions of the leaving chloride ion with water and that the FPMD results are more accurate than results using standard quantum mechanical calculations with continuum solvent models. Our simulation of an hydroxide ion reacting with dimethyl phosphate answers a long-standing question of whether the pentacoordinate phosphate is a transition state or an intermediate.

We also used classical molecular-dynamics simulations to analyze the structural and dynamical properties of several known variants of the DNA repair protein, Ape1. Results show that the mutations can be grouped into three categories: those that (1) interfere with the catalytic activity of the enzyme, (2) affect the structural stability of the protein, and (3) affect the binding of the damaged DNA.

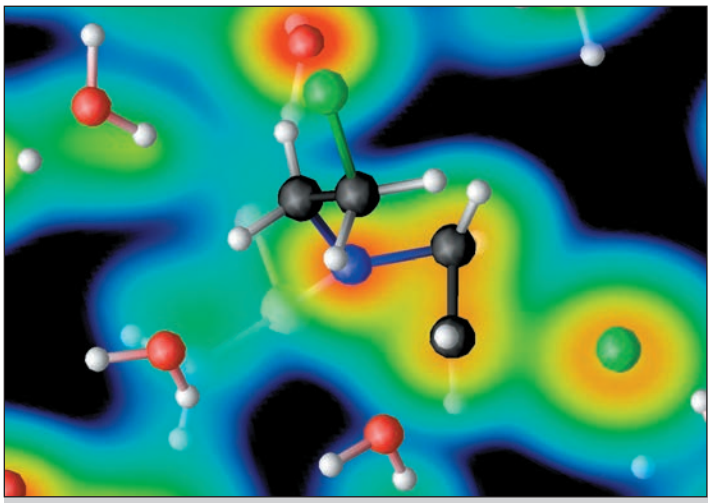

The electron density of the first-principles molecular dynamics (FPMD) simulation of the activating reaction of phosphoramide mustard, the active metabolite of a widely used anticancer drug. Spheres are atoms: carbon (black), hydrogen (white), oxygen (red), chlorine (green), and nitrogen (dark blue). Color shading indicates the electron density around the atoms.

We predicted a molecular model of the *Escherichia coli* "clamp-loading" complex, required for the assembly of a ring-shaped molecular "clamp" onto DNA during genome replication. The model was based on our discovery of a structural homology between the three major subunits of the clamp-loading complex—a prediction that was recently validated by experimental structural studies at New York University.

We also began several collaborations with researchers at the new University of California, Davis (UCD)/LLNL joint Cancer Center. With our collaborators we investigated the origins of the autoimmune liver disease, primary biliary cirrhosis, by developing a quantitative structure-activity relationship to understand which xenobiotic properties are most likely to cause self-proteins to be recognized as immunogens. We used computer modeling to predict the structure of an antibody fragment that targets a large glucoprotein that is overexpressed on the surfaces of many malignant cancers. The structure of our model shows that this interaction occurs on a specific part of the antibody that provides information for further refining of the antibody's structure.

We reported our work in a number of refereed articles that were either published or in press at the end of FY2001.

During FY2002, we will continue to apply the FPMD method to investigating biochemical reactions, including simulations of the phosphate hydrolysis reaction that include amino acids in the active site of an enzyme that catalyzes the reaction. We will build new collaborations with UCD, including the design of better chemical-delivery systems for radionuclide cancer therapies and the optimization of combinatorial libraries used to develop a wide variety of new drugs.

Energy and Environmental Technologies

Section 5

Section 5 Energy and Environmental Technologies

Palm power: A microelectromechanical systems-based fuel cell–integrated microfluidic fuel processor

J. D. Morse, A. F. Jankowski, R. T. Graff, J. F. Hayes

MAIN TOC

Portable power sources represent a critical need throughout the military, weapons-testing, and intelligence communities. Although their inherent limitations as a power source are a minor hindrance in consumer portable electronics, batteries are simply inadequate for advanced applications in remote reconnaissance, intelligence, and telemetry. A lighter-weight, longer-lasting power source would provide new functionality to missions of all kinds, yield long-term cost benefits to all government agencies, enable new levels of safety and security for personnel in the field, and contribute to general national security.

The miniature fuel cell developed in this project offers a compact, lightweight, long-lasting power source with higher specific energy than is available in established battery technologies. Its modular design is scalable over a wide range of output power to meet the requirements of a wide variety of portable electronics systems. Our targeted output is 0.1 to 0.5 W, and scaling to more than 10 W is possible. This fuel cell is based on LLNL-developed technology that combines thin-film expertise with microfabrication microelectromechanical systems (MEMS).

During FY2001 we focused on prototyping suitably packaged fuel cell devices that included internal resistive heating elements. Our design included a micromachined support structure fabricated from silicon in which the anode flow-field structure is designed. A thin-film electrode is patterned on the silicon surface in a manner similar to integrated-circuit processing. Next a catalyst layer is deposited, and then a layer of electrolyte. For the proton-exchange membrane fuel cell, the electrolyte is Nafion, a Dupont polymer. The catalyst layers were formed by depositing platinum coatings or inks on the support structure. Electrode meshes were fabricated to provide electrical conduction in a porous structure through which both fuel and air can flow.

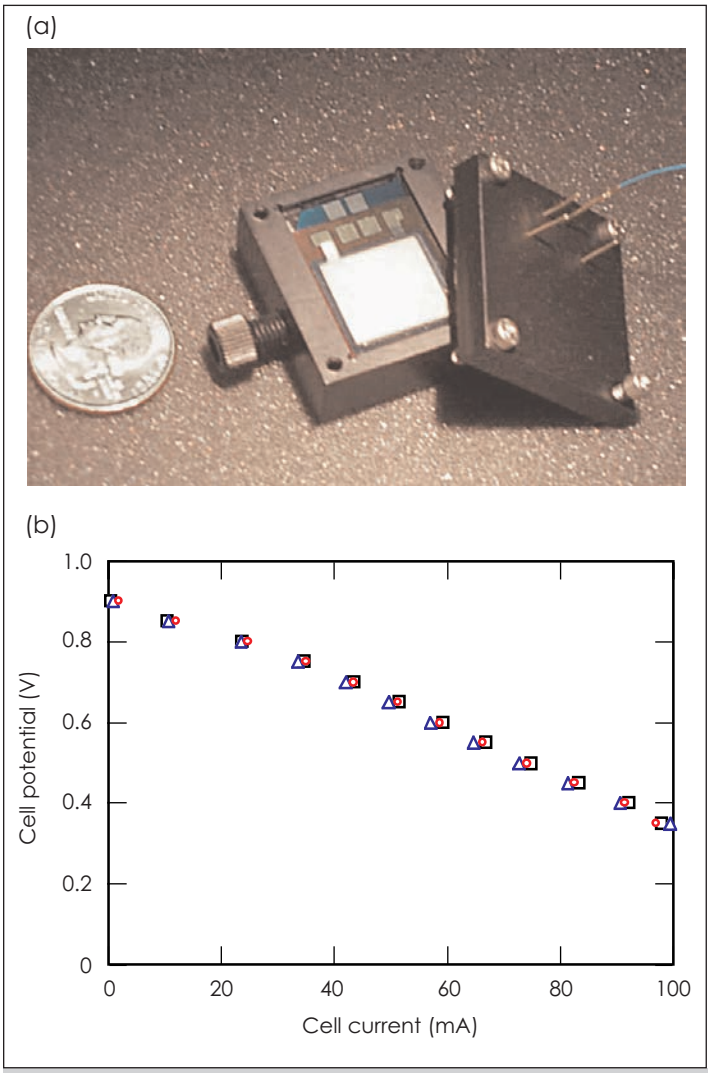

(a) Prototype fuel-cell package. (b) Current–voltage characteristic of fuel cell at 40°C with fuel flowing at 6 cm^3/min; cell output at about 0.5 V is satisfactory. The overlap of the curves for various heater power input suggests that operation at temperatures of about 40°C may be desirable for this fuel cell.

Figure (a) shows an example of a fuel cell package with integrated heaters. The package provides a manifold support for the MEMS-based fuel cell chip, inlet and outlet feeds for the fuel, an air breathing cap, and electrical connections for the heater and for the output power. Figure (b) shows an example of the fuel cell output.

This is a materials-flexible fuel cell architecture that enables the direct integration of flow field and manifold structures with the gas-diffusion electrode support structure. We have fabricated and tested both solid oxide and proton: exchange membrane fuel cells. The micromachined, microfluidic architecture of these cells offers further levels of integration with catalytic fuel processing and storage components for the realization of miniature power sources with high energy density.

Colloidal transport of actinides in the vadose zone

A. B. Kersting, P. Zhao, M. Zavrin, P. G. Allen, E. Sylwester, R. Maxwell, C. R. Carrigan

Toxic contaminants generated during the nuclear weapons program have resulted in more than six billion cubic meters of contaminated soil and rock at DOE facilities. Some 60 million cubic meters of soil and rock within the vadose zone (between the land surface and the underlying groundwater aquifers) are contaminated with radioactive waste or mixed low-level radioactive waste. Cleaning up the contaminated subsurface is a DOE responsibility. A better understanding of contaminant migration in the vadose zone will enable better, more effective and less costly cleanup and containment.

Because of laboratory observations that plutonium (Pu) and americium (Am) attach strongly to the rock surface and do not readily dissolve in groundwater, it has long been thought that such radionuclides do not migrate in the subsurface. Our earlier field studies suggest, however, that these radionuclides are in fact transported in groundwater. We detected Pu in groundwater more than 1 km downgradient from its source, the location of an underground nuclear test at the Nevada Test Site (NTS).

The Pu and other radionuclides (Am, europium, and cesium) were associated with the colloidal fraction of the groundwater. Colloids, naturally occurring submicrometer particles found in almost all surface water and groundwater, are formed through the weathering of rocks, soils, and plants; because colloids are so small, they can be transported in groundwater. Determining how colloids may transport low-solubility radionuclides is critical for developing reliable conceptual models for predicting contaminant transport. Models based solely on solubility measurements could underestimate the transport of low-solubility radionuclides.

In this project, we are studying geochemical controls on colloid-facilitated transport of actinides in the vadose zone at the NTS. We will integrate field and laboratory studies into a reactive-transport model of subsurface transport, with the ultimate objective of developing a framework for predicting when colloid-facilitated transport of actinides may occur, to quantitatively describe these results, and to develop a flow and transport model based on our experimental results.

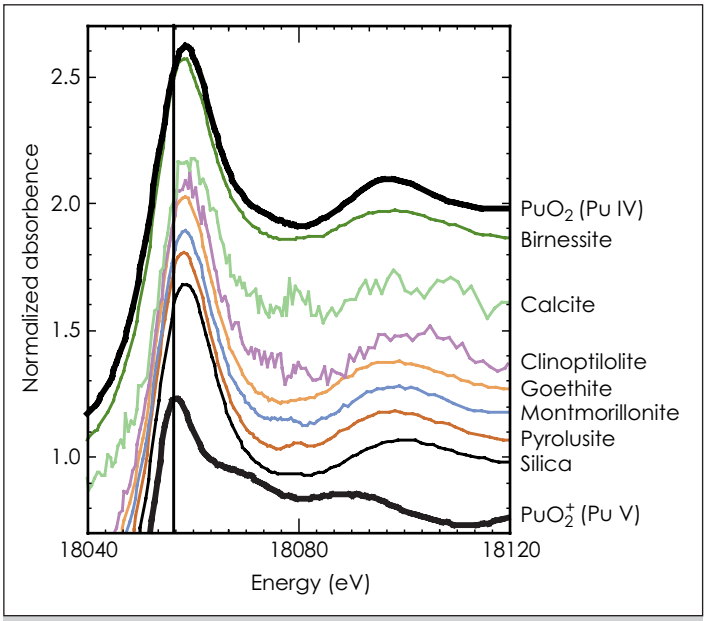

X-ray absorption near-edge structure (XANES) of plutonium (Pu) sorbed to various mineral surfaces. The shift in the main (and secondary) peaks of the spectra indicate that all Pu(V) in the initial solution sorbed as Pu(IV). (XANES studies carried out at the Synchrotron Radiation Laboratory, Stanford University.)

In FY2001 we completed a series of experiments on the sorption of Pu(IV) and Pu(V) on seven minerals we had earlier observed as colloids in NTS groundwaters: iron oxide (goethite), manganese oxides (birnessite and pyrolusite), clay (montmorillonite), zeolite (clinoptilolite) silica, and calcium carbonate (calcite). Plutonium can occur in various oxidation states. Understanding the oxidation state of the Pu is important for modeling its behavior both in solution and as a sorbed component. The sorption of Pu(IV) onto the minerals we have studied is quite strong and fast, whereas the sorption of Pu(V) is slow. The sorption rates varied from mineral to mineral, but Pu(IV) and Pu(V) sorbed on every mineral investigated. Initial x-ray absorption spectroscopy of the experimental-run products (see Figure) showed that Pu(IV) remained in the Pu(IV) oxidation state, but that Pu(V) was reduced and sorbed as Pu(IV) on every mineral investigated. This is the first documentation of this reduction process, which has important implications for modeling the transport of Pu.

In FY2002 we will investigate the sorption of Np (V) on the mineral colloids investigated in FY2001 and compare the results with those of the Pu sorption experiments. Using our experimental data, we plan to develop a mechanistic (surface complexation) description of Pu interaction with colloid minerals observed in our field studies in FY2000. Finally, we will link our model to a colloid transport code to help us understand when colloid-facilitated transport of actinides may occur in the subsurface.

Research on the direct conversion of carbon into electricity

N. J. Cherepy, K. Fiet, R. Krueger, D. Ahre, J. F. Cooper

Direct carbon conversion is a route to 70 to 80% efficient electricity generation (based on the heat of combustion of the fossil fuel used), which is more than twice the efficiency of coal–steam power plants. Direct conversion is pollution free—carbon dioxide is the only byproduct. We are working on developing practical, scaleable electrochemical cells for efficient conversion of carbon into electricity and are using these cells to identify suitable carbon fuels derived from diverse resources. The power densities we have demonstrated, over 100 mW/cm^2 of active area, are sufficient for base-load power applications.

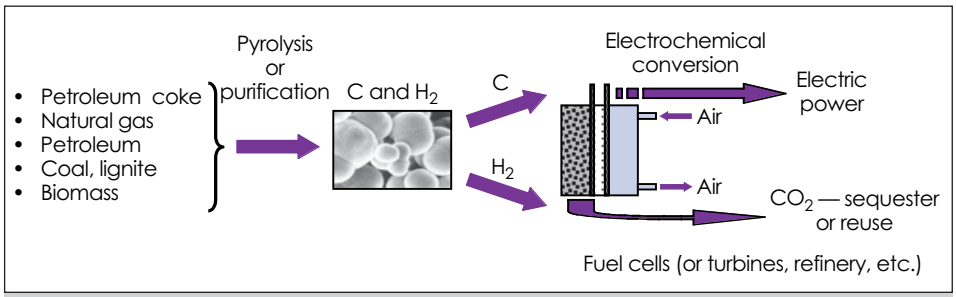

We envision a novel and highly efficient technology for electric power generation. The sequence (1) fossil fuel extraction, (2) pyrolysis to carbon and hydrogen, (3) electrochemical conversion of carbon and hydrogen into electricity in fuel cells. The net efficiency, 70 to 80%, is more than twice that of coal–steam power plants.

The strategic value of direct carbon conversion lies in its ability to address demands for very-high-efficiency conversion of fossil fuels to electricity while producing only a pure CO_2 byproduct capable of reuse or sequestration. Direct carbon conversion cells should be low-cost (our prototype design suggests costs of less than $300/kW) and could use inexpensive carbon fuels such as petroleum coke ($33 to $110/ton) and carbon blacks ($198 to $242/ton). At 80% efficiency, fuel costs would contribute $0.013 to $0.025/kWh to electricity costs. Further, we envision "clean coal" and biomass conversion processes using purified coal particles or biochars in a direct carbon conversion cell; the cool-refining processes required for purification are inexpensive.

Our electrochemical cell has a slurry of powdered carbon fuel in a molten carbonate electrolyte in the anode compartment, and air (to provide oxygen) flows through the cathode compartment. We operate the cell at temperatures from 700 to 850°C. A porous ceramic separator between the compartments allows carbonate transport, the cathode half reaction $O_2 + 2CO_2 + 4e^- = 2CO_3^{2-}$, and the anode half reaction $C + 2CO_3^{2-} = 3CO_2 + 4e^-$; the net reaction is $C + O_2 = CO_2$, with an electrochemical potential $E \approx 1.0$ V.

During FY2000 and FY2001 we studied the relation between carbon structure and discharge rate for low-cost particulate carbon fuels derived from biomass, coal, hydrocarbon pyrolysis blacks, and petroleum cokes. For a diverse set of carbon samples, we determined electrochemical discharge rate, particle surface area (by gas adsorption), primary particle size (from scanning electron microscopy), and nanostructure (by x-ray diffraction).

We obtained the highest discharge rate, 100 to 125 mA/cm^2 at 0.8 V, with biochar-derived carbons, the materials with most disordered nanostructure. Petroleum cokes yielded 50 to 60 mA/cm^2 at 0.8 V, and carbon blacks yielded 50 to 100 mA/cm^2 at 0.8 V.

In general, materials with disordered nanostructure had the highest reactivity, because of their high fraction of reactive sites. Relative electrical conductivity also seems to contribute to the discharge rate, however. For example, we found that particulate graphite (carbon with low reactivity) produced 20 to 50 mA/cm^2 at 0.8 V, because high electrical conductivity enhances current collection. Thus even graphitic carbon particles could be used as fuels in direct electrochemical conversion. All the carbons studied had small primary particle sizes (0.015 to 5 μm), and high specific surface areas (9 to 1500 m^2/g), but within these ranges particle size and surface area did not appear to significantly affect the electrochemical discharge rate.

In FY2001 we demonstrated linear scalability of power between 2.8-cm^2 and 60-cm^2 cells. In FY2002 we plan to test a stackable cell on the 1000-cm^2 scale as an industrial prototype. We will also improve our cell performance with the use of a cathode like those used in commercial hydrogen-fueled molten carbonate fuel cells (possibly doubling current densities). Finally, we will explore long-term performance of components.

Investigation of the effect of magnetic configuration on spheromak performance

D. N. Hill, H. S. McLean, B. W. Stallard, R. Wood, S. Woodruff

MAIN TOC

The Sustained Spheromak Physics Experiment (SSPX) device at LLNL was designed to study how well the spheromak can contain plasma energy while the confining magnetic fields are maintained by dynamo processes in the plasma. The SSPX design may greatly improve operation over previous spheromak experiments because it is compact, has no field coils linking the vacuum vessel, and can be operated in a steady state with voltage applied to external electrodes. The ability of the SSPX to contain the plasma thermal energy is predicted to increase with increasing plasma electron temperature; in other words, the hotter it is, the better it will work. Our near-term goal is to determine which of several magnetic field configurations works best to produce hot, well-confined spheromak plasmas. We also want to verify the predicted inverse relation between plasma temperature and heat loss, and to use these results to design an even higher-temperature follow-on experiment that will push closer to fusion conditions. New features of the SSPX include a large-radius coaxial plasma injector to improve efficiency, a conformal flux conserver to minimize open field lines around the plasma, a divertor to aid in cold-particle exhaust, and a set of programmable-bias magnetic-field coils to vary the magnetic geometry.

During FY2001 we carried out experiments in the SSPX device to explore how different vacuum magnetic-field configurations affect energy loss from spheromak plasmas. The primary attractive feature of the spheromak as a magnetic-confinement fusion device is that currents in the plasma itself (the so-called plasma dynamo) produce the confining toroidal magnetic field, rather than complex external coils. This design could lead to smaller, cheaper fusion power plants.

The SSPX spheromak was modified in FY2000 by the addition of six independently controllable magnetic field coils with associated power supplies. These coils, along with the original set of three bias coils, provide an initial seed magnetic field that is twisted and amplified by currents driven through the spheromak plasma by an external capacitor bank. The complete coil set gives us unprecedented flexibility in studying how the geometry of the initial vacuum field in the SSPX spheromak affects plasma formation and magnetic field amplification.

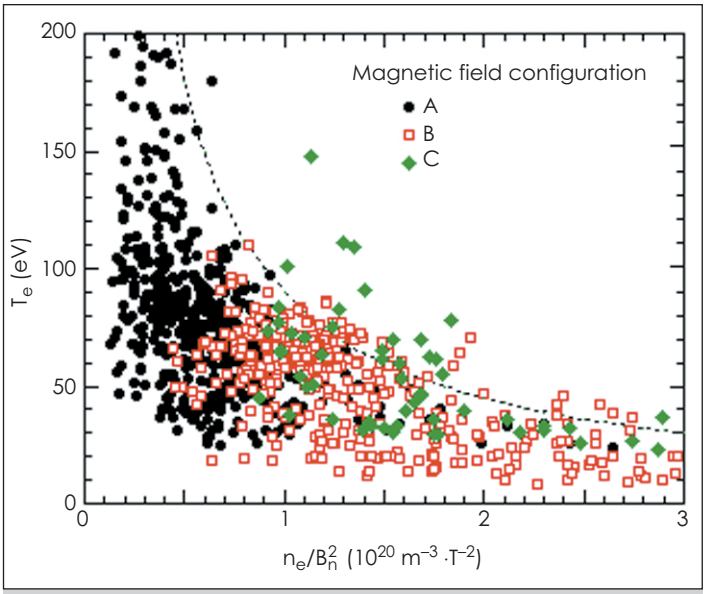

Plasma electron temperature vs plasma density for three magnetic field configurations in the SSPX spheromak. The points are roughly bounded by a maximum normalized electron pressure of 3.5% (dotted line).

The new coils also greatly expand the density range over which good spheromak plasmas can be formed in SSPX. This results from their ability to create an initial Penning discharge during spheromak formation, so that plasma discharges can be initiated with low gas pressure. Thus, we have found it possible to reduce the plasma density by factors of 2 to 3 and to increase the plasma electron temperature by similar factors. Lower plasma density reduces impurity radiation losses and allows the plasma temperature to rise without exceeding the fundamental pressure limits of the spheromak configuration. The relation between plasma density and temperature is shown in the Figure. Besides representing records high temperatures in driven spheromak plasmas, these data show that SSPX can operate with a normalized plasma pressure of 5 to 10%, comparable to tokamaks and other toroidal magnetic fusion devices.

We have made an initial comparison of six magnetic field configurations using the new bias field coils. These configurations fall into two categories: those with vacuum magnetic field lines lying parallel to the side walls of the SSPX chamber and those with diverging fields passing through the side walls of the chamber. Basic spheromak theory and SSPX data obtained before the installation of the bias coils suggested that up to three times higher field amplification could be expected with the field lines parallel to the walls. Contrary to predictions, however, we observed no increase in amplification with the parallel field. Surprisingly, we observed about 20% higher field amplification with the diverging magnetic field configuration. We believe that these differences lie in the detailed path of current flow during early formation and the resulting magnetohydrodynamic stability of the resulting current channel.

In FY2002, with funding from the DOE Office of Fusion Energy Science, we will continue using the bias coils to examine how current amplification depends on the vacuum magnetic field geometry. We plan to install new diagnostics to better measure radiation losses and the distribution of plasma current, and to upgrade our density measurements.

Resolving nuclear reactor lifetime extension questions: A combined multiscale-modeling and positron-characterization approach

B. D. Wirth, P. Asoka-Kumar, R. H. Howell, J. Marian, G. R. Odette, P.A. Sterne

Increasing U.S. and worldwide demand for electricity and the desire to reduce greenhouse gas emissions make it important to maintain and extend the operating lifetime of nuclear reactors. Doing this safely and reliably will require maintaining the integrity of structural materials, including the reactor pressure vessel, whose properties are degraded as a result of neutron- and gamma-ray exposure. Fundamental understanding of the chemistry and structure of nanometer features that form in steels during irradiation is required to resolve outstanding safety issues that bear on predictions of safe operating lifetimes.

This project builds on multiscale materials modeling capability developed under the Stockpile Stewardship Program, and state-of-the-art positron annihilation spectroscopy measurements. Our work will enhance the Laboratory's capability to characterize nanometer-scale features responsible for strength in structural steels and will contribute to the Laboratory's work in nuclear energy technology and stockpile stewardship.

In this project, we combine molecular dynamics modeling of defect production in high-energy displacement cascades with kinetic Monte Carlo simulations of the long-time evolution of defects. The combination provides a multiscale model with which to predict the formation of nanometer features in multicomponent ferritic steels. Complementary characterization of the nanometer features is performed at the LLNL positron facility. This facility has the unique ability to measure both the positron lifetime, which allows us to identify the defect type and size, and the orbital electron momentum spectrum, which provides information about the defect's chemical composition. The integration of modeling predictions with experimental characterization provides a validated, atomistic picture of the character and composition of the nanometer features and provides the basis for predicting mechanical property changes.

During FY2001, we studied the evolution of copper (Cu) precipitates and vacancy–solute clusters in binary and ternary iron (Fe)–Cu–manganese(Mn) alloys. The features that form under irradiation in these alloys are similar to those that form in more complicated, multicomponent reactor pressure-vessel steels, and they provide a model system on which to validate our modeling and characterization capability. The modeling studies predict the formation of Cu–Mn precipitates with a composition of about 90% Cu and 10% Mn, along with a spectrum of subnanometer vacancy–Cu–Mn clusters. The positron characterization confirmed the presence of Cu-rich and nonmagnetic precipitates in these alloys and of the existence of the smaller vacancy–Cu clusters.

The Figure shows (a) one of the subnanometer vacancy–Cu clusters predicted by modeling to form in an irradiated Fe–Cu alloy, in this case containing 17 vacancies and 5 Cu atoms. The atomic configuration of this cluster was input into a quantum mechanical code to calculate the positron probability density (wave function) shown in (b) and to predict the orbital electron momentum spectrum (OEMS) expected from positron annihilations, as shown in (c). Figure (d) shows the corresponding measured spectrum. Figure (c) and (d) plot the number of positron annihilations at a given electron momentum, normalized to pure, unirradiated Fe. Both the predicted and observed OEMS show a peak in the number of annihilations at low momentum, which is characteristic of vacancy clusters, and a second, broader peak at higher momentum, characteristic of Cu. The qualitative agreement between the predicted and measured OEMS provides a validation of our understanding of the features formed in this alloy under irradiation and the multiscale modeling to predict damage evolution.

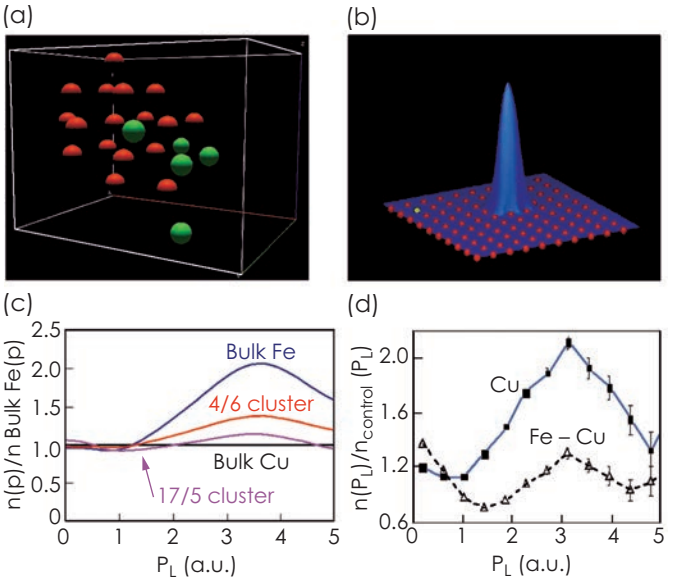

Comparison of modeling predictions and positron annihilation spectroscopy results: (a) 17 vacancy–5 Cu cluster, (b) positron wave function, (c) predicted orbital electron momentum spectra, (d) measured orbital electron momentum spectra. (See text for discussion.)

In FY2002, we will extend our modeling and positron characterization capability from binary and ternary Fe–Cu–Mn alloys to more complicated multicomponent Fe–Cu–Mn–nickel reactor pressure-vessel steels. We will continue to investigate the atomic structure and composition of the nanometer features, including identification of features expected to form at very high radiation exposures.

Novel approaches for monitoring intrinsic bioremediation

H. R. Beller

Because engineering approaches to groundwater cleanup at civilian and military sites throughout the U.S. would cost billions of dollars intrinsic bioremediation is becoming attractive as a cost-effective option for restoration of groundwater contaminated with organic pollutants. A primary impediment to the acceptance of intrinsic bioremediation is the difficulty of demonstrating that decreases in the concentrations of contaminants in groundwater truly represent biological metabolism of these compounds rather than abiotic processes.

Using detailed laboratory microbial studies and focused chemical analyses of groundwater from contaminated sites, we are identifying and then testing the usefulness of unique metabolites that environmental monitoring programs can use as distinctive indicators of in situ biodegradation of specific contaminants. Contaminants of concern at LLNL and other DOE and Department of Defense (DoD) facilities, include high explosives (HE) [such as RDX (hexahydro-1,3,5-trinitro-1,3,5-triazine)] and certain aromatic hydrocarbons [benzene, toluene, ethylbenzene, and xylenes, or (BTEX)] found in gasoline. The project is making a significant contribution to our understanding of the biological fate of HE compounds in subsurface environments and could dramatically enhance the effectiveness of in situ monitoring for BTEX degradation by taking advantage of recent groundbreaking findings in anaerobic hydrocarbon biochemistry.

This research is relevant to LLNL's mission because it both investigates cost-effective remediation of HE contamination at Site 300 and develops scientific knowledge that supports environmental remediation and regulation on a national basis.

In its first year, the project has resulted in significant findings concerning anaerobic RDX metabolism by bacteria in aquifers. Most notably, we detected three distinctive nitroso-substituted RDX metabolites in numerous groundwater samples collected from an Army Ammunition Plant. Their presence, confirmed by the appropriate mass/charge (*m*/*z*) ratio and chromatographic retention time (see Figure), provides strong evidence of in situ RDX transformation. A state-of-the-art analytical method developed for this project, which relies on liquid chromatography/mass spectrometry/mass spectrometry (LC/MS/MS), proved to be sensitive (detection limits ~0.1 μg/l) and accurate.

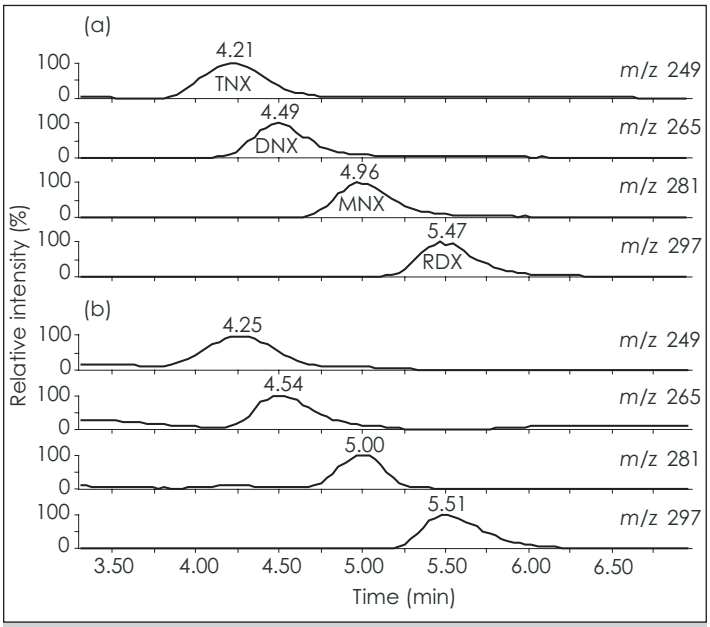

Liquid chromatography/mass spectrometry (LC/MS) chromatograms of adducts of RDX and three distinctive metabolites (mono-, di-, and trinitroso-RDX; MNX, DNX, and TNX, respectively) in (a) a standard, and (b) a contaminated groundwater sample.

In addition, notable results were obtained from laboratory studies of anaerobic RDX metabolism by bacteria enriched from LLNL's Site 300 aquifer material. The primary finding was that RDX can be transformed in a simple growth medium that contains hydrogen as the sole electron donor. Past studies of RDX degradation have typically involved complex, undefined media with multiple potential electron donors and acceptors. With hydrogen as the sole electron donor, we observed transient formation of the same metabolites detected in groundwater from the Army Ammunition Plant. Studies with carbon-14-labeled RDX suggested that mineralization to carbon dioxide by bacteria from the Site 300 aquifer was negligible (<2%), which is consistent with cometabolic transformation of the explosive.

For monitoring of in situ BTEX degradation, we developed an LC/MS/MS method for a distinctive class of metabolites (benzylsuccinates). The method was validated in studies with groundwater and proved to be sensitive and accurate. Articles describing our work are in press in refereed journals.

In FY2002, we plan to further assess the applicability of nitroso-substituted RDX metabolites and BTEX metabolites as indicators by performing LC/MS/MS analyses on groundwater from multiple contaminated sites. We will also conduct further laboratory research on the physiology of anaerobic RDX metabolism by aquifer bacteria.

Chemical deactivation of reactive uranium

D. D. Gates-Anderson, C. A. Laue

The U.S. Department of Transportation strictly controls the transport of pyrophoric materials, which are capable of igniting upon contact with air, and pyrophoric waste is not accepted at disposal sites for hazardous, low-level, and mixed waste. LLNL has an inventory of pyrophoric depleted-uranium (DU) waste of at least 11,700 kg (DU plus storage solutions and containers, with a total volume of about 33 m^3) that requires treatment to render it suitable for disposal. A further inventory of more than 40,000 kg of such waste across the DOE complex requires treatment.

Developing a technology to treat DU metal waste is essential for DOE sites to remain in compliance with regulatory agreements. The objective of this project is to develop an integrated process to convert pyrophoric metallic DU wastes to a nonpyrophoric waste that is suitable for disposal.

We are exploring the kinetics and thermodynamics of U dissolution and oxidation. These studies will allow us to scale the selected process from laboratory to full scale. We will conduct studies at scales ranging from 1 g to 5 kg to ensure that the process we develop can safely and efficiently treat the variety of DU waste found on site. Thermodynamic relations will be explored in calorimetric studies, in which we will monitor the exchange of heat during dissolution in a well-insulated system. Uranium dissolution reaction order and rate determination using real-time monitoring of U concentration will support the optimization of a fully integrated process.

During FY2001, we treated 1-g aliquots of U metal or U alloy with 5 to 50 ml of selected reagents used alone or in combination: hydrochloric, sulfuric, and phosphoric acids; and sodium hypochlorite, sodium hydroxide, and hydrogen peroxide. We evaluated reagent concentration, volume, and treatment temperature. Complete dissolution of U metal and U-molybdenum alloys with several acidic/oxidizing reagents was achieved within minutes at room temperature.

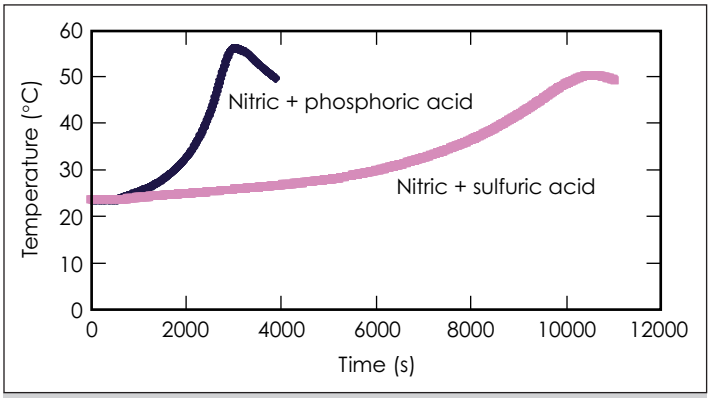

Calorimetric evaluation of depleted uranium dissolution in nitric acid. The heat generated during dissolution must be understood so that a safe, properly sized treatment system can be designed.

We chose four systems for more detailed studies: phosphoric acid with traces of hydrochloric acid, sulfuric acid alone and with an oxidizing agent (hydrogen peroxide or nitric acid), and nitric–phosphoric or nitric–sulfuric acid mixtures (see Figure). We based our selection of these dissolution systems on the desire to achieve a treatment time of less than 1 day, the need for flexibility when applying the process to actual waste, and the desire to minimize the corrosiveness of the process developed.

During FY2002, we will investigate the reaction kinetics and thermodynamic characteristics of the selected systems in detail. Key data to be established will be the molar heat of reaction, activation energy, rate, and reaction order. The desired outcome is a fully detailed reaction mechanism for each systems selected for scale-up. We will also conduct studies with actual mixed waste to determine pretreatment requirements and optimum reactor configuration. Our final task in FY2002 will be to identify the most effective stabilization methods for the dissolution products. Our goal is to identify stabilization media (clay, resins, or grouts) that yield a final product that meets regulatory requirements for land disposal.

Evaluation and optimization of methyl tert-butyl ether biodegradation in aquifers

S. R. Kane, T. L. Legler, C. J. Koester, W. J. Wilson

Methyl tert-butyl ether (MTBE) is a fuel oxygenate that has become a major threat to drinking-water supplies because of its release at numerous leaking underground fuel tank (LUFT) sites, its high mobility in groundwater, and its recalcitrance to biodegradation. Nationwide, an estimated 250,000 of the approximately 385,000 confirmed LUFT releases have contained MTBE. In addition to its suspected carcinogenicity, MTBE degrades drinking-water quality by negatively affecting taste and odor. Therefore, several states have set primary maximum concentration levels for MTBE at or below 20 mg/l and at 12 mg/l for the primary metabolite, tert-butyl alcohol (TBA), a known carcinogen.

Areas of insufficient information concerning MTBE biodegradation at LUFT sites include (1) the distribution of in situ aerobic MTBE degradation that would result in the most rapid removal rates; (2) MTBE-degrading bacteria in general—even less is known about their occurrence and degradative activity at LUFT sites; and (3) the effect of dissolved gasoline components—most notably benzene, toluene, ethylbenzene, and xylenes (BTEX)—on MTBE biodegradation in aquifer sediments.

We are focused on (1) defining site-specific factors that could determine if aerobic degradation could occur in situ, and (2) characterizing microorganisms responsible for MTBE degradation. Using purge-and-trap gas chromatography/mass spectrometry (GC/MS), we are monitoring MTBE consumption and the transient formation of TBA in microcosms containing aquifer sediment and groundwater from MTBE-contaminated LUFT sites. Our results will contribute to our understanding of processes that control MTBE biodegradation and will allow the development of bioremediation approaches—thereby directly supporting the DOE's mission in environmental restoration and management.

During FY2001, we examined the potential for aerobic MTBE degradation in sediments from four LUFT sites characterized by oxygen-limited conditions. MTBE depletion was observed for sediments from half the sites (e.g., see Figure), whereas no consumption of MTBE was observed for sediments from other sites after 75 days. For sediments in which MTBE was consumed, about half the added MTBE was completely degraded to carbon dioxide. When the water-soluble fraction of nonoxygenated gasoline was added to microcosms, MTBE metabolism was sometimes markedly inhibited and TBA accumulation was more pronounced—presumably because of exposure to BTEX. In contrast, in microcosms from another site, MTBE metabolism was not affected by the addition of water-soluble gasoline components. BTEX degradation was rapid and was not affected by the presence of MTBE.

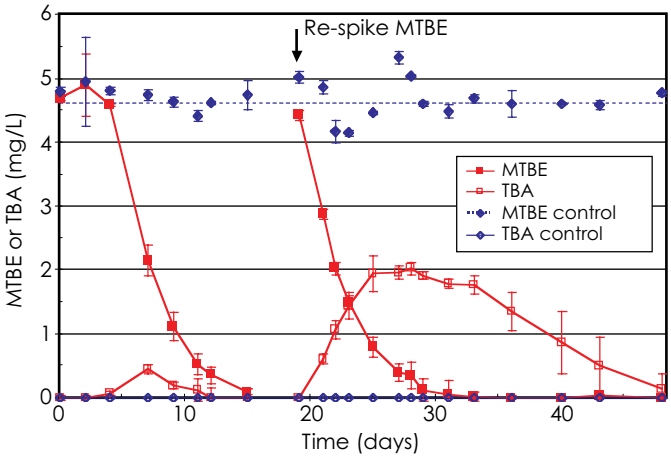

Aerobic methyl tert-butyl ether (MTBE) biodegradation and transient production of tert-butyl alcohol (TBA) in microcosms containing material from a leaking underground fuel tank site. After a 4-day lag period, about 4.6 mg/l of MTBE was depleted in 15 subsequent days.

Overall, our results suggest that the effects of dissolved oxygen levels and water-soluble gasoline components on in situ MTBE degradation will vary from site to site, and that more site-specific information is needed to predict the potential for MTBE biodegradation.

In FY2002, we will focus on the isolation and characterization of MTBE-degrading microorganisms present in sediments showing MTBE degradation activity. Using pure-culture bacterial strains, we will study genes involved in MTBE biodegradation. Information from pure-culture strains about factors controlling MTBE degradation can be used to optimize biotreatment approaches and to predict where aerobic bioremediation may be successful. In addition, to understand how the presence of other dissolved gasoline compounds will affect MTBE and TBA biodegradation rates, we will investigate the mechanism(s) of observed MTBE/BTEX interactions.

Stellarator divertor studies

M. E. Fenstermacher, D. N. Hill, A. E. Koniges, T. D. Rognlien, M. Umansky

MAIN TOC

At LLNL an ongoing set of research projects helps develop controlled fusion energy because of its potential both as a clean, abundant energy source and as a neutron source that could transmute present radioactive waste to much safer products. Large fusion experiments have become national projects developed and operated by many collaborating laboratories. The most scientifically advanced configuration is the torus-shaped tokamak, which uses a plasma with symmetry about a toroidal axis. Billion-dollar-class tokamaks operate in the U.S., the U.K., France, Germany, and Japan. The National Compact Stellarator Experiment (NCSX)—to be built at the Princeton Plasma Physics Laboratory (PPPL)—is a toroidal device with no axis of symmetry; it is expected to be the next major fusion experiment funded by the DOE.

This project is working to make major contributions to the design and operation of the NCSX, a challenging new configuration. First, we are using our recognized expertise for computational simulation of the edge plasmas in tokamaks to produce the fully 3-D modeling capability that is needed for more complex geometries such as the stellarator. Second, by using the specific geometry of NCSX for these studies, we plan to become an active member of the NCSX design and experimental teams through a collaboration with PPPL.

The two major components of this project are to (1) collaborate in the development of 3-D transport and field-line tracing codes, and (2) join in the NCSX design activities and become strong participants in the international stellarator community.

Field-line tracing is our first step in analyzing the edge plasma. However, our long-term goal is to build LLNL's core competency in state-of-the-art computer modeling by collaborating, with the five-person team at the Max Planck Institute for Plasma Physics (IPP) in Greifswald, Germany, on the development of BoRiS, a multispecies, 3-D, magnetized-plasma-fluid simulation code. This capability will give LLNL the 3-D computational techniques needed to design the plasma-interaction hardware (the divertor) for stellarators and other nonaxisymmetric plasma devices.

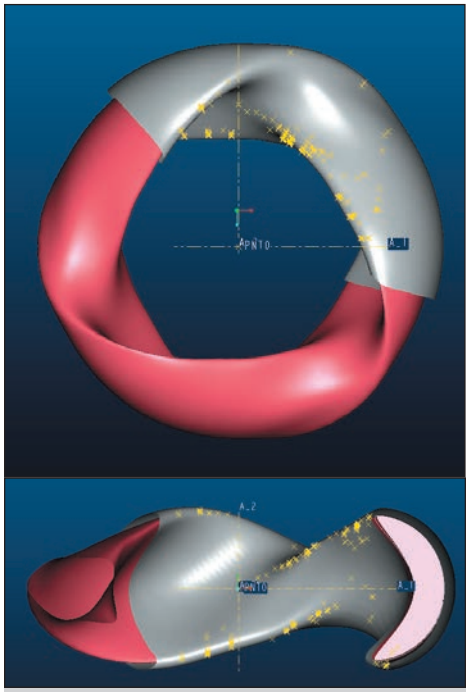

Plan view (top) and cross-sectional view (bottom) of the National Compact Stellarator Experiment (NCSX) vacuum vessel, showing core (pink) and edge (red) plasmas, vacuum vessel (gray), and predicted intersection points of magnetic field lines traced from near the core to the vacuum vessel (yellow crosses).

During FY2001, we developed the capability to trace magnetic-field lines in the stochastic-edge region and to roughly model the effects of turbulence diffusion in the stellarator-edge plasma. We also installed BoRiS at LLNL, tested it on NCSX configurations, and began benchmarking BoRiS solutions in 2D with UEDGE, our mature edge-plasma transport code. Finally, we used an analytic, fluid-plasma model to predict the electron temperature of the edge plasma for the NCSX. This work included data obtained from colleagues at the W7-AS stellarator experiment at IPP Garching and was part of our contribution to the NCSX physics basis, as documented in the NCSX Physics Validation Review. Results were also presented at the 2001 APS-DPP meeting.

The Figure shows our initial predictions of where the escaping plasma power will be concentrated on the NCSX vacuum vessel—as indicated by the density of yellow crosses. Our results are based on tracing magnetic-field-line trajectories in the complex 3-D fields. Such calculations will guide the NCSX project decisions regarding where to construct high-heat-flux target plates to protect the vacuum vessel from erosion.

In FY2002, we will contribute our numerical expertise in implicit solvers, interpolation methods, and fluid-neutral models to the development of the BoRiS code and apply it to the NCSX baseline design. BoRiS simulations will give a self-consistent plasma solution from the interior to the plasma–material interaction surfaces. This work will give us international exposure, provide LLNL with a unique tool within the U.S. fusion program, and position LLNL to become a major partner in the NCSX efforts.

Study of the direct oxidation of methane in solid-oxide fuel cells

A. Q. Pham

Although hydrogen is the preferred fuel for fuel cells, its widespread use is dependent on technological breakthroughs in its production cost and storage. For the immediate future, the fuels of choice are still hydrocarbons, especially natural gas. Unfortunately, methane, which is the main constituent of natural gas, has very low reactivity. As a consequence, all fuel-cell applications using natural gas currently have a fuel reformer to convert methane to more reactive products such as CO and H_2. However, the addition of a fuel reformer increases system cost and complexity while decreasing the overall energy efficiency.

In this project, we explored the possibility of direct oxidation of methane at the anode of a solid-oxide fuel cell (SOFC), thus eliminating the fuel-reforming step. Such technology would make significant contributions to the efforts to conserve natural resources and to reduce greenhouse-gas emissions. This project extends LLNL's capabilities in electrochemistry and fuel-cell technologies in support of the DOE's energy and environmental missions.

Two major issues are known to hamper the direct oxidation of methane at SOFC anodes: (1) carbon deposition resulting from cracking, and (2) low reactivity. During FY2001, we addressed both issues. First, we performed thermodynamic calculations to determine the stable species in a typical fuel-cell environment. Results indicated that coking of methane occurs at all temperatures of interest (400 to 800˚C) if no oxygen-containing species (such as water or oxygen) are present. Experimental thermogravimetric analyses confirmed the presence of carbon for all fuel-cell anodes that had been exposed to methane. The presence of steam reduced the carbon deposition; however, a large excess of steam with a steam-to-carbon ratio up to 3 was necessary to completely prevent methane coking. Such a large excess of steam is impractical in real applications, and would favor the steam-reforming reaction at the expense of direct oxidation.

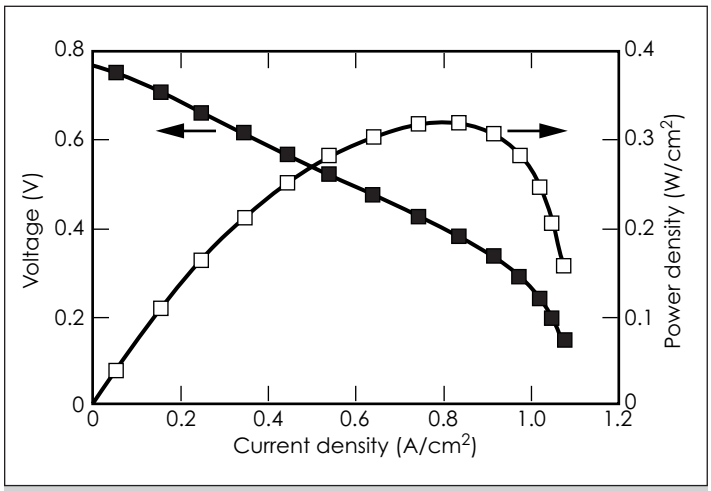

Successful operation of a solid-oxide fuel cell on methane fuel at 550˚C.

Although the thermodynamics may favor methane coking, it is still possible to alter the kinetics of the reaction to avoid carbon deposition. We found that the anode microstructure and materials can have significant effect on the amount of carbon deposited. Highly porous anode structures resulted in less carbon deposition. Employing mixed ionic–electronic conducting materials such as doped ceria at the ceramic matrix of the anode also yielded much lower carbon deposition than the conventional zirconia matrix.

Using the available information about steam-reforming kinetics, we demonstrated the occurrence of the direct oxidation of methane at the fuel-cell anode. With appropriate electrode materials, the direct-oxidation current can be very high, up to six to seven times the reforming reaction rate (at 550˚C). The Figure shows the performance of a fuel cell operating on direct oxidation of methane at 550˚C. The peak power density is 320 mW/cm^2, slightly higher than that of the Siemens Westinghouse fuel cell, which is operated at 1000˚C.

We have secured funding from the DOE to continue this development effort. Furthermore, we will work with Solid Oxide Systems, LLC, as our industrial partner, to bring fuel-cell technology to commercialization.

Genetic techniques for measuring microbial population changes caused by subsurface leaks of oxygenated fuels

A. M. Happel, T. C. Legler

MAIN TOC

As a result of amendments to the Clean Air Act in 1990, oxygenates were added to gasoline in the U.S. to decrease carbon monoxide emission from automobiles. These additives, mostly methyl tert-butyl ether (MTBE) and ethanol, along with other gasoline components, are now found at many leaking underground storage tank sites, of which there are about 400,000 nationwide.

Biodegradation of the major water-soluble components of gasoline (benzene, toluene, ethylbenzene, and xylenes, together called BTEX) is an important component of the remediation of these leaks. It is important to study the effects of oxygenates on the subsurface microbial populations responsible for BTEX degradation, because the size and activity of those populations affect the degradation rate and thereby affect the BTEX concentration in migrating groundwater plumes that could contaminate drinking water supplies. For example, oxygenates might increase the activity of oxygenate-degrading bacteria at the expense of BTEX degradation activity. Alternatively, the presence of oxygenates might fortuitously enrich bacteria that can degrade both oxygenates and BTEX.

Methods for quantifying the effects of oxygenates on microbial communities are limited by the absence of clear ways to identify and quantify the presence and activity of oxygenate-degrading microbes and of BTEX-degrading microbes. In this project, we have investigated the possibility of applying state-of-the-art molecular technologies to the quantitative detection of the organisms carrying these genes. This research supports DOE's mission in environmental restoration and waste management.

The use of molecular technologies is limited by the absence of genetic tools to characterize the microbial populations involved in oxygenate and BTEX degradation. Although the organisms and genes involved in MTBE degradation are unknown, many catabolic genes have been identified for the degradation of BTEX compounds. The focus of this partial-year LDRD project was to investigate the possibility of using genetic probes to quantify shifts in communities of BTEX-degrading microbes arising from releases of oxygenated gasoline. For the development of such probes, we selected seven microbial strains containing genes coding for various biochemical pathways of BTEX degradation.

From each of these genes, we selected distinctive regions (shorter than about 300 base pairs) that appeared to be specific to the associated pathway on the basis of comparisons with related genes and with the general gene bank. Gene probes were designed for conventional DNA:DNA hybridization analysis, which allowed us to determine how robust the probes are for identifying genes from diverse microbial groups that have the same function. From the seven selected microbial strains, individual probes were constructed and tested for cross-reactivity with catabolic genes coding for various biochemical pathways of BTEX degradation to ensure that the target probe would be useful for future studies involving heterogeneous populations of BTEX degrading bacteria. The powerful real-time polymerase chain reaction (PCR) technique was used to quantify low-level copies of target DNA (BTEX catabolic genes) within environmental samples. For this measurement, the environmental samples were spiked with bacteria containing a specific gene and detection limits were determined for hybridization and PCR-based methods.

These tests demonstrated that the laboratory tools developed in this project can be used to detect specific BTEX-degrading populations to very low concentrations (<100 organisms per gram of sediment). They can thereby provide information on the effect of oxygenates on the microbial community responsible for BTEX degradation. Rigorous studies involving materials from "real world" regulatory sites can now be performed to determine whether the presence of oxygenates in the fuel release will directly affect the population and catabolic activity of BTEX-degrading bacteria.

Electromagnetic imaging of carbon dioxide sequestration at an enhanced oil-recovery site

B. A. Kirkendall, J. J. Roberts

MAIN TOC

An effective means of decreasing surface-warming effects caused by increased levels of greenhouse gases is to sequester CO_2 in the subsurface. Moreover, the petroleum industry highly values CO_2 as a means of producing heavy oil—an abundant petroleum compound that is also expensive to process—more efficiently than other techniques during enhanced oil-recovery (EOR) efforts.

In this project, we are combining laboratory and field research to (1) image CO_2 injection and long-term sequestration at an EOR site using an electromagnetic (EM) imaging technique and system developed recently at LLNL, (2) improve and understand the data processing in CO_2 studies by coupling field results with these laboratory measurements during analysis, and (3) explore new techniques for imaging sequestrated CO_2. Our goal is to develop the ability to image subsurface, injected CO_2 during EOR processes while simultaneously discriminating between the injected CO_2 and pre-existing petroleum and water deposits.

Our work addresses national energy issues by developing field and laboratory techniques to improve in situ analysis of oil- and gas-enhanced recovery operations and also by providing a tool for in situ analysis of CO_2 sequestration—an international technical issue of growing importance.

During FY2001, we (1) acquired subsurface images and increased the accuracy and resolution of the processing method to produce difference images over time, and (2) built experimental equipment for the laboratory and conducted initial experiments. We acquired two complete tomographic data sets at multiple frequencies at an EOR site in Lost Hills, California. We then transformed these data sets in a mathematical process known as inversion—one obtained before CO_2 injection and one during—to a map of electrical resistivity using our newly developed routines to increase resolution and decrease calibration error.

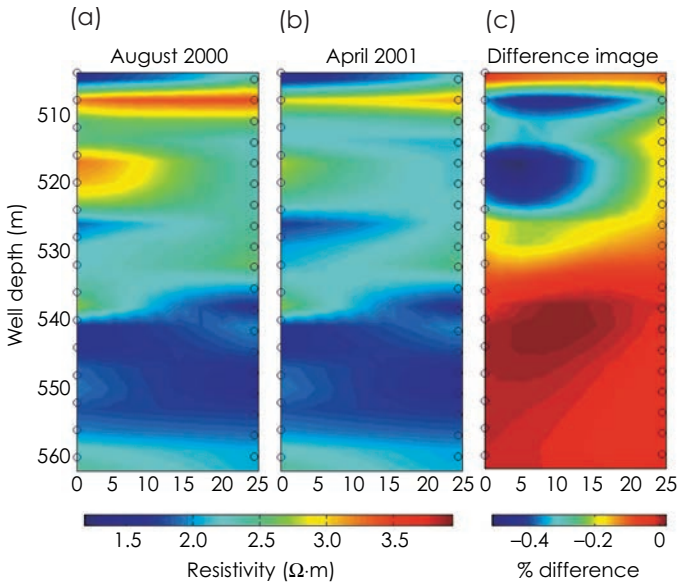

Two-dimensional images of the subsurface electrical resistivity in the plane between two observation wells (a) before, and (b) after CO_2 injection at 4.0 kHz. The difference image is shown in (c). The circles on the left side of each image represent the well containing the receiver antennae; those on the left represent the transmitting antenna. The difference image shows a decrease in resistivity between 500 and 525 m. Laboratory measurements confirm that this result indicates the presence of CO_2 or CO_2 byproducts.

Time-lapse results from 4.0-kHz data are shown in the Figure.

In the laboratory, under carefully controlled pressure and temperature conditions, we monitored the electrical properties of core samples from the same EOR site. Preliminary measurements indicate distinct electrical signatures for core samples saturated with brine, oil, and CO_2. Thus, EM images at appropriate frequencies should identify the different components.

We presented our initial results at the National Energy Technology Laboratory (NETL) First Annual Carbon Sequestration Conference, sponsored by the DOE, and also to our industrial partner, Chevron Heavy Oil Production, Bakersfield, California. Our work has been accepted for presentation at The International Gas Research Conference in FY2002.

Our focus during FY2002 will be on (1) improving the inversion process in CO_2 studies by coupling results with petrophysical laboratory measurements, (2) acquiring multiple-frequency data in the field, (3) developing techniques to estimate gas and oil saturation that are not currently possible, (4) continuing to acquire data at the EOR site, and (5) concentrating on frequency-dependent electrical properties of the ground and on how to best match electrical properties to gas and fluid content. To take advantage of the multiple-frequency data, we expect to develop a novel frequency-weighting technique to create higher-resolution images that are currently not possible using single-frequency data.

FLIRT: A magnetic field topology diagnostic for spheromaks and other self-organized magnetically confined plasmas

H. S. McLean, H. Chen, D. D. Ryutov

Tangled magnetic field lines are common in laboratory and space plasmas, but determining the geometrical structure of magnetic fields in the presence of plasma is a difficult and still unresolved problem. To address this open question, we are developing and testing a new technique for measuring the magnetic field-line topology in magnetically confined plasmas. Our field-line tracing diagnostic (FLIRT) uses a high-power, short-pulse laser to launch a burst of energetic (~100 keV) electrons from a target passing through the plasma. These electrons then generally follow magnetic-field lines until they strike a solid surface, where a burst of x rays is produced. The field-line connection length can be determined from the time delay between the laser pulse and the burst of x rays. The topology of the field lines can be inferred by measuring the connection length as a function of initial target location inside the plasma. Measuring the spatial distribution of x-ray production provides further information on the field topology, including the effects of magnetic field fluctuations and stochasticity.

This research includes testing the appropriate x-ray detectors; measuring the background x-ray emission in a spheromak plasma; measuring the energetic electron production by a short-pulse, high-power laser; and making preliminary measurements of the edge field line topology in the Sustained Spheromak Physics Experiment (SSPX). A pulsed electron-beam source is the prototype for a laser-based source. If successful, this technique will have broad application to a variety of plasma configurations and provide physics data applicable to many plasma-physics issues relevant to magnetic confinement fusion and space plasmas of interest to the DOE's fusion energy science program.

Since this project started in mid-FY2001, we have: (1) mounted a detector on the SSPX spheromak and compared plasma background x rays with those produced by the high-power laser system—measurements so far confirm the absence of x rays that would interfere with the goals of the diagnostic; (2) completed an electron spectrometer and electron-gun test stand and begun building prototype high-speed detectors and the electron gun; (3) begun to measure electron yield using the electron spectrometer on the JanUSP laser facility; (4) developed a theory of space-charge effects in the emission of fast electrons from the surface, which shows that the electron yield depends on the pulse-width and energy of fast electrons, but not on the focal spot size; the yield could be increased by a factor of ten by using a neutralizing plasma plume; and (5) performed an analytic study of the dynamics of fast electrons, accounting for the effects of magnetic mirroring and particle drifts.

During FY2002, we will further evaluate the background x-ray spectrum in SSPX and launch electrons into the edge plasma of SSPX taking x-ray measurements in vacuum and with plasma present. Our results will determine viewing geometry and requirements for detector sensitivity. The electron injection will test our ability to detect known quantities of electrons in an actual, self-organized plasma. Field line lengths will be measured and compared with 3-D magnetohydrodynamics computational modeling. Analytical electron-transport studies will be undertaken to quantify the relationship between field properties and quantities that can be measured. The results of our systematic study of electron production (efficiency, angular distribution, and space charge effects) with the high-power laser on solid targets will determine the minimum laser power required to produce sufficient quantities of electrons and measurable x-rays. These measurements will be compared with 3-D computational modeling of the laser–plasma interaction.

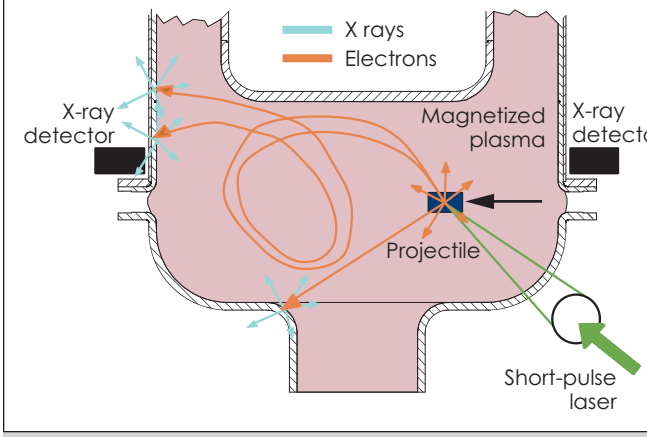

Electrons (red lines) generated by a high-power laser inside a magnetized plasma, shown in a spheromak configuration, are confined to magnetic fields lines and eventually strike the walls, generating x-rays (blue lines).

Chemical reactions controlling mobility of uranium in water in contact with apatite

M. J. Taffet, B. K. Esser, K. E. Roberts, B. E. Viani, J. Crispino

MAIN TOC

Uranium (U) contamination of groundwater is common at U mining, processing and disposal sites. In the U.S., 1.8×10^9 m^3 of groundwater are contaminated with radionuclides. Traditionally, U-contaminated groundwater is cleaned by "pump-and-treat" methods, which are expensive and of limited effectiveness in many situations. Passive, in situ methods may be more efficient, less expensive, and safer, e.g., installation of a reactive, permeable barrier to sequester dissolved U. Optimal design of a permeable reactive barrier, however, requires an understanding of the kinetics and thermodynamics of the U-removal mechanism.

Apatite [$Ca_5(F,Cl,OH)(PO_4)_3$] is known to remove U from groundwater. The mechanism, whether a surface process or precipitation of an insoluble phase (e.g. autunite: $Ca(UO_2)_2(PO_4)_2{\cdot}10H_2O$)], is not well-constrained, especially at dissolved U concentrations typical of groundwater plumes. Our goal is a mechanistic understanding of U removal by apatite by (1) documenting how variations in pH, dissolved CO_2, common ions, and apatite composition and surface area affect U removal; and (2) characterizing the structure and speciation of fresh and aged solid-phase U.

This project will provide insight and data about mechanisms that reduce U mobility in water. Elucidating these mechanisms requires controlled conditions plus the imaging and analytical facilities and expertise available at LLNL.

In mid-FY2001, we began batch experiments with four apatite forms: (1) amorphous ceramic hydroxylapatite, (2) crystalline hydroxylapatite, (3) coarse-fishbone apatite, and (4) fine-fishbone apatite. We measured surface areas of these apatites as 42.0, 82.7, 1.7, and 4.7 m^2/g, respectively. The apatites were pre-equilibrated with a phosphate buffer solution for several days at a solid:solution ratio of 1:1,000. Uranium was added to give an initial concentration of 10, 1,000, or 10,000 ppb. We measured pH and concentrations of U and anions and cations at intervals between 1 and 120 h. Equilibrium thermodynamic modeling indicates that, under these initial conditions and assuming no sorption, solubility with respect to precipitation/dissolution of autunite defines a maximum concentration of dissolved U at 2 to 3 ppm. Because many of the mixtures resulted in soluble U concentrations below 1 ppb, we hypothesize that sorption plays a major role in reducing dissolved U concentrations.

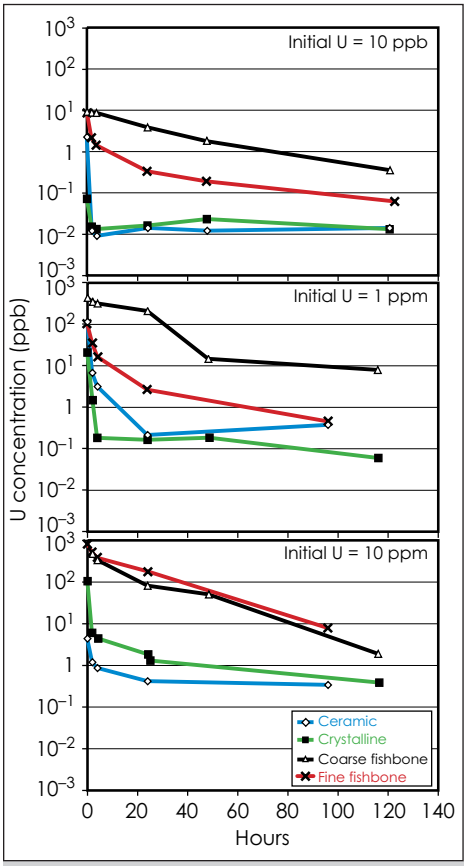

Concentration of uranium in water as a function of time for three initial concentrations and four different forms of apatite.

The Figure shows U concentrations over time for 12 batch experiments (four apatites at three initial U concentrations). Generally, fishbone apatite was less effective in removal rate and final equilibrium U concentration than crystalline or amorphous apatites, and coarse-fishbone was less effective than fine-fishbone apatite. In general, effectiveness is proportional to surface area. Within 5 min, ceramic and crystalline apatites reduced all U concentrations to below the 20 ppb Federal drinking-water standard. We anticipate that the fishbone apatite would be more effective if surface area was increased by grinding to a smaller particle size. In separate experiments, all four apatites reduced U concentrations from 45 ppb to less than 1 ppb in groundwaters at LLNL's Site 300 explosives test site.

During FY2002, we plan to (1) evaluate the effects of hydrolysis and schoepite [$UO_2(OH)_2$] precipitation on our results; (2) use reactive transport models to design column experiments; (3) perform batch and column experiments while varying dissolved CO_2 and pH to determine reaction-rate kinetics; (4) employ scanning electron microscopy/energy-dispersive spectroscopy (SEM/EDS) and x-ray diffraction (XRD) to characterize the solid phases of U; and (5) use x-ray absorption fine-structure (XAFS) spectroscopy to characterize sorbed species and coordination chemistry of U on apatite surfaces.

Removal of uranium from groundwater using granulated activated carbon modified with hydrophobic aerogels

S. J. Coleman, P. R. Coronado, J. G. Reynolds, M. J. Taffet, R. W. Williams

Uranium (U)-contaminated groundwater is a problem at some DOE sites and at other facilities that have had nuclear materials onsite. For example, at LLNL we have a regulatory-driven requirement to clean up contaminated groundwater at both the Livermore Site and at Site 300. In particular, Site 300 groundwater contains a variety of organic and radioactive contaminants, including U.

The goal of this project is to evaluate the feasibility and cost effectiveness of using hydrophobic-silica-aerogel-impregnated granular activated carbon (GAC) for treating groundwater contaminated with low concentrations of U. This project leverages LLNL's expertise in the research and production of aerogels and in groundwater remediation. The results will be useful in planning pilot studies at LLNL and at other sites with similar groundwater issues.

During FY2001, we conducted a bench-scale experiment to study the adsorption capabilities of an aerogel/GAC composite for low concentrations of U in groundwater. We began by preparing varieties of hydrophobic silica aerogel that had been modified with phosphoric acid (H_3PO_4), which has an affinity for U. These aerogels were then individually combined with GAC (in this case, virgin coconut shell is the source of the GAC) to produce composite samples. The GAC was chosen because it would continue to adsorb other contaminants from the groundwater (e.g., volatile organic compounds). Thus, the composite would take advantage of the infrastructure already existing for treatment technologies that utilize GAC, and would produce less waste than the amount of conventional GAC needed to treat an equivalent volume of groundwater.

The modified materials were formed by mixing $(CH_3O)_4Si$ with a hydrophobic sol-gel precursor. The phosphorus (P) was added during the aerogel reactions by using different P-containing precursors.

To simulate the conditions of treating groundwater, the sample composites were put into vials with laboratory-prepared solutions that contained either 50 or 100 ppb of U. We then (1) analyzed the simulated treated groundwater using inductively coupled plasma mass spectrometry (ICP-MS), and (2) calculated the amount of U that was absorbed by each composite. The most promising composites (those described below) were used with solutions of 100 ppb of U.

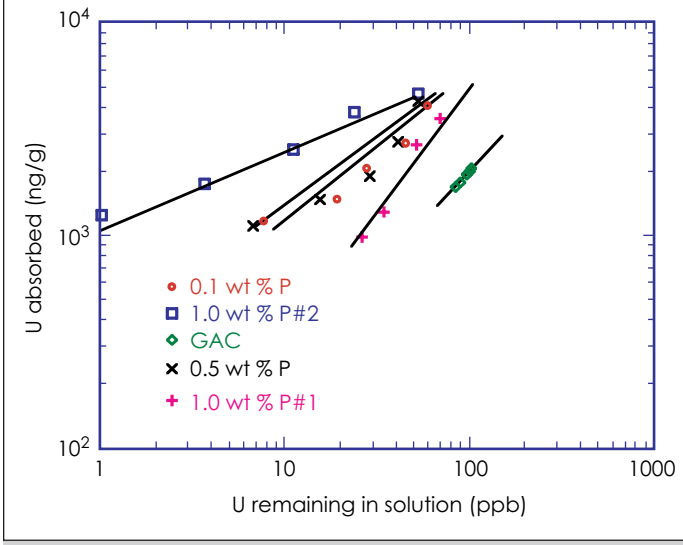

Effectiveness of aerogel/granular-activated-carbon (GAC) composites vs. GAC in removing low concentrations of uranium (U) from groundwater. The composites with varying amounts of phosphorus (P) incorporated into the aerogel (ranging from 0.1 to 1% P by weight) out-performed GAC. The slope of each line is an indicator of its adsorption intensity; its respective intercept is an indicator of adsorption capacity.

Using a modified ASTM D 3860-98 test method, we found that the composites were superior in removing U from solution compared to GAC alone (see Figure). These results show that GAC modified by hydrophobic aerogels can form a superior composite treatment material for adsorption of U in the aqueous phase and could have broad application in the cleanup of U-contaminated groundwater. A patent application has been filed.

In FY2002, we plan to evaluate and improve our method for increasing the affinity of the hydrophobic silica aerogel for U, conduct additional analyses by varying the concentrations of U, evaluate the effects of varying the water chemistry, and document our results and submit them to a peer-reviewed journal.

Isotopic tracing of fuel components in diesel emissions

B. A. Buchholz

Environmental and health concerns over engine emissions are leading to increasingly stringent emissions standards, which in turn drive research into the use of unconventional, cleaner-burning fuels. Beyond emissions concerns, U.S. dependence on imported oil makes transportation fuel a national security issue. If cleaner-burning, renewable fuels can be substituted for petroleum products, even in part, U.S. dependence on foreign oil can be reduced and the conversion of deep-reservoir carbon in fossil fuels to greenhouse gases can be slowed.

The addition of oxygenates, such as ethanol, to diesel fuel is known to reduce emissions of particulate matter (PM). The mechanisms responsible for this reduction are not fully understood because it is difficult to determine the origin of these and other undesired emissions, such as unburned hydrocarbons and CO, from among the various fuel components. The subattomole sensitivity of accelerator mass spectrometry (AMS) for measurement of radioactive carbon-14 (^{14}C)allows us to trace the C atoms from specific fuel components, such as ethanol, to soot or gaseous emissions. Radioactive materials are not required, because contemporary C (e.g., that in ethanol derived from grain) has 1000 times more ^{14}C than petroleum-derived fuels. The specificity and sensitivity of ^{14}C AMS makes it a powerful tool in acquiring data for validation of combustion modeling.

We will use data provided by our engine tests to validate combustion models developed at LLNL. In separate work stimulated by this research project, such data will provide insight into which parts of the molecular structures of fuels and additives most greatly influence emissions.

For our tests in FY2001, we ran our test engine, a six-cylinder, 6-l 1993 Cummins diesel (see Figure), at 1600 rpm and 210 ft·lb. Our test fuels were diesel blends with 10, 20, and 40% ethanol. We used an emulsifier or cosolvent to overcome the low solubility of ethanol in diesel fuel, and we supplemented the blends with an ignition improver to maintain the autoignition properties of the baseline diesel.

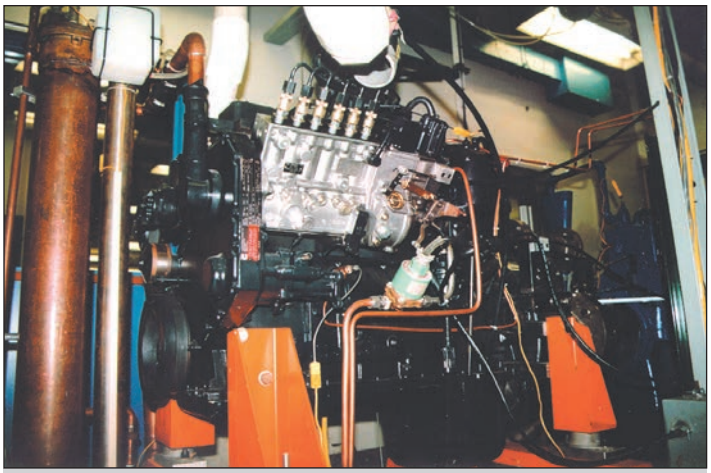

Diesel test engine at the University of California, Berkeley

We collected PM on quartz filters after passing the exhaust through a minidilution tunnel, which allows the formation of the PM actually observed in diesel exhaust. We separated the PM into volatile and nonvolatile organic fractions (VOF and NVOF) for AMS analysis. A fuel formulation that shifts PM to the VOF may be just as important as reducing overall soot mass, because the VOF is amenable to conventional catalytic conversion to CO_2.

In general, the addition of ethanol to diesel fuel reduced both PM and NO_x emissions with respect to those of baseline diesel fuel. The homogeneous cosolvent blends were more effective in reducing total PM mass, but the heterogeneous emulsified blends yielded a higher VOF. The chemical mechanisms that inhibit soot formation and/or promote soot oxidation appear to depend on the homogeneity of the ethanol–diesel blend. Ethanol-derived C tended to reside in the NVOF, especially for the cosolvent blends. The role of C_2 molecules in soot formation may account for the high level of ethanol-derived C in NVOF PM, and this suggests that fuel components with ethyl groups may be undesirable. We are preparing reports of this work for publication.

We plan to develop techniques for separating the small aldehydes (formaldehyde and acetaldehyde) in the VOF from the PM. Small aldehydes and CO are implicated in smog production and can serve as data validation endpoints for combustion models. Continuing our investigation of the origins of undesired engine emissions, we will run soy biodiesel–diesel, methanol–diesel and ethanol–diesel blends in FY2002. Only the C bound to oxygen will be labeled in the alcohols, allowing us to trace individual C atoms.

A laboratory approach relating complex resistivity observations to flow and transport in saturated and unsaturated hydrologic regimes

C. R. Carrigan, S. Martins, W. Daily, A. Ramirez

MAIN TOC

This project studied the feasibility of using two important imaging techniques— electric resistance tomography (ERT) and electric impedance tomography (EIT)— to learn about porous flow and transport in soils. The goal is to use these techniques for obtaining quantitative information about how a site will respond hydrologically to an infiltration event. In addition, this feasibility study initiated a collaboration with Rensselaer Polytechnical Institute (RPI) that will enhance LLNL's capabilities in subsurface imaging of flow and transport processes in support of DOE's environmental restoration and waste management program.

These two tomographic methods—ERT and EIT—involve passing currents (dc or ac) between two electrodes that are within or between electrode arrays while measuring the electric potential at the remaining electrodes. With the aid of an inversion scheme, the potentials are used to solve for the electrical conductivity distribution in the region bounded by the electrode arrays. Groundwater movement resulting from a leak or surface spill will produce measurable conductivity changes, which have been imaged using ERT. However, quantification of the groundwater flow remains open to interpretation of the imaged results.

In FY2001, we performed a series of experiments to evaluate the fundamental relationship between ERT and EIT images and targets of a given volume that approximate infiltration-induced conductivity anomalies. To pursue issues relating imaging of conductivity anomalies to quantification of groundwater transport, a test section was constructed that simulates the subsurface electrode distribution used at the LLNL Vadose Zone

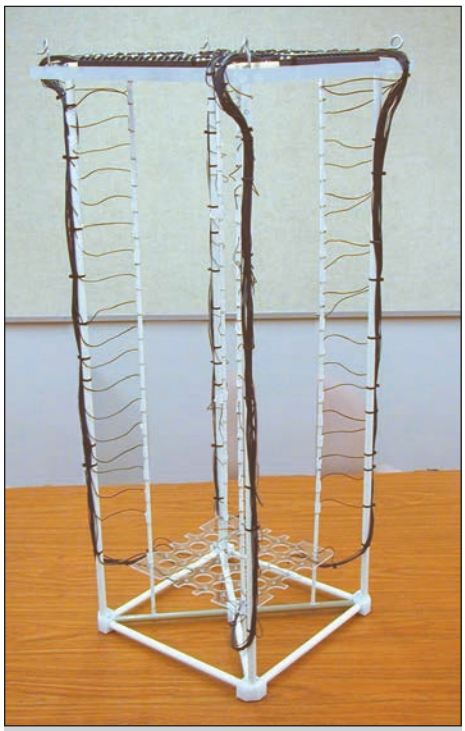

The four-electrode-well test section simulating the subsurface distribution of electrodes at the LLNL Vadose Zone Observatory (VZO). The test section is immersed in a large tank of water to simulate the conducting conditions of the soil at the VZO site. Stainless steel cylinders are suspended at different locations inside this test section to evaluate the characteristics of tomography and electric impedance tomography for imaging subsurface conductivity changes caused by groundwater flows.

Observatory (VZO). The four electrode arrays, each having 18 electrodes, are analogous to the four electrode wells at the VZO. Instead of using soil, we conducted the experiments in a 10,000-gal. tank of water, which provided the electrically continuous medium surrounding the four arrays. The Figure illustrates the electrode arrays used for the imaging study. The target used in this experiment, conductive metal cylinder of known conductivity, was suspended at varying locations between the electrode arrays and imaged. The images produced by the ERT and EIT techniques will be evaluated to determine the distortion of the conductivity anomaly as a function of its location between the electrode arrays.

The test section constructed for this study also included electrode arrays that resemble biomedical array distributions. Comparison of images of the same target produced with the four-array geophysical electrode distribution and the biomedical electrode array distribution will help us to better understand both the differences and advantages of the biomedical and geophysical electrode array patterns.

A secondary objective of this study was to initiate collaboration with researchers at RPI and the newly created National Science Foundation Center for Subsurface Imaging and Sensing Systems (CenSSIS). A major goal of CenSSIS is to promote collaborations among researchers with imaging backgrounds in different disciplines (geosciences, biomedical, civil engineering and biomedical) that will lead to new solutions of common subsurface imaging problems. Due, in part, to the results of this feasibility study, support for subsequent research will come from a DOE Office of Basic Energy Sciences project.

Feasibility of using chlorine-36 to depict water infiltration at the Pit 7 Complex at Site 300

G. J. Nimz

This feasibility study was designed to determine if variation in the abundance of fallout chlorine-36 (^{36}Cl) in soil profiles within the LLNL Site 300 Pit 7 Complex are of sufficient magnitude that chlorine and ^{36}Cl can be used to determine the sources of ground water invading the Complex. Physical measurements indicative of moisture movement and flux are prone to high degrees of uncertainty in the semi-arid unsaturated soils surrounding the Pit 7 Complex. In such situations, chemical methods have proven more useful than physical methods.

The Pit 7 Complex is a series of landfill pits in the northwest corner of Site 300 that contain waste debris from firing-table tests conducted from the late1950s to 1988. The pits were closed and capped, but today are responsible for a groundwater contaminant tritium plume. The source(s) of the invading groundwater is unclear. Water may enter the pits through their barrier caps, peripherally from surrounding hillslope surface runoff, or flow through the alluvial soils on these hill slopes. Tritium then enters into the bedrock aquifer, creating two tritium plumes: one migrating down valley (southeast) through saturated alluvium, and one migrating down dip (east-northeast) in bedrock. An engineering solution might prevent the pits from becoming saturated and releasing tritium. To assess this possibility, the sources of water invading the pits, the rate of migration of this water, and the degree and nature of local hydrologic connectivity must be determined.

Chlorine-36 derived from atmospheric nuclear testing (fallout) in the 1950s to 1960s can be used as a tracer to detect groundwater entering the system during that period. This includes water already at the water table as well as soil water currently infiltrating toward the water table. The measurements provide a means of identifying areas of high-infiltration flux. In unsaturated soils, they provide a measure of infiltration velocity by indicating the depth of water infiltration since the 1950s and 1960s. Information on lateral variations of infiltration volumes (flux) and velocities provides the foundation for identifying the sources of water within a basin. The purpose of this LDRD study was to determine if this method was applicable to the Pit 7 Complex basin. The results indicate that it is feasible to use bomb-pulse ^{36}Cl to depict infiltration flux and velocity because the bomb-pulse peak (1) is identifiable in Pit 7 Complex soil core profiles [Fig. (a)], (2) varies in magnitude at different locations (indicating variable water flux), and (3) occurs at varying depths at different locations (indicating variable water velocities).

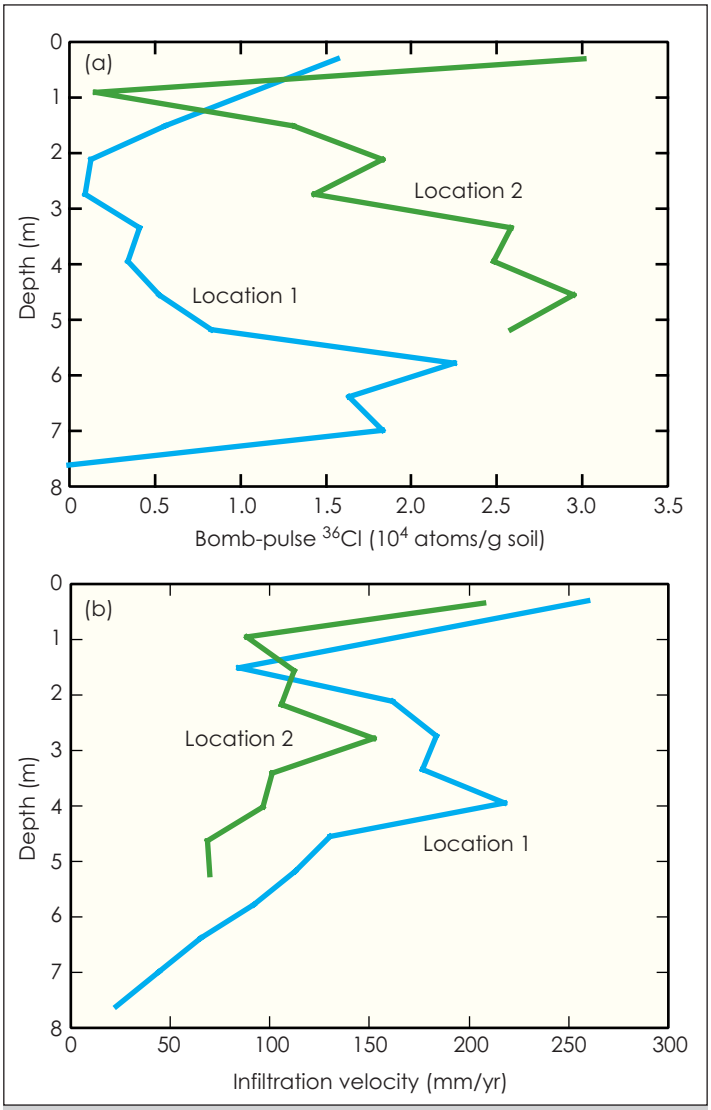

(a) Soil bomb-pulse ^{36}Cl at two Pit 7 Complex locations. Non-bomb-pulse ^{36}Cl, based on soil Cl concentrations and precipitation ^{36}Cl/Cl ratio ($150 \cdot 10^{-15}$), are subtracted. (b) Calculated infiltration velocities at two Pit 7 Complex locations. Profiles are independent of soil moisture content, which was not measured.

A simple numerical model for infiltration flux and velocity can be derived based on soil chloride concentrations. The model is based on atmospheric flux of chloride to ground surface and its accumulation in the soil column. At Site 300, the model can be calibrated using bomb-pulse ^{36}Cl. Figure (b) shows derived infiltration velocities at two Pit 7 Complex locations. While collecting the soil and hydrologic data necessary for a more rigorous numerical model was beyond the scope of this study, the results of this chloride accumulation model clearly demonstrate that chloride and ^{36}Cl data are useful in depicting infiltration at Site 300. In the continuing investigation of the origin and development of the Pit 7 Complex tritium plume, bomb-pulse ^{36}Cl will provide a useful tool for hydrologic characterization.

Lasers, Electro-Optics, and Beams

Section 6

Section 6 Lasers, Electro-Optics, and Beams

Computational and experimental development of a Compton x-ray source

H. A. Baldis, F. V. Hartemann

Recent technical advances in ultrashort-pulse laser technology, diode-pumped solid-state lasers (DPSSLs) and high-brightness electron sources offer the exciting opportunity to design novel, compact, monochromatic, tunable, femtosecond x-ray sources using Compton scattering. Such sources would enhance a number of important LLNL core competencies, including the study of fast structural dynamics, advanced biomedical imaging, and x-ray protein crystallography.

In FY2000, we met our goals of establishing a theoretical formalism capable of fully describing the 3-D nature of the interaction between electrons and photons, and the influence of the electron and laser-beam phase-space topologies upon the spectral brightness of the x rays.

During FY2001, we completed the interface between 3DCOMPTON and the Los Alamos National Laboratory's (LANL's) electron-beam design code PARMELA; completed the development of an innovative concept, the Ring Femtosecond Laser-Electron X-Ray (ReFLEX) source, for which a patent is being processed; commissioned and began operating a high-frequency (8.547 GHz), high-gradient (>150 MeV/m) X-band photoinjector; and further developed our chirped-pulse, inverse free-electron laser (CPIFEL) acceleration concept.

ReFLEX integrates a high-intracavity-power laser oscillator and a compact electron storage ring with unique features for stabilizing and maintaining very high-brightness electron bunches. The result is the production of tunable x-rays at high average flux. In turn, these enabling technologies open a new path to exciting modern applications, including macromolecule and protein crystallography, which are traditionally performed at national synchrotron facilities. The 3DCOMPTON–PARMELA code interface provides a new, flexible, and accurate tool for modeling the interaction of relativistic electrons with ultrahigh-intensity laser pulses. This tool is capable of providing an extremely detailed analysis of the x-ray phase space, as illustrated in Fig. (a–d).

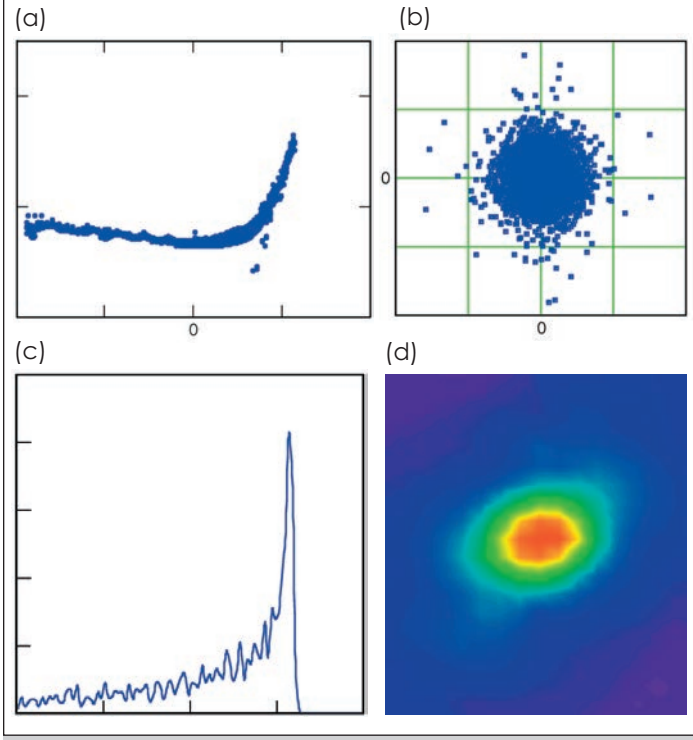

X-ray phase space, as modeled by 3DCOMPTON for the PLEIADES facility. The Figure shows (a) the electron-beam energy spectrum (horizontal scale: ±2 ps, vertical scale: $68 < \gamma < 75$), (b) the electron beam at focus (40×40-μm^2 frame), (c) the peak x-ray spectral brightness between 10 and 35 keV (vertical scale: 0 to 2.5×10^{20} photons/s/mm^2/mrad^2/0.1% bandwidth), and (d) the x-ray radiation pattern (10×10-mrad^2 frame).

Emittance is a measure of the transverse momentum spread of an electron beam, and ultimately limits its minimum spot size after magnetic focusing. Such high-quality electron bunches are required for efficient x-ray production via Compton scattering, where the size of the electron beam must match that of the focused laser, and where precise timing between the two subpicosecond pulses is of paramount importance. Using the X-band photoinjector commissioned during FY2001, we demonstrated the production of relativistic (2 MeV) electron bunches with very low emittance (measured at 1.65 π-mm·mrad). The beam also has an excellent energy spread of 1.8%—as obtained using a high-precision magnetic spectrometer, and extremely short duration (<2 ps)—as measured by a streak camera. The intrinsically synchronized production of electrons in the photoinjector enables experiments on both Compton scattering x-ray production and laser acceleration.

Finally, further developments in our CPIFEL acceleration concept include the detailed theoretical study of the interaction of an intense laser wavepacket with a relativistic electron in the presence of a dephasing static magnetic field, called a "delta-function wiggler." In this case, a new scaling law for the electron energy has been established for plane waves. The extremely favorable scaling may provide a practical approach to ultrahigh-gradient vacuum-laser acceleration.

An inner-shell photoionized x-ray laser at 45 angstroms

F. A. Weber, P. M. Celliers

The advent of advanced, chirped-pulse amplification techniques and their implementation into tabletop energy sources have rendered inner-shell photoionization (ISPI) x-ray laser (XRL) schemes increasingly attractive. Application of laboratory-generated short-wavelength and short-time-duration x-ray pulses in a variety of scientific disciplines—including biology, biomedical imaging, materials science, and plasma physics—is closer to realization than ever. In this project, we have attempted to design and build an ISPI XRL at 45 Å. The lasing transition is pumped in low-density carbon (C) by an incoherent x-ray source. This project will benefit the development of new diagnostic tools to probe the properties of high-density plasmas relevant to inertial fusion and stockpile stewardship. More broadly, it enhances LLNL's competency in high-energy-density physics, x-ray lasers, and optics.

The underlying concept for this project is based on the fact that the photoionization cross section is much larger for tightly bound inner-shell (1s) electrons than for more loosely bound outer-shell (2p and 2s) electrons. This consideration requires photon energies that are at least enough to photoionize the carbon K shell (~286 eV). As a consequence of the higher cross section, inner-shell electrons are knocked out, leaving a hole state $1s2s^22p^2$ in the singly charged C ion. This generates a population inversion to the radiatively connected state $1s^22s^22p$ in C^+, leading to gain on the 1s–2p transition at 45 Å. Competing processes that deplete the population inversion include auto-ionization, Auger decay, and, in particular, collisional ionization of outer-shell electrons by electrons generated during photoionization. Rapid termination of the gain mandates an ultrafast, high-intensity laser pumping system in traveling-wave arrangement.

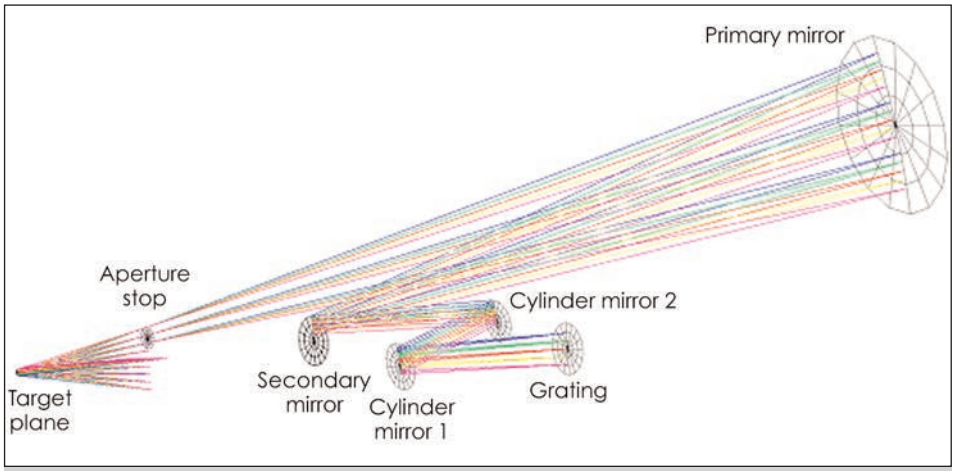

Near-diffraction-limited, traveling-wave, ultrashort-pulse laser pumping system in line-focus geometry. This novel scheme can create a traveling wave from a 30- to 50-fs pulse.

In the first two years of the project, we completed target design and static-target backside x-ray emission spectroscopy. In FY2001, we focused on developing a traveling-wave pumping system suitable for an ultrashort-pulse laser facility. A holographically generated grating serves both to produce the pulse front tilt needed for the traveling wave and to correct residual aberrations in the focusing system. An image of an incident 50-mm beam is projected onto the 10-mm target surface at 5× demagnification. Most of the focusing power is accomplished using a reflective, inverted, off-axis Schwarzschild microscope configuration, as shown in the Figure. The grating is centered on, and perpendicular to, the chief axis of the Schwarzschild system. The grating image is projected onto the target plane, which is also centered on and perpendicular to the chief axis. The required astigmatism is accomplished by using two additional cylindrical mirrors that are configured to produce the required line focus on target.

In FY2001, the system optics were built and tested. Characterization of the large mirror (12-in.-diam, gold-coated spherical optic) showed an extremely smooth surface, with a measured surface roughness on the order of only 5 Å and surface figure better than λ/20.

The shape of the pulse front can be adjusted to correct for its cylindrical appearance in the target plane by using a slightly cylindrical surface at the grating plane. The required grating surface curvature depends on the magnification and focal length of the Schwarzschild system. The remaining geometrical aberrations are corrected by generating the grating holographically. Back-illumination of the system with a diffraction-limited line focus at the target plane produces the grating by interfering the back-propagating beam with the incident beam at the grating surface. The back-propagating beam incorporates residual aberrations in the focusing system, thus allowing the production of a grating pattern that corrects for the aberrations. During operation, slight adjustments in the phase velocity of the pump at the target can be accomplished by slight tilts of the grating about an axis perpendicular to the plane of incidence.

Recreating planetary cores in the laboratory

G. W. Collins, P. M. Celliers, D. Hicks

The existence of life outside our Solar System relies partly on the probability of suitable host planets. What is known about the formation or interior properties of planets within or outside our Solar System is largely theoretical. At best, these models are constrained by the radius, atmospheric spectroscopy, gravitational moment, and magnetic field data. Integral to these models are the equation of state (EOS) and transport properties of the constituents at extreme conditions (about 10 Mbar and 10,000 K). However, very few materials have their high-pressure (>few Mbar), EOS, or transport properties experimentally validated—and even then, only on the principal Hugoniot. The Hugoniot is the locus of all final states achieved behind a single shock wave passing through a material from an initial state. Until recently, nuclear explosions were the only way to achieve the approximately10-Mbar pressures expected to persist at the core of giant planets (e.g., Neptune and Uranus).

Recently, we developed techniques to use high-energy laser facilities to produce and accurately characterize ultrahigh-pressure Hugoniot states. These data constrain EOS and transport models that enable the design of inertial-confinement fusion (ICF) experiments and are integral to models of planetary and stellar interiors. However planets, stars, weapons, and ICF all require EOS models at densities higher than can be achieved with single-shock Hugoniot techniques. Thus, a central theme of this work is to learn to use high-energy laser facilities to produce and characterize material states at densities even more extreme than those that can be achieved with single-shock techniques. We are now measuring Hugoniot and off-Hugoniot properties of materials to provide stringent tests of the material database required for the Stockpile Stewardship Program, ICF, and planetary models.

During FY2001, we developed and tested precompressed and multiple-shock techniques to recreate the extremely high-density core states of giant and extrasolar planets. Double-shock experiments show Sesame—an EOS database used world wide—accurately represents the EOS of water at 6 Mbar to densities near 4 g/cm^3. In addition, to test Sesame at densities higher than 4 g/cm^3, the first-ever precompressed-shock experiments were performed on water squeezed to high initial density in a diamond-anvil cell.

We are still analyzing the results of these experiments—but it appears that even with very modest precompression (10 kbar) there is a suppression of metallization pressure by about 100 Kbar. The Figure shows how shock-compressed reflectivity changes with pressure and temperature using Hugoniot and off-Hugoniot techniques. These results show that the water—metal insulator transition (the transition point at which water becomes a metallic conductor) is highly temperature activated.

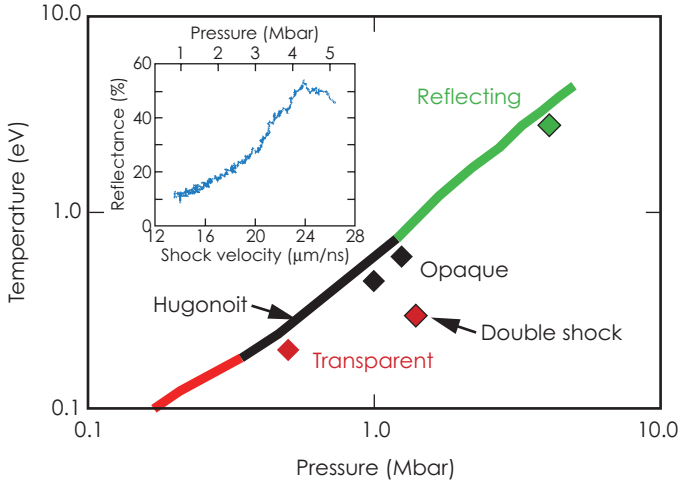

Results of first-ever precompressed-shock experiments on water together with reflectance measurements of water on the principal Hugoniot. The temperature–pressure axes indicate the states achieved in different experiments. Color designates whether the shock-compressed fluid is transparent (red), opaque (black), or reflecting (green) at λ = 532 nm (where λ is the wavelength of light used in the reflectance measurements). The line (diamonds) shows states achieved with the single-shock principal Hugoniot (precompressed single and double shock) measurements. The inset shows the shock reflectance of water on the principal Hugoniot at λ= 532 nm.

In FY2002, we will determine the limits of these techniques, complete off-Hugoniot measurements for water to 10 Mbar, and begin to determine planetary-relevant properties of N_2, O_2, C, and H_2. These materials are also of great interest to weapons physics because they are constituents and burn products of high explosives. Through the EOS and electronic properties, we will identify regions of molecular dissociation and association.

Ultrafast dynamics of plasma formation and optical materials modifications under high-fluence laser irradiation

S. G. Demos, H. B. Radousky, H. Baldis, M. Feit

Laser-induced damage in optical materials remains a problem in optical components of high-power, high-energy lasers. Such lasers have application to the Stockpile Stewardship Program and to inertial confinement fusion. It is believed that damage initiation is accompanied by the formation of plasma, which leads to localized high temperature and pressure that result in mechanical damage and the formation of defects. Our goal is to reveal the fundamental mechanisms by which laser damage occurs in transparent dielectric materials at relatively low fluences.

During FY2001, we used time-resolved spectroscopy to investigate the broadband flash of light that accompanies laser damage. The nature of this emission is still only partially understood. We also used electron paramagnetic resonance (EPR) spectroscopy and modeling to enhance our understanding of a possible mechanism leading to the plasma initiation. Spectra from the damage event—taking place in the bulk of KD_2PO_4 (DKDP) crystals—were recorded at different delay times with 10-ns temporal resolution. Immediately after damage initiation, the spectra were found to be roughly blackbody.

The Figure shows the evolution of measured temperature as a function of the delay time. An initial, rapid temperature drop is followed by a slower decrease. The observed temperatures can be related to the size and electron density of the plasma "fireball."

We observed that the temperature of the plasma decreases as fluence is increased. This could result from self-defocusing and shielding—the result being a larger ionized region that was heated to a lower temperature, accompanied by a slower cooling rate. The fact that the plasma reaches temperatures on the order of 10^4 K indicates that a substantial amount of energy (on the order of 20 kJ/cm^3) has been deposited. The initiating nanoparticles can be ruled out from this role because they are too small. This suggests that the absorption predominantly results from a high electron density. For the free electrons to appear opaque, their density would need to be above the critical density of 10^{22}/cm^3. These electrons are not thermal in origin because for a temperature of 10^4 K their density would be approximately 10^{17}/cm^3. This five orders-of-magnitude discrepancy suggests that impact ionization and electron avalanche are the dominant mechanism. Furthermore, the blackbody fit to the measured spectra at times after the laser pulse has terminated indicates that the electron density remains on the order of 10^{20} even tens of nanoseconds after the laser pulse has terminated.

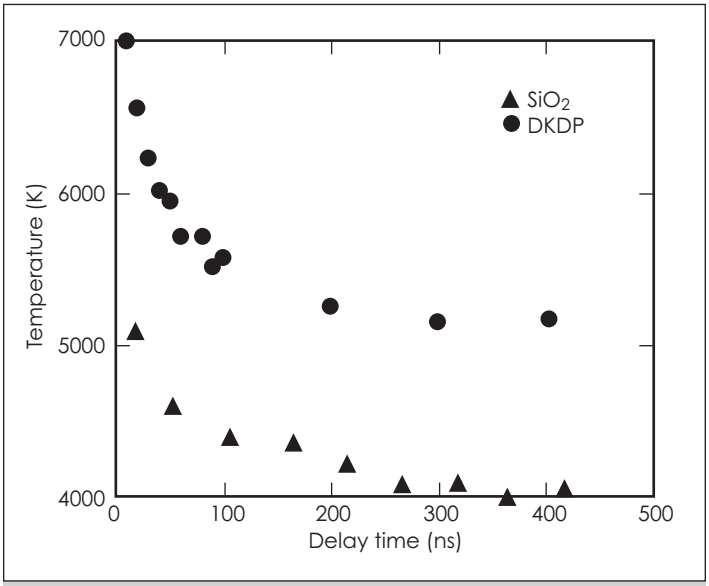

Temperatures obtained by fitting time-resolved emission spectra to blackbody emission. The spectra were recorded during laser-induced damage in the bulk of KD_2PO_4 (DKDP) crystals and fused-silica (SiO_2) samples.

The EPR study revealed new hole and electron traps in KH_2PO_4 (KDP) crystals that are stable at room temperature. These defects—present from the growth of the crystals—are converted to the paramagnetic forms by a 266-nm laser beam or x rays. We demonstrated that optical absorption extending from 200 to 700 nm accompanies the formation of these paramagnetic centers. In addition, using the pseudopotential method, we carried out (for the first time ever) first-principles calculations of electronic structure for the paraelectric and ferroelectric phases. These results provided a general picture for the ferroelectric phase transition of KDP and reconciled the previously proposed models.

Our goals for FY2002 include investigating the plasma emission on different materials and with different excitation wavelengths. For the first time, we will perform wavelength-dependant damage testing and also (1) further characterize the properties of defect centers observed with EPR spectroscopy, and (2) compare defect centers in KDP and DKDP crystals. Our experiments will be complemented by ab initio calculations to investigate the effect of point defects.

Large-aperture, lightweight space optics

R. A. Hyde, S. N. Dixit, A. H. Weisberg

Large, lightweight optics are important for many space-related missions. To develop such instrumentation, this research project has proposed a radically different approach for making them using diffractive optics instead of mirrors or conventional lenses. The specific goal of this project is to fabricate a diffractive lens that is lightweight, foldable, of high resolution, and the size class of lenses used in the Palomar and Hubble telescopes. Such an optic would be useful for the mission objectives of federal agencies responsible for deploying and using space-based assets, for example, the National Aeronautics and Space Administration and the National Reconnaissance Office.

In FY2001 our primary focus was to demonstrate that large, optical-quality, diffractive lenses can be successfully fabricated. The basic approach for building the lens was to assemble it by seaming together multiple thin-glass panels. This multipanel approach split the lens fabrication into two separate and feasible tasks: optical engineering to create meter-scale lens panels, and mechanical engineering to align and join panels across the full 5-m aperture. Accomplishing these tasks required a number of innovations in metrology and optical-component fabrication.

To make the lens panels, we needed meter-sized sheets of thin glass, each smoothed to an identical uniform thickness and patterned with the proper diffractive surface profile. The panels are smoothed by a two-stage process, based upon spatially controlled wet etching. Initial smoothing is performed by an interferometrically controlled line etcher, which removes the bulk of the surface ripples. During FY2001, we demonstrated the effectiveness of this process at subscale (see Figure) and built a production machine—currently being debugged—for scaling up to full-sized panels. Although the line etcher will perform the bulk of the smoothing, we are developing a second-pass etcher to remove any residual 2-D surface ripples. After the panels are smoothed, we will use lithographic surface patterning to make each panel act properly as a segment of the overall diffractive lens. Also in FY2001, we designed high-precision, panel-sized masks to define these patterns, which we then procured commercially. In FY2002 we will perform the lithographic processing necessary to transfer the lens patterns from these masks onto our thin-glass lens panels.

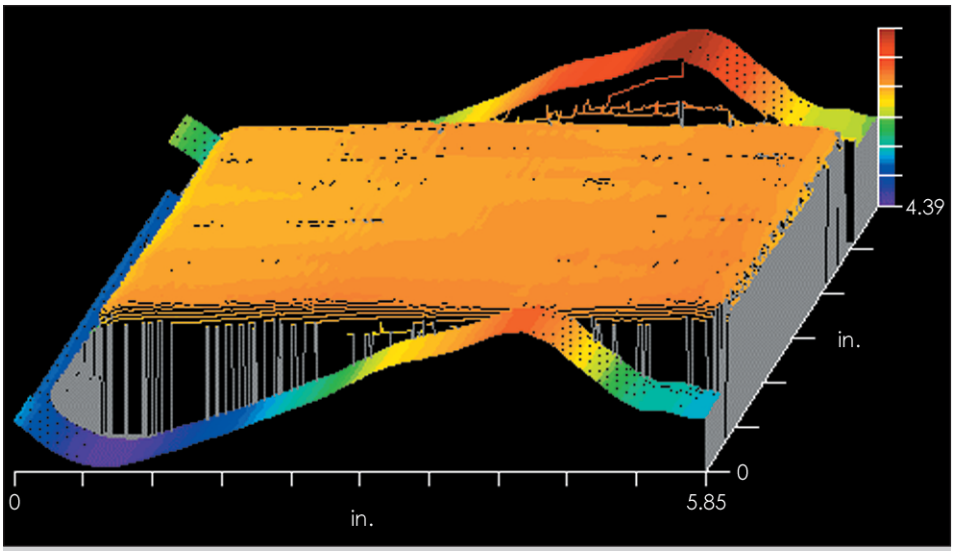

Glass smoothing achieved with spatially controlled line etcher

Once a full suite of lens panels is produced, the panels will be assembled into a complete lens. We will perform this assembly with the same panel-by-panel process demonstrated last year on our 75-cm lens, but upgrade the process to account for the larger size, panel-count, and tolerance requirements of our 5-m lens.

This high-precision assembly will be done on a large, semi-automated work station of our design, which is now under construction. Its work surface is 6 × 6 m in size and is thermally and vibrationally controlled. Each panel is aligned to its neighbors, first by monitoring fiducials along the common borders and then applying the proper 3 degrees-of-freedom adjustment to its position with a precision nudger. Once the panel is in the proper location, it will be joined to its neighbors with foldable metal seams. When all the panels are attached, we will determine the overall precision of the lens through global metrology.

Our goal during FY2002, the final year of this project, is to build a prototype large, lightweight, diffractive lens. We will first smooth and pattern a full suite of lens panels and complete the construction of our lens-assembly station. This station will then be used to align and join the separate panels into a diffraction-limited, 5-m lens.

Reconfigurable optical code division multiple access for fiber-optic networks

S. W. Bond, I. Y. Han, S. C. Wilks, E. M. Behymer, V. R. Sperry, S. J. Yoo, J. P. Heritage

MAIN TOC

High-speed, high-capacity fiber-optic communications networks, which allow multiple users to access the same network simultaneously by sharing the same transmission medium, have proliferated for long-distance, metropolitan, and local-area communications systems. Recently, a rapid expansion into wavelength division multiplexing (WDM) systems, which use multiple wavelengths to increase capacity, has been taking place. Code-division multiple-access (CDMA) techniques, which were originally developed for wireless communications, can also be used to further accommodate multiple users on an optical fiber. For the foreseeable future, fiber-optic networks utilizing WDM and CDMA will be the most important medium for the worldwide transfer of information.

This project entails the development of advanced technologies that have potential applications to national security and that position the Laboratory, in cooperation with government agencies, to better understand and utilize these systems. The project also enhances LLNL's competency in optoelectronics and high-speed communication technologies.

By applying innovations in WDM-component technology, we are developing a compact optical CDMA (O-CDMA) encoding and decoding device that would be adaptable to fiber-optic networks; be completely compatible with commercial coding schemes; and allow remote, rapidly reconfigurable user codes. Our goal is to apply the techniques of O-CDMA, where each user imprints his or her own message bits with a unique code, to spectrally phase-modulate (encode) a broadband, ultrashort, transmitted optical pulse that can only be decoded by the complementary phase modulation at the receiver end. The Figure, which is based on data measured by a collaborator, indicates the effectiveness of this type of transmission. On the basis of these results, we believe that integrated, monolithic semiconductor devices, which do the spectral slicing and phase modulation of the input pulse, can be devised that will allow for high-speed, remote reconfiguration of a user's O-CDMA code.

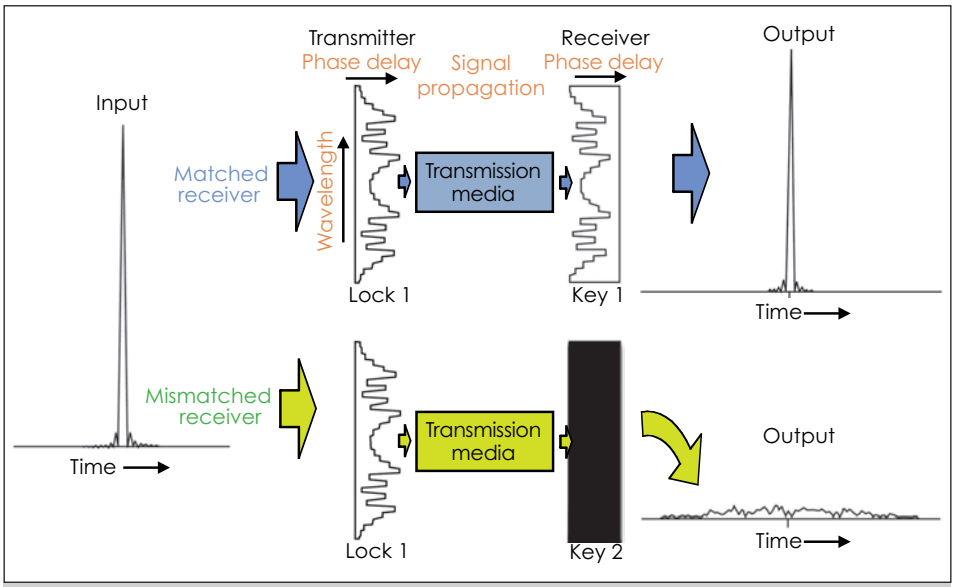

An example of the effectiveness of spectral phase encoding/decoding for a receiver when it is both matched and mismatched to the transmitter code.

Our approach uses broadband, ultrafast (300-fs) pulses from a mode-locked, erbium-doped, fiber-ring laser operating at 1.55 μm with a 2.5-GHz repetition rate that is equivalent to a commercial SONET OC-48 rate. These pulses are spectrally phase-encoded by transmitting them through a monolithically integrated semiconductor device comprised of two arrayed waveguide gratings (AWGs) and several phase modulators. The two AWGs do the spectral slicing and recombining of the pulse. Each spectral slice is phase-delayed using an electrically controlled waveguide phase modulator. Our device will allow remote phase trimming of each spectral slice of the input pulse at very high speeds. This compact device will allow long phase codes to be reconfigured rapidly by a network operator at a remote location.

In FY2001, we (1) used LLNL's Metal-Organic Chemical Vapor Deposition (MOCVD) facility to grow and characterize lattice-matched materials for our integrated AWG device; (2) through our collaboration with the University of California, Davis, developed several integrated device designs and fabrication methodologies; (3) began modeling the transmission of CDMA-encoded signals across standard fiber-optic networks and evaluating our ability to compensate for the cumulative propagation effects; and (4) designed, purchased, and aligned a free-space testbed for our O-CDMA devices. At year's end, we were aligning and characterizing our test system.

In FY2002, we plan to demonstrate remote configuration of spectral-phase-encoded signals and also fabricate, characterize, and package a prototype integrated semiconductor device.

Direct characterization of the electronic structure of shocked and heated materials

A. J. Nelson, J. Dunn, A. W. Van Buuren, R. F. Smith

LLNL's stockpile stewardship mission requires detailed knowledge of the response of materials to strong shocks or other extreme conditions (such as laser heating) on rapid time scales. This project began in FY2001 to develop and demonstrate a pump–probe characterization capability for investigating ultrafast changes in the chemical and electronic structure of materials under extreme conditions with picosecond time resolution.

The major initiative of the project is to use the COMET tabletop x-ray laser facility at LLNL to perform photoemission spectroscopy and to study the surface chemical and electronic structure of materials undergoing fast laser excitation or shocking. The source properties, including high photon flux (10^{12} photons per pulse), high energy monochromaticity ($\Delta E/E \approx 10^{-4}$), and short pulses (2 to 5 ps), are ideal for this technique when combined with time-of-flight photoelectron spectroscopy. Direct, time-resolved measurements of the electronic structure of the material will give us insight into the dynamic process and final states. The use of the x-ray probe also allows us to study much stronger nanoshocks than can be studied with optical probes and to further explore the physics of laser–matter interactions.

In this first year of our research we implemented and interfaced instrumentation with which we gave a proof-of-principle demonstration of the x-ray laser probe/time-of-flight photoelectron spectroscopy technique. This involved installing a ultrahigh-vacuum beamline and chamber on the COMET laser facility. Our design includes a differential vacuum pumping station, pinhole/filter isolation, and sample introduction. We rebuilt a photoelectron spectrometer obtained from Lawrence Berkeley National Laboratory.

We completed and tested a third COMET laser arm for use as the optical pump in our experiments. The laser output (1.2 J in a 500-fs pulse at 527 nm wavelength) exceeds our requirements. The pump beam and the two x-ray probe beams can be delivered simultaneously, because all three beams are derived from the output of a single oscillator.

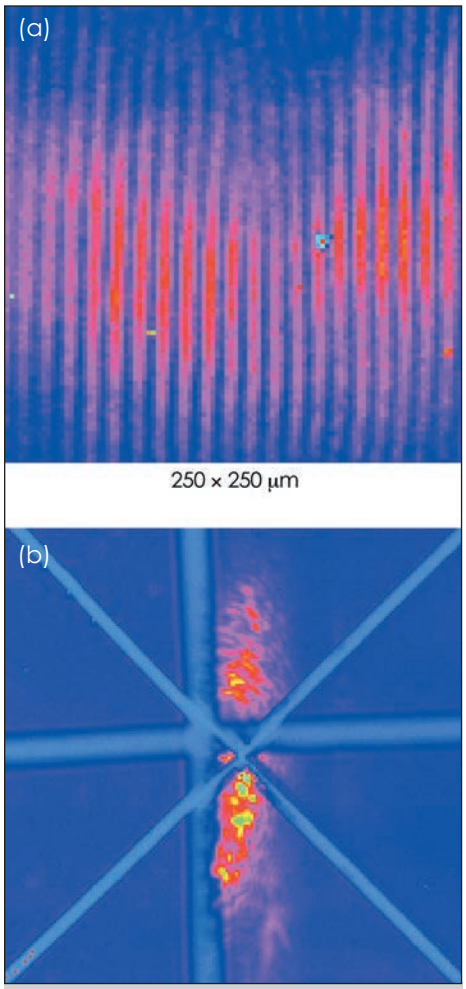

X-ray laser coherence and pointing. (a) Spatial coherence is demonstrated by the high fringe visibility (0.7) measured by interferometer, (b) near-field x-ray laser pattern aligned on 250-mm-diam crosshairs through beamline.

Routing the probe beam to the sample for surface analysis while discriminating against broadband spontaneous x rays from the plasma requires the use of molybdenum–silicon multilayer coated flat and spherical mirror optics fabricated for us at LLNL. Tests on COMET showed that these optics successfully relay and focus the 14.7-nm (85-eV) x-ray laser beam. The near-field exit footprint, far-field pattern, divergence, and pointing angle stability of the beam all satisfy the requirements of the project. The beam is partially coherent, exhibits a few tens of spatial modes, and has a 5× diffraction limited output (see Figure).

In FY2002, we will validate the x-ray laser/photoelectron spectroscopy technique by measuring the shallow 3d core (39.3 eV binding energy) and valence electron spectrum of bulk germanium (Ge) at room temperature. We will also investigate size- and phase-dependent changes in 3d core and valence electronic structure of Ge nanostructures. In addition, we will carry out the first dynamic pump–probe experiment of heating bulk Ge with a 500-fs laser pulse up to and beyond melt and determining the time-resolved changes.

Next, we will turn to more exotic materials of interest at LLNL and in the scientific community. We plan to probe the electronic structure of carbon, nanodiamonds, and carbon aerogels during fast melt and shock; of semi-metals bismuth, tin, and lead, which have low melting points and shallow d electrons, and tantalum.

High-pressure, high-strain-rate materials effects

D. H. Kalantar, M. Kumar, K. T. Lorenz, S. Pollaine, B. A. Remington, J. Stolken

MAIN TOC

Time-resolved dynamic x-ray diffraction provides a technique for studying the response of a crystal lattice under shock compression as the shock passes through the sample. Compression of the lattice spacing is observed as a shift of the Bragg diffraction angle, and a broadening of the signal may be characteristic of the dislocation and stacking fault density in the material. By recording x-rays diffracted from multiple lattice planes simultaneously, this technique provides information on the state of the shocked sample as it is compressed and subsequently relaxed. Optical and electron microscopy are used on recovered shocked samples to investigate the residual deformation structure that remains in the sample following the release of the shock.

The goal of this project is to study possible correlation of the lattice response under compression with this residual deformation microstructure. This research will provide information on how the microstructure affects the material response under shock loading at extreme conditions. The experimental results will directly benefit future experiments involving materials properties on advanced lasers and aid the development of improved models of the properties of shocked materials of interest to the Stockpile Stewardship Program.

During FY2001, we conducted a series of dynamic diffraction measurements of shocked single-crystal silicon (Si) and single-crystal copper (Cu) on the Omega laser at the University of Rochester. Direct laser irradiation was used to shock compress the crystal samples. The experiments with Si focused on the formation of multiple diffraction lines, which suggest a structured-wave profile. Experiments with Cu focused on developing a target configuration to record x rays diffracted from multiple lattice planes. We developed and demonstrated a large-angle film detector that recorded x rays diffracted into a large solid angle, extending up to 90 deg in one direction and 180 deg in the other, which provided information on the lattice response along many different lattice planes.

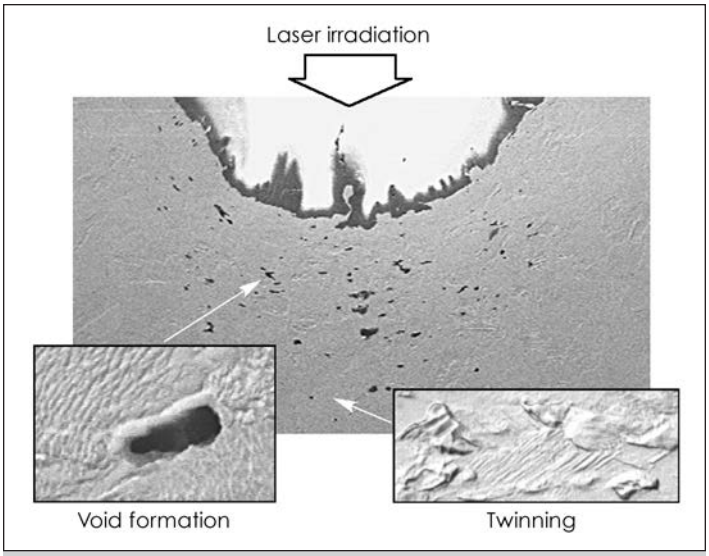

Section of a polycrystalline copper sample shocked by direct laser irradiation. The sample shows residual deformation, including the formation of twins and voids, that resulted from high-pressure loading.

We have demonstrated recovery of shocked single-crystal samples of Cu for postshock microstructural analysis on both the Omega and Janus (LLNL) lasers. Single-crystal Cu disks were placed within the tip of a recovery tube filled with a low-density aerogel foam. Direct laser irradiation generated a high-pressure shock that decayed as it propagated through the sample. Breakout from the free surface in some cases resulted in incipient spall due to void formation and coalescence. Optical and electron microscopy were used to investigate the residual deformation structure due to shock loading at a range of pressures. The lowest pressure shows the relaxation to a cell structure. As the pressure increases, the dislocations appear as a tangle between regions of twinning. At the highest pressures, large twin regions are formed as the temperature behind the shock is high enough to allow thermal recovery and evolution of the microstructure after the passage of the shock. The Figure shows examples of the deformation twinning and void formation.

Work in FY2002 will focus on refining the experimental technique to conduct three different measurements: (1) x-ray diffraction measurements of the lattice response during and after shock loading; (2) velocity interferometer system for any reflector-wave profile measurements; and (3) recovery and postshock microstructural-analysis measurements.

The combination of these techniques will provide information to compare detailed molecular dynamics modeling of the lattice response to correlate the dynamic diffraction data with the actual shock-wave profile, and the real-time lattice response with the residual deformation structure following recovery.

Development of wet-etching tools for precision optical figuring

S. N. Dixit, M. C. Rushford, J. A. Britten, C. R. Hoaglan, L. Summers

The four most common approaches used for figuring large aperture optics—grind-and-polish, small-tool figuring, magneto rheological finishing, and plasma etching—are expensive and involve large capital investment. A high degree of optical finish is needed for applications involving high-power lasers and in high-resolution imaging. Typically, the transmission wavefront is required to be of the order of λ/10 or better. Large apertures are also required in high-power lasers to minimize the laser damage and in space telescope applications to enhance the signal-to-noise ratio (achieved by virtue of increased light collection).

In this project, we are developing a low-cost etching process for figuring large-aperture, very thin (<< 1 mm) optic plates that cannot be processed by any other means. A patent on the wet-etch figuring approach is pending. These techniques will enable the fabrication of continuous-phase plate, diffractive optics, and disposable debris shields for the National Ignition Facility being built by DOE's Stockpile Stewardship Program. This enabling technology will be transferred to industry for use in low-cost production of high-quality optics for a wide range of national security and commercial applications.

The process involves the controlled application of a hydrofluoric acid etchant solution to the glass surface that is being figured. The etchant solution is pumped through a narrow tube and flows back down along the outer surface of the tube because of gravity. The tube is surrounded by an alcohol-containing region. Slight absorption of the alcohol in the etchant solution leads to a reduction of the surface tension between the etchant and the glass surface, which leads to a containment of the wetted region, known as Marangoni confinement. An in situ interferometer monitors the optical thickness from above in real time.

During FY2001, we built a point etcher (called the "fountain head tool") and a 1-D linear etcher. The linear etcher was used to flatten a 4 × 10 in. area of a 380-μm-thick glass sheet; the initial peak-to-valley thickness variation of over 10 μm was reduced to less than 0.1 μm. Using the fountainhead tool, we made a 1-in.-diam. aspheric lens on a 380-μm-thick glass sheet that converts a Gaussian profile into a flat-topped profile in the far field.

As a demonstration of a nonsymmetrical surface figuring, we fabricated a phase-correcting optic at 4-in. aperture. The surface figure variation is ~10 μm with fairly large (~50 mm) lateral scale lengths. The preliminary results of this effort are shown in the Figure, in which the nonsymmetric nature of the fabricated profile is evident. The difference between the input (desired) phase profile (not shown) and the fabricated phase is less than 100 nm. The similarity of the desired and the actual profiles demonstrates that the Marangoni confined wet etching is an effective surface-figuring tool.

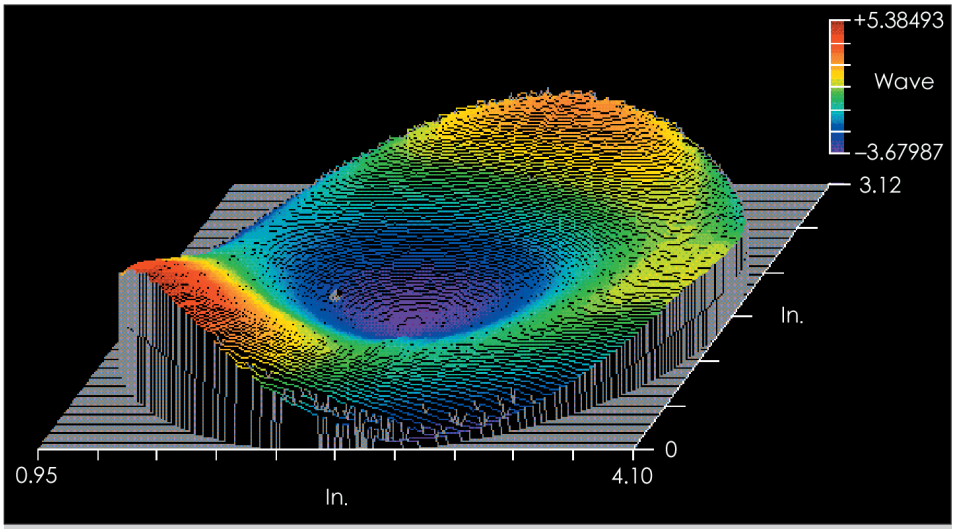

Interferogram of a complex, 80-mm-diam wavefront-correcting optic fabricated with a wet-etch figuring tool. The wavefront peak to valley is 12 mm, relatively high for optics of this sort.

In FY2002, we will develop a parallel etch process for simultaneous etching of the entire 2-D surface. This should lead to orders-of-magnitude reduction in the surface figuring time as compared to a fountainhead tool. We also plan to (1) take advantage of the temperature sensitivity of the etch rate to differentially control the local etch rate, (2) investigate direct heating of the etchant solution by irradiating it through a gray-scale mask or by using a rapidly rastered infrared laser beam, and (3) assess the effective figuring rates for both these approaches and evaluate their potential for scale-up to larger aperture sizes.

Developing a radiative-shock testbed

J. Greenough, B. Remington, T. Perry, R. P. Drake, P. Keiter

Radiative-precursor shock occurs when the flux of ionizing photons being radiated forward from the shock front exceeds the flux of atoms approaching the shock front.

Radiative shocks are of broad scientific relevance, particularly in astrophysics, and of generic interest in the Laboratory's stockpile stewardship mission. A dramatic example of radiative shock is the localized emissions emerging from the impact of ejecta from Supernova 1987A with its circumstellar ring nebula. This impressive display of radiative hydrodynamics is being played out in our nearest neighbor galaxy, the Large Magellanic Cloud (LMC), 160,000 light yr away. To interpret the events unfolding in the LMC, and for many stockpile stewardship applications a quantitative understanding of radiative shocks is needed. Yet comparisons of models and simulations with experimental data are not possible because relevant data do not exist. The goals of this project are to develop a radiative-shock, hydrodynamic testbed to rectify the lack of data, simulate effects of radiative shock on a high-Z metal signature layer, measure these effects, carry out detailed comparisons of the data with radiative-shock models and simulations, and develop scaling to relate results to astrophysics and regimes of interest to stockpile stewardship

The results of this research will have broad scientific impact in astrophysics and will benefit the Stockpile Stewardship Program.

To develop a radiative shock testbed, we are using state-of-the-art, Advanced Simulation and Computing-(ASCI-) level numerical simulations, experiments on the Omega laser, and theoretical scaling between regimes. At the conclusion of this project we will have developed a hydrodynamically driven, radiative-shock testbed, modeled its effects in various settings, and established appropriate scale transformations connecting regimes.

In FY2001, a series of 15 experiments on the Omega laser produced direct observations using x-ray absorption spectroscopy of a hydrodynamically driven, radiative-precursor in low-density SiO_2 aerogel foam. The peak temperature and the length of the radiative precursor from the shock were found to depend sensitively on the drive-beam power. Evidence of a threshold shock velocity to produce a radiative precursor was also observed. Comparing the observed silicon absorption to OPAL code calculations yielded an absolute temperature profile for the radiative precursor. We began simulations with the LASNEX, RAPTOR, CALE, and HYADES codes to compare with the data.

In FY2002, the length and temperature profile of the radiative precursor will be measured as the intensity of the laser and density of foam are varied. With these data, we will use ASCI simulations to develop the scale transformation connecting the shocks observed in the laboratory to astrophysical settings.

High-average-power, frequency-agile fiber lasers

D. M. Pennington, R. Beach, C. Ebbers, Z. Liao, C. Max, S. Payne

MAIN TOC

Development of versatile, compact, high-power, fiber laser technologies, tunable over the visible wavelength spectrum (500 to 700 nm) has the potential to enable a number of key Laboratory goals. We are developing a versatile laser technology based on diode-pumped fiber lasers, which are sum-frequency mixed in novel periodically poled nonlinear materials, to provide a broad range of visible laser frequencies. Initially the project will focus on high-risk technologies and then will explore the technical improvements required to produce significantly greater power levels required for high-average-power applications. A direct outcome of this research will be the development of a 589-nm laser for laser-guided adaptive optics for astronomy.

This project provides the means to develop a core competence in fiber lasers and periodically poled nonlinear materials at LLNL, which have been identified as strategic next-generation laser technologies. These technologies have the potential to impact several Laboratory missions, including national security and medical technology.

In FY2001 we concentrated on identifying and solving technical issues associated with the 1583-nm Er:doped fiber laser and the 938-nm Nd:doped silica fiber laser and scaling of periodically poled materials to high average power. The design for a 10-W, 1583-nm laser was completed, and we procured components for the prototype. The laser system design shown in the Figure is based on sum-frequency mixing a 1583-nm Er:doped fiber laser with a 938-nm Nd:doped silica fiber laser in a periodically-poled lithium niobate (PPLN) crystal to produce a continuous-wave output at 589 nm and greater than 10 W of power.

The 938-nm Nd:doped silica fiber laser is a more novel device, since the Nd^{3+} ions must operate on the resonance transition while suppressing amplified spontaneous emission losses at the more conventional 1080-nm transition. We identified several methods to circumvent competition from the 1080-nm transition. First, by pumping the amplifier with a high-power 938-nm seed pulse, we can extract gain preferentially at 938 nm. Second, losses at 1080 nm can be selectively induced by bending the fiber without negatively impacting the gain at 938-nm. Third, lowering the operating temperature of the fiber should provide a factor of 100 preference of the 938-nm over the 1080-nm transition. Finally, fiber Bragg gratings can be used to induce loss at 1080 nm. Fiber Bragg gratings are diffraction grating structures that are etched using ultraviolet light into a segment of optical fiber. These structures diffract unwanted wavelengths into the fiber cladding while transmitting the desired wavelength in the core. Based on modeling and experimental measurements of a single-core Nd: fiber, we produced a design for a cladding-pumped fiber amplifier that will deliver more than 10 W at 938 nm and procured the double-clad fiber and associated components necessary for testing our design. Work in FY2002 will concentrate on demonstrating the 938-nm and 1583-nm fiber laser systems at the 10-W design points.

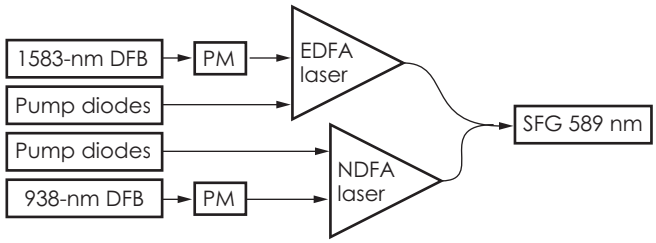

Laser system block diagram: A 1583-nm Er:doped fiber laser (EDFA) is sum-frequency-mixed with a 938-nm Nd:doped silica fiber laser (NDFA) in a periodically-poled material to produce continuous-wave output at 589 nm.

The final technical challenge is scaling periodically poled nonlinear materials to high average power. These materials have been demonstrated at 6-W continuous wave at visible wavelengths. However, special problems are encountered for producing higher average powers in the visible, due to green-induced infrared absorption. Due to the growth methods of these materials, PPLN crystals are limited to ~ 500 μm in the vertical dimension, though significantly larger in width and length. Higher powers should be achievable using an elliptical beam format to reduce the intensities in the material. In FY2001, we performed modeling to determine the optimal materials for sum-frequency generation to 589 nm, as well as direct harmonic conversion of the Nd:doped silica fiber laser to produce a blue source.

Experiments with the PPLN crystals will be performed in FY2002 to demonstrate the elliptical formatting technique. Once these materials have been demonstrated, we will sum-frequency mix the 938-nm and 1583-nm lasers in the periodically poled material to demonstrate a 589-nm laser source.

Ultrahigh-average-power inorganic liquid lasers

E. Ault, T. Baumann, B. Comaskey, K. Marsh

MAIN TOC

Fluid lasers based on rare-earth ions hold the promise of high average power and high optical beam quality, a combination that cannot be accomplished with glass and crystal lasers at the desired power levels. This project is aimed at developing a flowing-liquid host, high-power, near-infrared laser with high beam quality that will allow beam propagation over distances of tens of kilometers. Such a laser will have a host of military applications. In our laser, neodymium (Nd) salts are dissolved in a solution containing no free protons, which quench the laser levels of the ion, spoiling efficient laser action. Semiconductor diodes illuminate this solution to excite the Nd^{+3} ion. Subsequent extraction by stimulated optical emission produces power laser action.

For FY2001, we had the following four goals: (1) explore the solution chemistry of the desired aprotic solvent (thionyl chloride, sulfural chloride), including the coordination of Nd^{+3} ions with gallium chloride ($GaCl_3$); (2) measure the photophysical properties of these solutions; (3) set up a thermal test bed with a non-hazardous surrogate for thionyl chloride to measure the optical properties of the liquid under thermal loading by semiconductor diode light; and (4) begin the design of a 500-W demonstration laser and flow system.

Our laboratory has been producing sample quantities of the actual aprotic solutions for spectral analysis [see absorption spectra trace in Fig. (a)]. We are now studying the purity, solubility, and solution lifetime effects. Absorption spectra are in reasonable agreement with published spectra except for the ratio of peak heights in the 880-nm band. Further work is planned to understand this difference. Pure thionyl chloride is colorless and waterlike. When $GaCl_3$ is added, a light yellow color appears while the addition of $NdCl_3$ turns the solution gray-violet. We have found, however, that Nd salts and water solutions show that only the violet color is evident, which reduces the fluorescent lifetime. We are pursuing this issue because of the possible impact on absorption at the laser wavelength at 1.053 nm. Fluorescent lifetime is a critical parameter in this laser system. Measurements are being set up and results are expected in the coming months.

A small flow system has been obtained to provide steady, pulsation free flow to a small glass cell. All components are being integrated with semiconductor diodes to begin thermal loading tests. While we wait for health and safety approval to flow thionyl chloride solutions for the tests, we have begun working with low-hazard, proton-containing solvents (water, ethanol, ethylene glycol, etc.) for which fluorescent lifetime is not important. These measurements are aimed at comparing the calculated and measured optical path differences induced by steady heating of the solution by the pump laser light. Figure (b) shows the flow cell and pump/heat exchanger skid.

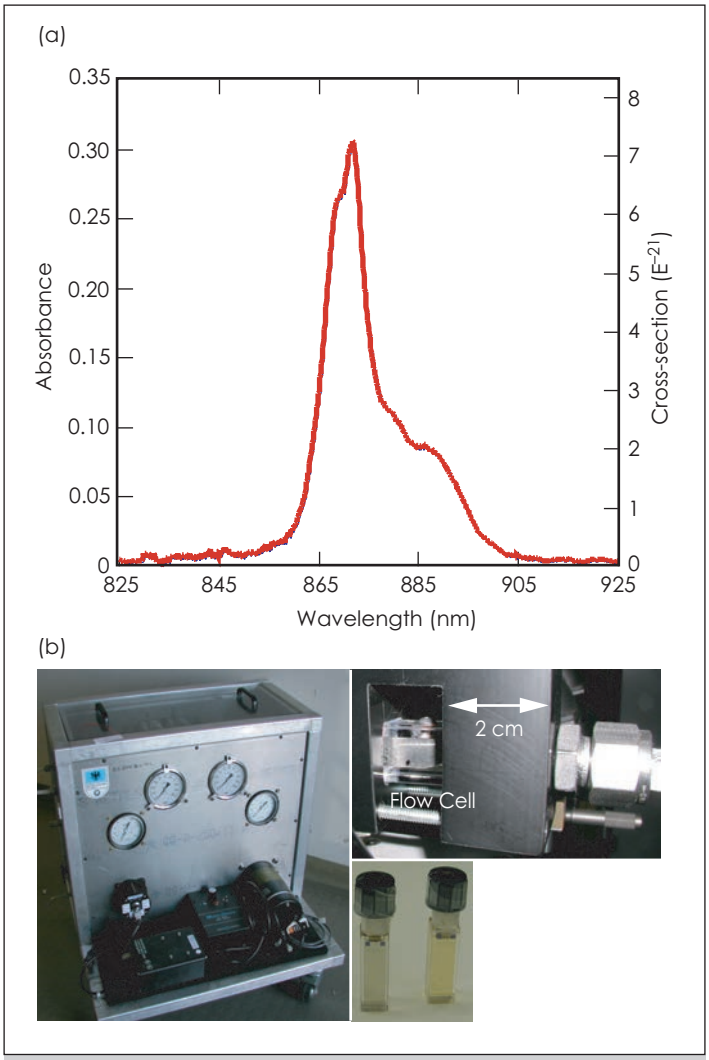

(a) Absorption spectrum of Nd^{+3} in thionyl chloride–$GaCl_3$ solution. (b) 500-W liquid laser components. On the left is the pump skid for flow tests; top-right, test cells of aprotic solutions; bottom-right, flow cell for thermal loading.

Design of a 500-W high-beam-quality demonstration laser has begun. We have completed an initial study of materials compatibility and have selected a commercial fluid pump and piping that can provide the required flow and resist corrosion by thionyl chloride. We have also completed design of a flow cell to be built of inert materials and have calculated the expected flow parameters.

During FY2002, we will complete the demonstration laser and will test it with an actual host liquid.

Precision hole drilling with a polychromatic, bimodal laser approach

H. W. Friedman

Rapid, precise drilling of precision, submillimeter holes is needed for many national security applications and industrial products, including turbine blades, aircraft wings, and fuel injectors. Recent results using ultrashort-pulsed lasers show promise, but problems remain associated with poor beam quality, unexplained phenomena, and the difficult task of scaling these lasers to high average powers.

This project makes use of results obtained with inexpensive diode-pumped solid-state lasers (DPSSLs) that operate in the near infrared (1.06 nm) and the second harmonic (532 nm) to drill precision submillimeter holes with arbitrary shapes in metal and ceramic substrates.

These lasers operate in the ablative regime (flux from 0.1 to 1 GW/cm^2), with short pulse duration (<100 ns) to minimize the heat-affected zone (HAZ) and at high average power (300W at 10 kHz) to achieve 1-s drilling times in millimeter-thick substrates. The infrared beam, sized roughly to the hole diameter, rapidly removes the bulk of the material and allows an escape path for debris in the second step. The second step uses a much lower power, but near-diffraction-limited laser beam at the second harmonic wavelength focused to one-tenth the beam diameter to clean, shape, and polish the sides of the hole. With this "trepanning" laser, both shape and cross section can be cut to the desired dimensions while maintaining a minimum HAZ.

If successful, this project will yield an improved technique for laser hole drilling that will produce high-quality holes with precise dimensions more quickly, cheaply, and reliably than previous methods. The techniques demonstrated in this project will find widespread use in LLNL's national security programs and in the aerospace and automotive industries.

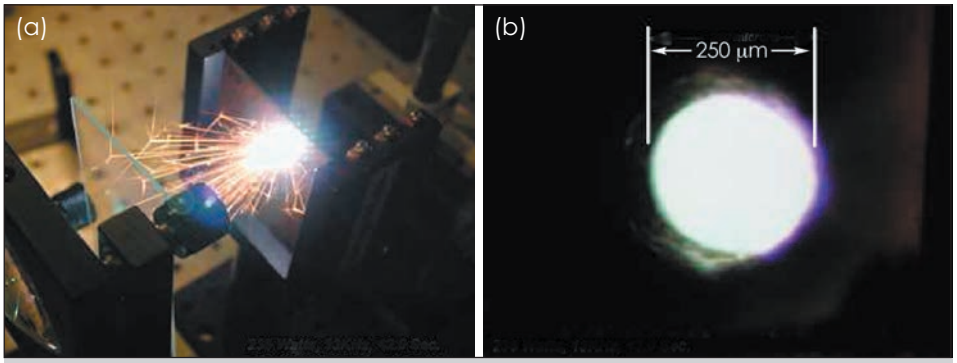

Hole-drilling experiments: (a) experimental setup and (b) photomicrograph of submillimeter hole in a 1.5-mm-thick steel substrate.

In FY2001 we concentrated on reactivating and optimizing the performance of two surplus DPSSLs. These lasers have produced over 500 W in the infrared and 300 W at the second harmonic and have been tested for several thousand hours. The infrared laser has been preliminarily optimized for beam quality and pulse duration to operate at 250 W, 13 kHz, and pulse duration of 85 ns. Under these conditions, the laser flux for a 300-μm hole is 0.3 GW/cm^2, well into the ablative regime. Cutting time for the setup shown in Fig. (a) is 1 s, which produces a well-rounded hole, as Fig. (b) shows. The DPSSL for the trepanning laser is working well. This experimental effort will continue in FY2002.

For FY2002, our research plans include (1) optimizing the cavity for operation in the infrared alone; (2) using a flowing Kerr cell as an electro-optic Q switch at a lower pulse-repetition frequency, with resultant increase in pulse energy, decrease in pulse duration, and therefore, a significant increase in peak power. We also plan to implement an electronic shutter to permit precise timing and/or pulse counting. This would leave a thin membrane intact at the bottom of the hole, thereby minimizing the amount of energy penetrating the hole, an important criteria for industrial applications. The membrane would be removed by the low-power trepanning laser at the conclusion of the hole-drilling process. The trepanning laser and the offset-enabling optics needed to shape the hole to final dimensions will be added. Finally we will demonstrate the precision hole-drilling process using both the infrared and visible lasers.

Nonlinear saturation of parametric laser–plasma instabilities

S. H. Glenzer, D. H. Froula, L. Divol

Plasma waves nonlinearly scatter laser light and cause instabilities in laser–plasma interactions. An improved fundamental understanding of ion and electron plasma wave saturation is important for high-energy laser experiments that require improved coupling of laser energy to targets. This understanding also has relevance to inertial confinement fusion, high-energy-density physics, and nuclear weapons physics. In this project, we propose to directly measure the amplitudes of plasma waves to obtain quantitative information about laser–plasma instabilities.

The instabilities of primary concern are stimulated Raman scattering (SRS) and stimulated Brillouin scattering (SBS). In these processes, ion acoustic (in the case of SBS) or electron (in the case of SRS) plasma waves are excited to large amplitudes by an incident light wave reflecting a large fraction of the incident laser energy. It is now well established that these instabilities will be saturated in the high-temperature, large-length-scale plasmas produced by the next generation of large lasers.

Experiments on the Nova and Trident lasers have shown that the location, amplitude, and saturation behavior of these excited waves can be measured with the Thomson scattering technique. Furthermore, the Thomson scattering experiments can provide data that are needed to develop the LLNL code pF3D into a predictive tool used to calculate plasma wave amplitudes and help design experiments with reduced SBS and SRS laser energy losses.

We have proposed a Thomson scattering experiment at the Omega laser at the University of Rochester. We will measure the spatial and temporal evolution of plasma waves and their correlation with time-resolved SRS and SBS reflectivity. The Thomson scattering diagnostics will be used to (1) provide independent measurements of plasma electron and ion temperature, plasma flow velocity, or electron distribution function, and (2) provide measurements of the primary plasma wave and the secondary, nonlinear decay wave products.

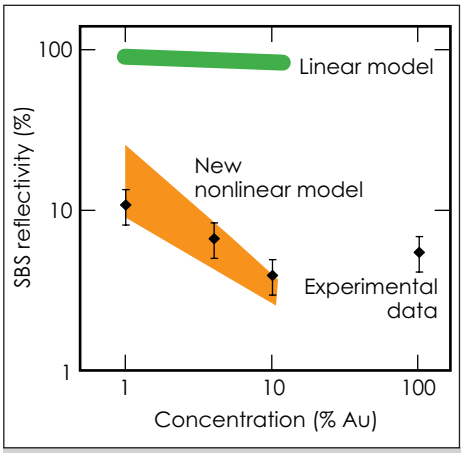

The stimulated Brillouin scattering (SBS) reflectivity from laser plasmas consisting of beryllium mixed with various amounts of gold (Au) ions. A newly developed nonlinear model that includes saturation of ion acoustic waves by ion trapping reproduces the trends and magnitude of previous expermental data. The classical linear model disagrees with the data.

In FY2001, we developed reduced models and pF3D simulations to design the experiments at the Omega laser that will begin in the second half of FY2002. We compared our results to the existing Nova and Trident data base and have successfully reproduced the SBS reflectivity from two ion-species plasmas. Thomson-scattering measurements from the same plasma have shown ion heating, which therefore strongly indicates ion trapping. The nonlinear model has included these trapping effects, and we find that the phase velocity of the ion acoustic waves are modified, thereby detuning the three-wave resonance and limiting the SBS reflectivity. The decoupling parameter has been calculated with first-principles wave equations. This has resulted in the first quantitative agreement of calculated values with experimental data without invoking multipliers (see Figure).

In FY2002, we will measure the decoupling parameter with Thomson scattering experiments. The experiments and the comparison with particle-in-cell simulations will establish the limit of this saturation model and will help in investigations of alternative models that might dominate in different plasma regimes.

Dense plasma characterization by x-ray Thomson scattering

O. L. Landen, S. H. Glenzer, S. M. Pollaine

The full range of plasmas, from Fermi-degenerate to strongly coupled to high-temperature ideal gas plasmas, are present at high density in a variety of laboratory and astrophysical environments. Material properties such as electrical and thermal conductivity, opacity, and equation of state (EOS) have been measured in this regime in an attempt to resolve theoretical and calculational uncertainties. The usefulness of such measurements has been limited by a lack of independent measurement of the key plasma parameters: temperature and density.

Surface probing of overdense plasmas is difficult to interpret because extremely small density-gradient scale lengths greatly modify observables such as optical reflectivity and phase modulation. Internal x-ray probing of plasmas at near-solid densities and above has relied on continuum-edge spectroscopy and extended x-ray absorption fine-structure (EXAFS), line-shape spectroscopy, or non-spectrally resolved x-ray scattering. However, the interpretation of results from all such techniques still relies on knowledge of the ionization balance, density, and temperature.

Such high-density plasmas are the principal state of matter in inertial confinement fusion (ICF) and high-energy-density physics (HEDP) research, the latter being an important component of LLNL's Stockpile Stewardship Program. This project is developing a novel characterization technique for low-atomic-number plasmas, which ultimately could be used to measure the density and temperature of compressed ICF fuel and could provide a noninvasive internal temperature measurement in radiatively and shock-heated materials for HEDP. This project is also extending the development of transient, hot laser plasmas as x-ray probes, a technique that has been a key part of the experimental expertise built up over decades at LLNL.

In this project, we are extending the plasma characterization technique of spectrally resolved optical photon scattering from free electrons (Thomson scattering) to the x-ray regime to obtain dense-plasma data unobtainable by other means. We use resonance-line emission from laser plasmas as a narrow-bandwidth transient x-ray probe that scatters from sample solid-density plasmas created by volumetric heating using x rays from other laser plasmas. The shape of the scattered spectra provide instantaneous information on the free-electron density and temperature of the sample plasma. We hope eventually to use this information for a proper interpretation of other plasma properties such as EOS and opacity.

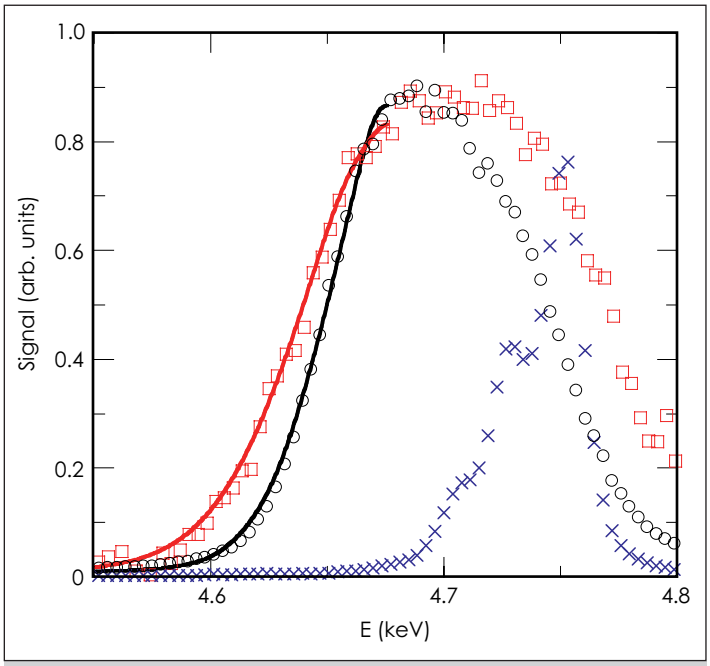

Normalized spectra of reference titanium line emission (crosses), scattering from cold beryllium (circles) and from heated beryllium (squares).

During FY2001, we demonstrated the feasibility of performing x-ray Thomson scattering. We optimized designs for two proof-of-principle experiments involving volumetrically heated solid beryllium (Be) and shocked LiH and plastic. The designs included 2-D radiation-hydrodynamic simulations of the expected test plasma conditions, which confirmed earlier analytic calculations of test plasma uniformity.

Experiments at the Omega laser facility (at the University of Rochester, New York) yielded high-quality scattered spectra on several shots. The Figure shows lineouts of the scattered spectra, which display the expected Compton down-shifted and Doppler-broadened spectral signatures. In particular, the comparison of the spectra of the heated versus cold Be sample shows increased broadening; this was the first demonstration of the sensitivity of x-ray Thomson scattering to plasma temperature. The spectra are well fitted by calculated spectra using the expected Fermi energy of 14 eV in both cases, and including an electron temperature of 10 eV in the heated case. This electron temperature is consistent with other observations, and is in reasonable agreement with a calculated electron temperature of 20 eV.

Time-resolved radiography of short-pulse plasmas and shock-compressed materials using laser-produced, multimegaelectron-volt ions

A. J. Mackinnon, D. Hicks, P. Patel

A recent development in the field of ultrahigh-intensity laser–plasma interactions is the use of laser-generated proton beams to probe extremely large, laser-pulse-generated electric and magnetic fields in plasmas. Electric fields as large as 10^{11} V/m and magnetic fields on the order of 100 to 1000 MG are believed to exist close to the surface of thin foils irradiated by laser pulses. These fields are located in regions of plasma that are difficult to access with conventional probe techniques. One new and powerful way of investigating these fields is to use a proton beam to form a proton radiograph of the plasma. Measurements of the proton deflections can be used to measure the magnitude of the electric or magnetic fields, which will test the validity of current theory in the area of relativistic plasma physics.

In this project, a theoretical and experimental feasibility study was carried out to investigate the utility of proton radiography. The theoretical study analyzed the effect of electric and magnetic fields on the structure of the proton probe beam. The experimental study was carried out on the JanUSP laser at LLNL, using static test targets and known electric field configurations. This project is important to the Stockpile Stewardship Program in a number of areas. First, strong electric and magnetic fields are thought to play an important role in energy flow inside the laser-driven hohlraums used in inertial confinement fusion. Second, proton radiography can be used to diagnose the position and ionization states of materials shocked to high pressures. This could be achieved in materials too dense for conventional x-ray radiography. Finally, as a compliment to existing neutron-based techniques, proton radiography could be used to directly measure areal densities inside imploded National Ignition Facility capsules.

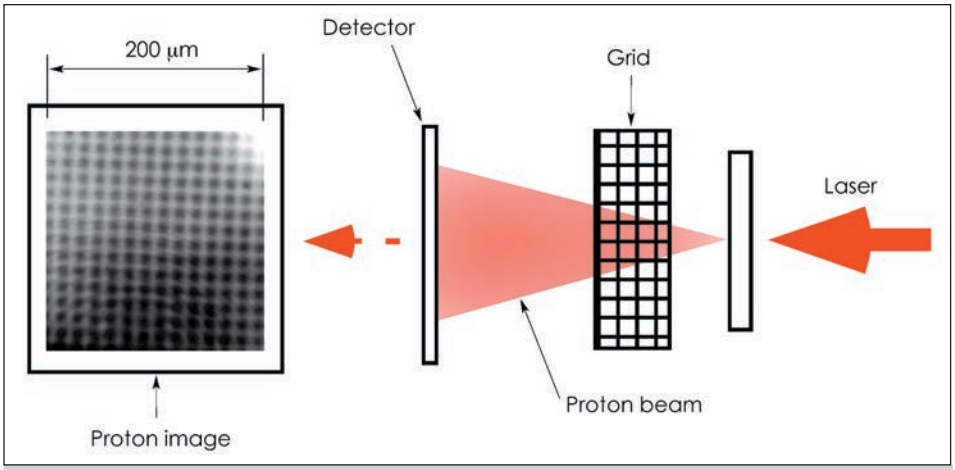

Proton radiography image of a 60-cycles/mm gold grid using a 10-MeV beam. The 5-μm gold wires are clearly resolved.

During FY2001 experiments were carried out on the single-beam JanUSP laser to produce a proton beam with a mean energy of 3.5 MeV and peak energy of 20 to 30 MeV. The resolution of the beam was characterized by imaging a 1,500-lines-per-inch gold mesh, which consisted of 5-μm wires, each separated by 17 μm. Images of the mesh at different proton energies were obtained using a multilayer proton-detecting film pack. The Figure shows a static 2-D pattern of the mesh imaged by a 10-MeV proton beam. The clearly visible pattern of the wire mesh demonstrates a resolution close to 5 μm. Importantly, the contrast of the proton images was consistent with deflections of the proton beam from the wires rather than slowing of the beam due to the material stopping. This beam deflection can be caused either by an electric field around the mesh wires or by multiple small-angle scattering. In either case, the diagnostic has been shown to measure very small proton-beam deflections. The analytical model showed that angular deviations can be impressed onto the proton beam by gradients in the electric field, which in turn are directly related to the local charge density in the probed target.

Proton radiography thus gives a direct mapping of the microscopic distribution of charge density, making it a very powerful diagnostic for investigating transient electric fields.

Ultrafast materials probing with the Falcon linac–Thomson x-ray source

P. T. Springer, G. P. le Sage, D. R. Slaughter, J. K. Crane, C. P. P. Barty, J. B. Rosenzweig, S. Anderson

MAIN TOC

Our goal is to develop a novel x-ray source and the experimental techniques that will enable unprecedented dynamic measurements in matter. Our project—dubbed Picosecond Laser Electron Interaction for Dynamic Evaluation of Structures (PLEIADES) is based on the scattering of a beam from LLNL's 35-fs Falcon short-pulse laser from a cosynchronous and highly focused relativistic electron bunch. PLEIADES will produce tunable, ultrafast, hard-x-ray (10 to 200 keV) probes that greatly exceed existing third-generation synchrotron sources in speed (100 fs to 1 ps), brightness (10^{20} photons/mm^2/s/mrad^2, 0.1% bandwidth, and >10^9 photons/pulse), and size (100-fold smaller). Such bright, ultrafast, high-energy x-rays will enable pump-probe experiments using radiography, dynamic diffraction, and spectroscopy to address the equation of state (EOS) and dynamics of phase transitions and structure in laser-heated and compressed metals of interest to the Stockpile Stewardship Program.

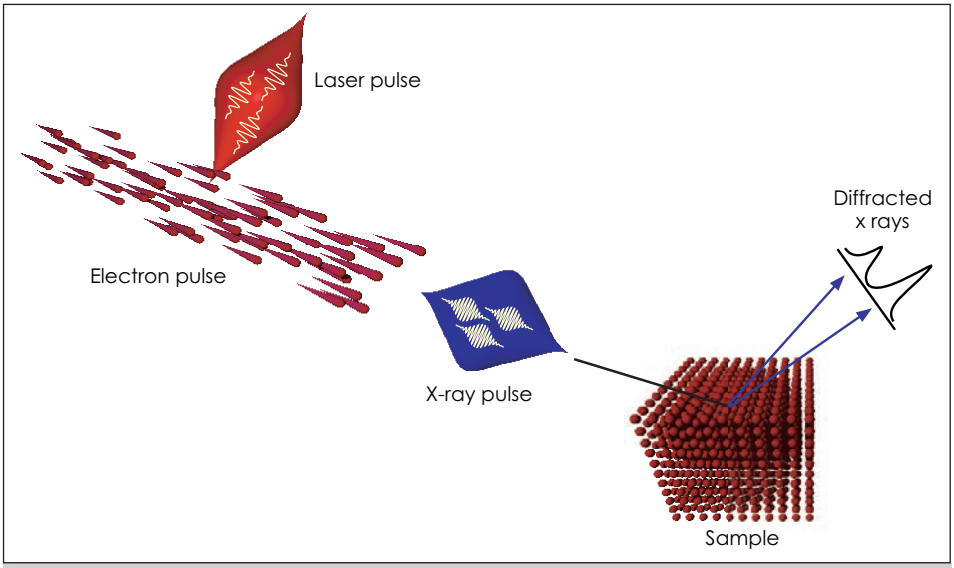

Scattering a short-pulse laser beam from a relativistic electron beam generates an ultrafast x-ray beam for dynamic materials experiments.

Our project also establishes LLNL leadership in research and development (R&D) related to advanced laser accelerators, with significant scientific spinoffs. With a compact accelerator, the Thomson source would provide a bright, tabletop x-ray source with widespread applications for protein crystallography and materials probes. The project also has strong ties to the efforts of the DOE's Basic Energy Science program in advanced light-source and accelerator development. As an integrated low-emittance beam and testbed for short-pulse laser and x-ray pump-probe experiments, PLEIADES could prove to be an important step towards the development of fast x-ray sources such as the Linac Coherent Light Source (LCLS), an x-ray free-electron laser. If proven feasible, PLEIADES can achieve x-ray fluences on materials comparable to those of LCLS, sufficient to perform essential R&D in x-ray optics and experimental techniques.

In collaboration with our colleagues at the University of California, Los Angeles (UCLA), in FY2001 we successfully completed the major laser and linear accelerator (linac) modifications required to produce a 100-MeV electron beam capable (with optics installed in FY2002) of a 1000-A current, a 1-ps pulse duration, and a 10-μm focal-spot radius. We integrated a low-emittance, laser-driven photoinjector in the LLNL's existing radio-frequency linear accelerator (RF linac) and demonstrated Thomson x rays at 600-eV photon energy—proving synchronization of the laser and the photoinjector. We also developed new probes capable of recording jitter below 3 ps—and used them to test and monitor synchronization of the Falcon laser and the photogun. Several sources of temporal jitter that were detected in both the laser and linac subsystems required reducing RF phase jitter and improving the stability of the Falcon laser's operation. This led to increased efforts in FY2001 to improve the Falcon laser's parameters to optimize x-ray production. At year's end, we were investigating the commissioning and characterization of a low-emittance beam.

During FY2002, our efforts will be devoted to the major technical challenges required to produce, characterize, and use the high-energy Thomson beam in pulse-probe experiments. We will install the final beam-delivery optics and, in collaboration with UCLA, investigate pulse-compression techniques for greatly increasing beam current, thereby realizing a 10,000-fold increase in electron current density over previous linac capabilities. We also plan to (1) optimize and stabilize critical beam parameters on the Falcon laser, including energy, pointing stability, and temporal jitter; (2) develop new architectures to improve reliability; (3) conduct a range of diagnostic analyses on the Thomson x-ray pulses for comparison with our 3-D simulations; (4) develop and install x-ray diagnostics for spectra and diffraction; and (5) perform the first dynamic experiment—in which we will test diffraction from a solid undergoing a laser-initiated phase transition.

Secure air-optic transport and routing network

A. Ruggiero

Information collection and communication technologies are crucial to our national security. Although new generations of U.S. sensor systems ensure our technological edge by enabling unprecedented quantities of data to be collected, communication bottlenecks limit timely data synthesis and interpretation. To maintain our information dominance in the next century, secure, high-capacity communication networks will be essential. These networks will require seamless data routing between permanent fiber infrastructures and deployable infrastructures, which include both mobile and temporary platforms. Open-air laser-communication (lasercom) links are a key enabling technology for fulfilling this vision.

Although the concept of free-space and air-optic lasercom has been around since the early 1960s, the functional use of lasercom is in its infancy. Commercial "last mile" lasercom links have recently demonstrated availabilities and bit-error-rates similar to fiber internets, but only over ranges of 100 to 500 m. To develop a long-range (tens of kilometers) lasercom technology, difficulties with optical-beam propagation through weather and turbulent atmospheric conditions must be overcome.

The objective of this Secure Air-Optic Transport and Routing Network (SATRN) project is to develop and demonstrate enabling technologies for long-range, secure, high-capacity, high-availability, air-optic lasercom links. Through a series of system-level, horizontal-path-link demonstrations, we will establish the viability of our concepts and techniques. Air-optic-link data from our horizontal lasercom demonstration testbed will be used to calibrate performance models and simulations of terrestrial links to airborne intelligence, surveillance, and reconnaissance platforms.

The key elements of this project involve the development and testing of (1) adaptive-optics (AO) receivers based on novel, nonlinear optical and micro-electromechanical systems (MEMS); (2) forward error-correction coding; (3) high-power, fiber-based transmitter technology; (4) custom transceiver components; (5) atmospheric and system-performance models; and (6) fiber Internet and radio-frequency wireless interfacing.

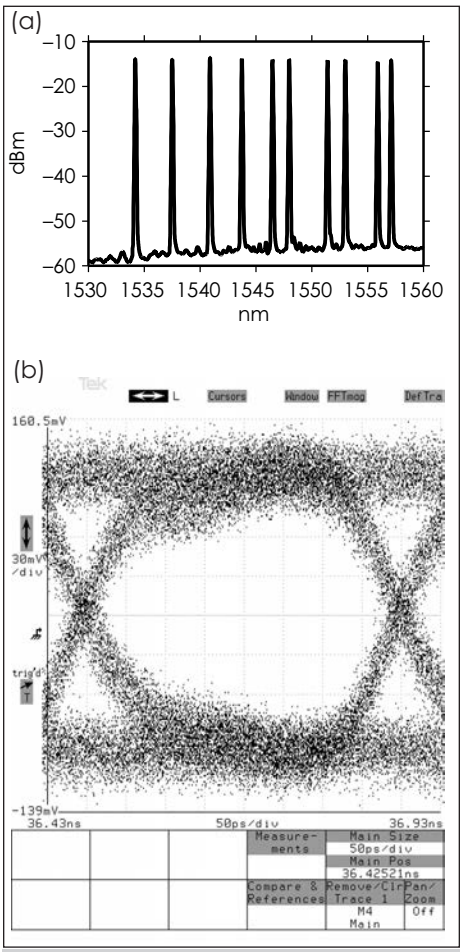

Characteristics of our baseline air-optic laser-communications link, showing (a) an optical power spectrum consisting of 10 optical channels, and (b) an eye diagram of optical modulation at 2.5 Gb/s on our 1.3-km link. (An eye diagram is a measure of communications quality; the more open the eye, the better the quality. The annotations involve the operational parameters of the oscilloscope.)

In FY2001, we assembled a baseline lasercom system and upgraded our 1.3-km outdoor building-to-building testbed to enable key subcomponent technologies to be routinely evaluated as part of their development process. The baseline system was configured with 10 optical channels that are combined into a single beam, as Fig. (a) shows, with single-channel data rates up to 2.488 Gbit/s. An eye diagram demonstrating the quality of the outdoor link at this single-channel bit rate is shown in Fig. (b). The transceiver can be operated with aggregate bit rates up to 25.4 Gbit/s.

Using this baseline system, we have begun investigating the lasercom-transmission characteristics of gigabit ethernet, and—for the first time— we are in the process of benchmarking the transfer of hyperspectral sensor data across an open-air laser link. We made progress on (1) modeling our photonics and atmospheric systems; (2) initial fabrication of both MEMS and nonlinear prototypes of optical AO-system prototypes; and (3) design, implementation, and assembly of the hardware for a novel, forward-error-correction technology.

In FY2002, we will focus on further development, demonstration, and evaluation of these new technologies on our baseline air link. Our plans also include beginning the (1) development of high-power photonic-crystal amplifiers, (2) assembly of a portable transceiver system for offsite deployments, and (3) extension of our testbed range from LLNL to the summit of Mt. Diablo, 29 mi away.

Tactical laser weapons for defense

R. J. Beach, L. Zapata

MAIN TOC

Pressing forward with laser weapons is emerging as a compelling national need, as articulated in a report recently issued by the High Energy Laser Executive Review Panel (HELERP). The HELERP report addresses near-term needs, strategic vision, and programmatic balance for a concerted national effort in laser weapons. Solid-state lasers are, for the first time, being actively considered as candidates for the "kill" weapon; previously, solid-state lasers were regarded only in supporting roles for missile tracking and for atmospheric correction.

Our technical focus is on demonstrating two innovative physics designs for laser systems that are appropriate for tactical laser weapons: (1) fiber lasers and (2) composite, ytterbium-doped, yttrium-aluminum-garnet (Yb:YAG) thin-disk lasers. Although these two pathways are independent, they share a common feature: thermal gradients are managed so that they do not preclude the generation of high-beam-quality laser radiation at single-aperture average powers in the 10-kW range.

In the fiber approach, a multiple-core structure is designed so it supports only a single transverse mode; this allows a simple phase plate at the output stage to generate a high Strehl beam (i.e., a beam capable of depositing substantial energy on a target at a distance). In the thin-disk approach, thermal gradients are constrained to be almost entirely parallel to the propagation direction of the laser radiation.

In FY2001, the key result for the fiber component of our project was the development of detailed models that validate our antiguiding approach for phase-locking, multiple-gain cores. The focus is on a ribbon-like geometry in which the waveguide region contains multiple-gain cores that alternate with nongain regions in a periodic array. An outer, lower-index cladding surrounds the entire ribbon structure. The distinguishing feature of the ribbon-laser design is a constant refractive-index profile across the waveguide region—as opposed to alternating higher- and lower-index regions. Modeling predicts that the constant-index design will provide modes that meet critical design requirements—strongly favored oscillation in a single transverse mode and good intensity uniformity across the waveguide structure. As a preliminary demonstration of our ribbon concept, we are fabricating the structure shown in Fig. (a), which consists of a rectangular, antiguiding core region surrounded by a lower-refractive-index region that is suitable for confining and transporting pump radiation.

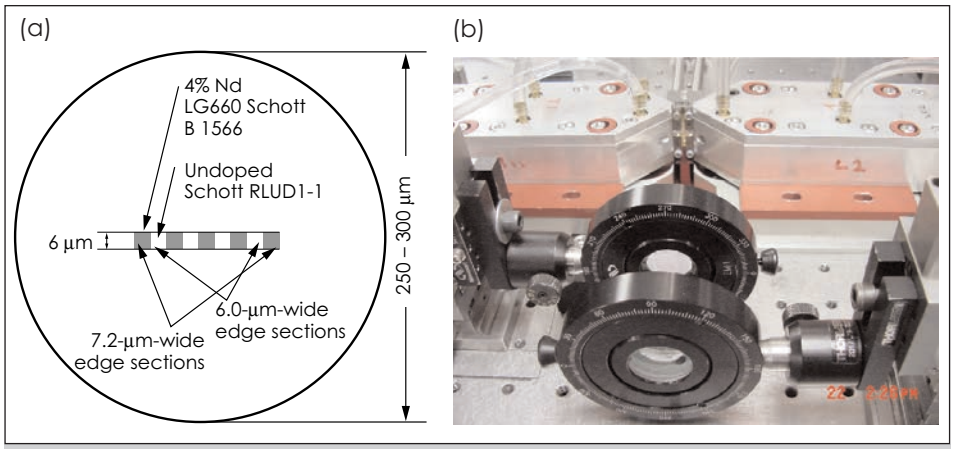

Two innovative physics designs for laser systems that are appropriate for tactical laser weapons: (a) our 5-core ribbon-fiber laser (fabricated with Schott glasses), and (b) the composite, ytterbium-doped, yttrium-aluminum-garnet (Yb:YAG) thin disk laser system.

In FY2001, we also experimented with thin-disk laser designs [Fig. (b)]. Our approach uses an index-matched, undoped, 1.3-mm-thick layer of YAG that has been diffusion-bonded to the top of a 200-mm-thick 15%Yb:YAG disk. At the bottom of the crystal is a high-reflector coating at both the pump and laser wavelengths. The thin-gain medium develops a thermal gradient identical to that of a capless thin disk, allowing the composite to maintain the thermal advantages of the conventional thin-disk lasers while enabling copious diode power to be injected through its edges. The thick, optically passive cap reinforces the thin disk, minimizing disk deformations and maintaining the contact between the thin-disk contact and the cooler. Optically, the diffusion-bonded, index-matched cap layer allows fluorescence decay to propagate freely out of the gain medium.

Materials Synthesis and Characterization

Section 7

Section 7 Materials Synthesis and Characterization

Chemistry and processing of nanostructured materials

G. A. Fox, T. F. Baumann, L. Hope-Weeks, A. L. Vance

Organic aerogels are typically prepared through sol-gel chemistry, a process that involves the condensation of reactive precursors into nanometer-sized clusters that crosslink to form a 3-D gel. Although sol-gel chemistry provides the opportunity to synthesize new material compositions, it suffers from the inability to separate the process of cluster (sol) formation from gelation. This limitation results in structural deficiencies in the gel that impact the physical properties of the aerogel or nanocomposite. Controlling the properties of these materials requires the ability to regulate the formation of the clusters and their subsequent crosslinking in the sol-gel process.

Dendrimers are 3-D, highly branched macromolecules that are prepared so that their size, shape, and surface functionality are readily controlled. To meet our goal of improving the sol-gel process, we used dendrimer chemistry to separate the cluster formation from the gelation so that new nanostructured materials were produced. In our procedure, the dendrimers are used as pre-formed sol clusters of known size that can be crosslinked to form the gel. Consequently, incorporation of dendrimers into the sol-gel process allows for greater control over both the composition and architecture of the resultant nanostructured materials.

Our research combined dendrimer chemistry with LLNL's expertise in organic aerogels for the design of novel nanostructured materials. This project strengthens LLNL's capabilities in both synthetic chemistry and organic aerogels, capabilities that support national security programs with the design of new materials.

In FY2001, we focused our efforts on the synthesis of larger dendrimers containing peripheral resorcinol units. Resorcinol is one of the main building blocks of organic sol-gel materials. One of the main challenges in the synthesis of the larger dendrimers was finding a suitable protecting group for the hydroxy groups of the resorcinol units. The protecting group had to be both robust enough to survive the synthesis of the dendrimer, and readily removed in high yield once the synthesis was complete.

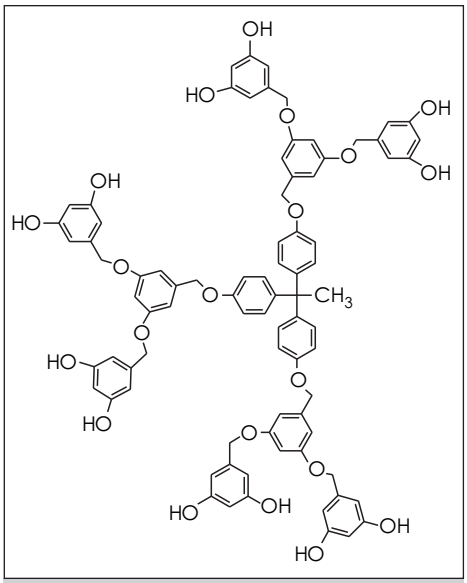

A Generation 2 dendrimer with peripheral resorcinol units that is used to prepare organic aerogels.

Because the allyl group fulfilled both requirements, we decided to protect the resorcinol groups with allyl ethers. Then, using a convergent growth method, we were able to synthesize Generation 1 and Generation 2 dendrimers that contained peripheral resorcinol units (see Figure). Once the protecting groups had been removed, these dendrimers were reacted under sol-gel polymerization conditions to generate new organic aerogels with densities, particles sizes, and surface areas similar to those of traditional organic aerogels. Having established a reliable synthetic protocol, at the close of the year we were investigating the synthesis of larger dendrimers with functional core molecules—such as metal complexes, binding sites, or sensing moieties.

This work has been presented at two conferences and has produced one publication, with three more manuscripts in preparation. Most importantly, on the basis of the work presented here we have obtained external funding from the DOE Joint Defense Program/Basic Energy Sciences (DP/BES) Nanoscience Network. This funding enables us to collaborate with groups at Los Alamos, Argonne, Sandia and Pacific Northwest National Laboratories (LANL, ANL, SNL, and PNL, respectively) with the goal of designing new, tailored nanostructured materials.

Kinetics of solid-phase reactions at high pressure and temperature

J. M. Zaug, D. L. Farber, C. K. Saw

Several decades of study have not yielded universal rate laws governing solid–solid structural phase transitions of polymer-blended explosive (PBX) materials. Each of the following parameters affects the solid phase transformation kinetics of energetic molecular crystals (EMCs), the explosive component of PBX, at fixed pressure and temperature: grain size, binder content, impurity content, and compaction density of the crystalline powder. To date no kinetic rate law incorporates these critical rate-limiting parameters for common stockpile EMC materials such as HMX (octahydro-1,3,5,7-tetranitro-1,3,5,7-tetrazocine) and TATB (1,3,5-triamino-2,4,6 trinitrobenzene). Given the importance of PBX to the stockpile safety initiative, we have developed and refined a series of experimental diagnostic tools that will result in a universal rate law.

We chose x-ray diffraction as the primary diagnostic tool because it provides accurate information concerning the lattice constants of the entire volume of a powdered sample. High-flux x rays can also be used to study the lattice constants of PBX materials held at high pressure in diamond anvil cells (DACs). Because x-ray diagnostics require 5 to 8 min of exposure time to develop an interpretable pattern, we began to search for an accompanying diagnostic tool that could provide a real-time probe of solid–solid structural transitions.

Second harmonic generating (SHG) was first demonstrated as an independent probe into the reaction kinetics of HMX and TATB phase transitions. To test the application of SHG to the study of EMC phase transitions, in FY2001 we developed a portable optical SHG and pressure measurement experiment that could utilize the DOE-supported x-ray beamline at the Stanford Linear Accelerator (SLAC). In FY01 we conducted simultaneous SHG/x-ray (XRD) experiments on DAC-encapsulated HMX and TATB. The data show that for a nonuniform grain-size distribution of pure HMX, the SHG and XRD results are temporally incongruent (see Figure). The x-ray and size distribution data show that HMX grains less than 10 μm in diameter have yet to phase convert.

The dramatic increase in surface area accounts for the primary contribution in SHG intensity observed. The break in inversion symmetry that occurs at the air–surface interface accounts for a significant contribution of SHG light. SHG is highly surface and temperature specific. As an example, SHG intensity was enhanced by a factor of ~10^4 on a roughened silver surface.

Simultaneous SHG/XRD experiments on HMX show that SHG can give misleading results, which brings into question the rates previously derived for HMX and TATB using only the SHG diagnostic. Studying uniforms grain-sized high explosives materials may prove to give SHG a foothold in more rigorous kinetic studies of PBX materials.

Our high-temperature TATB results do not indicate any solid–solid phase transformation occurrence, even up to 340°C, and this directly conflicts with the results of other researchers. Changes in XRD peak intensities are merely due to molecular re-arrangement and annealing effects. The molecular stacking distance relating to the c-lattice parameter increases with rising temperature. No major peak changes in the reflections are observed, suggesting that no change takes place in molecular conformation.

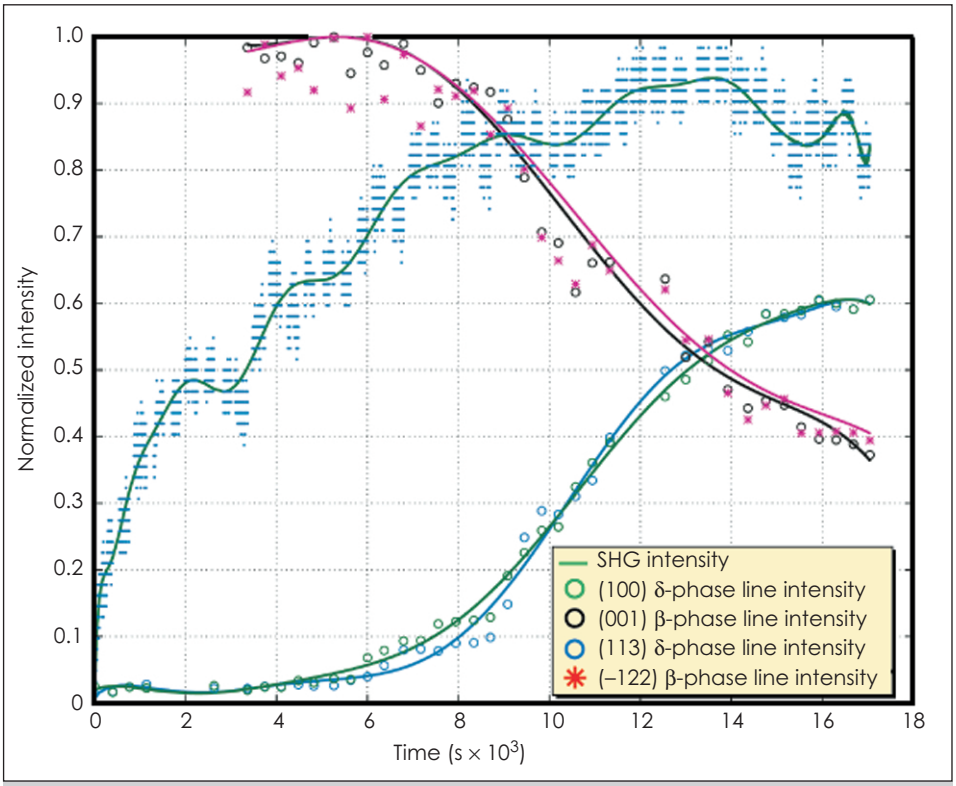

Second harmonic generating (SHG) and x-ray (XRD) time profile of HMX phase transition at 165°C.

Nanolaminate structures for bioelectrorecognition

W. D. Wilson

MAIN TOC

The ability to crystallize proteins—the chemical building blocks of the biological cell—is an important step in understanding their structure and function, but the process of protein crystallization is a trial-and-error procedure. Fewer than 1% of the approximately 100,000 proteins in the human body have been crystallized. Using current methods, finishing the job would take over 100 yr. A template at the nanoscale—similar in scale to biological building blocks—that would facilitate predictable, well-understood protein crystal growth could revolutionize the field of proteomics and a large segment of the pharmaceutical industry. This project puts such a possibility within reach by demonstrating both experimentally and computationally that a nanolaminate can capture and order proteins.

Nanolaminates, which have been constructed from over 72 chemical elements, are made by normal magnetron sputtering in the case of conducting materials (elements, alloys, and compounds) and by reactive magnetron sputtering in the case of oxides. A metal-oxide nanolaminate is built up layer by layer, like a deck of cards, by alternating the deposition of metal and oxide layers. The thickness of the layers can be varied from 1 nm to more than 200 nm, commensurate with many protein sizes. Precise control of nanolaminate size, composition, and functionalization—attaching a molecule to the nanolaminate to create a tailored binding site—could specify patterned binding not only of proteins, but of protein toxins (like botulinum ~10 nm), viruses (like smallpox ~220 nm), anthrax spores (~1 μm), and other pathogens on national security threat lists.

We have demonstrated the synthesis, characterization, modeling, and application of nanolaminate substrates for molecular self-assembly of protein layers. These substrates can be highly charged in electrolyte, which occurs naturally and is strongly dependent on the pH of the fluid. An understanding of the electrostatic potential near these structures requires solution of the nonlinear Poisson–Boltzmann equation, which we can use to compute the electrostatic potential, the energy, and forces for complicated surface geometries. Calculations of the force of interaction between a conical probe and a flat plate show excellent agreement with nanoscale measurements by the tip of a chemical force microscope.

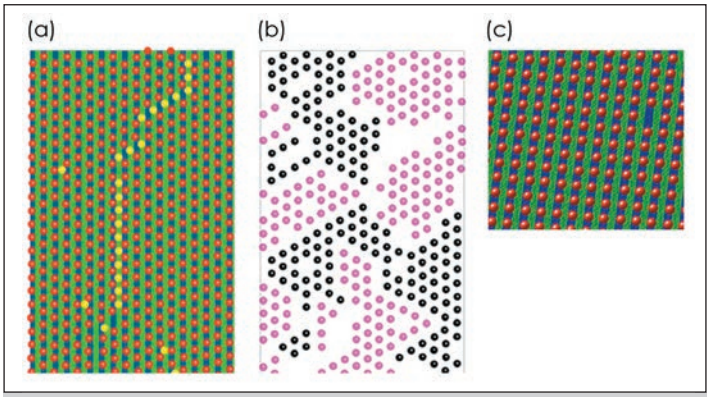

Simulation of the first and second layers of deposited proteins on a nanolaminate substrate (blue and green stripes). (a) The first layer (10-nm red spheres) deposited on a hexagonal face of a face-centered cubic (fcc) crystal reveals the high degree of order obtained with the template (the yellow atoms are defects). (b) The second protein layer forms numerous twinning domain defects (pink and black). These defects disrupt formation of the third layer and so inhibit bulk crystallization. (c) The first layer deposited on the square face of the fcc crystal on a different template. In this configuration, subsequent protein layers (not shown) do not form domain defects, thus yielding a more perfect 3-D protein crystal.

Atomic force microscopy reveals patterned protein adsorption after a silica–alumina nanolaminate substrate is exposed to an electrolytic solution of protein molecules to enhance protein crystallization. To guide this application, we developed a grand-canonical Brownian dynamics simulation. This models the solvation, diffusion, and adsorption of simple globular protein molecules onto patterned surfaces.

In FY2001, we extended the calculations to the study of protein growth beyond the first layer in order to understand the effect of the nanolaminate template layer spacings on the quality of crystal that would be produced. We find that growth on some crystal faces can lead to defects such as crystal twinning and domain formation [Figs. (a, b)]. Such defects can leave the crystal unsuitable for the high-resolution diffraction studies needed to experimentally deduce the protein structure. Fortunately, our heterogeneous, striped substrates can be designed to order the protein adlayer into other, higher-energy crystal planes. For example, growth on the square face [Fig. (c)] of our model face-centered-cubic crystal is resistant to twinning . Our theoretical work suggests additional techniques to further reduce the incidence of twinning and enhance crystal growth rates at low supersaturations.

Also in FY2001, we designed nanolaminate structures capable of manipulating analytes by electrophoretic transport in narrow channels in which a voltage gradient is induced along the metal-insulator layers of the nanolaminate. We designed structures that maximize the amount of exposed metal and minimize the diffusion distance, thus enabling electrochemical redox reactions to be used for detection purposes potentially replacing more costly laser detection of chemical species.

Determining the structure of biomaterials interfaces using synchrotron-based x-ray diffraction

M. T. McBride, J. J. De Yoreo

Many organisms exhibit control over biomineralization processes, resulting in exquisitely tailored crystalline architectures. Control may involve the introduction of acidic macromolecules that interact with growing crystals, the carefully timed introduction of ions or specific enzymes, or the removal of trace elements. These processes occur at crystal surfaces; specifically, they are mediated by atoms at the solid–solution interface.

Understanding such processes requires tools for probing the atomic ordering of crystal surfaces in liquids and the near-surface ordering of the liquid phase. Surface x-ray diffraction (SXRD) techniques are ideal for probing solid–aqueous interfaces because x- rays penetrate water with only limited attenuation. SXRD provides a dynamic picture of the system under study, giving crystal structure, surface molecular structure, the stereochemistry of adsorbates, and the stereospecifity of binding sites. It thus provides a crucial link between experimental surface techniques, such as scanned probe microscopy, and theoretical tools, such as the kinetic Monte Carlo method and molecular dynamics, that are together playing increasing roles in the detection, identification, and characterization of biological molecules and materials.

The purpose of this project is to explore the feasibility of using SXRD to determine the surface structure of biominerals in solutions and of the adsorbed layer of acidic amino acids that are believed to play a central role in the control of biomineral formation and function. Our work is a critical component in the development of an integrated picture of the physical and chemical bases for deposition and dissolution at solid–liquid interfaces in biological systems. This project will directly benefit investigations into the development of synthetic biomaterial implants in support of LLNL's biotechnology mission.

We chose as our model system calcium carbonate and calcium phosphate in aspartic and glutamic acid–bearing solutions. The calcium compounds are ubiquitous among biomineral structures; the two acidic amino acids are the dominant constituents of protein mixtures implicated in the control of biomineralization.

In FY2000 we determined that (1) aspartic acid strongly modifies calcite surfaces; (2) stereospecific binding interaction involves two sites on {hk0} faces, whereas interactions on {104} faces are insignificant; and (3) surface free-energy modifications are thermodynamically driven, not kinetically driven. We used sophisticated energy calculations to model the interactions of D- and L-aspartic acid with {*hk*0} faces of calcium carbonate; our results show that the differences in binding geometries are quite subtle. Building on our successful calcite studies, we proposed to investigate a protein-mediated calcite–aragonite phase transformation. Using SXRD, we sought to confirm the presence of two mineral phases, and to obtain structures of the mineral–protein, mineral–mineral, and mineral–liquid interfaces. We detected only calcite, casting doubt on the previously reported transition or the reproducibility of the protein mixture responsible for the transition. We proposed to extend our studies to calcium phosphates such as brushite and fluorapatite, but suitable crystals were not available.

In FY2001, we directed our efforts to the barite ($BaSO_4$)–water interface. This interface has been intensively studied because of the problem of barite scale formation in the petroleum industry. Similar to the calcite–aspartic acid system, barite also exhibits additive-induced shape modifications, and suitable crystals were readily obtained. High-resolution (1 Å) specular reflectivity was used to probe the step structures of cleaved {001} and {210} surfaces and the structure of water near the barite–water interface; these results are the subject of a recent report. We also studied the barite cleavage surfaces in the presence of the growth inhibitor HEDP (1-hydroxy-1,1-diethyl phosphonic acid); these results will be the subject of a future report. In a separate study, we presented results of an SXRD structural analysis of liquid tin (Sn) monolayers adsorbed on germanium{111} surfaces. We investigated the influence of temperature on the structure of liquid Sn. We found that at temperature above the melting temperature, Sn atoms displayed both liquid-like and solid-like behavior.

Smart membranes

T. van Buuren, S. Letant, T. Baumann, A. Vance

Our goal is to design a smart and selective membrane through the manipulation and control of the pore size of the membrane and the chemical groups coating the inside surface of the pores. With control over both the pore morphology and the chemical nature of the inside of the pore, we can tailor the chemical interaction and filtering capability of the smart membrane to selectively recognize and bind proteins, antibodies, and other biologically relevant macromolecules. Building such a device would constitute a step forward in membrane technology: most of the filtration membranes available on the market select molecules according to their size only and have no chemical functionality. Our approach is to etch pores in a silicon (Si) wafer to obtain a membrane; either coat the pore walls with gold (Au) or convert them to siloxane; and anchor functionalized, self-assembled monolayers (SAMs) designed to harvest targets.

This research will enhance both LLNL's capability in nanotechnology and bioscience in support of our chemical- and biological-weapon-detection programs.

During FY2001, we optimized the electrochemical parameters [photocurrent, voltage, and hydrofluoric-acid (HF) concentration] of the Si dissolution reaction and demonstrated the formation of pores with diameters ranging from 350 nm to 2.5 μm, a narrow size distribution (<50 nm), and a fast growth rate (1 μm/min). These pores can be strictly arranged according to the surface pattern that was created on the Si wafer by photolithography followed by a potassium hydroxide (KOH) etch. We now have control of pore size, length, and position—issues that remain to be addressed in commercially available membranes.

An electroless Au-plating technique deposits Au on the Si structures—a technique that is still under development in the plating industry. Although the nature and the geometry of our membrane constitute a challenge for this technique, we successfully plated large pores in Si substrates. The adhesion of the Au to the semiconductor surface was enhanced by electroless plating of a silver seed layer.

We prepared our first smart membrane during FY2001. This device was built in two steps: (1) 200-μm-deep pores were etched from the top of the wafer, and (2) the Si crystal lying underneath was removed by electropolishing from the bottom of the wafer. Characterization by scanning electron microscopy (SEM) showed that the membrane's surface area was 1 cm^2, the thickness was 200 μm, and the pore diameter was 800 nm.

In FY2001, we also synthesized SAMs with more complex terminal groups (e.g., biotin-terminated SAMs) and established a protocol for the synthesis of SAMs with different types of tethers. Characterizing and understanding these systems will allow us to design more complex and functional membranes.

At year's end, we were beginning first-order calculations of the gas flux through the Si membrane in the Knudsen diffusion regime (in which pore diameter and size of the target molecules are in the same order of magnitude). These calculations will allow us to adjust the pore size, length, and density.

For FY2002, our first goals are to (1) improve the robustness of our membrane; (2) complete our gas-flux calculations; (3) derivatize the pore walls; (4) test membranes with various pore size, thickness, and chemical functionality in liquid and gas environments; and (5) compare our experimental data to the results of our gas-flux calculations.

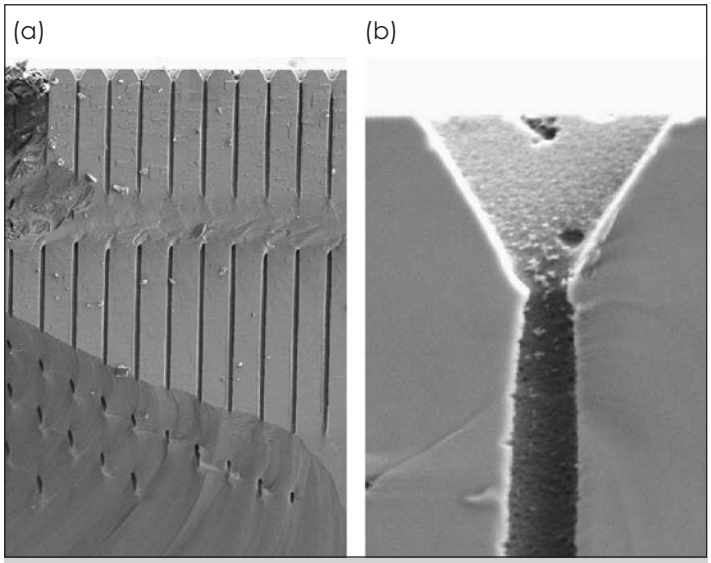

Scanning electron microscope (SEM) images of the cross section of a silicon membrane, showing (a) ten rows of pores, and (b) the detail of the top of a pore. The mean pore diameter is 500 nm.

Subcritical crack growth in silica glass

T. I. Suratwala, R. A. Steele

MAIN TOC

Fused silica glass (SiO_2) is a technologically important material because of its excellent optical qualities, low thermal expansion, and resistance to both high temperature and chemical corrosion. In many applications, fused silica glass parts are subjected to a range of mechanical stresses. Under such conditions, small, pre-existing flaws in the glass can grow at stresses below the critical stress needed to cause failure. This type of crack growth is often called subcritical crack growth (SCG) or slow crack growth. Despite the vast literature on SCG behavior, experimental data and understanding of environmentally assisted fracture in fused silica are surprisingly limited.

This project will lead to better scientific understanding of slow crack growth behavior in fused silica, an ideal glass to study scientifically because of its simple glass composition. Improved models will enable the quantitative prediction of crack velocities of fused-silica samples exposed to different environments encountered in a variety of applications, ranging from space exploration to military applications. This research enhances LLNL's competency in material behavior under stress and other extreme conditions, in support of the Laboratory's national security programs.

During FY2000, we designed and built a mechanical testing system and started measuring the SCG velocities of various types of fused silica using the double-cleavage, drilled-compression (DCDC) technique under various environments (i.e., different stresses, temperatures, and humidities). For our experiments, we mounted rectangular glass samples with a hole drilled through each center in a mechanical-testing setup within an environmentally controlled chamber in which a compressive stress was applied. Using a charge-coupled device (CCD) camera, we determined the velocity of the cracks originating from the sample hole by monitoring the position of each crack as a function of time.

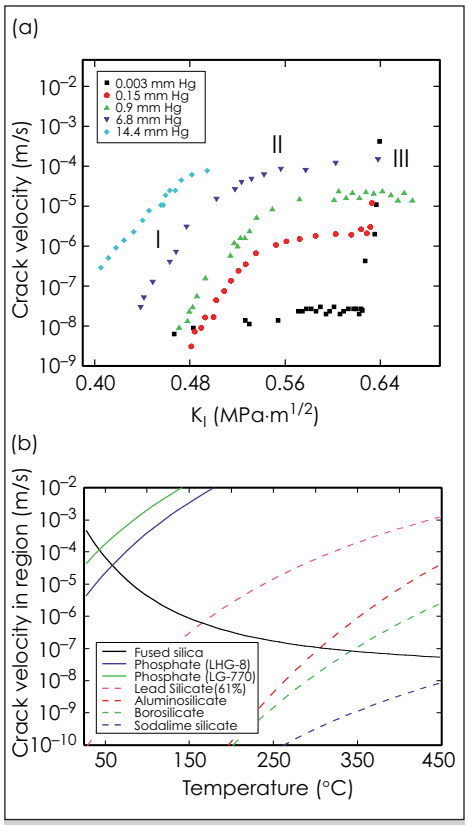

Results of experiments to determine subcritical crack growth (SCG) in fused silica glass: (a) crack velocity vs stress intensity (K_I) of fused silica glass at 25°C and various humidities; and (b) crack velocity vs temperature of various glasses.

During FY2001, we completed the matrix of crack-velocity measurements and then phenomenologically modeled the resultant data. Crack velocities expressed in plots of the log of the velocity vs stress intensity (K_I) commonly show three distinct Regions of behavior: Regions I, II, and III [Fig. (a)]. Region I, which refers to the range of conditions for which crack growth is reaction-rate limited, is characterized by a linear increase in the plots of log velocity vs K_I. In other words, enough H_2O is present at the crack tip such that crack growth is limited by the rate of reaction between H_2O and the Si–O–Si bonds in the glass structure. Region II refers to the conditions where the crack velocity becomes constant with increasing K_I; that is, where the velocity is mass-transport-limited by the rate of H_2O diffusion to the crack tip. Finally, Region III refers to the condition where crack velocity becomes independent of the H_2O environment as the K_I approaches the fracture toughness (K_{Ic}) of the glass.

We determined that—in contrast to what happens in other inorganic-oxide glasses—crack velocities in fused silica decrease with an increase in temperature [Fig. (b)]. Hence, a small temperature rise has the apparent effect of improving the mechanical strength of a stressed-glass part. Despite the anomalous temperature dependence, SCG in fused silica is still likely governed by the established, water-enhanced, stress-corrosion mechanism. However, another competing phenomenon (likely related to change in the glass structure with temperature and stress) is proposed to cause the observed temperature dependence. We then quantitatively described the measured crack velocities using an empirical model (for Region I) and a mass transport model (for Region II). Our results have been submitted to a refereed journal.

Successful completion of this project has provided a greater fundamental understanding of SCG behavior in fused silica and has allowed quantitative prediction of crack velocities of fused silica exposed to different environments.

Subpicosecond laser deposition of thin films

F. Y. Génin, B. C. Stuart, W. McLean, L. L. Chase

MAIN TOC

Understanding the interaction between materials and high-energy-density light is key to solving important scientific and engineering problems in both programmatic and fundamental research at LLNL. Following on more than a decade of developing high-power, short-pulse lasers at the Laboratory, this research is continuing the development of laser-based materials-processing techniques and accelerating progress in manufacturing smart materials for biosensors, detectors, and medical applications.

Although this project emphasizes aspects related to thin films prepared by ablation of material with intense, ultrashort laser pulses, the results also apply to the processing of nanoclusters. Work during FY2000 was fully devoted to building the foundation for our research by studying deposits of diamond-like carbon and aluminum produced using a titanium-sapphire laser operating at 1 kHz, 810 nm, and with pulse widths ranging from 150 fs to 0.5 ns. We then compared our results with those reported in existing literature and with earlier, LDRD-sponsored, nanosecond-pulse, laser-deposition work at the Laboratory. With the knowledge developed during the first year, we expanded our effort to include multielement systems of different natures and properties. This approach allowed us to better understand the differences between short-pulse and long-pulse laser deposition and to identify the advantages of each regime.

During FY2001, we investigated systems ranging from purely metallic and semiconductor materials to ceramics, aluminum nitride, boron nitride, cellulose from paper and wood, and polymers. Our investigation involved the full scope of morphology, phase, and microstructure analysis of the deposits using atomic force microscopy (AFM), scanning electron microscopy (SEM) or transmission electron microscopy (TEM), and x-ray diffraction (XRD). To relate the microstructure observations to the ablation events, we measured the ablated plume of selected systems using time-resolved imaging (TRI) and time-of-flight mass spectroscopy (ToF-MS).

The results of our physicochemical analysis of the films clearly demonstrated that ultrashort-pulse laser ablation allows the transport of molecules that would otherwise decompose using other deposition techniques. For example, cellulose films were deposited with pulses shorter than 10 ps. For the polyethylene system, Fourier-transfer infrared (FTIR) spectra proved that film chemistry is retained. At constant fluence, deposits were found to contain larger amounts of spherical particles when shorter pulses were used.

We also confirmed, using SEM, TEM, ToF-MS, and TRI, that shorter pulses tend to favor nanoparticle formation as a result of differences in light–matter interactions at the ablated target (see Figure). The TRI and ToF-MS measurements produced evidence of features that are specific to femtosecond laser-induced plasmas. In this ultrashort-interaction regime, three different plasma-expansion velocity populations are measured. First, a Coulomb explosion generates fast ions followed initially by atom neutrals, and later by submicrometer clusters. Under the same experimental conditions, nanocluster formation is not as pronounced for longer pulses. Femtosecond laser-induced plasmas are thinner and more directional than nanosecond plasmas. All these effects contribute to significant differences in deposition rate, thickness distribution profiles, and film morphology.

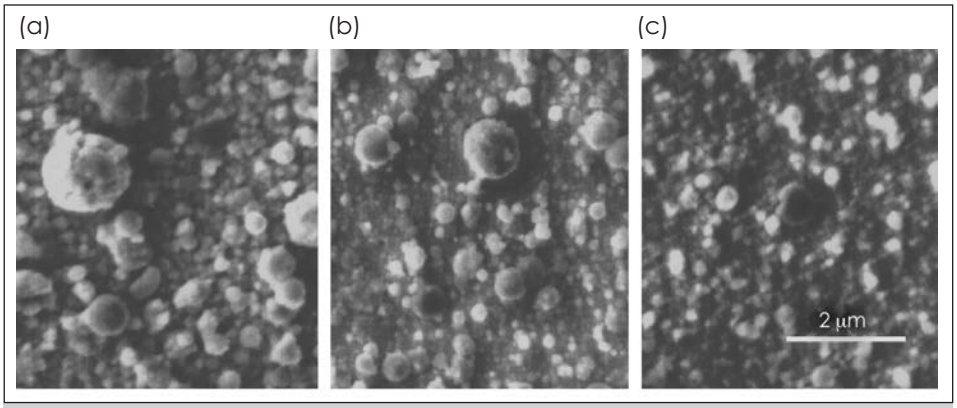

Scanning electron micrographs of pulsed-laser-deposited thin films. Laser pulse lengths were (a) 150 fs, (b) 1 ps, and (c) 20-ps. Shorter pulses tend to favor the formation of particles.

In conclusion, this research has clarified some of the advantages of ultrashort pulses for deposition on thin films. Femtosecond pulses allow faster and more directional deposition of materials. Their use tends to generate particles produced by phase separation of the irradiated surface layer, which sometimes lead to coarser films. Finally, femtosecond laser pulses can be used to deposit fragile molecules such as plastics, organic compounds, and biomolecules.

Next-generation nanoscale thermal imaging

D. J. Chinn, R. D. Huber, C. J. Stolz

Photothermal scanning microscopy (PTSM) is a powerful tool that can map optical absorption, scattering, and reflectivity as well as thermal absorption in materials—it has proven very useful in characterizing thin-film optical coatings. In PTSM, a raster-scanning technique is used in which a focused laser pump beam illuminates an approximately 5-µm-diam area of the test surface. Surface and subsurface defects within the test area absorb the light and cause a surface "bump" or lens to form from thermal deformation. The surface deformation changes the diffraction of the probe laser, which is recorded by a photodetector. By chopping the pump beam and locking in the photodetector to the chopping frequency, a photothermal signal is derived for one location. The pump and probe are then raster-scanned to generate a photothermal map of an area.

However, although the current PTSM technique shows excellent results in characterizing thin-film coatings, it is limited by extremely slow imaging times. For example, imaging a 1 cm^2 area of a thin-film coating at 10-µm resolution takes approximately 278 h—too long to make PTSM feasible for examining coatings on full-sized optics.

Our goal in this project was to advance the PTSM technique to enhance LLNL's capabilities in nondestructive characterization and testing in support of the Laboratory's national security programs.

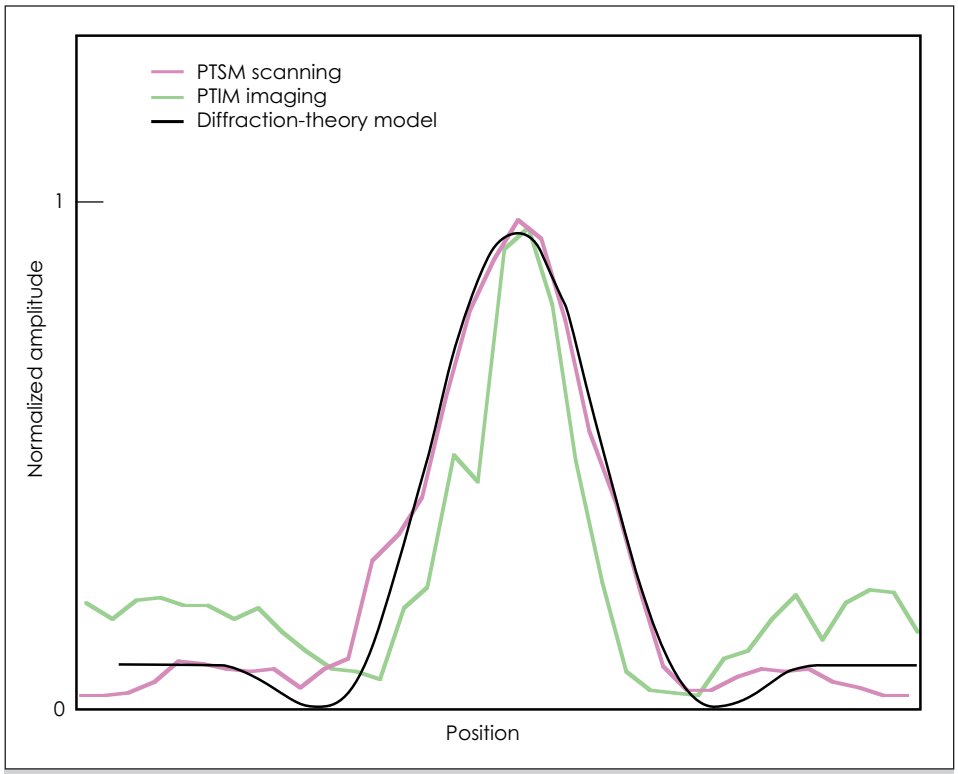

Normalized amplitude profiles across an aluminum dot show good agreement among photothermal imaging microscopy (PTIM), photothermal scanning microscopy (PTSM), and the diffraction-theory model.

During FY2001, with our collaborator at Wayne State University, we developed photothermal imaging microscopy (PTIM) into a viable technique for inspecting thin-film coatings on optics. PTIM is a rapid, photothermal imaging method that uses focal-array detectors and optical lock-in imaging techniques to increase the imaging speed of photothermal microscopy by 5 to 6 orders of magnitude over that of PTSM. In PTIM—instead of raster scanning as in PTSM—the pump and probe beams are expanded to about 5 mm. A megapixel charge-coupled device (CCD) camera detects the diffracted pump beam. By applying optical lock-in techniques to the camera images, we obtain a PTIM image. In 8 s, we generate a photothermal image of an area that would have taken 55 h to obtain with PTSM.

Our comparative tests proved the principle of PTIM. As shown in the Figure, PTIM gives comparable results to PTSM when imaging a glass sample with an antireflective coating that has sputtered aluminum dots on the glass substrate. The Figure compares—across one aluminum dot— normalized PTSM, PTIM, and theoretical amplitude profiles that are based on the diffraction-theory model of the photothermal response. The diffraction-theory curve assumes a Gaussian probe beam and a Gaussian-shaped lens resulting from heating of the aluminum absorber. Both PTSM and PTIM profiles correlate well with the modeled profile.

In summary, we developed a nondestructive testing capability that does not exist elsewhere. This capability will help (1) determine the source and characteristics of defects in (among other applications) thin-film coatings, and (2) reduce inspection time of photothermal microscopy by 5.5 orders of magnitude.

Structures of high-density molecular fluids

B. Baer, H. Cynn, V. Iota, C. S. Yoo

MAIN TOC

Material characterization under simultaneous conditions of high pressure and temperature would provide critical information for understanding the behavior of energetic materials in support of the Stockpile Stewardship Program, planetary structure, and the synthesis of novel materials under high pressure. However, until recently, experiments probing matter under such extremes were limited to dynamic compressions. Also, techniques for obtaining spectroscopic information under equivalent static conditions are still in their infancy.

Consequently, our goal in this project was to develop a technique for measuring the properties of simple molecules at high pressures and temperatures. For this purpose, we constructed a system that employs coherent anti-Stokes Raman spectroscopy (CARS) in a laser-heated diamond-anvil cell (LH-DAC).

Our challenge was to develop a robust spectroscopic method and a means to laser-heat a finite volume for investigation. Although high temperatures in a DAC have been reached using laser heating, very little spectroscopic information has been obtained in these experiments while the sample is hot. Two reasons account for this: (1) a tremendous amount of Planck radiation is emitted by matter as the temperature is markedly increased, and (2) generating "hot spots" in a DAC requires that the spectroscopic probe be spatially confined to that microscopic hot spot.

In FY2000, we constructed a laser system for CARS (see Figure), a four-wave mixing technique that gives vibrational information as a signal that is directional, coherent, and short pulsed so that it can easily be spatially and temporally resolved from the Planck radiation. In brief, two short-pulsed (30 to 100 ps) lasers are tuned so that their frequency difference is equal to the vibrational energy of the molecules to be studied. The higher-frequency laser is narrow band, while the other is broadband (i.e., broadband CARS). When the molecules are in resonance with the energy difference, two photons of the higher-energy laser become shifted in energy—one photon to the Stokes and the other to the anti-Stokes emission wavelength.

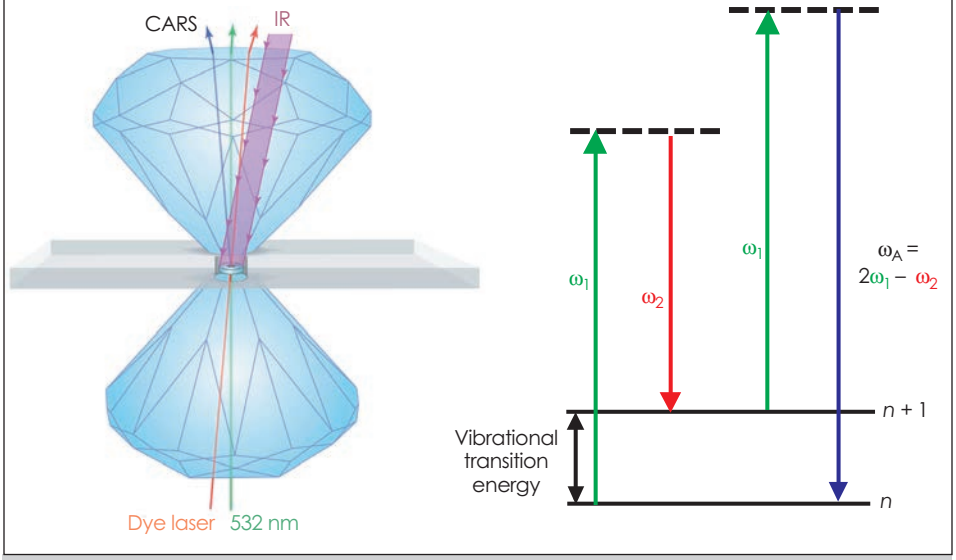

Simultaneous laser heating using coherent anti-Stokes Raman spectroscopy (CARS). (left) Diamonds, gasket, and beam configuration. (right) The CARS process for stimulating the anti-Stokes emission by using two different colors where ω_1 is the frequency of the narrow-band laser pulse (typically 532 nm), ω_2 is the frequency required from the broadband dye laser, n denotes the vibrational energy level, and ω_A is the anti-Stokes frequency.

During FY2001, our major achievements were to (1) devise a method that would create a well-established volume of pressurized, high-temperature material enclosed in a DAC; and (2) develop component technologies that enable CARS experiments on samples under simultaneous laser heating. The latter technology requires the microfabrication of toroids made of tungsten or tantalum. Even at ambient pressure, these materials have extremely high melting temperatures. The 15-μm-thick toroids have outer diameters of approximately 90 μm and inner diameters of 30 μm. The toroid allows the two laser beams used for the CARS experiment to cross inside the clear interior of the metal ring. The heating laser is focused to hit a broad area of the toroid's surface. This process generates a small volume of material within the sample that is at or near the temperature of the toroid's inner wall. This heating process, however, requires a large amount of laser power. FY2001 ended with the acquisition of high-power lasers for this application.

With these newly purchased lasers, we are in a position to examine the structure of nitrogen at detonation conditions. In fact, our work has already leveraged a new programmatic study of major detonation products.

Toward applications of quantum dots: Surface modification and novel electronic properties

B. R. Taylor, L. J. Hope-Weeks, S. M. Kauzlarich

Extremely small semiconductor particles, often called quantum dots, have unusual properties that differ from those of the bulk material. Our research addresses the initial work on some of the potential applications suggested by these properties, which include biological sensors and high-speed, all-optical switches.

Because these particles are so small, the number of atoms at or near their surface is much greater than is the case in bulk solids (see Figure). The surface plays a large role in the electrical and optical properties of quantum dots, whereas in bulk solids the surface plays a small role, or is neglected entirely. Quantum confinement, which occurs when the quantum dot is smaller than the radius of a bound electron–hole pair, changes the dot's electronic properties. Because most or all of the atoms in these dots interact with the surface, any charge carriers also interact strongly with the surface. Control of the surface termination changes both the physical and electronic properties of the dot. The surface termination chosen protects the dots from oxidation, permits them to form stable suspensions in organic solvents, and improves their luminescent efficiency by tying up dangling bonds.

Refinements in surface termination will permit attaching quantum dots to surfaces, chemically attaching them to proteins, and may permit making electrical connections to them. Because the quantum dots have such a large surface area per unit volume, attaching appropriate groups to their surface may permit the development of a sensitive sensor for pathogens or chemical agents, a possibility that is clearly relevant to the DOE's nonproliferation mission.

During FY2001, we continued chemically manipulating the surface of both silicon (Si) and germanium (Ge) quantum dots. With a simple modification of standard, published procedures, we achieved higher yields of Si quantum dots and demonstrated the ability to chemically manipulate the surface of quantum dots without affecting their desirable luminescent properties. The functional groups attached to the dots included alkyne, aromatic, and aliphatic hydrocarbons. A suitable choice of surface terminating groups permitted preparing Ge and Si dots with carboxylic acid groups chemically attached to the surface. This made the dots soluble in water and alcohols, an essential step for biological applications. We also demonstrated the attachment of Ge quantum dots terminated with carboxylic acid to mouse immunoglobulin through a routine biochemical coupling procedure, and prepared Ge and Si quantum dots with alkyne groups attached to the dot surface.

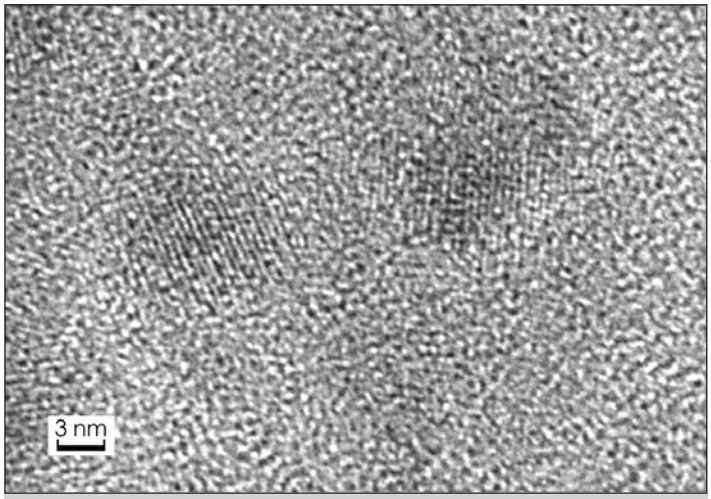

High-resolution transmission micrograph of germanium quantum dots. Bright and dark lines are rows of individual atoms in the crystal. Quantum dots have interesting potential applications in electronics, optoelectronics, and biology.

The smallest conducting systems prepared to date, called Tour wires after the first researcher to prepare them, consist of repeating alkyne and aromatic units. There is much interest in these molecular wires, because they are 1-D conductors, meaning that they constitute a correlated system, so that current flow involves the whole wire. Conduction is very different in such wires, which can behave as a switch, conducting at some voltage differences and not at others.

During FY2001, we developed much of the chemistry required to prepare Tour wires attached to quantum dots, which will permit us to make electrical connections to them. Wiring a system of quantum dots together chemically opens up a great number of possibilities, for example, creating a nanoscale analog of a random-access computer memory array.

In FY2002, we plan to continue chemical manipulation of the surface termination of quantum dots. Because the carboxylic acid-terminated dots have already been attached to a protein, our next step in their development will be to prepare them in a narrow size distribution; the properties of interest depend strongly on size. Size control can be obtained by varying the reaction conditions or by separating particles according to size.

Metal–Insulator transition in lithium and lithium hydride

M. Bastea

The transition of condensed matter between electrically conducting and insulating states is a topic of wide scientific interest. Its relevance has ranged from superconductivity to collosal magnetoresistance, to (more recently) thermoelectricity. The metal–insulator transition has received renewed attention during the past decade in the context of high-pressure research. Although much progress has been made in developing experimental, theoretical, and computational tools appropriate for the study of the metal–insulator transition at extreme conditions, our present understanding is mostly phenomenological and still incomplete. In this context, the recent prediction that lithium (Li) would transition to an atomically paired state with nonmetallic character posed a definite challenge to experimental physics.

Lithium is the archetype of a "simple" metal, that is, one in which the electronic valence states are well-separated energetically from the tightly bound core states. It has been known for a long time that the electronic properties of Li at ambient conditions are well described within the nearly free-electron picture, which is a cornerstone of the theory of metals. While it has been generally assumed that increased pressure would only improve the accuracy of this description, in recent years theoretical calculations have suggested that the opposite may be true. The best way to answer such questions is to measure the electrical conductivity of these materials at high pressures.

Our main goals are to search for a nonmetallic, high-pressure phase of Li—a first in the history of physics—and to find the metallization conditions for lithium hydride (LiH). Lithium hydride provides the unique opportunity to understand the effects of coupling two elements with opposite tendencies at extreme conditions and to study fundamental principles such as metallization and pairing. The materials we are focusing on—Li and LiH—have several technological applications and are also relevant to LLNL's stockpile stewardship mission. The expertise we are building for dealing with sophisticated target fabrication and experimental design issues will be transferred into broader projects.

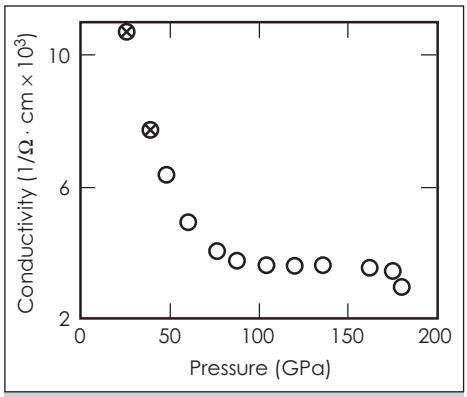

Electrical conductivity of lithium as function of pressure. The crossed symbols show data inferred from intermediate compression states.

In our quest for pressure-induced metal–insulator transitions, we have built upon existing LLNL experimental capabilities—such as the gas-gun facilities and the laser-induced shock facilities associated with LLNL's Janus laser. We have also developed collaborations with other DOE laboratories and with programs such as the Z-accelerator at Sandia National Laboratories (SNL).

During FY2001, we conducted multiple shock experiments and measured the electrical resistivity of Li at pressures up to 180 GPa. Our results show three regimes in the dependence of resistivity on pressure (see Figure). Up to about 100 GPa and threefold compression, the electrical conductivity of Li decreases steeply because of increased scattering of the charge carriers in the compressed material. This regime is followed by a much slower variation of the conductivity with pressure, which extends to approximately 160 GPa and almost fourfold compression. At the highest pressures, the conductivity drops sharply. The results are consistent with a departure of the electronic properties of Li from the nearly free-electron approximation at high pressures, and with ionic pairing correlations in the 100-GPa range.

We also conducted a successful experiment at SNL's Z-pinch accelerator in which our goal was to measure accurately the equation of state (EOS) of Li up to about 100 GPa and to identify the melting transition. The data analysis is in progress.

During the first quarter of FY2002, we will conduct laser-induced shock experiments up to several hundred GPa in LiH. To gain better understanding of the physics of these low-Z materials at extreme conditions, we will be combining EOS and optical-properties measurements with new investigating tools such as Thomson scattering.

Surface-enhanced Raman spectroscopy with high spatial resolution

T. Huser, C. Talley, C. Orme, W. Siekhaus

Identifying individual molecules and determining how these interact with their local environments are critical steps toward a better understanding of complex organic systems. Though optical detection techniques have always played a key role in the nondestructive and noninvasive analysis of complex materials, until recently optical microscopy has lacked the sensitivity to study biomolecular processes on the molecular scale.

This situation has changed with the recent development of new schemes that limit the optical detection volume and with the advent of new, highly quantum-efficient photon detectors. These inventions have enabled researchers to optically probe biomolecular processes at the single-molecule level by observing the fluorescence of specific marker molecules. However, the requirement to specifically label biomolecules and the fact that fluorescence emission is prone to photodecomposition of the marker molecules have limited this approach to a small number of well-characterized case studies. Raman scattering is one of the few optical techniques that can identify atomic species and determine their chemical bonds by observing their distinct vibrational fingerprints, but it is orders of magnitude weaker than fluorescence.

In this project, we are developing new optical probes that allow for the nondestructive characterization and identification of organic and inorganic matter at the single-molecule level using surface-enhanced Raman spectroscopy. This work will enhance LLNL's capabilities to characterize materials at the nanometer scale, which is very important to potential applications such as (1) identification of nanometric laser damage-initiation sites in optical materials for high-power lasers, (2) genomics and proteomics research at the single-molecule level, and (3) identification of spurious amounts of biological and chemical warfare (BW and CW) agents in forensics and counterterrorism.

Our approach combines confocal Raman microscopy with surface-enhanced Raman spectroscopy (SERS) generated by placing nanometer-size gold (Au) particles at the end of scanning-probe microscope (SPM) tips. The scanning SERS probe generates an image of the physical structure of a sample together with detailed chemical information about its composition.

During FY2001, we optimized our optical-detection setup to the maximum extent; we are now able to obtain Raman spectra with excellent signal-to-noise (S/N) ratios even from the interior of single biological cells.

We produced the first SERS tips by sputter-depositing Au onto commercially available SPM tips. Handling these tips is still complicated by the softness of the deposited Au layer and by the extreme sensitivity of the tips to contaminations. Furthermore, we measured the distance-dependence of SERS by comparing experimental glycine SERS spectra obtained from Au nanoparticles to molecular-dynamics calculations of glycine adsorption to Au surfaces [see Figs. (a,b)]. We also investigated the fluctuations of DNA hairpins attached to Au nanoparticles as a model system for macromolecular conformational changes. Our work was published in refereed journals.

In FY2002, we plan to (1) perfect the SERS-tip production by attaching Au nanoparticles to SPM tips, (2) use these tips to investigate DNA bound to glass surfaces and to explore the limits of resolution of these tips, (3) apply SERS to investigate the protein–DNA interaction of single molecules, and (4) obtain first results on the protein-folding dynamics of single proteins bound to Au nanoparticles.

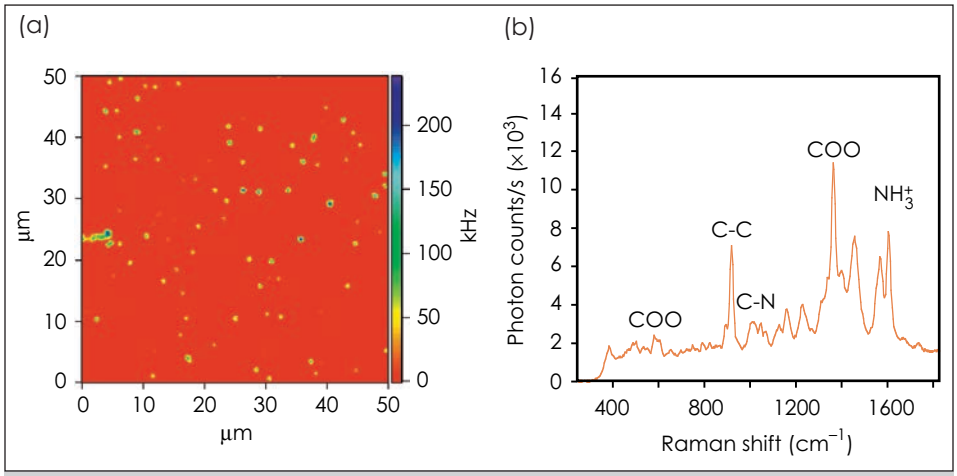

Results of surface-enhanced Raman spectroscopy (SERS), showing (a) a 50×50 µm^2 confocal-microscope image of glycine-loaded gold nanoparticles dispersed on a glass support, and (b) glycine adsorbate identified by the SERS spectrum of a single particle.

Shock recovery of organic liquids: From the origin of life to the defense of the nation

J. G. Blank

MAIN TOC

The origin of life on Earth remains one of the key questions in modern science, with far-reaching implications not only for our own origins but also for the prospects of life on other planets. The defense of the nation against ballistic missiles carrying chemical or biological agents is a major programmatic objective of the Department of Defense (DoD). These two disparate subjects are connected at a fundamental level by questions concerning the fate of organic liquids subjected to strong shock compression.

We are defining a new scientific niche, that of high-pressure-shock organic chemistry, with relevance to issues of national defense, the origins of life, and basic scientific research. This project will allow direct assessment of organic chemistry occurring under extreme pressures and temperatures relevant to cometary impacts and will improve our ability to model related dynamic scenarios. It will also provide, for the first time, laboratory simulations directly appropriate to real conditions of a missile interception and will allow us to gauge the chemical evolution of warheads interrupted en route to their target. The DoD, though the Ballistic Missile Defense Organization, is engaged in a massive effort to develop an effective defense against missile-borne weapons of mass destruction. LLNL has a substantial effort in this area, principally in modeling intercept scenarios.

The scope of our project is deceptively simple: shock organic liquids to extreme pressures, recover 100% of these liquids, and characterize their resulting chemical evolution as a function of pressure, temperature, and duration of the high-pressure impact pulse. Our objective is to determine the survivability of organic compounds delivered to Earth or other terrestrial bodies via a cometary impact, and the survivability of chemical-weapon (CW) simulants released in a ballistic-missile intercept scenario. Using aqueous solutions doped with organic compounds as a comet proxy, our results on amino acids will constrain models for the delivery of organic compounds to Earth. Our results on CW simulants will be used to determine whether part of a deadly payload may be rendered inert by shock, and whether chemical byproducts might be suitable for remote sensing of successful intercepts.

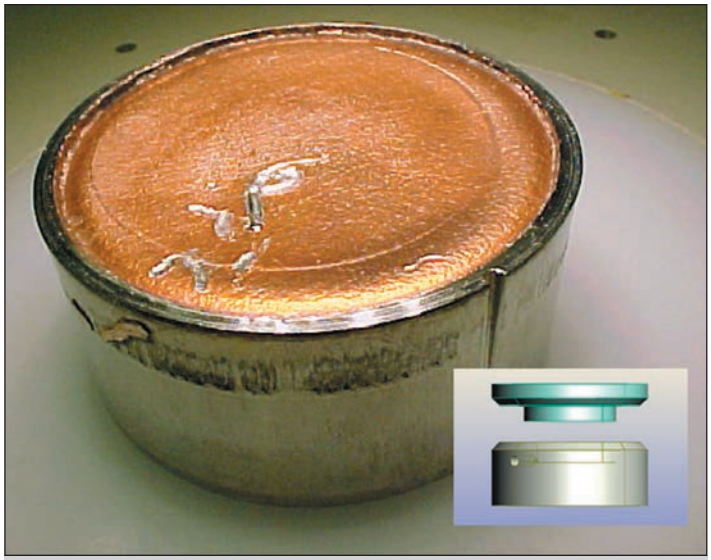

A Cu projectile disc caps a recovered, 42-mm-diam, stainless-steel capsule that held an aqueous solution of the amino acid glycine during an impact shock that reached 24.5 GPa. Inset shows the capsule before assembly.

To date, shock-recovery experiments have been conducted using LLNL's 6.5-m two-stage light gas gun. We designed sample capsules to hold roughly 0.05 cm^3 of liquid and to withstand the impact pressures up to 25 GPa that are generated by planar stainless-steel, cooper, and tantalum impactors. Initial calculations using hydrodynamic codes and supported by a companion LDRD (00-ERD-014) project suggest that (1) we will achieve uniform loading across most of the sample for times on the order of a millisecond; (2) peak pressure and temperatures of an experiment will last on the order of several microseconds; and (3) the duration of these peak conditions is directly proportional to the thickness of the metal impactor.

During FY2001, we developed procedures concurrently for (1) successful impact loading of a liquid solution to 25 GPa in a stainless-steel capsule (see Figure), (2) sample retrieval using a metal-piercing device, (3) quantitative measurement of 6-amino-acid aqueous solutions and, separately, of tributyl phosphate by liquid chromatography/mass spectrometry (LC/MS). Using the method of gradient-corrected density functional theory, we also established a protocol for conducting ab initio computational studies of the energetics involved in amino acid dimerization and ring formation in water.

In FY2002, we will expand our efforts to assess chemical changes in suites of liquids subjected to an array of shock conditions. Novel numerical modeling will address amino-acid polymerization and CW-simulant breakdown resulting from shock processing.

Microstructural origins of dynamic fracture in ductile metals

J. Belak, J. U. Cazamias, M. Fivel, D. L. Haupt, M. Kumar, R. Minich, R. E.Rudd, A. J. Schwartz

MAIN TOC

Shock waves in solids produce many interesting effects. One such effect, known as spallation fracture, occurs when a shock wave reflects from a free surface and produces extreme tension inside the solid. When this tension exceeds the internal rupture strength, the solid fails by nucleating voids in ductile metals and cracks in brittle solids. The growing voids quickly link together to fracture the solid. The origin of the voids is directly tied to the microscopic structure of the solid. Weak points in the microstructure, such as inclusions and grain boundary junctions, are the locations from which the voids are likely to nucleate. Improving our understanding of spallation requires correlating observed incipient damage with well-characterized microstructure.

One of the challenges facing LLNL's Stockpile Stewardship Program is the assessment of the stockpile using computational models. Changes in material properties due to effects such as aging and remanufacture are represented through constitutive models, which are sensitive to the microscopic structure or constitution of the material. This project integrates LLNL's experimental and modeling capabilities in material characterization and shock physics to enhance our understanding of constitutive properties required to model spallation fracture in ductile metals.

The project uses the LLNL gas gun facility to create a planar stress pulse with controlled pulse duration and stress amplitude in a metal with a known microstructure: single crystal and polycrystal without impurities; and copper (Cu) with internally oxidized inclusions. By studying light metals, we can use 3-D x-ray tomographic experiments to analyze the incipient damage. During an x-ray tomography experiment, an x-ray image is taken along many different directions. These images are then combined to compute the 3-D distribution of density throughout the material. Voids are identified with regions of very low density. The x-ray experiment gives both the size distribution and 3-D spatial distribution of the voids, which are essential input to constitutive models of spallation.

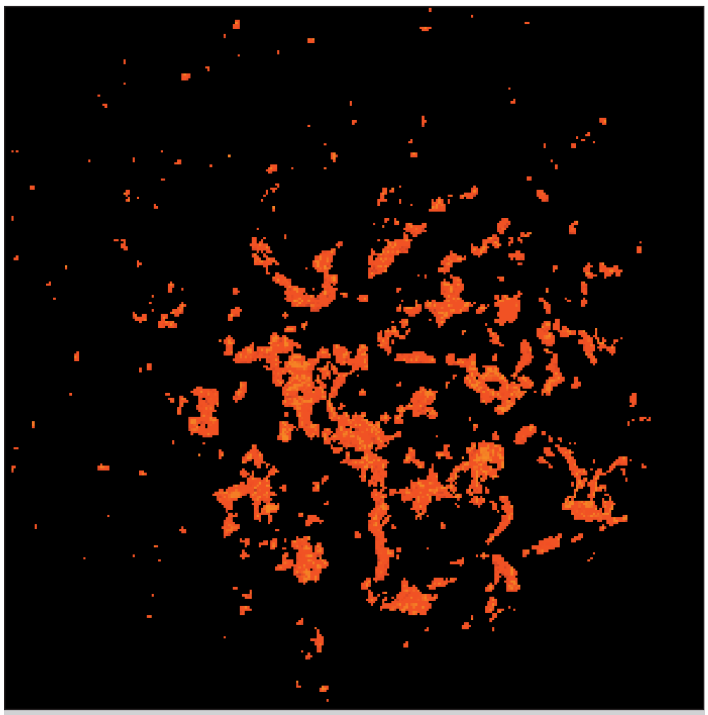

A 3-D tomographic image of the incipient spall plane in pure polycrystalline aluminum. In this 6 × 6-mm image voids appear as bright regions.

The Figure shows an example of the 3-D tomographic reconstruction. Viewed from above, the image is a 6 × 6-mm region of the spall plane in pure polycrystalline aluminum (Al) shocked at 160 m/s. Each bright voxel (3-D pixel) represents a 0.015-mm region where the material is voided. Larger voids are shown as connected voxels. The damage, far from homogeneous, is comprised of regions of isolated voids and a large region where the voids have begun to link together to form the fracture surface.

During FY2001, we demonstrated the capability to systematically shock samples and recover them with minimal further damage, while concurrently measuring the free-surface velocity wave profile. Although our primary goal is to characterize the incipient damage, the wave profile has long been used to characterize shock loading, including spallation. One of our secondary goals is to correlate features in the wave profile to the observed damage. Samples of commercial 1100 Al, pure polycrystalline Al, and Cu with internally oxidized inclusions were shocked to incipient spallation and recovered.

In FY2002, when the LLNL synchrotron beamline at the Stanford Synchrotron Radiation Laboratory returns to operation, we will analyze at increased resolution the samples we have in hand and correlate the observed void distribution with 2-D microscopy. We will also begin a series of gas-gun recovery experiments on single-crystal Al, titanium and vanadium. The experimental 3-D void distributions, in both size and space, will enable us to develop qualitatively new constitutive models of spallation fracture.

Metastability and δ-phase retention in plutonium alloys

A. J. Schwartz, J. J. Haslam, W. G. Wolfer, M. A. Wall, C. R. Krenn

MAIN TOC

Understanding the nature and details of the nondiffusive (displacive) martensitic phase transformation is among the most challenging problems in physical metallurgy. To understand this phenomenon, one must simultaneously deal with thermodynamics and kinetics controlled by materials properties. The most extreme example of a martensitic phase transformation is found in δ-stabilized plutonium (Pu) alloys. Here, the δ-to-α′ phase transformation results in a volume change of approximately 20%; this means that stress and plastic accommodation play central roles in governing the details of the transformation. In these kinetically dominated phase transformations, composition, microstructure, stress, and the effects of nuclear-decay radiation all play important roles in controlling dimensional stability of materials in a variety of defense, energy, and transportation systems.

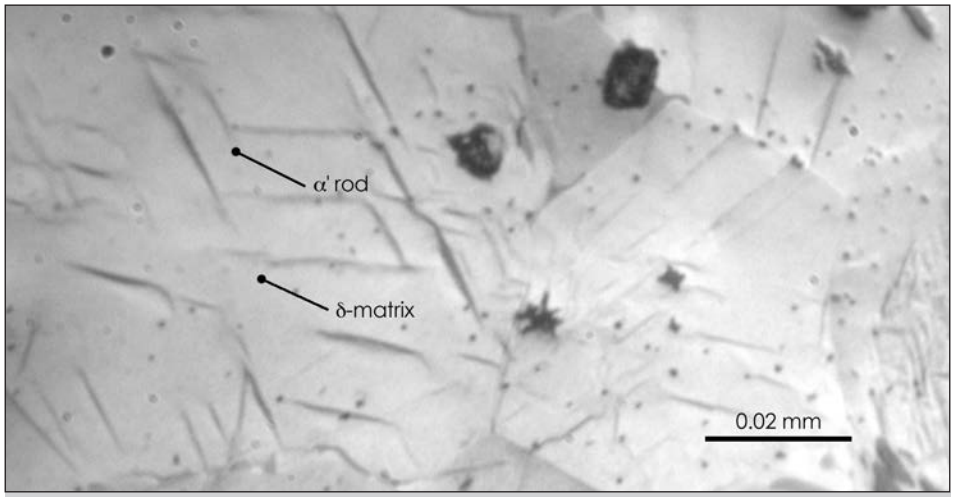

Optical micrograph of δ phase plutonium alloy cooled to –118°C to induce the δ-to-α′ phase transformation, showing α′ rods distributed along crystallographic directions within the δ matrix.

By engaging this basic scientific problem, we expect to make significant progress in developing the methodology for dealing with similar issues in other important technological areas including long-term storage of nuclear waste, fission and possible fusion reactor materials, and aging problems of interest to the stockpile stewardship program. An important result of this work will be a deeper understanding of the role of microstructure, solute content, and stress in the stabilization of the δ phase as well as the development of the scientific manpower base for future stockpile stewardship.

The goals of this research are to develop the physical framework needed to describe and predict the important features of the transformation, such as the martensite start temperature and the temperature width of the hysteresis, which corresponds to the reversion temperature to the δ phase. Our approach is based on historical experience with other metastable alloy systems undergoing martensitic transformations, but it recognizes the unique physics of the Pu alloy system. Our technical plan involves measurement of resistivity as a sensitive measure of α′-phase formation, microstructural characterization, and predictive modeling of the nucleation and kinetics of this displacive phase transformation.

In FY2001, we developed and tested experimental capabilities, cast reference alloys, and hired a full-time postdoctoral researcher and a term employee. We redesigned the resistivity specimen holder used for isochronal annealing in a previous LDRD project to accept 2.8-mm-diam specimens and performed finite-element method simulations of the effect of the specimen geometry on the resistivity measurements. To evaluate the resistivity system, we performed temperature cycles on aluminum. With our first reference alloy, we cooled low-solute alloys below the martensite start temperature and characterized the volume fraction and morphology with optical microscopy, as shown in the Figure. To characterize the interfaces and orientations of the δ and α′ phases, we used transmission electron microscopy (TEM) on the as-received reference alloy and on the sample cooled to induce the transformation. Our modeling efforts focused on coupling thermodynamics and mechanical properties to predict the width of the hysteresis loop and to better understand the mechanism of the transformation.

In FY2002, we will focus on the complete microstructural characterization by TEM and optical microscopy of the three reference alloys before any temperature cycling. We will use extensive thermal cycling to determine the phase transformation hysteresis loops, which will provide an indication of the mechanisms of the transformation. This will help elucidate the relevant parameters that affect the transformation. We will further model the width of the hysteresis loop by coupling thermodynamic and mechanical properties.

Thermodynamics and structure of plutonium alloys

P. G. Allen, P. E. A. Turchi, T. H. Shen, G. F. Gallegos

The underlying role of iron (Fe) impurities and gallium (Ga) atoms in Ga-stabilized δ-plutonium (Pu) is poorly understood. These elements may segregate either at grain boundaries or within the grains, where they may induce secondary phase formation in the nominal face-centered cubic (fcc) structure. The formation of undesirable phases, precipitates, and microstructural ordering can change mechanical behavior and influence long-term stability—with implications for any existing or future Pu–Ga materials. Thus, there is a need to understand and verify the thermodynamic behavior of Pu alloys through theoretical modeling and experimental techniques.

This work supports the NNSA missions in nuclear science (i.e., actinide metallurgy). The project will yield valuable information concerning the role of dopant atoms on the thermodynamics, secondary phase formation, and local structural effects in Pu alloys. The long-term benefit is development of state-of-the-art experimental and theoretical tools for studying nuclear materials. This research will form the basis for future predictive work needed to assess the impact of impurities in Pu–Ga alloys on their mechanical behavior and forms a scientific foundation for other areas of the Stockpile Stewardship Program, including metal dynamics and aging.

Our experimental approach includes (1) synthesizing alloys by melting and deposition techniques, (2) studying crystallographic structure using transmission electron microscopy (TEM) and x-ray absorption fine structure (XAFS) spectroscopy, and (3) characterizing thermochemistry of the samples using differential scanning calorimetry (DSC). Our experimental results will confirm or clarify regions on the phase diagrams and will provide suitable references. Our theoretical approach includes simulating alloy formation and thermodynamics by coupling information on alloy energetics (experimental and assessed thermochemical data) to the well-known calculation of phase diagrams (CALPHAD) approach.

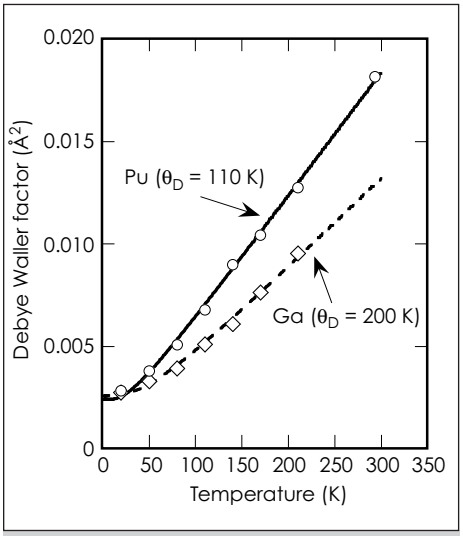

Bond displacements vs temperature obtained by x-ray absorption fine structure (XAFS) spectroscopy. The data are modeled to determine independent Debye-Waller temperatures (θ_D —a measure of bond stiffness) for Pu and Ga sites.

During FY2001, we used data obtained from the literature to develop thermodynamic models for Pu–Ga and Pu–Fe binary alloys over a wide composition range. The concentration and temperature dependence of the thermodynamic functions allowed us to reconstruct the phase diagrams. For Pu–Ga, the low-temperature models in the Pu-rich region predicted behavior similar to that suggested by a more recent Russian phase diagram. We initiated procedures for sample synthesis by laser melting and sputtering, and bought a new DSC workstation for online Pu thermochemistry. Information on the heats of formation of fully characterized samples of Pu_3Ga, Pu_6Fe, and others will allow us to validate the current theoretical assessments.

We also developed and tested XAFS instrumentation for variable temperature measurements (10 to 300 K) on Pu. The first Pu and Ga spectra for a test specimen were recorded in May 2001 at the Stanford Synchrotron Radiation Laboratory. Since XAFS measures local bonding, we can vary temperature and determine the motion for the Pu and Ga sites independently (see Figure). Our results reveal that the Ga sites experience stiffer local bonding relative to the Pu sites. This could have important implications for lattice-stabilization mechanisms in Pu and Ga alloys.

In FY2002, we will focus on (1) synthesizing Pu_3Ga and Pu_6Fe model compounds for model validation, and (2) performing full metallographic analysis using microprobe and scanning electron microscope techniques (in preparation for DSC). We will also test new synthetic methods to prepare uniform thin-film samples for analysis by TEM and XAFS. Our theoretical efforts will focus on completing assessments of Pu–Ga, Pu–Fe, and Ga–Fe phase diagrams and on beginning work on the ternary system, Pu–Ga–Fe.

Deformation-DIA: A novel apparatus for measuring the strength of materials at high strain to pressures of 15 gigapascals at elevated temperature

W. B. Durham, K. Bennett, I. Getting, D. Weidner, Y. Wang

MAIN TOC

The goal of this project is to develop a new experimental capability for validating models for material strength as an function of temperature, pressure, and plastic strain. The Deformation-DIA (D-DIA) is a new instrument designed to measure the strength of materials at confining pressures as high as 15 GPa under conditions that have been heretofore unobtainable in the laboratory. The problem of determining material properties at extreme conditions is of central importance to the Stockpile Stewardship Program.

The project combines state-of-the-art experimental techniques (e.g., laser shock, diamond anvil cell) with computationally intensive physics-based models. The D-DIA will allow us to characterize the rheology— the relationship between applied stress and rate of plastic deformation—of solid materials, while maintaining independent control of temperature, pressure, magnitude of deformation (i.e., strain), and rate of deformation. The D-DIA adds to our arsenal of new research tools, raising the pressure capability on high-precision rheological measurements by a factor of 5.

The D-DIA is a solid-medium press that applies a mechanical load to a 1-mm^3 single- or polycrystalline sample (see Figure). The key feature of the D-DIA is the coupled inward motion of deformation anvils, which move against the sample, and the outward motion of side anvils, which constrain the soft-pressure medium to keep the pressure constant. The measurements require state-of the-art, x-ray and neutron sources, which are available at DOE facilities at Argonne, Brookhaven, and Los Alamos National Laboratories. The x-ray and neutron beams are sufficiently bright to allow direct imaging of the sample to measure strain and to carry out diffraction, and to measure elastic distortions (hence pressure and stress) and crystalline texture.

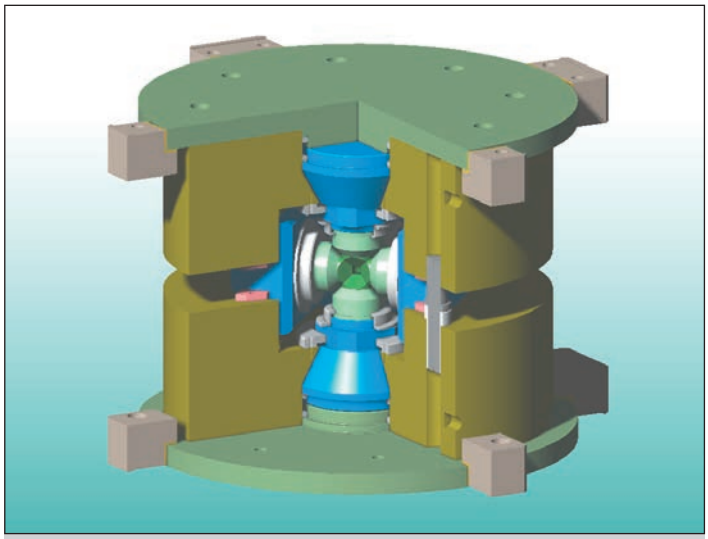

Cut-away view of the Deformation-DIA. The cubic volume defined by the tungsten carbide anvils (light green) at the center contains the sample assembly.

The project began in mid-FY2001 with the goal of taking the D-DIA from a concept to a working instrument to demonstrate its capabilities. Specialty steels and very close machining tolerances are required due to the very high stresses the machine generates at its nexus. During this first year, we took the rough plans for the D-DIA to final engineering drawings, went through the bidding process, located vendors willing and able to do the work, and had all parts of the D-DIA system delivered by the end of FY2001.

In FY2002 we will assemble and begin calibrating the D-DIA. The focus of the research will be to experimentally validate parameters used in models for material strength, such as the Steinberg–Guinan–Lund model. We will deform single-and polycrystalline samples of molybdenum and tantalum to strains approaching 1 at pressures to 15 GPa and temperatures to 1700 K. The first exercises are scheduled on the x-ray beamline at the National Synchrotron Light Source (Brookhaven National Laboratory) in late fall or early winter. We hope to produce the first measurements of the rheology at high pressure by the end of FY2002.

Designer diamond anvils for novel high-pressure experiments: Magnetic susceptibility experiments on actinides to multimegabar pressures

S. T. Weir, D. Jackson, C. Ruddle, V. Malba, J. Akella

MAIN TOC

Magnetism and magnetic order are manifested in a wide variety of materials. In materials exhibiting magnetic order, the order may assume one of a number of different forms—such as ferromagnetic ordering, antiferromagnetic ordering, and spin-density wave states. This rich variety of possible magnetic orders reflects the competing and often subtle electron–electron interactions at play in many materials. However, despite the widespread technological use of magnetic materials today, our understanding of the basic physics of magnetism and magnetic order is very far from complete, primarily because of the theoretical complexities associated with the electron–electron interactions in condensed matter.

Developing a better understanding of these electron–electron interactions is important for developing better models of magnetic materials and better models of materials (e.g., the actinide elements) that exhibit strong electron correlation effects. Information gathered by our ultrahigh-pressure magnetic-susceptibility experiments provides a strong foundation for developing better actinide equations-of-state (EOSs) and high-pressure phases of these materials, which are of critical importance to the Stockpile Stewardship Program.

To perform high-sensitivity magnetic experiments to ultrahigh static pressures, we are making use of a new high-pressure technology—designer diamond anvil technology—that was developed at LLNL. Designer anvils are specially fabricated diamond anvils with diamond-encapsulated, thin-film metal microcircuits. Our fabrication tools include 3-D optical lithography, metal sputter deposition, and epitaxial diamond chemical vapor deposition (CVD). For this project, we are fabricating designer anvils with multiple-turn microloops on the 300-μm-diam tip of the anvil. The Figure inset shows a designer anvil with a 10-turn microloop and a linewidth of 5 μm. Because of the close proximity of this magnetic sensing loop to the high-pressure sample (just a few micrometers), we can achieve extremely high signal sensitivities with very low background levels.

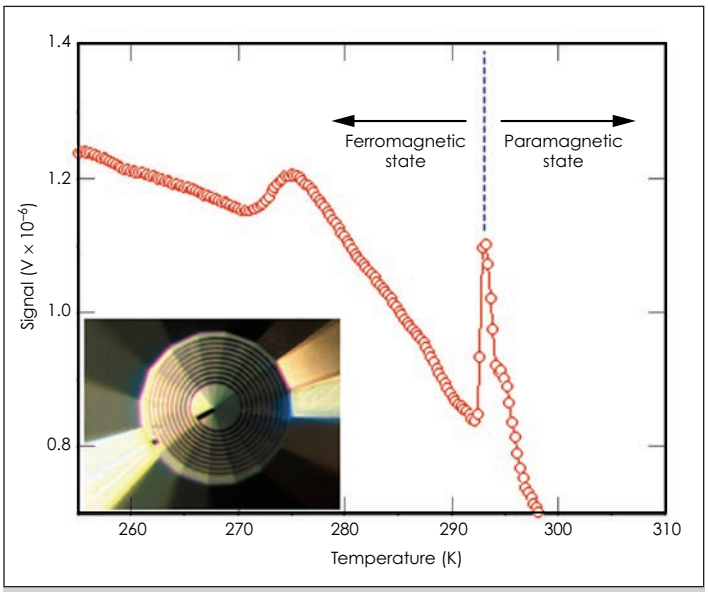

Signal voltage vs temperature of a gadolinium sample at zero pressure detected with a multiloop anvil (inset).

During FY2001, our focus has been on fabricating the first set of these new multiloop designer anvils, testing their performance and fine-tuning our electronics, and building up the needed experimental infrastructure (e.g., low-temperature cryostats and nonmagnetic diamond cells) to support these challenging experiments. The multiloop anvils perform as expected. The Figure shows a plot of the output voltage from a multiloop anvil that is examining a tiny sample of gadolinium (Gd) about 75 μm in diameter. The signal peak associated with the ferromagnetic-to-paramagnetic transition of the sample is clearly observable at 293 K, demonstrating the high sensitivity of the technique.

With the successful testing of the multiloop anvils and the completion of experimental infrastructure preparations, we are ready to embark on our FY2002 goal of performing ultrahigh-pressure magnetic susceptibility experiments on several lanthanide f-electron elements, including Gd and samarium. Gadolinium, for example, is of considerable interest because it undergoes a pressure-induced structural phase transition at 61 GPa in which the volume suddenly collapses by 10%, which is likely caused by the delocalization of the f-electrons. If so, we hope to confirm this by detecting the magnetic signature that should accompany the electronic delocalization. With successful detection, we will be ready to turn our attention to the actinide elements, including uranium and plutonium, in order to characterize their magnetic behaviors over a wide range of pressures and temperatures.

Direct and optically polarized nuclear magnetic-resonance methods for characterization and engineering of mesophased molecular structures

R. Maxwell, T. Baumann, B. Taylor

MAIN TOC

Nanoscale mesophase composite systems are organic/inorganic materials whose structural and motional properties span the definition of liquids and solids. Such materials are of broad programmatic and scientific interest. Often, they are heterogeneous, ill-defined, macromolecular structures with chemical and physical properties that may depend on nanoscale structural domains within the bulk material. Since mesophased materials and precursors generally lack long-range order, they are difficult to characterize beyond local, short-range structure. Nuclear magnetic resonance (NMR) shows great promise for characterizing intermediate- to long-range structure because NMR observables are sensitive to wide ranges of length and time scales.

This project is developing NMR methods for characterizing structure and dynamics in mesophase, nanoscale, composite systems. We will (1) develop NMR methods to measure short-, intermediate-, and long-range structure in a series of mesophase systems; and (2) construct correlations between NMR observables and molecular size, topology, and network structure. Both direct and optically polarized NMR will be applied. The resulting experimental protocols will provide LLNL with a unique capability to characterize this class of complex and important materials. Such in-depth characterization will allow us to understand relationships between synthetic variables, structure, and physical and chemical properties—an understanding that is necessary for the molecular manipulation of material microstructures.

This project exploits LLNL expertise in the synthesis of nanoscale materials, multiscale computational simulations and NMR spectroscopy of disordered materials to develop a strong LLNL capability in characterizing mesophased materials. The methods developed in the course of this study will find practical application to soft materials research in stockpile stewardship and in the biosciences.

During FY2001, we completed preliminary hydrogen-1 (^{1}H) and carbon-13 (^{13}C) NMR measurements of short-range order in (1) organic aerogels with varying porosity and density,

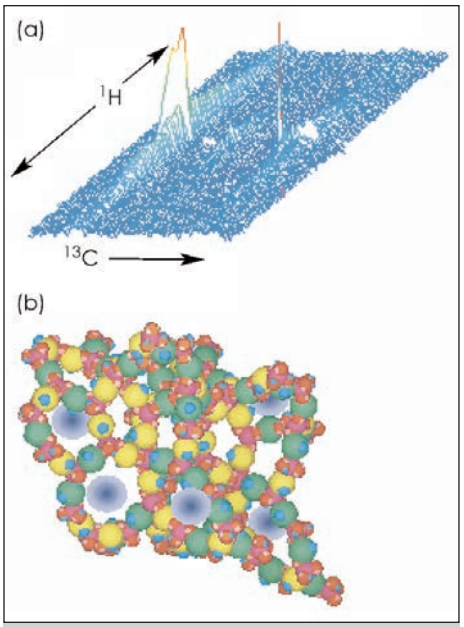

Results of diffusion-edited ^{1}H–^{13}C correlation NMR of (a) an organic aerogel showing (b) the effects of mobile, nanoscale inclusions in the network structure.

and (2) in surface-modified quantum dot surfaces functionalized with organic tethers. The Figure shows results of NMR measurements on an uncalcined organic aerogel material. The experiment was designed to correlate local structure (^{13}C dimension) with motional lifetimes (^{1}H dimension). The results of the experiment have allowed us to generate an estimate of the size of nanoscale inclusions of mobile species within the network structure [Fig. (b)]. We also (1) conducted dipolar-recoupling experiments and double-quantum experiments on a model system to assess intermediate-range structure, (2) began thermally polarized xenon-129/131 ($^{129/131}$Xe) baseline measurements of the organic aerogel's pore structure, (3) made initial diffusion measurement on both organic aerogels and functionalized nanoscale dots, and (4) obtained equipment for optically polarizing $^{129/131}$Xe gas.

At the end of FY2001, we were performing photoluminescence and optically detected NMR experiments on the quantum dots to gain a better understanding of the fundamental physics that will influence the coupling of the optical excitation and the silicon nuclear spins. Preliminary data suggest that efficient overlap of optical excitation with the adsorption spectrum of the quantum dots may result in a measurable nuclear polarization.

For FY2002, we propose to develop experimental protocols that correlate NMR observables with structure and dynamic properties on two baseline mesophased systems: organically functionalized nanoparticles and organic sol-gel-derived nanostructured materials. We will (1) measure short-, intermediate-, and long-range structure in these model systems by applying both solid-state and solution-state NMR methods; (2) measure speciation and the proximities and orientations of those species to each other; and then (3) use these data to construct models of molecular structure. Finally, we will investigate methods for enhancing the sensitivity and selectivity of optically polarized NMR. We expect that our work will lead to important developments in the ability of NMR to characterize disordered, large-molecular-weight, mesophased macromolecules.

Probing interactions in complex molecular systems through ordered assembly

J. J. De Yoreo, M. C. Bartelt

Emerging from the machinery of epitaxial science and chemical synthesis is a growing interest in self-organizing systems of complex molecular species. Self-organization in these systems spans the continuum from simple crystallization of macromolecules to assembly into organized networks of nanometer-scale structures such as quantum dots. The increasing activity in this area is testament to the success of the physical sciences in building a detailed understanding of crystallization and epitaxy rooted in thermodynamics and kinetics for simple atomic systems. A fundamental challenge of materials science in the coming decades will be to develop a similarly well founded understanding of assembly processes in these complex systems.

This project utilizes our unique capability to use in situ atomic force microscopy (AFM) for investigation of crystal growth, developed for research in support of LLNL's Laser Program and DOE's Office of Basic Energy Science. Crystallization of small molecules into crystals underlies the technology of KDP crystal growth, which is critical to advanced laser systems for inertial confinement fusion studies. The way in which biomolecules affect those controls is central to understanding the history of CO_2 sequestration in carbonate sediments as well as circumstances related to the origins of life. Extension of that understanding to complex molecular systems will affect our ability to perform high-throughput protein crystallization for proteomics and to develop the next generation of photonic solids based on assembly of engineered nanostructures.

In this project, we are combining AFM with molecular modeling to understand controls on self-organization in colloidal and dendrimer systems. We will learn how to extend models of epitaxy in small molecule systems to ordered assembly of supermolecular species and how systematic variations in the structure and bonding of the building blocks affect the kinetics and surface energetics that control the assembly process. Topographic AFM imaging provides experimental data on morphology and kinetics, while kinetic Monte Carlo (KMC) simulations predict morphology and kinetics. The potentials for the KMC simulations, provided by Poisson–Boltzmann calculations, are checked by measuring the force curve directly using chemically modified tips.

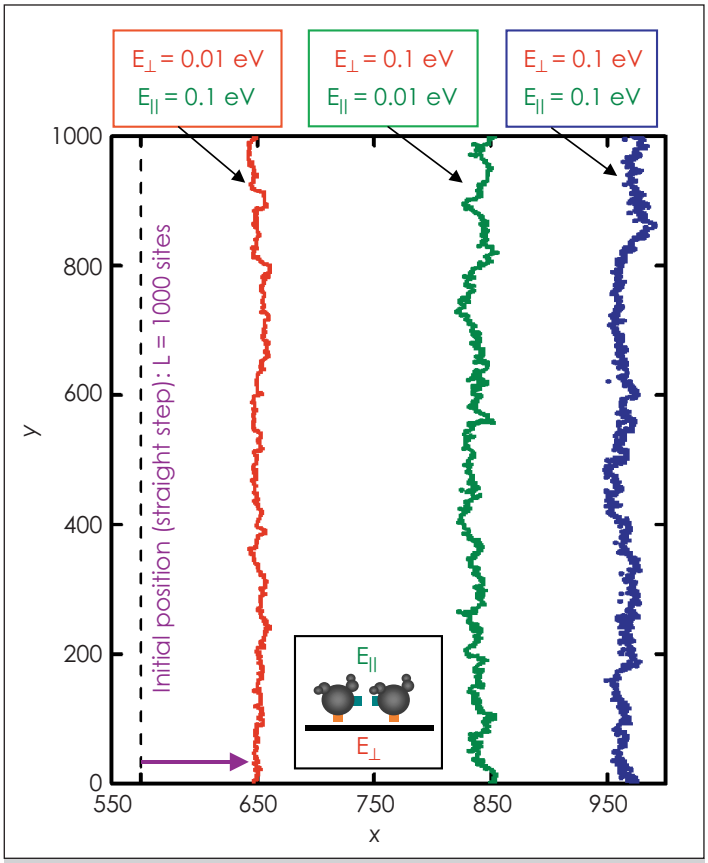

Result of kinetic Monte Carlo simulation indicating the dependence of step roughness and propagation speed on bond strengths $E_{||}$ and $E_\perp$, parallel and perpendicular, respectively, to an initial step (dotted line at left); the three jagged lines show the position of the step, at equal times, for the various bond strengths shown. Units of position x and y are number of lattice sites.

In FY2001, our activities focused on three areas. We used KMC methods to explore the role of anisotropy and intermolecular bond strength on step morphology and kinetics. The Figure shows an example for three combinations of bond strengths parallel and perpendicular to step. The higher the bond strength, the smoother the step and the slower the step motion. Bond anisotropy plays an important role, however: high bond strength along the step creates smoother, slower steps.

Our calculations also showed that when the bond strengths are much higher than the thermal energy *kT*, roughening at the step edges leads to nonlinear dependences of step speed on solute concentration. For numerous crystal systems, these results agreed qualitatively with AFM measurements on simple molecular systems.

We then analyzed terrace width distributions and measurements of step fluctuations to extract the basic physics of mass transport at step edges. Finally, we used the AFM to make chemical patterns as templates for initiating an ordered assembly of colloids. The goal is to use these assemblies of colloids as ideal systems for testing molecular scale calculations of interactions and growth dynamics.

Ligand design by combinatorial chemistry

D. Cary

Combinatorial chemistry or "parallel synthesis" allows large numbers of compounds to be synthesized concurrently and therefore quickly. The design and realization of multivalent ligands, which have the potential to act as synthetic antibodies able to sense or seek out specific targets, is the initial focus of this research project. This project involves more than the synthesis of the multivalent ligands, however. The design of the ligands for a specific target, usually a protein, involves the careful selection of two specific binding sites on the protein, followed by the identification of small molecules that bind to these sites. These molecules are identified through the uses of computational techniques followed by mass spectroscopy (MS). Synthetic chemistry is used to link the two small molecules together to realize a bivalent ligand, which can then be screened against the target protein to determine affinity and specificity using MS and nuclear magnetic spectroscopy (NMR).

The initial target of interest is botulinum toxin, a potential biowarfare agent. Work under this project could lead to the development of a practical sensor for the detection of this toxin. The structure of the botulinum toxin protein, determined by x-ray crystallography, is well documented in the literature and small molecules that bind to pockets on the surface of this protein have been identified at LLNL.

In FY2001 exploratory chemical reactions to establish synthetic procedures for the preparation of the multivalent ligands have been carried out. With the two semiautomatic synthesizers that have been installed (see Figure) up to 40 reactions can be run in parallel.

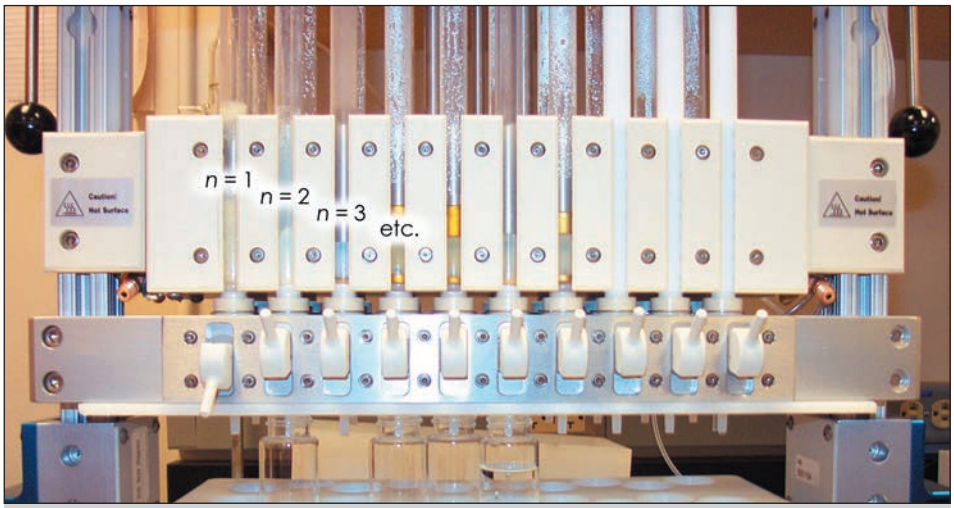

Ten reaction vessels on each side of a parallel synthesizer allow ten reactions (n = 1, 2, 3, etc.) to be carried out in parallel, increasing the productivity of the process.

The key to the rapid synthesis of compounds using the combinatorial approach is the use of so-called solid support chemistry, common in fully automated peptide synthesis, to support the synthesis product as the chemistry takes place. This technology allows the use of excess reagents to drive reactions to completion and facilitates the purification of the intermediate synthesis products.

The section of the ligand that links the small molecules together should have several important properties. It must be biologically inert, so that it does not interfere with specific binding of the small molecules; water soluble; and the length, shape, and rigidity of the linker section must be optimized for a specific target so that optimum binding of the ligand can be achieved.

The simplest way to meet these criteria is to synthesize many ligands (of differing length, rigidity, etc.) and experimentally determine their properties and affinity and specificity for the target protein to find the "best fit." The initial linkers will consist of a polyethylene/polyamide chain, and it is the synthesis of this type of molecule that is under investigation.

In FY2002, after identifiying the ideal procedures a set of ligands of varying length will be synthesized. These ligands will be screened against the target protein to determine their affinity and specificity. The results of these experiments will guide the direction of attempts to improve the specificity by changing the length, rigidity, and shape of the ligand.

Warm dense matter with energetic materials

J. D. Molitoris, W. M. Howard, R. W. Lee, J. W. Forbes, L. E. Fried and M. W. McElfresh

MAIN TOC

Understanding the properties of materials at high density and pressure is important to LLNL's stockpile stewardship mission. One of the least understood areas of density–temperature phase space is the region between solids and plasmas. Here, plasmas become strongly coupled and perturbation approaches fail as no small expansion parameters exist. This is the warm dense matter (WDM) regime, where standard theories of condensed matter physics and/or plasma statistical physics are invalid. Very little experimental data is available on this regime.

The objective of this research is to use energetic nanocomposite materials and new experimental techniques to produce the pressure and temperature conditions necessary to create a transition from molecular fluid to dense, low-temperature plasma. As any material being shock compressed from a normal solid to a plasma must transition through the WDM regime, this research provides new information about the physics and chemistry of detonations involving metal-bearing materials and probes the properties of matter under extreme conditions, which is relevant to LLNL's stockpile stewardship mission.

This project began as a Feasibility Study (01-FS-001) in which nearly planar shock waves generated from the detonation of an ideal high-explosive, LX-10, were used to compress tritonal, a typical metal-bearing energetic material composed of 20% aluminum. The tritonal was buffered on each side by a layer of Teflon. High-pressure shocks (on the order of a few hundred kilobars) initially created a hot (~7000 K) dense, plasma-like region followed by expansion, mixing, and combustion. The exciting results of the Feasibility Study merited a more in-depth investigation of WDM and led to this project, which focuses on shock compression of nanostructured materials.

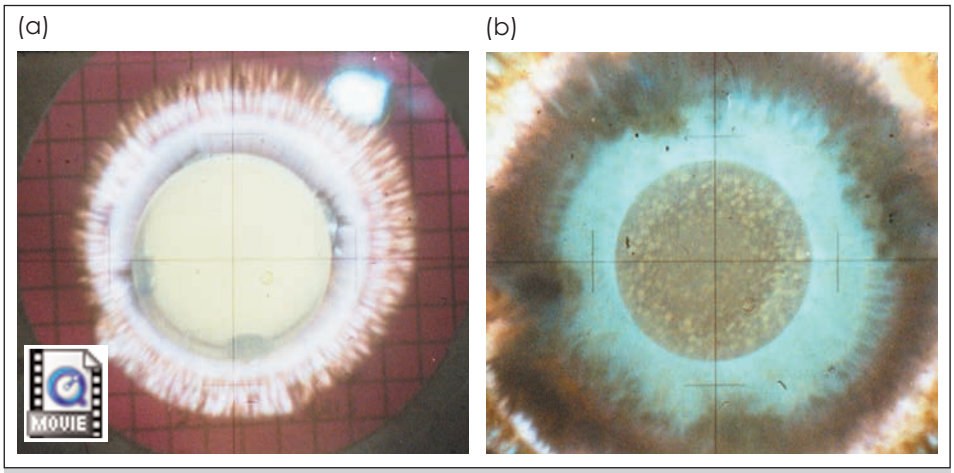

(a) The hot emission region, and (b) instability structure revealed after cooling in a shocked 130-mg/cm^3 silica aerogel. The image-exposure time is 0.42 ms in each frame.

In FY2001, we successfully developed a novel high-explosive technique to shock SiO_2 aerogel to densities and temperatures well within the WDM regime. The results of our experiments, conducted at LLNL's High Explosives Applications Facility, revealed the behavior and structure of transmitted shocks in aerogel and in the explosive driver. For example, Fig.(a) data show strong compression and emission as the shock is transmitted to the aerogel and establishes itself within the material. These data on shocks in aerogel represent a milestone in our fundamental understanding of the properties of matter under extreme conditions.

Temperatures approaching 1 eV were correlated with a dense, highly luminant region created after the shock was established in the aerogel. This accomplishment required diagnostic development in radiography and fast optical-radiance imaging. Radiography was critical in understanding the nature of the transmitted shock and in validating hydrodynamical aspects for comparison with the model. Fast imaging of the shock front revealed a steady reduction in emission (a cooling effect) which we know from the radiography correlates to dispersion of shock front. This is a somewhat surprising result, but the observation of structures within the shock front is even more surprising. The observed 0.5-mm structures, shown in Fig.(b), appear to be the result of Richtmyer-Meshkov instabilities. We used the ARES/CHEETAH thermochemical code to understand and interpret the data.

In FY2002, we will determine the extreme upper and lower density and temperature limits by using aerogels with initial densities well below 100 mg/cm^3 and well above 300 mg/cm^3. The desired result is to create densities approaching 5 mg/ cm^3 and temperatures approaching 2 eV. Our objective for FY2002 is to obtain a final set of data with the radiance imager and ascertain if the temperature can be pushed high enough to measure it with plasma spectroscopy.

Enhancement of strength and ductility in bulk nanocrystalline metals

T. G. Nieh, W. E. King, M. J. Caturla, C. A. Schuh

Nanocrystalline copper (Cu) is known to exhibit good mechanical characteristics at high strain rates. Thus, nanocrystalline materials are potential materials for shaped-charge liners and explosively formed penetrators.

Understanding and predicting the properties of nanocrystalline materials are important to the Stockpile Stewardship Program. LLNL's long tradition in electrodeposition technology, plus the availability of large-scale supercomputers, place LLNL in a unique position for conducting work on nanomechanics.

Our goal in this project is to develop a robust scientific and technological framework for designing nanocrystalline materials with high strength, ductility, and toughness. We are coupling experiments and simulations, with emphasis on materials of macroscopic dimensions (millimeter to centimeter scale) that are composed of nanoscale (<100 nm) grains.

During FY2001, we used x-ray diffractometry to finish the characterization of the crystallinity and grain size of nanocrystalline nickel (Ni) produced by electrodeposition techniques. Additional microstructural information—including grain size, shape, distribution, misorientation angle, and impurity—is expected from our future transmission electron microscopy (TEM) observations.

To evaluate the mechanical properties of nanocrystalline Ni, we used both instrumented nanoindentation and nanoscratch techniques to measure the material hardness, elastic modulus, and abrasive-wear resistance. Our data [Fig. (a)] indicate that as grain size of nanocrystalline Ni decreases, there is a characteristic large increase in hardness. However, at the smallest grain sizes (below about 20 nm), a reduction in grain size leads to a measurable decrease in hardness. This inverse Hall–Petch strengthening is of central interest,

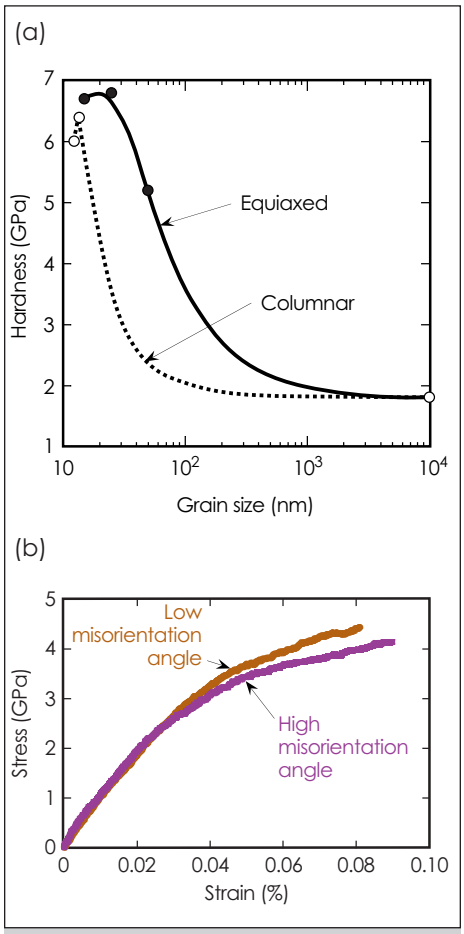

Characteristics of nanocrystalline nickel (Ni), showing (a) hardness of two forms of Ni as a function of grain size, and (b) simulated stress–strain curves at low- and high-misorientation angles in 24-grain Ni with 4-nm grain size.

because it defines a new regime of material behavior at the nanoscale.

Three main components are required to simulate the deformation of nanocrystalline materials at the atomic level: (1) initial conditions (i.e., grain size distribution and orientation), (2) interatomic potentials, and (3) boundary conditions (for either creep or tensile tests). Our experiments during FY2001 show that the grain distribution in nanocrystalline Ni follows a log-normal distribution. However, our simulation results show that grain distribution is close to Gaussian. Further, improvements are needed to achieve profiles closer to the experiments.

During FY2001, we also performed simulations with low- and high-angle grain boundaries to understand the effect of misorientation angle on deformation. Preliminary results [Fig. (b)] from Ni with a 4-nm grain size showed that the yield strength of a material consisting of low-angle grain boundaries is stronger than that for high-angle grain boundaries, suggesting dislocation does not play a significant role.

In FY2002, we will further explore the breakdown in Hall–Petch strengthening in nanocrystalline Ni and Cu, both prepared by pulsed-electrodeposition. We will also examine the effect of grain size upon the poorly understood tensile ductility of nanocrystalline materials.

The results of molecular-dynamics simulations depend upon the interatomic potentials used in the calculations. The role of impurities at grain boundaries on the deformation mechanisms is an important issue, especially for nanocrystalline materials. To understand this effect, we have obtained interatomic potentials for mixed systems such as iron in Ni or carbon in Ni. In FY2002, we will simulate the effect of impurity on grain-boundary sliding.

Dip-pen nanolithography for controlled protein deposition

J. J. De Yoreo, B. L. Weeks, A. Noy, A. Miller

MAIN TOC

The ability to deterministically organize molecules, nanometer-sized particles, cells, and spores is a major goal of nanoscience and technology, and that ability will have significant impacts on materials science, synthetic chemistry, biology, and medicine. For example, the deposition of proteins onto specific sites or into ordered arrays would facilitate detection and crystallization. The latter is a necessary step in structure determination and a daunting task for proteomics, which aims to elucidate the structure and function of the proteins expressed by the genome.

Unfortunately, despite their importance, there are essentially no practical, generic methods for controlling the organization of molecules and particles at surfaces. The purpose of this project is to use capabilities in atomic force microscopy (AFM) developed for LLNL's Laser Program and DOE's Office of Basic Energy Science to control the deposition of nanoparticles and macromolecules. The main result of this effort will be a new technology for protein trapping, detection, and assembly that will assist LLNL's work in biological nonproliferation and proteomics.

Detection of biological agents and investigation of protein–protein interactions will be advanced through the ability to fabricate ultrasmall, highly selective protein chips. Creation of ordered layers of proteins will eliminate the obstacle to protein structure determination presented by the need to crystallize proteins. The creation of colloid and quantum-dot arrays will enhance LLNL's ability to investigate the fundamental physics of particle interactions at the nanometer scale.

In this project, we are using dip-pen nanolithography (DPN) to create chemical patterns on gold and SiO_2 surfaces with feature sizes of 10 to 100 nm (Fig. (a)). In this technique, the atomic force microscope is used like a fountain pen. The tip is "dipped" into the desired chemical compound (the "ink"), and the pattern is produced by moving the tip across the surface in a predetermined trajectory. The ink diffuses from the tip to the surface through a naturally occurring meniscus of water.

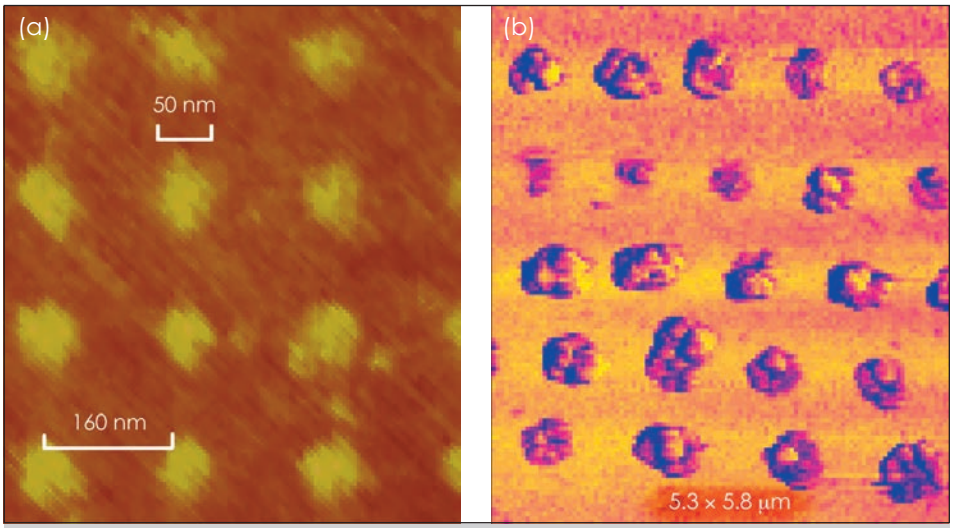

(a) Array of dots made by dip-pen nanolithography; (b) colloid clusters bound to dots like those in (a).

While a few groups are using DPN to pattern surfaces, our effort is unique because it is focused on organizing macromolecules and colloids into close-packed arrays. A patent disclosure has been filed on the use of DPN patterns as templates for macromolecular crystallization. We are collaborating with researchers from the Department of Biochemistry at the University of California, Irvine, whose expertise is in traditional methods of crystallizing macromolecules.

To make templates for the deposition of molecular or particulate species, we choose an ink that selectively binds to that species. Figure (b) shows an example of 40-nm amine-terminated colloids bound to a pattern of COOH-terminated dots. Because the amine group makes a strong bond with the COOH group, the colloids bind only at the dots.

The eventual goal of this project is to pattern surfaces with inks that ensure selective binding of proteins into specific orientations. In FY2001 we established the basic capability to pattern alkane thiol molecules on gold substrates and created a variety of patterns, including grids of dots, lines, and letters. We also showed that this method could be used to make patterns of photoluminescent molecules and antibodies on SiO_2 surfaces. Finally, we determined the dependence of feature size on tip speed, dwell time, and humidity for alkane thiols on gold. The results are well described by a model in which dissolution of the alkane thiols into the meniscus is the rate-limiting step during pattern formation.

In FY2002 we will template protein deposition using patterns of antibodies and other chemoselective inks. Using the AFM as a force sensor, we will then measure the strength of the interaction between the proteins and the pattern. These results will serve as input into kinetic Monte Carlo models of protein assembly.

Femtosecond laser synthesis of multi-element nanocrystals

M. Balooch, L. N. Dinh

The novel properties of nanocrystals—such as the quantization of the electronic density of states, blue shift of the dielectric band gap with reduced crystal size, high surface-to-volume ratio, and agile mobility—are radically affecting both the basic sciences and industry. Understanding the science of synthesizing nanocrystals (or crystalline nanoclusters) and nanostructures (including amorphous nanoclusters and any nanometer-scale structure) with specific sizes and properties and producing them at an industrial rate will revolutionize nanotechnology. Short-pulsed laser ablation offers a convenient way to produce a variety of nanoclusters with specific properties. By its energetic nature and with pulse lengths shorter than those of electron–phonon coupling, femtosecond-laser synthesis offers a unique thermodynamic pathway to the production of stoichiometric, multi-element nanocrystals.

Our goals are to achieve (1) a complete scientific understanding of the physical and chemical processes involved in femtosecond-laser synthesis of nanocrystals, and (2) a predictive capability of nanocrystal properties based on our experimental findings. We are building on experimental capabilities developed at LLNL. Our results will enhance our understanding of laser–target interaction and contribute to LLNL's solid-oxide fuel-cell (SOFC) program.

In FY2001, we investigated the properties of gallium arsenide (GaAs) nanoclusters deposited by a femtosecond-pulsed laser. Nanoclusters of GaAs were produced by laser-ablating single-crystal GaAs targets in vacuum or in argon (Ar) gas [Fig. (a)]. Atomic force and transmission electron microscopies (AFM and TEM, respectively) showed that most of the clusters were spherical and ranged in diameter from 1 to 50 nm, with a peak size distribution between 5 and 9 nm, depending on the Ar gas pressure and the laser fluence [Fig. (b)]. X-ray diffraction (XRF), solid-state nuclear magnetic resonance (NMR), Auger electron spectroscopy, electron-energy-loss spectroscopy and high-resolution TEM revealed that these nanoclusters were composed of randomly oriented GaAs crystallites. As a result of transportation in air, a 2-nm-thick oxide outer shell developed subsequently on the surfaces of the nanocrystals. Unpassivated GaAs nanoclusters exhibited no detectable photoluminescence. After surface passivation, these nanoclusters displayed photoluminescence energies less than that of the bulk GaAs from which they were made [Fig. (c)]. Our photoluminescence experiments suggest that—even after surface passivation—an abundance of electronic energy states are associated with surface species in the forbidden band gaps of these nanocrystals. The properties of the GaAs nanocrystals formed through laser ablation are independent of the laser pulse length from 25 ps down to 150 fs.

We also successfully laser-ablated In-doped zinc oxide (ZnO) targets in varying oxygen pressures to make In-doped-ZnO nanocrystal films with the same stoichiometry as the target. This was confirmed by x-ray diffraction (XRD) and x-ray fluorescence analysis (XRFA). By varying the oxygen pressure, we were able to make oxygen-deficient or Zn-rich,indium (In)–doped, ZnO nanocluster films suitable for fuel-cell application.

In addition to modeling the nonorthogonal tight-binding potentials for silicon and GaAs, we have begun testing the bulk phonon density of states, dielectric functions, and band structures. Photodissociation simulations of small clusters by 20- to 750-fs laser pulses were successful and compare accurately with available experimental data.

Plans for FY2002 include producing and studying indium phosphide (InP) nanocrystals by varying laser pulse length, laser power, and background pressure. Our focus will be on the laser–target interaction from femtosecond to picosecond timescales and on the passivation of the nanocrystals. We will investigate the surface morphology of the target, parameters affecting material removal, and in situ gas-phase surface passivation of the nanocrystals. These data—when analyzed in conjunction with the physical and chemical properties of the nanocrystals produced—will help to benchmark our predictive modeling efforts.

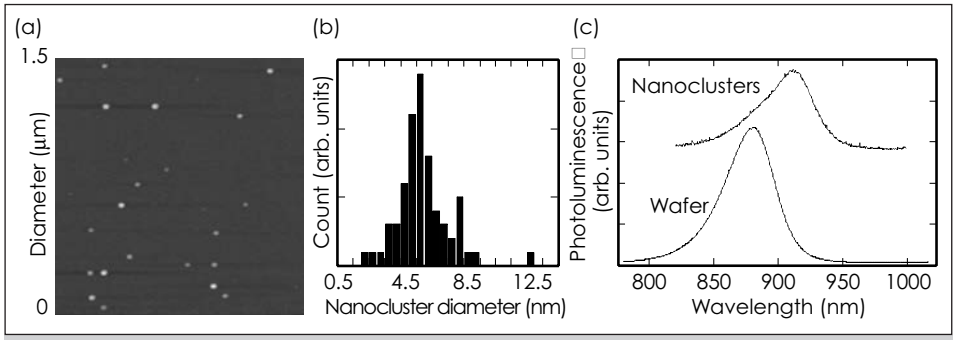

Gallium arsenide nanoclusters deposited by a femtosecond-pulsed laser ablation: (a) atomic force microscopy (AFM) image, (b) size distribution, and (c) photoluminescence properties.

High-accuracy tomography of mesoscale targets

W. Nederbragt, S. Lane, D. Schneberk, T. Barbee, J. Klingmann

MAIN TOC

High-energy-density experiments play an important role in corroborating the improved physics codes that underlie LLNL's Stockpile Stewardship mission. Conducting these experiments, whether on the National Ignition Facility or another national facility such as the Omega laser (University of Rochester) or the Z accelerator (Sandia National Laboratories), requires improving not only the diagnostics for accurate measurements, but also the fabrication and characterization of the target assemblies whose millimeter-size components typically have micrometer-size features. The precise characterization of the target assemblies with submicrometer accuracy is critical because the actual target assembly is the input to the experiment; the characterization of the as-built assembly is the input to the physics simulation. While sufficiently accurate measurements can be made with an enormous x-ray synchroton source, no laboratory-size technique exists for making the measurements we need to characterize target assemblies.

X-ray radiography/tomography is a technique that holds promise for characterizing the internal structure of target assemblies. Researchers have demonstrated submicrometer spatial resolution using a synchrotron x-ray source. However, this approach does not accommodate our requirements for a high-throughput and low-cost approach to characterizing production quantities of target assemblies.

This project is funding the development of a laboratory-scale Wolter x-ray microscope/tomoscope. Ideally, this instrument will be capable of producing 3-D tomographic images at 0.5-µm resolution, which we need to characterize target components. However, the resulting images are completely different from typical radiographic images. Evaluating and performing 3-D reconstruction of these images will require the development of new algorithms.

Work on the Wolter instrument began in April of FY2001 by determining the requirements for the instrument, including the x-ray energy needed to penetrate the targets. Based on these calculations, we will use 8-keV photons.

We also performed extensive tests on standard scintillator materials to determine the best material to use for our application. Since the scintillator adds to the blur captured by the charge-coupled device camera, it is essential to understand the properties of the available choices.

In FY2001, we simulated various aspects of the Wolter x-ray instrument using the IDL code. These simulations allow us to vary various parameters and find a suitable design that meets our goals. They also allow us to study the effects of the multilayer coatings that will be applied to our optics. These coatings increase the throughput of the instrument and limit the bandwidth of photon energies that are reflected. One problem with the limited bandwidth is that it reduces throughput of off-axis points. The simulations illustrate this effect (see Figure). By the end of FY2001, we had completed our preliminary simulations and had a preliminary optical design.

In FY2002, we will complete the optical design and the preliminary mechanical design, modify standard radiography codes so that this instrument can be used, and fabricate the optics—replicated multilayer Wolter imaging optics have never before been fabricated.

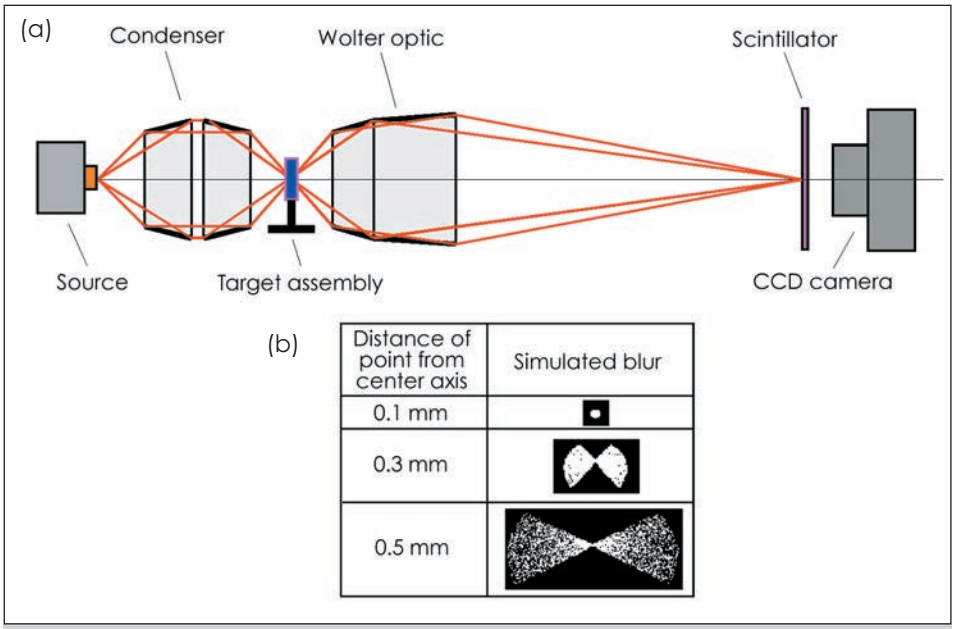

(a) Instrument layout, and (b) simulated blur characteristics of off-axis sample points projected through our x-ray microscope design. Simulation includes geometric and multilayer effects.

Probing the properties of cells and cell surfaces with the atomic force microscope

M. McElfresh, R. Balhorn, R. Rudd, J. Belak

MAIN TOC

Atomic force microscopy (AFM) has developed rapidly during the past decade, providing nanometer-scale resolution in the imaging of biological materials ranging in size from single molecules to intact cells, as well as other unique capabilities in the aqueous environment. By monitoring the cantilever deflection during approach–retraction cycles (i.e., force–volume curves), the unbinding forces have been determined for various ligand–receptor pairs. It is now possible to use a single receptor molecule bound to the tip of an AFM cantilever to map the locations of ligands bound on solid surfaces. This opens the door for new recognition-mapping methods. The goal of our project is to develop recognition mapping for living cells and cell membranes, a major step forward.

Our project contributes to LLNL's national security mission by creating a method for measuring the real-time response of individual living cells to a range of perturbations. The properties of living cells change in response to a wide variety of external stimuli, ranging from chemical and thermal changes in their environment to their response to infection or poisoning by bacteria and toxins, such as those manifested by bio- and chemical-warfare (BW/CW) agents. The technique we are developing provides a new, nondestructive means to detect resulting changes in the properties of the cell membrane at the nanoscale.

The current emphases of the project are on (1) an experimental technique to make recognition measurements on living cells, (2) a computational model to separate the local binding forces from gross cell deformations, and (3) a proof-of-principle application to a well-known cell system—a bovine sperm cell.

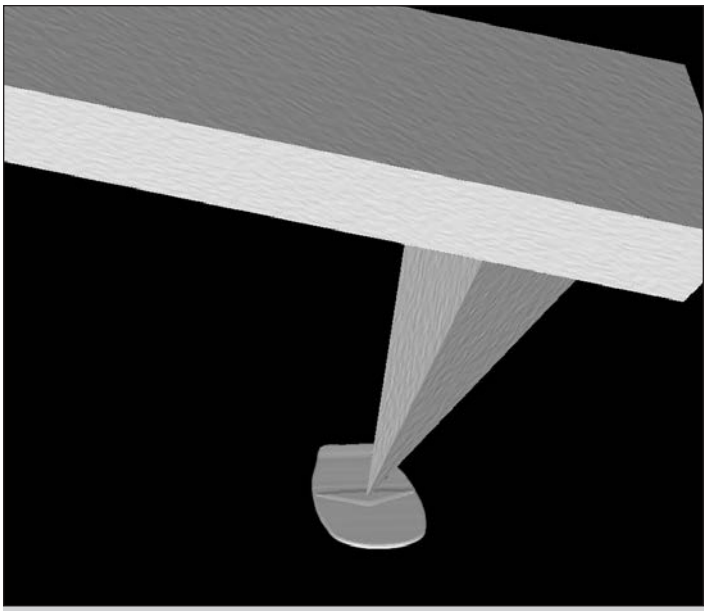

Indentation of a bull sperm cell by an atomic force microscope (AFM) tip, based on a 3-D finite-element model. The cell body is naturally flat, with dimensions of $10 \times 4 \times 0.5$ μm. The AFM tip is drawn to scale. The triangular acrosomal region is visible in the center of the cell, as is the raised posterior that couples to the tail (not shown). The deformation extends for about 1 mm from the AFM tip.

In FY2001, we produced significant results in three areas: (1) measuring the mechanical properties of cells using AFM, (2) building an analytical model to describe large deformations of the cell membrane, and (3) implementing numerical models of indentation.

For the first result, we obtained stunning topographic measurements of the shape of revitalized bull sperm cells, including hitherto unobtainable detail of the cell's equatorial segment, and made force-displacement measurements for all three segments.

For the second significant result, we developed a new analytical model for large deformations of cell membranes, and applied it to the bull sperm cell. This is a major step forward in the modeling of cell deformations, replacing the Hertz and linear-elastic models. Our model has been coded in smooth finite elements and applied to axisymmetric cell deformations.

Finally, we developed high-resolution, 3-D finite-element models of the cell that will be used to simulate more generic deformations (see Figure).

In FY2002, we will further parameterize our model by measuring the shape of a cell at the nanoscale while the cell is under load. We will also measure the changes in mechanical properties before and after the acrosomal reaction. Besides altering the number of membranes covering the acrosomal region, this reaction leads to expression of particular receptors that we will map using recognition microscopy.

Exhange coupling in magnetic nanoparticles to enhance magnetostrictive properties

H. B. Radousky, M. W. McElfresh, A. E. Berkowitz, G. P. Carman

The overall goal of this project was to investigate and improve the properties of magneto-elastomers—materials such as rubber, combined with magnetic materials—made with nanoparticles. In this feasibility study we demonstrated our ability to produce these particles using spark erosion, a versatile and economical method for producing particles of virtually any type of material that has a nominal conductivity. Particles can be prepared in sizes ranging from a few nanometers to tens of micrometers. Magneto-elastomers have applications to LLNL's national security missions that use magnetic sensors and magnetic actuators, and to vibration damping for automobiles, buildings and bridges.

The spark-erosion method uses a pulsed-power source to generate sparks between pieces of material that are immersed in a liquid or gaseous dielectric. Depending on the type of material being prepared, the dielectric liquid may be water, hydrocarbons, alcohols, or liquefied ammonia, nitrogen, or argon. The sparks, microplasmas that result from the breakdown of the dielectric liquid under high electric fields, cause transfer of the kinetic energy of the electrons and ions in the spark region, which creates localized superheated regions in the electrodes. When the spark collapses, molten droplets and vaporized material are ejected. In situ quenching of the droplets or condensed vapor is extremely rapid, as fast as 10^6 K/s, which facilitates the production of amorphous or nanocrystalline spherical particles. The average diameters of the particles can be controlled by selecting the duration and amplitude of the power pulses.

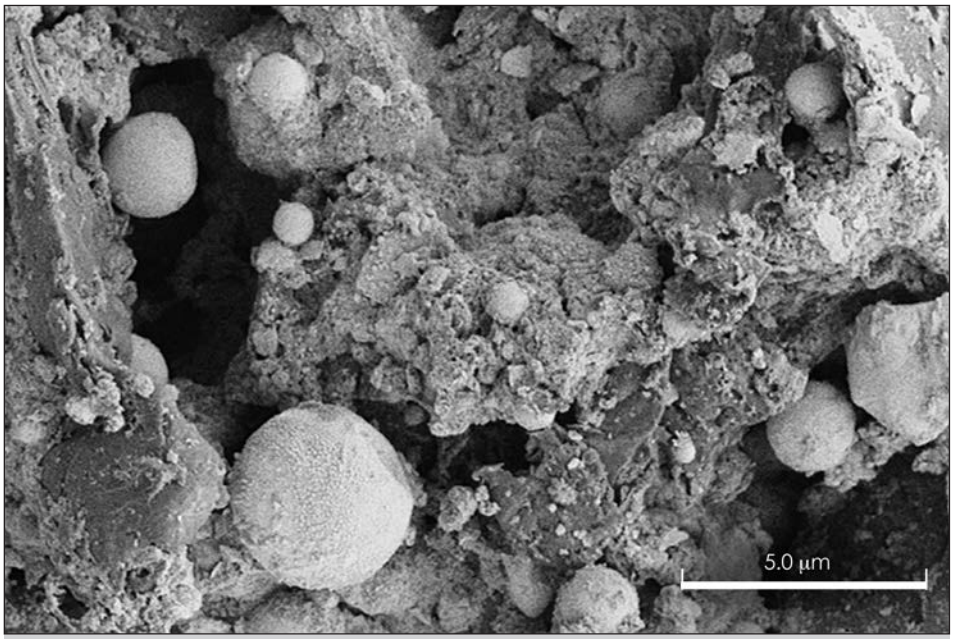

Scanning electron microscope image of (TbDy)Fe_2 (Terfenol-D) prepared by spark erosion. Note the formation of spherical particles, which are expected to produce improved mechanical properties when incorporated in elastomer composites.

We began with $Tb_{0.7}$ $Dy_{0.3}$ Fe_2 (known as Terfenol-D) because it is a giant magnetostrictive material. During this study we prepared spherical particles of Terfenol-D, as illustrated in the Figure, by the spark-erosion method. The shape of the particles is important because spherical particles hold the potential to make composites with much improved mechanical properties. We also demonstrated our capability to produce spherical nickel (Ni) particles as small as 10 nm. These Ni particles are suitable for incorporation into Ni–elastomer composites, which serve as a model system to study the effects of using spherical particles.

During this Feasibility Study, we also enhanced our basic understanding of the spark-erosion process, which will permit an optimization of this method for the controlled production of a wide range of materials in particulate form, with average sizes ranging from nanometers to tens of micrometers in diameter. In particular, we demonstrated that it is possible to dramatically reduce the size of the spark-erosion apparatus, while at the same time increasing the yield resulting from each run.

Based on the positive results from this Feasibility Study, we have an FY2002 LDRD project to produce spherical Ni and Terfenol-D particles ranging in size from a few micrometers to 10 nm, study their basic structural and magnetic properties, and produce/characterize mageto-elastomer composites incorporating these spherical particles.

Surface attachment of mechanically interlocking molecules

A. L. Vance, T. van Buuren

Recently, interest in mechanically interlocking molecules, known as catenanes and rotaxanes, has grown significantly—primarily because of their potential as building blocks of molecular-scale devices such as chemical sensors, microelectromechanical systems (MEMS), and molecular-scale machines. Catenanes consist of interlocking molecular rings, whereas rotaxanes are assembled by threading a linear molecule through a ring and capping both ends with "molecular stoppers" to prevent dethreading. Free (i.e., not surface-attached) molecules of this type are well documented, but the incorporation of mechanically interlocking molecules on surfaces is an area that remains virtually unexplored. Very few examples of surface-attached catenanes or rotaxanes have been reported in the literature.

We are working to develop new mechanically interlocking molecules for the formation of multifunctional and tunable self-assembled monolayers. Our long-term goal is the creation of sensors with properties that can be controlled at the molecular level (see schematic representation of a catenane in the Figure). These sensors will exploit three anticipated properties of surface-attached, mechanically interlocking molecules: (1) molecular recognition can occur within the pocket created by linking two molecular rings; (2) recognition elements can be placed on the exterior of the movable ring for tunable properties; and (3) terminal receptors can be combined with a molecular shuttle whose location on the surface-attached chain generates a unique signal. By using mechanical linkages in the monolayers, recognition can be switched on or off, thus allowing sensing to be controlled by changes in the configuration of the surface-attached species. With the flexibility of design inherent in these systems, detection can be carried out through a variety of methods such as electrochemistry or fluorescence.

This project expands efforts at LLNL to develop new types of self-assembled monolayers for improved detection and separation technologies and has the potential for making a significant impact on materials, nonproliferation, and environmental programs at LLNL.

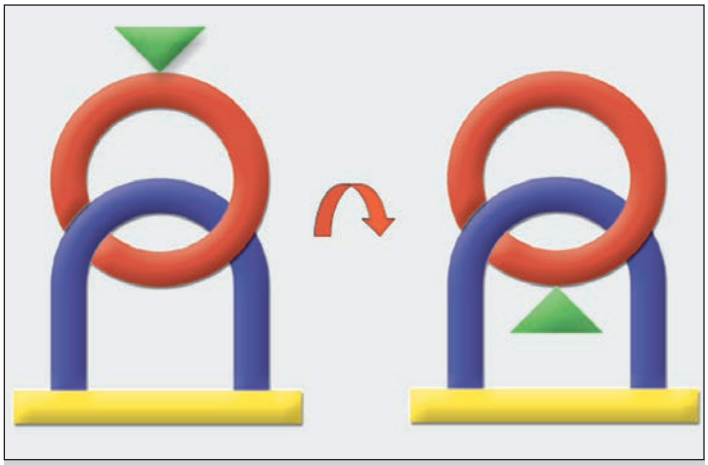

Representation of the rotation of surface-attached catenane. The red ring is a macrocycle that is mechanically restrained near the gold surface by the surface-attached loop (blue arch). The green triangle represents a functional group whose position is controlled by the rotation of the red ring.

During FY2001, we focused on the preparation and characterization of surface-attached molecular loops. These are monolayers that depart from the more traditional single attachment by binding to the surface of a gold-coated substrate through both ends of the molecule. Our first experiments involved a dithiol monomer and a disulfide-containing polymer. For the dithiol monomer, measurements taken using x-ray absorption and x-ray photoemission spectroscopy (XAS and XPS, respectively) showed only one sulfur atom attached to the gold surface. The same measurements on the polymer showed both sulfurs attached to the gold to form the desired surface-attached loop.

Our initial experiments highlighted the importance of designing molecules that incorporate turns to promote loop formation over single-site attachments, and we have prepared new compounds that successfully form loops. In addition to building capabilities in both synthetic chemistry and surface science, this work has led to a collaboration with the University of California, Los Angeles.

In FY2002, we will progress from work on model systems to the synthesis and characterization of surface-attached catenanes and rotaxanes. With the long-term goal being the creation of sensors with properties that can be controlled at the molecular level, we will investigate the surface-adsorption characteristics of nonfunctional, surface-attached, interlocking molecules. We plan to examine how these molecules order on surfaces and determine the stability of thiol- vs disulfide-surface attachment. This information will be used to help us design functionalized catenane and rotaxane systems for preliminary sensing.

Highly ordered, three-dimensional nanoscale structures with controlled surface chemistry

T. F. Baumann, J. H. Satcher, Jr., B. R. Hart, L. W. Hrubesh

MAIN TOC

Materials with defined pore sizes and shapes are important in applications where molecular recognition is required, such as catalysis, separations, selective adsorption, and chemical sensing. One method of forming uniform porous materials is the template approach—the use of an organic molecule or network to impart certain structural features to the solid under construction. An important extension of this approach is the preparation of porous inorganic materials that contain sites for catalysis or molecular recognition. Devices based on these porous solids require uniform pore networks and the ability to control the surface chemistry of the pores.

The goal of this project is the synthesis of ordered, 3-D, porous, inorganic solids with controlled surface chemistry. Such materials should exhibit unique optical, mechanical, thermal, and acoustical properties; they will provide novel chemical properties for general applications. This project couples recent advances in the design of extended structural networks with LLNL's expertise in molecular recognition and sol-gel chemistry. By establishing an entirely new and versatile route to ordered nanostructured materials, this project, if successful, could provide important new materials with application for LLNL's nonproliferation and environmental missions.

Our strategy for the design of these ordered, inorganic materials utilizes surfactant assemblies as templates. Surfactants are bifunctional molecules that, under the right conditions, assemble to yield 3-D hexagonal and cubic liquid-crystalline (LC) phases. The voids in these LC assemblies can then be infused with sol-gel precursors that are transformed into the inorganic framework.

For this project, we are using a new sol-gel technique, developed at LLNL, which will provide us with greater synthetic flexibility than that offered by traditional sol-gel methods. This new technique is inexpensive and allows for the preparation of a wider variety of metal-oxide materials than is accessible with traditional methods. Subsequent removal of the template produces a replicate inorganic solid containing an ordered array of pores. The porous solid can then be chemically modified by attaching specific functional groups to the surfaces of the pores, which allows us to tailor the properties of the material for a particular application. This functionalization can be performed either during the sol-gel polymerization process or following removal of the template.

In FY2001, our efforts were focused mainly on the synthesis of unfunctionalized, porous metal oxides, with the intent of establishing a reliable protocol for the synthesis of the more complex functionalized systems. As a first step in this process, we prepared templated silica containing a hexagonal array of cylindrical pores. The ordered pore network in this material was confirmed by small-angle x-ray scattering (SAXS) and transmission electron microscopy (TEM). On the basis of these initial experiments, we are extending this work to the preparation of other porous inorganic systems—including the oxides of iron, chromium, aluminum, and zirconium—using poly(alkylene oxide) block copolymers as our template surfactants. This particular class of surfactants forms both hexagonal and cubic LC phases that should be compatible with our new sol-gel process. The unfunctionalized, porous metal oxides prepared by this method will be of great interest—as new catalysts or as catalytic supports.

In FY2002, we will focus on the surface functionalization of the ordered pore networks in these solids. Utilization of functionalized monomers in the sol-gel reaction will allow for systematic control over the surface properties of the porous materials. For example, catalytic sites or sensing moieties could be tethered directly to the surfaces of the pores.

Nuclear and Atomic Science and Technology

Section 8

Section 8 Nuclear and Atomic Science and Technology

100-gigabar shock heating with the 100-terawatt JanUSP laser

P. T. Springer, P. K. Patel, D. F. Price

The latest generation of ultraintense, ultrashort-pulse lasers offers the possibility of creating states of matter with properties approaching those found in the interiors of stars and nuclear weapons. Producing plasmas at such ultrahigh temperatures and pressures under controlled conditions in the laboratory is a prerequisite for obtaining the physical data needed to test and validate atomic kinetics, equation of state (EOS), and opacity models. Developing such a capability therefore represents both a fundamental scientific interest and a key element of nuclear weapons stockpile stewardship.

Using the 100-TW JanUSP laser at LLNL, we are exploring the possibility of ion shock heating micrometer-sized plasmas to extremely high energy densities (approaching 1 GJ/g) on time scales of a few hundred femtoseconds. The JanUSP laser delivers 10 J of energy in a 100-fs pulse in a near diffraction-limited beam, producing a peak intensity on target of 10^{21} W/cm^2. The electric field of this beam ionizes and accelerates electrons to energies of millions of electron-volts (MeV). The sudden ejection of these electrons from the focal region produces tremendous electrostatic forces, which in turn accelerate heavier ions to MeV energies. The predicted ion fluxes of 1 MJ/cm^2 would be sufficient to heat solid-density targets to thermal equilibrium conditions at high temperature.

To test these predictions, we performed in FY2001 a set of experiments investigating the mechanisms for ion generation and acceleration in thin-foil targets irradiated at incident laser beam intensities above 10^{20} W/cm^2. In the experiments we used an ion time-of-flight magnetic spectrometer, radiochromic dosimetry film, nuclear activation detectors, and single-particle nuclear track detectors. Most of the energetic ions observed were in a highly directional beam emitted in the rear direction normal to the foil target surface. Although heavy target ions and lighter protons were detected, most of these particles appeared to originate not from the interaction region at the front of the target but rather from a thin adsorption layer on the rear surface as a result of rapid electrostatic acceleration. A large fraction of the incident laser energy (>1%) was coupled to the energetic protons. Since one expects the acceleration time to be of similar magnitude to the laser pulse duration, this suggests an extremely high particle flux at the source. The measured distribution was an exponential, typically containing 10^{11} particles with a mean energy of 3 MeV, comparable to the predicted hot electron temperature.

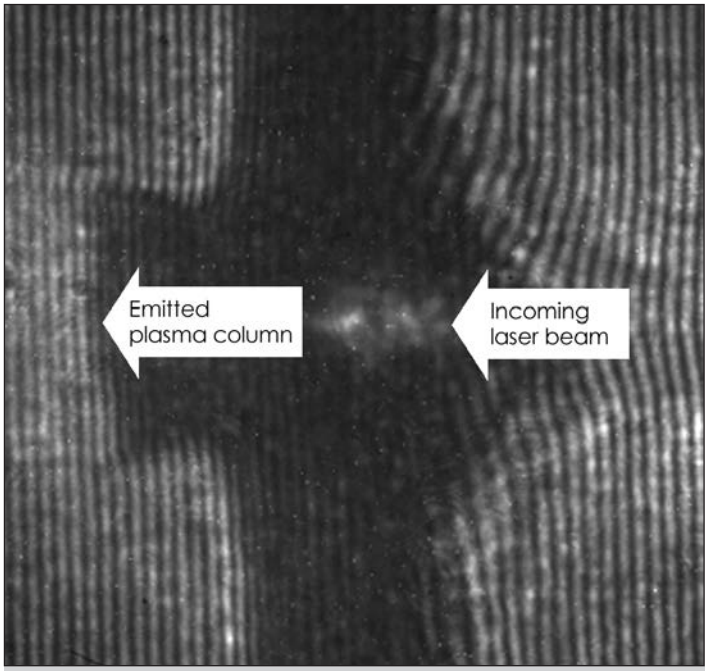

Interferometric image of a collimated plasma beam emerging from the rear of a foil irradiated with a high-intensity laser pulse.

Further data include interferograms taken with a 100-fs frequency-doubled probe beam. One such interferogram (see Figure), taken 150 ps after the main pulse, appears to reveal the ions as a well-defined column of plasma emerging from the rear of the target.

Detailed 3-D particle-in-cell simulations indicate that substantial ion acceleration is expected from both front and rear surface acceleration mechanisms. To isolate and measure the front surface–accelerated ions, we carried out experiments using deuterated buried layers to measure the ion emission as a function of depth within the target. Our findings related to the proton beam generation have resulted in two new projects funded in FY2002, to investigate proton radiography of laser-produced plasmas and proton heating for EOS studies.

X-ray optics and applications for fourth-generation light sources

A. J. Wootton, T. W. Barbee, R. M. Bionta, A. F. Jankowski, R. A. London, D. D. Ryutov, R. Shepherd, V. Shlyaptsev, A. Toor

MAIN TOC

The DOE's Office of Basic Energy Science has resoundingly endorsed research and development (R&D) towards a fourth-generation light source that would operate in an entirely new physics regime—a free-electron laser (FEL) with self-amplified spontaneous emission. A concept called the Linac (linear accelerator) Coherent Light Source (LCLS) has been identified as the best candidate and is the subject of a collaborative effort by a number of national laboratories and universities. The LCLS will produce a 0.8- to 8-keV, coherent x-ray beam with a 200-fs pulse length. It will have unprecedented brightness—10 orders of magnitude greater than existing sources.

Our goal is to develop methods to characterize and manipulate the intense x-ray free-electron laser (XFEL) beam, specifically, the x-ray optics and diagnostics. The source brightness presents demanding requirements and innovative design opportunities, which LLNL's historic expertise in x-ray optics, x-ray diagnostics, and FEL physics uniquely qualifies us to tackle. This particular light source has potentially large benefits for the Laboratory's biology and biotechnology research programs, and for the Stockpile Stewardship Program.

During FY2001, we researched and developed concepts for achieving some of the extreme requirements of the initial experiments: focusing the beam to submicrometer diameters at extra-ordinary energy fluences, time slicing and compressing the beam to 50 fs, and splitting and delaying the beam. Our modeling showed that grazing-incidence optics will work effectively. We developed a procedure for comparatively simple and inexpensive replication of these systems, based on the use of mandrels (see example in the Figure). The novel time-slicing concepts rely on chirping the accelerated electron-beam energy so that the photon pulses have a small wavelength spread in time (i.e., time and wavelength are now linked). Dispersive elements or multilayers are then used to separate colors, thereby producing time slices of the original beam. The temporal compression proposed would again be achieved with a chirped electron energy. A Bragg crystal with a variable lattice spacing would reflect different colors with different path lengths, and thus with different temporal durations. In this way, the different colors—corresponding to different times in a pulse—can be superimposed in space, and the pulse compressed.

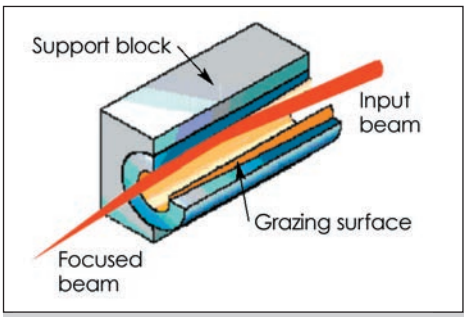

A tubular focusing mirror (lens) built by depositing material on a mandrel and then withdrawing the mandrel. This process allows simple replication of grazing-incidence optics that are suitable for high-energy loads.

We also developed and documented novel concepts for producing optical components in the x-ray region. These include using plasmas as lenses and electrostatically and magnetically controlled liquids as controllable mirrors. These liquid mirrors are formed by forcing liquid through a suitably shaped porous membrane (e.g., a microchannel plate). The liquid can be renewed if it is damaged by the high beam fluence.

In FY2002, we will focus on extending our photon–material interaction studies, both theoretically and experimentally, to learn if there will be effects that alter the optical properties of components during a subpicosecond x-ray pulse, even if the fluence is less than that required to cause long-term irreversible effects. Experimentally, we will extend the damage experiments into the x-ray regime, using either LLNL's Comet x-ray laser or a K_α radiation source. The latter we would develop ourselves, initially using Cu. We will initiate diagnostic R&D by developing a system to measure the profile of the x-ray beam. Finally, we will extend the model of the FEL beam to include the action of specific optical components such as mirrors and lenses. This code will then become a major design tool.

Exploring quantum chromodynamics at the relativistic heavy-ion collider with two-particle correlations

R. A. Soltz, E. P. Hartouni, S. C. Johnson, M. Heffner

The PHENIX experiment at the Relativistic Heavy-Ion Collider (RHIC), at Brookhaven National Laboratory (BNL), is one of two large experiments designed to detect and study matter at the highest energy densities attainable. Our scientific motivation, as participants in the experiment, is to measure the collision volume using Bose–Einstein correlations of identical pions. The source volume is one of several possible signatures of a quantum chromodynamics (QCD) phase transition in these collisions. QCD phenomenology theory predicts that a transition to a new phase of matter—a plasma of quarks and gluons—will lead to measurements of source radii that exceed typical radii for ground-state nuclei. This project also contributes to a broad range of physics goals by performing Monte Carlo simulations on the Livermore Computing (LC) cluster.

Our FY2001 accomplishments consisted of analyzing the first two-particle data set in PHENIX. We measured the source in three dimensions: along the beam axis, transverse to the beam axis but perpendicular to the mean pion momentum, and transverse to the beam but parallel to the pion pair momentum. All radii were measured as a function of the mean transverse pion momentum. The radii do not show a large increase, and the transverse radii are consistent with correlation measurements at lower energies. The longitudinal radius shows a slight increase with collision energy. Our results were presented at the Quark Matter 2001 Conference held at the State University of New York (SUNY) at Stony Brook/BNL to showcase the first results from RHIC.

The top of the Figure shows the measured sideward radius (R_S), which is a measure of the effective size of the source in the transverse direction perpendicular to the pion pair momentum. The fitted solid line is a prediction based on hydrodynamics for a source that is expanding in the transverse direction. Separate fits to data from two experiments, PHENIX and STAR, indicate the systematic errors. The bottom of the Figure shows the ratio of outward radius to sideward radius (R_O/R_S), which measures the duration of pion emission. All three radii are comparable to the radius of a gold (Au) nucleus, which is 5 fm. The results contradict most theoretical predictions, and they have presented the field with something of a puzzle.

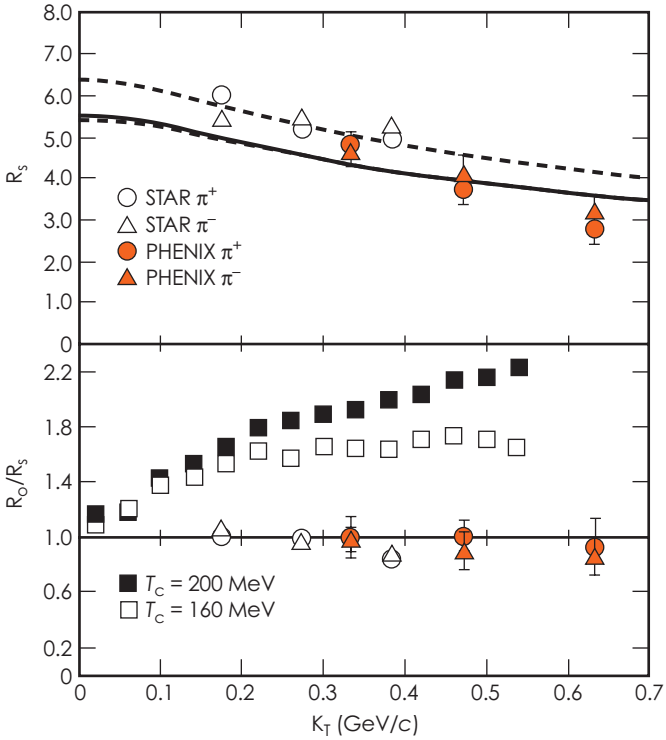

(top) Measured sideward radius (R_S) and (bottom) ratio of outward radius to sideward radius (R_O/R_S), which measures the duration of pion emission. Square data points are the results of a typical hydrodynamic model calculation for two critical temperatures (T_C) of the phase transition.

Our plans for FY2002 include extending the measured two-particle correlations to other species, namely kaons and protons. For pion correlations, the anticipated high-statistics data sets should enable the simultaneous fit of single-particle momentum distributions and two-particle correlations that will allow us to precisely determine the expansion velocity. Finally, we are developing new fitting techniques that will use the powerful LC cluster to fit the momentum dependence of the full data set. The latter advance will break new ground in using correlation functions to probe space–time dynamics of heavy-ion collisions, and it may provide insight into current contradictions between data and theory.

Ab initio nuclear structure from helium to oxygen

W. E. Ormand, P. Navratil

MAIN TOC

An important goal in the study of nuclear structure is to answer the question: Do we really understand how nuclei are put together? Towards achieving this goal, we wish to formulate a complete description of the properties of complex nuclei from first principles. In particular, we want to determine if our knowledge of the fundamental interaction between pairs of nucleons is sufficient to describe the rich and complex structure observed in nuclei. In this project, we are utilizing new developments in many-body theory and the exceptional computational power of LLNL's Advanced Simulation and Computing (ASCI) platforms to formulate a coherent picture of the structure of nuclei ranging from helium to oxygen.

Our starting point is effective interaction theory within the framework of the nuclear-shell model utilizing effective interaction theory. The most important aspect of effective-interaction theory is the presence of "induced" higher-body components, which arise even if the effective interaction is derived from a purely pairwise fundamental (bare) interaction. Our goal is to achieve an exact as possible treatment of nuclear structure by including these higher-body components of the effective interaction.

During FY2001, we carried out the first-ever ab initio calculations using three-body effective interactions for systems of more than four nucleons. Our results for beryllium-8 (^{8}Be) and boron-10 (^{10}B) are shown in the Figure, where they are compared with "exact" results obtained using the Green's Function Monte Carlo (GFMC) method. Clearly, faster convergence is achieved with the higher-body components. This achievement is significant because until now shell-model applications have been limited to the inclusion of only two-body effective interactions, and it is likely that computational restrictions will limit calculations for carbon-12 (^{12}C) (and heavier nuclei) to N_{max} = 4. Further, substantial evidence, which is also supported by our recent work for ^{10}B, exists for "true" three-body interactions in nuclei. The inclusion of a true three-body interaction will require that two-body interaction be treated at the level of a three-body cluster in the effective interaction. Our results indicate that a comprehensive study from first principles of the structure of nuclei up to oxygen-16 (^{16}O) is an achievable goal.

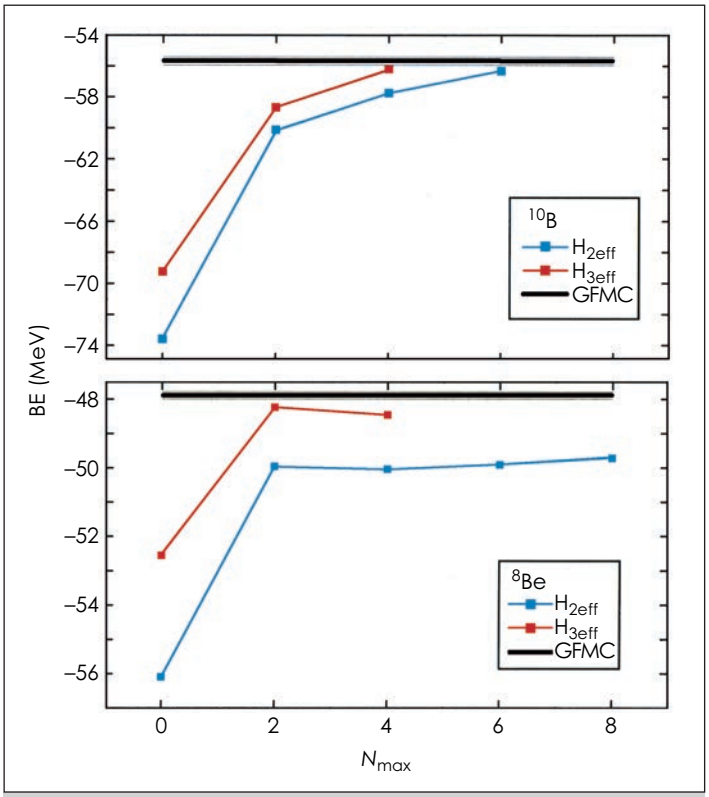

Binding energies of beryllium-8 (^{8}Be) and boron-10 (^{10}B) obtained with two- and three-body effective interactions (H_{2eff} and H_{3eff}, respectively) as a function of the model space (N_{max}) compared with results obtained using the Green's Function Monte Carlo (GFMC) method.

To carry out these new calculations, we undertook extensive software development during FY2001, including (1) new codes to evaluate the three-body effective interaction, and (2) a new shell-model code (REDSTICK) that is specifically designed to efficiently include three-body interactions. We also modified an existing code to handle three-body interactions. Our calculations were carried out primarily using the ASCI Pacific Blue computer and the Livermore Computing (LC) clusters.

Other scientific achievements for FY2001 include (1) participation in a validation of ab initio methods for helium-4(^{4}He); (2) an investigation of the low-lying structure of lithium-6 (^{6}Li); and (3) a detailed study of new states predicted in ^{8}Be. We also presented papers at a number of conferences.

During FY2002, we will utilize three-body effective interactions as well as a true three-body interaction to carry out systematic calculations for light nuclei. We will focus on studies in nuclear structure regarding the form of the nucleon–nucleon interaction, neutron-induced reactions on light nuclei and gamma production, fundamental studies of the electroweak interaction, neutrino absorption, and applications of our method to halo nuclei such as ^{11}Li. Throughout FY2002, we will investigate the computational feasibility of including four-body clusters in our calculations.

Developing radioactive ion beam capability

L. A. Bernstein, A. Schiller, J. A. Becker, P. E. Garrett, W. Younes, E. Tavukcu

Reactions involving radioactive nuclei play a central role in the formation of elements in both stars and nuclear devices. However, the abilities of reaction models to predict cross sections on radioactive nuclei are uncertain because of the lack of experimental data. The proposed Rare Isotope Accelerator (RIA) and existing radioactive ion beam (RIB) facilities offer an opportunity to fill in these gaps through the use of nuclear reactions with radioactive targets and/or beams. The primary goal of this project is to develop RIBs and new experimental capabilities for use with them.

Our three major accomplishments during FY2001 are described below.

Nuclear level densities are critical for accurate nuclear-reaction model calculations. In early FY2001, we collaborated with staff at the University of Oslo cyclotron to measure level densities in molybdenum-96 and iron-56. These experiments were the first attempts to measure level densities above the limits of discrete spectroscopy in these nuclei, which are important to astrophysics and stockpile stewardship. The measurements increased our understanding of the measurement technique—our goal is to use it with RIBs. The results from these experiments were presented at the International Nuclear Physics Conference in July 2001.

In February 2001, we collaborated with scientists at Michigan State University on a secondary RIB experiment. Secondary RIB experiments involve creating a radioactive nucleus in a nuclear reaction and allowing it to recoil onto a second. Our goal was to measure the deformation of the low-lying states in osmium-176. In this experiment, we successfully formed a RIB of osmium-176 using the titanium-48 (xenon-132, 4*n*) reaction at 640 MeV. The results of our work were presented at the American Physical Society meeting in April 2001.

In our third major accomplishment for FY2001, we and our collaborators at Lawrence Berkeley National Laboratory ran two experiments in which the selenium-74 + a reaction was used to make krypton-76 (half life = 14 h), bromine-76 (half life = 16.1 h), krypton-77 (half life = 1.24 h) and bromine-77 (half life = 2.4 d) using the "recyclotron" technique. In the recyclotron technique, radioactive krypton and bromine are formed in an 8 to 24-h production run using the cyclotron, removed from the target via heating, and transported via a helium gas line to the cryogenic traps (see Figure). The test runs successfully demonstrated that these radioactive beams could be produced using these reactions, and separated cryogenically. (In a third run, scheduled for FY2002, we will attempt to inject these nuclei back into the cyclotron for acceleration.

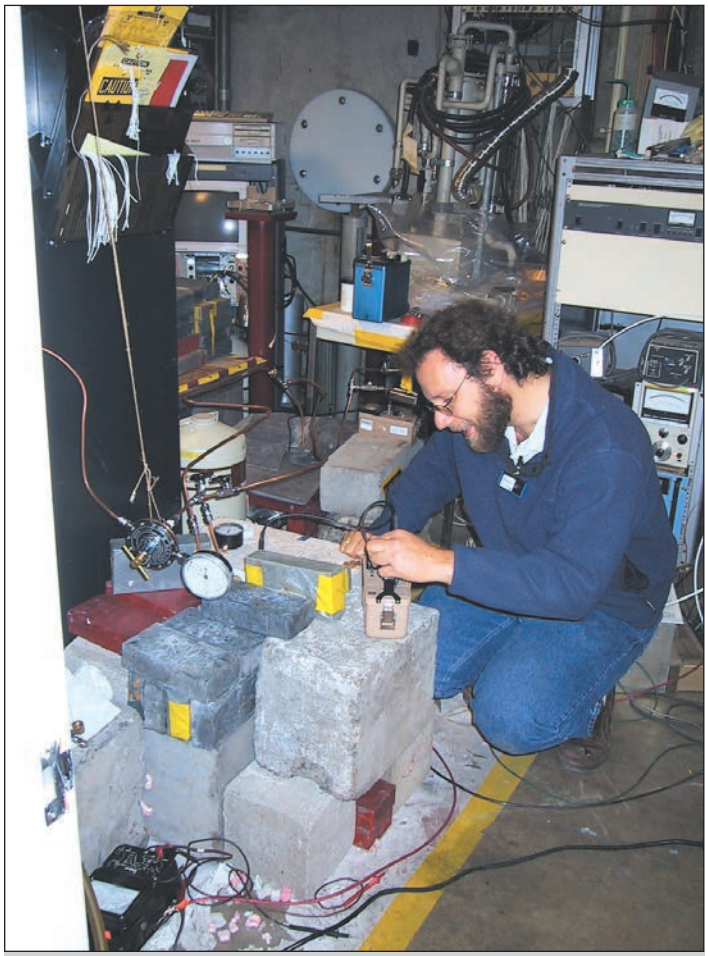

Principal investigator L. Bernstein measures prompt activity from the bromine and krypton cryotraps (dry ice and liquid nitrogen, respectively) at the Lawrence Berkeley National Laboratory 88-in. cyclotron.

Soft x-ray line emission from comets

P. Beiersdorfer

Recent x-ray satellite observations have firmly established comets as x-ray sources, a discovery that has far-reaching implications for understanding the interaction of comets with the inner Solar System. This discovery has opened up a new wavelength band for probing the solar wind—space weather—in real time, studying interactions between comets and the Sun, and understanding the composition of cometary atmospheres. However, because the charge transfer of solar-wind heavy ions, proposed as the comet's main x-ray production mechanism, is poorly understood, models of charge-transfer-induced x-ray emission are based on best-guess estimates. Improving our understanding of these x-ray production mechanisms greatly benefits LLNL's core mission in high-temperature plasma and atomic physics, and broadens our expertise in modeling short-wavelength radiation sources.

The goals of this project are to (1) simulate, in a controlled laboratory setting, the conditions that cause comets to emit x rays, (2) produce the necessary experimental database for describing charge-transfer-induced x-ray emission in low-energy collisions of highly charged ions with atoms and molecules, and (3) incorporate our results into models that accurately describe x-ray emission by comets.

In FY2001 we used high-resolution instrumentation to perform spectrally resolved measurement of the K-shell spectra of bare and hydrogen-like ions undergoing charge-transfer reactions. In collaboration with researchers from the NASA Goddard Space Flight Center, we installed a magnetically cooled x-ray microcalorimeter on our ion source. This calorimeter, a one-of-a-kind detector built at the Goddard Space Flight Center in the course of the Astro-E satellite mission, made possible a huge improvement in our data collection.

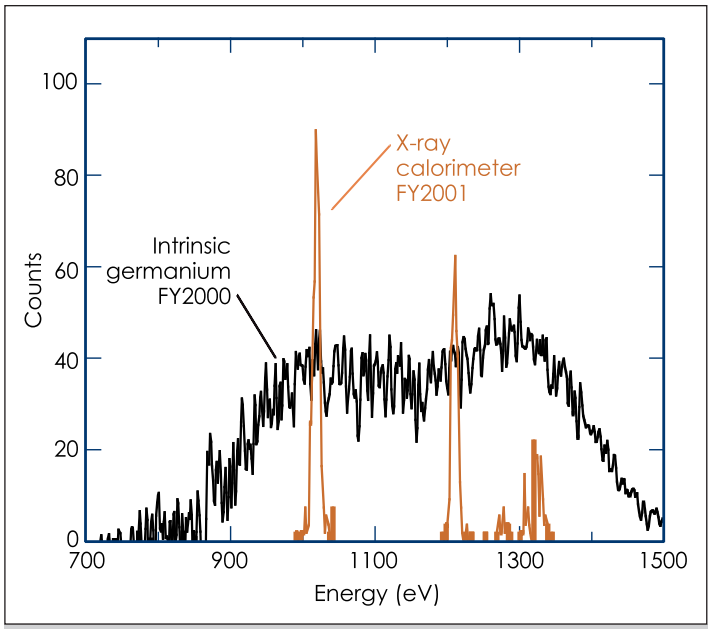

K-shell x-ray emission from Ne^{9+} following charge exchange of bare neon with atomic neon. The measurements recorded with the new microcalorimeter fully resolve the individual transitions. This is a major breakthrough over our previous measurements using an intrinsic germanium detector, which recorded only the overall shape of the emitted x rays.

Unlike our previous measurements, the data we collected in FY2001 with the help of the new microcalorimeter show all the x-ray transitions that are produced by charge exchange, as the Figure shows. This major breakthrough provides exactly the data needed to understand why theory has not been able to predict such spectral emission.

Our FY2001 data show that double electron capture is a major x-ray production mechanism, a process that has been left out in all previous x-ray models. Our FY2001 data also have provided the first spectroscopic evidence that x-ray emission can be used to probe the chemical composition of cometary atmospheres. This discovery will represent a major contribution to scientific understanding of primordial matter emitted by comets.

In the coming year, we will use the high-resolution capabilities afforded by the x-ray microcalorimeter to study chemical effects in detail. In FY2002, another major advance in experimental technique will be the implementation of an atomic hydrogen beam to study charge exchange in the absence of double capture. This will complete the data needed to build a complete x-ray emission model.

High-energy physics at the Next Linear Collider

K. A. van Bibber, J. Gronberg, E. Cook, W. Stein, J. Early

MAIN TOC

Worldwide consensus in the high-energy physics community points to an electron–positron linear collider in the teraelectron-volt range—called the Next Linear Collider(NLC)—as its next major project. Such a machine would reveal the mechanism of electro-weak symmetry breaking, whether through a Standard Model Higgs boson or a more exotic mechanism like Supersymmetry, to be studied.

The first discoveries of this new physics will probably be made in the next few years at proton colliders (Fermilab's Tevatron or CERN's Large Hadron Collider). However, the NLC will provide the large data samples that can produce the precision statistics needed to yield complete understanding of the new physics. The U.S. and Japan are carrying out research and development (R&D) towards a normal-conducting X-band (11.424-GHz) design for an NLC; the Europeans are working on a superconducting L-band (1.3-GHz) design.

This LDRD research project has two thrusts. The first is technology development to ensure that the main linear accelerator (linac) systems of the NLC are practical and affordable. The second is R&D and preliminary design of a gamma–gamma (photon) collider as an option for one of the interaction regions of the NLC. Study of high-energy photon–photon collisions will open an entirely new window to high-energy physics, complementary to that accessible through the study of electron–positron interactions. For example, the production rate of the Higgs boson in a photon collider (clearly distinguishable in the Monte Carlo simulation shown in the Figure) would be sensitive to new generations of quarks and leptons, including particles whose masses are far higher than can be created in any accelerator that will ever be built.

One of the primary challenges for the NLC's 20-km-long main linac systems will be efficient production of radio-frequency (rf) power of about 100 MW. There are four main systems in a high-gradient electron linac. The modulator takes power from the grid and produces fast, high-voltage pulses that drive klystrons, which produce microwave power at the accelerator's operating frequency. A pulse compressor temporally squeezes these rf pulses to achieve higher peak power. This power is fed to the accelerator structures, inside of which the electrons "surf." In FY2001, we built a fully solid-state prototype modulator capable of driving four klystrons. This modulator delivers greatly improved performance at lower cost than existing technology. In this work we made use of the Laboratory's expertise in the construction of an induction accelerators for stockpile radiography. In FY2002 we plan to produce a modulator capable of driving eight klystrons, which will be incorporated into a full-systems rf prototype at the Stanford Linear Accelerator Center (SLAC).

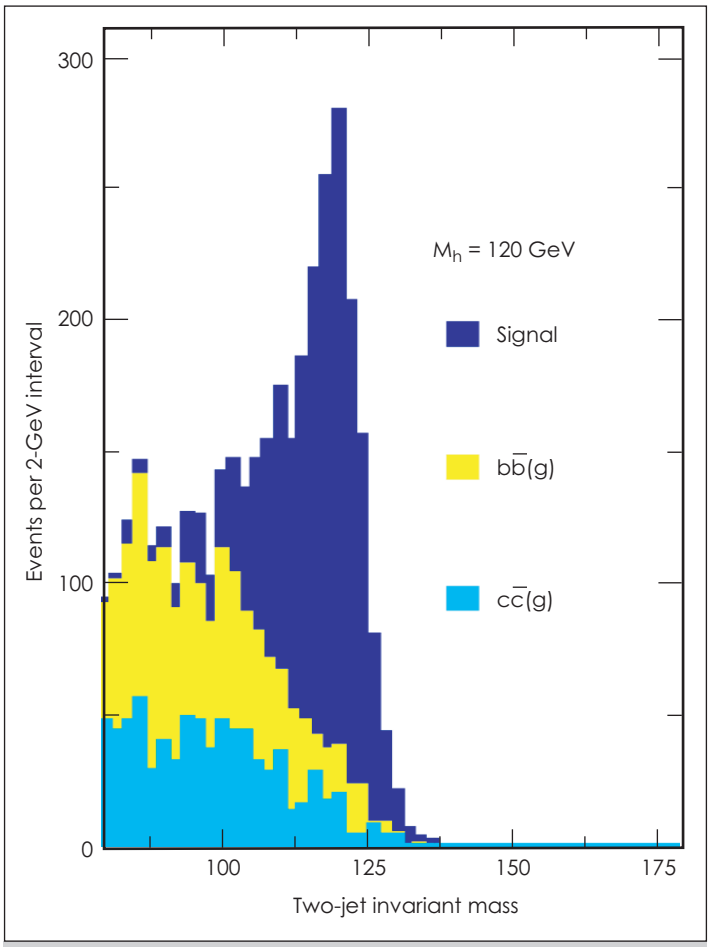

Monte Carlo simulation of the decay of a 120-GeV Higgs boson. Data obtainable from one year's running of the proposed NLC gamma–gamma collider would yield sufficient statistics to allow physicists to understand and quantify the nature of the Higgs boson.

In a photon collider, high-energy gammas would be produced by the Compton backscattering of short-pulse, high-intensity laser light from each electron bunch just upstream from the interaction point. This process upshifts low-energy laser photons to several hundred giga-electron-volts. In FY2001 we produced a preliminary design for a laser capable of delivering the high average power required, based on the Mercury laser developed for LLNL's Inertial Confinement Fusion Program. We also designed an optical system to transport the laser light into collision with the electron beams in the interaction region.

We have published this work in numerous refereed journals and have presented it in national and international meetings. The prominence of the work has allowed us to hire high-energy physicists in support of the Laboratory's national security mission.

In FY2002, we will carry out prototype design for the European version of a TeV linear collider and for a lower-energy prototype being proposed at SLAC.

First physics from BaBar

D. Wright, V. Brigljevic, D. Lange

The BaBar experiment at the Stanford Linear Accelerator Center (SLAC) is designed to observe or rule out charge/parity (*CP*) violation in the decay of *B* mesons. *CP* violation, an asymmetry in the decay of particles and their corresponding antiparticles, stands at a crossroads between particle physics and cosmology. Besides being one of the last major components of particle-physics theory that is not understood, *CP* violation is also required in cosmological models that explain the predominance of matter over antimatter in the universe, However, particle physics cannot yet explain the source of this effect in the evolution of the early universe. Until recently, there has been very little new experimental information about this fundamental phenomenon.

LLNL is part of the large international collaboration of physicists that built the BaBar detector and had several roles in the design and construction of the experiment. The purpose of this project is for LLNL to make major contributions to the first physics results of the BaBar experiment and to shed light on the mystery of *CP* violation. Observation of *CP* violation in the Babar experiments would be a major scientific discovery at the forefront of high-energy physics, a mission area of DOE's office of Science. The project will also extend Laboratory capabilities for handling and analyzing massive scientific data sets.

The first step in the broad physics program for BaBar is to unambiguously observe a *CP*-violation effect in *B* mesons. The *CP*-violation asymmetry will appear as a difference in the time dependence of the decays of *B* and anti-*B* mesons. The most sensitive tests of *CP* violation at BaBar can be made from the K_S decay channel of the *B* meson. This mode is easy to detect and has low background. Equally sensitive, but more challenging to detect, is the K_L decay channel. To make a convincing discovery, BaBar should observe a signal in both channels.

During FY2001, we developed the software tools to find the signal and measure the *CP* asymmetry in the K_L channel. This is particularly challenging because of competing physics backgrounds that also have *CP* asymmetries. We implemented a maximum-likelihood fit for the *CP*-asymmetry measurement in the presence of significant amounts of background. We did this in a completely general and flexible manner so that each signal and background category can have a different *CP* dependence, decay-time distribution, and tagging sensitivity. In addition, our fitting program can simultaneously fit the *CP* data with other control samples that measure *B*-meson oscillations and *CP* dilution resulting from errors in misidentifying the *B* meson. This effort resulted in our taking a leading role in fitting all the *CP* modes. To extract a *CP*-asymmetry measurement from all six *CP* modes—including the K_L channel—we performed the fit on the entire data set. The project was instrumental in studying the *CP* data and in producing the first BaBar publication. Our results were the first to establish a significant signal for a *CP*-violating effect in *B* mesons.

In FY2002, we will continue to enhance the software tools, analyze the data, study the systematic errors, and document our *CP*-violation measurements. To enhance our physics output, we will investigate ways to leverage our current role in data analysis. We will also (1) continue to take part in running the BaBar detector and acquiring the data, and (2) participate in a data-acquisition system and cosmic-ray test station to test new detector modules as part of a new effort to improve detector performance.

Multimegabar metal equation-of-state and material-property data using high-explosive pulsed power

R. C. Cauble, D. B. Reisman

The experimental determination of high-energy-density equations of state (EOS) and properties of metals is central to Stockpile Stewardship Program applications. These applications require EOS and material models that must be tested by experiment and constrained by data. For many applications, data in the few- to tens-of-megabar regime are needed. Strong shocks can generate these pressures; however, shocks produce unwanted high temperatures.

"Squeezing" a sample on an isentrope to a pressure produces lower temperatures than shocking it to that pressure, but "squeezing" is extremely difficult to do at high pressures without producing an unwanted shock. In earlier work with Sandia National Laboratories (SNL), we and SNL developed isentropic compression experiments (ICE) on their Z Accelerator, utilizing magnetic pressure to squeeze samples to high pressure. However, pulsed-power machines have limitations: the maximum pressure is only about 1 Mbar, the current pulse cannot be easily modified, and actinide sample materials are off limits.

Our goal in this project is to establish, in collaboration with Los Alamos National Laboratory (LANL), the use of high-explosive pulsed power (HEPP) for ICE. HEPP uses a set of explosives to provide a very large electrical current for a few microseconds and another set of explosives to shorten the current pulse to less than 1 μs. Though HEPP had never been previously considered for ICE, HEPP ICE has the potential to overcome the limitations of machine-based ICE, including the use of actinide samples. Our development plan is to start with conditions near those of the SNL experiments to validate the HEPP technique and then augment the current while optimizing load and target design. In the process, we must design and field an improved diagnostic, called a velocity interferometer system for any reflector (VISAR), for our measurements.

Detonation of a high-explosive, pulsed-power, isentropic compression experiment (ICE) at Los Alamos National Laboratory. The detonation of tens of kilograms of explosive generates an electrical current of several million amperes. The intense magnetic field associated with that current smoothly compresses a centimeter-size metal target to a pressure of hundreds of thousands of atmospheres.

In FY2001 we designed and began assembly of our new VISAR, scheduled for completion in FY2002. In the meantime, we modified part of the existing LANL diagnostic for higher efficiency. The better probes we built can be used on similar VISARs used at many facilities.

We fired three test HEPP devices to determine which of two basic HEPP designs we would use. Magnetohydrodynamic (MHD) codes were used to design the ICE load (which delivers current from the HEPP device to the samples) and the dimensions of the samples—critical to obtaining good results.

The first HEPP ICE shot (see Figure) proved that our new VISAR probes functioned well, although a HEPP component failed. A postmortem revealed a manufacturing defect, which was corrected. Additional HEPP design adjustments were made, and two HEPP ICE shots were conducted late in FY2001. The results showed that HE-driven experiments reproduced the Z Accelerator data, thereby validating the technique, but with larger samples. The larger sample size improves the accuracy of the EOS data.

In FY2002 , we will complete our VISAR and fire three HEPP ICE shots, optimizing for pressures in the few-megabar regime. These isentropic EOS data will be the first in this regime.

A highly efficient, fast-neutron threshold detector

P. L. Kerr

In this project, we are investigating new thorium-(Th)-based fast-neutron detector designs. These designs are more efficient than fission chambers and would be applicable in techniques that use active neutron interrogation to detect highly enriched uranium (HEU) in shielded containers. Due to the low-energy gamma rays that U emits, shielding easily reduces the gamma-ray signature from HEU, making it difficult to detect. This work supports the DOE nonproliferation and international security missions and homeland security by improving the ability to detect shielded HEU.

In addition to its low-energy gamma rays, U has little neutron signature due to the low rate of spontaneous fission. A threshold detector, such as a Th fission chamber, can distinguish fission neutrons (>1 MeV) from the lower-energy interrogating neutrons. The innovative designs explored in this project use a liquid or solid to detect the fission fragments instead of a gas, which is traditionally used in threshold detectors. Because liquids or solids have greater stopping power for fission fragments than a gas, they allow more Th per unit volume of the detector, thereby increasing the neutron-detection efficiency. The liquid design uses a liquid scintillator exchanged into a Th sol-gel. The solid design uses a slotted-silicon diode filled with a thoria aerogel (see Figure). Prototypes based on these concepts are being developed to demonstrate proof of principle. Subsequent work will improve the design to demonstrate that it is practical in terms of detection efficiency, ease of use, and construction cost.

During the first half of FY2001, good progress was made producing sol-gels containing liquid scintillators. These gels demonstrated good light transmission and the ability to detect gamma rays, as expected. Work was then directed to producing sol-gels containing silicon and Th. A testable prototype resulted from this work, but discoloration of the gel due to a pH mismatch resulted in quenched light and no signal from gamma rays or neutrons. This outcome suggested the need for a process of exchanging liquid scintillator for the solvent. The first such gels are now being processed. In addition, fully thoria gels (i.e., no Si) have been produced for the first time. These should provide even higher neutron-detection efficiencies. In addition, thorium nitrate dissolved in liquid scintillator provides an intermediate step to incorporating the scintillator into the sol-gel. The results from this work have identified a scintillator that does not change color when the thorium nitrate is added and maintains good pulse-shape discrimination properties. Most importantly, when the Th scintillator liquid is exposed to fast neutrons, a fission-fragment signal is indicated in the spectrum.

Good results were also obtained for the slotted-Si diode design. The diamond saw, an instrument well suited to making very small, sharp cuts into Si, produced 70 clean cuts (300-μm wide × 0.7-mm deep × 30-mm long) on a test piece of Si. Progress was made getting Th into the slotted Si. To build on our thoria sol-gel success, an aerogel technique was chosen to fill the slots with Th. Removing the solvent from the gel by super extraction gave better results than by evaporation. Slots were cut into a commercial Si diode detector to determine the effects on leakage current and other properties. The leakage current increased, but not significantly—a positive test of our cutting and cleaning technique.

In FY2002, we will focus on refining the sol-gel design, increasing the neutron detection efficiency by evaluating and optimizing various sol-gel techniques, scintillators, thoria concentrations, and detector geometries. We plan to initiate studies of detector lifetime versus neutron flux, and investigate combinations of other actinides that may enable neutron spectroscopy. In addition, we intend to publish our detector and chemistry accomplishments and pursue patents.

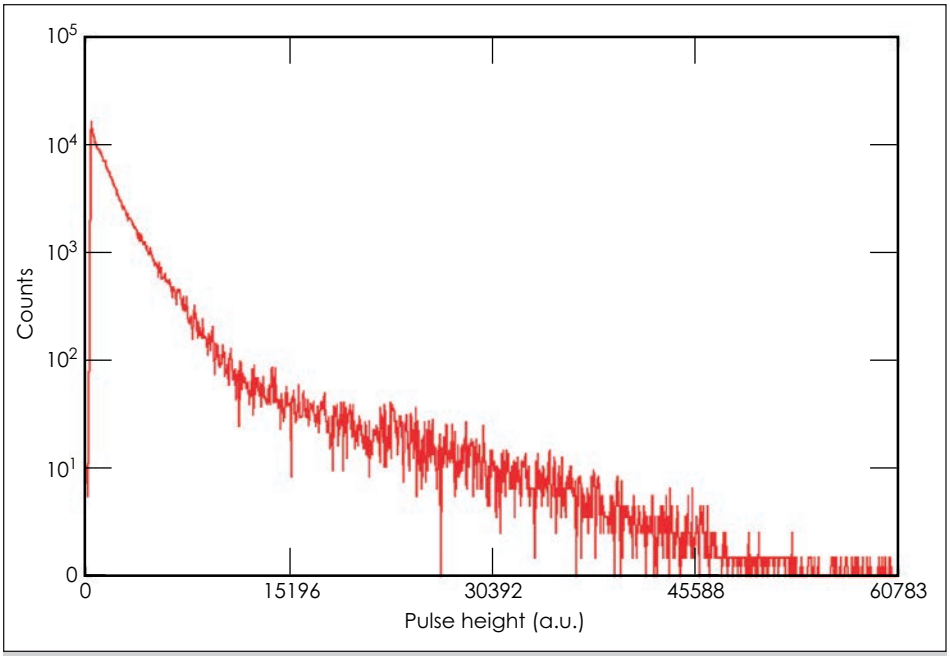

Energy spectrum (with background subtracted) from thoria-gel scintillator prototype showing successful light output.

Focusing hard x rays at current and future light sources for microscopy and high-power applications

R. M. Bionta

The goal of this project is to develop and demonstrate an x-ray microscope at the Stanford Synchrotron Radiation Laboratory (SSRL) that will operate at 8 KeV with a resolution of <1 μm. The critical element of this research is to develop and demonstrate a practical diamond-turning process to manufacture the microscope's x-ray lenses. The lenses will be of far superior quality compared to those previously reported, and they will be able to handle the extreme power densities expected from x-ray free-electron lasers (FELs) at proposed fourth-generation light sources.

At LLNL, the availability of high-performance x-ray lenses would enhance diamond anvil studies, National Ignition Facility research, and projects attempting to develop new x-ray sources through laser or electron interactions in support of the Stockpile Stewardship Program.

Our initial motivation for this project came from designs for 8-KeV x-ray optics for the warm, dense matter (WDM) experiment that will be conducted at the Linac Coherent Light Source (LCLS), which is a DOE Basic Energy Sciences initiative to develop an x-ray FEL at SSRL. The WDM experiment will study the interesting properties of an energetic plasma at near-solid density. WDM is believed to exist in the center of large planets, and the properties of this state of matter are important to astrophysics and to the production of inertially confined fusion reactions. To create WDM in the laboratory, the 8-KeV, 100-μm-diam LCLS X-FEL beam will be focused on a 2- to 10-μm-diam spot in the center of a sample of solid matter. The focusing element required for the experiment is a 200-μm-diam, blazed phase lens made of carbon and capable of withstanding the full, unfocused LCLS beam without sustaining damage. Our project uses single-point diamond turning to carve such lens profiles into the surface of thin disks of aluminum or carbon. The profiles are designed so that x rays from a diverging source experience a phase change through the lens that transforms the source wavefront to a spherical wave converging at the image point.

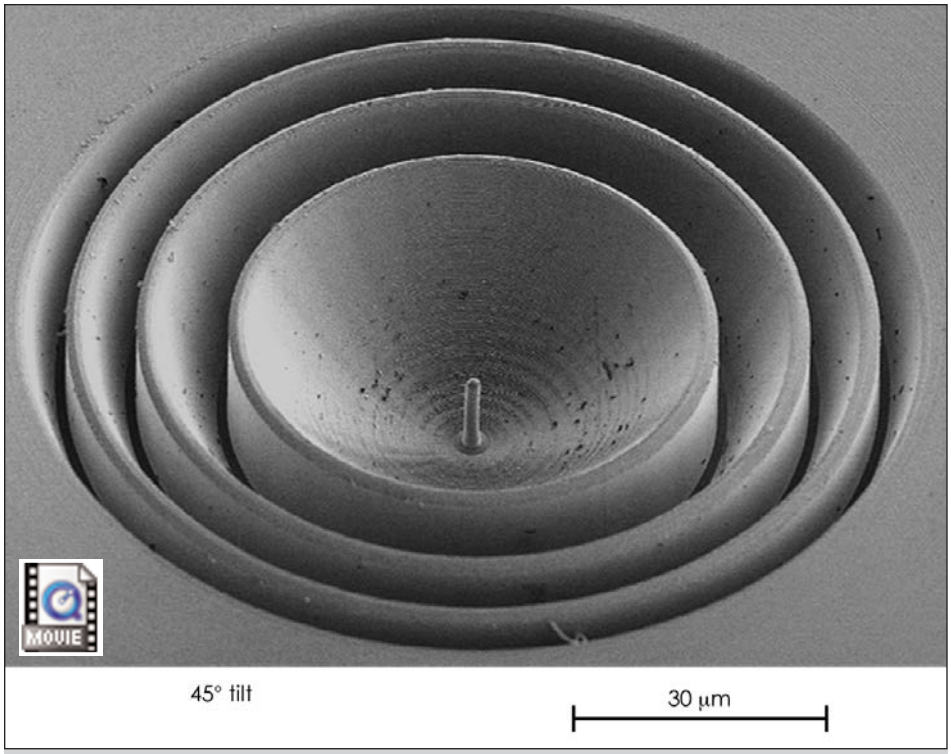

Picture of a lens carved into the surface of a flat aluminum disk by a special diamond-turning process.

During FY2001, we manufactured the first lens of the required type, shown in the Figure. The lens is made of aluminmum and is 100 μm in diameter. Each groove is 18.7-μm deep, which is the thickness in aluminmum at which 8-KeV x rays acquire an extra 2π radians of phase shift with respect to x rays traveling the same distance in vacuum. Although the small pillar in the center is difficult to remove, it has negligible effect on lens performance. The carved disk was subsequently flipped over and thinned down from the back side to a final thickness of 79 μm. Preliminary tests in the 8-KeV x-ray beam at the SSRL in July 2001 indicated that the lens performs as expected.

In FY2002, we will develop and test a 200-μm-diam lens to be used as a condenser lens in the microscope. We will also perform research and development to extend the process to fabricate carbon lenses.

Retrospective plutonium biodosimetry by modeling urinary plutonium-239 from archived occupational samples

K. T. Bogen, D. Hickman, T. Hamilton, T. Brown, A. Marchietti, C. C. Cox, R. Martinelli, J. Daniels

MAIN TOC

Uncertainty about plutonium- (Pu-) excretion biokinetics in humans limits retrospective Pu dosimetry; ^{239}Pu-detection for national security; and other potential uses of emerging, ultrasensitive Pu-detection technology. This project is investigating the feasibility of using accelerator mass spectrometry (AMS) to produce retrospective data on urinary excretion of Pu for two workers with relatively well defined ^{239}Pu exposures at LLNL. Using AMS to analyze archived alpha spectrometry (AS) plates will reveal previously undetectable patterns of urinary Pu excretion.

Archived data available for 15 to 20 LLNL Pu workers monitored periodically during 1981 to 2000 include AS plates as well as dosimetry records. During FY2001, we studied plates used to measure urinary Pu from one LLNL worker exposed via a suspected wound (Worker 1) and another exposed by inhalation (Worker 2). Records were searched for corresponding data on Pu-recovery efficiency (F_r), dosimetry, etc. Originally prepared using standard methods for Pu-separation chemistry, the plates contained electroplated ^{239}Pu as well as spiked ^{239}Pu used to determine F_r. When originally analyzed by AS, and then recounted by AS for this study, only three plates significantly exceeded AS Pu-detection limits (~130 mBq). Blank control plates prepared during 1981 to 2000 were also retrieved and recounted by AS. Background levels of less than 1 million atoms (<1 μBq) of ^{239}Pu were observed routinely, without interference from up to 10^{13} coprocessed uranium atoms. Of 43 archived AS and 3 control plates spanning years 1981-2000 evaluated by AMS, plates with AS counts well above background yielded similar ^{239}Pu levels by AMS, and AMS measures of ^{239}Pu in the 3 blanks indicate a detection level of 8.1 μBq (~20-fold more sensitive than AS).

AMS results obtained for Worker 1 (see Figure) indicate a chronic, nearly linear increase in urinary ^{239}Pu activity, consistent with nearly constant but previously nondetectable leakage from a previously unsuspected ^{239}Pu-injection wound. AMS data for Worker 2 also show a significant—again previously unsuspected and nondetectable—increase in urinary ^{239}Pu after about 10 yr of nearly constant low levels. Although no known occupational Pu intakes have occurred at LLNL during the past 20 yr, recent radiography revealed Pu at a potential wound site in Worker 1 as well as Pu in corresponding auxiliary lymph nodes. Neither safety records nor the worker can establish when a wound may have occurred. It is impossible to confirm any Pu intake for Worker 1 using AS, whereas the AMS data obtained clearly indicate an internal Pu source in this worker, and additionally indicate an approximate date of accidental Pu injection.

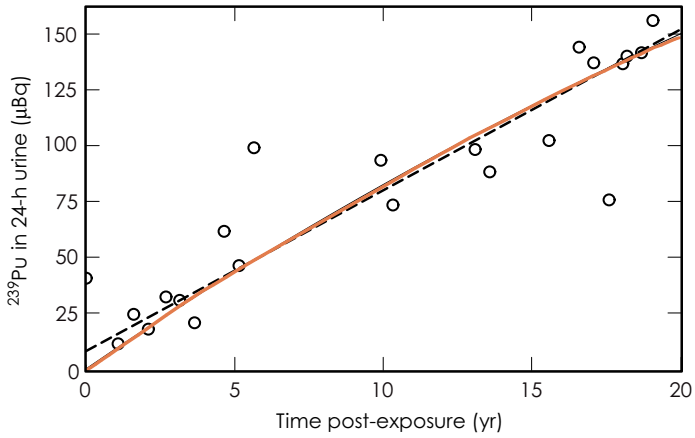

Elevated levels of urinary plutonium-239 (^{239}Pu) measured by accelerator mass spectrometry (AMS) analysis of archived material from a LLNL Pu worker (data points). Routine monitoring has never detected elevated levels in samples from this worker. Dashed line vs red curve compare best linear vs exponential-saturation fits, respectively, to data shown for times t after the estimated date of a previously unsus-pected internal Pu contamination event at $t \approx 0$ yr.

Our results during FY2001 have clearly demonstrated that AMS analysis of archived AS plates is directly applicable to occupational Pu risk management. We have thus demonstrated that this method can be used to better characterize human Pu-excretion biokinetics, and so facilitate applications of this ultrasensitive Pu-detection technology to important occupational safety and nuclear security goals of the broader DOE community—particularly in view of lower Pu-analysis costs using AMS compared to other methods with comparable Pu-detection sensitivity.

In FY2002, we will perform similar AMS analyses on archived AS plates pertaining to additional LLNL Pu workers and, using these data, fundamentally improve current biokinetic models of Pu excretion in humans.

Study of the ionization dynamics and equation of state of a strongly coupled plasma

R. Shepherd, P. Audebert, J. P. Geindre, J. Dunn, S. Moon, C. Iglesias, F. Rogers, P. Springer

MAIN TOC

Understanding radiation cooling of white dwarfs is important for estimating the age of star clusters. Because the majority of stars end their life as white dwarfs (e.g., our Sun), by knowing the number of white dwarfs as a function of brightness within a star cluster (and the brightness as a function of evolutionary track), one can infer the age of the star cluster. However, the age estimate is strongly dependent on understanding the internal cooling dynamics of white dwarfs. Much of the outer structure of a white dwarf consists of strongly coupled matter, with temperature regimes from 1 to 100 eV and densities between $0.5\rho_0$ and $3\rho_0$. Matter becomes strongly coupled when the potential energy of the particles becomes large compared to the kinetic energy. A thorough understanding of radiation transport through strongly coupled matter is necessary to understand the cooling of white dwarfs. Although an abundance of theoretical models exist for this regime, experimental data to test the models are scarce.

This project tests radiation transport models in strongly coupled matter by utilizing the unique capabilities of ultrashort-pulse lasers and fast x-ray detection pioneered at LLNL. The technique relies on the method of generating high-density, low-temperature plasma using ultrashort laser pulses (<1 ps). This project will be the first application of this technique to understanding energy-loss mechanisms in matter. If successful, this technique of studying radiation transport will support the Laboratory's national security mission by furthering our understanding of matter under extreme conditions.

During FY2001, we met two major milestones: we (1) built the hardware for the experiments and (2) performed the initial target characterization experiments using Fourier domain interferometry (FDI). Designing and building the experiment hardware required building and fabricating diagnostics and targets for the experiment, and making changes to the multibeam Comet facility where the experiments were to be performed. For our experiments, an air compressor was added for the FDI diagnostic and the three laser beams were rerouted for our geometry. Also, a large throughput optical delay line was added to achieve precise relative timing between the beams. All hardware was successfully installed and timing completed.

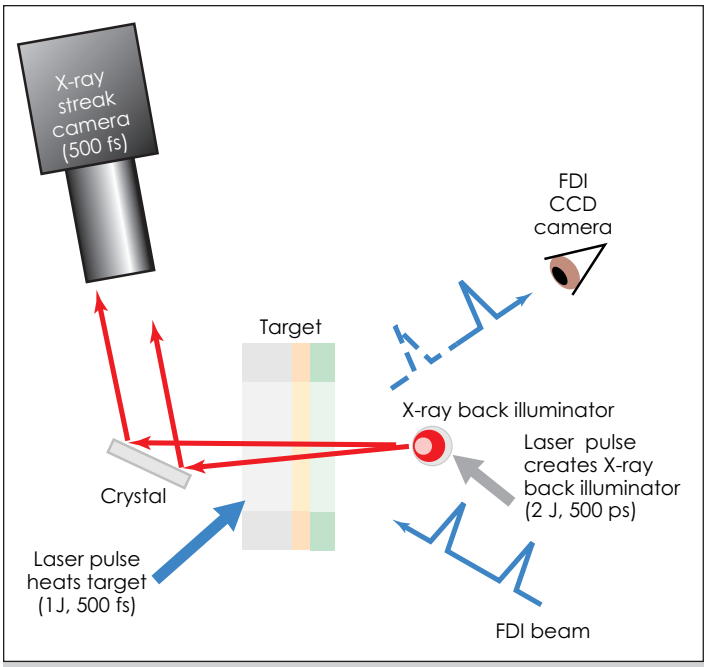

The layout for the experiment. The long-pulse laser creates the x rays (red lines)that are absorbed in the target while being heated by a short-pulse laser (blue arrow). The transmitted x rays are dispersed with a crystal and time-resolved with subpicosecond resolution using an x-ray streak camera. Simultaneously, Fourier domain interferometry (FDI) is performed by reflecting a pulse before heating and during heating to measure the relative fringe shift of the heated target.

The initial target characterizations were performed with FDI on untamped and tamped aluminum targets. The goal of the experiment was to verify the equation-of-state (EOS) information used in the simulations. Since the density and temperature are integral parts of the EOS, measuring the expansion velocity allows us to test the accuracy of the model used in the code. With simulations as a guide, targets were illuminated with laser intensities between 5×10^{14} and 5×10^{15} W/cm^3 at the Comet laser facility. The data are still being analyzed. However, initial results suggest that with a heating pulse intensity of 1×10^{15}, the plasma temperature for the untamped targets reaches roughly 40 eV after 1 ps while maintaining a density of approximately 3×10^{23} e/cm^3. This suggests a peak strong-coupling parameter, $\Gamma \approx 4$. Due to the rapid decrease in temperature, the strong-coupling parameter remains above 1 even after 10 ps. However, simulations suggest a substantial gradient is present after 4 ps but the tamped target will minimize the effects of the gradient. Tamped target data are still being analyzed.

For FY2002, we will characterize the long-pulse, laser-generated x-ray back-illuminator, back illuminate aluminum and selenium targets, and begin comparisons with code predictions for the x-ray absorption. Once completed, we will reconfigure the x-ray spectrometer to begin studying material of direct astrophysical interest (e.g., iron).

Space Science and Technology

Section 9

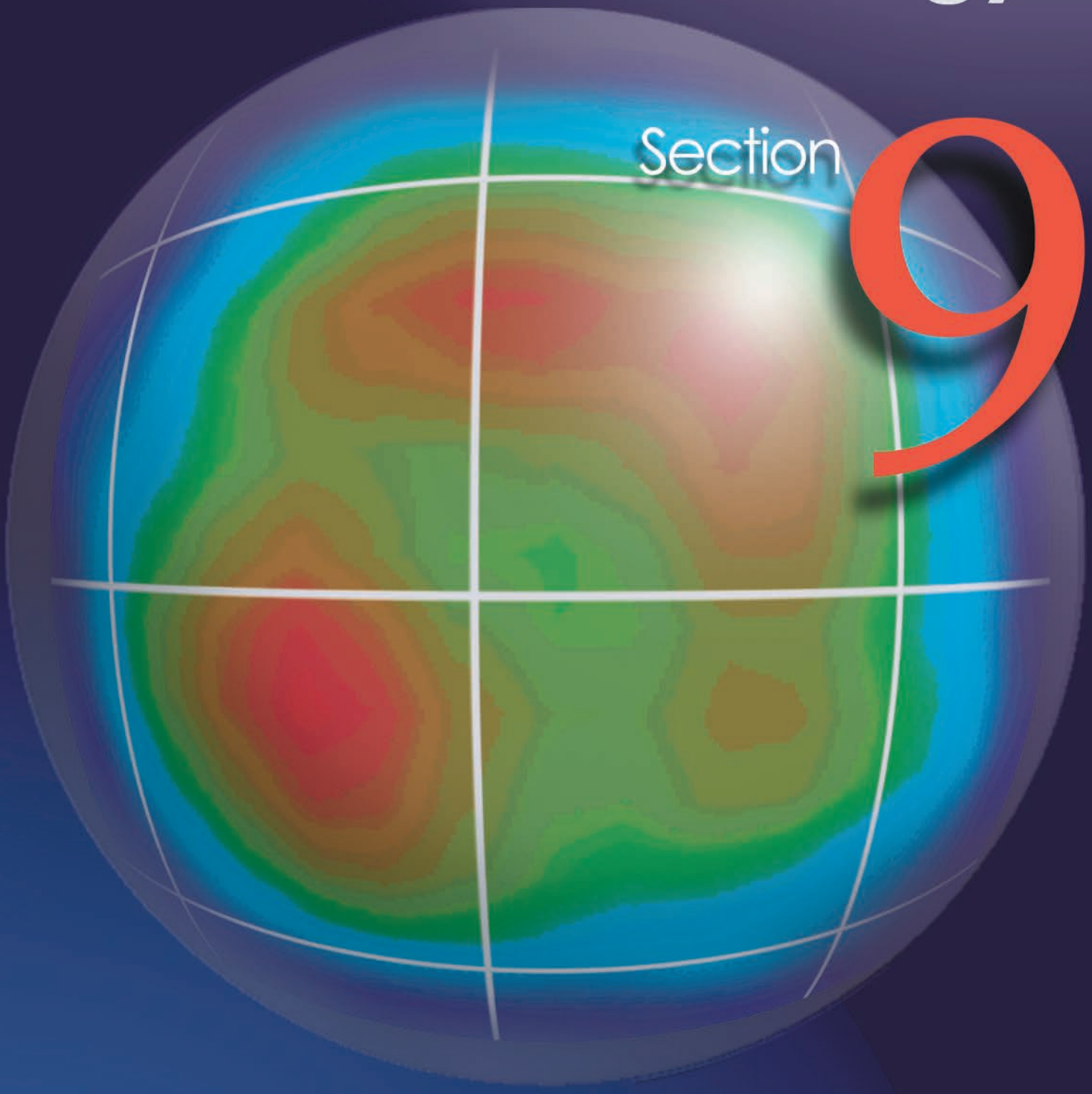

Section 9 Space Science and Technology

The size, shape, and composition of the Milky Way

K. H. Cook, P. Popowski

After decades of study, astronomers do not know the exact extent, mass, or make-up of the Milky Way. Most of the mass of Milky Way comprises some form of dark matter, thought to be distributed in a large, spherical halo made up of planets, brown-dwarf stars, black holes, or other massive compact halo objects (MACHOs) ranging from the mass of Mercury to solar masses. Because dark matter emits no detectable radiation, gathering information about dark matter presents an ongoing challenge for astronomers.

The goal of this project is to significantly improve our knowledge of the size, shape, and composition of the Milky Way and cosmic dark matter in general by using the gravitational microlensing effect to draw conclusions about the abundance of MACHOS along different lines of sight through our galaxy.

Microlensing of stellar light occurs when a MACHO passes very close to the line of sight between a distant star and the observer. The signature of the simplest microlensing is a characteristic magnification of the source star's light, which is time-symmetric with respect to the time of highest magnification. Even if all the dark matter were MACHOs, the probability of a detectable microlensing event is very low.

To detect microlensing events, we are exploiting our unique resource, the MACHO Lightcurve Database. The Database contains 7 terabytes of data from measurements of the light emitted by millions of stars in our nearest galactic neighbors, the Large and Small Magellanic Clouds (LMC and SMC). These measurements were conducted over an 8-yr period by the MACHO Project, an international collaborative effort between LLNL, six universities and two observatories to use the gravitational microlensing effect to measure the abundance of massive objects along different lines of sight.

The image-analysis techniques developed under this project will enhance LLNL's competencies in automated analyses and visualization of very large datasets and complex 2-D images. These capabilities are applicable in remote sensing for nonproliferation missions.

In FY2001, the MACHO Project released a number of exciting data analyses to determine the nature and masses of microlenses. On the basis of follow-up observations of our LMC microlensing events with the Hubble Space Telescope (HST), we constrained the locations of the source stars. Most of these stars are located in the LMC, which suggests that most microlenses are in the Galactic halo (see Figure).

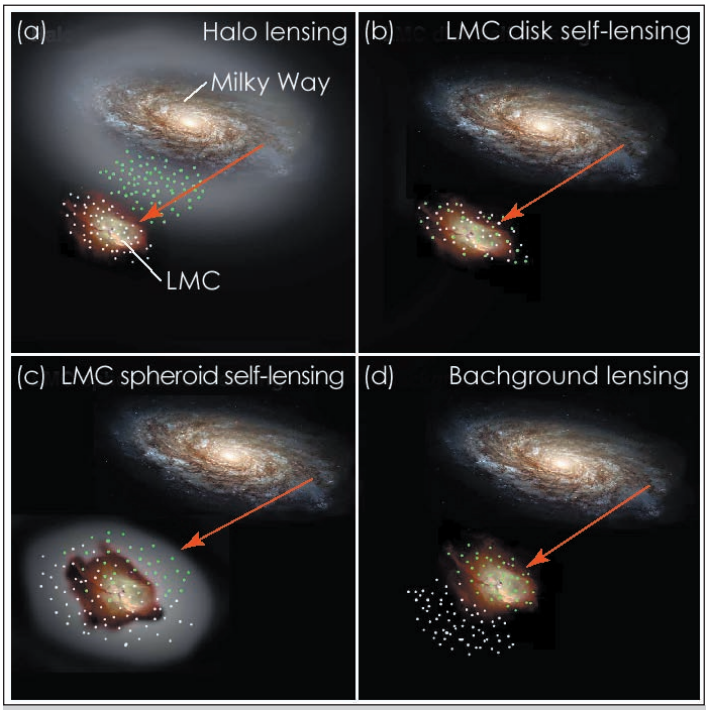

The Large Magellanic Cloud (LMC) galaxy, source star (white dots), and lens (green dots) placements in four microlensing models. (a) For halo lensing, the source stars are in the LMC and the lenses are in the halo; (b) and (c) for self-lensing, the source stars as well as the lenses are in the LMC disk or spheroid; (d) for background lensing, the source stars are behind the LMC while the lenses are in the LMC. The halo lensing model fits the data best.

Although we still do not know what type of objects dominates the lensing toward the LMC, we were able to directly detect one microlens. This lens is located in the Galactic disk. Using our multicolor HST images, the lens appears as a very red object extremely close to the line of sight to the magnified star. Using constraints from the microlensing fit and colors from HST, we concluded that this lens is a low-mass star.

On the opposite end of the mass spectrum, we identified several events along a line of sight toward the central regions of our galaxy that are likely due to a population of Galactic black holes. Such a population of black holes and other massive stellar remnants would explain the long duration of many microlensing events toward the Galactic bulge, which—on the basis of standard Galactic models—is not expected from normal stars. We had shown in FY2000 that when these long events are interpreted as being due to stellar remnants, the microlensing seen toward the Galactic bulge is consistent with all observational data and theoretical models.

During FY2001, we also identified a large number of high-proper-motion (HPM) stars in the crowded stellar fields we monitor. HPM stars appear to move with respect to the general star field because they are relatively near. Before this project, finding HPM stars was limited to searches in very uncrowded fields. The future National Aeronautics and Space Administration (NASA) Space Interferometry Mission (SIM) will be able to monitor the gravitational effect of these HPM stars on the field stars and directly determine the mass of the HPM stars—direct stellar-mass measurements are extremely rare.

Laboratory simulations of accretion-powered x-ray sources

M. E. Foord

The fundamental process for generating many bright x-ray sources in the universe is accretion. During the process of accretion, in-falling matter onto massive compact objects like neutron stars or black holes is heated and strongly radiates as the mass quickly decelerates and accretes onto the surface. Examples of accretion-powered x-ray sources include binaries and active galactic nuclei (AGN). Recently launched x-ray observatories—the Chandra X-ray Observatory (CXO) and the Newton X-Ray Multi-Mirror Mission (XMM-Newton)—are providing, for the first time, high-resolution spectral data from these objects. However, interpreting this unique high-resolution data requires developing better photoionization and spectral-synthesis models.

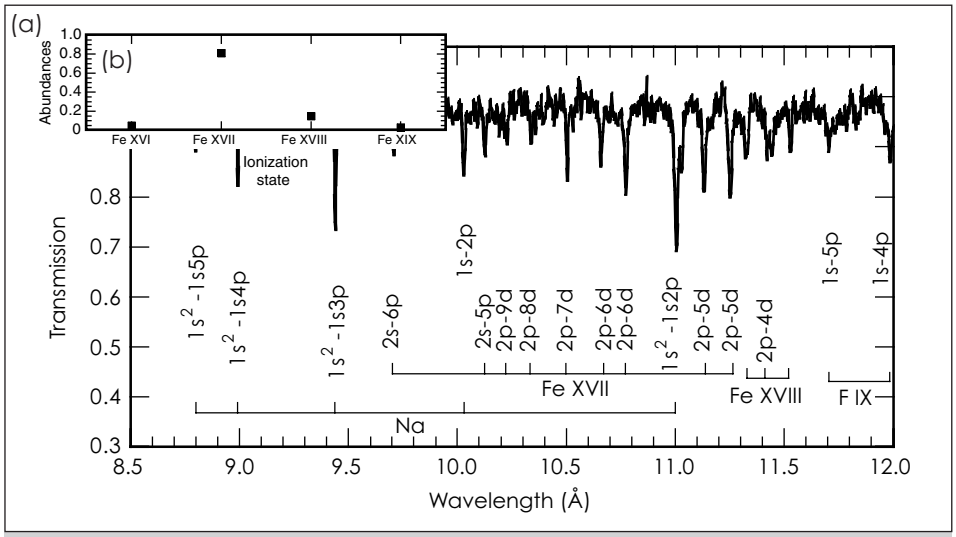

Spectral signature of a strongly photoionized plasma, showing (a) measured absorption features for L-shell iron (Fe) and K-shell sodium (Na) and fluorine (F) absorption features, and (b) the derived Fe ion-charge-state distribution.

In this project, low-density samples are strongly photoionized in the laboratory, allowing the simulation of conditions found near accretion-powered objects. Absolute measurements of the radiation field, conditions in the sample, and the resulting emission spectra allow these models to be tested in detail and improved where needed.

Our project builds on the experimental capabilities developed over many years for LLNL's Stockpile Stewardship Program and enhances the Laboratory's competence in x-ray spectroscopy, radiation modeling, and non-local thermodynamic equilibrium (non-LTE) physics, all important components for fulfilling the future requirements of advanced laser systems.

Recent improvements in Z-pinch technology now provide sufficiently high x-ray fluxes for reaching photoionization regimes of astrophysical relevance. In these experiments, we employed the Sandia National Laboratories (SNL) Z-pinch, which produces a 10-ns, 120-TW, 170-eV blackbody radiation source. A time-resolved, three-crystal, Johann x-ray spectrometer was developed for this project during its first year, and it has been used to obtain much of our spectroscopic data. This spectrometer was designed to simultaneously measure the spectral absorption of the pinch radiation through a sample along the line of sight (LOS) to the pinch as well as the spectral emission from a photoionized sample offset from the LOS. In these experiments, thin foils containing various materials such as iron (Fe), magnesium (Mg), oxygen (O), sodium (Na), and fluorine (F) are radiatively heated by the Z-pinch radiation; the foils subsequently expand to become highly photoionized, low-density plasmas. Emission and absorption spectra, as well as the electron temperature, density, and absolute x-ray flux from the pinch, are measured independently. Absorption spectra are used to determine the degree of ionization and the distribution of the charge states in the plasma.

Figure (a) displays absorption spectra measured during FY2001 from a photoionized plasma containing Fe, Na, and F. Analysis of the Fe spectra yields the ion charge-state abundances shown in Fig. (b). Time-resolved x-ray emission spectra were also obtained, and at year's end were being compared with an LLNL spectral-synthesis code. Analysis of the free-bound continuum edge of F VIII yielded an electron temperature near 35 eV, which is consistent with the low electron temperatures expected in a strongly photoionized plasma. In other experiments conducted at the end of FY2001, we obtained data using Mg and O dopants; these were also being analyzed at year's end.

Our work has led to a number of ongoing collaborations with astrophysical and atomic-physics groups around the world. For example, comparisons are underway with widely used photoionization codes XION, GALAXY, CLOUDY, and XSTAR. Preliminary comparisons between the codes showed substantial differences in the predicted degree of ionization. More recent comparisons of the data with GALAXY still show substantial differences. We are also using other codes [R-Matrix and the Hebrew University—Lawrence Livermore atomic code (HULLAC)] to study the effects of collisional processes on excited-state populations and the resulting emission spectrum. To provide the necessary data to benchmark and improve our capabilities to model strongly photoionized plasma, we plan to continue these types of experiments at SNL and in the future on the National Ignition Facility.

An imaging Fourier transform spectrometer for astronomy

R. Wurtz, C. L. Bennett, S. Blais-Ouellette, J. R. Graham, K. Cook, E. H. Wishnow

The astrophysics community is beginning to exploit data-mining of vast datasets. To date, datasets available for mining have been a patchwork of imaging and spectroscopy. Experience has shown that the most efficient use of the photons striking a telescope's aperture would be to produce true 3-D imaging—a hyperspectral data cube, consisting of two spatial dimensions and one spectral dimension—that could later be investigated in detail. Although there is no shortage of new ideas for acquiring these datacubes, most techniques are still in their infancy.

LLNL's pioneering, recently-developed, hyperspectral infrared imaging spectrometer (HIRIS) now offers the greatest promise for obtaining astronomical hyperspectral imaging in the immediate future. HIRIS obtains datacubes by means of an imaging Fourier transform spectrometer (IFTS) in the thermal infrared. This project advances the skill and knowledge base for the use of IFTS for remote sensing in support of NNSA's nonproliferation program.

In this project, we are extending the HIRIS technique to image faint objects that are emitting visible light. Our IFTS produces a spectrum for every spatial pixel. Our instrument has generated significant interest among astrophysicists and is attracting collaborators. The success of this project will demonstrate the viability of IFTS for astronomy and lead to the implementation of IFTS for first-rank ground-based and space-based optical and infrared telescopes.

During FY2001, we refurbished the interferometer at the heart of the instrument. Our first test of the instrument on a telescope in April 2000 showed that the LLNL-designed optical sections worked well but that the servocontrol system supplied by our industrial collaborator required a serious redesign in order to function in any orientation and while exposed to the out-of-doors at night. We modified and replaced hardware and software, eventually demonstrating, at the 1-m Nickel observatory on nearby Mount Hamilton, that the IFTS could perform in the adverse conditions encountered at astronomical observatories. During this same period, we also made our off-the-shelf charge-coupled device camera systems more rugged.

The instrument-development phase culminated in June 2001 with two commissioning runs of 3.5 nights of total observation time at the 3.5-m telescope at the Apache Point Observatory (APO) in New Mexico. One of our collaborators, Professor Christopher Stubbs of the University of Washington, is the Telescope Scientist at APO. We successfully operated the IFTS in several modes and under several observing conditions. Although no new science was acquired, we demonstrated the power of IFTS. The Figure shows an image of a well-studied emission nebula, the Ring Nebula. The original dataset contains 220 distinct color planes, enabling us to determine the material composition and energy density of the gaseous envelope expelled by this dying star. We now plan regular observation runs at APO to perform scientific investigations that were never before possible.

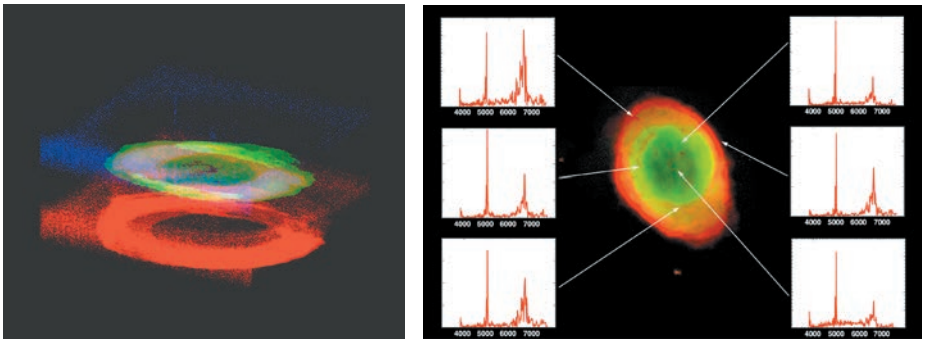

Two views of a spectral-spatial datacube of the Ring Nebula, M57, obtained with the Livermore IFTS at Apache Point Observatory. Figure (a) shows the cube in 3D, with the increasing spectral frequency along the vertical axis. Each 3-D pixel in the cube is color-coded with its true color. Figure (b) is a three-color image created from the spectral data, and the spectra associated with six selected image pixels.

Final projects involving data reduction and interpretation are underway. For example, we found that conventional methods of 2-D data visualization are inadequate for understanding the information content in datacubes. On example is the use of color, which has been historically used in "false-color" mode to indicate intensity. For viewing a datacube, color can be keyed instead to spectral bin—the actual color—but transparency must also be assigned to the 3-D pixels so that the whole cube can be examined at once.

As FY2001 proceeded, more collaborators were drawn to this project. LLNL is now the premier institution for collaborating on astronomical IFTS.

Primitive planetary systems via the Keck Telescope

B. A. Macintosh

MAIN TOC

One of the most fundamental questions in astronomy is the existence of other planetary systems like our own—those with potentially habitable planets. Although many other planetary systems have now been detected through indirect methods, all are quite different from our Solar System. These other extrasolar planetary systems have massive Jupiter-like planets occupying the inner part of the system, the same place Earth occupies in our own Solar System. It is unclear which type of planetary system is more common; current theories of star and planet formation have not yet found a compelling explanation.

This project uses the adaptive optics (AO) system on the 10-m W. M. Keck Telescope, which represents the most significant advance in astronomical capabilities since the launch of the Hubble Space Telescope, to study the formation and evolution of planetary systems like our own. The angular resolution of the Keck AO system allows us to study processes taking place in young stellar systems on distance scales comparable to that of our Solar System. This project enhances LLNL's competency in AO, a technology relevant to national security applications. Being at the forefront of a highly visible and exciting area of scientific inquiry, this research will also attract new talent to LLNL.

We are studying young stellar systems in the process of formation, especially in the one-million-year-old Trapezium region in Orion, which represents the closest large-scale star formation site to the Sun—approximately 1300 light yr away. Our AO survey of stars in the Trapezium, carried out in FY2000 and FY2001, is providing evidence that star formation on such massive scales represents the dominant mode of star formation in our galaxy and produces many fewer planet-disrupting binary systems than the smaller but closer star-forming regions studied to date. We have also imaged several of the Orion proplyds—protoplanetary disk envelopes surrounding young stars that are being disrupted by intense radiation from nearby supermassive stars (Figure 1).

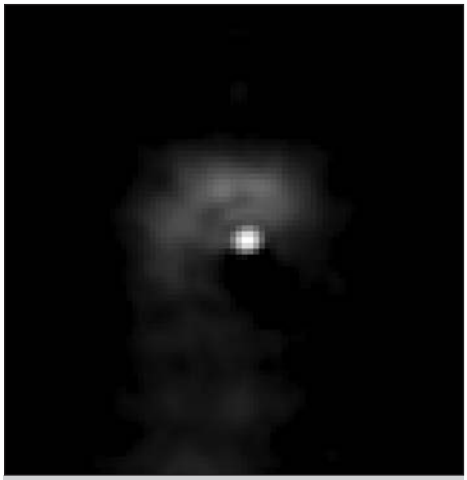

Keck adaptive optics image of a protoplanetary disk envelope surrounding a young star in the Trapezium region in Orion.

In addition to studying extremely young but distant stars, we are imaging older (10 million yr) but closer (150 light yr) stars in regions such as the TW Hydrae association. Together with our collaborators at the University of California, Los Angeles, we are imaging these stars to study a young brown dwarf, an object intermediate between stars and planets. This brown dwarf orbits a binary star system, and will ultimately provide the first age and mass determination of such an object.

At these young ages, Jupiter-sized planets will still be warm enough (1100°C) to emit infrared radiation. Though they will still be much dimmer than their parent stars, their infrared emission is much brighter than the sunlight reflected by mature cool planets like Jupiter. We carried out follow-up observations of a much dimmer object that could be such a planet in a distant orbit around a TW Hydra star, in an attempt to use its motion over several years to distinguish a true companion from a chance background star. Our most recent observations, in February 2001, are beginning to indicate that this tantalizing companion is merely a background star. Nonetheless we have demonstrated that Keck AO has the capability to detect companions up to a million times fainter than their parent stars, showing that these techniques could lead to the first true image of a planet outside our Solar System.

Our group has been using the Keck telescope to achieve the highest contrast ratios ever. We have been modeling the performance of the Keck AO system to understand how small imperfections in the primary mirror scatter light into patterns that can hide faint extrasolar planets. Our models verify the main sources of scattered light and demonstrate the ability to understand the interactions between optical aberrations and AO systems. Using these models, we can devise observing strategies to minimize such effects and improve the design of future cameras and AO systems optimized for planet detection or for fine control of wavefront errors in AO applications for national security missions.

Planetary interiors in the laboratory

R. Chau

The recent discovery of extrasolar planets whose masses are comparable to those of the giant planets in our own Solar System has focused attention on the nature of giant planets such as Jupiter and Uranus. To understand the formation and properties of these planets, we must determine the composition and nature of the hot, dense fluids within their interiors. For example, the electrical conductivities of planetary materials is needed to understand the generation of magnetic fields. Unfortunately, the extreme conditions within the planets and the large distances from Earth make direct probes of the planetary interiors impossible; ground-based observations and space probes provide only limited information.

In this project, we are using gas-gun drivers to generate—for a short period of time—high pressures (>300 GPa) and temperatures (>10,000 K). We can subject planetary materials to conditions found deep within giant planets, upwards of 7000 K and 200 GPa, and measure their electrical transport properties. This unique set of capabilities exists only at LLNL. Our project is the only one of its kind to provide the necessary experimental data on planetary materials under conditions actually found within giant planets.

This project builds on the experimental capabilities developed for stockpile stewardship and will enhance LLNL's competency in shock physics, an area very important to the DOE's national security mission. Planetary materials such as hydrogen, methane (CH_4), and water (H_2O) are also important to LLNL's work in inertial confinement fusion and energetic materials.

During FY2001, we completed electrical conductivity measurements on all the simple planetary fluids. Thus far, we have focused on understanding the behavior of the elemental components of basic molecular constituents. During FY2000, we found that fluid N_2, O_2, and H_2 all become metallic under high pressures and temperatures and can be explained universally with a simple model. Our preliminary results have been reported in *Physical Review Letters*.

In FY2001, we measured the conductivity of CH_4, which is a major component of Uranus and is predicted to dissociate. We found initially that the conductivity of CH_4 was low and similar to that of polyethylene. However, CH_4 was observed to dissociate, presumably into hydrogen and carbon, after 80 to 100 ns (see Figure). The dissociation was observed by the rapid decrease in the electrical resistivity. This result implies that any primordial CH_4 in the deep interior of Uranus or Neptune will have dissociated into hydrogen and carbon and also gives a time scale for the chemical reaction.

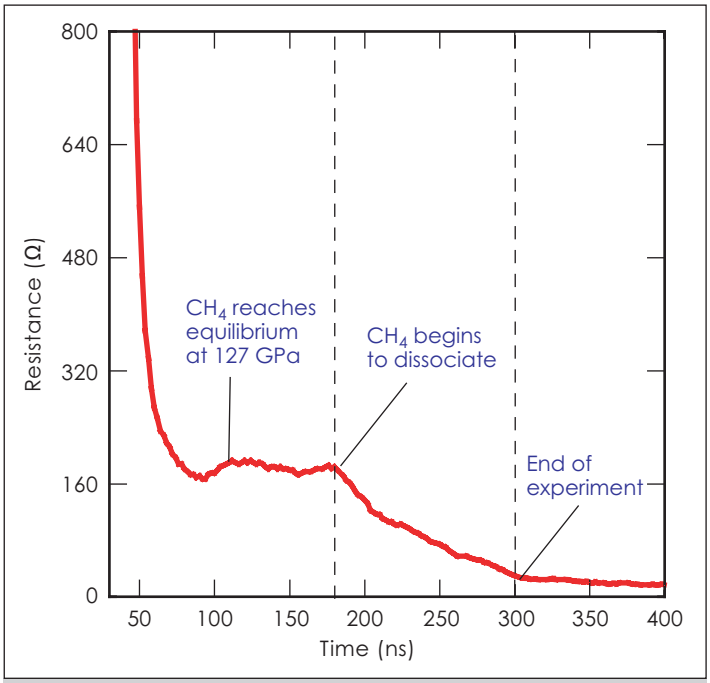

Resistance vs time for methane (CH_4) shocked to 127 GPa. The decrease in the resistance of the CH_4 after 200 ns results from dissociation of CH_4 into hydrogen and carbon.

Our goal for FY2002 is to address the question of mixtures of H_2O, CH_4, and ammonia (NH_3) at high pressures and temperatures. The chemistry between different atomic species will have a strong effect on the state of the fluid and the equation of state. The primary mixture will be "synthetic Uranus," which is representative of the expected composition of the deep interior of Uranus. Our measurements will provide a benchmark electrical conductivity for modeling planetary magnetic fields and will give insight into the effects of chemistry.

Nearby active galactic nuclei

C. E. Max, D. Gavel, B. Bauman, D. Pennington, W. van Breugel, J. Patience, G. Canalizo, W. de Vries

In some galaxy cores, a region well less than a cubic parsec in size—known as the Active Galactic Nucleus (AGN)—emits up to 10,000 times a normal galactic luminosity. The high luminosity, small volume, and nonthermal spectra of AGNs have led to the hypothesis that accretion onto supermassive black holes (mass more than a billion times that of the Sun) provides their energy source.

For more than 30 yr, DOE laboratories have researched the physics of black holes. DOE computer simulations were the first to describe how black holes form. However, only recently has direct evidence for the existence of supermassive black holes emerged via astronomical observations with very high spatial resolution.

In this project, we are using adaptive optics (AO) and laser guide stars—developed using LLNL technology on telescopes at Lick and Keck Observatories—to measure properties of these AGNs. To date, we have exploited the very high spatial resolution made possible by AO (e.g., 0.05 arcsec at the Keck Observatory) to obtain images of the central few hundred parsecs in 11 AGNs, and detailed spectra for two of these.

Adaptive optics technology is now used witin virtually all new DOE high-power lasers and is important to other national security applications that involve high-power lasers propagating through the atmosphere. This project enhances LLNL's and the DOE's expertise in AO, precision optics and controls, and exploits these technologies for studies of high-energy astrophysical phenomena.

Figure (a) shows a Keck Telescope AO image of the nucleus of Cygnus A, the most powerful nearby AGN, at a wavelength of 2 μm. This image, taken during FY2001, shows a bright, point-like source (size <40 parsecs) in the region very close to the central black hole. The black hole itself is too small to be resolved here. Also seen is a V-shaped emission region below and to the left of the black hole, and a fainter V-shaped region above and to the right. These "ionization cones" appear to correspond to gas illuminated by intense radiation from very close to the black hole. In comparison with Fig. (b), taken at the same wavelength with the Hubble Space Telescope, AO on a ground-based, 10-m-diam telescope produces more spatial detail than the 2.4-m-diam space telescope.

Figure (c) is a cartoon of the inferred AGN geometry. The black hole (tiny black dot in the center of the cartoon) is thought to be surrounded by an opaque toroidal disk of gas and dust. Intense radiation from very near the black hole illuminates surrounding gas in two cone-shaped regions above and below the opaque disk—it is obscured in the plane of the disk. The V-shaped emission corresponds to what would be observed when the ionization cones are viewed from the side. In FY2002, we will enlarge our AGN sample and make quantitative models for our spectral data.

At Lick Observatory, during FY2001 automation and engineering improvements in laser operation and in the AO system made it possible for astronomers from throughout the University of California to participate in laser guide star astronomical observations. Performance of the Lick laser guide star AO is now the best in the world. In FY2002, we will incorporate, at Lick, innovations developed for the Keck laser, and will finish adapting our image-processing algorithms for use with the laser guide star.

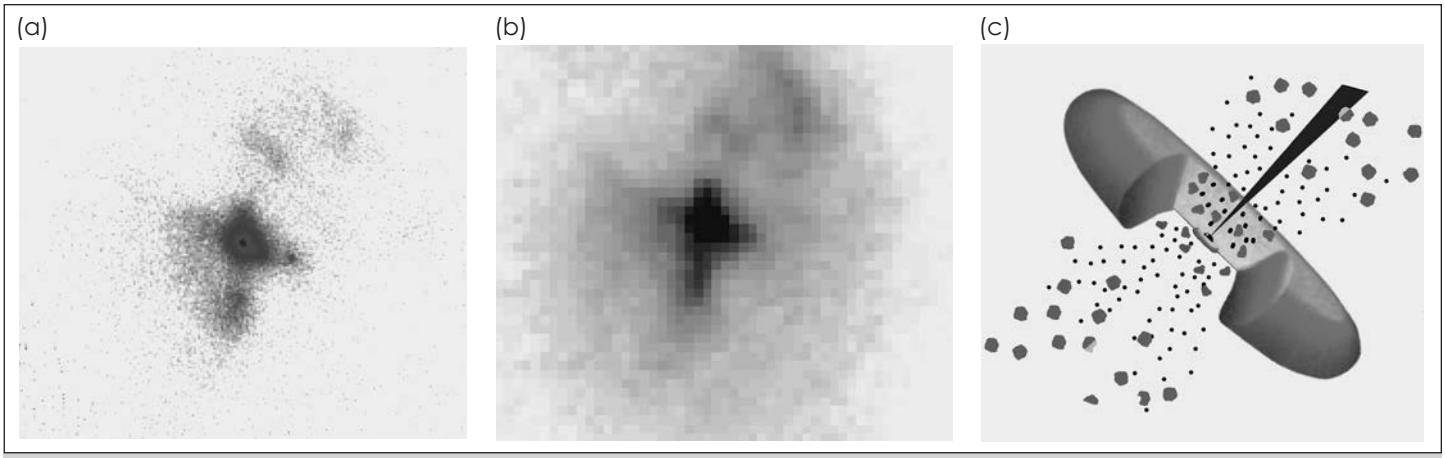

The active galactic nucleus (AGN) at the core of Cygnus A, seen in infrared light: (a) an adaptive optics (AO) image at Keck Observatory, and (b) a Hubble Space Telescope image. The cartoon in (c) shows the opaque torus and illuminated ionization cones inferred from (a) and (b).

Surveying the outer Solar System with robotic telescopes

S. Marshall, K. Cook, R. Porrata

The region of the solar system beyond the orbit of Neptune has become an area of increasingly active research since 1992, when the first detection of planetary material was reported. Today over 400 members of a newly discovered disk-like population of planetary remnants, called trans-Neptunian objects (TNOs), have been cataloged in this region. Now known as the Kuiper Belt, the region contains preserved clues about the early Solar System and about planet formation in general. The Kuiper Belt is the source reservoir of short-period comets and hence determines the rate and threat of comet collisions with the Earth. The distribution of orbits, sizes, and physical properties of this population are rich probes of planetary system physics.

The search for TNOs is difficult, because the objects are small, and the brightness of reflected sunlight declines rapidly. Modern surveys using sensitive charge-coupled devices (CCDs) have enabled the tremendous pace of TNO detections but they cover a limited area of the sky. Large TNOs are very rare while small TNOs are too faint to detect using reflected sunlight. The resulting size distribution of TNOs is limited to objects that are relatively bright but not too rare.

This project is developing two novel surveys for TNOs. These surveys provide data at both the bright (large) and faint (small) ends of the range of object sizes, where existing data are sparse. Our work extends LLNL's competency in advanced sensors, system integration, and processing large data sets for remote sensisng in support of nonproliferation missions.

Using an occultation technique that we have pioneered, the Taiwanese American Occultation Survey (TAOS) will probe for objects at much fainter magnitudes than any other survey, and will be able to detect objects as small as 2 km. The Massive Compact Halo Objects (MACHO) Telescope System in Canberra Australia will be used to probe for objects as large as Pluto. With it, we can search much larger areas (and hence detect much rarer objects) than is possible with existing CCD-based surveys.

The TAOS project is making progress toward the installation of four telescopes at Lulin mountain in Taiwan. Two of the TAOS telescopes, which are currently at LLNL, are being used to develop and test the various hardware and software facets of the survey system. New CCD cameras, delivered during summer 2001, are being integrated into the system. The system will begin routine operation in FY2002.

The large-object TNO survey on the MACHO telescope started taking data in January 2000, as work began to automate the telescope. By the end of FY2001, useful 3-epoch observations covering approximately 1700 square degrees near the ecliptic plane were obtained. Since March 2001, the incoming data stream has been processed by our photometry pipeline and automatically placed into a photometry database. The next stage of the pipeline searches for objects that are present in only one of the first or second epochs. These objects then are placed in candidate lists. By applying a set of filters to these candidates, we will choose objects that warrant further investigation. By matching up objects in epochs 1 and 2, and predicting positions in epoch three, we will obtain a final candidate list. These final objects will then have orbits fitted and follow-up observations planned. These results will be published during 2002.

Adaptive optics imaging and spectroscopy of the Solar System

S. G. Gibbard, B. Macintosh, C. E. Max, D. Gavel

The goal of this project is to observe planets and satellites in our Solar System and to compare them to each other and to the Earth. With this in mind, we are using the adoptive optics (AO) system and the near-infrared spectrograph (NIRSPEC) installed at the Keck Observatory to observe Solar System bodies with interesting atmospheric or surface features and time-variable behavior. We are then using simulations to interpret the results of our observations.

We are studying weather on the planets Uranus and Neptune and on Saturn's moon Titan—all of which have methane-rich atmospheres and complicated atmospheric dynamics. We are also investigating the largely unknown surface of Titan, where methane photolysis products may rain down to the surface and form "lakes" or "seas" of liquid hydrocarbon not seen on any other Solar System body. On Jupiter's moon Io—the most volcanically active body in the Solar System and only place other than the Earth where we can make real-time observations of volcanic eruptions—we are observing massive volcanic outbursts as they occur.

This project is aligned with several of LLNL's core competencies, including astrophysics, space science and technologies, information science and technologies, and advanced detectors and remote sensing. It draws together specialists in planetary science, atmospheric modeling, AO, image processing, and information science and technologies. We are among the first to use the updated AO technology at the Keck Observatory; this spectacular new science is generating much positive publicity for LLNL.

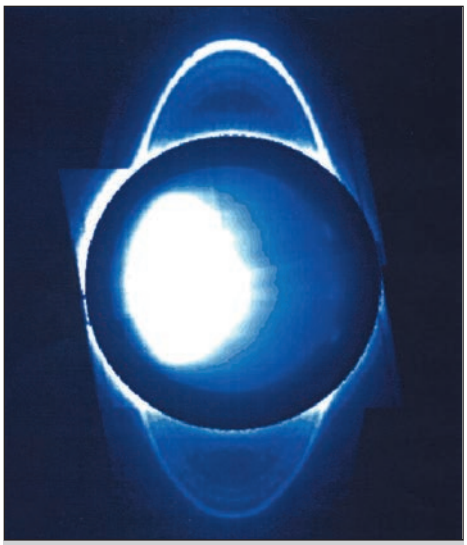

Infrared adaptive optics (AO) image of Uranus and its rings taken at the Keck Observatory. This is the first ground-based detection of the inner rings.

Our observations of Neptune during FY2001 showed a complicated cloud structure with vortices and wavelike motions that indicate complex atmospheric dynamics. In observing Titan in special, atmosphere-probing filters, we observed an infrared- (IR-) bright "polar hood" that had not previously been seen at IR wavelengths. Our images of Uranus (Figure) provided the first ground-based detection of that planet's inner rings.

During FY2001, we also observed the intriguing, oddly-shaped asteroid 216 Kleopatra. By modeling the data, we are able to reconstruct the asteroid's shape, which places constraints on its composition and formation history.

The planets Neptune and Uranus are similar in size and composition but very different in atmospheric dynamics. To understand the vertical structure and time evolution of these planets' atmospheres, during FY2001 we developed and began using a new radiative-transfer model. Because Saturn's moon Titan has an atmosphere similar to the upper atmospheres of Neptune and Uranus, its atmosphere can be modeled using a modification of the same code. We also began modeling the volcanic eruptions on Io. Our modeling of these eruptions seeks to understand the size, morphology, and temperature of these events.

In FY2002, we will continue our observations with the Keck AO system. To obtain quantitative information on the atmospheres of Titan and Neptune, we will increase our focus on radiative-transfer models. To obtain quantitative estimates of the brightness of each ring, we will also continue our modeling of the Uranus ring structure. By studying the dynamic behavior of cloud features on Neptune, we will attempt to connect the behavior of that planet's upper stratosphere to events occurring deeper within its atmosphere.

Constraining nucleosynthesis models: Mapping titanium-44 in Cassiopeia A

W. W. Craig, M. Devlin, K. Gunderson, P. Pinto, S. Woosley, K. Ziock

Supernovae produce and disseminate most of the elements in the universe. Supernova explosions are also among the most energetic in the universe, and the amount of light they emit has recently been established as an extremely sensitive measure of the size and geometry of the universe.

The study of supernova remnants using the light from radioactive isotopes has long been a goal of astrophysics and is now recognized as one of the highest priority scientific objectives for high-energy astrophysics in the next decade. Radioactive titanium-44 (^{44}Ti) (half-life of 52 yr) is perhaps the most important isotope available for the postmortem analysis and study of the events that occur during a supernova. This element is produced at the boundary between the material ejected during the explosion and the material that falls back into the neutron star or black hole left behind when a massive star explodes; its distribution is an ideal diagnostic of the details of the supernova event.

Cassiopeia A (Cas A), the remnant of a supernova that occurred 300 yr ago at a distance of 9000 light yr, is an ideal object in which to study ^{44}Ti. Cas A has been the subject of intense study over the last 20 yr because its ^{44}Ti emission is expected to be strong due to its age and proximity to the Earth. Modeling programs have made great progress and have made very specific predictions of the ^{44}Ti mass fraction and its spatial distribution in Cas A (see Figure). To make the crucial next step in our understanding of supernovae we must now actually measure and make the first-ever map of the ^{44}Ti distribution in a remnant; this is the ultimate goal of our efforts under this research project.

Our work builds on decades of LLNL expertise in supernova modeling and will provide the first true experimental verification of the details of these models. The observations will offer a direct path to validation of explosive nucleosynthesis and mixing models. These models are of particular importance because explosions of Supernovae produce a great many of the isotopes heavier than oxygen. The optics that make the observations possible will directly benefit LLNL's national security mission in the area of remote sensing from airborne platforms.

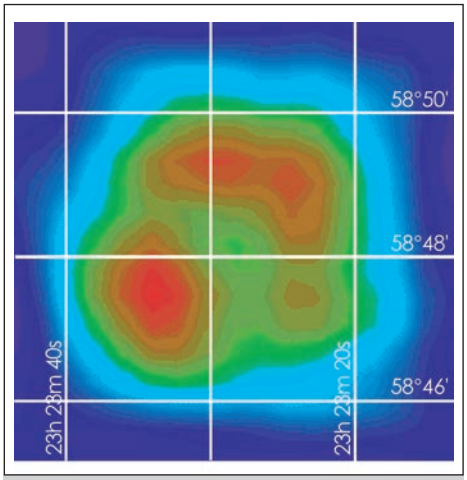

Simulation of a possible distribution of titanium-44 (^{44}Ti) ejected in the supernova Cassiopeia A (Cas A). Such a map would allow modelers to determine key details about the original supernova explosion. The High-Energy Focusing Telescope will probe the spatial distribution of ^{44}Ti in Cas A with unprecedented sensitivity and angular resolution.

Our observations of Cas A will be made possible by a new generation of instruments, under development, which have the potential to perform sensitive measurements of nuclear line emission for the first time. Of these new instruments, only the High-Energy Focusing Telescope (HEFT) experiment, led by California Institute of Technology will have the angular resolution required to measure the Cas A ^{44}Ti distribution.

The ^{44}Ti observations we propose would be impossible using the originally planned HEFT platform. These observations require a very long exposure time and unprecedented pointing stability for the gamma-ray telescope. Neither the 24-h flight nor the 10-arcsecond pointing required for a Cas A map was possible with the original HEFT gondola design. The pointing system lacked the crucial daytime tracking ability and was limited to no better than 30 arcsecond pointing performance. Our goal is to completely redesign and build a new kind of gondola to improve the pointing accuracy by a factor of 3 and to develop a system to permit accurate daytime pointing by designing and building an extraordinarily sensitive dual-camera daytime star-tracking system.

During FY2001 we built and performed initial testing on the balloon gondola that will support the HEFT telescope. Engineering tests showed the structure to be very stiff with an overall flexure of less than 0.001 in. throughout the 17-ft-high gondola under flight-like loads, a critical requirement for the 10-arcsecond tracking goal. We have modeled, designed, and are now testing a star-tracking system (a sensitive set of cameras with multistage 10-ft-long baffles to block scattered solar radiation) capable of observing stars during a daytime flight.

In FY2002 we will complete construction of the gondola and will establish 10-arcsecond tracking capability in a flight configuration. The star tracker will be field-tested and the final flight models built and integrated. We will also complete modeling of supernovae that will guide the observation during the planned FY2003 flight.

Spectroscopy of shock-compressed deuterium

N. Holmes, G. Collins

The properties of shock-compressed hydrogen are currently an area of intense scientific interest. At extremely high pressures, near 100 GPa, the Hugoniot function is still controversial. A sound understanding of deuterium (D_2) is important for planetary interiors and inertial confinement fusion. Our ability to understand shocked molecules has applications ranging from high explosives to the elimination of weapons of mass destruction containing chemical or biological agents. The results of this project also relate to another LDRD project (01-ERD-017) on the origins of life on this planet.

In recent experiments to measure sound velocity in shocked D_2, we found that the optical properties are highly unusual at low shock pressures, 11 to 20 GPa, suggesting the presence of large, unpredicted, intermolecular interactions that significantly perturb electronic states of the molecule. In fact, we observed that the emission intensity of shocked D_2 increased as pressure and temperature decrease near 11 GPa, a behavior previously unseen in any other molecular or atomic system. Bulk property measurements such as equation of state, temperature, sound velocity, or electrical conductivity give no clues as to the reason for this unprecedented behavior, although we do find that the sound velocity at these pressures is anomalously high.

This project's goal was to study shocked D_2 with a range of time-resolved spectroscopic methods over the pressure range of 5 to 25 GPa to investigate the vibrational and electronic (i.e. optical) properties. By doing this, we hope to substantially increase our understanding of shocked molecular systems and D_2 in particular.

We are planning to use spontaneous Raman spectroscopy to observe the D_2 stretching vibration from 13 to 20 GPa, and absorption spectroscopy over the range 5 to 25 GPa in an effort to gain understanding of the intermolecular interactions and their influence on electronic states. These experiments will be done on a two-stage gas gun, with the goal of developing the techniques to the extent that the pressure range could be expanded to be used with laser-driven shock experiments. These would be the first experiments of their type.

We started this project in mid-FY2001. The main results of the work to date are preparation of the spectroscopy laboratory, procurement of optical and mechanical components, and prototype target designs for shock wave experiments. In FY2002 we will complete the experimental system to perform Raman spectroscopy. Initial bench tests will test the new target design using unshocked fluid nitrogen (N_2), followed by initial experiments in shocked N_2 and then D_2. We will also begin development of the absorption spectroscopy hardware.

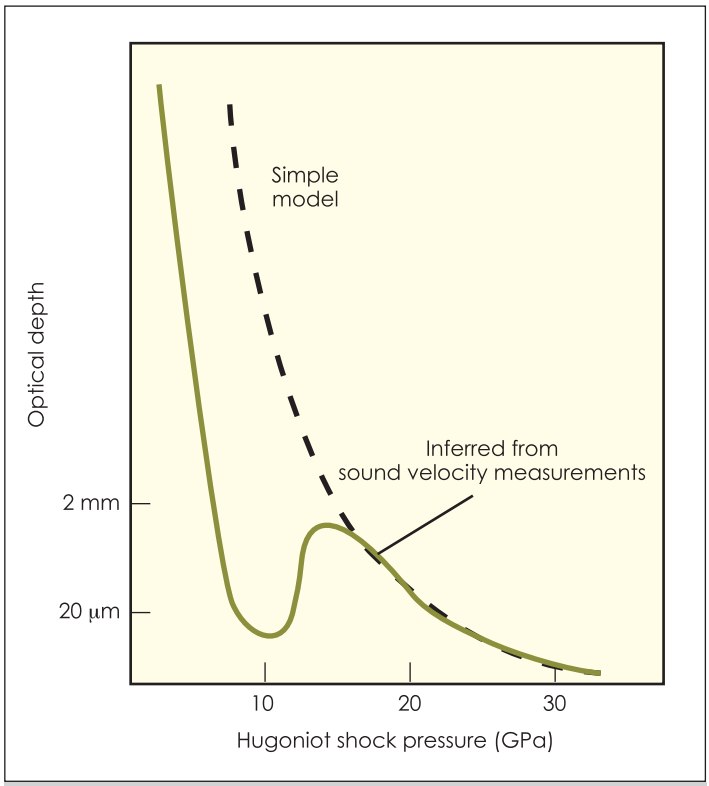

The optical depth of shock-compressed deuterium as a function of shock pressure, as inferred from sound velocity measurements.

Starburst galaxies

W. J. M. van Breugel

Starbursts—short periods (a few million years) of intense star formation in the central regions of galaxies—occur throughout our universe and signal important episodes in the life cycles of galaxies. The near-simultaneous explosions of millions of stars drive superwinds that enrich the intergalactic medium and may feed massive black holes triggering high-energy jets. In the early universe starburst galaxies provide the building blocks for larger galaxy systems. In the local universe they represent a large component of the total star-formation activity, and provide nearby analogs of their more distant counterparts. By studying starbursts and starburst galaxies we can learn more how galaxies form and what triggers high-energy activity from their central black holes.

This comprehensive research effort uses multiwavelength observations with ground-based telescopes to establish a possible causal connection between galaxy interactions, starbursts and the evolution of massive galaxies and active black holes. Our work provides a strong scientific rationale for continued development at LLNL of multiwavelength imaging devices (tunable filters) and capitalizes on LLNL-developed adaptive optics (AO) techniques. The observations of jets and starburst outflows in multiphase (hot and cold), dusty plasmas will be analyzed using hydrodynamics and radiation-pressure-dominated photoionization model simulations. This work may be used to define laser experiments to help validate complex hydrodynamic computer codes for stockpile stewardship. Our university collaborations include researchers from the University of California at Berkeley, Davis, and Santa Cruz; the University of Montreal, Canada; Leiden University, the Netherlands; California Institute of Technology; Australian National University; the University of Rochester, New York; and Cardiff University, U. K.

In our research we focus on the most luminous starburst galaxies, both near and far, to obtain the best data. To help us understand the starburst phenomenon we use narrow-band and tunable-filter emission-line imaging of jets and superwinds, and high-resolution AO imaging of their central galaxy morphologies.

Distant, ultraluminous starburst galaxies can be found through near-infrared (IR) identification of steep-spectrum radio sources found in large surveys such as the Faint Images of the Radio Sky at Twenty centimeters (FIRST) survey at the Very Large Array in New Mexico. These sources are thought to be powered by supermassive black holes and thus provide excellent beacons to study the connection between starburst and black-hole activity, and galaxy formation.

We discovered a gigantic emission-line nebula (see Figure) around a massive galaxy, which is less than one-billion-years old and still forming. The observations were made using a custom-made narrow-band filter and the world's largest (10-m) telescope at the W. M. Keck Observatory. The nebula is about 10 times the size of our own galaxy and shows a wealth of structure: a bright central region that is closely associated with a radio jet, and a one-sided cone and long filaments. The emission-line nebula signals the presence of a large reservoir of gas from which the galaxy may be forming. The nebula may be ionized by ultraviolet continuum radiation from a central, active black hole and massive young stars in the forming galaxy, or by shocks from their associated jet and superwind outflows.

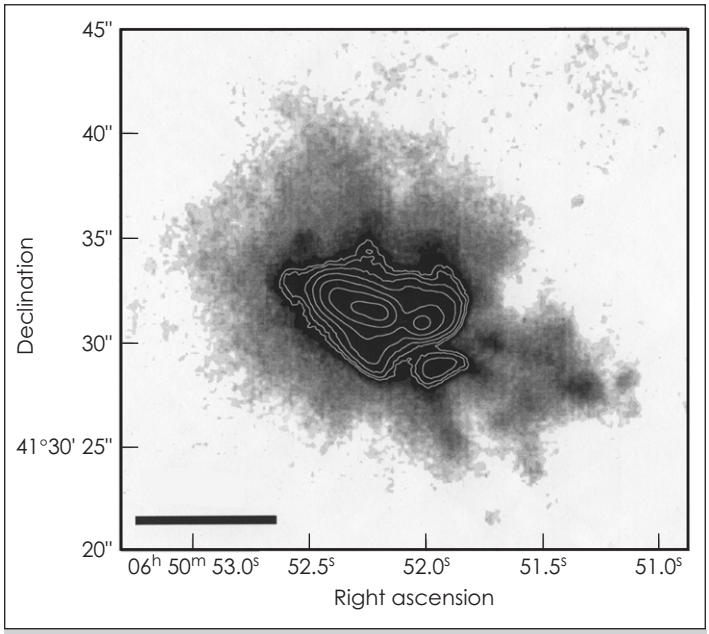

Huge Ly-a emission-line nebula associated with a massive forming galaxy. The filamentary structure may be caused by a starburst superwind emanating from the center.

In FY2002 we plan to (1) obtain observations of a few key targets to study the nature of the emission-line nebulae in detail, (2) begin numerical simulations of shocks in dusty plasmas to help interpret our data, and (3) undertake a narrow-band and tunable-filter survey to determine how common emission-line nebulae are. We believe that we have found evidence for over-densities of star-forming galaxies in some of our radio galaxy fields and will obtain spectra of these objects to determine whether they are at the same distance as the radio-galaxies. These data would provide important support for cosmological models, which assume that large structures, such as clusters of galaxies, are built up hierarchically.

Lithic astronomy: Absolute chronometers and correlated isotopic anomalies in meteorites

I.D. Hutcheon, R. Williams, F. J. Ryerson, K. D. McKeegan

One of the major discoveries in planetary science during the past 30 yr is the observation that major, rock-forming elements like oxygen, magnesium and silicon have isotope abundances that vary significantly within the Solar System. These isotopic anomalies are most pronounced in calcium-aluminum-rich, refractory inclusions (CAIs) in chondritic meteorites, the oldest known solid objects in our Solar System. While their existence is well documented, the origin of isotope anomalies remains highly controversial and the subject of intense scientific scrutiny. One model, the supernova trigger model, claims that nearby nucleosynthetic events could have seeded the solar nebula with exotic nuclei prior to gravitational collapse. Alternatively, according to the X-wind model, exotic species may have been produced within the solar nebula through irradiation by cosmic rays from the protosun. These two alternative models lead to radically different constraints regarding the time scales of gravitational collapse and the formation of solid materials within the solar nebula and, by extension, all planetary system around Sun-like stars. The goal of this project is to obtain new cosmochemical and cosmochronological constraints to distinguish between these two models.

This project, with the participation of collaborators from the University of California, Los Angeles, will develop a new radiochemical technique to determine the age and source of refractory inclusions in meteorites. The results of this research will allow us to constrain the collapse of the early Solar System and to provide better comparisons between astrophysical and cosmochemical models of the evolution of Sun-like stars. This project mass spectrometry uses special LLNL capabilities in mass spectrometry to pursue a forefront scientific problem. It will extend the Laboratory's competency in advanced instrumentation and nuclear chemistry, areas of importance to the stockpile stewardship mission.

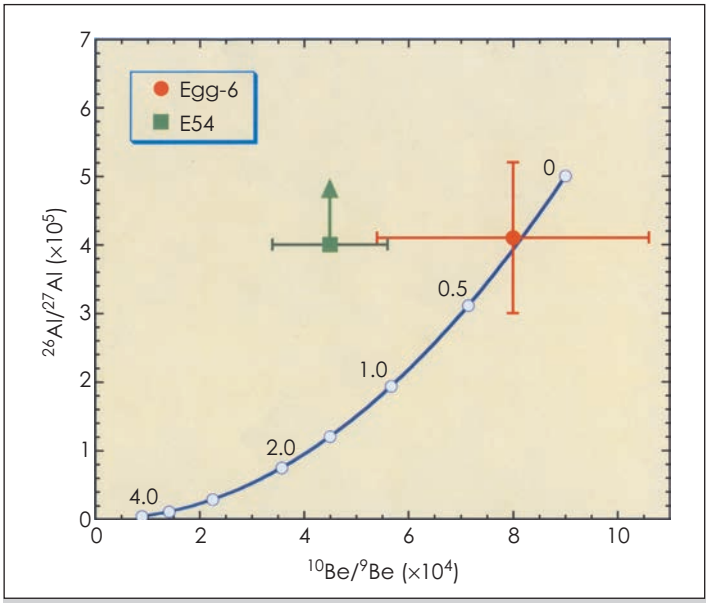

Correlated abundances of short-lived radionuclides plotted at 0.5 million-year intervals, predicted by the supernova trigger model (blue), compared to CAI data from meteorites Egg-6 and E54. The displacement of E54 implies that aluminum-26 (^{26}Al) and beryllium-10 (^{10}Be) were not produced at the same time.

Our approach takes advantage of the fact CAIs are host to the short-lived radionuclides calcium-41 (^{41}Ca), aluminum-26 (^{26}Al), and beryllium-10 (^{10}Be), and their respective daughter products: phosphorous-41 (^{41}K), magnesium-26 (^{26}Mg) and boron-10 (^{10}B). The short half-lives of these radionuclides (<1.5 million yr) makes them unique chronometers of events occurring during the first few million years of Solar System history.

During FY2001, using secondary ion microscopy (SIMS), we determined the B and Mg isotope compositions of two CAIs in primitive carbonaceous chondrite meteorites, Allende Egg-6 and Efremovka E54. Both CAIs show large excesses of isotopes ^{26}Mg* and ^{10}B*, which are produced by the in situ nuclear decay cascades of ^{26}Al and ^{10}Be, respectively. These new data confirm that CAIs formed very early in Solar System history, before ^{26}Al and ^{10}Be decayed significantly.

Our initial results suggest that the relative abundances of ^{10}Be and ^{26}Al in two CAIs are decoupled and do not behave in the self-consistent manner expected for a chronological interpretation. This behavior argues against the external nucleosynthesis model and in favor of a local irradiation origin for ^{10}Be and , by inference, the other short-lived radionuclides found in CAIs.

In FY2002 we will extend the study to include new CAIs and chondrules from primitive meteorites. Chondrules are more representative of normal solar system material than CAIs—up to 75% of the rock mass in the Solar System may have originated as chondrules. Understanding the time scale of chondrule formation is crucial to models of nebula evolution.

Appendix

Publications

The publications listed here report on LDRD research conducted in FY2001. Publications are listed by Section, and within each Section by project tracking code. The unique document number (beginning with UCRL) at the end of each publication reference indicates that the document was published under the auspices of the DOE in compliance with Contract W-7405-Eng-48.

Section 1
Advanced Sensors and Instrumentation

98-ERD-097

Ullom, J. N. et al. (2001). "Discrimination between bacterial spore types using time-of-flight mass spectrometry and matrix-free infrared laser desorption and ionization." *Anal. Chem*. **73**, 2331. UCRL-JC-141802.

99-LW-045

Berryman, J. G. (in press). "Time-reversal acoustics and maximum entropy imaging." *J. Acous. Soc. Am*. UCRL-JC-145156.

Borcea, L. et al. (2001). *Imaging and time reversal in random media*. UCRL-JC-145123.

Candy, J. (in press). "Time-reversal signal processing: An overview." *J. Acous. Soc. Am*. UCRL-JC-144863.

Candy, J. V. et al. (2001). *Dynamic acoustic focusing for noninvasive treatments*. UCRL-PROP-145316.

Chambers, D. H. (in press). "Spectrum of the time-reversal operator." *J. Acous. Soc. Am.* UCRL-JC-144905.

Chambers, D. H. (2001). *Time reversal for a general compact scatterer*. UCRL-JC-144392.

99-SI-016

Albala, J. S. (2001). "Array-based proteomics: The latest chip challenge." *Expert Rev. Mol. Diagn*. **1**(2), 145. UCRL-JC-144155.

Albala, J. S. (2001). "Beyond our genome: The application of proteomics in molecular diagnostics." *Expert Rev. Mol. Diagn.* **1**(3), 243. UCRL-JC-145286.

Albala, J. S., and I. Humphrey–Smith. (1999). "Molecular applications in proteomics." *Curr. Opin. Mol. Ther.* **1**, 680. UCRL-JC-136751.

Albala, J. S. et al. (2000). "High-throughput expression and purification of the human proteome." *J. Cell. Biochem*. **80**, 187. UCRL-JC-135571.

Venkateswaran, K., F. Milanovich, and R. Langlois. (2000). "Novel method for multiplex high-throughput flow cytometric analysis." *Cytometry Suppl.* **10**, 40. UCRL-JC-137432.

00-ERD-023

Cunningham, C. T., and R. S. Roberts (2001). "An adaptive path planning algorithm for cooperating unmanned air vehicles." *Proc. 2001 IEEE Conf. Robot. Automation*. UCRL-JC-140415-REV-1.

01-ERD-054

Reynolds, J. G. (2001). "Hydrophobic aerogels for oil-spill cleanup—synthesis and characterization." *J. Non-Cryst. Solids* **292**, 127. UCRL-JC-144150.

Reynolds, J. G. (in press). "Hydrophobic silica aerogels." *Recent Res. Adv. in Non-crystalline Solids* **1**. UCRL-JC-137059.

01-LW-036

Wilks, S. C. et al. (in press). "A test-bed for vision science based on adaptive optics." *Proc. SPIE*. UCRL-JC-145578.

01-LW-054

Cunningham, M. F. et al. (in press)."Dc and ac biasing of a transition edge sensor microcalorimeter." *AIP Conf. Proc.* UCRL-JC-143636.

001-SI-003

Levine, R. A. (2001). *A note on Markov Chain Monte Carlo sweep strategies.* UCRL-JC-145678.

Levine, R. A., and G. Casella. (2001). *Optimizing random scan gibbs samplers*. UCRL-JC-145679.

Newmark, R. N. et al. (in press). "Stochastic engine: Direct incorporation of measurements into predictive simulations." *Proc. Int. Groundwater Assoc. Meet*. UCRL-JC-145116.

Nitao, J. J., and W. G. Hanley. (2001). *Metropolis-type chains with finite memory and an averaging algorithm to promote mixing*. UCRL-ID-145680.

Nitao, J. J., and W. G. Hanley. (2001). *Use of averaged densities to promote mixing of the metropolis MCMC algorithm*. UCRL-ID-145681.

Section 2
Atmospheric and Geosciences

00-ERD-055

Bergmann, D. J., and P. Cameron-Smith. (2001). *^{7}Be and ^{10}Be tracer simulations using IMPACT, the LLNL atmospheric chemical transport model: An analysis of the sensitivity to source distribution and meteorological data*. Presented at the American Geophysical Union 2001 Spring Meeting. UCRL-JC-142953.

Cameron-Smith, P. J. et al. (2001). *Ensuring mass conservation in offline CTMs: The GMI approach*. Presented at the American Geophysical Union 2001 Spring Meeting. UCRL-JC-142943.

Chuang, C. et al. (2000). *Toward a new era of research in aerosol/cloud/climate interactions at LLNL*. UCRL-ID-140570.

Chuang, C. C. et al. (2001). *Global modeling of tropospheric aerosols by LLNL IMPACT and comparisons with field measurements*. Presented at the American Geophysical Union 2001 Fall Meeting. UCRL-JC-145282.

Dignon, J. C. et al. (2000). "Analysis of the non-linear effects of the diurnal cycle on the sulfer cycle." *J. Geophys. Res*. UCRL-JC-140339.

00-ERI-010

Masiello, C. A., O. A. Chadwick, and M. Torn. (2001). *Soil organic radiocarbon and mineralogy at two coastal California sites*. Presented at the December 2001 American Geophysical Union Meeting. UCRL-JC-146392.

Masiello, C. A. et al. (2000). *Effects of mineralogy on the storage rates of organic carbon classes across a soil chronosequence*. Presented at the 17th International Radiocarbon Conference. UCRL-JC-137642.

Masiello, C. A. et al. (2000). *Mineralogy and carbon storage across a soil chronosequence*. Presented at the American Geophysical Union 2000 Fall Meeting. UCRL-JC-137642.

01-ERD-024

Bradley, M. M. et al. (in press). "A national wildfire behavior prediction initiative: Full-physics models on supercomputers." *California's 2001 Wildfire Conf*. UCRL-JC-147051.

Hanson, H. P. et al. (2000). "The potential and promise of physics-based wildfire simulation." *Environ. Sci. Policy* **3**, 161. UCRL-JC-147078.

01-ERD-091

Rau, G. H. et al. (2001). "Enhanced carbonate dissolution as a means of capturing and sequestering carbon dioxide." *First Natl. Conf. on Carbon Sequestration* **1**, 1. UCRL-JC-143242.

01-ERI-009

Guilderson, T. P., M. Kashgarian, and D. P. Schrag. (2001). "Biogeochemical proxies in scleractinian corals used to reconstruct ocean circulation." *IAEA Tech. Document Ser.* **80/81**. UCRL-JC-141557.

Section 3
Biotechnology and Health Care Technologies

99-LW-004

McCutchen-Maloney, S. et al. (2001). *Chimeric proteins to detect damage and mismatches*. UCRL-ID-146788.

00-ERI-006

Bearinger, J. P., C. A. Orme, and J. L. Gilbert. (2001). "Direct observation of hydration of TiO_2 on Ti using electrochemical AFM: Freely corroding versus potentiostatically held." *Surf. Sci.* **491**, 370. UCRL-JC-143561.

Vogel, J. S., and P. G. Grant. (2001). "Attomole quantitation of protein separations with accelerator mass spectrometry." *Electrophoresis* **22**, 2037. UCRL-JC-141801.

00-ERI-009

Catlos, E. J. et al. (2001). "Geochronologic and thermobarometric constraints on the evolution of the main central thrust, central Nepal Himalaya," *J. Geophys. Res.* **106**, 16177. UCRL-JC-142115.

Dettman, D. L. et al. (2001). "Seasonal stable isotope evidence for a strong Asian monsoon throughout the last 10.7 Ma." *Geology* **29**, 31. UCRL-JC-136548.

Harrison, T. M. et al. (2000). "The Zedong window: A record of superposed tertiary convergence in southeastern Tibet." *J. Geophys. Res.* **105**, 19211. UCRL-JC-139079.

Ryerson, F. J. et al. (2001). "P-T-t path discontinuity in the MCT zone, central Nepal." *Geology* **29**, 571. UCRL-JC-136548.

Van der Woerd, J. et al. (in press). "Rapid active thrusting and river incision of the Tanghenan Shan, a consequence of transfer of sinistral slip from the Altyn Tagh Fault." *J. Geophys. Res.* UCRL-JC-134629.

Van der Woerd, J. P. et al. (in press). "Uniform post-glacial slip-rate along the central 600 km of the Kunlun Fault from $^{26}A1$, ^{10}Be, and ^{14}C dating of riser offsets, and climate origin of regional morphology." *Geophys. J. Int.* UCRL-JC-137203.

01-ERD-016

Mundy, C. J. et al. (2001). *Irradiated guanine: A car-parrinello molecular dynamics study of dehydrogenation in the presence of an OH radical.* UCRL-JC-145509.

01-ERD-045

Beernink, P. T. et al. (2001). *Development and use of in vitro expression systems for human proteomics.* Presented at the 15th Symposium of the Protein Society. UCRL-JC-144128.

01-LW-066

Mesleh, M. F. et al. (in press). "Marmoset fine B-cell and T-cell epitope specificities mapped onto a homology model of the extracellular domain of human myelin oligodendrocyte glycoprotein reveals potential sites antibody binding." *Neurobiol. Dis*. UCRL-JC-145179.

01-SI-002

Fitch, J. P., J. Ng, and B. A. Sokhansanj. (2001). "Matrix formulation of a universal microbial transcript profiling system." *Proc. IEEE Int. Conf. Acous., Speech, Signal Proc*. UCRL-JC-141175.

Fitch, J. P., and B. Sokhansanj. (2000). "Genomic engineering: Moving beyond DNA sequence to function." *Proc. IEEE* **88**(12), 1949. UCRL-JC-139410.

Fitch, J. P. et al. (2000). "Informatics and simulation in a genomic approach to understanding virulence." *Proc. IEEE Info. Tech. Applications Biomed*. UCRL-JC-140318.

Forde, C. E. et al. (2001). *Methods to identify transcription factors by SELDI mass spectrometry*. Presented at the Fifth International Symposium on Mass Spectrometry in the Health and Life Sciences: Molecular and Cellular Proteomics. UCRL-JC-144163.

McCutchen-Maloney, S. L. et al. (2001). *Cancer proteomics and differential protein profiling by SELDI mass spectrometry*. Presented at the Fifth International Symposium on Mass Spectrometry in the Health and Life Sciences: Molecular and Cellular Proteomics. UCRL-JC-144156.

McCutchen-Maloney, S. L. et al. (2001). "Proteomic analysis of *Yersinia pestis* by SELDI mass spectrometry." *Tri-Genome Conf. Abs*. UCRL-JC-142009.

Motin, V. L. et al. (2001). *A global view at the virulence process of* Yersinia pestis *through DNA microarray technology. (Une vue globale sur les processus de virulence de* Yersinia pestis *a travers les methods des puces a ADN.)* Presented at the International Congress on the Evolution and Paleoepidemiology of Infectious Diseases Plague: Epidemics and Societies. UCRL-JC-143678.

Murphy, G. et al. (2001). *Differential protein profiling in* Yersinia pestis *by SELDI mass spectrometry*. Presented at the Fifth International Symposium on Mass Spectrometry in the Health and Life Sciences: Molecular and Cellular Proteomics. UCRL-JC-144160.

Sokhansanj, B. A., and J. P. Fitch. (2001). *Practical modeling of* Yersinia *regulation with union-rule-configuration fuzzy logic*. Presented at the 2001 Annual Fall Meeting of the Biomedical Engineering Society. UCRL-JC-144081.

Section 4
Computing, Modeling, and Simulation

98-SI-008

Fattebert, J.-L., and F. Gygi. (2001). "Continuous solvation model for ab initio molecular dynamics simulations." *Tech. Proc. 2001 Int. Conf. Comput. Nanoscience.* <http://www.cr.org/publications/ICCN2001/index.html>. (Retrieved April 2002). UCRL-JC-140605.

99-ERD-015

Aufderheide, M. B., III et al. (2001). "Studies of dynamic failure of steel pipes using x-ray radiography." *Rev. Prog. Quant. Nondestructive Eval.* **21**. UCRL-JC-143473.

Logan, C. M., and A. E. Schach von Wittenau. (2001). "Effects of backshield albedo on imagery with a dpiX Flashscan20 using a 9-MV Bremsstrahlung spectrum." *Mater. Eval.* **59**(5), 617. UCRL-JC-136055.

Schach von Wittenau, A. E. et al. (2001). *Blurring artifacts in megavoltage radiography with a flat-panel imaging system: Comparison of Monte Carlo simulations with measurements*. UCRL-JC-144247.

99-ERD-016

Clague, D. S., and E. K. Wheeler. (2001). "Dielectrophoretic manipulation of macromolecules: The electric field." *Phys. Rev. E* **64**(2). UCRL-JC-142486.

Clague, D. S., and E. K. Wheeler. (2001). *Dynamic simulation of dielectrophoretic manipulation of spherical macromolecules in microflows*. Presented at the First Gordon Conference on the Chemistry and Physics of Microfluidics. UCRL-PRES-144857.

Weisgraber, T. H., E. K. Wheeler, and D. S. Clague. (2001). *Dynamic simulation of fluids and suspensions in microflows*. Presented at the AIChE Annual Meeting. UCRL-PRES-137061.

99-ERI-009

Bennett, J. et al. (2001). "Parallelizing a high accuracy hardware-assisted volume renderer for meshes with arbitrary polyhedra." *Proc. IEEE Symp. Parallel and Large-Data Visualization and Graphics.* UCRL-JC-143127.

Bertram, M. et al. (2001). "Wavelet representation of contour sets." *Proc. IEEE Visualization*. UCRL-JC-144651.

Bethel, W., R. J. Frank, and J. D. Brederson. (2002). *Combining a multithreaded scene graph system with a tiled display environment*. Presented at the Engineering Reality of Virtual Reality Conference. UCRL-JC-143204.

Duchaineau, M. A. et al. (2001). "Interactive display of surfaces using subdivision surfaces and wavelets." *Proc. 16th Spring Conf. Comput. Graphics.* UCRL-JC-145745.

Duchaineau, M. A. et al. (in press). "Dataflow and remapping for wavelet compression and view-dependent optimization of billion-triangle surfaces." *Hierarchical and Geometrical Methods in Scientific Visualization*. G. Farin, B. Hamann, and H. Hagen, Eds. (Springer-Verlag: Heidelberg, Germany). UCRL-JC-140718.

Laney, D., M. Duchaineau, and N. Max. (2001). "A selective refinement approach for computing the distance functions of curves." *Proc. IEEE TCVS Symp. Visualization*. UCRL-JC-142632.

LeMar, E. C., B. Hamann, and K. I. Joy. (2001). "A magnification lens for interactive volume visualization." *Proc. Pacific Graphics*. UCRL-JC-144766.

LeMar, E. C., B. Hamann, and K. I. Joy. (in press). "Efficient error calculation for multi-resolution texture-based volume visualization." *Hierarchical and Geometrical Methods in Scientific Visualization*. G. Farin, B. Hamann, and H. Hagen, Eds. (Springer-Verlag: Heidelberg, Germany). UCRL-JC-145831.

Lindstrom, P., and V. Pascucci. (2001). "Visualization of large terrains made easy." *Proc. IEEE Visualization 2001*. UCRL-JC-144753.

Max, N., P. Williams, and C. Silva. (2000). "Approximate volume rendering for curvilinear and unstructured grids by hardware-assisted polyhedron projection." *Int. J. Imaging Systems Tech.* **11**, 53. UCRL-JC-134175.

Pascucci, V. (2001). "On the topology of the level sets of a scalar field." *Proc. 13th Canadian Conf. Comput. Geometry*. UCRL-JC-142262.

Pascucci, V. (in press). "Multi-resolution indexing for hierarchical out-of-core traversal of rectilinear grids." *Hierarchical and Geometrical Methods inScientific Visualization*. G. Farin, B. Hamann, and H. Hagen, Eds. (Springer-Verlag: Heidelberg, Germany). UCRL-JC-140581.

Pascucci, V., and R. J. Frank. (2001). "Global static indexing for real-time exploration of very large regular grids." *Proc. Supercomput. 2001 Conf.* UCRL-JC-144754.

Sigeti, D. E. et al. (in press). "Approximating material interfaces in two-and three-dimensional meshes during data simplification." *Hierarchical Approximation and Geometrical Methods in Scientific Visualization*. G. Farin, B. Hamann, and H. Hagen, Eds. (Springer-Verlag: Heidelberg, Germany). UCRL-JC-145747.

Tsap, L. V. (2001). "Feedback from video for virtual reality navigation." *Proc. Int. Workshop on Digital and Comput. Video*. UCRL-JC-141131.

Tsap, L. V. (2001). "Gesture-tracking in real time with dynamic regional range computation." *Real-Time Imaging*. UCRL-JC-137651-REV-1.

Tsap, L. V., D. B. Goldgof, and S. Sarkar. (2001). "Fusion of physically based registration and deformation modeling for nongrid motion analysis." *IEEE Transactions on Image Processing*. UCRL-JC-136349-REV-1.

Tsap, L. V., and M. C. Shin. (2001). *Improving the quality and speed of range data for communication*. Presented at the IEEE Workshop on Cues in Communication. UCRL-JC-145664.

99-ERI-009

Lindstrom, P., and C. T. Silva. (2001). "A memory insensitive technique for large model simplification." *Proc. IEEE Visualization 2001*. UCRL-JC-144550.

99-ERI-010

Cantu-Paz, E. (2001). *Single vs. multiple runs under constant computation cost.* Presented at the Genetic and Evolutionary Computation Conference. UCRL-JC-142172.

Cantu-Paz, E. (2001). *Supervised and unsupervised discretization methods for evolutionary algorithms*. Presented at the Genetic and Evolutionary Computation Conference 2001 Workshop on Optimization by Building and Using Probabilistic Models. UCRL-JC-142243.

Cantu-Paz, E., and C. Kamath. (2000). *Improving the performance of linear decision trees with evolutionary algorithms*. Presented at the Center for Advancement of Signal and Image Sciences Workshop at LLNL. UCRL-JC-141297.

Cantu-Paz, E., and C. Kamath. (2001). *Inducing oblique decision trees with evolutionary algorithms*. UCRL-JC-143718.

Cantu-Paz, E., and C. Kamath. (2001). *Sapphire: Mining scientific datasets*. Presented at the Joint Statistical Meetings. UCRL-JC-142044.

Fodor, I. K. (2001). *Statistical issues in data mining*. Presented at the Fifth North American Meeting of New Researchers in Statistics and Probability. UCRL-JC-142212.

Fodor, I. K., and C. Kamath. (2000). *Wavelet-based denoising techniques in Sapphire*. Presented at the Center for Advancement of Signal and Image Sciences Workshop at LLNL. UCRL-JC-141298.

Fodor, I. K., and C. Kamath. (2001). *Denoising through wavelet shrinkage: An empirical study*. UCRL-JC-144258.

Fodor, I. K., and C. Kamath. (2001). *On denoising images using wavelet-based statistical techniques.* UCRL-JC-142357.

Fodor, I. K., and C. Kamath. (2001). *On the use of evolutionary algorithms in data mining*. Presented at the MSRI Workshop on Nonlinear Estimation and Classification. UCRL-JC-141738.

Fodor, I. K., and C. Kamath. (2001). "The role of multiresolution in mining massive image datasets." *Symp. Adv. Multiscale and Multiresolution Methods*. (Springer-Verlag Lecture Notes). p 307. UCRL-JC-139713.

Fodor, I. K., and C. Kamath. (in press). "A comparison of denoising techniques for FIRST images." *Proc. Third Workshop on Mining Scientific Datasets*. UCRL-JC-142085.

Fodor, I. K., and C. Kamath. (in press). "Dimension reduction techniques and the classification of bent-double galaxies." *Comp. Stat. and Data Anal.* UCRL-JC-144209.

Grossman, R., C. Kamath, and V. Kumar. (2001). *Data mining for scientific and engineering applications*. Presented at Supercomputing 2001. UCRL-JC-145087.

Kamath, C. (2001). *Data mining for science and engineering applications*. Presented at the First SIAM Conference on Data Mining. UCRL-JC-142626.

Kamath, C. (2001). *Mining science data: The Sapphire approach*. Presented at the Computer Science, Electrical Engineering Department Colloquium, University of Nevada, Reno. UCRL-JC-143254.

Kamath, C. (2001). "On mining scientific data sets." *Data mining for scientific and engineering applications*. R. Grossman et al., Eds. (Kluwer: New York). p 1. UCRL-JC-141709.

Kamath, C. (Ed.). (2001). *Proceedings of the Fourth Workshop on Mining Scientific Datasets*. UCRL-ID-144763.

Kamath, C. (2001). "The role of parallel and distributed processing in data mining." *Newslett. IEEE Tech. Committee on Distributed Processing*. UCRL-JC-142468.

Kamath, C., and E. Cantu-Paz. (in press). "Creating ensembles of decision tress through sampling." *Proc. 33rd Symp. Interface Comput. Sci. Stat.* UCRL-JC-142268.

Kamath, C. et al. (2001). "Searching for bent-double galaxies in the FIRST survey." *Data mining for scientific and engineering applications*. R. Grossman et al., Eds. (Kluwer: New York). p 95. UCRL-JC-140418.

Kamath, C. et al. (2001). "Using data mining to find bent-double galaxies in the FIRST survey." *SPIE Proc. Astro. Data Anal*. **4477**, 11. UCRL-JC-143458.

99-SI-005

Sackett, D. E., and B. E. Anderson. (2001). *Network mapping and vulnerability assessment*. UCRL-ID-145348.

00-ERD-007

Fattebert, J.-L., and F. Gygi. (2001). "Continuum solvation model of ab initio molecular dynamics simulations." *Proc. 2001 Intl. Conf. Comput. Nanoscience* **1**, 185. UCRL-JC-140605.

Fattebert, J.-L., and F. Gygi. (2001). *First principles molecular dynamics simulations in a continuum solvent*. UCRL-JC-146694.

Fattebert, J.-L., and F. Gygi. (in press). "Density functional theory for efficient ab initio molecular dynamics in solution." *J. Comput. Chem.* UCRL-JC-143326.

00-ERD-016

Dorr, M. R., F. X. Garaizar, and J. A. F. Hittinger. (2001). *Adaptive mesh refinement in laser plasma simulation*. Presented at the 30th Anomalous Absorption Conference. UCRL-PRES-143652.

Dorr, M. R., F. X. Garaizar, and J. A. F. Hittinger. (in press). "Simulation of laser plasma filamentation using adaptive mesh refinement." *J. Comput. Phys.* UCRL-JC-138330.

Hittinger, J. A. F. (2001). *On the use of adaptive mesh refinement in laser plasma simulation*. Presented at the DOE Computational Science Graduate Fellowship Conference. UCRL-PRES-143656.

00-ERD-017

Carlsson, L., and N. A. Petersson. (2001). *Optimizing chimera grids using genetic algorithms*. UCRL-JC-143856.

Chand, K. (2001). *Unstructured hybrid mesh support for Overture: A description of the Ugen and Advancing Front classes and documentation for additional support classes.* UCRL-MA-144020.

Fast, P., and W. D. Henshaw. (2001). *Time-accurate computation of viscous flow around deforming bodies using overset grids*. Presented at the 15th American Institute of Aeronautics and Astronautics (AIAA) Computational Fluid Dynamics Conference. (AIAA Paper 2001-2604). UCRL-JC-140714.

Henshaw, W. D. (2001). "An algorithm for projecting points onto a patched CAD model." *Proc. 10th Intl. Meshing Roundtable*. <http://www.andrew.cmu.edu/user/sowen/imr10.html>. (Retrieved April 2002). UCRL-JC-1440106.

Petersson, N. A., and K. Chand. (2001). "Detecting translation errors in CAD surfaces and preparing geometries for mesh generation." *Proc. 10th Intl. Meshing Roundtable*. <http://www.andrew.cmu.edu/user/sowen/imr10.html>. (Retrieved April 2002). UCRL-JC-144019.

00-ERD-018

Brezina, M. A. et al. (2000). "Algebraic multigrid based on element interpolation (AMGe)." *SIAM J. Sci. Comput.* **22**, 1570. UCRL-JC-131752.

Cleary, A. J. et al. (2000). "Coarse grid selection for parallel algebraic multigrid." *Lecture Notes in Comput. Sci.* **1457**, 104. UCRL-JC-130893.

Cleary, A. J. et al. (2000). "Robustness and scalability of algebraic multigrid." *SIAM J. Sci. Comput.* **21**, 1886. UCRL-JC-130718.

Henson, V. E., J. K. Kraus, and P. S. Vassilevski. (2001). "Element-free AMGe: General algorithms for computing the interpolation weights in AMG." *SIAM J. Sci. Comput.* **23**, 629. UCRL-JC-139098.

Henson, V. E., and U. M. Yang. (in press). "BoomerAMG: A parallel algebraic multigrid solver and preconditioner." *Appl. Num. Math.* UCRL-JC-141495.

Jones, J. E., and P. S. Vassilevski. (2001). "AMGe based on element agglomeration." *SIAM J. Sci. Comput.* **23**, 109–133. UCRL-JC-135441.

00-ERD-031

Galli, G., and F. Gygi. (2001). *Electronic excitations and the compressibility of hydrogen*. UCRL-JC-145048.

Galli, G., E. Schwegler, and F. Gygi. (2001). *First principles simulations of shock front propagation in liquid deuterium*. UCRL-JC-145224.

Galli, G. et al. (2001). *Hydrogen bonding and molecular dissociation in water under pressure*. Presented at the American Physical Society Meeting. UCRL-JC-143276.

Lightstone, F. C. et al. (2001). "A first-principles molecular dynamics simulation of the hydrated magnesium ion." *Chem. Phys. Lett.* **343**, 549. UCRL-JC-141754.

Schwegler, E. et al. (in press). "The dissociation of water under pressure." *Phys. Rev. Lett.* UCRL-JC-145220.

00-ERD-056

Vincent, P. (2000). "Aseismic Mw = 5.3 and 5.6 slip events along the southern San Andreas fault system captured by radar interferometry," *Proc. Third Conf. on Tectonic Problems of the San Andreas Fault System.* (Stanford UP: Stanford, CA). p 193. UCRL-JC-145561.

Vincent, P., K. Tiampo, and J. B. Rundle. (2000). *Aseismic, potentially pre-cursory slip in southern California imaged by InSAR correlated with high probability regions produced by a new seismicity-based space-time pattern dynamics with high probability regions predicted by new seismicity-based space.* Presented at the American Geophysical Union Meeting Fall 2000. UCRL-JC-140233.

00-ERD-057

Johnson, J. W., and J. J. Nitao. (2002). *Enhanced cap rock integrity and self-sealing of the immiscible plume through mineral trapping duration prograde and retrograde CO_2 sequestration in saline aquifers*. Presented at the Annual Meeting of the American Association of Petroleum Geologists. UCRL-JC-146931.

Johnson, J. W., J. J. Nitao, and C. I. Steefel. (2000). *Reactive transport modeling of geologic CO_2 sequestration: Identification of optimal target formations based on geochemical, hydrologic, and structural constraints.* Presented at the Annual Meeting of the Geological Society of America. UCRL-JC-146930.

Johnson, J. W., J. J. Nitao, and C. I. Steefel. (2002). *Fundamental elements of geologic CO_2 sequestration in saline aquifers*. Presented at the Annual Meeting of the American Chemical Society. UCRL-JC-146929.

Johnson, J. W., C. I. Steefel, and J. J. Nitao. (2000). *Reactive transport modeling of geologic CO_2 sequestration to identify optimal target formations: Quantifying the relative effectiveness of mitigation and sequestration processes as a function of reservoir properties.* Presented at the Annual Fall Meeting of the American Geophysical Union. UCRL-JC-146928.

Johnson, J. W. et al. (2001). "Reactive transport modeling of geologic CO_2 sequestration in saline aquifers: The influence of intra-aquifer shales and the relative effectiveness of structural, solubility, and mineral trapping during prograde and retrograde sequestration." *Proc. First Natl. Conf. Carbon Sequestration*. UCRL-JC-146932.

Johnson, J. W. et al. (2001). *Reactive transport modeling of geologic CO_2 sequestration to identify optimal target formations: Quantifying the relative effectiveness of mitigation and sequestration processes as a function of reservoir properties*. Presented at the First National Conference on Carbon Sequestration. UCRL-JC-146928-REV-1.

00-LW-068

George, J. A., M. E. Colvin, and V. V. Krishnan. (2001). *A simulator for ensemble quantum computing*. UCRL-JC-143936.

Krishnon, V. V. (2001). "Estimating the efficiency of ensemble quantum computing." *Phys. Lett. A*. UCRL-JC-144113.

00-SI-002

Epperly, T., S. Kohn, and G. Kumfert. (2000). "Component technology for high-performance scientific simulation software." *The Architecture of Scientific Software*. R. F. Biosvert and P. T. P. Tang, Eds. (Kluwer: Norwell, MA). p 69. UCRL-JC-140549.

Kohn, S. et al. (2001). "Divorcing language dependencies from a scientific software library." *Proc. 10th SIAM Conf. Parallel Processing*. UCRL-JC-140349.

00-SI-004

Cavallo, R. et al. (2001). "DJEHUTY, a next-generation stellar-evolution code." *BAAS* **198**, 6513. UCRL-JC-143194.

Eggleton, P. P., and L. Kiseleva-Eggleton. (2001). "Not-so-simple triple systems." *ASP Conf. Proc*. **229**, 91. UCRL-JC-144485.

Eggleton, P. P., and C. A. Nelson. (2001). "Case A binary evolution." *ASP Conf. Proc.* **229**, 205. UCRL-JC-143307.

Eggleton, P. P., and C. A. Nelson. (2001). "A complete survey of case A binary evolution with comparison to observed Algol-type systems." *Astrophys. J.* **552**, 664. UCRL-JC-140453.

Turcotte, S. (2001). "Chemical inhomogeneities and pulsation." *IAU Coll.* **185**. (PASP Conf. Ser.). UCRL-JC-144692.

Turcotte, S. (2001). *The evolution of the solar composition and possible implications on the study of interplanetary particles*. Presented at the Amercian Geophysical Union Spring Meeting. UCRL-JC-144123.

Turcotte, S. et al. (2001). "DJEHUTY, a code for modeling whole stars in three dimensions." *IAU Coll.* **185**. (PASP Conf. Ser.). UCRL-JC-144483.

01-ERD-008

Paglieroni, D. W. (2001). *Hyperspectral image-based broad area search (HIBAS), FY01 final report*. UCRL-ID-145666.

Paglieroni, D. W., and D. E. Perkins. (2001). "Automatic extraction of spectrally homogeneous closed pixel clusters for target cueing in hyperspectral images." *Proc. SPIE 46th Annual Meet. Int. Symp. Opt. Sci. Tech.* UCRL-JC-141883.

Paglieroni, D. W., and D. E. Perkins. (in press). "Spatial constraints on segmented regions for target cueing in hyperspectral images." Presented at the 2001 Meeting of the MSS Specialty Group on Passive Sensors. UCRL-JC-142307.

01-ERD-010

Bond, T. C. et al. (2001). "Performance investigation of all-optically controlled multi-section MQW laser for digital logic applications." *Proc. OSA Annual Meeting 2001*. UCRL-JC-143625.

Bond, T. C. et al. (2001). "A time-domain model for optically controlled multi-section MQW lasers for digital logic applications." *Proc. Fourth Biennial Tri-Laboratory Engineering Conf. on Modeling and Simulations*. UCRL-JC-144689.

01-ERD-015

Asoka-Kumar, P. R. et al. (2001). *Opportunities for materials characterization using high-energy positron beams*. UCRL-JC-145018.

Eshed, A. et al. (2001). *Gamma spectra resulting from the annihilation of positrons with electrons in a single core level*. UCRL-JC-145231.

Hartley, J. H. et al. (2001). *Positron annihilation with the anion in alkali halides*. UCRL-JC-145398.

Hastings, P., A. L. R. Bug, and P. A. Sterne. (2001). *Stimulation of positronium in silica sodalite*. UCRL-JC-143554.

Hunt, A. W. et al. (2001). "Doppler-broadening of in-flight positron annihilation radiation due to electron momentum." *Phys. Rev. Lett.* **86**, 5612. UCRL-JC-143552.

Larrimore, L. et al. (2000). "A two-chain path-integral model of positronium." *J. Chem. Phys.* **113**, 10642. UCRL-JC-140277.

Pask, J. E. et al. (2001). "Finite-element methods in electronic-structure theory." *J. Comput. Phys. Commun.* **135**, 1. UCRL-JC-139563.

Sterne, P. A., P. Asoka-Kumar, and R. H. Howell. (2001). *Atomic-based calculations of doppler broadening spectra*. UCRL-JC-144719.

Sterne, P. A. et al. (2001). *A finite-element approach to large-scale electronic calculations*. UCRL-JC-145227.

01-ERD-017

Williamson, A. J., R. Q. Hood, and J. C. Grossman. (2001). "Linear scaling quantum Monte Carlo calculations." *Phys. Rev. Lett.* **87**, 246406. UCRL-JC-143811.

01-ERD-033

Amendt, P. et al. (in press). "Hohlraum-driven noncryogenic double-shell ignition target designs for the National Ignition Facility." *IFSA 2001 Conf. Proc.* UCRL-JC-143188.

01-ERD-043

de Supinski, B. R. et al. (2001). *Benchmarking SMP memory system performance*. Presented at the International Business Machine SP Scientific Computing User Group, SciComp 4, Meeting. UCRL-JC-145223.

Mohan, T. et al. (2001). *Dynamic detection of streams in memory references*. Presented at the Los Alamos Computer Science Institute Symposium 2001. UCRL-JC-144546.

Mueller, F. et al. (2001). *Partial data traces: Efficient generation and representation*. Presented at the Workshop on Binary Translation, Parallel Architectures and Compilation Techniques. UCRL-JC-144405.

Parker, E., B. R. de Supinski, and D. J. Quinlan. (2001). *Measuring the regularity of array references*. Presented at the Los Alamos Computer Science Institute Symposium 2001. UCRL-JC-144545.

01-ERD-044

Buongiorno-Nardelli, M., J.-L. Fattebert, and J. Berholc. (2001). "An O(N) real-space method for ab initio quantum transport calculations." *Phys. Rev. B* **64**, 245423. UCRL-JC-142038.

Fattebert, J.-L. (2001). "Linear multigrid techniques in self-consistent electronic structure calculations." *NATO Sci. Ser. III* **177**, 104. UCRL-JC-140210.

Fattebert, J.-L. (2001). *Multigrid preconditioning for large-scale electronic structure calculations*. UCRL-JC-141988.

Lightstone, F. C. et al. (2001). "A first-principles molecular dynamics simulation of the hydrated magnesium ion." *Chem. Phys. Lett.* **343**, 549. UCRL-JC-141754.

Pizzagalli, L. et al. (2001). "Structure and stability of germanium nanoparticles." *Phys. Rev. B* **63**, 5324. UCRL-JC-140787.

Schwegler, E., G. Galli, and F. Gygi. (2001). "Conformational dynamics of the dimethyl phosphate anion in solution." *Chem. Phys. Lett.* **342**, 434. UCRL-JC-141047.

01-LW-040

Kalos, M. H., and F. Pederiva. (2000). "Exact Monte Carlo for continuum fermion systems." *Phys. Rev. Lett.* **85**, 3547. UCRL-JC-136917.

01-LW-068

Koning, J. M., G. Rodrigue, and D. White. (2001). *Linear magnetohydrodynamics using the vector finite element method*. Presented at the SIAM Annual Meeting. UCRL-MI-142200.

01-SI-012

Balu, N. et al. (in press). "Modified guanines representing O^6-alkylation by the cyclophosphamide metabolites acrolein and chloracetalkdehyde: Synthesis, stability, and ab initio studies." *Chem. Res. Toxicol.* UCRL-JC-145823.

Hatch, F. T., M. G. Knize, and M. E. Colvin. (in press). "Extended QSAR for 80 aromatic and heterocyclic amines: Structural, electronic and hydropathic factors affecting mutagenic potency." *Environ. Mol. Mitagen*. UCRL-JC-141893.

Lee, B. et al. (in press). "Molecular interactions of human exol with DNA." *Nucleic Acids Res*. UCRL-JC-146093.

Lightstone, F. C. et al. (2001). "A first principles molecular dynamics simulation of the hydrated magnesium ion." *Chem. Phys. Lett.* **343**, 549. UCRL-JC-141754.

Long, S. A. et al. (2001). "Immunoreactivity of organic mimeotopes of PDC–E2: Connecting xenobiotic with primary biliary cirrhosis." *J. Immunol.* **167**, 2956. UCRL-JC-143324.

Schwegler, E., G. Galli, and F. Gygi. (2001). "Conformational dynamics of the dimethyl phosphate anion in solution." *Chem. Phys. Lett.* **342**, 434. UCRL-JC-141047.

Tran, N. L. et al. (in press). "Experimental and simulation studies of heat flow and heterocyclic amine mutagen/carcinogen formation in pan-fried meat patties." *Food Chem. Toxicol.* UCRL-JC-142434.

Wilson, D. M., III, and D. Barsky. (2001). "The major human abasic endonuclease apel: Formation, consequences, and repair of abasic lesions in DNA." *Mutat. Res.* **485**, 283. UCRL-JC-140433.

Section 5
Energy and Environmental Technologies

00-ERD-011

Kersting, A. B. (in press). "Colloids and radionuclide transport." *Uncertainty Underground: Dealing with the Nation's High-Level Nuclear Waste*. A. Macfarlane and R. Ewing, Eds. (MIT Press: Boston). UCRL-JC-147028.

00-ERD-059

Cherepy, N., R. Krueger, and J. F. Cooper. (2000). "Direct electrochemical conversion of carbon anode fuels in molten salt media." *Proc. Fall Meet. Electrochemical Soc., Power Sources for the New Millenium*. **PV 2000-22**. UCRL-JC-139288.

Cherepy, N., R. Krueger, and J. F. Cooper. (2001). "Evaluation of direct electrochemical conversion of carbon anode fuels in molten carbonate electrolyte in a novel configuration." *Fall 2001 Meet. Electrochemical Soc.* UCRL-JC-143398.

Cooper, J. F., N. Cherepy, and R. Krueger. (2000). *Direct electrochemical conversion of carbon: Systems for efficient conversion of fossil fuels to electricity*. Presented at the Fuel Cell 2000 Conference. UCRL-JC-138900.

Cooper, J. F. et al. (2000). "Direct carbon conversion fuel cells: Application to the efficient conversion of fossil fuels to electricity." *Proc. Fall Meet. Electrochemical Soc., Electrochemistry and Global Warming*. **PV 2000-20**, 78–90. UCRL-JC-140629.

01-ERD-041

Wirth, B. D. et al. (2000). "Positron annihilation spectroscopy and small angle neutron scattering characterization of nanostructural features in irradiated Fe–Cu–Mn alloys." *Mater. Res. Soc. Fall 2000 Symp. R Proc.* **R**, 6.5. <http://www.mrs.org/members/proceedings/fall2000/r/R6_5.pdf>. UCRL-JC-139402.

01-ERD-042

Marian, J. et al. (2001). Dynamics of self-interstitial migration in Fe–Cu alloys. *Phys. Rev. B* **64**, 094303. UCRL-JC-141715.

Odette, G. R. et al. (2001). "Multiscale-multiphysics modeling of radiation damaged materials: Embrittlement of pressure vessel steels." *Mater. Res. Bull.* **26**, 176. UCRL-JC-142559.

01-ERD-063

Beller, H. R. (in press). "Anaerobic biotransformation of RDX (hexahydro-1,3,5-trinitro-1,3,5-triazine) by aquifer bacteria using hydrogen as the sole electron donor." *Water Res*. UCRL-JC-141362.

Beller, H. R. (2001). *Detection of distinctive indicators of intrinsic RDX metabolism in groundwater at an army ammunition plant*. Presented at the Tri-Service Environmental Technology Symposium. UCRL-JC-142677.

01-ERD-065

Kane, S. R. et al. (2001). "Aerobic biodegradation of methyl tert-butyl ether by aquifer bacteria from leaking underground fuel tank sites." *Appl. Envir. Microbiol.* **67**(12), 5824. UCRL-JC-143865.

Kane, S. R. et al. (2001). *Aerobic metabolism of methyl tert-butyl ether by aquifer bacteria*. UCRL-MI-143791.

Kane, S. R. et al. (2001). *Evaluation of MTBE biodegradation in commercial LUFT sites: Microcosm studies*. UCRL-JC-140662.

01-ERD-106

Reynolds, J. G., P. G. Coronado, and S. J. Coleman. (2001). *Removal of uranium from groundwater using granulated activated carbon modified with hydrophobic aerogels*. Presented at the DOE Technical Information Exchange Conference. UCRL-JC-145512.

01-LW-002

Benedetti, L. C. et al. (2000). "Earthquake time-slip histories determined from in situ ^{36}Cl cosmogenic dating of limestone fault scarps: The Sparta Normal Fault (Greece)." *Eos Trans. AGU Fall Meet. Suppl. Abs.* **81**(48), T71E-10. UCRL-JC-140389.

Section 6
Lasers, Electro-Optics, and Beams

99-ERD-049

Mackinnon, A. J. et al. (2000). Effect of plasma scale length on multi-MeV proton production by ultra-short laser pulses. *Phys. Rev. Lett.* **86**, 1769. UCRL-JC-139273.

99-ERI-008

Gibson, D. J. et al. (2001). "Electron beam and RF characterization of a low-emittance x-band photoinjector." *Phys. Rev. Spec. Top.—Accelerators and Beams* **4**, 090101. UCRL-JC-143435.

Hartemann, F. V., and D. J. Gibson. (2001). *Experimental measurements of coherent synchrotron radiation in an x-band photoinjector*. Presented at the Annual Meeting of the American Physical Society Division of Plasma Physics. UCRL-JC-144646.

Hartemann, F. V. et al. (2000). "The chirped-pulse inverse free-electron laser: A high-gradient vacuum laser accelerator." *Phys. Plasmas* **6**, 4104. UCRL-JC-134073.

Hartemann, F. V. et al. (2000). *Three-dimensional theory of emittance in Compton scattering*. Presented at the Annual Meeting of the American Physical Society Division of Plasma Physics. UCRL-JC-140224.

Hartemann, F. V et al. (2001). *Experimental characterization of a high-brightness x-band photoinjector*. Presented at the Annual Meeting of the American Physical Society Division of Plasma Physics. UCRL-JC-144648.

Hartemann, F. V. et al. (2001). *Nonlinear laser acceleration in a magnetic field and the chirped-pulse inverse free-electron laser*. Presented at the Annual Meeting of the American Physical Society Division of Plasma Physics. UCRL-JC-144647.

Hartemann, F. V. et al. (2001). *Three-dimensional computer modeling of Compton scattering*. Presented at the Annual Meeting of the American Physical Society Division of Plasma Physics. UCRL-JC-144676.

Hartemann, F. V. et al. (2001). "Three-dimensional theory of emittance in Compton scattering and x-ray protein crystallography." *Phys. Rev. E* **64**, 016501. UCRL-JC-140944.

00-ERD-044

Celliers, P. M. et al. (2000). "Shock transformation of deuterium from molecular fluid insulator to liquid metal." *Phys. Rev. Lett.* **84**, 5564. UCRL-JC-130339-REV-1.

Collins, G. W. (2000). "Laser-shock-driven laboratory measurements of the equation of state of hydrogen isotopes in the megabar regime." *High Pressure Res.* **16**, 281. UCRL-JC-135406.

Collins, G. W. et al. (2001). "Shock temperature of liquid deuterium up to 2.4 Mbar pressures." *Phys. Rev. Lett.* **87**, 165504. UCRL-JC-131955.

Gold, D. M. et al. (2001). "Optical interferometry diagnostics in laser-driven equation-of-state experiments." *Astrophys. J.* **127**, 267. UCRL-JC-134798.

00-ERI-004

Demos, S. G. et al. (2001). "Mechanisms to explain damage growth in optical materials." *SPIE* **4347**, 277. UCRL-JC-139771-REV-1.

Demos, S. G. et al. (in press). "Imaging of laser-induced defect reactions of individual defect nanoclusters." *Opt. Lett*. UCRL-JC-138882-REV-1.

Garces, N. Y. et al. (2001). "Identification of electron and hole traps in KH_2PO_4 crystals." *J. Appl. Phys*. **89**, 47. UCRL-JC-139770.

Zhang, Oing et al. (in press). "Ab initio study of the electronic and structural properties of the ferroelectric transition in KH_2PO_4." *Phys. Rev. B*. UCRL-JC-144359.

01-ERD-031

Kalantar, D. H. et al. (2001). *Laser-driven high pressure, high strain-rate materials experiments*. UCRL-JC-141824.

01-ERD-072

Rushford, M. R. et al. (2001). "Wet-etch figuring: Optical surfacing by controlled application of etchant solution using the Marangoni effect." *Proc. SPIE* **4440**. UCRL-JC-143914.

01-ERD-107

Froula, D., L. Divol, and S. H. Glenzer. (2001). "Growth of ion acoustic waves in plasma." *Bull. Am. Phys. Soc*. UCRL-JC-144575.

Glenzer, S. H. et al. (in press). "Anomalous absorption of high-energy green laser light in high-Z plasmas." *Phys. Rev. Lett.* UCRL-JC-145287.

Glenzer, S. H. et al. (2001). "Ionization balance in inertial confinement fusion hohlraums." *Phys. Rev. Lett.* **87**, 045002. UCRL-JC-139505.

Glenzer, S. H. et al. (2001). "Reduction of stimulated scattering losses from hohlraum plasmas with laser beam smoothing." *Phys. Plasmas* **8**, 1692. UCRL-JC-141689.

01-SI-007

Anderson, S. G. et al. (2001). "Space-charge effects in high brightness electron beam emittance measurements." *Phys. Rev. Special Topics: Accelerators and Beams*. UCRL-JC-145571.

Slaughter, D. et al. (2001). *Development of a sub-picosecond tunable x-ray source at the LLNL electron linac*. UCRL-JC-144637.

01-SI-010

Thompson, C. A. et al. (2001). "Horizontal path laser communications employing MEMS adaptive optics correction." *SPIE Proc*. **4494**. UCRL-JC-145326.

01-SI-011

Beach, R. J. et al. (2001). *Scalable antiguided ribbon laser concept*. UCRL-JC-143422.

Section 7
Materials Synthesis and Characterization

99-ERD-004

Baumann, T. F., G. A. Fox, and A. L. Vance. (2001). *Dendritic methodology applied to the prediction, design, and synthesis of sol gel materials*. Presented at the American Chemical Society Symposium Series, Division of Polymer Chemistry. UCRL-JC-133875.

99-ERD-007

Saw, C. K. et al. (2001). "Using simultaneous time-resolved shg and xrd diagnostics to examine phase transitions of HMX and TATB." *Am. Phys. Soc. Proc. 2001*. UCRL-JC-142332.

99-ERD-066

Shestakov, J., L. Milovich, and A. Noy. (in press). "Solution of the nonlinear Poisson-Boltzmann equation using pseudo transient continuation and the finite element method." *J. Colloid Interface Sci.* UCRL-JC-139342.

99-ERI-011

De Yoreo, J. J. et al. (2000). *Force microscopy investigation of trends in surface dynamics during crystal growth from solution*. Presented at the 2000 Materials Research Society Spring Meeting. UCRL-JC-133041.

Fenter, P. et al. (2001). "Structure of barite (001)- and (210)-water interfaces." *J. Phys. Chem. B* **105**, 8112. UCRL-JC-142042.

McBride, M. T. et al. (2000). *Surface investigations of amino acid binding on calcite*. Presented at the 2000 Materials Research Society Spring Meeting. UCRL-JC-136683.

Noy, A. et al. (2000). *Morphological changes in calcite induced by amino acids: emergence of chirality*. Presented at the 2000 Materials Research Society Spring Meeting. UCRL-JC-135308.

Orme, C. A. et al. (2000). *Selective binding of chiral amino acids to atomic steps of calcite.* Presented at the 2000 Materials Research Society Spring Meeting. UCRL-JC-135307.

Orme, C. A. et al. (2001). "Formation of chiral morphologies through selective binding of amino acids to calcite surface steps." *Nature* **411**, 775. UCRL-JC-135307.

Reedjik, M. F. et al. (2001). "Structure of liquid Sn on Ge(111)." *Phys. Rev. B* **64**, 033403. UCRL-JC-142042.

00-ERD-012

Suratwala, T.I., and R. A. Steele. (2001). *Anomalous temperature dependence of sub-critical crack growth in silica glass.* UCRL-JC-145105-REV-1.

00-ERD-013

Génin, F. Y. (2001). "Surface morphological evolution of thin films under stress and capillary forces." *Interface Sci.* **9**, 81. UCRL-JC-141512.

McCormick, M. A. et al. (2001). *Pulsed laser deposited ferroelectric Pb (Zr,Ti)03 thin-film oxygen sensors*. Presented at the Material Research Society Spring Meeting. UCRL-JC-142195.

Salleo, A. et al. (2001). "Energy deposition at front and rear surfaces during piosecond laser interation with silica." *Appl. Phys. Lett.* **78**, 192840. UCRL-JC-141784.

00-ERD-033

Bastea, M., A. C. Mitchell, and W. J. Nellis. (2001). "High pressure insulator-metal transition in molecular fluid oxygen." *Phys. Rev. Lett*. **86**, 3108. UCRL-JC-141433.

Chau, R. et al. (2001). "Electrical conductivity of water compressed dynamically to pressures of 70–180 GPa (0.7–1.8 Mbar)." *J. Chem. Phys.* **114**, 1361. UCRL-JC-135379.

00-LW-010

Taylor, B. R. et al. (in press). "Solution preparation of Ge nanoparticles with tailored surfaces." *Mater. Sci. Eng. B*. UCRL-JC-145430.

00-LW-037

Bastea, M. (2001). *New physics at extreme conditions—outstanding results on shock compressed molecular fluids and lithium.* Presented at the Biennial International Conference of the American Physical Society Topical Group in Shock Compression of Condensed Matter. UCRL-JC-142785.

Bastea, M., and S. Bastea. (2001). "Electrical conductivity of Li at Mbar pressures." *Phys. Rev. Lett.* UCRL-JC-144385.

00-LW-058

Huser, T., and M. Yan. (2001). "Aggregation quenching in thin films of MEH-PPV studied by near-field scanning optical microscopy and spectroscopy." *Synth. Met.* **116**, 333. UCRL-JC-138638.

Huser, T., M. Yan, and L. J. Rothberg. (2000). "Single chain spectroscopy of conformational dependence of conjugated polymer photophysics." *Proc. Natl. Acad. Sci. USA* **97**, 11187. UCRL-JC-138711.

01-ERD-022

Rudd, R. E., and J. Belak. (in press). "Void nucleation and associated plasticity in dynamic fracture of polycrystalline copper: An atomistic study." *Comp. Mat. Sci*. UCRL-JC-144339.

01-ERD-029

Haslam, J. J. et al. (in press). "Phase transformation hysteresis in a plutonium alloy system: Modeling the resistivity during the transformation." *Mater. Res. Soc. Symp. Proc.* UCRL-JC-144283.

01-ERD-030

Allen, P. G. et al. (2001). *Studies of vibrational properties in Ga-stabilized d-Pu by extended x-ray absorption fine structure*. UCRL-JC-146442.

Section 8
Nuclear and Atomic Science

99-ERD-044

Foord, M. E. et al. (2001). "Photoionization and heating of a well characterized iron plasma, in spectroscopic challenges of photoionized plasmas." *Astron. Soc. Pacific Conf. Ser.* **247**, 117. UCRL-JC-143067.

Heeter, R. F. et al. (2000). *Iron photoionization experiments to benchmark models of the spectra of accretion-powered sources*. Presented at the High Energy Astrophysics Division of the American Astronomical Society Meeting. UCRL-JC-141129.

Heeter, R. F. et al. (2000). *Photoionization equilibrium of iron radiative properties of hot dense matter*. UCRL-JC-141116.

Heeter, R. F. et al. (2000). *X-ray photoionized plasmas in the laboratory*. Presented at the Atomic Data Needs for X-ray Astronomy Workshop. UCRL-JC-137493.

Heeter, R. F. et al. (2000). *X-ray spectroscopy of astrophysically relevant photoionized iron plasma at Z*. Presented at the 12th APS Conference. UCRL-JC-137660.

00-ERD-025

Chapman, H., and K. A. Nugent. (in press). "X-ray pulse compression using strained crystals." *Opt. Commun.* UCRL-JC-145127.

London, R. et al. (2001). "Computational simulations of high-intensity x-ray matter interaction." *Proc. SPIE Annu. Meet.* UCRL-JC-142074.

Ryutov, D., and A. Toor. (2001). "Optical elements based on the use of renewable liquid films with magneto-electrostatic control." *Rev. Sci. Instr.* **72**, 4042. UCRL-JC-141538.

Ryutov, D., and A. Toor. (2001). "Renewable liquid optics with magnetoelectrostatic control." *Proc. SPIE Annu. Meet.* UCRL-JC-142094.

Wootton, A. et al. (2001). "Research and development for x-ray optics and diagnostics on the Linac Coherent Light Source (LCLS)." *Proc. FEL 2001 Conf. User Workshop.* UCRL-JC-145122.

Wootton, A. et al. (2001). "X-ray optics and diagnostics for the first experiments on the Linac Coherent Light Source." *Proc. SPIE Annu. Meet.* UCRL-JC-144183.

00-ERD-026

Johnson, S. (2001). "First measurements of pion correlations by the PHENIX experiment." *Nuc. Phys. A* **A698**, 603C. UCRL-JC-143580.

00-ERD-028

Barrett, B. R., P. Navratil, and J. P. Vary. (2001). *Ab initio shell model and its application to A=6 systems.* Presented at the Meeting of the American Physical Society. UCRL-JC-142079.

Barrett, B. R. et al. (2001). *Ab initio large-basis no-core shell model and its application to light nuclei*. Presented at Mazurian Lakes Summer School. UCRL-JC-145062.

Barrett, B. R. et al. (2001). *Ab initio no-core shell model*. Presented at the International Symposium on Nuclear Structure Physics. UCRL-JC-142761.

Barrett, B. R. et al. (2001). *Large-basis ab initio no-core shell model.* Presented at the International Nuclear Physics Conference. UCRL-JC-143431.

Caurier, E. P. et al. (2001). "Intruder states in ^{8}Be." *Phys. Rev. C* **64**, 051301. UCRL-JC-144859.

Kamada, H. et al. (2001). "Benchmark test calculation of a four-nucleon bound state." *Phys. Rev. C* **64**, 04401. UCRL-JC-143602.

Marsden, D. B. et al. (2001). *The Tucson-Melbourne three-body force in a translationally-invariant harmonic oscillator basis*. Presented at the Meeting of the American Physical Society. UCRL-JC-142078.

Navratil, P. (2001). *A > 4 systems with the harmonic oscillator effective interaction method*. Presented at the ECT Workshop on Few-Body Systems at Low and Moderate Energies: Open Questions beyond Computational Problems. UCRL-PRES-144317.

Navratil, P., W. E. Ormand, and J. P. Vary. (2001). *Ab initio shell model with three-body interactions for p-shell nuclei: I. Three-body effective interaction calculation.* Presented at the Topical Meeting of the Division of Nuclear Physics of the American Physical Society. UCRL-JC-144862.

Navratil, P. et al. (2001). "Six nucleon spectroscopy from realistic non-local Hamiltonian." *Phys. Rev. Lett.* **87**, 172501. UCRL-JC-143670.

Navratil, P. et al. (2001). *Solving system of six nucleons interacting by a realistic non-local potential*. Presented at the International Nuclear Physics Conference. UCRL-JC-143430.

Ormand, W. E. (2001). *Ab initio nuclear structure from helium to oxygen*. Presented at the Nuclear Theory Workshop on Rare Isotope Physics. UCRL-PRES-144658.

Ormand, W. E., P. Navratil, and B. R. Barrett. (2001). *Ab initio shell-model with three-body interactions*. Presented at the International Nuclear Physics Conference. UCRL-JC-143433.

Ormand, W. E., P. Navratil, and J. P. Vary. (2001). *Ab initio shell model with three-body interactions for p-shell nuclei: II. Codes and results for ^{8}Be and ^{10}B*. Presented at the Topical Meeting of the Division of Nuclear Physics of the American Physical Society. UCRL-JC-145695.

Vary, J. P., P. Navratil, and B. R. Barrett. (2001). *Properties of ^{12}C in the ab-initio nuclear shell model*. Presented at the Meeting of the American Physical Society. UCRL-JC-142078.

00-ERD-035

Fischer, S. M. et al. (2001). "Alignment delays in the N = Z nuclei ^{72}Kr, ^{76}Sr, and ^{80}Zr." *Phys. Rev. Lett.* UCRL-JC-144442.

Garrett, P. E. et al. (2000). "Observation of ^{46}Cr with GAMMASPHERE+FMA." *Bull. Am. Phys. Soc.* UCRL-JC-139555.

Garrett, P. E. et al. (2001). *Nuclear structure of the A = 45, T = 1 triplet*. UCRL-JC-142679.

Garrett, P. E. et al. (2001). "Observation of ^{46}Cr and testing of the isobaric multiplet mass equation at high spin." *Phys. Rev. Lett.* **87**, 132502. UCRL-JC-142634.

Garrett, P. E. et al. (2001). "Spectroscopy of the T = 1 band in the N = Z nucleus ^{46}V." *Bull. Am. Phys. Soc.* UCRL-JC-144441.

Schiller, A. et al. (2001). *Radiative strength function in deformed rare earth nuclei below the neutron binding energy*. UCRL-JC-142880.

Schiller, A. et al. (2001). *Thermodynamical properties of rare earth nuclei: The melting of pair correlations.*" UCRL-JC-142881.

Tavukcu, E. et al. (2001). *Thermodynamical properties of ^{56}Fe*. UCRL-PRES-143032.

Younes, W., J. A. Becker, and L. A. Bernstein. (2001). "Transition from asymmetric to symmetric fission in the 23 5U(n,f) reaction." *Phys. Rev. C*. UCRL-JC-143586.

00-ERD-037

Beiersdorfer, P. (2001). *Laboratory simulation of charge exchange induced x-ray emission from comets*. Presented at the International Seminar on Atomic Collisions. UCRL-JC-144976.

Beiersdorfer, P. et al. (2000). "X-ray signatures of charge transfer reactions involving cold, very highly charged ions." *AIP Conf. Proc.* **500**, 626. UCRL-JC-136569.

Beiersdorfer, P. et al. (2001). *Charge-exchange-induced K-shell x-ray line emission from highly charged ions*. Presented at the International Conference on the Physics of Electronic and Atomic Collisions. UCRL-JC-143174.

Beiersdorfer, P. et al. (2001). "X-ray velocimetry of solar wind ion impact on comets." *Astrophys. J. Lett.* **549**, L147. UCRL-JC-141555.

Perez, J.A., R. E. Olson, and P. Beiersdorfer. (2001). "Charge transfer and x-ray emission reaction involving highly charged ions and neutral hydrogen." *J. Phys. B* **34**, 3063. UCRL-JC-141894.

Schweikhard, L., P. Beiersdorfer, and E. Träbert. (2001). "EBIT in the magnetic mode: Mass spectrometry, atomic lifetime measurements, and charge transfer reaction of highly charged atomic ions." *Proc. 2001 Workshop on Non-Neutral Plasmas*. UCRL-JC-143990.

00-SI-005

Abe, T. et al. (2001). *Linear Collider Physics Resource Book for Snowmass 2001*. (American Linear Collider Working Group). UCRL-ID-143810.

Elmer, J. W., J. Klingmann, and K. van Bibber. (in press). "The effect of surface condition on the strength of diffusion bonded copper for linear collider accelerator structures." *Sci. Tech. Welding and Joining.* UCRL-JC-141309.

Elmer, J. W. et al. (2001). "Diffusion bonding and brazing of high purity copper for linear collider accelerator structures." *Phys. Rev. Special Topics: Accelerators and Beams*. **4**(5). UCRL-JC-135547.

Gronberg, J. (2001). "The NLC photon collider option, progress, and plans." *Proc. Int. Workshop on High Energy Photon Colliders 2001.* UCRL-ID-140291.

Gronberg, J. (2001). "Gamma–gamma interaction region design issues." *Proc. Linear Collider Workshop.* UCRL-JC-142080.

Gronberg, J. (2001). "NLC Interaction Region Layout and Background Estimates." *Proc. Linear Collider Workshop.* UCRL-JC-142271.

Gronberg, J. et al. (2001). "Lasers and optics for a gamma-gamma collider." *Proc. Particle Accelerator Conf. 2001.* UCRL-JC-144228.

Stein, W. et al. (2001). "Thermal shock structural analyses of a positron target." *Proc. Particle Accelerator Conf. 2001.* UCRL-JC-143893.

01-ERD-014

Wright, D. R. (2001). "Measurement of CP-violating asymmetries in B_o decays to CP eigenstates." *Phys. Rev. Lett.* **86**, 2515. UCRL-JC-142746.

01-ERD-025

Cauble, R. et al. (2001). *Isentropic compression experiments to 1 Mbar using magnetic compression*. Presented at the Association for the International Advancement of High Pressure and Technology Conference. UCRL-JC-143364.

Reisman, D. et al. (2001). *MHD modeling of isentropic compression experiments*. Presented at the Annual Meeting of the American Physical Society Division of Plasma Physics. UCRL-JC-144794.

01-ERD-097

Bionta, R. M. (2001). *Prototype focusing element for the LCLS warm dense matter experiment.* <http://www-ssrl.slac.stanford.edu/lcls/LCLS_X-RAY-OPTICS_Fotos02.HTML>. (Retrieved April 2002). UCRL-MI-144723.

01-FS-003

Glenzer, S. H. (in press). "Dense plasma characterization by x-ray Thomson scattering." *Bull. Am. Phys. Soc.* UCRL-JC-144574.

Landen, O. L. et al. (in press). "Dense matter characterization by x-ray Thomson scattering," *J. Quant. Spectros. Radiat. Transfer*. UCRL-JC-141055.

Section 9
Space Science and Technology

99-ERD-041

Alard, C. et al. (2001). "Mass-losing semiregular variable stars in Baade's windows." *Astrophys. J.* **552**, 289. UCRL-JC-143278.

Alcock, C. et al. (2001). "MACHO Project limits on black hole dark matter in the 1–30 m solar range." *Astrophys. J. Lett.* **550**, L169. UCRL-JC-141915.

Alcock, C. et al. (2001). "The MACHO Project LMC variable star inventory: IX. Frequency analysis of the first-overtone RR Lyrae stars and the indication for nonradical pulsations." *Astrophys. J.* **542**, 257. UCRL-JC-140202.

Alcock, C. et al. (2001). "The MACHO Project LMC variable star inventory: X. The R Coronae Borealis stars." *Astrophys. J.* **554**, 298. UCRL-JC-141879.

Alcock, C. et al. (2001). "The MACHO Project: Microlensing optical depth toward the galactic bulge from difference image analysis." *Astrophys. J.* **541**, 734. UCRL-JC-139846.

Alcock, C. et al. (2001). "The MACHO Project: Microlensing results from 5.7 years of Large Magellanic Cloud observations." *Astrophys. J.* **542**, 281. UCRL-JC-137592.

99-ERI-003

Macintosh, B. et al. (2001). "Keck adaptive optics observations of the TW Hydrae association members." *Astron. Soc. Pacific Conf. Ser.* **244**, 309. UCRL-VG-138074.

Macintosh, B. et al. (2001). "Practical high-order adaptive optics systems for extrasolar planet searches." *Proc. SPIE* **4407**. UCRL-JC-145248.

Patience, J., B. Macintosh, and C. E. Max. (2001). "High resolution imaging with AEOS." *Proc. SPIE*. UCRL-JC-145321.

Roe, H. G. et al. (2001). "Observations of Neptune's tropospheric cloud layer with the Lick Observatory adaptive optics system." *Astron. J*. **122**, 1636. UCRL-JC-137754.

00-ERD-037

Beiersdorfer, P. (2001). *Laboratory simulation of charge exchange induced x-ray emission from comets.* Presented at the International Seminar on Atomic Collisions. UCRL-JC-144976.

Beiersdorfer, P. et al. (2000). "X-ray signatures of charge transfer reactions involving cold, very highly charged ions." *AIP Conf. Proc*. **500**, 626. UCRL-JC-136569.

Beiersdorfer, P. et al. (2001). *Charge-exchange-induced K-shell x-ray line emission from highly charged ions*. Presented at the International Conference on the Physics of Electronic and Atomic Collisions. UCRL-JC-143174.

Beiersdorfer, P. et al. (2001). "X-ray velocimetry of solar wind ion impact on comets." *Astrophys. J. Lett.* **549**, L147. UCRL-JC-141555.

Perez, J. A., R. E. Olson, and P. Beiersdorfer. (2001). "Charge transfer and x-ray emission reaction involving highly charged ions and neutral hydrogen." *J. Phys. B* **34**, 3063. UCRL-JC-141894.

Schweikhard, L., P. Beiersdorfer, and E. Träbert. (2001). "EBIT in the magnetic mode: Mass spectrometry, atomic lifetime measurements, and charge transfer reaction of highly charged atomic ions." *Proc. 2001 Workshop on Non-Neutral Plasmas.* UCRL-JC-143990.

00-ERD-049

Canalizo, G. (2000). "Age-dating of interaction-induced starbursts in QSO host galaxies and companions." *Bull. Am. Astron. Soc.* **32**, 20.06. UCRL-JC-145781.

Canalizo, G. (2001). "The merger-starburst-AGN connection in QSOs." *Bull. Am. Astron. Soc.* **33**, 34.08. UCRL-JC-145780.

Canalizo, G., and A. Stockton. (2000). "Low-ionization BAL QSOs in ultraluminous infrared systems." *Astron. Soc. Pacific Conf. Ser.* UCRL-JC-144487.

Canalizo, G., and A. Stockton. (2001). "Quasi-stellar objects, ultraluminous infrared galaxies, and mergers." *Astrophys. J.* **555**, 719. UCRL-JC-143060.

Max, C. E. (2001). "Laser beacons for adaptive optics (star light star bright)." *OE Mag.* **1**, 30. UCRL-JC-141697.

Max, C. E. et al. (2001). "Adaptive optics observations of NGC 6240 at the Keck and Lick Observatories." *Bull. Am. Astron. Soc.* **32**, 52.07. UCRL-JC-145779.

01-ERD-013

Roe, H. G. et al. (2001). "Near-infrared observations of Neptune's tropospheric cloud layer with the Lick Observatory adaptive optics system." *Astron. J.* **122**, 1636. UCRL-JC-144352.

01-ERD-100

McLean, H. S., H. Chen, and D. D. Ryutov. (2001). "FLIRT: A magnetic field topology diagnostic for self-organized magnetically confined plasmas." *Bull. Am. Phys. Soc.* **46**. UCRL-JC-144624.

Ryutov, D. D. (2001). "The dynamics of fast electrons in a spheromak." *Bull. Am. Phys. Soc.* **46**. UCRL-JC-144605.

Ryutov, D. D. (2001). *Space-charge effects in the emission of fast electrons generated by a short laser pulse*. UCRL-JC-144196.

Principal Investigator Index

Project Title Index

Tracking Code Index